Fast Shearing Of Cohesive Soils Using Ring Shear Apparatus

Volume One Of Two

Paul Taylor

Thesis submitted to the University of Warwick
for the degree of Doctor of Philosophy

Department of Engineering
University of Warwick

September 1998

Abstract

Residual shear strength is a fundamental property of cohesive soils and is the governing parameter in many slope stability problems, particularly the reactivation of landslides. Traditionally, residual strengths are determined in the laboratory at slow drained rates of shearing using either shear boxes with reversals or ring shear apparatus. Many catastrophic landslides have been triggered by seismic loading inducing fast rates of shear. Interest has therefore developed in laboratory shear testing at faster rates and over greater displacements to establish fast residual shear strengths.

This thesis presents results from testing using the Imperial College–Norwegian Geotechnical Institute Ring Shear Apparatus modified to conduct shearing at velocities up to 1 m/min. The variation of residual strengths as shear rate increases is investigated in association with soil grading and plasticity and also with the morphology of the shear zone. A novel set of undulating interfaces are used to investigate the influence of shear zone waviness.

The research concludes that as shear rate is increased three types of fast residual shear strength variation may occur: (i) little variation from the slow residual shear strength, (ii) a continuous increase above the slow residual shear strength or (iii) an initial increase followed by a decrease to levels significantly below the slow residual shear strength. Increases in fast strength are attributed to particle disorientation and viscous effects. Falls in fast residual shear strength are attributed to the generation of positive pore water pressure in the shear zone, as a result of a pumping effect induced by wavy or inclined shear zones. Computational modelling of this pumping effect is undertaken using consolidation theory.

Fast peak strengths and slow peak strengths after fast shearing are also investigated. Finally, the influence on slow residual shear strength of shear zones with undulations parallel to the shear direction are studied both mathematically, and using the Bromhead Ring Shear Apparatus.

Contents

List of Figures

List of Tables

Notation

Symbol	Definition
A	Pore pressure parameter
A_v	Area of a vertical annular element
a	Geometric factor
a_e	Effective gradient
B	Mean landslide width
b	Geometric factor
C	Correction factor
C_n	Constant
C_p	Correction factor for a parabolic wave-form
C_s	Correction factor for a sine wave-form
C_v	Correction factor for a v-shape wave-form
CF	Clay fraction
c	Geometric factor
c'	Effective cohesive strength
c'_r	Effective residual cohesive strength
c_v	Coefficient of consolidation
c_{vswell}	Coefficient of consolidation for swelling
c_{v50}	Coefficient of consolidation determined from t_{50}
c_{v90}	Coefficient of consolidation determined from t_{90}
D	Mean landslide depth
D_p	Particle diameter
d	Drainage path length
e	Void ratio
e_g	Granular void ratio
e_0	Initial void ratio
e_1	Void ratio at the end of the preceding consolidation phase
F_h	Force generated from horizontal annular elements
F_{total}	Down slope force at failure
F_v	Force generated from vertical annular elements
F_1	Force recorded on one shear force proving ring
F_2	Force recorded on the other shear force proving ring
H	Sample depth

Symbol	Definition
H	Average sample depth during one consolidation phase
H_s	Height of solids
H_0	Initial sample depth
H_1	Sample depth at end of preceding normal stress increment
H_2	Sample depth at end of current normal stress increment
h	Height of wave-form
h_{max}	Maximum height of wave-form
h_p	Maximum height of parabolic wave-form
h_s	Maximum height of sine wave-form
h_v	Maximum height of v-shape wave-form
h_1	Height of sample at wave trough
h_2	Height of sample at wave peak
I_p	Plasticity index
i	Angle of shear plane inclination to the horizontal
K	Earth pressure coefficient
k	Lateral earth pressure coefficient
k_a	Active lateral earth pressure coefficient
k_p	Passive lateral earth pressure coefficient
k_0	At rest lateral earth pressure coefficient
L	Load on hanger
LL	Liquid Limit
l	Distance between torque arm abutting points
l_{max}	Slope length
M	Moment of resistance from an annular sample
$M_{element}$	Moment developed from an annular element
M_{np}	Moment of resistance from a non-planar annular sample
$M_{np_{parabolic}}$	Moment of resistance from a parabolic annular sample
$M_{np_{sine}}$	Moment of resistance from a sine wave-form annular sample
$M_{np_{vshape}}$	Moment of resistance from a v-shape annular sample
M_v	Moment of resistance from the vertical components of the shear zone
m	Depth ratio of phreatic surface
m_v	Coefficient of volume compressibility
m_{vswell}	Coefficient of volume compressibility for swelling
N_{pt}	Number of peaks and troughs on a wave-form
n	Number of model steps on one up or down slope section
n_{int}	Integer value
P	Weight of upper loading platen
P_{disp}	Dispersive pressure
PL	Plastic limit
p	Pressure
R	Constant
R_a	Average surface roughness

Symbol	Definition
r	Radius
r_a	Average radius
r_{vc}	Volume ratio of clay and water to total volume
r_1	Inner radius
r_2	Outer radius
s	Shear stress
s_c	Compression distance
s_p	Peak shear strength
s_r	Residual shear strength
T	Dynamic shear stress
T_v	Time factor
t	Time
t_{50}	Time for 50% pore water pressure dissipation during consolidation
$t_{50swell}$	Time for 50% pore water pressure dissipation during swelling
t_{90}	Time for 90% pore water pressure dissipation during consolidation
$t_{90swell}$	Time for 90% pore water pressure dissipation during swelling
U	Percentage of pore water pressure dissipation during consolidation
U_0	Free stream velocity
u	Flow velocity
u	Pore water pressure
V	Turbulent flow velocity
V_l	Rate of normal loading
V_s	Rate of shearing
v	Particle concentration
W	Weight of soil strip
W_n	Normal load on sample
w_{max}	Slope width
Z	Depth of shear zone
α	Dynamic angle of shearing resistance
β	Slope angle
γ	Unit weight of unsaturated soil
γ_{sat}	Unit weight of saturated soil
γ_w	Unit weight of water
Δe	Change in void ratio
ΔH	Change in height
ΔW	Side friction force
$\Delta\sigma'_n$	Change in effective normal stress
δ	Shear displacement
$\dot{\delta}$	Rate of shear
δe	Incremental change in void ratio
$\dot{\delta}_0$	slow rate of shear
δp	Incremental change in pressure
θ	Angular displacement

Symbol	Definition
λ	Wavelength
μ	Dynamic viscosity
μ_s	Rate dependent shear stress
ν	Kinematic viscosity
ρ	Mass density
ρ_p	Individual particle mass density
σ_n	Normal stress
σ'_n	Effective normal stress
σ'_n	Average effective normal stress
σ'_{nmin}	Minimum effective normal stress
τ	Shear stress
$\tau_{apparent}$	Apparent shear stress
τ_{dsz}	Shear stress from a disorientated shear zone
τ_r	Residual shear stress
τ_{total}	Total shear stress
τ_u	Shear stress from an undulating shear surface
τ_v	Shear stress from the vertical components of the shear zone
$\tau(v)_{coulomb}$	Rate independent shear stress
ϕ	Angle of shearing resistance
ϕ'	Effective angle of shearing resistance
ϕ_{cv}	Constant volume angle of shearing resistance
ϕ'_{mob}	Mobilised effective angle of shearing resistance
ϕ_p	Peak angle of shearing resistance
ϕ'_p	Effective peak angle of shearing resistance
ϕ_r	Residual angle of shearing resistance
ϕ'_r	Effective residual angle of shearing resistance
ϕ_{range}	Range of angles observed on the failure envelope
$\phi_{rapparent}$	Apparent residual angle of shearing resistance
ϕ'_{rplane}	Planar effective residual angle of shearing resistance
ϕ'_{rs}	Effective residual angle of shearing resistance at start of displacement
ϕ_μ	Angle of inter-particle friction
ϕ'_μ	Effective angle of inter-particle friction

Acknowledgements

The research contained in this thesis would not have been possible without the help and support of many of my colleagues at Warwick University, the majority of whom I now also consider to be my friends.

My supervisor, Dr D.J. Petley, has provided continuous support and encouragement throughout my studies. I am grateful to him for letting me follow my own ideas and letting the research evolve. His guidance has lead to the successful completion of this research and helped me to reject some of the crazy ideas I am occasionally prone to. None of this research would have been possible without the influence of Dr A.P. Boldy, my undergraduate tutor, who guided me towards studying for a PhD over four years ago. I wish to express my gratitude to Dr Boldy and also to Professor D. Anderson who helped me to obtain funding from the Engineering and Physical Science Research Council without whom none of this would have been possible.

Beyond Warwick I wish to thank Dr A. Ridley of Imperial College for his discussions on modifying the ring shear apparatus, Professor M.C.R. Davies of the University of Dundee for his ideas on improving the reliability of the pore pressure transducers and Professor D. Muir Wood of Bristol University for his comments and views on my research.

I wish to extend my thanks to Eurotherm Drives at Rugby for their help with supplying a new motor and drive unit and to Dennis Smith, Malcolm Whitehouse and Stuart Idriss for helping me to install the new equipment on the ring shear apparatus. I am also indebted to Peter Meesum for his skills in manufacturing the undulating interfaces and to Dave Robinson for helping with the measurement of the interfaces surface roughness. I would also like to thank Colin Banks, Gary Hackett and Dennis Smith for their support and friendship around the lab.

Over the past three years I have lived with a number of different people all of whom I wish to thank. Special thanks go to Ross Bannister who was not only a great house mate, but a top notch physicist who provided guidance with some of the mathematics in Chapter 8 of this thesis.

My fellow engineering doctoral students have made working at Warwick great fun and I wish to thank them all for their friendship both at work and at play. Special

mentions are owed to Martin for buying a book on LaTeX and then permanently lending it to me, Russell for his constructive comments and terrible jokes and Jo for being a fellow Civil Engineer who appreciates a fairly regular tea break. I wish you all happiness in your futures which ever paths you choose to follow.

I'd also like to acknowledge the role my other friends have played in maintaining my peace of mind and progress: Saranne for providing an artistic view in an engineers life and Matt for providing lots of stress relief on the squash court

Finally I am permanently indebted to my parents for their continued guidance and support throughout my life and also to Lesley for her help in preparing this thesis and her commitment over the past three years.

Chapter 1

Introduction

1.1 Background And Aims Of This Research

The slow drained residual shear strength of a soil has been established as a fundamental geotechnical parameter for many years. The main credit for this goes to Professor Skempton, who related the property to case studies and analysed its variation with respect to clay fraction and stress history in the Fourth Rankine Lecture [1]. Professor Skempton noted that the slow residual strength was independent of stress history. Furthermore he attributed the loss of strength down to the slow residual level to orientation of the plate like clay particles parallel to the direction of shear, thus reducing particle interlocking and therefore shear stress transmission.

Recently much research has been undertaken into the variation of the residual shear strength with increasing shear velocity. Three effects are possible at faster rates of shearing.

- A Neutral Rate Effect–where the fast residual strength is the same as the slow residual strength.
- A Positive Rate Effect–where the fast residual strength is higher than the slow residual strength.
- A Negative Rate Effect–where the fast residual strength is lower than the slow residual strength.

Negative rate behaviour is claimed to be the cause of many rapid landslides. These normally, but not exclusively, occur when pre-existent shear zones are reactivated by events such as earthquakes or periods of heavy rain. Such landslides tend to have long run-out distances in association with high velocities and therefore potentially catastrophic effects on inhabited regions.

Whilst this research involves the study of all the typical strengths observed in association with fast shearing, its main objective is to resolve the mechanism behind negative rate behaviour in cohesive soils. Extensive research has been undertaken globally into long run-out landslides and this is reviewed in Chapter 2. The specific aim is to investigate two separate schools of thought which have emerged from the Soil Mechanics Department of Imperial College London as a result of twenty years research.

Tika [2] presented a PhD thesis in 1989 which included test results and research from a decade of previous investigations along with her own testing. She concluded that five types of fast residual strength behaviour could occur with increasing shear rate, where the likely type was a function of the soils grading, plasticity and shear mode. The major conclusion of this research was published in 1996 [3] and stated that negative rate behaviour was a result of massive particles dilating in the shear zone, yielding an increased water content and therefore an increased ability for the soil to flow.

Parathiras [4] presented another PhD thesis in 1994, the main focus of which was the development of new confining rings to prevent soil loss from the Imperial College/Norwegian Geotechnical Institute (IC/NGI) ring shear apparatus. As part of his research, he noted that negative rate behaviour occurred in the absence of massive particles, but in association with undulating shear zones and free water. He postulated that negative rate behaviour occurred as a result of a pumping effect from the undulating shear zones, generating positive pore water pressures which reduce the effective normal stress and therefore the fast residual strength.

The research reported in this thesis has been conducted using the IC/NGI ring shear apparatus in association with controlled grade artificial soils and undulating rigid interfaces. Furthermore computational modelling of the pumping effect has been

undertaken and compared to test results. In addition to this, a numerical assessment of the influence of shear zones with undulations parallel to the shear direction has been conducted and experimental work using undulating interfaces in the Bromhead ring shear apparatus has been performed to validate the numerical investigation. Finally the results of this additional work have been extrapolated to study the influence of undulations parallel to the shear direction on the analysis of translational landslides.

1.2 Layout Of The Thesis

The thesis consists of ten chapters and four appendices. Following this introduction, Chapter 2 provides a review of the previous research in this field. This chapter includes the study of slow residual strength, the development of a number of different ring shear apparatus, the mechanisms behind both positive and negative rate effects and long run-out landslides and studies relating to shear surface undulations.

Chapter 3 presents a summary of all the different types of testing undertaken in this research, including the IC/NGI Ring Shear Apparatus Tests, Bromhead Ring Shear Apparatus Tests, Standard Oedometer Tests and Soil Classification Tests. The chapter includes descriptions of additional pieces of apparatus such as the rigid interfaces used with both types of ring shear apparatus, the instrumentation and data logging systems employed, the analysis of the data and a discussion of testing errors.

Chapter 4 contains a summary of the IC/NGI apparatus testing in association with the aims of the testing and reports on the different testing methods employed. Detailed analysis of all the test results are then included in four separate sections, each one relating to the four phases of testing.

Chapter 5 commences with a detailed discussion of all the difficulties encountered during testing in the IC/NGI apparatus. This is followed by a discussion on the different types of typical strength observed, including the slow residual strength, the fast peak strength, the fast residual strength and the slow peak strength after fast shearing . The time taken to induce negative rate behaviour is also discussed. The chapter concludes with a summary of the likely behaviour of the typical strengths as the shear rate is increased.

Chapter 6 presents the hypotheses and mechanisms that have been deduced from this and previous research to account for fast peak strengths, slow peak strengths after fast shearing, positive rate effects and negative rate effects. The sections on positive and negative rate effects are divided into subsections; these discuss individual potential mechanisms in more detail and conclude with an assessment of the likely occurrence of each mechanism.

Chapter 7 is an attempt to validate and model the pore pressure pumping effect first proposed by Parathiras [4]. The chapter commences by introducing the concept behind the model and then presents results from oedometer tests determining coefficients of volume compressibility and consolidation for remoulded kaolin, information which is required for the model. The development of three C programs is then covered using flow charts to explain how each one works. This is followed by an assessment of the performance of each model. The best model is then used to determine the influence of shear rate, wave height, wavelength, sample depth and total normal stress on pore water pressure magnitude and distribution. Finally, comparisons are made between predicted and observed pore water pressures and rate effects along with an assessment of the usefulness of the model. Throughout this chapter the influence of the model assumptions and the limitations are considered continuously.

Chapter 8 contains a study of the influence of shear surface undulations parallel to the shear zone. Initially a general solution based on lateral earth pressure theory is derived. This solution is then implemented to give a number of specific solutions for different wave-forms including v-shapes, parabolas and sine curves. Correction curves are then generated for each specific solution and from these it is concluded that the V-shape solution is suitable for most wave-forms.

Chapter 9 includes the comparison of the results obtained in Chapter 8, to those obtained using the Bromhead ring shear apparatus in conjunction with non-planar interfaces. Then the specific solution for the V-shape wave-form is expanded to cover any number of wave cycles by introducing the concept of effective gradient. This expansion and simplification of the idea then allows the theory to be expanded to cover translational landslides with undulating shear surfaces parallel to the shear direction, thus concluding this chapter.

Finally, Chapter 10 presents the conclusions drawn from this research. These include the likely rate behaviour of any cohesive soil, the implications of this research to field problems and suggestions for further work.

Chapter 2

Literature Review

2.1 Introduction

The aim of this chapter is to present a summary of the current knowledge available in this field. The chapter has been split into five sections, the first one being this brief introduction. The second section reviews the development of ring shear apparatus and presents the progression of understanding with regards to residual strength. The third section provides a summary of the investigation into the effect of rate of shearing on the residual strength of soils. This is followed by the fourth section which analyses the mechanisms that have been hypothesised to account for falls in residual strengths at faster rates of shearing. The last section presents studies that have investigated undulating shear surfaces, thus concluding this review and providing the background for this research.

2.2 Ring Shear Apparatus And Residual Strength

2.2.1 Introduction

The post-peak drop in strength of cohesive soils at drained rates of shearing has been the focus of significant attention for many years. It has also recently been recognised by Skempton [5] that the displacements required to observe this behaviour fully are in the range 100 mm to 500 mm.

Early insights into the applicability of a variety of shear tests to the study of stress-strain relationships in soils were provided in 1939 by Hvorslev [6]. His work concluded that the majority of investigations could be adequately conducted in triaxial testing apparatus. However, he noted that the large displacements required to study post-peak behaviour rendered the main shear tests impractical. Hvorslev recognised that knowledge of the post-peak drop in strength would be necessary to calculate factors of safety in earth structures where failure could not be prevented and proposed that such information could be obtained using a torsion shear test. Such testing apparatus would allow large displacements, thus initiating the inherent relationship between the study of residual strength and the ring shear apparatus. This early work by Hvorslev should not be underestimated. His observations and conclusions have been confirmed by many later researchers and to a large extent still hold true today.

2.2.2 Early Types Of Ring Shear Apparatus

An excellent summary of early ring shear apparatus designs was provided by Bishop et al in 1971 [7]. The earliest types were very basic affairs, composed of a laterally confined disk or cylinder which is normally loaded through the top platen, then either the top or bottom platen is twisted to obtain the shear strength. Examples of these designs are provided by The American Society of Civil Engineers [8], Streck [9], Franzius et al [10] , Tiedmann [11] and Ghani [12]. The simplicity of these designs is advantageous and they do provide the potential for virtually infinite shearing without a change in shear surface area. Uncertainties arise, however, whenever disks or cylinders are sheared because of the variation in shear stress across the radius of the sample. Also the shear surface is generated between the main body of the sample and the platen, whereas ideally it would be situated in the middle of the sample.

An improved design using split confining rings to allow shear surface formation in the middle of the sample was advanced by Langer in 1938 [13]. Unfortunately the design did not solve the problem of the uneven stress distribution. A more even stress distribution can be achieved using an annular sample, this was recognised in the 1930s by Cooling and Smith [14] [15]. Their design also solved the problem of side friction by using an unconfined sample. This severely limited the normal stress

range at which tests could be conducted and Bishop felt that shear stress transmission would also be problematic.

Divided annular confining rings were first introduced by Gruner and Haefeli in 1934 [16],similar designs were then put forward by Tiedmann [11], Hvorslev [17] [6] [18] and Hvorslev and Kaufman [19]. The designs of Tiedmann and Hvorslev were of similar dimensions and appear to minimise stress variations and side friction whilst promoting mid-sample shearing.

2.2.3 Early Studies On Residual Strength

The Fourth Rankine Lecture presented by Professor Skempton in 1964 [1] was a definitive landmark in the study and understanding of residual strength and its applications to slope stability. After their development of successful ring shear apparatus in the 1930s, Professor Skempton credited Tiedmann [11] and Hvorslev [17] with the first determinations of residual strength. Skempton also highlighted the work of Professor Haefeli [20] who introduced the term *"residual strength"* into the English Language in 1950 and continuously maintained its practical relevance when little attention was paid to shearing over large displacements.

When introducing the term *"residual strength"*, Professor Haefeli used his earlier work of 1938 [21] to draw many significant conclusions. He postulated that residual strength was associated with a static condition involving relieved pore pressures, where no further vertical or horizontal displacements were observed after the cessation of shearing. Perhaps more significantly he noted that the attainment of residual strength is linked to the development of a shear surface and a corresponding loss of cohesion. Owing to these factors Haefeli considered that residual strength was a governing factor where progressive slope failures occur, a similar conclusion to the earlier work of Hvorslev [6]. Professor Skempton's praise for Haefeli was well placed, despite his hypothesis about pore pressures. These observations have provided the foundation of knowledge from which todays understanding of residual strength has been constructed. As reported by Lupini et al [22], Professor Haefeli [20] also conducted a study of brittleness in 1950. Although this work was conducted on a stress controlled ring shear apparatus on which post-peak movements were retarded

by a spring, Haefeli found that the magnitude of the drop in strength from peak to residual increased with liquid limit of the soil, which of course is directly related to the clay fraction.

Despite the suitability of ring shear apparatus for studying residual strength, the problems associated with side friction had not been solved. Despite Hvorslev's earlier conclusions, Professor Skempton based his Rankine Lecture [1] around slow drained shear box tests with reversals, rather than ring shear apparatus. This is probably because direct shear tests were easily available and well established where as ring shearing was still very much in its infancy. In his introduction Skempton stated the long established Coulomb-Terzaghi equation for determining the shear strength of a soil as:

$$s_p = c' + (\sigma_n - u)\tan\phi'_p. \tag{2.1}$$

As the lecture progressed, the point was highlighted that the equation could be expressed in terms of the residual strength, thus:

$$s_r = c'_r + (\sigma_n - u)\tan\phi'_r. \tag{2.2}$$

Furthermore from available test results Professor Skempton proposed that the value of c'_r varied insignificantly from zero and therefore residual shear strength could be determined from:

$$s_r = (\sigma_n - u)\tan\phi'_r. \tag{2.3}$$

This relationship is fundamental to the study of residual shear strength, even though test results never perfectly reproduce this linear relationship.

Professor Skempton proposed that the post-peak loss of strength was due to two factors. Firstly, dilation of the shear zone with continued shearing causing an increase in water content. Secondly, reorientation of the clay particles until they are all aligned parallel to the direction of shearing. Skempton also postulated that the residual strength was independent of stress history and that testing illustrated its value decreased with increasing clay fraction, see Figure 2.1, where the residual angle ϕ'_r would equal the angle of inter-particle friction ϕ'_μ in a pure clay with perfect particle

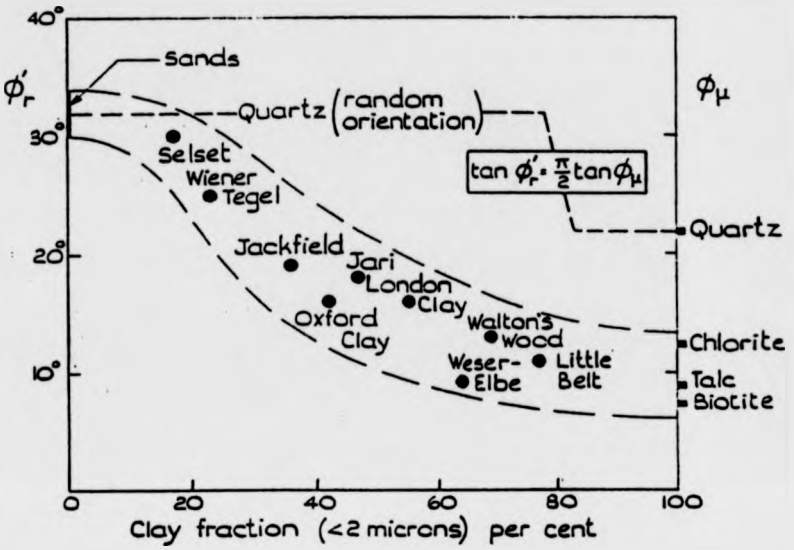

Figure 2.1: Decrease in ϕ'_r with increasing clay fraction, from Skempton 1964 [1].

alignment, assuming that ϕ'_μ for Kaolinite and Illite minerals is similar to ϕ'_μ for layer-lattice materials such as Biotite, Talc and Chlorite as predicted by Horn and Deere [23]. Whilst he acknowledged the work of Goldstein et al [24] revealed the probability of the formation of orientation domains at small strains, he also cited Astbury in 1960 [25] as providing decisive evidence that continuous bands of almost perfectly aligned particles existed at large strains. Further evidence of particle orientation was reported by Lupini et al [22] who noted that orientation had been observed with an optical microscope by Mitchell [26] and Morgenstern and Tchalenko [27]. Similar observations were made by Yong and McKyes [28] using electron microscopes. Skempton also stated that for more rotund particles with random orientation, the approximate relationship for constant volume shearing proposed by Caquot in 1934 [29],

$$\tan \phi'_r = \frac{\pi}{2} \tan \phi'_\mu \tag{2.4}$$

applies. For soils which are a mixture of plate like and rotund particles, the residual angle could not fall to the friction angle as the rotund particles would disrupt particle

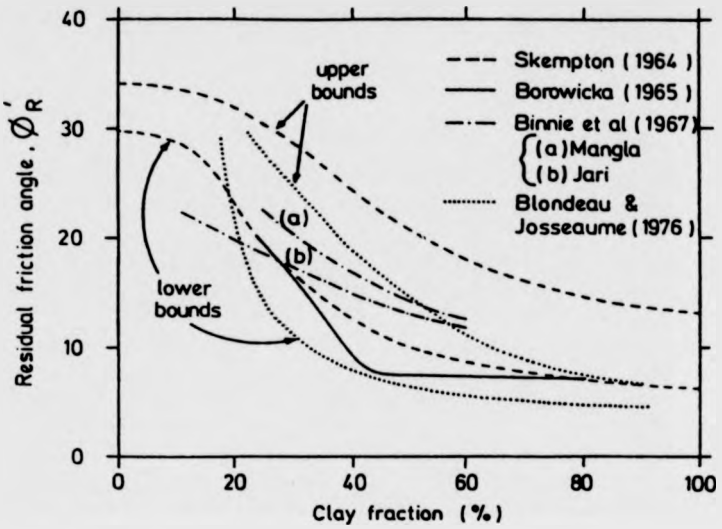

Figure 2.2: Residual strength: correlations with clay fraction, from Lupini et al 1981 [22].

orientation and add their own frictional component. The main conclusions of Skempton's lecture focused on the levels of strength applicable to unstable slopes. In newly excavated cuttings he concluded that the slow peak strength applied, then depending on the age of the cutting and the amounts of displacement the strength falls to the slow residual value, where a progressive failure has been occurring for many years.

2.2.4 New Impetus And Discovery

Professor Skempton's Fourth Rankine Lecture [1] increased awareness of the residual strength and its importance in slope stability problems. A significant number of papers were reported by Lupini et al [22] and Parathiras [4] after 1964, most of which seem to have been encouraged by Skempton's work.

Borowicka [30] conducted investigations with different artificial soil mixtures by means of shear box testing with reversals. The results of his work are shown in Figure 2.2, revealing that as clay fraction increased the residual angle of shearing resistance decreased. This work also illustrated that the brittleness (or magnitude of the post-peak fall in strength) of soils increases with increasing clay fraction.

Chandler in 1966 [31] and 1969 [32], conducted studies on Keuper marl, a soil

composed of clay particles which are aggregated in stable silt sized particles, thus giving the soil a low plasticity in spite of its mineralogy. Using shear box tests with reversals and pre-cut specimens in triaxial apparatus, Chandler found that the clay fraction of the soil increased in the residual shear zone, henceforth indicating that the stable aggregated particles had broken down into there component clay size particles. Chandler's work with respect to the variation of residual strength with clay fraction was in agreement with Skempton [1].

Herrmann and Wolfskill [33] reported tests on weak clay shales in 1966. They conducted experiments using shear box tests with reversals and triaxial tests, with and without pre-cut failure planes. They also conducted some tests using ring shear apparatus in which it was discovered that ring shearing and shear boxes gave residual values in close agreement whereas triaxial testing always gave higher strengths.

In 1967 Skempton and Petley [34] studied the development of shear surfaces in direct shear apparatus. They noted that if a well developed slip surface was re-sheared, peak strength was diminished and that the residual strength was attained in relatively short displacements. Their work also involved a comparison between direct shear tests on field shear surfaces and shear box tests with reversals on intact samples. Intact samples were also tested in triaxial apparatus, the results were in close agreement, suggesting that the residual strength available in the field was very similar to that measured on intact clays in the laboratory. Moreover they noted a significant non-linearity of the stress envelope at low levels of normal stress.

Other testing on samples containing field shear surfaces were conducted on the Mangla and Jari clays by Binnie et al in 1967 [35], see Figure 2.2, and also by Early and Skempton (1972) [36] on the Waltons Wood clay. All these clays had a high plasticity and illustrated low residual values. In all cases the correlation between field shear surface strength, measured in shear box tests, and residual strength, measured by shear box tests with reversals, was good. Thus providing further evidence that not only was residual strength the controlling parameter in many landslides, but that it could be obtained with relatively simple laboratory testing.

Skempton [5] reported on Sinclair and Brooker [37], whom in 1967 studied the shear strength of Edmonton Shale. They found that residual strengths were attained

at much shorter displacements if the normal stress was increased, logically implying that under high normal stress particle reorientation takes place more rapidly. They found that at $\sigma_n = 100kPa$ residual strength was reached within 60 mm, however at $\sigma_n = 2000kPa$ residual strength was reached within 25 mm. This has important implications with respect to shear surface depth and a landslide masses potential for progressive failure.

In 1967, Kenney [38] was concerned with the effects of mineralogy on residual strength of soils. Initial tests on undisturbed samples resulted in irregular shaped shear planes, which he believed lead to an apparent increase in residual strength. The problem was overcome by the use of pre-cut planes. The results of his test on natural soils lead him to conclude that the residual strength is not related to plasticity, clay fraction or water content, but instead is dependent on the mineral composition of the soil. This is in direct opposition to one of Skempton's conclusions in 1964 and all the authors listed on Figure 2.2, who postulated that residual strength decreases with increasing clay content. Subsequently, Skempton's ideas have been proved correct, however the mineral composition does play a role in soils where there is a high clay content. Different clay minerals have different angles of inter-particle friction, therefore when the shear mode is pure sliding and the particles are orientated in the direction of shear, the residual angle should approach the angle of inter-particle friction [1]. Kenney extended his testing to pure minerals. From this he concluded that for massive particle minerals, residual strength depended upon the shape and angularity of the particles not particle size. Moreover, for layer-lattice minerals, residual strength is a function of system chemistry, increasing with ion concentration in the pore fluid and inter-particle bond formation.

A later paper by Cullen and Donald [39] in 1971 presented results from a rigorous investigation into the determination of residual shear strength using direct shear apparatus. Cullen and Donald made a significant contribution to testing procedure by proposing that multi-stage testing, where residual conditions are established at one normal stress level and then the normal stress is increased and further residual shearing takes place, can be performed to obtain perfectly valid results in a significantly shorter time period.

2.2.5 New Ring Shear Apparatus

Once again, further developments in this area of research appear to have been triggered by Professor Skempton's Fourth Rankine Lecture [1]. It lead to renewed interest from Professor Casagrande at Harvard and Professor Bishop at Imperial College. They both encouraged the development of new ring shear designs.

The Harvard design was presented at a conference in Mexico in 1969 by Sembenelli and Ramirez [40] and more fully by La Gatta in 1970 [41]. This *"rotation shear machine"* illustrated in Figure 2.3 was a fixed rate of shearing device comprising of a *"shearing unit"*, a *"vertical loading system"* a *"torque application system"* and a *"moment measuring system"*. This apparatus is capable of shearing either disks of diameter 71.1 *mm* or annuli with inner and outer dimensions 50.8 *mm* and 71.1 *mm* respectively. The sample height can be varied from 25 *mm* down to thin smears of as little as 1 *mm* in depth. Bishop et al in 1971 [7] reported that usually small samples in the range 1 *mm* to 3 *mm* deep were used in PTFE confining rings to minimise the effects of side friction. Normal stress was applied to the sample via a loading yoke connected to a counter balanced dead load lever system. Rotation of the base of the shearing unit was achieved by a geared motor connected through a worm gear. The shearing forces were measured by transducers positioned on the top plate.

Parathiras [4] produced a summary of the development of the Harvard apparatus. Initially a split confining ring system was used to encourage shearing at mid-height of the sample. However with a fixed gap of 0.005 *in* between the upper and lower confining rings excessive soil extrusion occurred at large rotational displacements. What is more, the shear surface did not always develop at mid-height, when the surface developed adjacent to a platen, the difference between the recorded strength here and at the middle of the sample was insignificant. Henceforth a solid confining ring system was employed. This simplified the design and the testing procedure and eliminated uncertainties about friction between the upper and lower confining rings. Whilst assessing the errors associated with this rotation shear machine, La Gatta concluded that soil extrusion can lead to an uneven normal stress distribution, which leads to an underestimation of residual strength. He estimated that this may be as

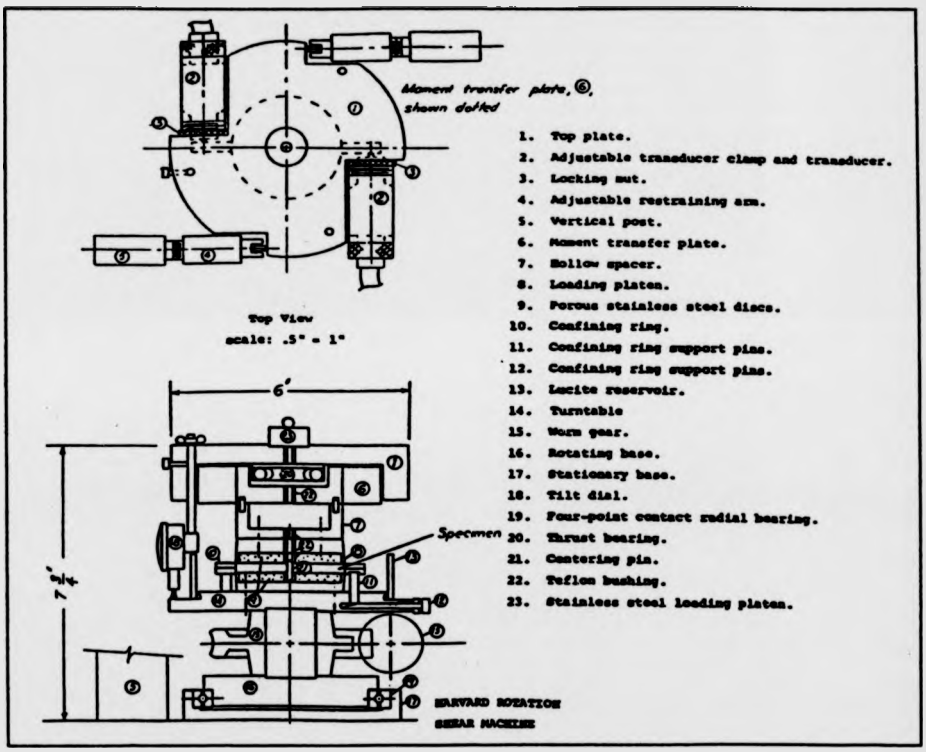

Figure 2.3: Harvard rotation shear machine, La Gatta 1970 [41], from Parathiras 1994 [4].

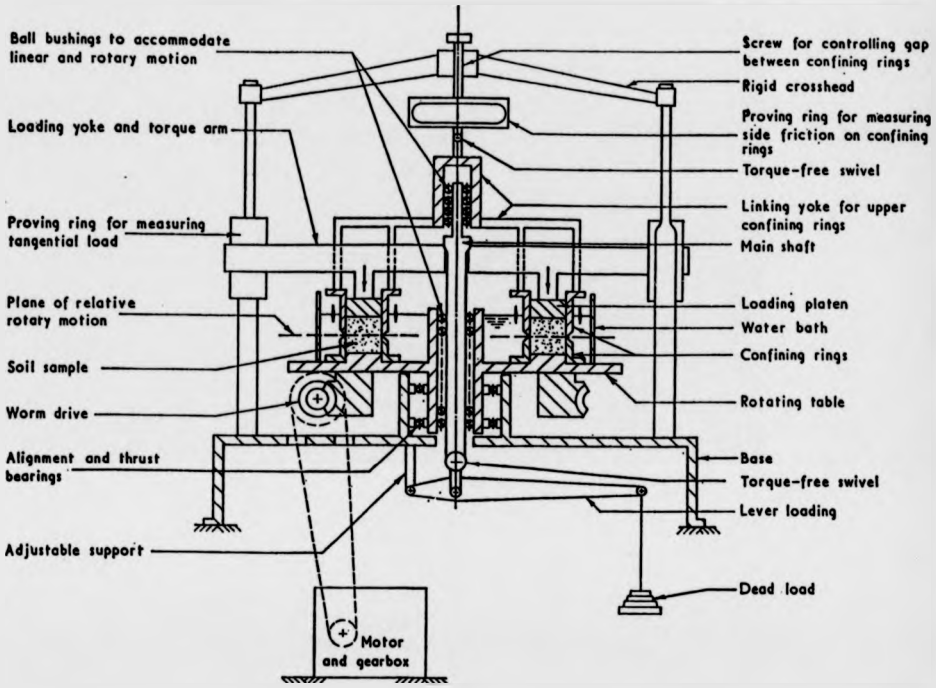

Figure 2.4: Principles of operation of Imperial College-Norwegian Geotechnical Institute ring shear apparatus (simplified section), from Bishop et al 1971 [7].

large as 12% in disk samples. Also he studied the errors induced by failure near the platen, inaccuracy of the lever system, side friction and friction between still and rotating parts. He estimated that these errors were of the order of 0.1% to 1.4% and as such were insignificant.

The result of the collaborative work between Imperial College and the Norwegian Geotechnical Institute lead by Professor Bishop was a machine termed the *"new ring shear apparatus"* which is now known as the IC/NGI ring shear apparatus. The machine was presented by Bishop et al in 1971 [7] and Garga in 1970 [42], it is illustrated in Figure 2.4. As with Hvorslev's earlier designs, the apparatus was of the annular format with split confining rings. The inner and outer diameters of the annulus are 101.6 *mm* and 152.4 *mm* respectively, the initial sample is 19 *mm* deep. The sample is sheared at a fixed rate across a plane of relative rotary motion. It

is normally loaded by a dead load lever via the main shaft which is mounted on bearings to allow both rotational and linear movements. The bottom half of the sample is mounted to a rotating table which is driven by one of two electric motors (one for the slow range, the other for the fast range) via two gear boxes and a worm gear with a ratio of 170:1. The upper half of the sample is restrained by a torque arm abutting against two tangential proving rings, these measure the shear load transmitted through the sample. Side friction has always posed a problem in previous designs and the IC/NGI apparatus provides a novel solution. The gap between the upper and lower pairs of confining rings is controlled by a differential screw mounted in the rigid cross-head. Placed in series between the screw and the confining rings is a proving ring which is used to measure the side friction on the sample resulting from shearing, consolidation or gap size adjustment. The main assumption with this is that a proving ring of suitable stiffness can be found to maintain an approximately constant gap, yet be flexible enough to allow accurate measurement of the side friction. Later works reported problems with gap control, especially at faster rates of shearing. Lemos [43] attempted to solve the problem by clamping the proving ring prior to fast shearing and then back calculating the side friction. Tika [2] used two proving rings of differing stiffness to alleviate the problem. Other solutions have been attempted such as inserting cast iron blocks into the proving rings. In the authors experience it has not been a significant problem, although adjustments to the gap size are sometimes necessary during fast shearing, which causes only minor short term fluctuations in test results.

Bishop et al [7] also conducted an investigation into the effects of non-uniform normal stress distribution. This lead them to conclude that even the most extreme and unlikely stress distributions cause a variation of less than 2° in the residual angle of shearing resistance when compared with a uniform normal stress distribution. Therefore they concluded that the assumption that stresses are evenly distributed across the plane of relative rotary motion should always be made when processing data from the IC/NGI ring shear apparatus. The paper also went into significant detail about the placement of undisturbed samples in the apparatus. This appears to make an already complicated test, more intricate and its benefits appear limited.

Peak strengths can be obtained more easily from direct shear or triaxial testing and it is now known that residual strength can be found from remoulded samples and is independent of stress history. In direct shear apparatus field shear surfaces are sometimes tested, yet there is no point in doing this in ring shear apparatus as the nature of shearing is rotational not linear as in actual surfaces.

Finally by carrying out tests on Blue London clay from Wraysbury and finding their results to be directly comparable to tests carried out on the same soil by La Gatta at Harvard, Bishop et al concluded that the IC/NGI ring shear apparatus enable the *"correct measurement of residual strength"* and offered a better method than the shear box with reversals, which gave a wider range of results and could not produce long unidirectional shearing often observed in the field.

2.2.6 Further Progress On Residual Strength

A thorough review of the research into residual strength during and after the development of the IC/NGI apparatus is provided by Lupini [44] and Lupini et al [22] both from 1981. A summary of their report is provided here along with some additional studies.

In the second paper produced using results from the Harvard ring shear apparatus, La Gatta [45] proposed residual strength to be the drained shear strength of a specimen undergoing *"continuous deformation under a constant state of effective stress and at a constant void ratio"*. La Gatta believed that in normally consolidated soils the strength decrease to the residual value was a result of bond breakage and particle orientation, whereas in over consolidated soils it was also a result of an increase in void ratio. It was also suggested that the residual and critical states are identical. Current knowledge on this subject was comprehensively summarised by Professor Skempton in 1985 [5]. Although most of La Gatta's ideas were correct, one was fundamentally incorrect. The critical state definitely does not correspond to the residual condition, an explanation of this will be provided shortly as part of the review of Skempton's work. Finally La Gatta suggested that a logarithmic scale should be employed when plotting shear strength against displacement to prevent the overestimation of residual strength.

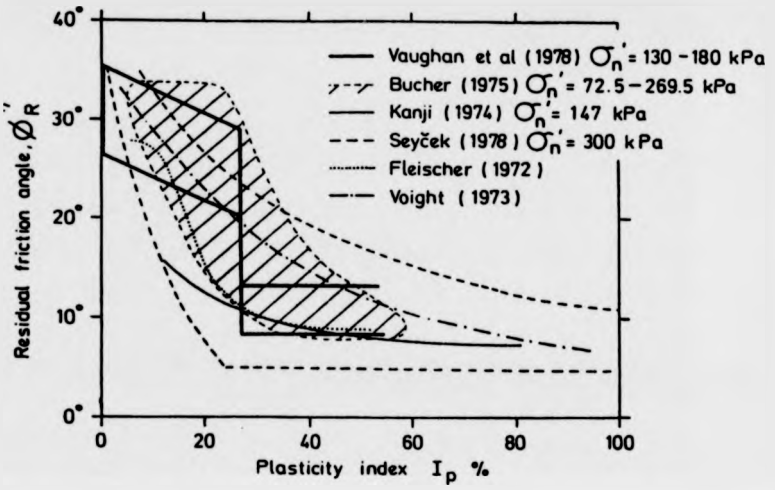

Figure 2.5: Residual strength: correlations with plasticity index, from Lupini et al 1981 [22].

Other works reviewed by Lupini et al from 1972 included Spears and Taylor [46] and Fleischer [47]. Spears and Taylor conducted shear box tests on mudstones and related the residual strengths to proportions of quartz to clay minerals. Fleischer [47] conducted strain controlled ring shear tests on stiff clays and then related the plasticity index of the clays, I_p, to the residual strength. This relationship is illustrated on Figure 2.5 along with further studies from other authors including Voight [48]. According to Lupini et al, further testing was conducted in 1979 by Fleischer and Scheffler [49] using *"modified ring shear equipment"*, no further details were given.

Townsend and Gilbert published a series of papers in the 1970's [50] [51] [52] concerned with ring shear and direct shear testing of clay shales. They found that in hard highly over consolidated materials results from both types of testing are in close agreement, however they expressed doubts as to whether or not this is the case in softer materials. They also concluded that variations in stress history, the initial soil structure and normal stresses above 150 kPa do not affect the linearity of the residual strength envelope. This also suggests that they had evidence of the non-linearity of the residual strength envelope at lower normal stresses. An interesting observation was made in their 1974 publication. During tests on Dawson clay-shale, a material

which has variable properties, they found a sharp increase in residual strength when the plasticity index fell below a threshold value.

The previous observation about the behaviour of Dawson clay-shale appears to be in good agreement with the hypothesis of Vaughan and Walbancke in 1975 [53] and Vaughan et al [54] in 1978, who presented results from the IC/NGI apparatus on natural clays of medium activity. From these results they proposed a discontinuous relationship between plasticity index and residual strength with the threshold value between the two separate zones being of the order of $I_p = 27\%$, this can be seen on Figure 2.5. They also proposed that the governing parameter was likely to be the proportion of plate like clay minerals present and that for clays of similar activities this would correlate with I_p.

A further correlation was proposed by Kanji in 1974 [55] and Kanji and Wolle in 1977 [56] after conducting a series of shear box tests with reversals on interfaces between soils and polished rock surfaces. The relationship they proposed between residual strength and plasticity index can be seen on Figure 2.5 and is in general agreement with the other correlations, lying close however to the lower boundaries of the other relationships. It was noted by Littleton in 1976 [57] that when shearing was conducted against hard polished surfaces such as the rock interface used by Kanji, residual values were encouraged and attained at shorter shear displacements.

Bucher in 1975 [58] conducted strain controlled ring shear tests to investigate the influence of plasticity, temperature, shear rate and stress history on residual strength. He found that temperature had no effect in the range $10°C$ to $60°C$, however rate did influence the strength and this will be covered in Subsection 2.3.1. The relationship proposed by Bucher [58] between plasticity and residual strength is illustrated in Figure 2.5 and can be seen to follow the trends of the other works shown.

In 1976 Blondeau and Josseaume [59] conducted triaxial tests and shear tests with reversals on samples with and without pre-cut surfaces. As with many other studies they found that triaxial testing usually gave higher strengths than the direct shear tests. They did conduct one ring shear test on a highly plastic clay which gave a result in close agreement with the direct shear test. As a result of their work they postulated a relationship between clay fraction and residual strength and this can be

seen in Figure 2.2.

In 1977, Kenney [60], continued his studies on the effects of mineralogy on residual strength. He found that the residual strength would depend on the mineral mixture composition and the chemical state of the clay mineral. Moreover he postulated that the residual strength would be inversely proportional to the ratio of the volume of clay minerals and water to the total sample volume (which he called the volume ratio, r_{vc}). This is in close agreement with test results in Skempton's Fourth Rankine Lecture on a number of different soils containing varying quantities of clay. As the clay fraction percentage of the soils increased, the residual angle fell in a non-linear fashion. Kenney also argued that in mixtures of water, clay particles and relatively massive particles (in this case quartz), the clay and water would form a cohesive matrix in which the quartz particles would be discretely included. In soils where 40% to 50% or more of the total volume is clay and water, the shear strength of the sample will be given by the shear strength of the cohesive matrix. However, as the percentage of massive particles increases they will form a structure within the matrix which will control the ultimate residual strength and the strength of the matrix will offer only a small contribution to the residual strength.

Finally, Seyček in 1978 [61] produced a summary of results from direct shear tests and a variety of tests reported by other researchers. It was concluded that there is a better correlation between residual strength and plasticity index than with any other parameters. The correlation proposed by Seyček is also illustrated in Figure 2.5.

2.2.7 Two Further Ring Shear Apparatus

Although the IC/NGI apparatus did lead to the correct measurement of residual strength, it was felt by many people to be overly complicated for industrial use. Its worth as a research instrument, however, is without doubt. The next ring shear apparatus to be developed was presented by Mandl et al in 1977 [62] and is illustrated in Figure 2.6. Parathiras reported that the aim of the design was to investigate the structure of shear zones in soils. The machine contained an annular sample, inner diameter 350 *mm*, outer diameter 450 *mm* and height 46 *mm*. The lower section of the device was rotated by a constant speed motor and the gap between the upper

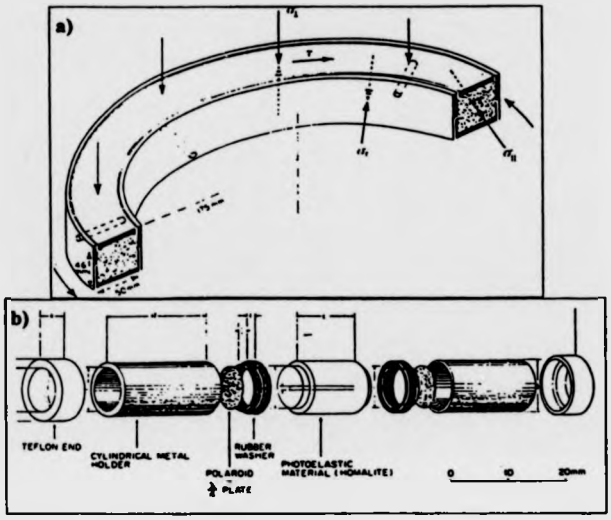

Figure 2.6: Cambridge load cells in ring shear apparatus, Mandl et al 1977 [62], from Parathiras 1994 [4].

and lower rings is maintained closed by springs and adjustment screws to prevent soil extrusion. The design has some novel features including the application of normal stress by means of gas pressure and the measurement of normal and shear stresses using Cambridge load cells and photo-elastic meters.

In 1979 Professor Bromhead [63] presented a compact design for ring shearing, illustrated in Figure 2.7, which was aimed at a commercial as well as an academic market. Bromhead described the design as *"simple, robust and inexpensive"* which, in recent years, has proved to be the case. A detailed description of the apparatus is provided in Subsection 3.3.1.

The key to the success of this apparatus is the depth of the sample. As it is only 5 *mm* deep, drainage is more rapid thus reducing consolidation times and allowing the use of faster rates of drained shearing. This significantly reduces the test time in comparison with other ring shear designs. Bromhead realised that peak strengths could not be accurately measured owing to the progressive nature of ring shear failures. He also concluded that the potential sources of error, which included friction transmitted

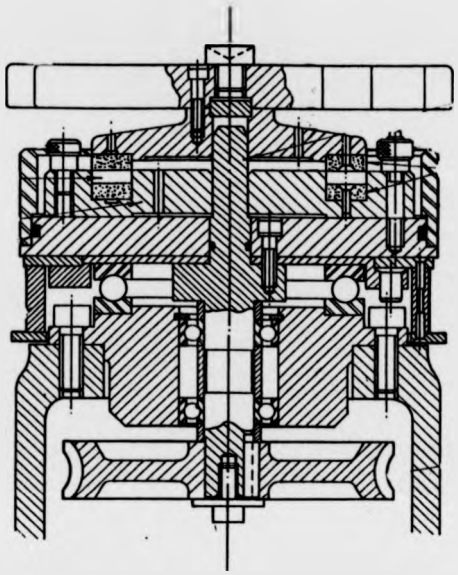

Figure 2.7: Bromhead ring shear apparatus, section through sample turret, from Wykeham Farrance Engineering Ltd instruction manual.

between the confining rings and top platen by extruded soil, side friction between the sample and confining rings, tilting of the top platen leading to non-uniform stress distributions, soil extrusion and inaccuracies in force measurement, had only minor effects on recorded results and therefore may be safely ignored.

2.2.8 Current Knowledge Of Residual Strength

Lupini [44] and Lupini et al [22] in 1981 presented studies which gave a good overview of all previous attempts to correlate residual strength with properties such as clay fraction and plasticity index. They also presented a wide variety of test results from the IC/NGI apparatus on natural soils and mixtures of sand and bentonite. From their work they concluded that there are are three modes of drained residual shear behaviour, *turbulent*, *sliding* and *transitional*, where the mode depends on the dominant particle shape and the magnitude of inter-particle friction.

- (i) The *turbulent mode* occurs in soils with a high percentage of rotund particles, or possibly in plate like soils where the coefficient of inter-particle friction is

high, where presumably groups of plates stick together to form rotund particles. There is no preferred particle orientation and the drained residual strength tends to be high (usually greater than 25°). Once a shear zone is formed, it is defined by an area of increased porosity, as a result of the rotund particles riding over one another. Strength is dependent on the shape and packing of the particles, not on inter-particle friction.

- (ii) The *sliding mode* occurs in soils which mainly consists of plate like low friction particles. Particles become strongly orientated in the shear zone, and align themselves parallel to the direction of shear. The residual strength is dependent on mineralogy, pore water chemistry and the inter-particle friction.

- (iii) The *transitional mode* where a combination of the turbulent and sliding modes occurs across the shear surface. Residual strength in this mode tends to be very sensitive to small changes in the soils grading.

Whilst concluding their work, it was stated that the type of shear mode and, to a lesser extent, the residual strength could be correlated to the granular void ratio, e_g, that is the ratio of the volume of plate like particles and water to the volume of rotund particles. This work is a development of the ideas proposed by Kenney in 1977 [60] and in fact the relationship between e_g and Kenney's volume ratio r_{vc} can be expressed as,

$$e_g = \frac{r_{vc}}{1 - r_{vc}}. \tag{2.5}$$

The relationships between e_g, ϕ_r and shear mode are illustrated in Figure 2.8. Lupini and Lupini et al also proposed correlations to rate effects, this will be covered in Subsection 2.3.2.

Yet again another landmark publication was produced on residual strength by Professor Skempton in 1985 [5]. This lecture to the British Geotechnical Society updated and revised the Fourth Rankine Lecture, incorporating new ideas that had been developed during the twenty years between the two lectures. The opening paragraphs of the lecture focused on highlighting the difference between the fully softened (critical state) strength and the residual strength. In over consolidated clay, Skempton con-

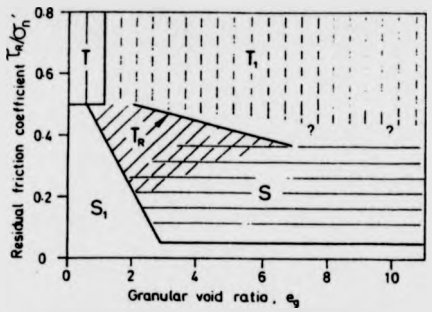

T	Turbulent shear
T_1	Turbulent shear for platy particles if $\phi_R > \phi'_{cv}$. Also for soils containing non-platy clay particles if these are excluded from the volume of rotund particles in calculating e_g
S	Sliding shear
S_1	Possible sliding shear when soil is failed against a smooth interface
T_R	Transitional shear. Part turbulent and part sliding. Location of a particular soil within this zone depends on residual friction factors of rotund and platy particles, tested separately, and on soil grading. Platy clay particles mixed with well-graded sand/silt rotund particles fall to left of zone. Gap graded fine clay and sand mixtures fall further right in direction of arrow. Mixtures of platy and rotund particles of comparable size fall to right of zone

Figure 2.8: Residual shear mechanisms as a function of particle packing: summary of conclusions, from Lupini et al 1981 [22].

sidered the post-peak drop in strength to be initially caused by dilatancy (resulting in an increase in water content) until the fully softened strength is reached, further reductions in strength he attributed to particle reorientation. At larger displacements when particle reorientation is complete, the soil strength will have fallen to its residual value. In normally consolidated clays Skempton stated that *"the post peak drop in strength is due entirely to particle reorientation"*. These observations are illustrated in Figure 2.9. Skempton also provided a summary of the various stages of shearing and the displacements at which they could be observed, this is illustrated in Table 2.1. As with his previous lecture in 1964 [1], Professor Skempton presented studies of actual landslides as well as test results. He found that comparisons made between measured strength and predicted strength from back analysis of reactivated landslides revealed good correlation. He did note however that ring shear apparatus may lead to an underestimation of field residual strength by 1° to 2°. A further summary of the influence of clay fraction on residual strength is presented for tests on sand-bentonite mixtures, kaolin and field residual strengths. These all follow the trends highlighted

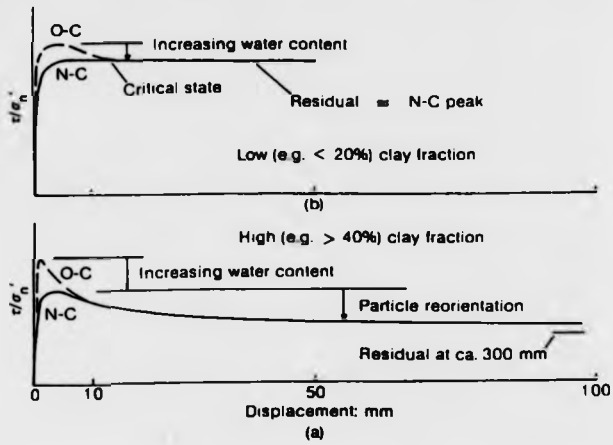

Figure 2.9: Diagrammatic stress-displacement curves at constant σ'_n, from Skempton 1985 [5].

previously. Skempton sounded a note of caution that not all clay sized particles are plate like, take halloysite and allophane for example, and will not therefore behave as clays usually do, having residual angles greater than 25°. Finally Professor Skempton noted that the relationship between normal effective stress and residual strength is not always linear, therefore he proposed that when comparing strengths of two different clays a standard normal stress of 100 kPa should be adopted.

Since 1985 a few more developments have arisen, however Professor Skempton's summary is excellent and really defines the knowledge available on residual strength.

Table 2.1: Typical displacements at various stages of shear in clays having $CF > 30\%$, from Skempton 1985 [5].

Stage	Displacement: mm	
	O-C	N-C
Peak	0.5-3	3-6
Rate of volume change approximately zero	4-10	
At $\phi_r + 1°$	30-200	
Residual ϕ_r	100-500	

Further works on residual strength reported by Parathiras include those by Bromhead and Dixon, Moore and Yagi et al.

In 1986 Bromhead and Dixon [64] made a valid point in relation to the necessity for accurate measurement of ϕ_r in ring shear apparatus when studying field residual strength. They postulated that long term stability is much more dependent on pore water pressure changes at the shear surface than knowledge of the exact drained residual strength.

In 1991, Moore [65] studied the importance of pore water chemistry and mineralogy. He proposed that weathering of soil reduces its residual strength and that remoulding samples with distilled water results in higher residual strengths than when natural water is used.

Finally Yagi et al in 1991 [66] conducted ring shear tests suggesting that the reason why residual strengths predicted by back analysis are sometimes greater than laboratory strengths is due to the development of slickensides, which are promoted in the laboratory but not always present in actual landslides.

2.2.9 Recent Developments Of Ring Shear Apparatus

Recent research in the field of ring shearing can be split into two categories. Firstly, works aimed at improving the Bromhead apparatus and secondly works presenting new ring shear devices. As reported by Parathiras [4], Anayi et al in 1989 [67] reiterated the point that in the Bromhead ring shear apparatus, the failure surface develops very close to the top sintered bronze porous platen. They believed that the application of shear stress depended on the adhesion between the sample and the top platen. On testing Lias clay samples they observed unbalanced readings on the torque proving rings, which they claimed lead to *"friction on the centre pivot and tilting of the loading platen"* as well as undulation of the failure surface. The author has experienced similar problems with the IC/NGI apparatus, however it was found that such imbalance appeared to have no effect on recorded strength [68]. In order to overcome this problem, they suggested the uniform placement of vanes around the top and bottom platen and increased sample depth from 5 *mm* to 10 *mm*. They then suggested that the sample should be placed in two layers each 5 *mm* deep, thus

encouraging a planar shear surface in the middle of the sample. In conclusion, they found that this would reduce the rate of soil extrusion and any errors associated with it. Much discussion has taken place over the relative merits of shear surfaces at or close to platens. One point that appears to have been overlooked in this case, however, is that if such modifications did successfully achieve mid-sample shearing, the measured shear strength would contain a component from side friction between the top 5 *mm* of the sample and the confining ring, the magnitude of which depends on the lateral earth pressure. It is difficult to imagine that this effect would be insignificant.

Stark and Vettel in 1992 [69] came to similar conclusions with regards to the influence of vanes. They also postulated that as the top platen descends into the confining rings as a result of soil extrusion, the influence of side friction may lead to an overestimation of residual strength by as much as 25%. They proposed a new testing procedure where after shearing the sample is topped up with new soil and then both the sample and the new soil is reconsolidated. This technique may have some merit but appears to be time consuming, as topping up would lead to the loss of the residual state at the interface between the soil and the platen.

Parathiras considered another paper by Stark and Eid [70] which introduced a new *"specimen container"* for the Bromhead apparatus, this enables the specimen to be over consolidated and pre-cut prior to shearing. The position of the shear surface is unclear. They also presented a *" modified ring shear test procedure"* which they claimed substantially reduced test duration and errors in test results. Parathiras however judged this new procedure to be *"rather complicated and test operator dependent"*.

Another ring shear apparatus was presented in 1984 by Hungr and Morgenstern [71]. This design, illustrated in Figure 2.10, was specifically aimed at testing granular materials. The apparatus is of a now familiar concept consisting of an upper and lower box containing an annular sample with inner and outer diameters of 220 *mm* and 300 *mm* respectively. The sample is 20 *mm* deep and not submerged. The lower box is rotated by an electric motor and the upper box is attached to a stiff load cell. This load cell controls the gap between the upper and lower boxes and measures the side friction, basically replacing the side friction proving ring in the IC/NGI apparatus,

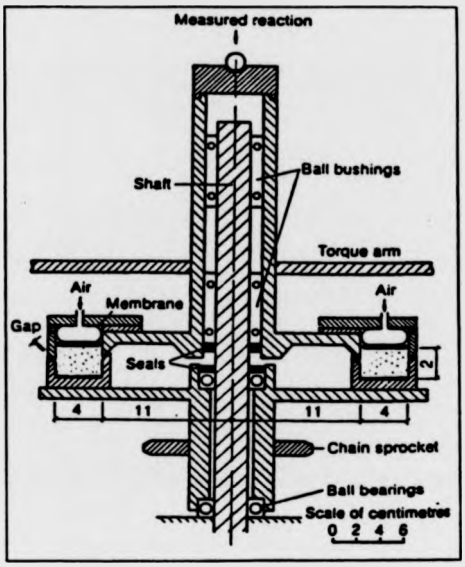

Figure 2.10: Cross section of ring shear apparatus used by Hungr and Morgenstern 1984 [71], from Parathiras 1994 [4].

which some reporters have found problematic at fast rates of displacement. Normal stress is applied via pressurised air contained in an annular rubber membrane and shear stress is measured by a strain gauged torque arm attached to the upper box. Hungr and Morgenstern anticipated shearing granular materials at displacement rates up to 2 m/s, however they limited testing to rates up to 0.9 m/s, above this speed excessive vibrations were observed which they feared would damage the apparatus.

Professor Sassa and his team [72] [73] [74] developed and described the first of a new generation of high speed ring shear devices in 1984 and 1985. The first design is illustrated in Figure 2.11 and shared many of the characteristics of Hungr and Morgenstern's machine. The normal stress is applied via an inflatable rubber membrane and is measured by a load cell mounted beneath the rotating bottom confining rings. Shear stress is monitored by a torque arm reacting against a load cell. It is reported that the apparatus permits constant volume shearing at fast rates of shearing up to 0.9 m/s. Volume changes can be monitored by a dial gauge located at the top of the apparatus. The gap between the upper and lower boxes is sealed by silicon rubber rings and the edges of the boxes are individually machined to ensure a perfect fit with

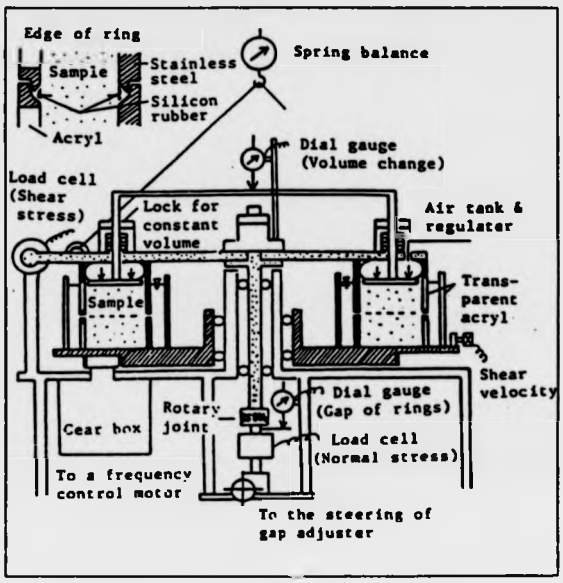

Figure 2.11: Ring shear apparatus presented by Sassa 1985 [74], from Parathiras 1994 [4].

minimum friction.

The second generation of Sassa's ring shear devices was introduced by Sassa et al [75] [76] in 1989 and a paper was produced by Sassa et al in 1991 [77] which utilised this new apparatus. Landslides are a significant problem in Japan and substantial funding is available to help investigate and prevent potential disasters. This is evident from the levels of technology employed in this apparatus. This *"high-speed high-stress ring shear apparatus"* has many interesting features. The normal stress is applied via six air pistons and is measured by a load cell whose signal constantly maintains the level of normal stress via an air servo-valve. The gap between the upper and lower confining rings is continuously monitored and maintained with an accuracy of 1/1000th of a millimetre by a servo-motor. Another servo motor rotates the bottom half of the sample. As in the earlier design shear strength is measured by a load cell mounted to a rigid vertical arm. All output signals and servo-motors are constantly monitored and controlled via a personal computer, making the equipment state of

the art. The outer confining rings are acrylic glass to allow visual observation of the shear zone. The sample has an outside diameter of 330 *mm*, an inner diameter of 210 *mm* and a height of 60 *mm*. It is submerged and drainage is facilitated by porous metal plates at the top and bottom of the sample. Soil extrusion is prevented by a rubber edge mounted on the upper confining ring which is always compressed against the lower confining ring.

A completely new and very complicated design developed by Sassa in 1991 and presented with results in 1992 [78] is now reviewed. A very similar test rig was used by Shoaei and Sassa in 1994 [79] and a brief description of this new design is provided here. The general layout of the apparatus is shown in Figure 2.12. The sample (L) is confined in the shearing rings, where the lower rings are rotated by a servo-motor. Cyclic normal loading comes from the air piston (B) and the cyclic shear loading from the torque controlled servo-motor (V), which shears the sample at a constant rate. With this equipment it is possible to perform a constant volume test, by securing the top platen to the main stable frame at (D). This has little relevance to the Bishop apparatus. Vertical load is measured by the load cell (E) and the side friction by load cell (R), where the difference between these recordings gives the correct vertical load. The shear load is monitored by load cell (I) and the shear torque from a servo-motor is monitored by a torque converter (T). The horizontal displacement of the bottom ring is monitored by displacement transducer (K). When fast rate tests are conducted, not all the pore water pressure in the sample will be dissipated, the pore water pressure may even build up. Recent thinking suggests that the role of pore water pressure in rate effects is important. Therefore three needles connected to pressure cells (H) are inserted into the centre of the sample. The load cell (F) monitors the change in sample height, if a constant volume test is not being performed.

Perhaps the most interesting feature on this apparatus is the gap control mechanism. The gap between the rings is automatically maintained constant by a servo-motor (S) through a feedback signal from the precise gap sensor (W) which detects changes down to 1/1000th of a millimetre. A Teflon coated rubber edge 9 *mm* thick is stuck to the upper ring. This edge is always compressed by about 0.2 *mm* using a weight of 25 *kgf* during cyclic and high speed loading, thus preventing soil loss

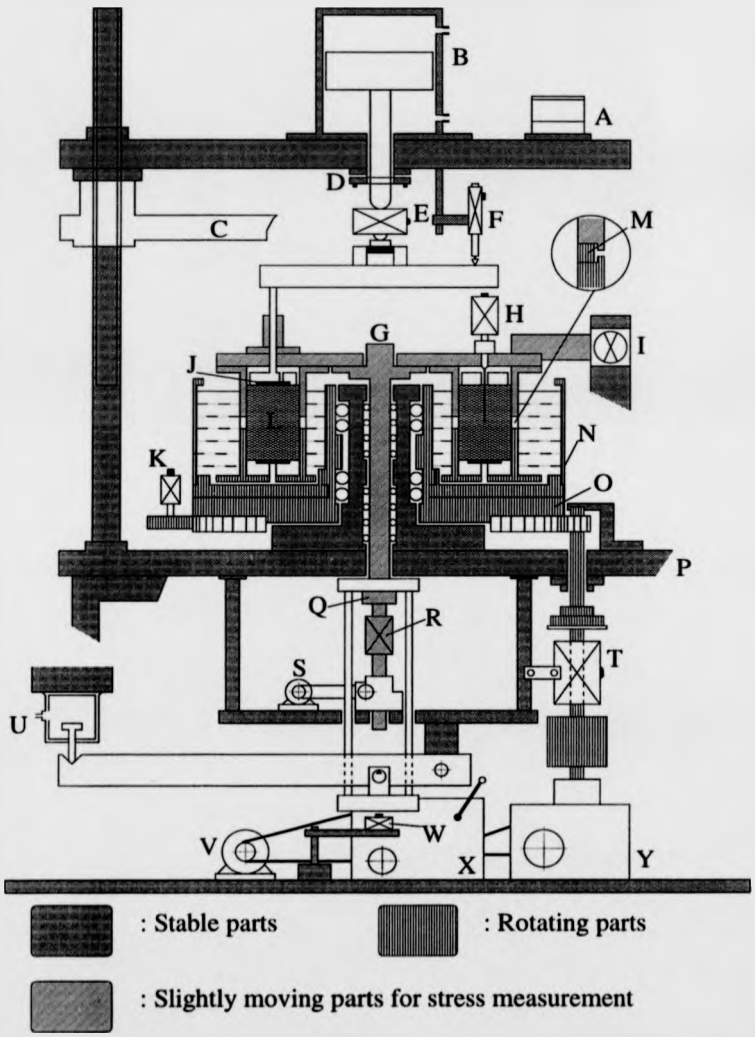

Figure 2.12: Structure of a new cyclic loading high-speed ring shear apparatus. Parts identified by letters are referred to in the text.

through the gap.

Many major landslides in Japan are earthquake induced. The function of Sassa's design is to simulate earthquake induced shearing. In Sassa's 1992 study [78], the cyclic loads were applied at a frequency of 0.1 Hz (once every 10 seconds), this appears to be the limit of this design as allowances had to be made to model real earthquakes which have frequencies one or two orders higher than 0.1 Hz. Sassa's work is bordering on seismology and as such has important links to the initiation of long run-out landslides. It is interesting to note many features of this new design and the levels of technology used in comparison with the IC/NGI apparatus. It has many advantages for the study of rate effects including the range of speeds available, the prevention of soil loss, the precise gap control and the ability to apply cyclic stresses.

As reported by Parathiras [4], Nieuwenhuis in 1991 [80] introduced a new ring shear device designed at the University of Utrecht, see Figure 2.13. This device functions as either a strain or stress controlled system. The normal load on the sample is applied by an axial motor and is measured at three points around the edge of the top platen. The bottom rings are fixed to a rotating table and the shear stress is measured through vertical supports. The gap can be controlled by a set of three clamps that appear to be manually operated. Parathiras [4] does not mention how or indeed if side friction is measured. The sealing of the gap between the confining rings is interesting, as it might be possible to adapt it to work on the IC/NGI apparatus. The gap is sealed by a flexible hollow lubricated O-ring which is kept in place by two lubricated steel rings, see Figure 2.14. The friction created by this seal is measured using a dummy sample and then the necessary correction can be calculated and applied to actual test results. The author suggests that this friction may be minimised by the application of a Teflon spray coating. Parathiras [4] indicated that Nieuwenhuis [80] claimed that positive or negative pore water pressures could be introduced to samples in this apparatus. A comprehensive presentation of this was not provided.

According to Parathiras, Yagi et al [66] introduced two new devices aimed at the investigation of stability analyses on landslides. A brief description of the equipment was provided along with the diagrams shown in Figures 2.15 and 2.16, which

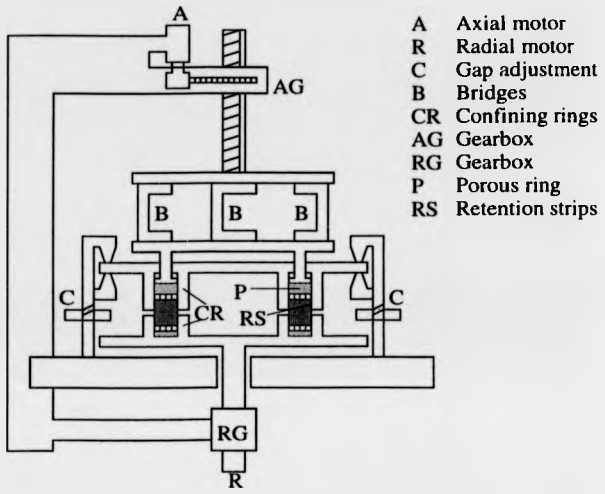

Figure 2.13: Utrecht University ring shear apparatus, Nieuwenhuis 1991 [80].

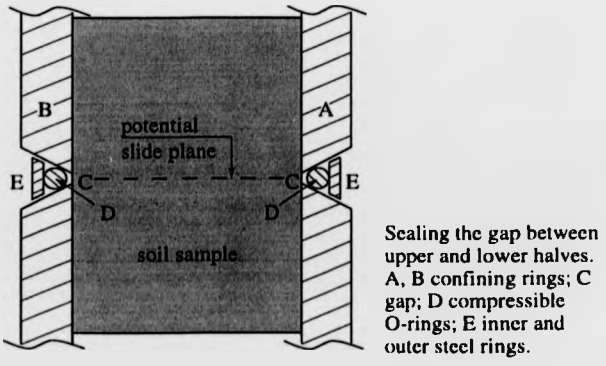

Figure 2.14: Gap sealing mechanism for Utrecht University ring shear apparatus, Nieuwenhuis 1991 [80].

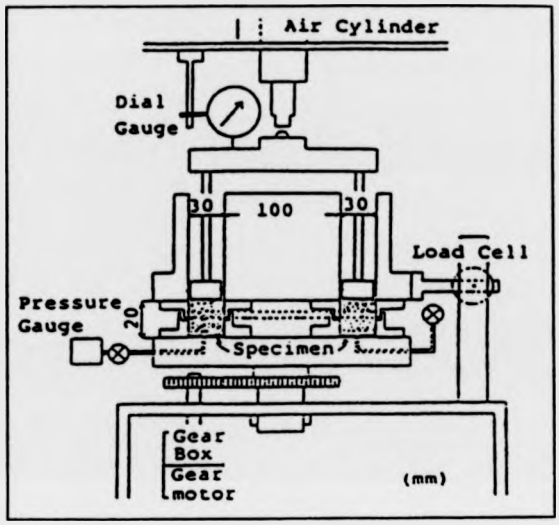

Figure 2.15: B-type ring shear apparatus, Yagi et al 1991 [66], from Parathiras 1994 [4].

highlight the main differences which related to the shearing conditions placed on the sample. The B-type apparatus encourages shearing along a plane where as the S-type apparatus applies uniform shear conditions throughout the sample. As mentioned in Subsection 2.2.8, Yagi was concerned about the development of slickensides in shear boxes, the aim of the S-type apparatus was to prevent slickensides developing. In the B-type apparatus, the normal load is applied by an air cylinder, the sample height is 20 mm and it is not submerged. Shear stress is recorded with a torque arm load cell arrangement, whilst pore pressures are recorded in the base of the sample. Parathiras noted that the bottom confining rings have tooth like edges, the aim of this is to reduce soil extrusion. The S-type design is similar to the B-type, however the sample is 10 mm high submerged yet unconfined in an effort to prevent single plain failure. Finally, all of Yagi's tests were conducted at a rate of 0.21 mm/min because at this rate measured pore water pressures were considered insignificant.

The next development to be reviewed is that provided by Parathiras [4], who was concerned that it was difficult to progress through more than two levels of normal stress in a test, without significantly losing accuracy because of soil loss.

Initially Parathiras [4] considered the technique of clamping the proving ring,

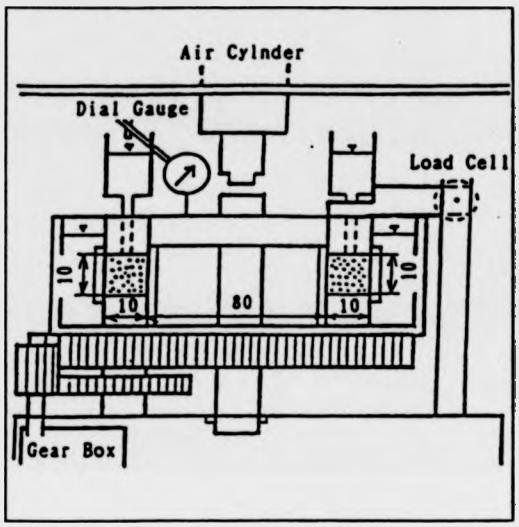

Figure 2.16: S-type ring shear apparatus, Yagi et al 1991 [66], from Parathiras 1994 [4].

but concluded that Lemos's attempts at this in 1986 [43] had been exhaustive and had had minimal levels of success. Parathiras then considered, designed and tested three modified sets of rings, which would fit the IC/NGI apparatus. These new rings, illustrated in Figure 2.17, had overlapping flanges, so that there would be no direct gap between them. However on testing Parathiras discovered that soil particles entered between the flanges, causing a build up of friction and an eventual jamming together of the upper and lower rings.

So Parathiras [4] designed a new set of confining rings that would fit into the standard ring shear apparatus. The first design had a constant gap width of 0.02 *mm*. This was achieved by fixing the top rings to the rotating base, by means of ball bearings. This modification allowed the top ring to rotate with respect to the bottom ring, but did not allow any relative vertical or horizontal movement of the rings that could promote soil loss.

After gaining some experience with the new rings, Parathiras [4] decided that in order to completely minimise soil loss, the gap had to be kept closed by an elastic system which would not create large amounts of internal friction. This problem was solved using a spring mounted carbon flange positioned in what had been the

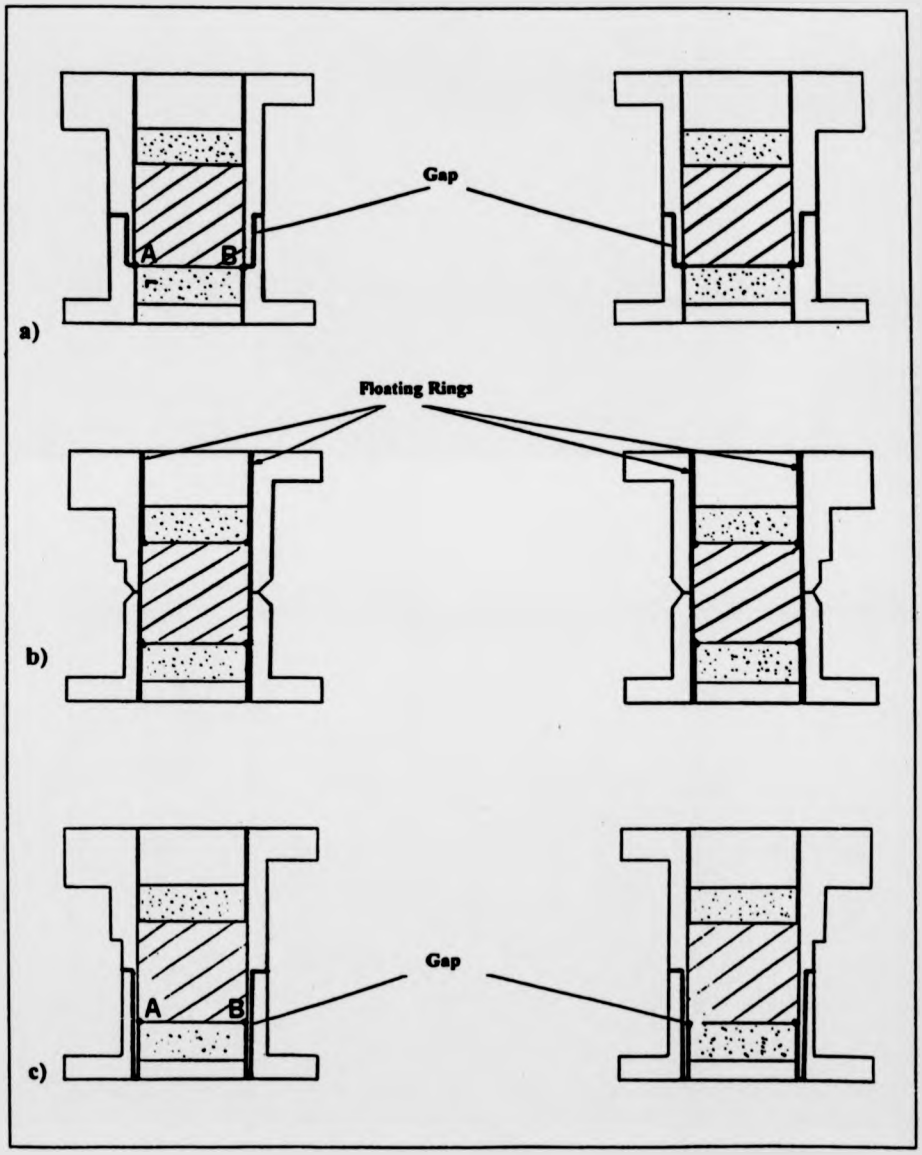

Figure 2.17: Sets of modified confining rings, from Parathiras 1994 [4].

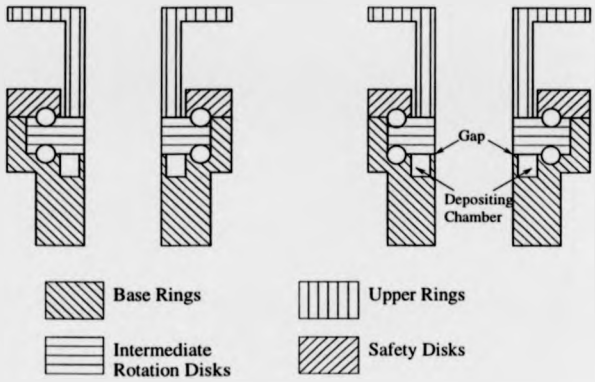

Figure 2.18: Cross section of new confining rings (assembled).

deposition chamber in the first version of the new rings. Cross sections through both versions of the new rings can be seen in Figures 2.18 and 2.19.

Two factors had to be considered before a thorough testing program could begin. Firstly, the gap friction had to be quantified. This was carried out by using a dummy sample, similar to that used in the University of Utrecht apparatus.

Secondly and perhaps more significantly, it was not possible to directly measure the side friction with the new rings designed by Parathiras. This problem was solved by testing identical samples to those being tested in the new rings in the standard rings. This allowed the side friction created in the old rings to be recorded along with the associated displacement of the upper loading platen. Once a database of this information had been established, it was possible to monitor the change in sample height in the new rings and therefore obtain the side friction by cross referencing with the database.

Unfortunately Parathiras [4] did not have enough time to use the carbon flanged rings in his main testing program. However when summarising tests with both sets of rings, he claimed that the limitations of the standard rings owing to soil loss had been overcome, that the new rings estimated residual shear strength to within 0-2% of the old rings and that the new rings lose up to seven times less soil and allowed prolonged fast shearing. Parathiras concluded that *"the new ring design provides the*

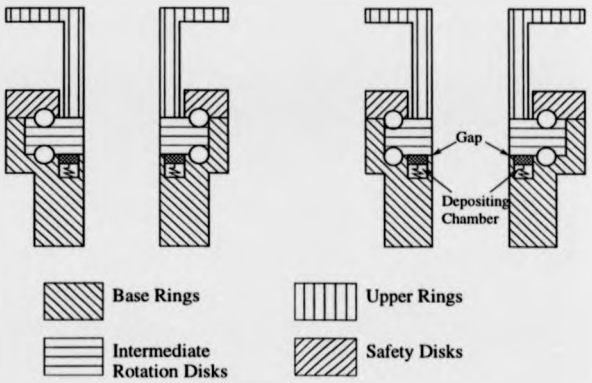

Figure 2.19: Cross section of new confining rings - version 2.

most efficient means of minimising soil loss and testing samples in prolonged stages at earthquake-induced rates of displacement" in the IC/NGI apparatus.

The most recent ring shearing equipment has again been developed by Sassa and his team at Kyoto University [81]. The apparatus is designed to simulate earthquake induced landslides with shear zones up to 200 *m* deep. The scale of the apparatus is impressive, occupying two floors in its current building, the size of the apparatus is clearly visible in Figure 2.20. This new intelligent-type dynamic-loading ring shear apparatus is the culmination of a decade of research and development at Kyoto which started in 1988 with the first high-speed high-stress apparatus [75] [76]. This new apparatus was briefly presented in 1997, according to Sassa [81] the main characteristics of the apparatus are:

- Annular shear box with inner and outer radii of 250 *mm* and 350 *mm* respectively.
- 37 *kW* servo-control motor, where both torque and speed control are possible.
- Two 20 *ton* servo-control oil pistons, one for normal stress application and the other for gap control.
- High precision (1/1000th *mm*) gap control system.

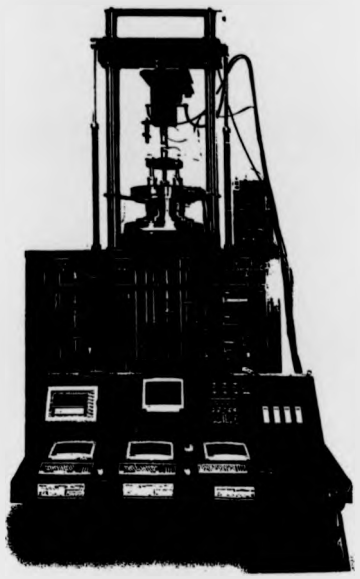

Figure 2.20: Photo of Sassa's new apparatus and its control and data-acquisition, Sassa 1997 [81].

- Fast data sampling at speeds up to 200 *samples/second.*
- Maximum mid-annulus shear speed of 220 cm/s.
- Maximum normal stress is 40 kgf/cm^2.
- High frequency of normal and shear loading up to 3 Hz.
- The ability to apply normal and shear loads identical to those monitored in actual earthquakes.
- Finally, owing to the complexity of the apparatus, a number of warning and safety systems exist to ensure correct operation.

2.3 The Effects Of Rate Of Shearing On The Residual Strength Of Soils

2.3.1 Early Investigations

Early investigation into rate effects on soils began in the 1960s. The main aim of these investigations was to conduct tests in a shorter time period by maximising rates of shear. This would save time in the laboratory and therefore have commercial advantages. The majority of these early works were conducted in triaxial and direct shear testing apparatus, mainly because these were more widely available and easier to use and interpret in comparison with ring shear apparatus.

The earliest study into rate effects was reported by Parathiras [4] and appears to have been produced in 1962 by Horn and Deere [23]. In their study of the frictional characteristics of minerals, they conducted tests on smooth and roughened quartz and phlogopite mica in both the dry and saturated condition. As part of the testing they varied the rate of shearing from 17.78 mm/min to 152.4 mm/min, this variation resulted in a 12% increase in residual strength in the dry condition and a 28% increase in residual strength in the saturated condition for phlogopite mica. For the quartz no change in residual strength was observed.

The first major investigation by Lupini [44] and Lupini et al [22] into rate effects was conducted using the IC/NGI apparatus in 1981. Prior to this, several studies were conducted which included as a part of the research an investigation into the effects of rate of shearing. The majority of these works were reported in 1989 by Tika [2] and can roughly be divided in two. Approximately half of the studies found residual strength to be independent of rate of shearing whereas the other half generally found increases in strength with increasing rate of shearing.

Firstly the rate independent reports. In 1964, Novosad [82] conducted a study using a modified Hvorslev ring shear apparatus and granular materials. Despite using a large range of rates from 300 mm/min up to 30000 mm/min, Novosad found no variation in the residual strength. He also reported that during fast shearing, the granular material was in motion at distances up to 3 mm above or below the shear

plane.

Scarlett and Todd [83] studied the behaviour of sand in an annular shear cell and reported measurements of dilatancy and critical porosity using the gamma ray attenuation technique. They found that the thickness of the shear zone increased with both increasing particle size and normal stress. The number of particles in the shear zone (usually 5 to 10), however, decreased as particle size increased. The study concluded that the critical porosity of a flowing sand decreases as normal stress increases and is also dependent on particle shape and size. With regard to rate effects they found that variations of rate in the range 1.3 rad/min to 5.1 rad/min had no effect on the measured strength.

Kenney in 1967 [38] conducted direct shear tests on a range of materials as reported in Subsection 2.2.4. He found no variation in residual strength with shear rates varying from 10^{-3} mm/min to 0.17 mm/min.

In 1970 Ramiah et al [84] performed tests on a silty clay using direct shear apparatus. They varied the rate of shearing from 0.023 mm/min to 10.2 mm/min and found no corresponding variation in residual strength.

Garga [42], using an early version of the IC/NGI apparatus, conducted tests on Blue London clay and found it to be rate independent in the range 0.0038 mm/min to 0.0076 mm/min. Meanwhile La Gatta [41] conducted tests on Blue London clay using the strain controlled ring shear apparatus developed at Harvard, he came to the same conclusion as Garga, finding no variation in residual strength at rates varying from 0.0048 mm/min to 0.48 mm/min. La Gatta performed tests on Pepper shale and Cucaracha shale too, finding these materials also to be insensitive to rate of shearing.

The first study to report a variation in residual strength with rate of displacement was produced in 1966 by Petley [85]. The conclusions with regard to rate effects were based on shear box tests with reversals, using samples of Brown London clay. He found that an increase in residual strength of approximately 4% occurred, when the rate of displacement was increased from 0.00004 mm/min to 0.10 mm/min.

De Beer [86] carried out a series of tests on both pre-cut and remoulded samples of Boom clay using a torsion shear test. These lead him to conclude that at a rate of

0.035 mm/min the residual strength is lower than that at a rate of 0.0066 mm/min. Tika [2] questions the validity of this study because truly residual conditions may not have been established as the actual shear displacements were small.

La Gatta in 1971 [45] conducted additional tests on Blue London clay and Bearpaw shale using the Harvard ring shear device at rates ranging from 0.0048 mm/min to 2.4 mm/min. From these tests he postulated that for Blue London clay an increase in residual strength occurs as rate of displacement increases. However for the Bearpaw shale no significant strength variation was apparent.

Cullen and Donald in 1971 [39] performed direct shear tests with reversals on a silurian clay, whilst they only varied the rate of shearing between 0.017 mm/min and 0.025 mm/min it appears they may have made the first observation of what is now known as the threshold strength, after Martins in 1983 [87]. When the rate of shearing was rapidly increased they found that at zero relative displacement a strength 10% to 15% higher than the slow residual strength was attained and then a steady value was gained at the faster rate. On the resumption of slow shearing they observed that the slow residual strength was 0% to 15% lower than the steady value which occurred at the fast rate.

In a similar fashion to Cullen and Donald, Gostelow in 1974 [88] appears to have observed what is now known as the fast peak strength, after Martins in 1983 [87]. Whilst conducting a ring shear test on Penwortham Upper till they observed a slight peak in residual strength if the rate of shearing was increased rapidly. They also found that as the rate of shearing was increased from 0.0145 mm/min to 1.35 mm/min a slight decrease in residual strength occurred.

Bucher [58] carried out similar tests in 1975 using a medium plasticity clay in a ring shear device at rates ranging from 0.0145 mm/min to 14.6 mm/min. Bucher found that an increase in residual strength was observed with increasing rate of shear.

It is noteworthy that the highest rate of displacement used up to this point with cohesive soils is 14.6 mm/min. At this rate significant rate effect was reported, whereas studies carried out at much lower rates did not generally report any significant rate effects. Where rate effects were reported at much lower rates of shearing, credit must be paid to the test operators for there careful testing procedures and observations.

It now appears likely that for the majority of cohesive materials mentioned above, rate effects would have been observed by everyone if testing had been conducted at rates above a level of approximately 10 mm/min. These early results lead people such as Lupini in 1981 [44] to carry out tests at much higher rates of displacement and therefore start to obtain data about the variations of residual strength with rate of displacement.

2.3.2 A Decade Of Progress

The first extensive study of rate effects using the IC/NGI apparatus was reported by Lupini [44] and Lupini et al [22], who carried out tests at rates up to 177 mm/min. Lupini postulated a link between the drained residual shear mode and rate effects, as described in Subsection 2.2.8 and illustrated in Figure 2.8.

Lupini postulated that soils with a sliding residual shear mode would exhibit an increase in residual strength as the rate of shear was increased. He proposed that as the rate of shearing increased so would viscous effects which lead to an increase in inter-particle friction, ϕ_μ. As the residual angle ϕ_r is a function of ϕ_μ, this leads to an increase in residual strength. If the rate effect is large enough to allow the viscous effects to make $\phi_\mu = \phi_{cv}$ then the plate like particles will start to become disorientated and a turbulent shear mode will occur, thus leading to a further increase in the residual strength. Whether or not disorientation occurs depends on the magnitude of the viscous effect and therefore the rate of shearing and also the difference between the residual angle ϕ_r and the constant volume angle ϕ_{cv} which for normally consolidated clays is equal to the peak angle ϕ_p. A good indication of particle disorientation is supplied by the phenomena of *"renewed brittleness"* observed after some stages of fast shearing. When slow shearing is recommenced, a slow peak strength is observed if the particles have been disorientated owing to the higher resistance obtained in comparison with the aligned particles.

If soils had a turbulent shear mode, Lupini found that their residual strengths fell as rate increased. This negative rate effect may be a consequence of increasing dilatancy with displacement and therefore an increase in the granular void ratio, which means that the degree of interlocking between particles is reduced and therefore so is

the residual strength.

A theoretical and experimental study of rapid granular flows was conducted by Savage in 1982 [89]. The experimental work involved testing of single sized spherical particles, mixtures of different sized particles and angular particles in an annular shear cell. He found that both normal and shear stress increased with concentration (volume of grains divided by total volume). The shear and normal stress tended to vary with the square of the shearing rate at low concentrations. At higher concentrations however he postulated that the dynamic friction angle is insensitive to shearing rate. Savage believed that the shear strength, τ_{total}, had two components, the first being rate independent and the second being the rate dependent or dynamic part, thus:

$$\tau_{total} = \tau(v)_{Coulomb} + \mu_s(v)\rho_p D_p^2 \left(\frac{du}{dx}\right)^2 \tag{2.6}$$

where τ and μ_s are functions of the concentration, v, ρ_p is the individual particle mass density, D_p is the particle diameter and du/dx is the average rate of shearing. At high concentrations and low rates of shearing the rate independent part dominates, the shear strength is developed as a result of dry friction and the over riding action of the particles. By contrast, at low concentrations and high shear rates the rate dependent part is dominant, the shear strength is generated as a result of the transfer of momentum during particle collisions. Savage's equation implies that shear strength is generated simultaneously by both mechanisms but it is difficult to visualise the combination of over riding and collisions occurring at the same time in the same area of the shear zone.

Martins in 1983 [87] carried out investigations on weathered Panama Tuff. He studied the effects of rapid shearing on pre-existent shear surfaces, using the IC/NGI ring shear apparatus at rates up to 100 mm/min. Martins [87] recognised that there were four rate dependent strength effects, also see Figure 2.21:

- (i) A threshold effect prior to any relative displacement across the shear surface.
- (ii)An increase in strength across the shear surface, presumed to be associated with the restructuring of the particles in the soil matrix.

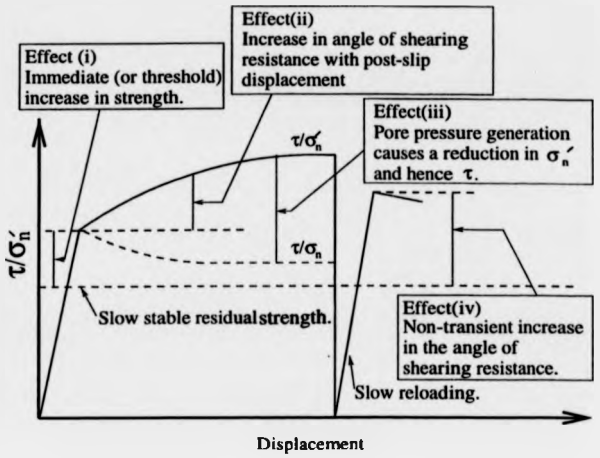

Figure 2.21: Summary of rate-dependent phenomena, Martins 1983 [87].

- (iii) A pore pressure build up that reduces the effective normal stress and therefore the residual shear strength.
- (iv)A non-transient increase in strength when a sample is sheared slowly after a period of fast shearing. This increase in strength increases with the fast rate of shearing prior to the current slow shearing. Resulting from this behaviour Martins suggested that a critical rate exists below which the particles in the shear zone do not become disorientated.

Hungr and Morgenstern conducted two series of experiments on the behaviour of granular materials at high velocities. In the first tests [90] they used a flume to study the behaviour of dry sand and concluded that at rates up to 5 m/s the material behaved in a perfectly frictional fashion, thus implying that no rate effects occurred. In the second series of tests [71] Hungr and Morgenstern decided to investigate the influence of higher levels of normal stress. They used the ring shear apparatus described in Subsection 2.2.9 and illustrated in Figure 2.10, again the sand illustrated neutral rate behaviour at speeds in the range 0.1 cm/sec to 98 cm/sec and at normal stresses between 20 kPa and 200 kPa.

As reported by Tika [2], Osipov et al [91] conducted experiments which simulta-

neously involved soil shearing and vibration. The aims of these tests were to study the microstructural changes associated with thixotropic flow phenomena in clay soils. Pure clay minerals (kaolinite and montmorillonite), silty clay and loess were used in the tests, prepared as pastes, with moisture contents in the range 0.8 to 2.2 times the liquid limit of the soil. Initially a steady residual strength was obtained at a rate of 15 mm/min then the sample was vibrated for 5 minutes as the shearing continued. Finally after the cessation of vibration a steady residual value was reattained. Osipov et al found that the vibrations caused a significant reduction in the strength of the soil, depending on the parameters of the vibration. Microstructural changes were observed in the soils by rapidly freezing them with liquid nitrogen during the test and then studying the samples with a scanning electron microscope. During shearing they observed that deformation occurred over a limited volume in the shear zone and is associated with significant changes in the microstructure in this zone. When the pastes were composed of small particles only, they observed that any deformation is volumetric and does not lead to the structural discontinuities (shear planes). Although in coarser clays they observed both volumetric deformation and disruption of the structure along developing shear planes. The application of vibrations to the sample results in a dynamic state where all the particles are oscillating. This prevents the development of structural discontinuities and leads to a homogeneous condition. The drop in strength is associated with the disruption of particle structure, a loss of inter-particle cohesion and an increase in soil dispersion. When the vibrations cease an increase in strength is observed above the initially observed residual strength, this they proposed was a result of mutual fixation of the particles and coagulation contacts between them. Henceforth the soil structure after thixotropic flow shows a marked similarity with its original state.

Bernander [92] presented results in 1985 on the testing of soft Swedish clays in direct shear apparatus. It was reported that the residual strength decreased with both increasing rate of displacement and over consolidation ratio. Bernander attributed the loss of residual strength at faster rates to a decrease in effective stress caused by localised increases in pore pressure. Owing to the localised nature of these pressure increases Bernander postulated that they could not easily be observed as most systems

measure mean pore pressure. Tests were conducted at rates similar to those observed in actual landslides in this material and the residual strength was compared to the critical state strength. The ratio of these strengths was as low as 0.3 and therefore Bernander proposed that this negative rate effect explained the large planar landslides often observed in Sweden, which could not be accounted for by using the slow drained residual strength in analysis. Tika [2] questioned the validity of Bernander's work because the reported displacements are short and *"it is doubtful whether real residual conditions had been achieved"*.

Another study reported by Parathiras [4] was published in 1985 by Idriss [93]. Idriss was concerned with the large shear displacements that can occur as a result of earthquakes. He investigated large displacements using vane shear tests, direct shear tests and cone penetration tests on Bootlegger Cove clay. As a result of his studies he proposed that earthquakes may lead to the complete reorientation of clay particles and a change in pore water pressure conditions, henceforth establishing undrained residual conditions. Whilst acknowledging a wide scatter among the results Idriss claimed that at displacements of 150 *mm* the strength would have fallen to around 70% of the peak strength where as at large displacements the strength would have fallen to around 30% of the peak strength. These ideas are illustrated by the step type function shown in Figure 2.22.

In 1985 Professor Skempton [5] presented information on rate effects as part of his study of residual strength, noting that landslides move at a wide range of velocities and therefore *"a knowledge of the effects produced by different rates of shearing is therefore a significant part of residual strength studies"*. Firstly Skempton reported on slow tests in the range 0.0001 *mm/min* to 1 *mm/min*. He concluded that in London clay and kaolin whilst residual strength did increase with rate the change was small, of the order of 2.5% per log cycle and as such could be regarded as insignificant. However as an interesting corollary of this, Skempton noted that this meant small changes in strength could lead to significant changes in the speed of landslides, thus indicating why many instabilities are sensitive to piezometric level and can be stabilised by drainage which only slightly increases the factor of safety. At much faster rates Skempton reported tests on soils from the Kalabagh Dam project, in clays he

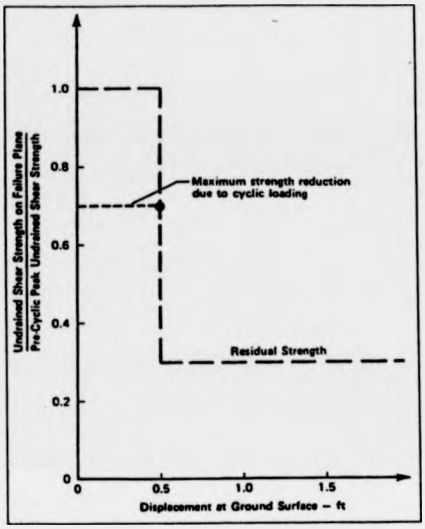

Figure 2.22: Variation of undrained shear strength on potential failure surface, Idriss 1985 [93], from Parathiras 1994 [4].

proposed that significant increases in residual strength would be observed at rates above 100 mm/min, in low clay fraction siltstone he reported that no rate effects had been observed at rates up to 800 mm/min and perhaps most significantly that a *"a remarkable drop in strength"* was observed in a clayey siltstone (CF=25%) at a rate of 400 mm/min. Nevertheless Professor Skempton readily acknowledged that only a small number of tests had been reported and much more research work was necessary to make definite conclusions.

Lemos et al [94] presented some typical results from rate effect tests performed in the IC/NGI apparatus, using a standard testing procedure. This work recognised that five different strengths could be observed during a combination of fast and slow shearing, also see Figure 2.23:

- (a) the *drained residual strength*,
- (b) the *threshold strength* which is mobilised prior to any shear movement when fast shearing occurs after slow shearing,

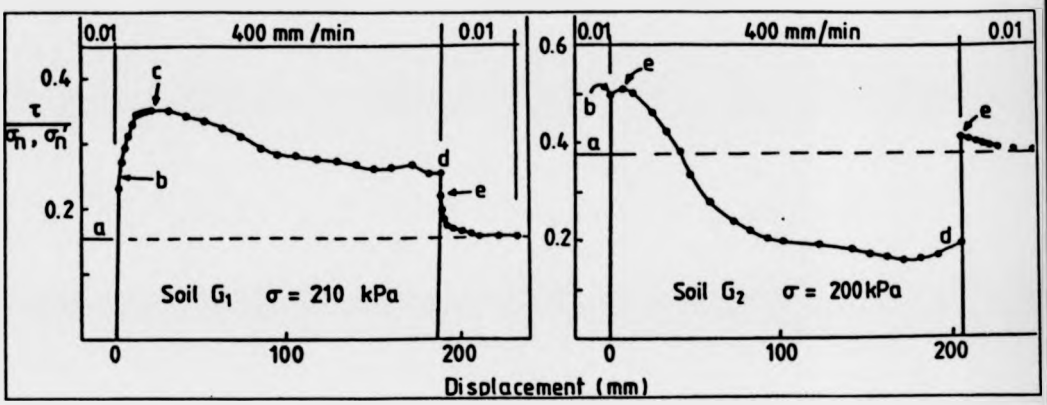

Figure 2.23: Typical behaviour during fast shear tests, Lemos et al 1985 [94], from Parathiras 1994 [4].

- (c) the *peak strength* which is attained after the threshold strength,
- (d) the *ultimate fast strength* which is the steady value of shear strength during fast undrained loading, and
- (e) the *peak strength after fast shearing* which is mobilised when slow shearing follows fast shearing.

Lemos et al [94] postulated that increases in residual strength with rate of shearing would be observed in soils exhibiting a sliding shear mode [44]. They proposed that this gain in strength may be associated with disordering of the clay particles which may be triggered by the presence of rotund particles in the shear zone. Finally they stated that dramatic drops in strength will occur if positive pore pressures are generated in the shear zone by rapid shearing.

In 1986 Lemos [43] carried out an in depth study of rate effects on residual strengths at rates up to 6000 *mm/min*. To an extent this work merged the ideas developed in Lupini [44], Lupini et al. [22] and Martins [87]. Both Parathiras [4]

and Tika [2] recognised that the following observations and conclusions summarise the results of Lemos's investigation.

- (i) Soils which have a very low clay fraction and a turbulent shear mode, exhibit negligible rate effects with an increasing rate of shear (Figure 2.24a).
- (ii) Rate effects suddenly become significant with an increasing clay fraction. Soils with a turbulent or transitional shear mode and a higher clay fraction have a lower fast residual strength than their slow residual strength (Figure 2.24b).
- (iii) Soils with an increasing clay fraction and a sliding shear mode exhibit an increase in residual shear strength with an increasing rate of shearing (Figure 2.24c).
- (iv) The slow peak strength that occurs after a period of fast shearing is attributed to the disordering effect of the fast shearing on the particles in the shear zone. This effect does not occur in soils with a turbulent shear mode, as its strength does not depend on particle orientation.
- (v) The threshold strength is an intercept to the failure envelope, not an increase in the actual friction angle.
- (vi) The fast peak strength rises above the threshold strength because of the disordering effect on the particles in the shear zone.

Tika [2] attempted to amalgamate all the ideas developed by Lupini [44], Lupini et al [22], Martins [87], Lemos et al [94] and Lemos [43]. She managed this successfully by further testing on natural and artificial soils, to verify Lemos's work and develop a classification which links types of soils to their likely responses to different rates of shearing.

The five types of variation of residual strength with an increasing rate of displacement can be seen in Figure 2.25. Type I shows no significant rate effect. Types II and III show that at higher rates of shearing, the residual strength is lower than the slow residual strength, whereas Types IV and V show that at higher rates of shearing, the

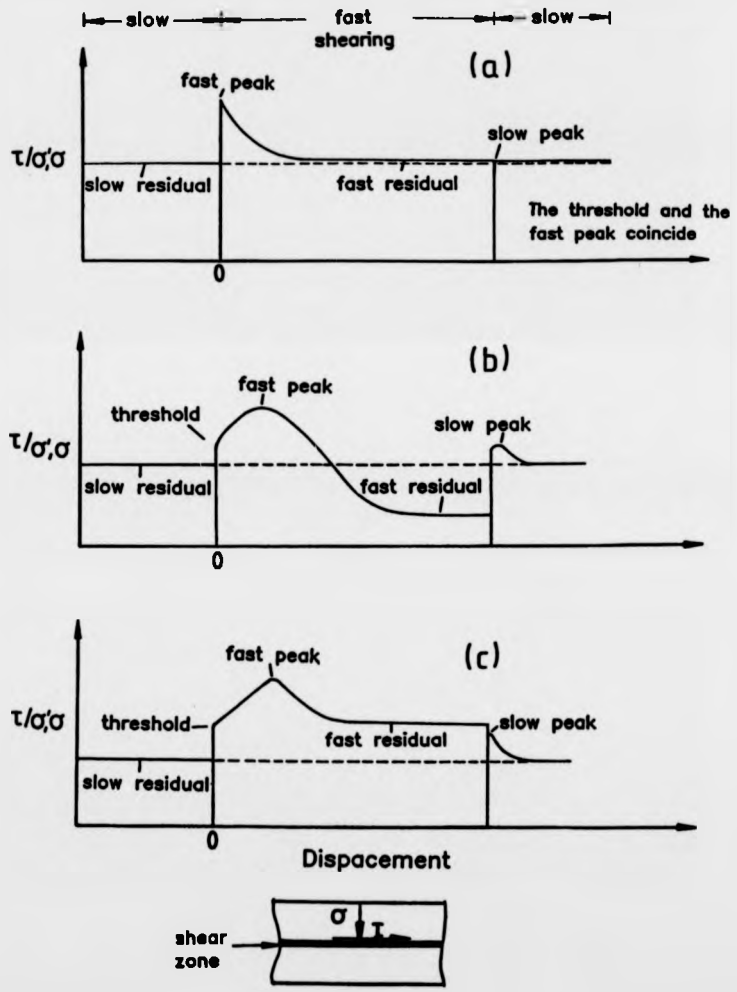

Figure 2.24: Typical behaviours of pre-existing shear zones/surfaces at fast rates of displacement, Lemos 1986 [43], from Tika 1989 [2].

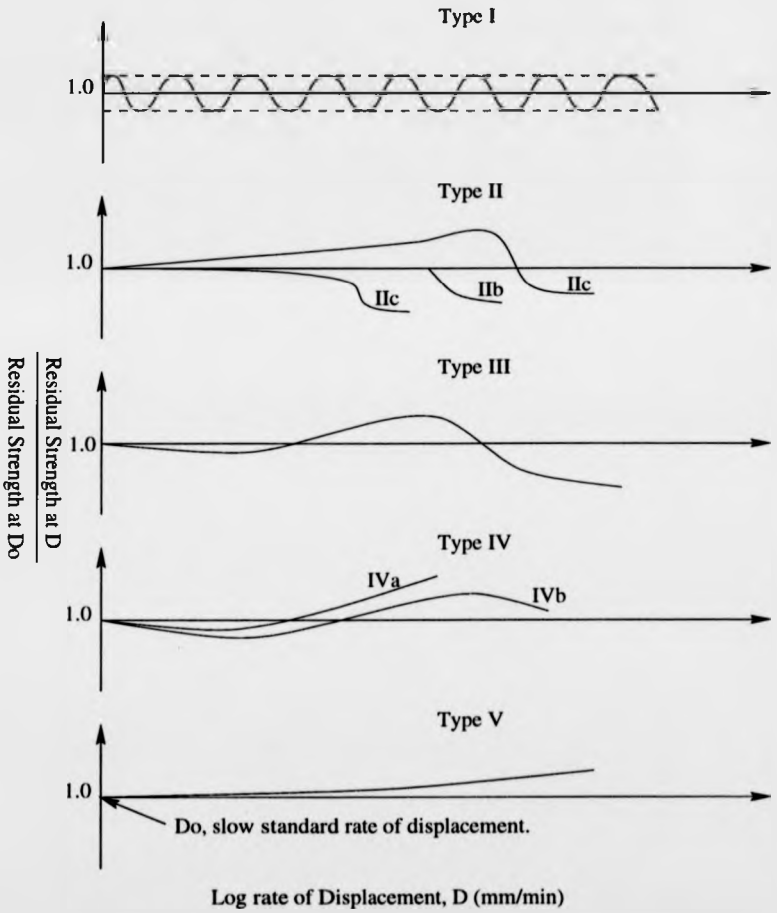

Figure 2.25: Variation of residual strength of soils with an increasing rate of displacement, from Tika 1989 [2].

residual strength is higher than the slow residual strength. Tika noted the following properties about each of the following types:

- Type I soils had a turbulent shear mode. They were sands and silty sands, with a plasticity index below 9%, a sand content above 20% and a clay content less than 10%.
- Type II soils had a turbulent or transitional shear mode. Their plasticity indexes fell between 9% and 21%. These soils had a silt content greater than 60%.
- Type III soils were silty clays exhibiting transitional or sliding shear modes. Their plasticities fell between 24% and 26%.
- Type IV soils were silty clays and low plasticity clays. The silty clays exhibited transitional or sliding shear modes and had a plasticity between 26% and 36%. The low plasticity clays had a turbulent or transitional shear mode and a plasticity between 10% and 21%. They generally had either a granular phase or were very well graded.
- Type V soils were clays exhibiting sliding shear modes, they had high plasticities between 36% and 51% and a clay content greater than 48%.

Tika attributed the increase in residual shear strength in mainly turbulent shear mode soils to viscous effects. In soils with mainly sliding shear modes it was attributed to structural changes in the shear zone. She attributed the drop below the slow residual strength in Types II and III to a decrease in the soils viscosity in the shear zone, allowing the particles to flow over one another. She reinforces this by observing that once fast shearing has stopped, the shear zone attempts to contract, this results in the build up of pore water pressures, which maintain this lower shear strength if the sample is sheared at a slow rate until the excess pore water pressure dissipates. Tika also states that *"the type of behaviour does not relate to the type of drained residual shear mode or the index properties of the soil, but rather to the grading of their granular phase"*. This appears to contradict a lot of the early work conducted using the IC/NGI apparatus.

2.3.3 Recent Discoveries

Lemos [95] produced more arguments on the effects of fast shearing on cohesive soils. He defined the effects as either neutral, positive or negative depending on whether the strength remained roughly constant, underwent a net increase, or a net decrease when subjected to faster rates of shearing. He also defined the boundaries of these effects. A neutral effect would occur in a soil with a clay fraction below 5%, whereas a negative effect occurs in soils with clay fraction between 5% and 40% and a positive rate effect will be observed in soils with a clay fraction greater than 50%. As part of his study, Lemos [95] also developed ideas on why the soils behave in such a way. He attributes the immediate and maximum increase in strength on fast shearing to viscous effects and he notes that the threshold strength increases with the rate of shearing. The positive rate effect is associated with the disturbance of the shear zone on fast shearing and the effect will be more apparent in clayey soils which contain massive particles. The negative rate effect is attributed to increased porosity and water content in the shear zone. Lemos attempted to confirm this by noting different results between a full and an empty water bath test. He also discounted the possibility of excess pore pressures during fast shearing of a submerged sample. Previously it had been postulated that because the time for the slow residual strength to be regained after fast shearing was equal to the time for consolidation, there must have been excess pore pressure during shearing. Lemos however points out that this observation is largely correct, but that the pore pressure is generated immediately after the cessation of fast shearing as the shear zone contracts from its dilatant condition and not during the process of fast shearing. Lemos should be commended in his attempts to simplify the situation and his boundaries for the types of rate effect are considerably simpler than the five types suggested by Tika [2]. On the other hand Lemos did note that there were several soils which did not comply with his boundaries and these include some tills and some residual soils.

Bracegirdle et al [96] presented a case study of a shipping berth, located above an active shear surface on the banks of the River Tyne in North East England. They conjectured that the displacement of the landslide could be predicted over a single

tide cycle using rate effects. They proposed the following relationship between shear strength, ϕ'_{mob}, and the rate of shearing, $\dot{\delta}$:

$$\dot{\delta} = \dot{\delta}_0 . e^{C_n \Delta^R} \tag{2.7}$$

where C_n and R are constants and $\dot{\delta}_0$ is a low rate of shearing and Δ is given by:

$$\Delta = \frac{\tan \phi'_{mob} - \tan \phi'_{rs}}{\tan \phi'_{rs}} \tag{2.8}$$

where ϕ'_{rs} is the residual strength at the initiation of movement, in practise they used ϕ'_r. Having established these equations Bracegirdle et al integrated the equation with respect to time, thus resulting in an equation to predict the actual displacement, δ:

$$\delta = \int_{t_1}^{t_2} \dot{\delta}_0 . e^{C \Delta^R} . dt \tag{2.9}$$

where t_1 and t_2 are functions of the tide cycle at this particular location. In conclusion they proposed that in the long term, movements of existing landslides can be explained by triggering actions (in this case low tides) with displacements being controlled by rate effects. Therefore they proposed that if a knowledge of the rate effects could be obtained, future predictions of movement were possible. Similar predictions for landslide displacement were made by Skempton et al in 1989 [97] using rate effects on the Mam Tor Landslide in Derbyshire, UK.

Tika in 1991 [98] presented clay on steel ring shear tests and discussed the results implications to displacement piles. She found that after a series of fast stages (simulating pile driving) or after a fast stage preceded by a slow stage (representing loading of a pile before further driving) that the coefficient of friction is highly dependent on the shear rate (penetration rate). When the pile is finally loaded, thus simulating slow shearing, Tika reported that the slow peak strength will be attained and further displacements will result in a drop in strength towards the slow residual value. The magnitude of the slow peak increases with the fast rate of displacement prior to the loading of the pile. Finally she noted that at rates above 110 mm/min results suggested a viscous effect may be occurring as well as a change in the shearing

mechanism.

Fukuoka [99] presented test results from the high speed high stress ring shear apparatus introduced by Sassa et al in 1989 [75] and [76] on a variety of granular soils. This series of tests lead him to conclude that the strength of the granular soils was affected very little by the rate of shearing, however variations in strength did depend on normal stress and shear displacement.

Sassa et al. in 1991 [77] and Sassa in 1992 [78] reported results from the high speed cyclic loading ring shear device on the testing of weathered pumice from the Ontake Landslide site. It was reported that no significant pore water pressure build up occurred in the shear zone on fast shearing. It was postulated that this lack of pressure may result from opposing dilating and contracting mechanisms that are a result of the cyclic loading. However, when the normal stress was decreased and the shearing velocity was increased, pore water pressures rose significantly, thus generating a negative rate effect. Finally Sassa noted that under continued cyclic loading the sample strengths tended to rise above the slow residual strength.

Parathiras [4] reported on two recent studies, firstly, Yagi et al. in 1991 [66]. They conducted ring shear tests in apparatus where pore pressures were measured during shearing. They claimed a boundary rate of 0.35 mm/min exists above which pore water pressures significantly influence soil strength. Yagi et al. [66] were also concerned with the variation of pore water pressure with displacement. They found that excess pore pressures reach a maximum value within the first 80 mm of shearing, these then decrease by up to 80% in the next 80 mm, beyond this point the remaining excess pressure falls slowly until it is only 10% of maximum value. This usually occurs after around 400 mm of shearing, further displacements show that the pressure level remains at this 10% mark.

Secondly, Steenfelt in 1992 [100] presented results from field studies and large shear box tests on a remoulded clay till. He reported that at a rate of 120 $mm/hour$ soil behaviour changed from being elastic to elastoplastic. Below 120 $mm/hour$ he claimed strength increased with a decreasing rate of displacement, whereas above 120 $mm/hour$ strength increased with an increasing rate of displacement. This behaviour is illustrated in Figure 2.26. Moreover Steenfelt made comparisons between load and

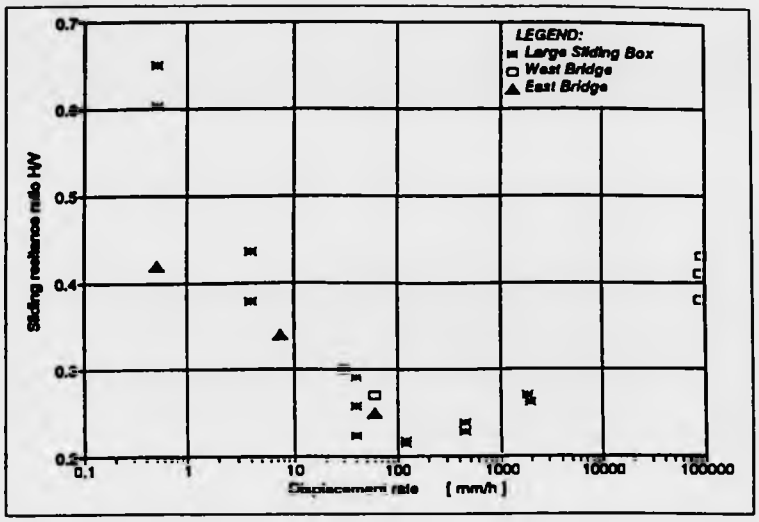

Figure 2.26: Sliding resistance as a function of the rate of displacement, Steenfelt 1992 [100], from Parathiras 1994 [4].

strain controlled tests. He found that although the load controlled tests lead to lower strength values, see Figure 2.27, both tests indicated similar types of rate behaviour.

Sassa and Fukuoka [101] presented a further study entitled *"Measurement of the Internal Friction Angle of Soils during Motion by the High-Speed Ring Shear Apparatus"*. Although the paper was presented in Japanese, it was possible to attain the following information from the abstract. Sassa and Fukuoka noted that the friction angles mobilised during landslide motion would not be the same as the conventional friction angles measured in slow (almost static) shear tests. Using the ring shear apparatus they sheared granular samples at a constant rate in the range 6 mm/min up to 60000 mm/min under both dry and drained conditions. To record the angle of friction they changed the normal stress during continual shearing, a new approach which would appear to shorten testing time. As a result of their studies they found that whilst granular soils were relatively insensitive to rate of shearing, there was a variation of $-3.2°$ to $+3.7°$ from the slow residual value across the above range of shear speeds.

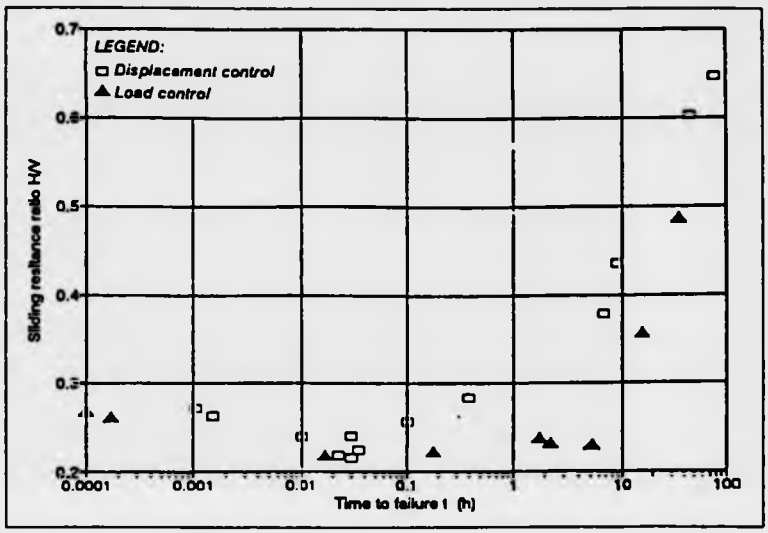

Figure 2.27: Comparison between displacement controlled and load controlled tests, Steenfelt 1992 [100], from Parathiras 1994 [4].

Shoaei and Sassa in 1994 [79], using a cyclic loading high speed ring shear apparatus, presented further results on pumice, loess and Toyoura sand. The aim of this research was to study the shear behaviour of landslides during earthquakes. They came to many conclusions on seismic stress levels and speeds at which landslides would move. It is interesting to note however, that they attributed great importance to pore water pressures, noting that rapid landslides in pumice should occur due to a great build up of pore water pressure. They also noted that the seismic coefficient necessary to cause failure in a drained slope, will be different from that in a saturated one. Many current ideas on negative rate effects are based around the build up of pore water pressures.

The next study to be reviewed is Parathiras, 1994 [4]; this thesis is the most recent and perhaps the most relevant work in relation to the authors research project. Parathiras [4] carried out a range of tests using new modified rings in the IC/NGI [7] type apparatus. He confirmed the presence of positive and negative rate effects, proposed by Lemos in 1991 [95] and also studied the threshold strength and the post threshold strength decrease. Parathiras noted that the post threshold strength decrease is accompanied by an increase in sample height. Therefore he postulated

that the strength decrease is associated with dilation or an increase in porosity in the shear zone. That is, voids will form between the rotating and stationary particles in the zone and an increase in pore water pressure will occur.

Parathiras observed that the behaviour of soils during fast shearing depends on their plasticity, the shape of the shear surface and the presence of water in their environment. He defines the positive rate effect as Type I behaviour. Type I behaviour occurs in plastic soils (where $I_p > 12\%$, $LL > 27\%$ and $CF > 30\%$) which are not submerged in water, whatever the shape of the shear surface is. If such a soil is submerged, a nearly planar surface must develop for Type I behaviour to occur. The maximum fast residual strength occurs at a rate of about 900 mm/min, at rates above this, the strength remains constant around this level. Parathiras observed that fast residual strengths may be 150% to 250% higher than slow residual strengths, but the magnitude of Type I behaviour decreases as normal stress increases. Parathiras defined a negative rate effect as Type II behaviour. He claims Type II behaviour occurs in all non-plastic soils (where $I_p \approx 0\%$ and $5\% < CF < 9\%$) except sands and with plastic soils that have a non-planar undulating shear surface. Type II behaviour in non-plastic soils is attributed to an increase in porosity of the shear zone during fast shearing (this agrees with Lemos [43] and Tika [2]) and that the fall in strength may be 4% to 12% below the slow residual value. Parathiras presented a hypothesis for the generation of Type II behaviour which is covered in Subsection 2.4.6. Parathiras also defined two hybrid types of more unusual behaviour, both of which he attributes to the circumstances involved with ring shear testing. Finally it was noted in Parathiras [4] that reversing the direction of shear did not effect the strength properties of any of the samples.

To conclude this section an excellent summary of all the work completed in the 1980s using the IC/NGI apparatus was provided by Tika et al in 1996 [3]. All the salient points highlighted by Lupini [44], Martins [87], Lemos [43] and Tika [2] are reiterated and all of the test data is presented. Reports were made on the variation of threshold strength, fast peak strength, and slow peak strengths after fast shearing, with respect to rate of shearing and the properties and shear modes of the soils.

With respect to fast residual strengths some new ideas were postulated and some

old ones were restated. They appeared to have abandoned Tika's [2] five types model and have gone with Lemos's [95] definitions of positive, neutral and negative rate behaviour, which they correlated with shear mode, clay fraction, plasticity and granular void ratio, a summary of their boundaries is shown in Table 2.2. Tika et al

Table 2.2: Relationships between shear mode, clay fraction, plasticity index and granular void ratio to type of rate behaviour.

Soil Property	Positive Effect	Negative Effect	Neutral Effect
Shear Mode	Sliding	Turbulent, Transitional or Sliding	Turbulent
Clay Fraction		$3\% < CF < 55\%$	
Plasticity Index		$10\% < I_p < 37\%$	
Granular Void Ratio e_g Natural Soils	$e_g > 2.590$	$0.688 < e_g < 2.590$	$e_g < 0.688$
Granular Void Ratio e_g Residual Soils	$e_g > 5$ (approx)	$1.726 < e_g < 4.640$	$e_g < 1.726$

[3] acknowledged, however, that these properties alone are not sufficient to predict behaviour. They admitted that other factors may be involved including the grading of the granular phase, the shape of the granular particles and the relative sizes of the rotund and plate like particles. As with previous studies Tika et al concluded that positive rate effects can be related to two components, firstly disordering of the shear zone by fast shearing increasing the structural shearing resistance of the soil and viscous effects. They stated that the presence of the viscous component is confirmed by the immediate loss of strength after fast shearing. It could also be argued that as the magnitude of the slow peak after fast shearing rarely attains the levels of the preceding fast residual strength, a second component of resistance such as viscous effects must be in operation as well as the disruption of the shear zone orientation. They also proposed a mechanism for negative rate effects which is covered in Subsection 2.4.6. Finally they postulated that above rates of 1 mm/min a knowledge of rate effects is necessary when studying the kinematics of a potential landslide. Furthermore, in first time landslides, they proposed that the loss in strength from peak to residual usually exceeds the reduction in shear stress owing to geometric changes, therefore if positive

rate effects occur the strength increases as the slide starts to accelerate and would usually decelerate the mass until the slow residual strength is in operation, allowing slow progressive movements until the point of equilibrium is reached. If a negative rate effect occurs it is possible that the slide will gain enough velocity and therefore momentum, to carry it beyond its equilibrium point. In reactivated landslides where residual conditions already exist, positive rate effects mean that extra strength can be mobilised at all displacements and rates. Therefore the mass is likely to be relatively stable, whereas if negative rate effects are operating displacements lead to a fall in strength and the slide accelerates to potentially catastrophic failure.

2.4 Hypotheses Explaining Strength Loss At High Rates

This subject area has provoked much discussion ever since the early research of the 1930s. No general agreement appears to have been made about the mechanisms at work in long run-out landslides. The problems appear to stem from the striving of each paper to postulate the theory which provides a solution to the behaviour of all recorded long run-out slides. In the authors opinion this is not possible, as no two landslides take place under exactly the same conditions and therefore where pore water pressure can account for one slide, mechanical fluidization may well account for another. It is of course also possible to postulate that a combination of two or three of the theories reviewed here may occur in any given landslide event. The author therefore believes that in order to gain further knowledge of these potentially catastrophic events, a wider more open view needs to be taken. A very thorough review of this subject was presented by Tika in 1989 [2] and provides the basis for many of the following reviews.

2.4.1 Lunar And Martian Landslides

In 1973, Howard [102] presented research illustrating the presence of large rock avalanches on the Moon. More recently probes sent to Mars have supplied photo-

graphic evidence of vast landslides [103]. This creates a significant problem for many of the theories postulated on earth, which rely on the presence of a lubricating fluid such as air or water, these are not readily available on the Moon or Mars. As a result of this, Tika [2] reported that theories of *"mud-lubrication"* by Heim in 1932 [104], *"air-fluidization"* by Kent in 1966 [105], *"vapour-fluidization"* by Habib in 1967 [106], 1976 [107], Goguel in 1978 [108] and finally *" entrapped-air cushion"* by Shreve in 1966 [109] and 1968 [110] [111] which all related to large scale rock avalanches, could be discounted. These projects are not closely relevant to this study, so further analysis will not take place. However it is dangerous to conclude that these mechanisms could not have taken place on Earth simply because they could not have taken place on the Moon or Mars, even if they appear to be implausible. Furthermore whilst evidence has been provided by Heim [104], Sharp and Nobles [112] and Kojan and Hutchinson [113] that long run-out landslides have occurred on earth in the absence of water, there is also a large number of theories relating to the generation of pore water pressures. These will be reviewed presently. This section is now divided into categories according to the proposed theories, these include *"Mechanical Fluidization"*, *"Acoustic Fluidization"*, *"Pore Water Pressure owing to Frictional Heating"*, *"Liquefaction"*, *"Thixotropy and Rheological Effects"*, *"Dissociation due to Rock Melting"* , *"Other Pore Water Pressure Effects"* and finally *"Further Potential Mechanisms"*.

2.4.2 Mechanical Fluidization

The term Mechanical Fluidization was introduced in 1978 by McSaveney [114] and all works in this area have been developed from the concepts postulated by Bagnold in 1954 [115] who studied the dispersive grain flow of cohesionless materials. Bagnold conducted tests on gravity free dispersions of large spheres in Newtonian fluids using a rotary viscometer. As a result of his work, Bagnold [115] [116] reasoned that the behaviour of a granular material would vary depending on the rate of shearing. He postulated that at slow rates the shear zone would dilate to facilitate frictional shearing with continuous particle contacts, while at faster rates dilation increases

and particle contacts become brief collisions which transfer momentum and therefore the shear and normal stresses. As a result of the dilation, Bagnold proposed that a significant dispersive pressure, P_{disp}, is exerted between the grains and that this related to the shear stress, T, by the following equation:

$$\frac{T}{P} = \tan \alpha \tag{2.10}$$

where $\tan \alpha$ is the dynamic analogue of the static friction coefficient. Furthermore in the inertial or fast shearing condition he postulated that the diffusion of the momentum from the grain collisions may increase P_{disp} by a factor of two. Therefore this means that when the shearing switches from being continuous frictional contacts to a series of collisions, a significant drop in the angle of resistance is observed. In his tests Bagnold recorded a value of $\tan \alpha = 0.75$ during slow frictional shearing compared with a value of $\tan \alpha = 0.30$ during fast inertial shearing. Finally he applied his test results to the cases of flowing sands and gravels under the effects of gravity.

In 1973 Howard [102] stated that the mechanism behind the lunar avalanches was likely to be that postulated by Bagnold [115]. Howard believed that mechanical fluidization was the only likely mechanism that could account for the low apparent friction angles that must have been in operation.

A fine example of a catastrophic rockfall which had a long run-out distance occurred in Elm, Switzerland in 1881. Heim described the rockfall in 1932 [104], it did not slide, it *"crashed"* and the resulting debris flow travelled down the flat bottom valley and up the slope on the other side. Hsü in 1975 [117] studied Heim's account and concluded the event could be accounted for by the dispersed flow theory postulated by Bagnold [115]. In this paper Hsü [117] also suggested that flowing debris can move down gentle slopes because of the presence of a dense fluid in between the grains, which reduces the effective normal stress and therefore the available frictional resistance, a theory also advanced by Sassa in 1985 [74]. Hsü also claimed that in the Elm rockfall such a fluid could have existed in the form of water saturated mud and compressed air. In the lunar environment dispersion of fine particles between the grain structure was used as an explanation for the observed rock avalanches.

In 1977, Körner [118] developed a rolling model for avalanches, which utilised the concept of mechanical fluidization. Körner postulated that dispersion occurs beyond the critical density at rates of shearing observed in flows. This loose state allows particles to move past each other more easily, resulting in a low shear strength.

As well as introducing the term *"Mechanical Fluidization"*, McSavaney [114] reinforced the idea first introduced by Hsü about the effects of fine particles in the debris flow. McSaveney believed that fine particles not only increased the number of particle collisions, but they also increased the dispersion of the larger fragments, allowing flow to take place more readily with a corresponding loss of strength.

Further papers in support of Mechanical fluidization were reported by Lee and Sassa in 1996 [119], they included Körner from 1980 [120] and 1982 [121] and Davies also in 1982 [122]

Finally despite the evidence that has been produced for the process of mechanical fluidization, Hungr and Morgernstern [90] [71] discounted the theory saying that they could not produce a breakdown in the Coulomb relationship for granular materials. However Tika [2] speculated that they had not used fast enough shearing rates to reach the inertial condition of particle collisions instead of continuous contact friction, which Bagnold [115] specified as the crucial change to allow falls in shear strength.

2.4.3 Acoustic Fluidization

The theory of acoustic fluidization was proposed in 1979 by Melosh [123] and according to Tika [2] was applied to a range of geological processes. The theory assumes that an acoustic wave can be generated in the rock mass. This wave is strong enough to temporarily relieve the normal stress in regions of the debris mass, henceforth allowing sliding to occur in this expanded fluidized region. Melosh postulated that the energy required to create such an acoustic wave could be generated by the initial rockfall down a steep slope, and that when this critical energy is reached the slide literally flows and travels as a fluid.

Similar basal waves were postulated by Kobayashi in 1994 [124], who proposed that the waves would be generated by high velocity motion and trigger mechanical fluidization thus decreasing the shear strength of the sliding zone.

2.4.4 Pore Water Pressure Owing To Frictional Heating

The theory that positive pore water pressures can be established by frictional heating along the shear surface is based on the works of Habib in 1967 [106] and 1975 [107], who proposed that a thermodynamic process could offer an explanation for long run-out landslides. When a landslide event occurs, the energy generated by the moving mass is dissipated along the shear surface resulting in heat. If the slide is large and the velocity is high, enough energy may be available so there could be sufficient heating to cause differential thermal expansion of the soil and water, thus generating increased pore pressures, these reduce the effective stress causing the mass to accelerate. Habib postulated that in some cases there may be sufficient energy for the water to vapourize, which creates a high pressure cushion on which landslide mass rides, a process referred to as *"vapour-fluidization"*

An example of a disastrous high speed landslide event occurred in the Vaiont Valley in Northern Italy in 1963. A large block slid from Mont Toc and crashed into a reservoir creating a wave which over topped the dam and swept down the valley claiming approximately 2000 lives. Romero and Molina in 1974 [125] and Anderson in 1985 [126] studied the kinematic aspects of this catastrophic slide with respect to the effects of water heating and pore pressure increase in the shear zone. Prior to this, Anderson [127] had presented a mechanism which suggested that earthquakes may cause frictional heating and this might be an explanation for many of the large landslides and flows that are triggered by earthquakes.

Voight and Faust in 1982 [128] speculated that vapourization need not occur to trigger rapid landsliding. They believed that an increase in pore pressure would be sufficient in most cases and developed an analytical model which accounted for the strength loss in many rapid landslides. In particular they applied their model to the Vaiont Landslide. However, whilst studying their work, Tika noted several errors and entered into private correspondence with Voight and Faust in 1991, this resulted in a number of corrections being published by Voight and Faust in 1992 [129]. In this paper they also noted that further independent evidence for frictional heating had been provided by a number of authors including Nonveiller [130] and Davis et al [131],

who presented theoretical papers. Another large landslide that may be attributed to frictional heating is the East Abbotsford slide in New Zealand. Voight and Faust [129] reported that Salt et al in 1980 [132], Salt in 1984 [133] and finally Smith and Salt in 1988 [134] all reported frictional heating as a potential mechanism for this rapid failure. In conclusion Voight and Faust made sensible conclusions about the mechanism of the Vaiont Landslide: *" Vaiont was a complex landslide, and surely no single mechanism can account fully for its dynamic processes"*. This view is also held by the author.

2.4.5 The Viability Of Heat Generation

Before a discussion on the likelihood of the heating mechanisms is undertaken, one further theory should be reviewed. In 1979, Erismann [135] proposed the hypothesis of *"dissociation due to rock melting"* which, according to Tika [2], was later supported by Voight and Faust [128]. The title of the hypothesis is self explanatory, Erismann thought that the high concentrations of energy near the shear surface create heat causing the rock to melt and allow the landslide to become *"self-lubricating"*.

Tika [2] produced a strong discussion with respect to frictional heating. She postulated that the main problems associated with these mechanisms is their sensitivity to the input parameters such as angle of friction and normal stress as well as properties of the shear zone like thickness, porosity and compressibility. The problem with the theoretical predictions is that it is virtually impossible to gain information about the state of the shear zone during motion in the field, so precise modelling is difficult. The results of the best methods available all depend on the assumptions made for the controlling parameters. It was also noted by Tika that none of the studies had allowed for the rate dependence of residual strength for the soils involved. If the soils had illustrated negative rate behaviour the energy dissipated by frictional heating would be significantly reduced, thus limiting the potential for pore pressure generation and leading to overestimations of the reduction in effective stress by the frictional heating models. Finally, whilst frictional heating may provide a possible solution for long run-out distances, it does not appear to relate to the triggering mechanism of large landslides which presumably start with slow rates of displacement.

Three differing sets of experimental work also seem to question the validity of this theory. Atakol and Larew conducted simple shear tests on dry sands in 1970 [136]. They conducted tests at rates of shearing up to 1000 cm/sec, under normal stresses of 570 kPa, with thermocouples installed in the apparatus. The sensitivity of the thermocouples was $0.3°C$, but they found no measurable increase in temperature in the soil. Secondly Lemos [43] conducted an IC/NGI ring shear test on a clayey siltstone, which illustrated negative rate behaviour. The tests were conducted at rates of 800 mm/min and 6200 mm/min and under a normal stress of 500 kPa, the maximum temperature increase Lemos observed was $2.5°C$, which is no where near the magnitude required for the generation of pore pressure to account for the negative rate behaviour. Finally Tika [2] conducted additional IC/NGI ring shear tests on a clayey siltstone and a claystone, using a glass interface containing thermocouples. In one case she recorded a temperature increase of $2.4°C$ although most of the increases were less than $1°C$. It is debatable whether temperature measurements made in the laboratory can be directly compared to those predicted from theoretical work based on field observations, owing to the differing scale and thermodynamic conditions, however these tests do illustrate that heat is not readily generated by fast shearing.

2.4.6 Liquefaction

The concept that *"liquefaction"* could be responsible for highly mobile landslides was first introduced by Terzaghi in 1956 [137]. He postulated that if a loose metastable structure occurred in cohesionless or only slightly cohesive soils, it was possible for this structure to collapse and contract resulting in the generation of high positive pore water pressures. This could result in a flow slide as the drop in effective stress leads to a fall in strength well below the slow drained residual angle. It was anticipated by Terzaghi that the slide would then travel until the degree of consolidation approached one and most of the excess pore water pressures had been dissipated.

In 1986, Hutchinson [138] developed a sliding-consolidation model, which he postulated could be applied to flow sides, which had a constant depth of debris sheet. The model assumes an excess pore water pressure in the base of the debris sheet thus allowing the flow to accelerate down the slope. He then stated that the displacement

of the debris could be calculated using consolidation theory if the thickness of the liquefied layer and the coefficient of consolidation for the material were known. Furthermore he postulated that when the slope was in motion, the maximum velocity would be attained when the acceleration was zero and the factor of safety equalled one, beyond this point the slide would then decelerate and come to rest. Finally Hutchinson used his model to predict the run out distance of the colliery tip at Aberfan in South Wales and produced predictions in close agreement with the actual disaster. This appears to be a work of considerable merit and provides very interesting results. However it does have a limitation similar to one for the frictional heating models. It is virtually impossible to know the exact dimensions of the shear zone and therefore, in this case, the depth of the liquefied zone, which if the model is based on consolidation theory and henceforth drainage path distances must have a significant bearing on the results.

A number of other authors have conducted research on the subject of liquefaction and these were reported by Tika [2]. They included Seed [139], Hutchinson and Bhandari [140], Casagrande [141] and Sassa [72]. Seed postulated in 1968 [139] that in many soils, drainage would be too rapid for flow slides with large displacements and high velocities to develop. From field descriptions of flow slides, Seed reported the types of material involved are normally loose to medium dense sandy saturated soils and rain soaked loess.

In 1971, Hutchinson and Bhandari [140] conducted research on the high mobility of mud flows on slopes with lower declines than those corresponding to the limiting equilibrium for residual strength conditions. They noted that these slopes tended to be saturated with the ground water flowing parallel to the direction of the mud flow. They concluded, that the high mobilities were associated with undrained loading of these slopes as material descended from steeper back scarps, thus generating high pore water pressures and a corresponding drop in shear strength below the drained residual level.

In 1975 Casagrande [141] proposed a change in the effective friction characteristics of sand when it is liquefied and flowing. He postulated that this change is due to a change in the soil structure, whilst the sand is flowing each particle is constantly

rotating relative to the other surrounding particles. Casagrande believed that this rotation lead to a loss of frictional resistance and spread through a flow structure as a chain reaction. Lastly he stated that when the flow ceased and the excess water pressures had drained, the soil would attain a static structure slightly denser than the one prior to the flow.

Sassa in 1984 [72] and 1985 [74] conducted tests on glass beads under either constant normal stress or constant volume. In the dry condition he found that the shear strength of the granular material was rate independent and, as was noted by Parathiras [4], Sassa therefore postulated that the *"flow condition"* proposed by Casagrande may not be of use as an explanation for the shear strength decrease observed in debris flows at high velocities. During constant volume tests with a damp condition (moisture content 1%–3%) however, a fall in strength was noted at a rate of 907.6 mm/min. Sassa attributed this to liquefaction of the shear zone when the beads effectively float in the water thus increasing its specific gravity and henceforth causing a decrease in the effective stresses and a corresponding loss of soil strength.

Cruden and Hungr [142] reporting on the Frank Slide in Canada, noted that the rock mass had fallen onto alluvial deposits where the ground water level is at relatively shallow depths. Lee and Sassa proposed that undrained loading was very likely and that this may well have accounted for the distance of run-out.

Tika [2] presented an analogy for undrained loading proposed by Sassa in 1987 [143], [144]. Sassa speculated that the high mobility of the Ontake landslide was due to undrained loading of deposits as the landslide mass spread onto them. According to Tika, he likened this to the hydro-planing phenomena of a car on a wet speed-way. As the car moves along, water flows into the tyre grooves from the front and is drained to the sides, as the cars velocity increases so does the rate at which water enters the tyre. However the drainage rate cannot increase beyond a maximum value and when this is exceeded, a film of water develops between the tyre and the track surface, thus supporting part of the weight of the car. This results in a loss of friction between the tyre and the track.

Parathiras [4] has developed an interesting theory relating to his Type II (negative rate effect) behaviour in plastic soils. He claims that the presence of water and an

undulating shear surface combine in a pumping action that builds up pore water pressure across the shear surface thus reducing the strength. Liquefaction in the shear zone is confirmed by water content tests. He claims that the pumping action (and hence the magnitude of the pore water pressure) is a function of the amplitude of the undulations and that in tests where the amplitudes decreased, the pore water pressures start to dissipate and therefore the shear strengths start to rise. This pumping effect is claimed to reduce strength to a level up to 78% lower than the slow residual strength, where rate of shearing and normal stress have minimal effects on this value. Parathiras postulated that a Type II effect in a plastic soil relates to the morphology of the shear surface, not to any intrinsic properties of the soil.

Sassa et al in 1994 [145] conducted a case study on the Sale landslide in China of 1983. This disaster was used as an example of a large scale long travelling landslide with an initial height of 40 m but a run-out distance of 1 km. Sassa produced results correlating field observations with laboratory results. The distance travelled by this landslide indicated that the mobilised friction angle on the shear surface was much lower than the slow drained strength of the soil. Sassa claimed that the reason for this was that the initial landslide mass slid onto saturated alluvial deposits, thus rapidly increasing the normal stress and therefore generating significant pore water pressures creating a large reduction in effective stress and a corresponding drop in shear resistance. This was confirmed in the laboratory. At drained rates of shearing (0.014 cm/sec) an angle of shearing resistance of 23.5° was recorded. When the rate was increased to 8.8 cm/sec and the normal stress was rapidly increased up to 366 kPa whilst the drainage was shut of, this angle fell to only 5.2°. This case study illustrates one mechanism for the generation of positive pore water pressures and therefore long run-out landslides. However, there are many arguments for the development of such landslides without the presence of water, so Sassa's paper whilst providing a solution to some problems does not provide the complete answer.

Lee and Sassa [119] conducted tests on landslide debris from the Sale and Ontake slides. The alluvial deposits taken from the Sale Landslide tended to be a fine silt and when subjected to undrained testing under an increasing normal load (representing the slide mass moving onto the alluvial deposits) significant pore pressures were gen-

erated. Lee and Sassa reported that their tests closely resembled the field conditions and that the resulting drop in effective normal stress and therefore, the fall in the available angle of friction recorded in the ring shear apparatus, accounted for the run-out distance observed in the Sale Landslide. Nevertheless the Ontake slide did not have its shear surface on alluvial deposits and its soil was a coarse grained volcanic pumice so the first theory could not realistically be applied in this case. However whilst testing the pumice under a constant normal stress Lee and Sassa recorded significant increases in pore water pressure large enough to result in a very low apparent angle of friction, which could account for the displacement of the Ontake slide. They postulated that the positive pore water pressures were generated by grain crushing in the shear zone, leading to negative dilatancy and consolidation due to the constant normal stress. So in conclusion Lee and Sassa have proposed two realistic mechanisms to account for long run-out landslides, both of which rely on the availability of water and henceforth pore water pressure generation.

Finally, a body of evidence which does not support liquefaction of the shear zone as a potential mechanism for loss of strength was gathered by Tika et al in 1996 [3]. They summarised many tests which were aimed at investigating whether or not positive pore pressures could account for negative rate effects. This included direct measurement of pore pressures by means of an instrumented glass interface, measurement of temperatures using thermocouples to see if frictional heating could generate significant pore pressures. They concluded that the measured and calculated pore pressures could at most account for only 28% of the observed loss of strength. They noted that at first sight indirect procedures like carrying out dry tests, or testing with water and noting that the time for strength recovery after fast shearing is close to the consolidation time of the soil, indicated the development of positive pore pressures. Nevertheless they concluded that positive pore pressures were only generated when shearing ceased as a result of contraction of a saturated shear zone of increased porosity. Tika et al [3] speculated that negative rate effects were not due to a reduction in effective stress as a result of positive pore pressures, but were associated with increased porosity and water content in the shear zone.

2.4.7 Thixotropy

According to Tika [2], Freudlich [146] in 1935 used the term *"thixotropy"* as a description of the *"isothermal reversible soil-gel transformation"*. In a thixotropic material the process of softening and stiffening is totally reversible and with particular reference to soils does not involve any changes in water content. Freudlich [146] postulated that this type of behaviour was dependent on repelling and attracting forces between the soil or gel particles.

In the same year Freudlich [147] produced another study focused on a quicksand from Knott end, Fleetwood. This soil exhibited thixotropic behaviour which Freudlich attributed to the presence of 2.1% fine clay, compared with only 0.3% fine clay in the ordinary sand. Freudlich removed all particles smaller than $10\mu m$ from the quicksand and found that this prevented it from behaving thixotropically. However when these fine particles were remixed with the sample the thixotropic behaviour reoccurred.

Freudlich and Jones in 1936 [148] conducted a study of concentrated mineral suspensions with particle sizes in the range $1\mu m$ to $10\mu m$. They studied the sedimentation volume and the dilatant, thixotropic and plastic properties of the sediments. They concluded that the level of independence of the particles (where non adhering particles are totally independent) correlates best with the type of behaviour observed. They believed that independent particles will tend to form dilatant soil structures, where as particles which are not independent but not necessarily plastic always exhibit thixotropic behaviour to some degree. Moreover in plastic sediments, thixotropic behaviour was always observed and tended to be associated with large sedimentation volumes. Finally they proposed that adhesion varied with particle size, above $10\mu m$ adhesion cannot overcome gravitational forces, at around $2\mu m$ to $3\mu m$ adhesion reaches a maximum level, but when particle sizes fall below these levels thermal agitation reduces adhesive forces.

The thixotropic behaviour of a compacted silty clay (LL=38% and PL=24%) was studied by Seed and Chan in 1957 [149] and Mitchell in 1960 [150]. They found that the degree of thixotropy was significant at high degrees of saturation, where as when water contents were lower than the optimum for compaction, little thixotropic

behaviour was observed. Mitchell [150] postulated that thixotropic behaviour is a result of a soil structures response to a change in its external conditions. For example, when a soil is compacted or remoulded a new structure is induced which results from the applied shear forces. When shear ceases, the soil structure is holding an excess of internal energy. This energy is dissipated by water redistribution and small particle movements, resulting in thixotropic phenomena until a new stable soil structure is attained.

Mitchell [150] also reported on the work of Day in 1955 [151] who studied water tension changes in clays with water contents around their liquid limits, before and after stirring by means of a simple tensometer. Day reported that immediately after stirring tension dropped to a minimum value and then slowly returned to a level approaching the tension prior to the disturbance. Tika [2] reported that similar observations had been made by Bishop et al in 1960 [152] after the remoulding of London clay at a constant moisture content. Mitchell [150] proposed that these observations resulted from changes in the levels of *"double layer interaction"* between particles and a decrease in free energy in the sample with time after stirring.

Kerr and Drew in 1968 [153] investigated the behaviour of a so called *"quick clay"* from the USA. The clay was known to be sensitive in the field and was prone to thixotropic flow type behaviour. On stirring or shaking, the clays strength fell to virtually zero, but after being left to stand for 40 minutes, the initial water-saturated strength was recovered. Kerr and Drew proposed that the loss of strength was associated with the collapse of the initial *"card-house"* structure which converted the clay into a virtual fluid. The fact that the strength is recovered when the material is left stationary suggests that the *"card-house"* structure may be reconstructed, but it is difficult to imagine a mechanism which allows this to happen.

Osipov et al [91] studied thixotropic behaviour in association with microstructural changes, as reported in Subsection 2.3.2.

Finally Tika [2] reported two further papers, Ward and Whitmore [154] and Chong et al [155] who both reported on the viscosity of suspensions containing unflocculated spheres and as such have little relevance to this research project.

2.4.8 Further Potential Mechanisms

Casagrande and Wilson [156] conducted constant water content, unconfined compression tests on an undisturbed sandy clay (LL=32% and PL=21%) and two compacted soils one a clayey sand (LL=18% and PL=16%) the other a silty clay (LL=37% and PL=23%). They found the peak strength to be variable with the time taken to load the sample. With a loading time between 10 minutes and 1 day, they found strength was lower with a loading time of 10 minutes. Above 1 day, however, they found strength increased above the level recorded at the 10 minute loading time. Casagrande and Wilson postulated that this rate behaviour may be a result of only partial soil saturation. They thought it probable that the increase in strength was a result of a decreasing void ratio at constant water content, implying that internal consolidation had occurred with the gas in the voids compressing and being absorbed by the water.

A few studies using triaxial apparatus have reported rate effects on peak strengths, these include Bishop et al in 1960 [152] and Richardson in 1961 [157]. Bishop et al found that shear strength decreased with time to failure and reported that the pore pressure parameter A increased with time to failure. However, according to Blight [158], the pore pressure parameter A, for heavily over consolidated clays should increase as time to failure decreases because of a tendency for slow dilation under load.

Richardson [157] conducted tests on a saturated loess (LL=37%, PL=26% and CF=14%), using three different times to failure, 1000 seconds, 11 seconds, and 10 milliseconds. It was reported that the strength increase compared with the 10000 second test was greater in the 11 seconds test than in the 10 milliseconds test. Richardson claimed that this behaviour could have two explanations, firstly because of the change in pore pressure parameter A owing to water migration to or from the shear zone, or secondly due to scatter in his experimental results.

To conclude, a recent study in 1996 from the Disaster Prevention Institute at Kyoto University was presented by Lee and Sassa [119], who conducted tests using an improved version of their high-speed high-stress apparatus capable of undrained testing and pore pressure measurements close to the shear zone. They conducted dry

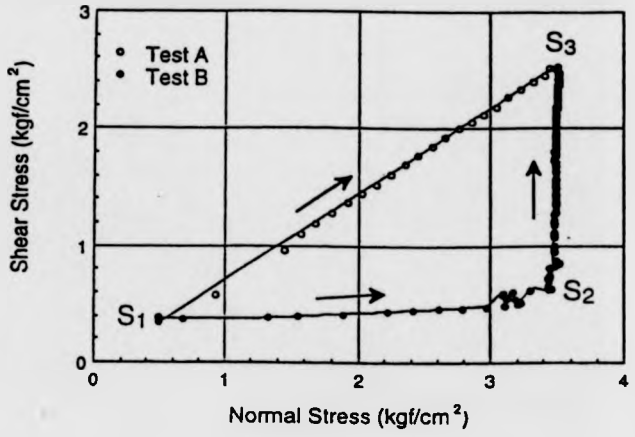

Test A (S1→S3): Shear speed = 1.2 cm/sec
Loading time (S1→S3) = 8 seconds
Test B (S1→S2→S3): Shear speed = 0.01 cm/sec
Loading time (S1→S3) = 7 seconds

Figure 2.28: Test results of the rapid loading ring shear tests on dry sample from Kyoto University campus at two different shearing speeds, from Lee and Sassa 1996 [119].

tests on a granitic sand from the campus of Kyoto University, undrained tests on soils from the Sale Landslide in China (1983) and soils from the Ontake Landslide in Japan (1984). Their testing followed a standard procedure. Initially, drained residual conditions are established at a slow rate of shearing and a constant normal stress. Then fast shearing is commenced and the normal strength is increased quite rapidly giving a stress path similar to those shown in Figure 2.28. Figure 2.28 illustrates how a dry granular soil can produce low mobilised angles of friction, if shearing is not conducted at a high enough rate. In Test A the stress path follows the plastic failure line and this means that the rate of shearing, 720 mm/min, was high enough to allow the displacement required for mobilisation of the full shear strength along the plastic failure line. In this case the angle of friction from the origin to S_1 (the slow residual angle) is almost identical to the angle of friction from the origin to S_3, indicating neutral rate behaviour, a result to be expected after the works of Hungr and Morgernstern [90] [71] and Fukuoka [99] for example. However, the stress path illustrated in Test B appears to represent the behaviour that would be expected

if pore pressures had been generated, even though it is known that this was not possible as the sample was dry. The only significant difference between Tests A and B was the rate of shearing. In Test B the rate was only 6 mm/min whereas in A it was 720 mm/min. Lee and Sassa [119] postulated that this explained the stress path of Test B. In any shear test a certain displacement is required to mobilise the available shear strength, with this in mind they realised that if normal stress was being continuously increased, a boundary shear rate would exist below which the available full shear strength would not be mobilised and therefore the stress path would be below the plastic failure envelope. Lee and Sassa called this behaviour the pre-failure deformation state, in which the available shear stress is lower than the shear strength. In this case the granular material appears to be showing marked negative strength effects, the apparent friction angle from S_2 to the origin is obviously significantly lower than the slow residual angle. As a result of this work, Lee and Sassa carried out an analysis and stated for that particular soil, to ensure the shearing is always on the plastic failure envelope the rate of shear V_s (cm/sec) should not be less than 1.25 times the rate of normal loading V_l $(kgf/cm^2/sec)$. Whilst this offers a potential source of negative rate effect in the laboratory, it is difficult to envisage how such a situation could arise in the field.

2.5 Undulating Shear Surfaces

2.5.1 Introduction

The initial impetus for a study of undulating shear zones was provided by the work of Parathiras [4], who postulated that undulations perpendicular to the direction of shearing could be a mechanism for the generation of negative rate effects, refer to Subsection 2.4.6. It was also noted early in this research that non-planar shear surfaces develop parallel to the direction of shearing in the IC/NGI apparatus and are also quite common in field failure surfaces [159]. As a result of these observations, this section is divided into two, the first part refers to undulations parallel to shear direction, the second refers to undulations perpendicular to shearing direction. Before

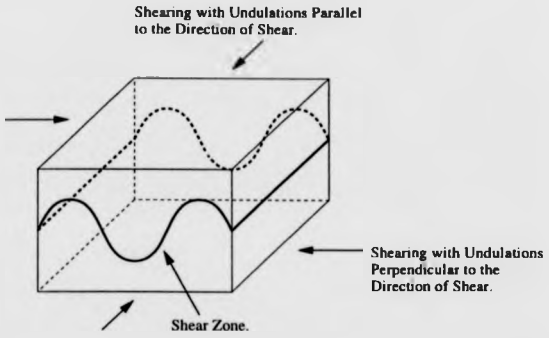

Figure 2.29: Definition of undulation orientation.

commencing this section, it is important to define the meaning of *"parallel to"* and *"perpendicular to"* the direction of shearing, this convention is illustrated in Figure 2.29.

2.5.2 Undulations Parallel To The Shear Direction

It appears that little consideration has been given to the influence of undulating surfaces which are orientated parallel to the shear direction. This would seem quite surprising given that Dounias et al [159] stated that *"When a shear zone or surface is formed in the field, it is usual for it to undulate, with the axes of the undulations parallel to the direction in which it was sheared."* However when it is considered that most of the standard limit equilibrium analyses for Landslides are conducted in two dimensions using a central cross-section and that any undulations would tend to increase the factor of safety, it is perhaps not surprising that very limited research has occurred.

Bromhead in 1992 [160] reported that when significant lateral variations occurred across a failure surface, a series of techniques were available which combined the analysis of a number of two-dimensional cross-sections using a weighted average system to calculate the factor of safety. Bromhead noted that a good example of this technique was provided by Hutchinson in 1969 [161].

Whilst not directly relevant to undulating shear surfaces, Professor Skempton

[5] postulated that the influence of side shear could be allowed for by the use of a reduction factor for the shear stress,

$$\frac{1}{1+\frac{KD}{B}} \tag{2.11}$$

where D and B are the mean depth and width of the slide respectively and K is described as an earth pressure coefficient.

2.5.3 Undulations Perpendicular To Shear Direction

An early and significant contribution was made to the understanding of undulating surfaces by Patton in 1966 [162] [163], who, as part of his work, conducted direct shear tests on inclined shear surfaces and *"sawtooth"* joints. He used plaster of paris casts to make these joints and drew many conclusions in relation to his test results and field observations. With respect to the inclined failure surfaces he speculated that the ratio of shear stress to normal stress could be represented thus,

$$\frac{\tau}{\sigma_n} = \tan(\phi + i). \tag{2.12}$$

Where ϕ is the angle of shearing resistance and i is the angle of inclination of the shear surface. Patton postulated that undulating surfaces in the field may have a sawtooth morphology and this was also noted by Goodman in 1970 [164] and Barton in 1971 [165] and 1974 [166] as reported by Dounias [159]. Patton [162] [163] believed that two modes of failure could occur along a sawtooth joint.

- (i) If the strength of the intact rock mass is very high compared with the strength of the joint or the confining stresses are low, failure may occur with the rock mass dilating significantly with the upper mass moving over the sawtooth joints.
- (ii) If the strength of the rock mass is comparable to the joint strength, shearing of the saw-teeth may occur resulting in a planar failure with little dilatancy.

In the first mode the governing factors will be the strength of the infill in the rock joint and the geometry of the surface, whereas in the second mode the intact rock

strength is the controlling parameter. Dounias [159] reported that a third failure mode had been proposed by Davis and Salt [167] which involved the elastic flattening of the joint undulations.

In 1967 Skempton and Petley [34], investigated the development of shear surfaces under direct shear and found that during the process of shear zone formation undulating surfaces develop perpendicular to shearing direction. They postulated that there are five stages in the formation of a shear surface. Initially shearing involves a *"continuous non-homogeneous strain"*, followed by the development of *"Riedel shears"*. With further displacement the Riedel shears gradually extend into *"displacement shears"*, these then merge together to form an undulating shear surface. Continued shearing leads to the achievement of maximum particle orientation whilst the surface becomes sub-planar, at this stage residual strength is attained. The fact that the surfaces only became sub-planar may be of great importance in the light of recent studies, Parathiras [4] stated that undulations with amplitudes as low as 0.3 *mm* may induce negative rate behaviour.

Morgernstern and Tchalenko [168] produced a similar study in the same year. They conducted drained direct shear tests on identical samples of kaolin prepared from a slurry condition and terminated the tests over a range of displacements. The samples were then impregnated with Carbowax 6000 to allow studies of the microstructure of each sample. Illustrations of a series of tests halted at different stages are shown in Figure 2.30. It can be seen from this illustration that at small displacements after peak strength has been attained, *" displacement discontinuities"* develop close to the edge of the shear box, at angles which significantly deviate from the horizontal. As shearing progresses these discontinuities extend and increase in number until eventually some of the discontinuities at lower angles of inclination link somewhere in the middle of the shear box, creating an undulating failure surface, whilst the other higher angle discontinuities still remain. Morgernstern and Tchalenko postulated that the displacements in the shear box were not large enough to obtain the structure that controls the residual strength and they also noted that high stress concentrations may occur around the perimeter of the shear box, leading to a non-uniform distribution of shear strength.

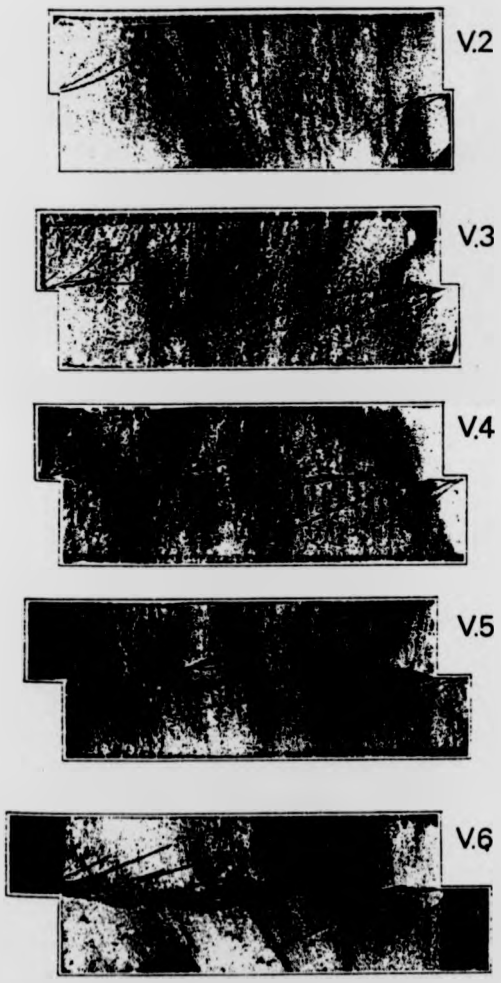

Figure 2.30: Sequence of structures in specimens sheared normal to original fabric. Entire longitudinal sections 1 × 2.35 *in.* Crossed polars. From Morgernstern and Tchalenko 1967 [27].

Whilst undulating shear surfaces usually develop parallel to the direction of shearing, it is possible for shearing to occur in other directions as a result of engineering works. Two examples were reported by Dounias et al [159]. The first occurred in the upper Lias clay foundation of Emphingham Dam and was reported by Bridle et al [169]. The construction of the Dam resulted in perpendicular shearing of undulations initially formed as a result of valley-ward movements including bulging and contouring. A further example was reported by Skempton and Coats [170] at Carsington Dam. The pre-existent shear surfaces developed as a result of solifluction, however the construction of the dam lead to loading in a differing direction to which the surface was formed. According to Skempton and Coats, the thin layer of soliflucted material allowed the undulating shear surface to be seen clearly. Another possiblity for the formation of undulations perpendicular to the direction of shearing was reported by Bromhead in 1992 [160]. He noted that in many tectonically sheared clays, numerous shear zones exist which continuously merge and diverge, resulting in a highly irregular shear zone, containing undulating surfaces and lenticular masses of clay.

Dounias et al [159] produced results of a finite element study of an undulating shear surface in a plastic clay under direct shear. After several trial runs they optimized there model for accuracy and economy to a size of 4.2 m long by 1 m thick. They set the wavelength of the undulations to 0.6 m and varied the thickness and amplitude of the shear zone between 15 mm to 60 mm and 0 mm to 150 mm respectively. As a result of their modelling they concluded that only a small shear zone amplitude was necessary to increase the shear strength to about halfway between that of the shear zone itself and the intact strength of the material outside the shear zone. As amplitudes were increased further the shear strength approached and became assymptotal to the intact strength of the material outside the shear zone. Finally, whilst their study was conducted mainly in terms of peak strength, in some tests they allowed strain softening to occur, resulting in progressive type failures. They anticipated that their results could be used as a guide to the strength of materials which contain non-planar shear zones.

Chapter 3

Apparatus And Methodology

3.1 Introduction

The objectives of this chapter are to provide a description of the apparatus used in the investigation and the testing techniques employed. The main section of testing was performed using the IC/NGI ring shear apparatus, with smaller sections performed on the Bromhead ring shear apparatus and standard oedometer test apparatus. A brief description is also included on the instrumentation of the apparatus and on the techniques utilised to determine particle size distribution and soil classification.

3.2 Imperial College–Norwegian Geotechnical Institute Ring Shear Apparatus

3.2.1 Brief Description

A comprehensive description of the IC/NGI ring shear apparatus was given by Garga in 1970 [42] and Bishop et al in 1971 [7]. The apparatus is illustrated in Figure 2.4 and reviewed in Subsection 2.2.5. The apparatus is a controlled rate of shearing device which ruptures annular soil samples across a plane of relative rotary motion. The soil is confined between upper and lower confining rings which usually have a small gap between them to prevent friction transmission. At the top and bottom of the sample are annular porous plates which have small brass fins projecting from them.

These plates facilitate drainage of the sample and the brass fins prevent slippage of the sample at the soil-plate interface. A constant normal stress is applied to the sample via a loading platen. The desired normal stress level is applied by placing dead weights on the hanger of the lever system which operates with a 10:1 ratio. The lower section of the sample is rotated on a table which is driven by a low ratio (170:1) worm gear. The upper section of the sample is restrained by a torque arm abutting against two tangential load cells which are mounted on separate rigid posts, thus providing the shear force required to rupture the sample.

The main point of interest on the IC/NGI apparatus is its ability to monitor the side friction which is produced between the upper confining rings and the sample. The upper rings are attached to a rigid cross head via a differential screw and a proving ring. The differential screw allows the upper rings to be raised and lowered, thus allowing the operator to control the size of the gap between the two sets of rings. This proving ring allows the measurement of the side friction which develops as a result of opening and closing the rings or as a result of dilation or contraction of a sample during testing. The gross normal force is constant as a result of the load on the hanger. On the other hand the applied normal force varies and is obtained by adding or subtracting the side friction, depending on its direction, to the gross normal force. Provided the proving ring is stiff enough, this system should allow a relatively constant gap to be maintained during shearing.

The IC/NGI apparatus is best suited to testing remoulded samples, although Bishop et al [7] discuss the preparation of undisturbed samples at length. It is therefore generally limited to the measurement of remoulded peak and residual strengths of shear surfaces or zones. The sample has an outer diameter of 152.4 *mm* (6 *in*) and an inner diameter of 101.6 *mm* (4 *in*). In a standard test the sample is initially 19 *mm* deep. In this study many shearing interfaces were used and when using a planar interface the sample was initially 8.5 *mm* deep, where undulating interfaces were used the maximum and minimum depths were 9.5 *mm* and 8.5 *mm* respectively. The sample is enclosed in a perspex water bath, thus allowing the sample to be submerged during all stages of testing.

3.2.2 Modifications To Allow Faster Shearing Rates

To permit a study of soil strength behaviour at faster rates of shearing, it was necessary to upgrade the drive system on the IC/NGI apparatus. The standard top rate of shearing is usually 66 mm/min, however as a result of previous investigations [43] [2], it was felt that a top rate of 1000 mm/min would be required. It was decided to leave the standard motors and drive system in place and install another motor and drive system onto the apparatus, thus allowing a choice of using the apparatus as supplied or using the new system to conduct faster shearing.

A 0.37 kW geared DC motor fitted with a tachogenerator was mounted directly behind the standard control panel. The motor was mounted in line with the worm gear that drives the rotating table. The coupling of the motor to the worm gear requires the standard drive chain to be removed and is performed by a shaft containing two universal joints. These accommodate a difference in height and any misalignment between the new motor and the worm gear.

The electrical signal from the tachogenerator is continuously monitored by the drive system which maintains the motor speed to within 0.2% of its top speed, 417 rpm, even under variable loading. The drive system allows the rate of shearing to be accurately set anywhere in the range 10 mm/min to 1000 mm/min. The drive system also outputs a signal in the range 0 V to 10 V DC which corresponds to 0% to 100% of the top speed. This permits the rate of shearing to be monitored externally. The new control panel associated with this system is conveniently mounted above the original controls. It is a simple unit composed of a display showing the motor speed in rpm, a dial potentiometer which allows accurate setting of the required shearing rate and forward, reverse and stop buttons.

One further option is available on this package. As the motor has sufficient excess torque it is possible to double the top shearing rate to 2000 mm/min by switching to a different gearbox. This has not been used in this study and may not be advisable as it could cause excessive vibration in the apparatus.

3.2.3 Shearing Interfaces With Undulations Perpendicular To The Direction Of Shearing

A significant part of this research has focused upon the influence of non-planar shear surfaces and as a result of this a system was required which would allow the shape of the surface to be controlled. It was decided to conduct tests against a variety of different interfaces, all of which were directly screwed to the confining ring base, whilst the lower confining rings remained in position to aid with the location of the upper rings and the placement of the sample.

Initially two interfaces were manufactured in perspex. Interface 1 was planar and protruded 1 *mm* above the lower confining rings. Interface 2 had an undulating waveform, the base of the waves coinciding with the tops of the lower confining rings. The waves were 1 *mm* high and on this interface there were 4 wave cycles. Illustrations and the exact dimensions of these interfaces can be found in Figures 3.1 and 3.2. After some preliminary testing further interfaces were required. Interfaces 3 and 4 were of a similar format to Interface 2, they featured 2 and 8 wave cycles respectively. These can be observed in Figures 3.3 and 3.4. Interface 5 was identical to Interface 1 except for being manufactured in stainless steel, the objective of this interface was to maintain a planar shear surface in soils where undulations tended to occur in the sample.

The strength developed around the interface will be partially dependent on the surface finish of the interfaces. As a result of this, surface roughness measurements were taken in the direction of shearing using a Taylor-Hobson Form Talysurf profilometer at six points around each interface. This permitted the average surface roughness, R_a, to be calculated for each interface. A summary of each interface is provided in Table 3.1. The objective of the interfaces was to control the shape of the shear surfaces, so that the influence of differing shapes could be investigated. This had two repercussions for the surface of the interfaces. Firstly, all interfaces were of a similar roughness so that any variations in strength could not be attributed to small scale variations in roughness, and, secondly, the surfaces were not rough enough to trap significant quantities of soil particles thus varying the shape of the shear surface.

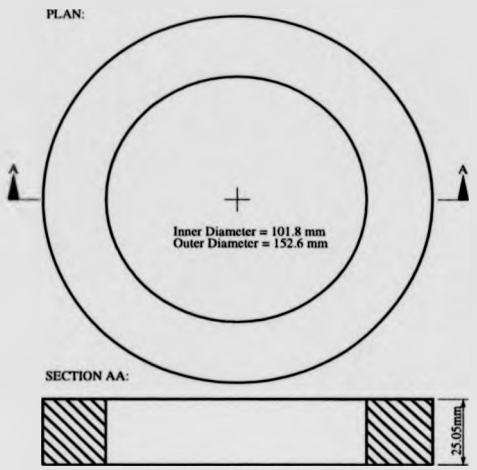

Figure 3.1: Interface 1.

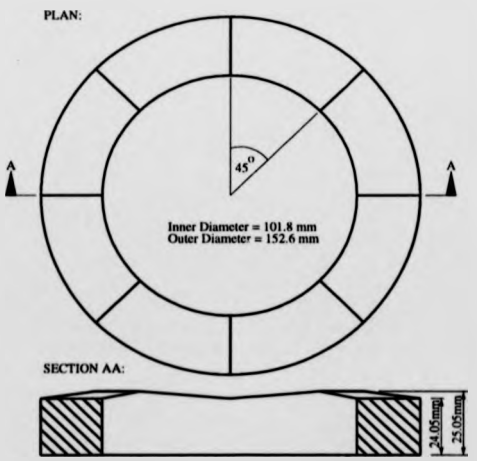

Figure 3.2: Interface 2.

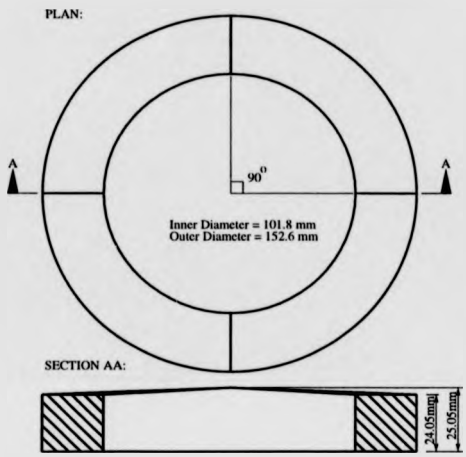

Figure 3.3: Interface 3.

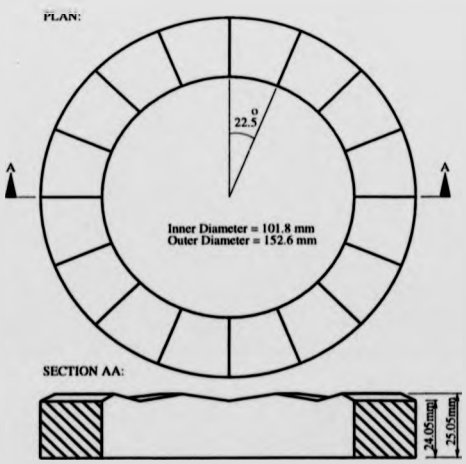

Figure 3.4: Interface 4.

Table 3.1: A summary of the shearing interfaces.

Interface Number	Material	Wave Cycles	Wave Height (mm)	Average Roughness μm
1	Perspex	0	0	0.450
2	Perspex	4	1	0.515
3	Perspex	2	1	0.771
4	Perspex	8	1	1.616
5	Stainless Steel	0	0	0.157

As a result of these requirements all interfaces were machined to approximately the same quality of finish and were then left unroughened.

3.2.4 Modifications To The Interfaces To Accommodate Pore Pressure Transducers

As testing progressed, it became obvious that the ability to measure pore water pressures in the shear zone could be fundamental to the understanding of negative rate effects. So four miniature pore pressure transducers were purchased and fitted into Interface 2. An illustration of the modifications made to Interface 2, to accommodate the pore pressure transducers and their positioning, is supplied in Figure 3.5.

To fit one transducer, a single hole just large enough to slide the transducer into was drilled into the interface. Then a small channel was added to the top of the hole to accommodate an O-ring which sealed the transducer into the surface of the interface. A slot was then machined into the side of the interface to allow the cable to be lead out of the apparatus and a small grub screw was added to hold the transducer firmly in place. Another alteration had to be added to the ring shear apparatus to allow the cables to be lead out. The lower outer ring had four small tapped holes placed in it, these were plugged by small flat screws during standard testing. Also four channels were cut in the alignment ring which slides down over the lower outer confining ring prior to shearing. Finally four grooves were filed into the inside edge of the perspex water bath, without lowering its height, these reduced the risk of friction

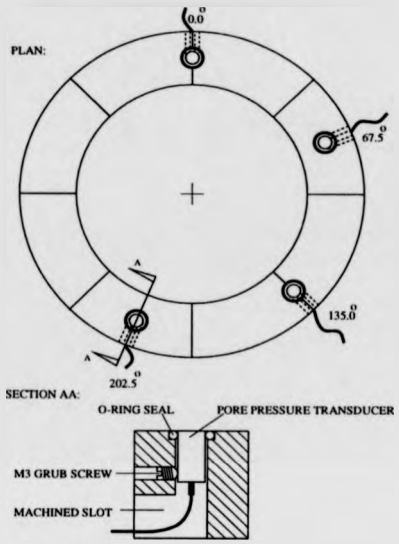

Figure 3.5: Modifications to interface 2 to accommodate pore pressure transducers.

developing between the cables and the upper confining rings.

3.2.5 Instrumentation And Data Acquisition

The testing described in this study involved the measurement of linear and rotational displacements, forces and pore water pressures. All of these were recorded using electronic transducers connected to the data recording unit with the exception of rotational displacements. This allowed the data collection to be fully automated and therefore allowed continuous monitoring to take place.

All linear displacements were measured using Strain Gauge Displacement Transducers (SGDT). These measure the displacement of the spindle using a 350 Ω full strain gauge bridge giving them infinite resolution. The transducers were powered by 10 V (AC or DC) and gave a linear voltage output throughout the 26 mm range of the spindle. The calibration of all seven SGDTs is supplied in Appendix A. Direct measurements of linear displacements were made using the SGDTs at four points on the IC/NGI apparatus. Two were positioned diametrically opposite one another at the points where the upper rings are connected to the side friction proving ring. These

were set to zero once the sample was in place but before any consolidation occurred and therefore when testing commenced provided a direct reading of the gap between the upper and lower confining rings. The other two were also placed opposite one another on top of the torque arm which is connected by four torque pins to the top platen. These were zeroed at the same time as the other pair of SGDTs and provided a direct reading of the movement of the top platen. It should be noted that the displacements recorded by this pair of transducers could not be used to accurately calculate volume changes of the sample, because in addition to recording consolidation and dilation they also recorded the loss of the sample through the gap between the confining rings.

Rotational displacements were measured using the vernier scale mounted on the IC/NGI apparatus. These recordings were taken manually and were then compared to the displacements calculated from the rate of shearing and the time of shearing. This allowed the calibration of both the IC/NGI drive system and the new fast drive system to be monitored. A small discrepancy was expected as the vernier measures shear displacement whereas the calculation provided the displacement of the bottom half of the table which may have included small movements prior to shearing. As the difference was small of the order 1 to 2 mm, the displacements produced in the test results were obtained using rate and time calculations, this allowed the processing of test results to be completely automated.

Forces were recorded at three separate points on the apparatus using proving rings. Two of these rings were mounted on the vertical rigid posts against which the torque arm reacts. These provide measurements of the shear force transmitted through the shear zone and were calibrated in compression only. The third ring was mounted in series between the rigid cross head and the upper confining rings. It provided measurements of the force generated by side friction between the upper confining rings and the sample as described in Subsection 3.2.1 and was calibrated in both tension and compression. Proving rings are designed to function in accordance with Hookes Law, i.e. the relationship between the compression or extension of the ring and the compressive or tensile force acting on it is linear. The three proving rings used on this apparatus were brand new prior to testing and were already calibrated,

the displacement across these proving rings were recorded by the SGDTs described previously. The combination of the calibrations for the rings and the SGDTs is provided in Appendix A and allowed the data logging unit to produce the measured forces in Newtons.

Pore water pressures were measured at four points on the shearing interfaces as shown in Figure 3.5, using miniature pore water pressure transducers. The transducers consisted of a machined silicon diaphragm mounted behind a ceramic porous plate. Semiconductor strain gauges were diffused into the diaphragm in a Wheatstone bridge format. The transducers required a 5 V supply and produced a linear output voltage with increasing pressure. The transducers were delivered with calibration certificates containing the conversion factors in the form $x\ mV/V/bar$. Copies of the calibration certificates are provided in Appendix A. With future testing in mind, two different types of these pore pressure transducers were bought. Two operating in the 3 bar range and two in the 7 bar range, the trade off for the extension of range being a loss of sensitivity. Great care was needed when using the transducers to ensure that they had been de-aerated properly and that a reference pressure was available from the casing of the wires.

All of the electrical signals generated by transducers were converted into displacements, forces and pressures and then recorded on to 3.5 in disks via an Orion Data Logger. The maximum speed at which readings could be taken was 0.1 $s/channel$, this meant that the minimum scan interval was 0.8 s for standard tests and 1.3 s for tests involving pore pressure transducers. Minimum scan intervals were adopted to ensure full data capture, these being 1 s and 2 s for the standard and pore pressure tests respectively. A summary of the signals and channels is provided in Table 3.2.

Table 3.2: A Summary of the signals received and converted by the Orion data logger.

Channel	Type of Transducer	Position of Transducer	Conversion Factor $y(UNITS) = mx + c$ Where $x = signal$ and $y = output$
1	SGDT HS25/7721 in P-Ring 100458/3	Right Shear Proving Ring	$y(N) = 0.648135x$
3	SGDT HS25/7716 in P-Ring 100458/1	Left Shear Proving Ring	$y(N) = 0.656280x$
5	SGDT HS25/7715 in P-Ring 100458/2	Side Friction Proving Ring	$y(N) = 0.631541x$
7	SGDT HLS25/10527	Right Side of Torque Arm	$y(mm) = 0.001886x$
9	SGDT HLS25/10525	Left Side of Torque Arm	$y(mm) = 0.001889x$
11	SGDT HS25/4815	Front of Upper Conf-Rings	$y(mm) = 0.001864x$
13	SGDT HS25/4829	Rear of Upper Conf-Rings	$y(mm) = 0.001846x$
15	New Drive System Speed Output	In New Drive System	$y(mm/min) = 99.31325x$
16	Supply Voltage to Pore-Press Trans	External Supply 5 V	$y(V) = x$
Variable Position	Pore Pressure Transducer 7762	Variable Position	$y(kpa) = 3421.41x + c$
Variable Position	Pore Pressure Transducer 7838	Variable Position	$y(kpa) = 3553.39x + c$
Variable Position	Pore Pressure Transducer 9019	Variable Position	$y(kpa) = 7956.42x + c$
Variable Position	Pore Pressure Transducer 9020	Variable Position	$y(kpa) = 8211.10x + c$

3.2.6 Sample Preparation

All of the soils used in this study were artificial and were available in a powdered format. The Fine Sand, Kaolin and Ball Clay were all dry powders but the Crushed Flint was in a damp condition to minimise the safety hazard from the dust. When only one type of soil was in use, a quantity of the powder was placed in a mechanical mixer with some distilled water. The top of the mixer was then covered with plastic to minimise dust emissions and the sample was mixed until the risk of dust had diminished. Further distilled water was then added until the soil had reached a state just above its plastic limit. Following this, the mixer was left on for an extra two minutes to ensure thorough mixing.

When using mixtures of soils, Ball Clay and Crushed Flint for example, the soils had to be accurately weighed to attain the correct quantities of sand, silt and clay particles. Therefore the powders were oven dried for 24 hours at a temperature between $100°C$ and $110°C$. The dry powders were weighed and the correct proportions were placed in a large plastic bag which was sealed. The powders were then mixed thoroughly by turning the bag, this mixture was placed into the mechanical mixer and the process outlined in the previous paragraph was followed.

Once a soil had been mixed thoroughly to a point just over the plastic limit, it was sealed in plastic for at least 24 hours and left to hydrate. The plastic limit was attained to ensure that the soil could be moulded into the confining rings with out excessive crumbling. It was important that it was not significantly wetter than the plastic limit, this allowed dilatant behaviour during shearing and also reduced the amount of consolidation that took place. The soil was placed in accordance with the method for remoulded samples described by Bishop et al in 1971 [7]. It was compacted into the confining rings by hand, avoiding the entrapment of air whilst trying to achieve an even density, allowing relatively uniform consolidation around the annular sample. Care was taken to prevent the sample from drying.

3.2.7 Testing Techniques

Once the sample had been moulded into the confining rings, the top was levelled using the scraper supplied with the IC/NGI apparatus. This allowed a constant depth of soil to be achieved all the way around the annulus. In stiffer clays, the scraping process was difficult, only very small quantities of clay could be removed each time, otherwise the scraping action tended to open fissures in the sample. Scrapings from the top of the sample were retained for moisture content investigation.

All testing commenced with the first phase of consolidation taking place with 10 kg on the hanger, giving a normal stress of 98 kPa. Immediately before the 10 kg was placed, all proving rings were checked to ensure no stress was being applied to the sample, all data channels were initialised to zero and finally the water bath was filled with distilled water. Consolidation took place for at least 24 hours, until the primary consolidation phase was complete. The majority of testing was conducted with 10 kg on the hanger, but in Tests 1 and 2 a further 10 kg was added to the hanger half way through the tests. Before the extra weight was added all shear stresses were removed from the sample, then, when the extra weight was added the sample was left to consolidate for 24 hours. Testing over consolidated soils was not part of this investigation and therefore no swelling stages occurred. In Test 22 weights were added and removed to and from the hanger during a phase of fast shearing, the aim of this being to study the effects of rapid loading and unloading, this was a non-standard testing procedure.

In preliminary testing, drained rates of shearing were calculated according to Gibson and Henkel [171], this method tended to give relatively fast rates of shearing. As the slow drained residual strength was a benchmark around which much of this work was based, a slow standard rate of shearing, 0.005 mm/min, was adopted in all testing to ensure the integrity of the results. Before shearing commenced the upper rings were raised to create a gap between the two sets of confining rings. In soil on soil tests this gap was approximately 0.3 mm to 0.5 mm and in the interface tests it tended to be between 1.2 mm and 1.4 mm, this prevented a friction build up between the two sets of rings. Raising the upper rings generated a side friction force which

decreased the applied normal stress, therefore the soil was left for at least 1 hour before shearing commenced to allow swelling of the sample to take place.

Before any shearing stage commenced, the base table was rotated until the clearance between the torque arm and the shear force proving rings was minimal. Any difference in this distance was corrected by adjusting the position of the shear force proving rings. If readjustment occurred, the relevant channels were reset to zero. The hardened steel wheels which provide the contact between the shear force proving rings and the torque arm, were mounted slightly off centre. This allowed them to be rotated until they just touched the torque arm without applying any significant shear stress. At this point shearing commenced.

Slow shearing at 0.005 mm/min was conducted at the beginning of every test to establish the remoulded peak strength. In lower plasticity soils this slow stage was generally continued until residual conditions had been established. In higher plasticity soils, because of the large distances required to establish residual strength, the speed up slow down method described by Bishop et al [7] was used. This involved closing the confining rings to prevent soil loss and increasing the rate of shearing to acquire the displacement necessary to attain residual strength. This faster rate of shearing was usually in the range $0.1mm/min$ to 1 mm/min. When this faster shearing was complete the rings were reopened and slow shearing recommenced until a residual value had been obtained.

Fast shearing was conducted at a range of rates from $1mm/min$ to 1000 mm/min. During both slow and fast shearing the gap was maintained at the distances described previously in this section. At fast rates soil loss increased and this had the effect of closing the rings, it was found however that by adjusting the differential screw the gap could be maintained during both slow and fast shearing with limited adverse effects on the test results. A discussion of this and other problems encountered during fast shearing is provided in Section 5.2. One benefit of opening the rings further during a shearing stage was that it provided a check to see if friction had been building up between the upper and lower confining rings. If the recorded strength fell considerably below the previous value over a long period, it was a good indication that friction had been creating a problem.

Finally, the slow shearing stage was conducted at a drained rate of shearing and therefore no pore water pressures were likely to develop which could affect the following stage of shearing. Positive pore pressures may have been generated directly during fast shearing or when the sample attempted to contract when shearing ceased, hence after every stage of fast shearing the sample was left to consolidate for at least 1 hour before the next stage of shearing commenced.

3.2.8 Data Processing

The data placed on to 3.5in disks by the Orion Data Logger needs processing to allow the study of rate effects. The calculations for the average normal stress, average shear stress and the stress ratio, $\tan\phi$, are well documented by Tika [2] and Parathiras [4]. The calculations assume the normal stress to be evenly distributed across the shear surface and an indepth analysis of the errors associated with this assumption was conducted by Bishop et al in 1971 [7]. The average normal stress is found thus:

$$\sigma_n = \frac{W_n}{\pi(r_2^2 - r_1^2)}, \tag{3.1}$$

the average shear stress is given by:

$$\tau = \frac{3M}{2\pi(r_2^3 - r_1^3)}, \tag{3.2}$$

and the stress ratio is found from:

$$\tan\phi = \frac{\tau}{\sigma_n} = \frac{3M(r_1 + r_2)}{2W_n(r_1^2 + r_1 r_2 + r_2^2)}. \tag{3.3}$$

Where,

W_n is the applied normal load on the sample,

M is the torsional moment on the sample,

r_1 is the inner radius which equals 50.8 mm and

r_2 is the outer radius which equals 76.2 mm.

The applied normal load on the sample is calculated from:

$$W_n = 10L + P \pm \Delta W \tag{3.4}$$

and the torsional moment is calculated thus:

$$M = \frac{(F_1 + F_2)}{2} l. \tag{3.5}$$

Where,

L is the load on the IC/NGI apparatus hanger,

P is the weight of the upper loading platen (11 Newtons),

ΔW is the side friction force recorded on Channel 5, see Table 3.2,

F_1 and F_2 are the forces recorded on Channels 1 and 3, see Table 3.2 and

l is the distance between the two shear force proving rings which equal 480 $mm \pm 0.2mm$ according to Tika [2].

Combining Equations 3.3, 3.4 and 3.5 yields:

$$\tan \phi = \frac{\tau}{\sigma_n} = 3.7298 \frac{F_1 + F_2}{10L + P \pm \Delta W}. \tag{3.6}$$

Finally, the relative displacement around the shear surface is given by,

$$\delta = \frac{(r_1 + r_2)}{2} \theta \tag{3.7}$$

or

$$\delta = 1.10828\theta^{\circ}(mm). \tag{3.8}$$

Where,

θ is the angular displacement in radians and

θ° is the angular displacement in degrees.

As soon as preliminary test results were obtained on 3.5in disk it became apparent that it would be necessary to produce some software to rearrange the data and conduct the calculations outlined in Equations 3.1 to 3.8. The first version of this software was produced using Turbo Pascal and was entitled, Convert. The programme read

the data file from the 3.5in disk produced by the Orion data logger, removed all the unwanted text and aligned all the values from channels 1-15 (see Table 3.2) into columns. The data from the channels was also processed to provide columns for the time in minutes, t, average displacement in millimetres, δ, normal stress, σ_n, shear stress, τ, angle of shearing resistance, ϕ, stress ratio, $\tan\phi$, average gap size and finally average settlement of the top platen. The result was exported to a text file. This file was flexible and could be read into spreadsheets or software like Matlab, thus allowing the data to be plotted and analysed. A second version of the programme entitled Convertp became necessary when the extra data from the pore pressure transducers was available on Channels 16-20. This version included these extra channels in the output file and also calculated the average pressure from the four monitoring points. A further development was made with the programme Wavehunt. During testing unusual variations in sample height had been noted during fast shearing, the Wavehunt programme produced results in a separate file showing actual settlements and settlements corrected for soil lost through the gap between the upper and lower rings. All three programmes are listed in full in Appendix B.

To prevent confusion when analysing the data a standard file naming system was adopted. Each shearing stage of a test was treated as a separate unit and given an individual name, t2410b.txt, for example. This is the name of the Orion data logger file for Test 24 with 10kg on the hanger, the b refers to Stage B of the test and the txt indicates that it is a text only file. The output file from the software described previously for this data file would be named, t2410bc.txt, the c standing for converted and finally if a Wavehunt file had been generated this would be named t2410bw.txt. This system proved successful and relatively easy to use.

Once all the data had been manipulated into text columns, it was loaded into Matlab to allow graphical plotting. The main graph produced from the data was a plot of the angle of shearing resistance, ϕ, against linear displacement from the start of the test, also a plot of the consolidation of the sample against the log of time was produced. Both these graphs are produced in Appendix D for every test conducted. It is important to note however that there were many more results which needed to be studied, these included all the settlement and gap size data, side friction and

normal stress data and finally shear stress and shear force data. It was not possible to reproduce all this information owing to the length constraints on this work, but to give an idea of what was available a comprehensive set of results for Test 7, excluding the variable rate investigation at the end of the test, is supplied in Appendix C.

3.2.9 Testing Errors

The IC/NGI apparatus has been in use for over 25 years and it is now generally accepted that it provides accurate measurements of residual strength. However, uncertainties arise as a result of several of the features of the apparatus.

The largest area of uncertainty comes from the assumption that normal stress is uniformly distributed. This assumption is implicit to Equations 3.1 to 3.3 and to all further equations derived from them. A closer analysis of the actual stress distribution reveals a more complicated picture, which, whilst worthy of further research, is beyond the scope of this study given the proven track record of the apparatus. The shear stress is not uniform because of the increasing radius across the annulus of soil. This means that displacements, rates of displacement and shear forces are 50% higher at the outer edge of the sample than at the inner edge. This is accounted for in Equation 3.2. Levels of normal stress tend to fall around the peripheries of the annulus as a result of two causes. One is the loss of soil through the gap between the upper and lower rings. The second is a result of the side friction forces which are exerted on the edges of the sample as a result of raising the upper rings. The opposite effect would be observed if the side friction had a downward action. The problems are increased further by the presence of brass fins which help to hold the sample in place. Bishop et al [7] were aware of these potential sources of error and conducted some investigations into a variety of stress distributions. They concluded that whilst the stress distributions were not uniform, assuming that they were uniform induced only small errors into the test results.

Soil loss through the gaps between the upper and lower confining rings provides a medium through which friction can be transmitted, thus increasing the recorded shear forces. Tika [2] reported that Hvorslev and Kaufman [19], Garga [42] and Lupini [44] estimated this error by considering the width of the edge of the confining rings, thus

yielding an increased apparent area. It was assumed that the normal stress acting across the rings and the extruded soil was equal to the applied normal stress and that the friction coefficient of the soil-steel interface was the same as the coefficient for the soil itself. As with all calculations, the results are dependent on the assumptions employed. In these cases, the assumptions on normal stress and friction are extreme and would result in a worst case estimate. A more realistic and refined approach was utilised by La Gatta [41], who assumed that the normal stress on the extruded soil is provided by the side friction force. Tika [2] presented this analysis in full, but in the majority of testing conducted in the IC/NGI apparatus, the direction of the side friction force is upwards, thus relieving the extruded soil of normal stress according to La Gatta's assumption.

It has been noted previously that there is a tendency for an imbalance in shear loads across the torque arm to occur during testing. With reference to the Bromhead ring shear apparatus, Anayi et al [67] proposed that this may generate friction around the central shaft and cause tilting of the top platen. It is possible for this to occur in the IC/NGI apparatus, especially as provision has been made within the apparatus for tilting of the torque arm. However in a previous report by Taylor and Petley [68] it was noted that even when all the shear force was provided by one proving ring only, there was no significant effect on the recorded ratio. Furthermore many of the designs produced by Sassa [73] [76] [78] have only one rigid post for the torque arm to abut against.

Uneven settlement of the sample may be a result of uneven sample density, soil extrusion, or non-uniform shear stress and it could potentially decrease the applied normal stress on the sample. The clearance around the top loading platen and the upper rings is small, therefore uneven settlement may generate a frictional force between the platen and the upper rings which will relieve some of the applied load. If uneven settlements occur, it is best to regularly check the stress ratio to see if it is falling unexpectedly and to monitor the change in height of the sample for stick-slip patterns.

Assessments of the errors in the measurement of the forces and displacements are provided in conjunction with the calibrations supplied in Appendix A.

3.3 Bromhead Ring Shear Apparatus

3.3.1 Brief Description

Whilst it is widely accepted that the IC/NGI apparatus [7] offers an accurate laboratory method for determining residual shear strength, it has to be acknowledged that the tests are intricate and time consuming. With this in mind, Professor Bromhead designed a more compact ring shear unit, in which tests were easy to conduct and took significantly less time than in the IC/NGI apparatus. The Bromhead apparatus is suitable for use with remoulded samples and can accurately define residual strengths only.

The Bromhead ring shear apparatus was presented in 1979 [63]. It is illustrated in Figure 2.7 and reviewed in Subsection 2.2.7. The sample is confined in the sample container, which holds an annulus of soil with an inner diameter of 70 mm, an outer diameter of 100 mm and has a depth of 5 mm. In the base of the container beneath the sample is a sintered bronze porous plate. The top platen consists of another annular sintered bronze plate mounted on the torque arm assembly, this is located on top of the sample by means of a centring pin. Normal stress is applied to the sample via a dead load lever system operating with a 10:1 ratio. Consolidation and swelling of the sample is recorded by a dial gauge placed on top of the loading yoke. The sample container is surrounded by a perspex water bath which is usually filled to prevent the sample drying out. Shear forces are measured by the torque arm abutting at 90° against two rigidly mounted tangential proving rings, which supply the resistance that shears the sample. The sample container is rotated at a constant rate by a variable speed motor-gearbox combination and the shear stress developed across the shear surface is calculated from the shear forces recorded on the tangential proving rings.

There are three interesting points to note about the Bromhead apparatus. The first, which is its main advantage, is a shorter testing time. This is a result of the shallow depth of the sample, the two way drainage path supplied by the pair of porous plates and the fact that the shear surface forms close to the upper plate. The depth and drainage of the sample allows faster rates of drained shearing and

the proximity of the top plate encourages the development of residual strength at shorter displacements. The second point to note is the position of the shear surface directly beneath the top platen. This has been highlighted as a potential problem by some researchers who have tried to encourage mid-sample shearing in the Bromhead apparatus, see Anayi et al [67], Stark and Vettel [69] and Stark and Eid [70] in Subsection 2.2.9. However providing that the upper plate traps some of the soil particles, which it is likely to do because of its rough surface, the residual strength should not be affected by the presence of the plate. It may have some advantages as it is less likely that non-planar shear surfaces will develop in the Bromhead apparatus in comparison with the IC/NGI apparatus. The third and final point is that side friction forces are not developed or recorded because there is no raising or lowering of rings. Side friction may develop from two sources when soil is extruded between the sample container and the upper plate. One being the contact between the container, the extruded soil and the upper plate, the second being a result of the upper plate sinking into the sample container. During this testing, results suggested that these potential sources of error did not have a significant effect.

3.3.2 Shearing Interfaces With Undulations Parallel To The Direction Of Shear

One of the significant features of the Bromhead ring shear apparatus mentioned in Subsection 3.3.1 becomes a distinct advantage in testing non-planar shear surfaces. As the shear surface is generated adjacent to the top plate, the shape of the shear surface is defined by the shape of the top plate. Therefore five new interfaces were designed which would allow the investigation of the effects of non-planar shear surfaces on the drained residual strength. These are illustrated in Figure 3.6, described in Table 3.3 and are used in place of the plane sintered bronze top plate. Ideally these would have been manufactured in sintered bronze, but to reduce costs and to allow them to be made at the University of Warwick, these new interfaces were machined in perspex. Accompanying the five new interfaces were four scrapers which had the same waveforms on their bases as the interfaces. This allowed the soil to be formed in the

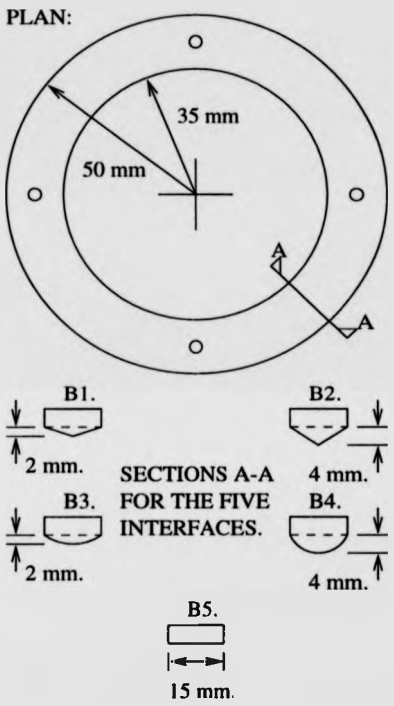

Figure 3.6: The shearing interfaces used in the Bromhead apparatus.

Table 3.3: A summary of the shearing interfaces used in the Bromhead apparatus.

Interface Number	Wave-Form	Wave Height (mm)	Average Roughness μm
B1	V-shape	2	0.054
B2	V-shape	4	0.054
B3	Circular	2	0.049
B4	Circular	4	0.086
B5	Plane	0	0.083

sample container with the wave-form on its top surface ready to receive the interface. This helped to reduce the amount of sample that would be extruded in establishing a wavy shear surface at residual conditions and therefore reduce the potential for side friction to develop. The maximum depth of wave-form on the interfaces is 4 *mm* and in the standard Bromhead sample container this would have severely limited the test as it only gives 1 *mm* of clearance between the lower porous plate and the base of the wave. Henceforth a new sample container was manufactured in brass, which was identical to the standard container except that the sample depth had been increased to 9 *mm*, giving 5 *mm* of clearance. The adverse side effect of this is that it lengthens the drainage path and therefore may increase testing time.

There are two main effects to be considered as a result of using perspex in place of sintered bronze. Firstly, the sample can now only drain in one direction through the planar sintered bronze plate in the base of the sample Therefore the length of the effective drainage path is now doubled, resulting in two variations during testing, the time for full primary consolidation will now be significantly longer and also the rate of shearing may need to be lower to ensure that drained residual conditions are maintained at all times during shearing. The second effect of using perspex in place of sintered bronze, is that virtually no clay particles will be trapped on the perspex interface. This means the recorded residual angle of friction may be different to the actual angle of friction from a standard Bromhead test, as it will represent the friction between the clay and the perspex not the friction within the clay. This is not a problem in this series of tests as all the perspex interfaces are manufactured to the same quality of finish, see Table 3.3, hence the results from all the tests are directly comparable and any variations in the recorded shear strengths will be due to the different wave-forms on the interfaces, not due to small scale differences on the surfaces of the interfaces.

3.3.3 Instrumentation And Data Acquisition

Owing to the shorter time scales involved and the limited data available when using the Bromhead apparatus, all of the readings were taken by hand and placed in a standard table, an example of this from Test WF1 is supplied in Appendix C. The

consolidation, swelling and loss of the soil sample was recorded in millimetres from a dial gauge, on which one division corresponded to 0.002 *mm*. The shear force proving rings contacted the torque arm in the centre of the abutting zone, the distance between the two contact points was always maintained at 152 *mm*, thus allowing one standard set of equations to be used when processing the data. The deflections of both rings was recorded on dial gauges, with the same resolution as the settlement gauge. The gauges and rings had been calibrated together yielding the following calibration factors, on ring 9717A, 1 division = $0.18818N$ and on ring 9717B, 1 division = $0.19120N$. These readings combined with the weight on the hanger provided all the data necessary to calculate shear strengths, normal stress and angles of shearing resistance. Displacement was calculated from the rate of displacement and time, thus involving the same assumptions outlined in Subsection 3.2.5. Regular comparisons were made between actual rotations measured using the dial on the apparatus and the calculated displacement to check that significant discrepancies did not occur.

3.3.4 Sample Preparation

The kaolin used in all five tests was mixed from a dry powder with distilled water until the soil sample was just above the plastic limit. The sample was then sealed in plastic and left to hydrate for a minimum of 24 hours before the first test commenced. A more detailed description of the preparation is supplied in Subsection 3.2.6.

The sample was moulded into the sample container, taking care not to trap air in the sample whilst trying to achieve relatively uniform compaction around the annulus. The sample container was initially overfilled, the excess material was removed using a straight edged bar, thus ensuring a planar level starting surface. When necessary, the appropriate wave-form was scraped into the top of the sample by removing small quantities each time with the scraper and completing 3 or 4 circuits of the annulus before the wave-form was fully developed. The prepared sample was placed on the rotating table of the Bromhead apparatus ready to receive the top plate and torque arm.

3.3.5 Testing Techniques

Before testing commenced the appropriate interface was screwed to the top loading platen and the torque arm. The countersunk screw holes were filled with small quantities of the soil sample. The whole top plate assembly was then weighed so that the exact normal stress could be calculated. The top plate assembly was then gently located on the sample by means of the centring shaft.

Before any shearing took place the sample was consolidated under the lowest normal stress. Before the consolidation was allowed to start the load was supported by a threaded post, this was wound down to commence the consolidation of the sample. A dial gauge was set on top of the loading platen so that the consolidation could be recorded. The water bath surrounding the sample was filled with distilled water and the threaded post was wound down. This was the start of the test and readings were taken at exponential intervals as in the standard oedometer consolidation test, until the sample was fully consolidated.

The shear force proving rings were then carefully aligned, so that they were perpendicular to the torque arm, thus ensuring that the spacing between the two would be 152 *mm*. They were then adjusted so that the distance of torque arm travel before contact was made was minimised. The first stage of shearing involved the establishment of near residual conditions, this was achieved by setting the rate of shearing relatively fast and allowing the sample to be sheared over 4 or 5 revolutions. No readings were taken during this phase of shearing on the shear force proving rings. The shear force was then removed and the sample was left overnight to allow any pore water pressure which may have developed during this fast shearing to dissipate.

The apparatus was set to a slow drained rate of shearing and the shear force proving rings were readjusted as described in the previous paragraph. Slow drained shearing then commenced and readings were taken at intervals of 1 or 2 minutes until the shear strength started to level off towards the residual value. Shearing continued until a stable residual shear strength was attained, usually within a displacement of 6 to 8 *mm*. During this stage readings were taken at intervals of 30 minutes to 1 hour. As soon as shearing stopped the shear stress was removed.

This completed one stage of testing where the residual shear strength was obtained at one level of normal stress. The sample was then consolidated to the next level of normal stress and the slow drained shearing process was repeated. Consolidation of the sample always took place in the absence of shear stress, over-consolidation was not required and therefore no swelling stages occurred.

3.3.6 Data Processing

Because the quantities of data produced by the Bromhead tests were significantly smaller than in the IC/NGI tests, the results were calculated by hand in the standard table provided in Appendix C. The normal stress, shear stress and stress ratio, were calculated using Equations 3.1 to 3.3 respectively. The only modifications being that in the Bromhead apparatus the total normal load is given by,

$$W_n = 10L + P, \tag{3.9}$$

not as stated in Equation 3.4. Where,

L is the load on the Bromhead apparatus hanger and

P is the weight of the interface, top plate and torque arm assembly (variable depending on the interface).

The dimensions of the annular sample are different in the Bromhead ring shear apparatus, therefore Equation 3.6 can not be used. Using the dimensions from the Bromhead apparatus,

r_1 the inner sample diameter, equal to 35 mm,

r_2 the outer sample diameter, equal to 50 mm and

l the distance between the proving rings, equal to 152 mm,

in Equations 3.1 to 3.3 yields,

$$\sigma_n = 2.4491(10L + P), \tag{3.10}$$

where σ_n is in kPa and L and P are in kg,

$$\tau = 0.44185(F_1 + F_2), \tag{3.11}$$

where τ is in kPa and F_1 and F_2 are in Newtons and finally,

$$\tan\phi = \frac{\tau}{\sigma_n} = 1.7699\frac{(F_1 + F_2)}{10L + P}, \tag{3.12}$$

where the units of all the variables must be identical. The relative displacement around the shear surface in the Bromhead apparatus can be calculated using Equation 3.7, or by using the following equation,

$$\delta = 0.7418\theta^{\circ}(mm). \tag{3.13}$$

Where, θ° is the angular displacement in degrees. The difference between Equations 3.8 and 3.13 is again a result of the differing dimensions on the two sets of ring shear apparatus.

When the results have been produced using the above equations, the data was fed onto the computer system, thus allowing the rapid plotting of the graphs in Matlab. Two main types of graph were produced as part of the analysis of the test results, one a plot of shear strength against cumulative displacement the second being plots of shear stress against normal stress. The first plot allowed studies of the attainment and levels of residual strength for the different interfaces, the second plot allowed a study of the variation of the stress ratio and the non-linearity of the failure envelope.

3.3.7 Testing Errors

Many of the uncertainties described in Section 3.2.9 for the IC/NGI apparatus apply equally to the Bromhead Apparatus. The normal and shear stress distributions are again assumed to be uniform. In the Bromhead apparatus, the displacements, rate of displacements and shear forces are 43% larger at the outer radius than at the inner one, thus reducing the variation in shear stress in comparison to the IC/NGI apparatus, but not to an insignificant level. Variations in normal stress are also likely

to be lower because there is no side friction force from the opening or closing of split confining rings, some variation may occur as a result of soil loss around the edge of the annulus. Perhaps a larger influence on shear and normal stress is provided by the settlement of the top platen into the sample. This will have the effect of increasing the shear strength and possibly reducing the normal stress because friction will develop between the vertical edges of the top platen, the extruding soil and the sample container. Quantifying this effect would be difficult and would generally require some broad assumptions regarding the stress patterns in the sample and the extruding soil. However, as a test proceeds and the platen moves lower into the sample container the effect of this friction is going to become more significant.

On the standard Bromhead apparatus it is not possible to measure uneven settlements, yet it has been proposed by Anayi et al [67] that these may occur as a result of uneven loading of the shear force proving rings. They postulated that this could cause undulating shear surfaces and friction around the central guiding pin. Visual checks and test results did not indicate that this was a problem during this series of tests.

3.4 The Oedometer Tests

A series of three Oedometer tests were conducted on kaolin samples. The objective of these tests was to supply data on the coefficient of volume compressibility, m_v, and the coefficient of consolidation, c_v, across a range of normal stresses for remoulded kaolin. At the end of the three tests, average values of m_v and c_v were obtained. This information was later utilised in modelling pore pressures on undulating shear surfaces. The tests were conducted according to BS1377:Part5:1990 Clause 3 [172], however, the British Standard does not provide guidelines on the preparation of remoulded samples, therefore the sample preparation is outlined below.

The kaolin powder was mixed with distilled water to a point just above its plastic limit and was then sealed in plastic to hydrate for at least 24 hours. The consolidation rings were removed from the apparatus and placed on a flat glass plate, after hydrating the kaolin was then carefully moulded into the rings trying to achieve a similar density

in each of the three rings. The samples were levelled with the tops of the rings using a straight edge. Each of the three rings containing the samples was sealed in plastic for a further 24 hours. The aim of this preparation procedure was to simulate the densities achieved when placing the sample in the IC/NGI ring shear apparatus.

3.5 Soil Classification Tests

3.5.1 Moisture Content

All moisture content tests were conducted according to BS1377:Part2:1990 Clause 3 [173].

3.5.2 Index Properties

The liquid limit tests were performed using the cone penetrometer test in accordance with BS1377:Part2:1990 Clause 4 [173]. The plastic limit and the plasticity index were determined in accordance with Clause 5 of the same document.

3.5.3 Particle Size Distribution

The particle size distributions of the fine particle soils, kaolin, ball clay and crushed flint were determined in accordance with BS1377:Part2:1990 Clause 9 [173]. The soils were pre-treated with a dispersant and then wet sieved through a $63\mu m$ sieve, generally only very small quantities were retained on this sieve. The particle size distribution of the soil suspension was then determined using the hydrometer method.

Chapter 4

Summary And Analysis Of Tests Conducted In The IC/NGI Ring Shear Apparatus

4.1 Introduction

The research conducted in the preparation of Chapter 2 revealed a diverse range of studies into rate effects. According to several studies, including Hungr and Morgernstern [71], Fukuoka [99] and Lee and Sassa [119], sands were going to illustrate neutral rate behaviour at the range of shear velocities available in the University of Warwick apparatus and therefore further investigations were not conducted. Another major progressive investigation has been conducted at Kyoto University by Professor Sassa and his team; this work has focused on the development of new ring shear apparatus, seismic loading and negative rate effects caused by undrained loading as a result of rapid increases in normal stress. Such investigations are currently beyond the scope of the IC/NGI apparatus at Warwick University.

The foundations of this research are based on investigations conducted at Imperial College over the past twenty years. These investigations have lead to two schools of thought on the understanding of rate effects. In the first four studies, Lupini [44], Martins [87], Lemos [43] and Tika [2] lead to the conclusion that rate effects were

dependent on soil shear mode, plasticity, grading and more specifically the granular void ratio, e_g. They also developed terminology describing the behaviour associated with fast shearing. Different theories were developed by Parathiras [4] who attributed negative rate behaviour to the morphology of the shear surface, postulating that negative rate effects would be generated by undulations perpendicular to the direction of shear if water was available to the shear zone. Henceforth this research has focused on investigations using artificial soils with controlled gradings with both soil on soil shear zones and artificial shear zones with clearly defined wave-forms running perpendicular to the direction of shearing.

4.2 Summary And Aims Of The Tests

The main body of this research has been split into four phases,

- Phase 1 :- Preliminary Tests
- Phase 2 :- Investigating Waves Running Perpendicular To The Direction Of Shearing
- Phase 3 :- Investigating Mixtures
- Phase 4 :- Strength Recovery With Time

The objectives of Phase 1 (Tests 1, 2, 3 & 4) were to try to establish both positive and negative rate effects, according to the theories enhanced and summarised by Tika [2] and those proposed by Parathiras [4]. The results of this phase of testing were then used to decide which theories would be initially investigated.

Tests 1 and 2 were conducted on two soil mixtures of differing grading which were designed to illustrate positive and negative rate behaviour respectively, according to Tika [2]. Unfortunately, the gradings attained in Tests 1 and 2 were not ideal, this was a result of two factors associated with the early stages of testing. At the time no silt sized particles were available and therefore a fine sand was used in place of silt, secondly it was assumed that the kaolin used in these tests had a high clay fraction ($> 80\%$), subsequent grading tests have revealed the actual clay fraction of the kaolin

dependent on soil shear mode, plasticity, grading and more specifically the granular void ratio, e_g. They also developed terminology describing the behaviour associated with fast shearing. Different theories were developed by Parathiras [4] who attributed negative rate behaviour to the morphology of the shear surface, postulating that negative rate effects would be generated by undulations perpendicular to the direction of shear if water was available to the shear zone. Henceforth this research has focused on investigations using artificial soils with controlled gradings with both soil on soil shear zones and artificial shear zones with clearly defined wave-forms running perpendicular to the direction of shearing.

4.2 Summary And Aims Of The Tests

The main body of this research has been split into four phases,

- Phase 1 :- Preliminary Tests
- Phase 2 :- Investigating Waves Running Perpendicular To The Direction Of Shearing
- Phase 3 :- Investigating Mixtures
- Phase 4 :- Strength Recovery With Time

The objectives of Phase 1 (Tests 1, 2, 3 & 4) were to try to establish both positive and negative rate effects, according to the theories enhanced and summarised by Tika [2] and those proposed by Parathiras [4]. The results of this phase of testing were then used to decide which theories would be initially investigated.

Tests 1 and 2 were conducted on two soil mixtures of differing grading which were designed to illustrate positive and negative rate behaviour respectively, according to Tika [2]. Unfortunately, the gradings attained in Tests 1 and 2 were not ideal, this was a result of two factors associated with the early stages of testing. At the time no silt sized particles were available and therefore a fine sand was used in place of silt, secondly it was assumed that the kaolin used in these tests had a high clay fraction ($> 80\%$), subsequent grading tests have revealed the actual clay fraction of the kaolin

Table 4.1: The artificial soils used in the tests.

Soil Code	Soil Description (Tests Used In)	Clay %	Silt %	Sand %	Liquid Limit %	Plasticity Index %	B.S. Class.
KBS1	60 % Kaolin 40 % Buckland Sand (1)	18	42	40	31	13	CL
KBS2	27 % Kaolin 73 % Buckland Sand (2)	8	19	73	19	6	ML
K	100 % Kaolin (3,4,5,6,7,8,9,11, 12,14,15)	30	70	0	48	18	MI
BC	100 % Ball Clay (10,16,17,18)	80	20	0	62	31	CH
CRF	100 % Crushed Flint (13,23,24,25)	10	80	10	34*	6*	ML*
BCF1	67 % Ball Clay 33 % Crushed Flint (19,20)	57	40	3	44	20	CI
BCF2	33 % Ball Clay 67 % Crushed Flint (21,22)	33	60	7	32	13	CL
* Non-standard results owing to time dependent behaviour of the soil							

to be only 30%. However these tests provided some information on the influence of grading and provided valuable experience to the author in the use of the IC/NGI apparatus. A description of all the artificial soils used in this study is provided in Table 4.1.

Tests 3 and 4 were conducted using plain kaolin against perspex interfaces. Test 3 was conducted against Interface 1 (planar), see Figure 3.1 and Table 3.1. Test 4 was conducted against Interface 2 ($4 \times 1mm$ wave-form), see Figure 3.2 and Table 3.1. According to the theories put forward by Parathiras [4], Test 3 would yield a positive rate effect where as Test 4 would yield a negative one. Such behaviour was observed and, as a result of Phase 1, it was decided that the investigation of undulations was perhaps more significant and therefore further investigations with mixtures were deferred until a suitable artificial silt had been obtained.

The main objective of Phase 2 (Tests 6, 7, 8, 9, 11, 12, 14 & 15) was to investigate further the influence of wave-forms running perpendicular to the direction of shearing. All testing in Phase 1 had been conducted with a full water bath, therefore Test 6 used Interface 2 as in Test 4, however, the water bath was left empty, thus allowing the assessment of the influence of water availability on rate behaviour. Tests 7 and 8 were conducted using Interfaces 3 ($2 \times 1mm$ wave-form) and 4 ($8 \times 1mm$ wave-form) as illustrated in Figures 3.3 and 3.4 and outlined in Table 3.1 respectively. The water bath was full throughout the duration of these tests, whose aims were to show the influence of wavelength on rate behaviour in comparison with Test 4. Two further results of Tests 4, 7 and 8 were, one, it became apparent a critical rate of shearing existed below which negative rate effects appeared not to occur and two, that larger displacements would be needed to ensure that fast residual strengths had been established. Tests 9, 11 and 12 were conducted using Interface 2 ($4 \times 1mm$ wave-form), over larger displacements at a number of different rates in the region of the critical value. This allowed the critical value to be established and also allowed a study of the time taken to attain negative rate effects at speeds above the critical value. Finally, in Phase 2, monitoring of pore water pressures around the surface of Interface 2 was attempted in Tests 14 and 15 using miniature pore pressure transducers. The installation of these transducers is described in Subsection 3.2.4 and illustrated in Figure 3.5. The aim of Tests 14 and 15 was to investigate whether pore pressure reducing the effective normal stress could be a potential mechanism for the loss of shear strength at faster rates. Furthermore the positioning of the transducers allowed pore water pressure to be monitored on both the up slope and down slope sections of the waves as well as on the peaks and in the troughs.

As Phase 2 neared completion, two new artificial soils were attained, a Ball Clay, containing a very high clay fraction and a Crushed Flint, containing a very high silt fraction. A summary of all the artificial soils used is provided in Table 4.1. This allowed Phase 3 (Tests 13, 16, 17, 18, 19, 20, 21, 22, 23, 24 & 25) to commence. The aim of Phase 3 was to study the influence of grading and plasticity on the rate behaviour of soils. A variety of mixtures of Crushed Flint and Ball Clay were used, giving a grading range from 80 % clay, 20 % silt to 10% clay, 80% silt and 10% sand.

As a consequence of the results observed in Phase 2, all the mixtures were subjected to soil on soil testing and testing against a planar stainless steel interface.

Finally Phase 4 (Tests 5 & 10) was conducted as an addition to the main study, mainly to make use of the IC/NGI apparatus during vacation periods. The aim of Phase 4 was to discover whether any shear strength is regained above the slow residual strength if the shear surface is left stationary for extended periods of time. Test 5 involved pure kaolin, subjected to no shear stress throughout a 10 day pause and Test 10 involved Ball Clay, subjected to residual stress throughout a 19 day pause.

4.3 Testing Procedures

4.3.1 Standard Test

The placement and consolidation of the samples in the IC/NGI apparatus are described in Subsection 3.2.7 as are descriptions of the attainment of the remoulded slow peak and slow drained residual strengths using either one slow stage of shearing or the speed up slow down method described by Bishop et al [7]. Subsection 3.2.7 also describes standard procedures for slow and fast stages of testing. Once residual conditions are established in the shear zone, the shear stress is removed from the sample whilst the speed setting is changed to a faster rate, this pause is generally of the order of 10 to 20 minutes. Fast shearing is then conducted over a displacement of at least 100 mm and in some cases over many metres until a fast residual strength is attained. Then follows a pause of at least 1 hour to allow any pore pressures generated as a result of the fast shearing to dissipate. Residual conditions are re-established by a further stage of slow shearing. Residual conditions were always established prior to the commencement of a stage of fast shearing. As stated in Subsection 3.2.7 slow shearing was always performed at a rate of 0.005 mm/min usually over a period of two or three days to ensure that the slow residual strength had been regained. A typical test was likely to include fast stages at rates of 10, 50, 300 and 1000 mm/min interspersed with slow stages at rates of 0.005 mm/min. In some tests other fast rates may have been used if soil loss allowed further testing or if a critical rate was

being searched for. Some non-standard testing procedures also occurred and these are outlined in the following subsections.

4.3.2 Variable Fast Speed Method

It is possible to gain valuable information regarding rate effects by deviating from the standard test procedure, the variable fast speed method is one example of this. Monitoring the time taken for a drop in shear strength owing to fast shearing (a negative rate effect) to recover when fast shearing ceases, may provide information which could help reveal the mechanism involved with rate effects. The variable fast speed method was incorporated into standard tests during some fast stages of shearing. The method was only used in conjunction with the new drive system. If a negative rate effect occurred, in some tests the rate was decreased during fast shearing to the lowest constant rate available. This was achieved by turning the speed control potentiometer by hand at a rapid relatively constant rate. The lowest rate attainable was around 8 mm/min which was not ideal but was a level at which most soils illustrate mainly neutral rate behaviour. This slower shearing was then continued for several minutes until a strength approximating the slow drained residual strength was regained. This procedure would be followed by a true slow stage and the standard test pattern would be followed. When processing the results the rate of shearing was plotted as well as the variation in the effective angle of shearing resistance ϕ', this allowed the rate at which strength started to recover to be attained. An example of this can be seen in Appendix D in Figure D.27.

4.3.3 Variable Normal Stress Method

The majority of testing conducted during this research was performed at one nominal normal stress, 98 kPa. In Test 22 however, a procedure inspired by Professor Sassa's rapid normal loading testing [77] [78] was used as part of a standard test. The sample showed a marked negative rate effect at 1000 mm/min under 98 kPa, and while fast shearing continued another 10 kg was added to the hanger (increasing the normal stress by 98 kPa) until a new fast residual strength was obtained. Further weights

were then added to the hanger until the behaviour became neutral, once this had occurred all of the additional weights were removed so that the sample was again subjected to the nominal normal stress of 98 kPa. Shearing continued until a further fast residual strength occurred. This was the last stage of testing in Test 22.

4.3.4 Strength Recovery Tests

Phase 4 (Tests 5 & 10) involved the investigation of long pauses in movement on shear zones at the residual condition. These tests followed the standard test until residual strength had been developed for the first time. The samples were left stationary for a prolonged period of time either with or without an applied shear stress. When slow shearing recommenced the object of the tests was to see if any increase in the slow residual strength occurred during the long pauses.

4.4 Analysis Of Results

This section presents the results of the testing performed in the IC/NGI ring shear apparatus. The levels of the fast peak, fast residual and slow peak strengths after fast shearing are assessed in comparison with the slow drained residual strength. It should be noted that, owing to the limited rates of data scanning available, the threshold strength has not been recorded. This also presented a problem with the fast peak strengths and thus any data presented on fast peaks is liable to moderate inaccuracies as a result of the sampling interval. However the data available can be studied for trends and patterns but not for accurate values. The data is presented in this chapter in tables and as plots of the ratios of typical strength to slow residual strength against the log of the rate of displacement. Full plots of shear resistance against shear displacement are provided in Appendix D.

4.4.1 Phase 1–Preliminary Tests

Test 1 was conducted on Soil KBS1, a mixture of kaolin and fine sand, as defined in Table 4.1. The sample was placed at a moisture content of 23% and was sub-

merged throughout the test. The shear surface under investigation was formed at the mid-height of the sample. Results from the consolidation and shearing stages are illustrated in Figures D.1 to D.5. The sample was initially compacted under a normal stress of 98 kPa and Figure D.1 illustrates that the consolidation was relatively even around the ring.

Test 1 was the first full test performed in the IC/NGI apparatus at Warwick University and therefore the quality of the results were not as high as they are in later tests. In Test 1, during some of the shearing stages, problems were encountered with the data logger and some data was lost, henceforth the displacement scale in Figures D.1 to D.5 is discontinuous. Also in the test, the periods of slow shearing were conducted over short periods of only 5 hours in some cases. It was subsequently found that this does not provide sufficient displacements to ensure that slow drained residual strengths had been recovered.

An inspection of Table 4.2 and Figure 4.1 reveals that Soil KBS1 in Test 1 illustrated a considerable positive rate effect under normal stresses of 98 kPa and 196 kPa. The fast residual strength was approximately 25% higher than the slow residual strength at a rate of 1000 mm/min. The slight negative rate effect illustrated at 50 mm/min under 98 kPa can be attributed to discrepancies between the average slow residual strength and the actual slow residual strength attained before this particular stage of shearing. The results illustrated in Figure 4.1 suggest that at these relatively low levels of normal stress, the positive rate effect is independent of stress level, it also reveals an apparently smooth continuous relationship between residual strength and rate of shearing.

Owing to the problems outlined previously in this section, the data available on fast peak strengths and slow peak strengths after fast shearing is sketchy. Figure 4.2 reveals that only one fast peak strength was recorded during Test 1. It is almost certain that other fast peaks occurred during the test, but they were not recorded. However at 196 kPa a definite increase in slow peak strength after fast shearing can be observed in Figure 4.3, with slow peak strengths occurring after 300 mm/min and 1000 mm/min shearing. The size of these peaks also increased with rate, until after shearing at 1000 mm/min the slow peak was 5% higher than the slow residual

Table 4.2: A summary of phase 1 tests.

Test No. (Stage)	Soil Code	Interface Number	Normal Stress (kPa)	Slow Res. Angle	Fast Rate mm/min	FP/ SR	FR/ SR	SP/ SR	Notes
1 (B)	KBS1	None	98	23.3	50	0.99	0.94	1.00	1.
(D)					303	1.00	1.13	1.00	2.
(F)					1000	1.00	1.25	1.00	
(H)			196		50	1.00	1.04	1.00	
(J)					303	1.17	1.13	1.03	
(L)					1001	1.00	1.22	1.05	
2 (D)	KBS2	None	98	30.7	50	1.14	0.98	1.00	
(F)					302	1.10	0.96	1.00	
(H)					1000	1.00	1.03	1.00	
(J)			196		50	1.02	0.98	1.00	
(L)					300	1.00	1.01	1.06	
(N)					996	1.00	1.02	1.05	
3 (B)	K	1. Plane	98	9.6	10	1.00	1.21	1.02	
(E)					50	1.00	1.32	1.08	
(G)					303	1.00	1.40	1.09	
(H)					1002	1.61	1.50	-	
4 (B)	K	2. 4x1mm	98	10.8	10	1.00	1.19	1.00	
(D)					50	1.33	1.19	1.04	
(F)					302	1.49	0.80	1.09	
(H)					1000	1.56	0.36	1.10	

Where: SR = Slow Residual Angle, FP = Fast Peak Angle,
FR = Fast Residual Angle and SP = Slow Peak Angle After Fast Shearing.

Notes:
1. Actually illustrated +ve rate effect. FP/SR and FR/SR are less than one because the slow residual angle was averaged across the whole test.
2. Fast Peak Strengths may have been missed owing to slow rate of sampling throughout Tests 1,2 and 3.

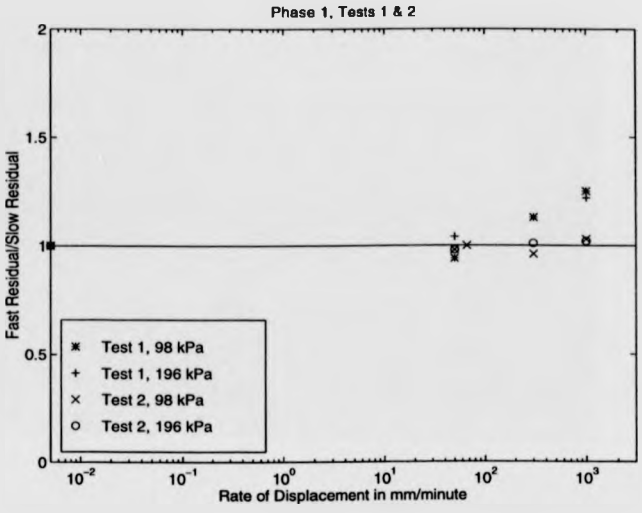

Figure 4.1: Variation of the fast residual strength with rate in phase 1, tests 1 and 2.

strength.

Some further problems were encountered in Test 1, the main one being the change in slow residual strength during the test. Initially the slow residual angle appeared to be 16°, after Stage B (50 mm/min) the slow residual strength increased to a value of 23.3° and remained there throughout the rest of the test. Reasons for this are considered in in Subsection 5.2.3. In addition, friction was encountered as soil was extruded during fast shearing thus helping to close the gap between the upper and lower confining rings. This generates an apparent increase in recorded strengths, which can be alleviated by raising the upper confining rings slightly. A good example of this increase in strength can be seen during Stage B of Test 1 on Figure D.1.

Test 2 was conducted on Soil KBS2 a lower plasticity mixture of kaolin and fine sand in comparison with Test 1, see Table 4.1. The sample was placed at a moisture content of 15% and was always submerged during the test. The shear surface was formed at the mid-height of the sample. Detailed results can be found in Figures D.6 to D.10. The sample was subjected to the same stress conditions as Soil KBS1 in Test 1, again the consolidation around the annulus was relatively uniform.

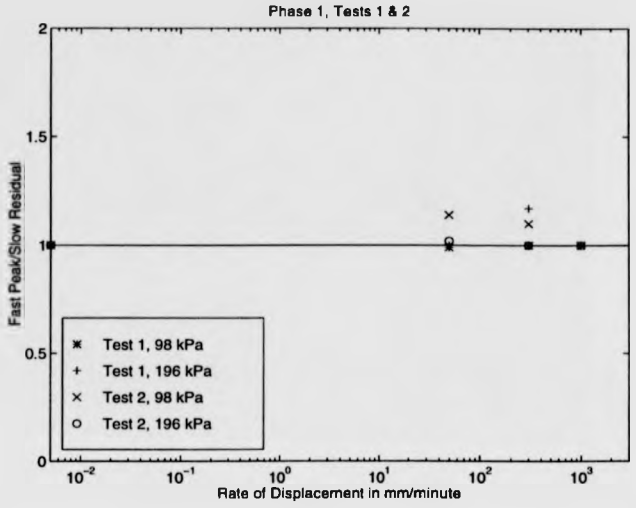

Figure 4.2: Variation of the fast peak strength with rate in phase 1, tests 1 and 2.

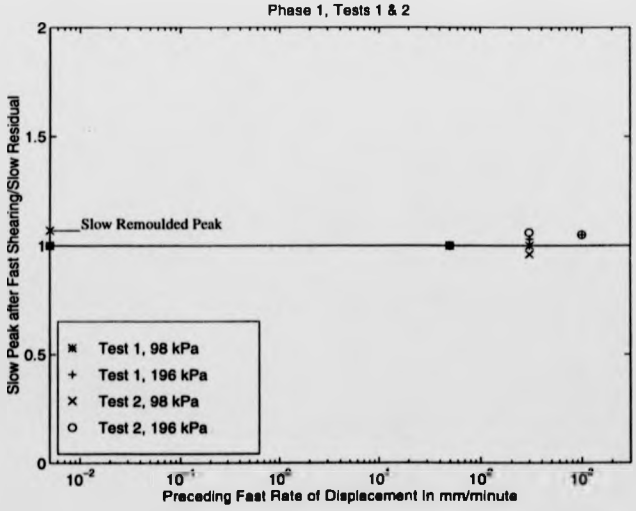

Figure 4.3: Variation of the slow peak strength after fast shearing with rate in phase 1, tests 1 and 2.

Many of the problems associated with inexperience outlined for Test 1 were diminished in Test 2. Slow drained shearing started to take place over longer displacements in Test 2, but the attainment of fast peak strengths and slow peak strengths after fast shearing was still not ideal. Table 4.2 and Figure 4.1 illustrate that Soil KBS2 exhibited predominantly neutral rate behaviour during Test 2. Small variations of the fast residual strength above and below the slow residual strength can be observed at both 98 kPa and 196 kPa, these are never more than $\pm 4\%$ of the slow residual value and as such can be regarded as relatively insignificant.

Fast peak strengths were observed more successfully in Test 2 under 98 kPa than in Test 1, see Figure 4.2. The trend observed was in opposition to current well established knowledge on fast peak strengths [3], which states that the magnitude of the fast peak increases with rate of shearing. At a rate of 50 mm/min a fast peak strength 14% higher than the slow residual strength was observed, at 300 mm/min this had fallen to 10% and at a rate of 1000 mm/min no fast peak was observed, this again may be attributed to the slow rate of data sampling. No fast peaks were observed under a normal stress of 196 kPa.

Slow peak strengths after fast shear were observed in Test 2 and seemed to follow the trend noticed in Test 1, see Figure 4.3. Under 98 kPa no significant slow peaks were noted, however, under 196 kPa slow peak strengths were noticed after shearing at 300 mm/min and 1000 mm/min, these were 5% and 6% higher than the slow residual strength respectively. Fewer problems were encountered during Test 2, although it should be noted that differential settlement of 0.35 mm had occurred by the time the second level of normal stress was applied.

Test 3 was performed on Soil K, pure kaolin, see Table 4.1. The sample was placed at a moisture content of 36% and was submerged for the duration of the test. The shear surface in Test 3 was formed between the sample and Interface 1 (planar), thus encouraging the shear surface to be truly planar. Consolidation and shearing results are provided in Figures D.11 to D.13, these illustrate that consolidation was relatively uniform around the annulus, under a normal stress of 98 kPa. Both Tests 3 and 4 provided quality results with the majority of the problems encountered in Tests 1 and 2 being eliminated, they also provided some interesting results.

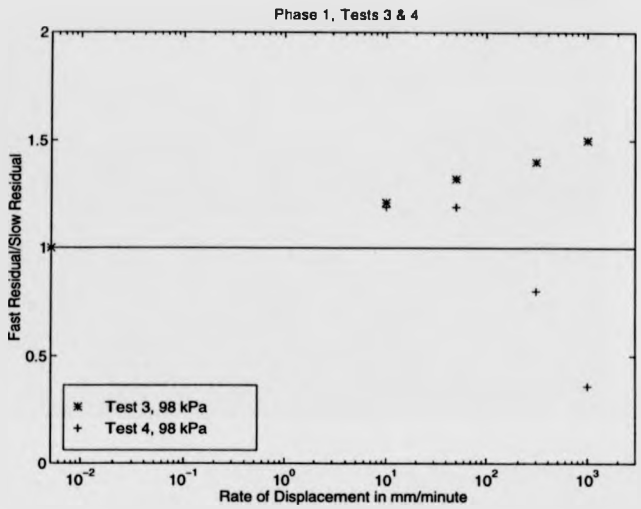

Figure 4.4: Variation of the fast residual strength with rate in phase 1, tests 3 and 4.

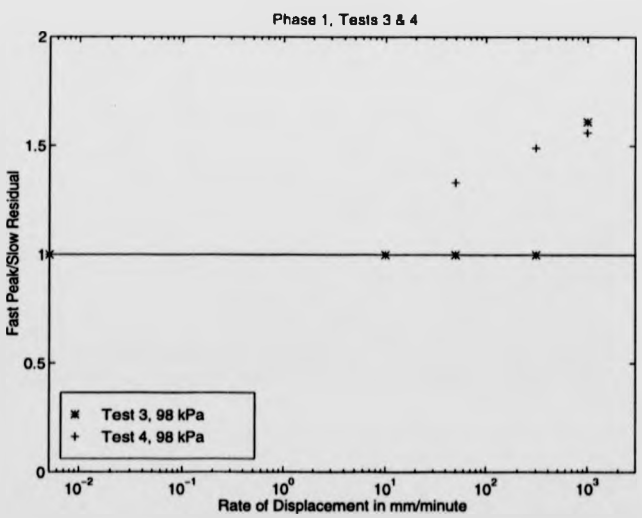

Figure 4.5: Variation of the fast peak strength with rate in phase 1, tests 3 and 4.

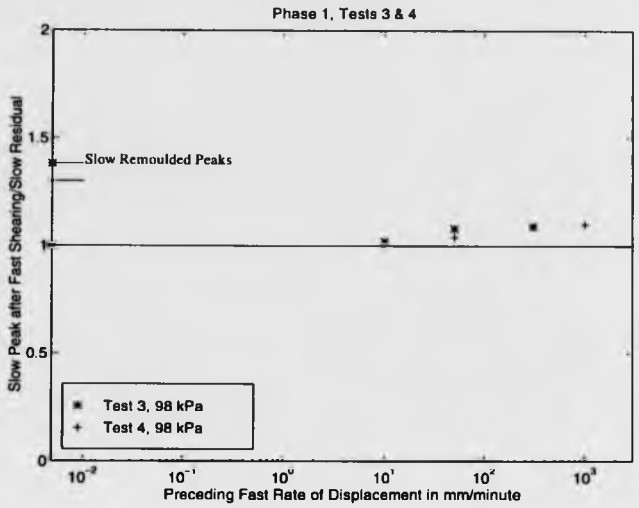

Figure 4.6: Variation of the slow peak strength after fast shearing with rate in phase 1, tests 3 and 4.

A study of Table 4.2 and Figure 4.4 reveals that Test 3 illustrated a distinct positive rate effect with the kaolin against the planar interface. The fast residual strength was 21% higher than the slow residual strength at rates of shearing as low as 10 mm/min, as the fast rate of shearing increased, the fast residual strength increased correspondingly, until at a rate of 1000 mm/min the fast residual strength was 50% higher than the slow residual strength.

Fast peak strengths were not recorded during Test 3 until shearing took place at 1000 mm/min, when a peak was observed 61% higher than the slow residual value. The discontinuous behaviour illustrated on Figure 4.5 suggests that fast peaks may have occurred at lower rates of shearing, but again were missed by the data logging system. Slow peak strengths were successfully observed after all stages of fast shearing, with the exception of Stage H (1000 mm/min) where the test was stopped prematurely because of excess soil loss. A slow peak 2% higher than the slow residual strength was observed after shearing at 10 mm/min and this peak increased to 9% after shearing at 303 mm/min. Whilst these slow peak strengths are significant, they

do not approach the magnitude of the remoulded slow peak strength which is 38% higher than the slow residual strength, thus indicating that the shear zone has not been completely disrupted by the fast shearing.

Test 4 was conducted in an identical fashion to Test 3, the only difference being the interface used. Test 4 involved shearing against Interface 2 which was composed of 4, 1 mm wave-forms. Further results from Test 4 can be found in Figures D.14 to D.16. Table 4.2 illustrates that the undulations of the interface lead to an increase in the average slow residual strength of 1.2° as would be expected. Surprisingly however, a similar effect was not noted in the remoulded slow peaks, in fact the remoulded slow peak in Test 4 was measurably lower than that in Test 3. One problem was encountered during Stage A of Test 4, see Figure D.14, in that friction was generated between the interface peaks and the upper confining rings. This was alleviated by raising the rings to give a gap width of 1.3 mm, however this did encourage soil loss during the test.

Despite the problems encountered in the first stage, Test 4 produced some interesting results. At a rate of 10 mm/min the test appeared to be similar to Test 3, with a fast residual strength 19% higher than the slow residual strength. At 50 mm/min a further increase in strength was not observed, the fast residual strength remained 19% higher. Then at 302 mm/min it decreased to only 80% of the slow residual strength and a study of Figure D.15 suggests that it may still have been falling when Stage F was halted. Moreover, when shearing commenced at 1000 mm/min the fast residual angle fell to less than 5°, 64% lower than the slow residual angle, thus providing evidence that undulations may induce dramatic and potentially catastrophic negative rate effects.

Test 4 produced some excellent results on fast and slow peaks. These did not illustrate any unusual behaviour even though a strong negative rate effect had been observed. A fast peak strength was first observed at a rate of 50 mm/min, 33% higher than the slow residual strength, this peak then increased to a level 56% higher upon shearing at 1000 mm/min. The slow peak strengths after fast shearing illustrated a trend very similar to that observed in Test 3, with the slow peak after fast shearing being 10% higher than the slow residual strength after shearing at 1000 mm/min.

Test 4 concluded the first phase of testing in the IC/NGI apparatus and provided the direction for the next phase of testing, the investigation of undulating shear surfaces.

4.4.2 Phase 2–Investigating Waves Perpendicular To Shear Direction

Test 6 was initially performed on a non-submerged sample of Soil K, pure kaolin, placed in the confining rings at a moisture content of 34%. The soil was consolidated under a normal stress of 98 kPa and the shear surface was then formed between the sample and Interface 2 ($4 \times 1mm$ wave-form). Figures D.19 to D.23 and Table 4.3 provide results from the consolidation and shearing stages. Figure D.19 reveals that problems were encountered during the initial consolidation of the sample. The top loading platen appears to have stuck in the upper confining rings limiting the consolidation. After approximately 1.5 minutes, however, the test operator managed to release the top platen so that full consolidation could be achieved. Further problems occurred during the non-submerged phase of Test 6. The slow residual strength gradually increased during the course of the test until the water bath was flooded. The range of slow residual angles during the non-submerged testing spanned 10.8° and is probably associated with the soil drying out as testing progressed.

Despite these problems, Test 6 provided valuable insights into the negative rate behaviour illustrated in Test 4. Test 6 was identical to Test 4 with the exception that water was not freely available to the sample and, as a result of this, the strong negative rate effect from Test 4 was not observed in Test 6. In fact the sample showed positive rate behaviour at rates from 1 mm/min up to 1000 mm/min, at which point the fast residual strength was 57% higher than the slow residual strength. Figure 4.7 is misleading in this case, the apparent negative rate behaviour shown at rates of 1 mm/min and 10 mm/min is a result of the use of the average slow residual strength, which, because of the wide range of values obtained in this test, is not a close representation of the slow strengths recorded prior to the fast shearing at 1 mm/min and 10 mm/min. Further evidence that water was required to produce negative rate

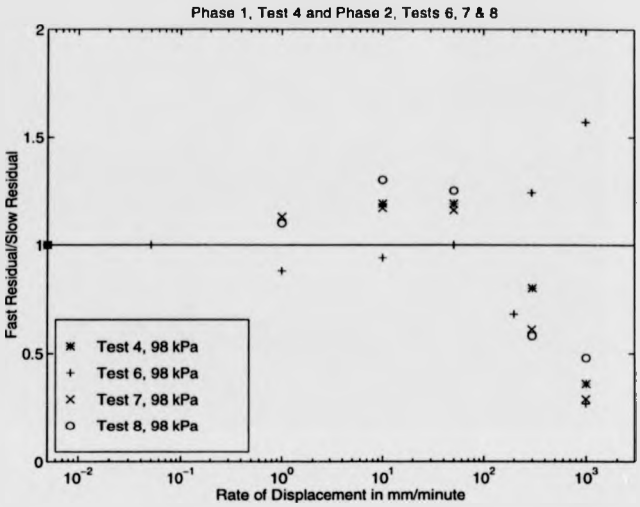

Figure 4.7: Variation of the fast residual strength with rate in phase 1, test 4 and phase 2, tests 6, 7 and 8.

behaviour was provided by flooding the water bath towards the end of the test. Fast shearing performed after the flooding resulted in significant losses of strength, with fast residual strength falling to 68% and 27% of the slow residual strength at rates of 200 mm/min and 989 mm/min respectively. During Stage O (989mm/min, with the sample now submerged) the variable fast speed method described in Subsection 4.3.2 was implemented. This revealed that the strength did not start to recover until the speed fell below a value in the region of 200 mm/min, see Figure D.23. The time taken from when the strength started to recover until the slow residual strength was reattained was approximately 25 seconds. One further point noted during the non-submerged phase of Test 6 was that when positive rate effects occurred, the fast residual strength did not reach a constant value, a good example of this can be seen in Stage J on Figure D.21. The strength appears to fluctuate in a cyclic manner corresponding to the wave-form on the interface, that is, both the length of the strength cycle and the wavelength of Interface 2 are approximately 100 mm.

The fast peak strengths observed in Test 6 also appeared to be a function of the

Table 4.3: A summary of phase 2 tests.

Test No. (Stage)	Soil Code	Interface Number	Normal Stress (kPa)	Slow Res. Angle	Fast Rate mm/min	FP/ SR	FR/ SR	SP/ SR	Notes
6 (D)	K	2. 4x1mm	98	18.5	1	1.00	0.88	0.78	1, 2.
(F)					10	0.91	0.94	1.00	2.
(H)					50	0.95	1.00	1.00	2.
(J)					297	1.00	1.24	1.00	
(L)					990	1.00	1.57	1.41	
(O)				14.6	989-8	1.73	0.27	1.00	3, 4.
(Q)					200	1.15	0.68	-	
7 (B)	K	3. 2x1mm	98	11.2	1	1.00	1.13	1.00	
(D)					10	1.00	1.17	1.01	
(F)					50	1.27	1.16	1.03	
(H)					298	1.54	0.61	1.15	
(J)					988-8	0.96	0.29	1.07	4, 5.
8 (B)	K	4. 8x1mm	98	12.4	1	1.00	1.10	1.00	
(D)					10	1.00	1.30	1.00	
(F)					50	1.37	1.25	1.00	
(H)					300	1.51	0.58	1.04	
(J)					1000	1.11	0.48	-	5, 6.
9 (B)	K	2. 4x1mm	98	11.5	65	1.29	0.87	1.03	
11(B)	K	2. 4x1mm	98	11.4	90	1.30	0.81	1.10	
(D)					150	1.32	0.54	-	6.
12(B)	K	2. 4x1mm	98	11.3	50	1.28	0.98	-	6.
14(D)	K	2. 4x1mm	98	12.9	10	1.00	1.16	1.05	7.
(F)			98		50	1.38	0.24	-	8.
15(C)	K	2. 4x1mm	98	11.3	50	1.15	0.62	1.00	7.
(E)					300	0.85	0.25	-	8.

Where: SR = Slow Residual Angle, FP = Fast Peak Angle,
FR = Fast Residual Angle and SP = Slow Peak Angle after fast shearing.

Notes:

1. The sample was not submerged during Stages A to M.
2. Actually illustrated +ve rate effect. FP/SR and FR/SR are less than one because the slow residual angle was averaged across the whole test.
3. Sample is now submerged.
4. Stage O included the Variable Fast Speed Method described in Subsection 4.3.2.
5. The fast peak may not be accurate due to slow sampling rate.
6. Test halted because of soil loss.
7. Pore pressure transducers installed in interface.
8. Test abandoned pore pressure transducers failed.

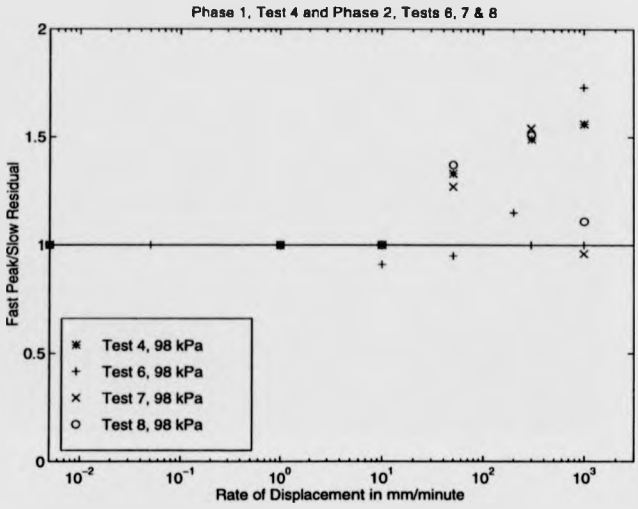

Figure 4.8: Variation of the fast peak strength with rate in phase 1, test 4 and phase 2, tests 6, 7 and 8.

availability of water. A study of Figure 4.8 and Table 4.3 reveals that no fast peaks occurred at rates up to 1000 mm/min when the sample was not submerged. However when the water bath was flooded and shearing commenced at a rate of 989 mm/min a fast peak 73% higher than the slow residual value occurred, then a further stage of shearing at 200 mm/min exhibited a fast peak 15% higher. Slow peaks were not widely observed during Test 6, one however is illustrated on Figure 4.9 which occurred after Stage L (990 mm/min). At this point the sample was still non-submerged and a slow peak after fast shearing was attained at a level 41% higher than the slow residual strength. In conclusion, Test 6 provided useful information regarding the influence of water, however, the results are slightly misleading because of the variation observed in the slow residual strength.

Test 7 was conducted on a submerged sample of pure kaolin, Soil K, which was placed in the confining rings at a moisture content of 34%. The sample was placed against interface 3 ($2 \times 1mm$ wave-form) and consolidated under a normal stress of 98 kPa. Figures D.24 to D.27 and Table 4.3 provide a summary of the consolidation and

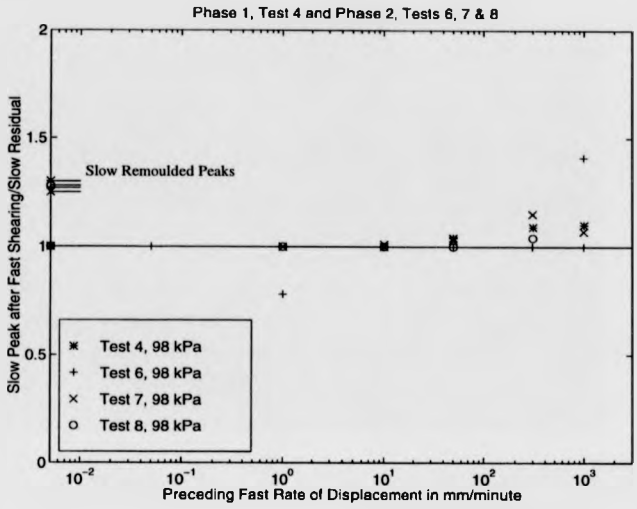

Figure 4.9: Variation of the slow peak strength after fast shearing with rate in phase 1, test 4 and phase 2, tests 6, 7 and 8.

shearing stages of Test 7. Test 7 provided an excellent set of results and no significant problems were encountered during the test. The initial consolidation of the sample resulted in a differential settlement of less than 0.2 *mm* and the first shearing stage established a well defined slow remoulded peak strength and a steady slow residual strength. No significant variations in slow residual strength were observed during Test 7, the range of recorded angles being only 0.8°.

Test 7 was performed in a similar fashion to Test 4, the main difference being the shearing interface whose undulations had double the wavelength in Test 7. The behaviour of the fast residual strength with increasing rate of displacement was also similar to Test 4, see Figure 4.7. The fast residual strength was 13% and 17% higher than the slow residual strength at rates of 1 *mm/min* and 10 *mm/min* respectively. However at 50 *mm/min* a subtle change in behaviour can be observed, the fast residual strength has not increased further, it has fallen slightly below the 10 *mm/min* level to 16% higher than the slow residual value. A change in behaviour can also be observed in Figure D.25, a constant fast residual strength is not attained almost

immediately or after a fast peak as usual. Initially the fast residual strength is higher than that at 10 mm/min, however this falls slowly but steadily over the next minute until a lower fast residual strength is attained. At rates of 298 mm/min and 988 mm/min a strong negative rate effect is observed, similar to that observed in Test 4. At 298 mm/min the fast residual strength was 39% lower than the slow residual strength and at 988 mm/min the fast residual strength was 71% lower. During Stage J (988 mm/min) the variable fast speed method was implemented. In this test strength started to recover at a rate of approximately 150 mm/min, see Figure D.27 and then took a further 42 seconds to recover to the slow residual strength. No significant cyclic variations in strength were observed during Test 7.

During the early stages of Test 7 at rates of 1 mm/min and 10 mm/min no fast peak strengths were recorded. However it can be seen on Figure 4.8 that at 50 mm/min the fast peak was 27% higher than the slow residual strength then at 300 mm/min a further increase to 54% higher was noted. It was expected that another increase in fast peak strength would be observed at a rate of 988 mm/min, yet this did not occur. At 988 mm/min the fast peak strength was recorded as 96% of the slow residual angle. Such behaviour may be attributed to the short time taken for a negative rate effect to occur and therefore the true fast peak may not have been recorded.

Figure 4.9 illustrates that slow peak strengths were recorded after all the stages of fast shearing in Test 7, with the exception of the 1 mm/min stage. Increases of 1%, 3% and 15% above the slow residual strength were observed at rates of 10, 50 and 300 mm/min respectively. A further increase was not observed after shearing at 988 mm/min because the variable speed method was implemented towards the end of this stage. It is interesting to note that none of the slow peaks after fast shearing approach the level of the initial slow remoulded peak strength.

Test 8 was performed on a submerged sample of pure kaolin, Soil K, which was placed in the confining rings at a moisture content of 33%. The sample was then consolidated under a normal stress of 98 kPa against Interface 4 ($8 \times 1mm$ waveform). The results from the consolidation and shearing stages can be seen in Figures D.28 to D.30 and in Table 4.3. Test 8 presented more problems than Test 7, this

was probably a direct result of the increased number of waves and therefore the shorter wavelength, which appeared to promote soil loss through the gap. Stage A in Figure D.28 has a clearly defined slow remoulded peak strength, however, this was followed by a build up of friction which was then released after a displacement of approximately 8 *mm*. This was a result of trying to minimise soil loss by maintaining a smaller gap between the upper and lower confining rings, resulting in the wave peaks protruding into the upper confining rings. The build up of friction rendered the attempt a failure and the gap was enlarged so that the upper confining rings cleared the wave peaks. Further problems were encountered towards the end of the test because soil loss limited the duration of the fast shearing at rates of 300 *mm/min* and 1000 *mm/min*, this made the assessment of the fast residual strength difficult.

Test 8 was designed to be similar to Tests 4 and 7, with the exception of having 8 waves around the shearing interface instead of 2 or 4. The behaviour of the fast residual strength with increasing rate of shearing during Test 8 is shown in Figure 4.7 to follow the same trend as Tests 4 and 7. At rates of 1 *mm/min* and 10 *mm/min* increases in strength of 10% and 30% above the slow residual value were observed respectively. At 50 *mm/min* a positive rate effect was also observed, however, this strength was lower than the preceding one at 25% higher than the slow residual strength. Similar behaviour was observed at this rate to that noted in Test 7, where the fast residual strength appeared to fall slightly during the first 80 *mm* of shearing. Furthermore, a cyclic pattern in strength can be observed during Stage F, see Figure D.29, which appears to have a wavelength of around 50 *mm*, identical to the wavelength of the undulations on the shear surface. At rates of 300 *mm/min* and 1000 *mm/min* strong negative rate behaviour was recorded although the exact levels of the fast residual strength were uncertain. At 300 *mm/min* the fast residual strength appeared to be 58% of the slow residual strength and at 1000 *mm/min* the fast residual strength was approximately 48% of the slow residual strength.

A study of Figure 4.8 reveals that fast peak strengths were recorded during Test 8 and appear to follow the same trend as Test 7. At rates of 1 *mm/min* and 10 *mm/min* no fast peak strengths were observed, at rates of 50 *mm/min* and 300 *mm/min* increases above the slow residual strength of 37% and 51% were observed

respectively. At 1000 mm/min a fast peak strength 11% higher than the slow residual strength was recorded, again uncertainties exist over the accuracy of this value because of the slow sampling rate of the data logger.

Figure 4.9 reveals that no slow peaks were observed after shearing at rates up to and including 50 mm/min. After shearing at 300 mm/min a slow peak 4% higher than the slow residual strength was observed. Unfortunately, as a result of soil loss slow shearing could not be performed after Stage J (1000 mm/min). This test concluded the investigation using the 2 and 8 wave-form interfaces, all further testing during this phase was performed against the 4 wave-form interface.

Tests 9, 11 and 12, were performed on pure kaolin, Soil K, placed in the confining rings against Interface 2 ($4 \times 1mm$ wave-form) at moisture contents of 33%. Each of the three samples was consolidated under a normal stress of 98 kPa. So far Tests 4, 6, 7 and 8 have indicated that the change from positive to negative rate behaviour occurs, when water is available to the sample, at rates between 50 mm/min and 300 mm/min relatively independently of the wavelength. The objectives of Tests 9, 11 and 12 were to establish exactly the rate at which this change from positive to negative occurred, that is, the shear speed at which neutral rate behaviour was observed. Also in previous tests some uncertainties arose because of the limited shear displacement available, therefore these tests involved only one or two stages of fast shearing with much greater shear displacements.

Test 9 included one stage of fast shearing at a rate of 65 mm/min, see Figure D.31, over a displacement approaching 800 mm. This resulted in a negative rate effect after a displacement of around 400 mm, with the fast residual strength appearing to be around 87% of the slow residual strength towards the end of the shear stage. Again a cyclic variation in strength can be observed in Figure D.31 which has a wavelength similar to that of the undulations on the interface. Test 11 included two stages of fast shearing at rates of 90 mm/min and 150 mm/min both over displacements of 450 mm, see Figures D.35 and D.36, these both resulted in negative rate effects. At 90 mm/min the fast residual strength was recorded as 81% of the slow residual value and may have been lower if further displacements had been permitted. Also strong cyclic behaviour was observed with the angle of shearing resistance varying by as much as

2° over a 100 *mm* cycle. At 150 *mm/min* the fast residual strength fell further to only 54% of the slow residual value, this stage illustrated more typical behaviour with no cyclic variations in strength. Test 12 involved only one stage of fast shearing at a rate of 50 *mm/min* over a displacement of 850 *mm*. Figure D.37 illustrates that this stage of shearing produces a virtually identical strength to the slow residual strength at displacements in excess of 450 *mm*. In fact Table 4.3 and Figure 4.10 shows that the fast residual strength at 50 *mm/min* is 2% lower than the slow residual strength, with such a small discrepancy it is reasonable to conclude that over large displacements ($> 400mm$) 50 *mm/min* is the boundary between positive and negative rate effects for Soil K against a $4 \times 1mm$ wave-form interface. Figure 4.10 illustrates the excellent relationship between fast residual strength and rate of displacement obtained from Tests 9, 11 and 12. It can be seen that the fast residual strength falls linearly as the log of the rate of displacement increases. These tests cast doubt on the accuracy of previous testing at 50 *mm/min* because of the displacements required to establish true fast residual conditions. However at slower rates positive rate behaviour was observed where no sign of a slow decrease in strength was observed, therefore these results are regarded as accurate. At rates above approximately 100 *mm/min* fast residual strengths are attained relatively quickly and therefore results obtained at rates around 300 *mm/min* and 1000 *mm/min* should also be regarded as accurate.

Tests 9, 11 and 12 also provided an excellent set of results for fast peak strengths, these are illustrated in Figure 4.11. At a rate of 50 *mm/min* a fast peak 28% higher than the slow residual strength was observed during Test 12. The fast peak strength then increased linearly with the log of the rate of shearing until it was 32% higher than the slow residual strength at a rate of 150 *mm/min* in Test 11. Extrapolating this relationship backwards suggests that the onset of fast peaks would occur at rates lower than 0.1 *mm/min*. Previous testing has revealed that no fast peaks were observed at rates at or below $10mm/min$, so it cannot be assumed that the relationship is linear across a wide range of shearing rates.

Further investigation of slow peak strengths after fast shearing was not the objective of Tests 9, 11 and 12 and therefore a period of slow shearing was not always performed at the end of each test. However, Figure 4.12 illustrates that slow peaks

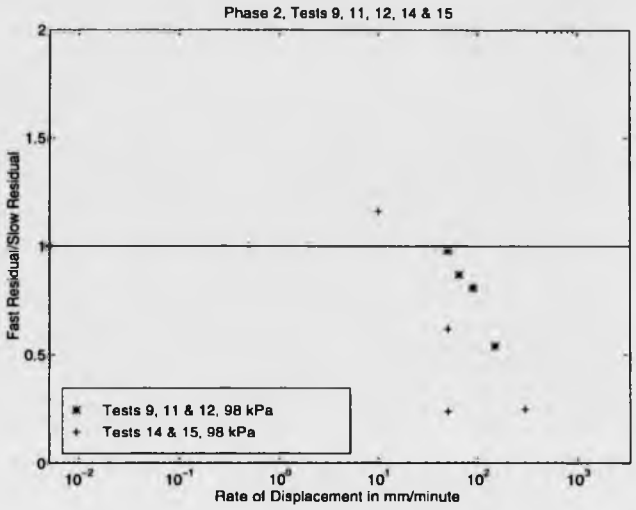

Figure 4.10: Variation of the fast residual strength with rate in phase 2, tests 9, 11, 12, 14 and 15.

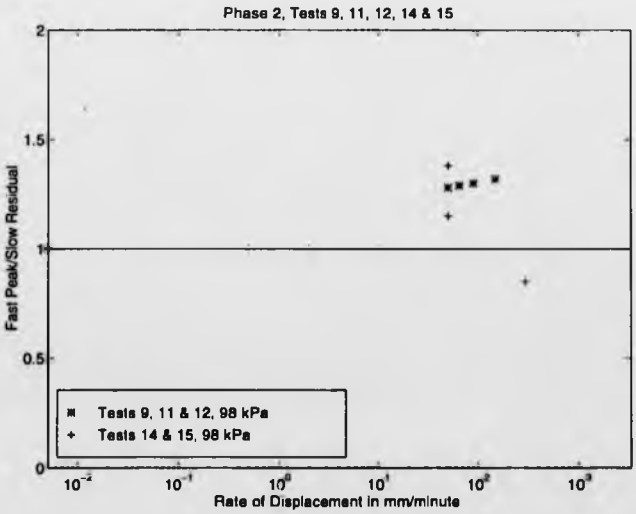

Figure 4.11: Variation of the fast peak strength with rate in phase 2, tests 9, 11, 12, 14 and 15.

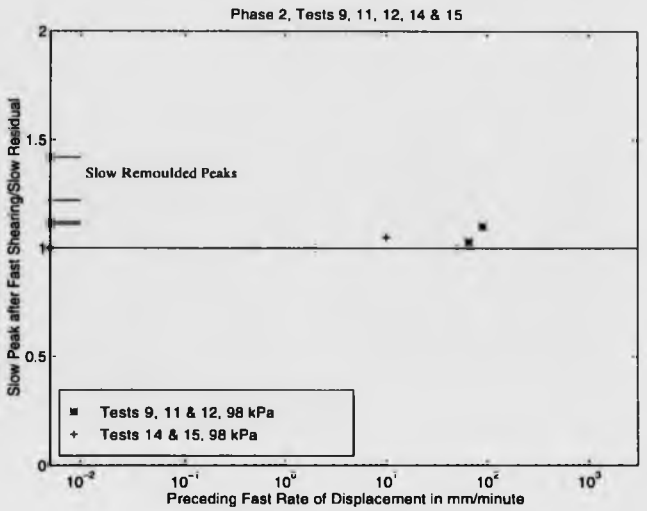

Figure 4.12: Variation of the slow peak strength after fast shearing with rate in phase 2, tests 9, 11, 12, 14 and 15.

were observed after shearing at rates of 65 mm/min and 90 mm/min and that the trend was an increase in slow peak strength with increasing preceding rate of shearing. After shearing at 65 mm/min and 90 mm/min slow peaks 3% and 10% higher than the slow residual strength were recorded respectively.

Tests 14 and 15 were designed to monitor pore water pressures around the interface during slow and fast shearing. The tests were performed on pure kaolin, Soil K, placed against modified Interface 2 ($4 \times 1mm$ wave-form), see Figure 3.5, at a moisture content of 33%. Both samples were initially consolidated under a normal stress of 98 kPa and this process was used to check that all four pore pressure transducers were functioning correctly.

Test 14 involved two phases of fast shearing at rates of 10 mm/min and 50 mm/min, further testing was not performed because of the pore pressure transducers malfunctioning. Test results for the consolidation and shearing stages are illustrated in Figures D.40 to D.43. It can be seen in Figure D.40 that the initial consolidation of the sample was quite uneven across the ring, with a difference of 0.5 mm in

height recorded around the top of the annulus. This may also be reflected in the recorded pore pressures which initially varied around the annulus between 65 kPa and 130 kPa. When consolidation was complete however all the transducers read approximately zero.

The first phase of fast shearing was performed at a rate of 10 mm/min, this yielded a positive rate effect with the fast residual strength being 16% higher than the slow residual strength, see Figure 4.10 and Table 4.3. A study of the pore pressures during this stage, see Figure D.42 reveal that at the wave peak and wave trough the pore pressures remained close to zero. On the up slope, a positive pore pressure was recorded which fluctuated continuously during shearing with an average value of approximately 25 kPa and on the down slope a negative pore water pressure was recorded. The negative pressure fluctuated less and had an approximate value of -80 kPa. Assuming similar behaviour was occurring on all the wave-forms this yielded a net negative pore pressure of approximately -20 kPa. It is tempting to conclude that this net negative pore pressure has generated a positive rate effect by increasing the effective normal stress, particularly as the plot of average pore pressure with displacement appears to mirror the plot of angle versus displacement. This may not be the case as the previous slow stage of shearing reveals that an offset error appears to have developed with the downslope pressure transducer, so that at the end of the slow drained stage and the beginning of the 10 mm/min shearing the transducer is already recording pressures of -35 kPa. Correcting for this error returns the average pore pressure during the 10 mm/min shear to approximately zero. The fact that the angle is mirrored by the average pore pressure should not, however, be disregarded.

At a rate of 50 mm/min unusual behaviour was observed, during the first 75 mm of shearing a positive rate effect was observed, then suddenly a dramatic decrease in strength was observed until at the end of the shearing stage the fast strength had fallen to only 24% of the slow residual value, see Figure 4.10. Unfortunately the offset error on the downslope pressure transducer had increased by this stage so that when the fast shearing commenced at a rate of 50 mm/min this transducer was already reading -55 kPa. When shearing commenced the peak and upslope pressure transducers dipped to give negative readings of the order of -40 kPa, the transducer on the downslope

gave a reading of -125 kPa and the one in the trough showed little change from 0 kPa. As shearing progressed, the up slope and peak transducers started reading positive pressures which continually fluctuated but averaged around a value of 25 kPa for the rest of the stage. The transducer in the trough illustrated very little change from zero throughout the rest of the stage and unfortunately just before the dramatic drop in strength the transducer on the downslope stopped functioning and gave a constant reading of -55 kPa. This again resulted in an average pressure of zero, however the true pressures on the downslope were unknown. Prior to the transducer malfunction, the angle again appeared to mirror the recorded angle, suggesting that variation in effective stress may account for the rate behaviour. It is possible to expand the results and suggest that the pressure on the downslope transducer was increasing and would have given a positive pore pressure if it had continued to function. This would account for the drop in strength, but it is pure speculation as the true pressure is unknown. Test 14 was terminated at this point because of the malfunction in the pore pressure transducer.

Test 15 also involved two phases of fast shearing at rates of 50 mm/min and 300 mm/min. Results for the consolidation and shearing stages including pore pressure measurements are provided in Figures D.44 to D.46 and Table 4.3. The initial consolidation of the sample was problematic. The top annular platen became stuck in the upper confining rings when the normal stress was applied, thus preventing consolidation. The marked spikes on the graphs in Figure D.44 are a result of unjamming the platen, by raising it above the sample and then relowering it. Once this procedure was complete consolidation occurred as usual. All the pore pressure transducers were functioning and recording no pore water pressures when primary consolidation was complete.

During the first stage of fast shearing at 50 mm/min a marked negative rate effect occurred, with the fast residual strength falling to only 62% of the slow residual strength, this is illustrated on Figure 4.7. As soon as shearing commenced, negative pore pressures of the order of -20 kPa were recorded on the peak and down slope transducers, though no variations occurred on the other two transducers. From this point on, three of the transducers produced constant signals around 0 kPa, with

no fluctuation suggesting that they were no longer working. The only transducer generating a signal was the one located at the peak of a wave, during the 50 mm/min this recorded positive pore pressure throughout varying between 0 kPa and 65 kPa with the average value being of the order of 25 kPa. The next stage of fast shearing at 300 mm/min illustrated an even bigger loss of strength, where the fast residual angle was only 24% of the slow residual angle. During this stage only the one transducer was working. This recorded a negative pressure of -70 kPa initially and as the fast residual strength was attained a positive pressure which varied between 30 kPa and 100 kPa with an average of approximately 50 kPa. Just on the end of this stage a dramatic increase in pore pressure can be observed, this is associated with the contraction of the shear zone once rapid shearing has stopped. This was only recorded because shearing was stopped momentarily before the data logger. Before Test 15 was abandoned, a further 10 kg was added to the hanger and the pore pressure transducer readings were monitored, no increases were recorded by three of the four transducers, thus proving that they were not working.

The observation of slow peak strengths after fast shearing was not the objective of Tests 14 and 15, therefore slow shearing was not performed after every fast stage. One slow peak was recorded, however, during Test 14 after shearing at 10 mm/min, the magnitude of the peak was 5% higher than the slow residual strength. No changes in pore pressure were noted in association with this slow peak.

Fast peak strengths were noted in both Tests 14 and 15. In Test 14 no peak was recorded at a rate of 10 mm/min, at 50 mm/min a fast peak 38% higher than the slow residual value was recorded this is illustrated on Figure 4.11. Also associated with this peak are significant decreases in pore water pressure on three of the four pore pressure transducers, see Figure D.43. In Test 15 at a rate of 50 mm/min a fast peak 15% higher than the slow residual strength was recorded and again this was accompanied by negative pore pressure measurements, this time on two of the four pressure transducers. At a rate of 300 mm/min it appears that the instrumentation has again missed the true fast peak, a value of 85% of the slow residual strength being recorded. By this stage only one of the pore pressure transducers was functioning in Test 15, but this one recorded a negative pore water pressure of -70 kPa in associ-

ation with this peak, see Figure D.46. Tests 14 and 15 have provided some useful results with regards to pore pressures during testing. They have, however, proved temperamental and difficult to install and use, it may be difficult to draw significant conclusions from the results obtained.

4.4.3 Phase 3–Investigating Mixtures

The analysis of Phase 3 testing will be divided into two parts, the first part will consider the soil on soil shearing of the mixtures, Tests 13, 16, 17, 19, 21 and 23, the second part will consider the tests performed with mixtures against the planar stainless steel interface (No. 5), Tests 18, 20, 22 and 24. Both parts of the analysis will be performed in order of increasing silt content. The water bath was flooded during all the testing performed as part of Phase 3.

Test 16 was performed on pure ball clay, Soil BC, which was placed in the confining rings at a moisture content of 34%. The sample was then consolidated under a normal stress of 98 kPa. Details of the consolidation and shearing phase can be found in Figures D.47 to D.50 and also in Table 4.4. A study of these results illustrates that fairly erratic behaviour was illustrated during the early stages of this test, after stage F, the results become less unusual. Test 16 did reveal some unexpected results at faster rates of shearing; with such a high clay content, current knowledge suggested a strong positive rate effect would occur. However, a negative rate effect was observed with an unstable fast residual strength, a behaviour which had not been observed previously in this research.

The variation of the fast residual strength with rate of shearing for Test 16 is illustrated in Figure 4.13. It shows that a strong positive rate effect occurs at rates up to 50 mm/min, at which point the fast residual strength is 78% higher than the slow residual strength. At rates of 1 mm/min and 10 mm/min, Figure D.48 shows that no stable fast strength was attained and therefore the values given in Table 4.4 are an estimate of the average value. At a rate of 300 mm/min a change in behaviour was noted, initially the fast residual strength appeared to attain a similar level to that at 50 mm/min, however, after a displacement of 300 mm the strength started to fall steadily. Unfortunately this stage was stopped before a stable lower strength was

Table 4.4: A summary of phase 3 tests.

Test No. (Stage)	Soil Code	Interface Number	Normal Stress (kPa)	Slow Res. Angle	Fast Rate mm/min	FP/ SR	FR/ SR	SP/ SR	Notes
13(B)	CRF	None	98	36.6	10	1.08	1.04	1.00	
(D)					50	1.12	1.04	-	1.
16(D)	BC	None	98	18.2	1	1.00	1.24	1.03	
(F)					10	1.00	1.48	1.12	
(H)					50	1.00	1.78	1.13	
(J)					300	1.00	1.30	1.05	
(L)					1000	1.59	0.38	-	
17(C)	BC	None	98	18.4	300	1.54	0.98	1.10	
(E)					1003	1.73	0.82	-	
18(D)	BC	5. Plane	98	15.0	10	1.17	1.11	1.04	
(F)		Stainless			50	1.49	1.43	1.09	
(H)		Steel.			300	1.64	1.60	1.16	
(J)					1000	1.72	0.93	1.03	
(L)					600	1.65	1.20	-	
19(D)	BCF1	None	98	24.3	10	1.29	1.19	1.07	
(F)					50	1.38	1.34	1.05	
(H)					301	1.44	1.15	1.08	
(J)					1000	1.48	0.37	-	
20(D)	BCF1	5. Plane	98	15.0	10	1.31	1.21	1.07	
(F)		Stainless			50	1.31	1.17	1.05	
(H)		Steel.			300	1.57	1.38	1.04	
(J)					1000	1.79	1.25	0.93	
(L)					600	1.47	1.27	1.12	
(N)					1000	1.81	1.10	-	
21(B)	BCF2	None	98	35.7	10	1.24	1.12	0.96	
(D)					50	1.42	1.32	1.05	
(F)					300	1.61	0.53	1.00	
(H)					1000	1.54	0.25	-	
22(D)	BCF2	5. Plane	98	21.4	10	1.13	0.81	1.00	
(F)		Stainless			50	1.17	0.98	1.00	
(H)		Steel.			300	1.42	0.74	1.16	
(J)					1000	1.57	0.66	-	2.
(K)			196		1000	-	1.03	-	
(L)			294		1000	-	1.18	-	
(M)			98		1000	-	1.25	-	

Where: SR = Slow Residual Angle, FP = Fast Peak Angle,
FR = Fast Residual Angle and SP = Slow Peak Angle After Fast Shearing.

Notes:
1. Test aborted, confining ring gap could not be maintained.
2. Additional weight added to hanger whilst 1000 mm/min shearing in progress

Table 4.5: A summary of phase 3 tests continued.

Test No. (Stage)	Soil Code	Interface Number	Normal Stress (kPa)	Slow Res. Angle	Fast Rate mm/min	FP/ SR	FR/ SR	SP/ SR	Notes
23(B)	CRF	None	98	36.6	10	1.14	1.00	1.01	
(D)					50	1.22	1.00	1.03	
(E)					300	1.23	1.01	1.01	
(H)					1000	1.22	0.87	-	
24(B)	CRF	5. Plane Stainless Steel.	98	29.8	10	1.00	0.92	1.00	1.
(D)					50	1.08	0.97	-	
25(B)	CRF	5. Plane Stainless Steel.	98	29.5	1000	1.05	1.00	-	1.

Where: SR = Slow Residual Angle, FP = Fast Peak Angle,
FR = Fast Residual Angle and SP = Slow Peak Angle After Fast Shearing.

Notes:
1. Short tests because of excessive soil loss.

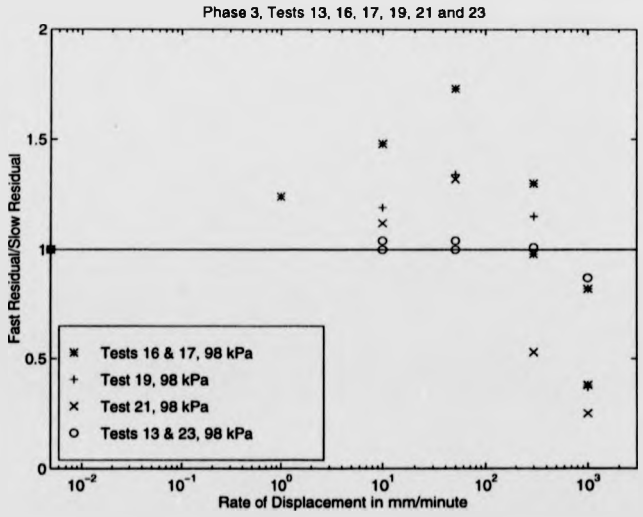

Figure 4.13: Variation of the fast residual strength with rate in phase 3, tests 13, 16, 17, 19, 21 and 23.

attained. Table 4.4 provides the value to which the strength had fallen when the stage was stopped. At 1000 mm/min typical negative rate behaviour was initially observed, with a fast peak strength followed by a steady drop to a fast residual value 62% lower than the slow residual value. This strength was maintained for a shear displacement of around 1000 mm and then the strength started to recover again, the fast angle doubling in the space of 500 mm. During these fast shearing phases resulting in negative rate behaviour unusual vertical displacements were noted of the top platen and these are illustrated in Figure 4.14. All of these Figures have been corrected for soil loss, using the wavehunt program provided in Appendix B, which assumes the rate of soil loss to be constant throughout the fast shearing. The wavelength of these cycles appears to be the same as the circumference at the mid-width of the annulus and comparison between the two readings suggest that one wave-form may have developed around the annulus, so that when one side was at the peak the other was in the trough. The wave height is approximately 0.5 mm but is not strictly constant. At 1000 mm/min the wave height appears to decrease as the shear strength starts to recover.

Figure 4.15 illustrates that fast peaks were not readily apparent during Test 16, only one was recorded, at a rate of 1000 mm/min, the magnitude of the peak being 59% higher than the slow residual strength. Slow peaks after fast shearing did occur and these are illustrated in Figure 4.16. They appear to follow the pattern of the fast residual strength, increasing with rate up to speeds of 50 mm/min and then showing a decrease in magnitude at 300 mm/min.

Test 17 was performed on pure ball clay, Soil BC, placed in the confining rings and consolidated under a normal stress of 98 kPa, as in Test 16. The objective of Test 17 was to repeat the 300 mm/min and 1000 mm/min stages of Test 16 over long displacements. All the consolidation and shearing stages are illustrated in Figures D.51 and D.52 and summarised in Table 4.4.

As with Test 16, typical fast residual strengths were not observed, however estimates of an approximate fast residual value were made, see Figure 4.13. At 300 mm/min, the strength fell to around 98% of the slow residual value and at 1000 mm/min the strength fell to 82% of the slow residual value. The 300 mm/min stage

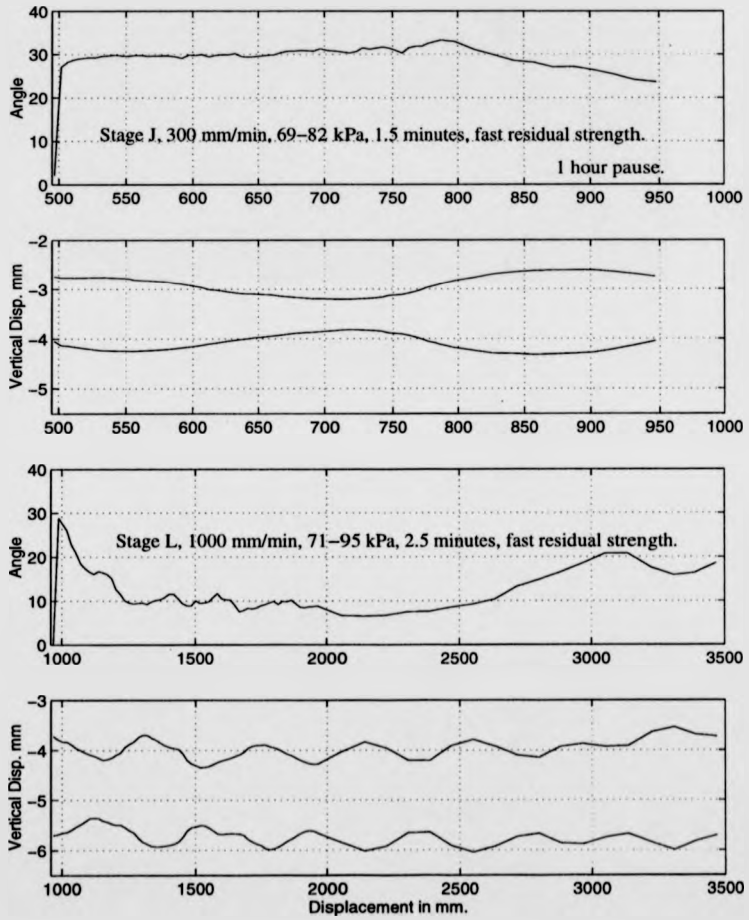

Figure 4.14: Vertical displacement of two opposite points on the top loading annulus during fast shearing in test 16.

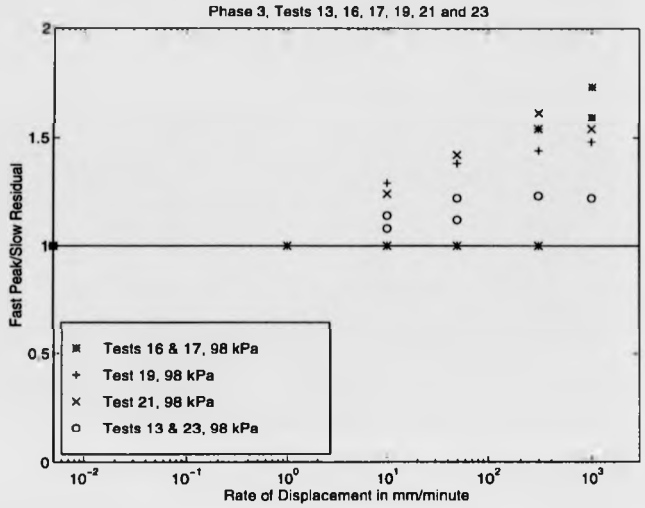

Figure 4.15: Variation of the fast peak strength with rate in phase 3, tests 13, 16, 17, 19, 21 and 23.

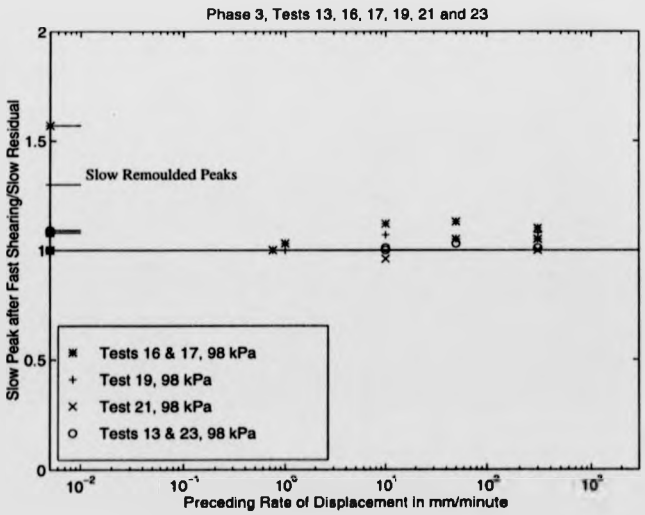

Figure 4.16: Variation of the slow peak strength after fast shearing with rate in phase 3, tests 13, 16, 17, 19, 21 and 23.

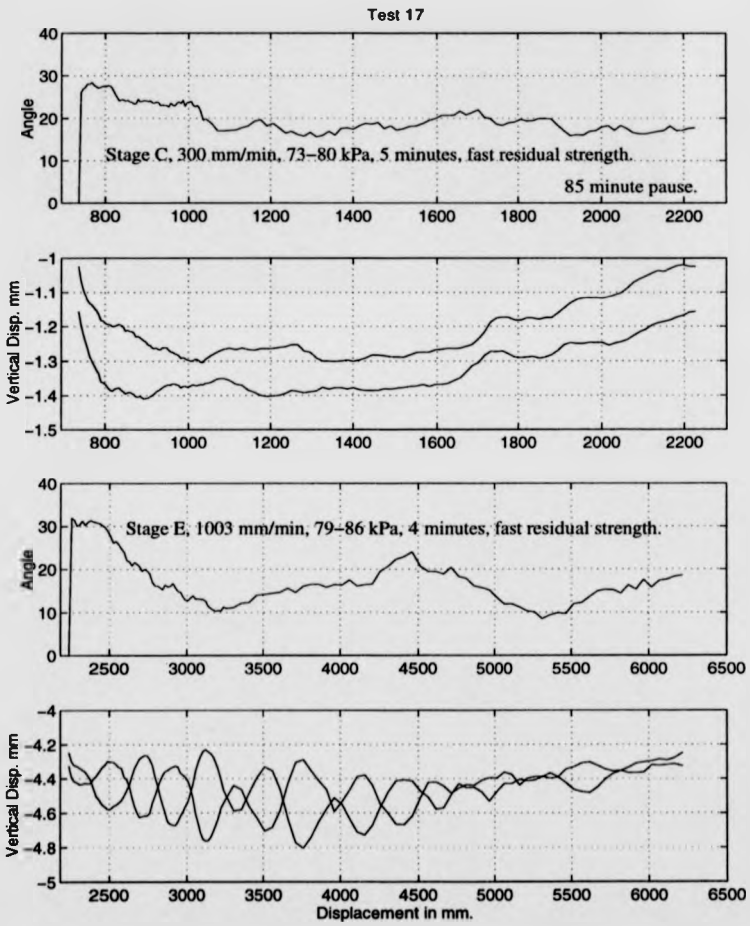

Figure 4.17: Vertical displacement of two opposite points on the top loading annulus during fast shearing in test 17.

illustrated a moderately stable strength, however at 1000 mm/min, the strength appeared to vary cyclically, by as much as 13° over a displacement of 2000 mm. This results in a mixture of positive and negative rate behaviour, which averages out to negative. Furthermore, significant vertical displacements were noted on the top platen, see Figure 4.17, which are similar to those observed in Test 16, in places their wave heights approach 0.8 mm, the wavelengths vary slightly but are of the order 400 mm to 500 mm. The wave height does tend to decrease as strength recovers, but does not increase when the strength falls for a second time.

Figures 4.15 and 4.16 show that both fast and slow peaks were recorded during Test 17. Fast peak strength increased with rate of shearing to 73% more than the slow residual strength at 1000 mm/min. A slow peak strength 10% higher than the slow residual value was noted after shearing at 300 mm/min.

Test 19 was performed on a mixture of ball clay and crushed flint, Soil BCF1, the silt content of this soil being 40%, 20% higher than the pure ball clay. The sample was placed at a moisture content of 29% and consolidated under 98 kPa. Results from the consolidation and shearing phases can be seen in Figures D.57 to D.59 and are summarised in Table 4.4.

The fast residual strengths obtained during Test 19 displayed similar behaviour to Tests 16 and 17. At rates up to 50 mm/min positive rate effects occurred with the fast strength at 50 mm/min being 34% higher than the slow residual strength. At 300 mm/min the behaviour changes, the fast strengths become less stable and do not illustrate true residual values, at 300 mm/min the residual strength is also less at approximately 15% higher than the slow residual strength. At 1000 mm/min the fast strength is even less stable, starting off with a fast peak, followed by a negative rate effect at 38% of the slow residual value followed by a recovery in strength to a slightly positive rate effect. Figure 4.13 illustrates that the magnitudes of the positive rate effects have decreased in Test 19 compared with Test 16, above 50 mm/min the change in behaviour appears similar for both tests. Accompanying these fast stages are further vertical displacements of the top platen, shown in Figure 4.18. These are not as pronounced in this test as they were in Tests 16 and 17, however they do follow the same format for wavelength and alignment of peaks and troughs.

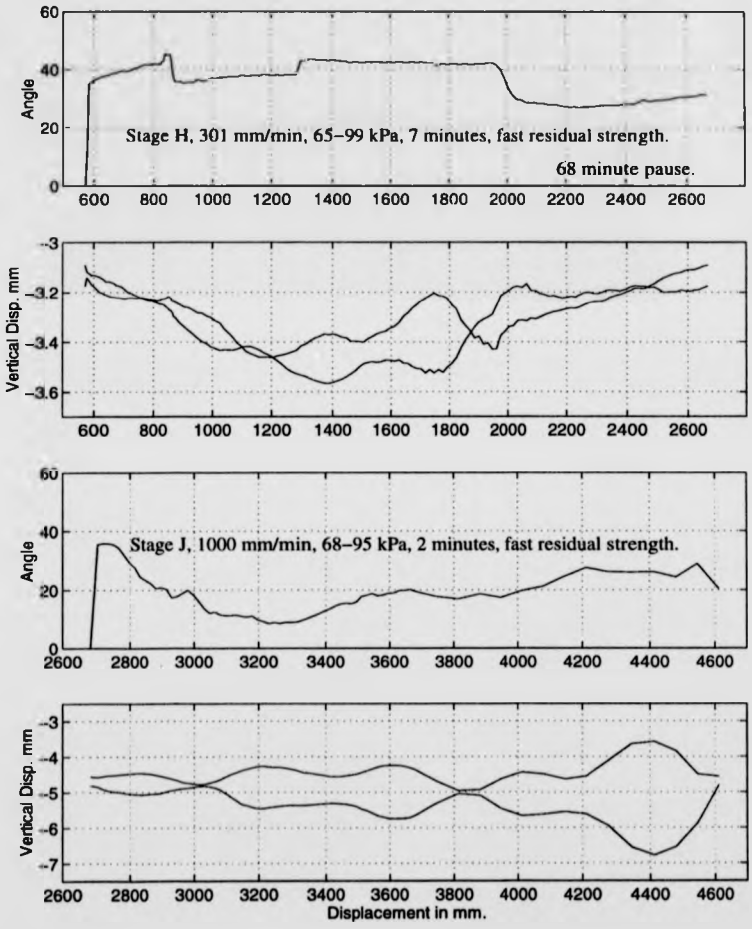

Figure 4.18: Vertical displacement of two opposite points on the top loading annulus during fast shearing in test 19.

Fast peak behaviour during Test 19, follows the trend set in previous testing. During this test however the peaks are well defined and provide an excellent set of results. At a rate of 10 mm/min a peak 29% higher than the slow residual value was attained, the magnitude of the peak then increased through the 50 mm/min and 301 mm/min stages until at 1000 mm/min it was 48% higher than the slow residual value. This behaviour is illustrated in Figure 4.15.

An excellent set of results was also obtained for the slow peaks after fast shearing, these are displayed in Figure 4.16. The peaks were clearly defined but did not really increase with rate of shearing. A peak 7% higher was recorded after shearing at 10 mm/min; this was followed by peaks 5% and 8% higher after rates of 301 mm/min and 1000 mm/min respectively.

Test 21 was also performed on a mixture of ball clay and crushed flint, Soil BCF2, the silt content of this soil being 60%, 40% higher than the pure ball clay. The sample was placed at a moisture content of 22% and consolidated under 98 kPa. Results from the consolidation and shearing phases can be seen in Figures D.64 to D.66 and are summarised in Table 4.4.

Test 21 illustrated exactly the same behaviour as all the previous soil on soil tests in phase 3. The fast residual strength increased with rate of shearing up to a rate around 50 mm/min showing stable residual values. At 300 mm/min a change in behaviour occurs where the strength is less stable and lower. Finally at 1000 mm/min a strong negative rate effect is observed at a level of only 25% of the slow residual strength. A study of Figure 4.13 now reveals a trend in the positive rate effects, as the silt fraction of the soil is increased the magnitude of the initial positive rate effects decreases, a trend which is also followed with Tests 13 and 23. With regard to shearing at 300 mm/min and 1000 mm/min, the level of fast residual strength is more random, not appearing to directly correlate with any soil properties. As a result of the significant movements of the top platen noted in previous tests, this test was examined more closely. The movement of the top platen is shown in Figure 4.19 and does not appear to show any significant variations. However, a close study reveals that slight waves do exist, which are more prominent when strength is falling and become less obvious when or if fast residual conditions are attained. As previously

their wavelength remains approximately 400 *mm*.

The slow peak strengths observed after fast shearing in Test 21 are illustrated in Figure 4.16. A 5% increase in strength was noted after shearing at 50 *mm/min*, however more unusually, no slow peak was observed after shearing at 300 *mm/min*. Another distinct trend emerges with the fast peak strengths, see Figure 4.15. In Test 21 the magnitudes of the fast peaks tends to increase with rate of shearing up to a rate of 300 *mm/min* where they are 61% higher than the slow residual strength, at 1000 *mm/min* the fast peak is not quite as high at 54% more than the slow residual.

Tests 13 and 23 were performed on crushed flint, Soil CRF, the silt content of this soil being 80%, 60% higher than the pure ball clay. The sample was placed at a moisture content of 32% and consolidated under 98 *kPa* in both tests. Results from the consolidation and shearing phases of both tests can be seen in Figures D.38 and D.39 and Figures D.71 to D.73, they are also summarised in Table 4.4.

A study of Figure 4.13 reveals that Soil CRF behaved totally differently to all the others used in phase 3, at rates up to 300 *mm/min* the behaviour was essentially neutral in both tests, that is the fast residual strength equalled the slow residual strength. One negative rate effect was observed at 1000 *mm/min* in Test 23, where the fast residual strength was 13% lower than the slow residual strength. This may have been the start of a negative trend which would increase with faster shearing, however, this was beyond the capabilities of the apparatus. No significant vertical displacements of the top platen occurred during the test, except the ones associated with soil loss.

Only minor slow peaks were observed after fast shearing during Tests 13 and 23, these being of the order 1% to 3% above the slow residual value with no apparent trend, see Figure 4.16. Fast peaks did occur with Soil CRF and these are displayed on Figure 4.15. The trend here is for the fast peaks to increase in magnitude up to rates of 50 *mm/min* at which point they have reached a plateau value at around 22% higher than the slow residual strength, a level at which they remain at rates of 300 *mm/min* and 1000 *mm/min*.

This concludes the first part of the analysis of Phase 3 which considered soil on soil shearing. The next part covers soil against planar interface shearing, the objective

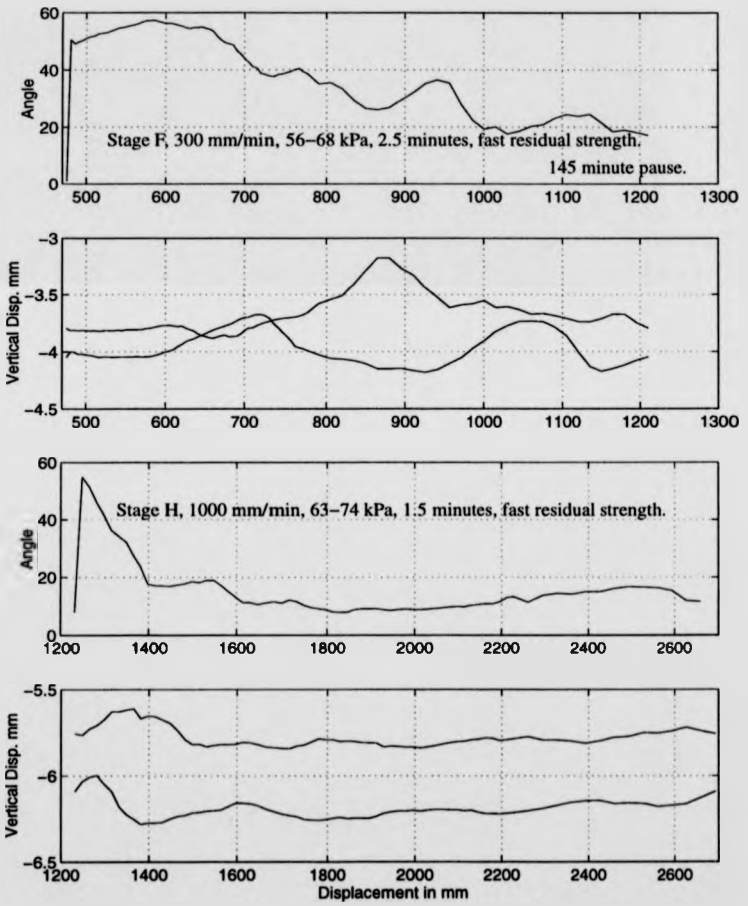

Figure 4.19: Vertical displacement of two opposite points on the top loading annulus during fast shearing in test 21.

of the tests being to try to prevent the displacements of the top platen which are presumably associated with an undulating shear zone and see what affect this has on the rate behaviour.

Test 18 was performed on ball clay, Soil BC, placed against Interface 5 (planar stainless steel) at a moisture content of 34%. The sample was then consolidated under a normal pressure of 98 kPa, results from the consolidation and shearing stages are provided in Figures D.53 to D.56 and summarised in Table 4.4. One of the advantages of shearing against an interface is that it tends to drastically reduce the rate of soil loss from the gap between the upper and lower rings, this has permitted longer fast shearing stages in this series of tests.

The variation of the fast residual strength with increasing rate of shearing is illustrated in Figure 4.20. A positive rate effect occurs with clearly defined fast residual strengths at rates up to 300 mm/min, at which point the fast residual strength is 64% higher than the slow residual strength. At 600 mm/min the behaviour is slightly different, the fast residual value is more variable and is lower than that at 300 mm/min, the strength having fallen to only 20% higher than the slow residual strength. Furthermore, at 1000 mm/min the results are highly variable, see Figure D.55; initially there is a fast peak strength, followed by a slight drop in strength, this is short lived however, as the strength then rises above the fast peak strength and fluctuates between 20° and 33° during the next 4000 mm of shearing. Over the next 1000 mm of shearing, the fast strength falls steadily until a relatively stable fast residual strength is attained at a level 7% below the slow residual value. Comparing Tests 16 and 17 on Figure 4.13 with Test 18 on Figure 4.20, it is apparent that the interface has reduced the magnitude of both the positive and negative rate effects, and has also increased the rate at which the change in behaviour from increasing strength with increasing rate to decreasing strength with increasing rate occurs. A study of Figure 4.21 provides compelling evidence that the fall in strength to a fast residual value in the ball clay is accompanied by a *"wobble"* of the top platen. The start of the drop in strength during Stage J corresponds exactly to the onset of considerable vertical displacements of the annulus, approaching 1 mm. Similar but less obvious behaviour can also be seen during the early part of stage L. It is interesting and potentially important to

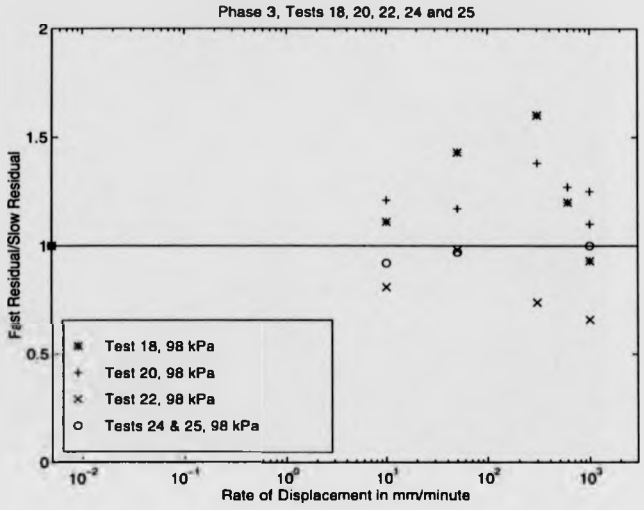

Figure 4.20: Variation of the fast residual strength with rate in phase 3, tests 18, 20, 22, 24 and 25.

note that once a relatively stable fast residual value is attained, the magnitude of the oscillations falls considerably until they become either very small or non-existent. Because the planar stainless steel interface was used, which has a considerably lower angle of friction than the internal friction of the soil, it is very unlikely that any shear surface would develop in the soil and not against the interface, thus questioning the possibility of an undulating surface.

Excellent data was also obtained for fast and slow peaks, with the general trends observed in previous testing being followed. Figure 4.22 shows that fast peak strengths increased with rate in the range 10 mm/min to 1000 mm/min, being 17% and 72% higher than the slow residual strength respectively. These compare closely to the soil on soil values obtained in Test 17. Figure 4.23 illustrates the variation of slow peaks after fast shearing with rate for Test 18. Slow peaks occurred after every fast shearing stage, rising to 16% higher than the slow residual strength at 300 mm/min. At 1000 mm/min however, a fall in the slow peak occurred so that it was only 3% higher than the slow residual strength. Figure 4.23 shows that at 300 mm/min the slow peak

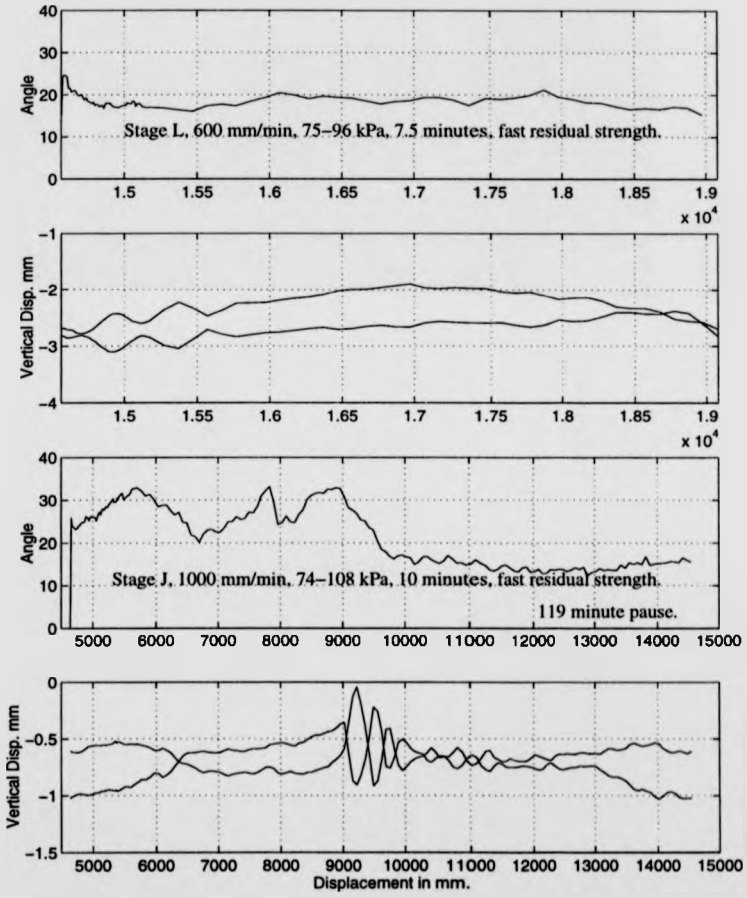

Figure 4.21: Vertical displacement of two opposite points on the top loading annulus during fast shearing in test 18.

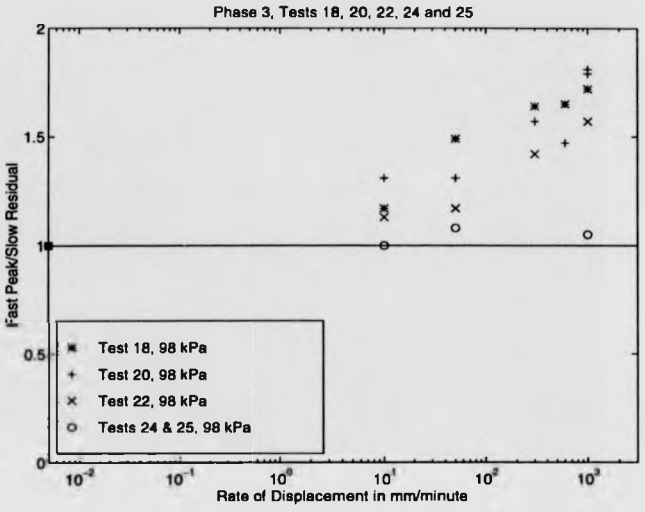

Figure 4.22: Variation of the fast peak strength with rate in phase 3, tests 18, 20, 22, 24 and 25.

observed exceeded the slow remoulded peak strength, this is unusual and suggests that the fast shearing disrupted the shear zone to a condition more disorientated than the remoulded soil. This sounds unlikely and may suggest that this measurement of the slow peak strength is inaccurate.

Test 20 was performed using a mixture of crushed flint and ball clay, Soil BCF1, which contained a silt fraction of 40%. The sample was placed against Interface 5 (planar stainless steel) at a moisture content of 29%, it was then consolidated under a pressure of 98 kPa. The results of the consolidation and shearing are displayed in Figures D.60 to D.63 and are summarised in Table 4.4.

The fast residual strengths obtained in Test 20 are illustrated in Figure 4.20. There was no negative rate behaviour observed during the test and stable fast residual values were attained in each fast stage of shearing. The variations in strength did not, however, follow the usual pattern quite so closely. An increase in strength to 21% more than the slow residual level was observed at 10 mm/min, a further increase did not occur at 50 mm/min the strength being only 17% higher. The fast residual

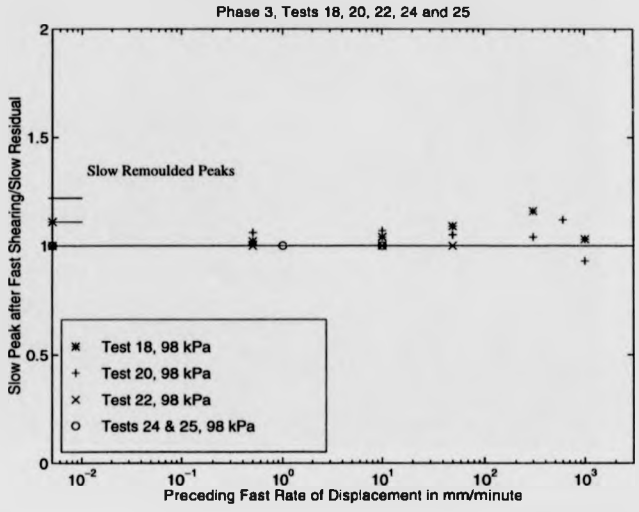

Figure 4.23: Variation of the slow peak strength after fast shearing with rate in phase 3, tests 18, 20, 22, 24 and 25.

strength reached a maximum at 300 mm/min where it was 38% higher, from this point it fell to around 10% more than the slow residual strength at a rate of 1000 mm/min. The magnitude of these positive rate effects is generally lower than those observed with the ball clay until a rate between 300 mm/min and 600 mm/min is exceeded. Comparing Tests 20 and 19 reveals that the effect of the interface was to prevent the onset of negative rate effects at speeds between 300 mm/min and 1000 mm/min, however, Figure 4.20 suggests that at higher rates negative behaviour may occur even against the planar interface. No unusual vertical displacements of the top platen were observed during Test 20.

The fast peak strength tended to increase with rate of shearing in Test 20, see Figure 4.15, although the increase in strength was not as linear with the log of the rate of displacements as it had been in some previous tests. A fast peak strength 31% higher than the slow residual strength was recorded at rates of 10 mm/min and 50 mm/min, from here the trend was generally upward until at 1000 mm/min the fast peak strength was 81% higher than the slow residual strength. These levels are

similar to those observed in the interface test on ball clay, Test 18 and significantly higher than those recorded in Test 19, on Soil BCF1 without an interface.

Slow peak strengths occurred after every stage of fast shearing without showing a particular trend. They varied between 4% higher than the slow residual strength after shearing at 300 mm/min and 12% higher after shearing at 600 mm/min. The value for the peak after 1000 mm/min may be neglected because there was no real peak and the value falls slightly below one because of minor variations in the slow residual strength.

Test 22 was conducted using a mixture of crushed flint and ball clay with a silt content of 60%, Soil BCF2. The sample was placed against Interface 5 (planar stainless steel) at a moisture content of 22% and was consolidated under 98 kPa. The results from this test are displayed in Figures D.67 to D.70 and are summarised in Table 4.4. These figures illustrate that all the fast residual strengths had very stable values and did not fluctuate as dramatically as they did during some of the more clayey tests.

Figure 4.20 illustrates negative rate behaviour at 10 mm/min, an unusual result, an inspection of stages C and D on Figure D.68 shows that the rate behaviour was actually neutral. This misleading information occurs due to the averaging of the slow residual strengths. Neutral rate behaviour is then displayed again at a rate of 50 mm/min. At 300 mm/min and 1000 mm/min negative rate behaviour is observed with the strengths falling to only 74% and 66% of the slow residual value respectively. This is completely different behaviour to Tests 18 and 20 and is not accompanied by vertical *wobbles* of the top platen. One of the advantages of using the interface is reduced soil loss, this allows longer shear stages. This results in a need for the gap between the rings to be adjusted during fast shearing, a good example of this is provided in stage F, Figure D.68. The small peaks on this graph around 1150 mm and 1800 mm are a result of opening the gap, which will create small negative pore water pressures in the sample leading to increases in the effective stress above the recorded normal stress and therefore increases in the shear strength of the shear zone. The small decrease in strength just above 2000 mm is a result of the opposite mechanism, closing the rings slightly increases the pore pressures in the shear zone.

It can be seen from Figure D.68 that the fast residual strength is reattained as these water pressures dissipate and the actual variation of the fast residual strength as a result of these adjustments is minimal. A further investigation was conducted as a result of low soil loss, the variable normal stress method outlined in Subsection 4.3.3 was implemented, the results of which are shown in Figure D.67. This revealed that the fast residual angle actually increased with normal stress, once most of the excess pore water pressures were dissipated. More interestingly it showed that once the extra normal stress was removed resulting in an over-consolidated sample the angle ϕ'_r did not return to its original value, instead it stayed at the valued attained when the increased normal stress was in position.

The slow peak strength results for Test 22 are shown in Figure 4.23. These reveal that the onset of slow peak development after fast shearing is later in this soil than in the more clayey soils. No slow peaks were recorded after rates up to 50 mm/min, then after shearing at 300 mm/min a slow peak 16% higher than the slow residual value was recorded. Fast peak strengths were recorded during each fast shearing stage of Test 22, see Figure 4.22. These started of at a level 13% higher than the slow residual angle at 10 mm/min and steadily rose to 57% higher at 1000 mm/min. The magnitudes of these fast peaks is lower than the more clayey soils and also lower than the peaks recorded with the same soil with no interface.

Tests 24 and 25 were performed on crushed flint, Soil CRF (80% silt), placed against Interface 5 (planar stainless steel) at a moisture content of 32%. The sample was then consolidated under a normal stress of 98 kPa. The results from Tests 24 and 25 are given in Figures D.74 to D.76. The crushed flint proved very difficult to use against an interface and soil loss was rapid, this was probably because of the low levels of cohesion in the soil. Hence, Tests 24 and 25 were severely restricted.

The fast rate behaviour illustrated in both these tests is essentially neutral. There may be some evidence on Figure 4.20 that negative behaviour occurred at rates of 10 mm/min and 50 mm/min but this is not conclusive. There was no sign of the onset of significant negative rate effects at 1000 mm/min during this test unlike the soil on soil test using the crushed flint, Test 23. Relatively stable fast residual values were attained, however the 50 mm/min stage in Test 24 and the 1000 mm/min stage in

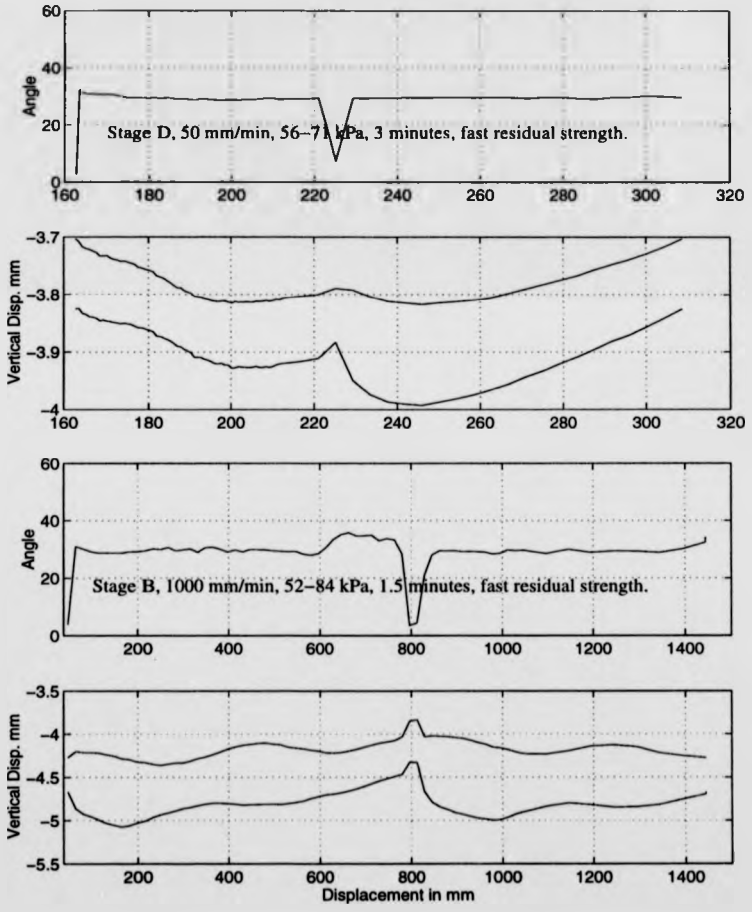

Figure 4.24: Vertical displacement of two opposite points on the top loading annulus during fast shearing in tests 24 and 25.

Test 25 contained significant short term dips in strength, behaviour that had not been observed previously. Figure 4.24 has been produced in an attempt to explain this, the figure illustrates that significant upward vertical displacements occurred at the same time as the dips in strength. It is possible to draw analogies with the behaviour observed earlier in phase 3, but this appears to be different. The movements are in the same direction on diametrically opposite points of the annulus and appear to be unique and not associated with any cyclic behaviour. It may be analogous to the initial drops in strength seen in previous tests but this poses the question why did true cyclic behaviour not occur, the other problem is that the triggering mechanism of all these *"wobbles"* is unknown and appears to be chaotic.

The information gathered from these tests regarding slow and fast peaks is limited due to the short duration of the tests, this is illustrated in Figures 4.23 and 4.22. No slow peaks were observed and only slight fast peaks were observed at levels significantly lower than the other soils tested and also lower than the peaks observed during soil on soil testing with the crushed flint.

This concludes Phase 3 which has seen a thorough investigation of four different soils with silt contents ranging from 20% to 80%. The effects of these variations and of the use of a planar interface on the rate behaviour of the soils have been reported. Finally, the next phase reports on a short investigation into whether or not strength is regained across a shear surface if it is left stationary for long periods.

4.4.4 Phase 4–Does Residual Shear Strength Recover During Long Static Pauses?

Test 5 was conducted on pure kaolin, Soil K, placed in the confining rings at a moisture content of 36%. The soil was submerged and consolidated under a normal stress of 98 kPa. Test results for Test 5 can be found in Figures D.17 and D.18

Initially the slow remoulded peak was recorded at a rate of 0.005 mm/min within a displacement of 3-4 mm. Then, a well orientated shear surface was produced using the speed up slow down method described by Bishop et al [7]. At a slow rate of 0.005 mm/min the slow residual strength was found to be 12°. Once slow

residual conditions were well established shearing was stopped and the shear stress was immediately removed. The sample was left submerged under a normal stress of 98 kPa but with no shear stress for a period of 10 days. Slow shearing was resumed at 0.005 mm/min, this resulted in a slight slow peak of 12.7°, 6% higher than the slow residual value.

Test 10 was performed on the ball clay, Soil BC, placed in the confining rings at a moisture content of 34%. The soil was submerged and then consolidated under a normal stress of 98 kPa, the results from the consolidation and shearing stages are shown in Figures D.33 and D.34.

The first stage of the test involved the measurement of the slow remoulded peak strength at a rate of 0.005 mm/min, once this was obtained the confining rings were closed and a shear surface was established at a rate of 0.1 mm/min. The rate was then reduced to 0.005 mm/min the rings were opened and the slow residual angle was found to be 18°. The test was stopped and in this test the shear stress continued to be applied by the compression in the proving rings. The soil was then left in this condition with a well defined shear surface under a constant normal stress for a period of 19 days. When slow shearing at 0.005 mm/min was resumed a slight slow peak was observed reaching 19.3°, beyond this the strength varied slightly around 18°. This means that a 7% rise in strength was observed.

The slow peak angles recorded after the pauses are relatively insignificant and it would not be prudent to use these 6% and 7% margins in design calculations for the reactivation of landslides. Especially as the slight peak in Test 10 may be due to particle disorientation as a result of small quantities of reverse shear as the shear strength relaxed during the pause. It is difficult to predict whether further increases would be possible if the pauses were longer. Generally it is the author's opinion that they would not, unless some form of chemical bonding occurred.

This concludes Chapter 4. The next chapter looks at these results in more detail and assesses what can be learnt and postulated from them.

Chapter 5

Discussion Of Test Results

5.1 Introduction

The aim of this chapter is to collate and discuss the results of the series of tests performed in the IC/NGI apparatus, explanation of the observed behaviour is undertaken in Chapter 6. This chapter commences with reports on the difficulties faced during testing and any limitations these problems may have caused. This is followed by discussion of the typical strengths observed during the tests, including the slow residual strength, the fast peak strength, the fast residual strength and the slow peak strength after faster shearing. The chapter concludes with a study of the time scales and velocities needed to induce negative rate behaviour when non-planar shear surfaces exist, the long term aim of this being to predict earthquake magnitudes and durations which may trigger long run-out landslides.

5.2 Testing Difficulties

5.2.1 Soil Loss

One of the inherent problems with many ring shear apparatus is soil loss, either from between split confining rings or between a loading platen and the confining rings. The IC/NGI apparatus is no exception. Many potential solutions have been developed for this problem, notably by Parathiras [4], Nieuwenhuis [80] and Sassa et al [76].

All of these involve designs that seal the gap with O-rings or flanges and do have the potential to prevent soil loss. However, all of the designs have the potential to transmit shear stress from between the rings via frictional forces and therefore affect the accuracy of results. The problem may be resolved by measuring friction using dummy samples, but the accuracy attained is questionable. Such designs may also inhibit the measurement of side friction, Parathiras [4] for example, whose design relies upon predicting side frictions using databases developed during previous testing.

From the outset of this study, the author was aware that soil loss may be a problem. However, substantial quantities of research had already been successfully performed without preventing soil loss, notably Lupini [44], Martins [87], Lemos [43] and Tika [2]. Henceforth the approach of this research was that soil loss would only become a problem if its effects were not fully considered.

Soil loss prevents the direct measurement of volume changes within the sample during shearing and therefore also prevents calculations of the change in void ratio. Displacements at the top platen are a result of both soil loss and volume change in the shear zone during shearing. It is possible to correct for soil loss by knowing the initial and final sample depths before and after a stage of shearing once primary consolidation is complete and then assuming that the rate of soil extrusion is constant throughout the stage. All of the settlement data for the fast rates of shearing was corrected in this fashion using the wavehunt program supplied in Appendix B. It was noted during this research that the rate of soil extrusion varied with the rate of shearing. The fastest losses occurred at speeds of 50 mm/min and 300 mm/min with rate of soil extrusion decreasing either side of these values. Similar observations have been made by Lemos [43] and Tika [2]. Furthermore it is reasonable to expect rates of soil extrusion to increase with increasing normal stress and gap size.

Soil extrusion has some potentially serious effects on the accuracy of testing. Firstly the extrusion of the soil tends to relieve normal stresses around the peripheries of the soil annulus, thus invalidating the uniform normal stress assumption made in Equation 3.1. A variety of normal stress distributions were analysed by Bishop et al [7], who concluded that even large variations in normal stress across the annulus had little effect on the accuracy of test results. Secondly when soil is extruded between the

rings, it provides a medium through which frictional forces can be transmitted and if this occurs the recorded strength of a soil may be artificially high. The problem can be alleviated by periodically opening and closing the confining rings and monitoring any variations in recorded strength as a result of this action. Further details concerning uneven stress distributions and soil loss can be found in Subsection 3.2.9.

Soil extrusion severely limited the duration of the fast stages of shearing. In some cases, Test 4 for example, this inhibited the attainment of true fast residual strengths because sufficient displacements could not be permitted. This problem occurred during soil on soil tests and tests using undulating shearing interfaces. One solution to the problem was to perform only one or two fast stages of shearing in a test rather than the standard multi-stage tests. This could provide more accurate fast residual strengths, see Tests 9, 11 and 12, but did involve more laboratory time. Another way of reducing soil loss was to perform tests against planar interfaces. Similar observations had been made previously by Lemos [43] and Tika [2]. During this research the use of a planar stainless steel interface allowed displacements of up to 100 m. Speculatively this reduction in soil loss may be attributed to the planar nature of the shear surface. In soil on soil testing there is a tendency for a slight upward bulge in the shear surface towards the centre of the annulus and it may be that this promotes soil loss as the upper half of the specimen flows down the sides of the bulge under the normal stress. With undulating shear surfaces there will be significant plastic deformations and flow type movements in the sample which may promote soil loss. Generally it is felt that the planar interface discourages internal movements of the sample away from the shear zone. It should be noted that the use of the planar interface did not reduce soil loss in the case of the pure silt which was almost non-cohesive.

5.2.2 Confining Ring Gap Control

The gap between the upper and lower confining rings is controlled via the differential screw which lifts or lowers the top rings via the side friction proving ring. The mechanism is attached to the top rings at two points directly opposite each other. At these two points the gap between the two sets of rings is monitored by SGDTs,

as outlined in Subsection 3.2.5. The gap size needs to be maintained at a level that does not promote excessive soil loss and prevents friction between the upper and lower rings. In this research the gap was normally maintained between 0.3 mm and 0.5 mm during soil on soil testing and between 1.2 mm and 1.4 mm during interface testing, where the top of the interface protruded 1 mm above the lower confining ring.

Once the preliminary consolidation of a sample was complete, the rings were opened. At this stage in some of the tests the gap opened unevenly around the annulus of soil. There are many possible consequences as a result of this behaviour, one being that friction between the sample and the upper and lower rings may be difficult to eliminate on one side without promoting excessive soil loss on the other side. Another consequence is an irregular distribution of side friction and hence another opportunity to develop an irregular normal stress distribution. If the gap has opened less on one side than the other, it must be logically assumed that the side friction force generated between the top ring and the sample on this side must have been greater than on the opposite side and therefore the normal stress at this point will be higher or lower depending upon whether the side friction proving ring is in compression or tension respectively. Yet again the calculated normal stress must be treated as an average stress over the shear surface not a uniform stress.

Gap control tended to be relatively easy with pure clays and mixtures of clays, silts and sands. However, the pure silt proved to be very problematic. The dilatant and time dependent behaviour of the silt meant that the side friction developed between the upper rings and the sample could not be overcome by the maximum upward force from the side friction proving ring of 700 N. This meant that the rings could not be opened. The problem was partially solved by compressing the upper proving ring with a lever system until the side friction was overcome and the rings opened. However the silt was prone to fast rates of soil loss because it was only semi-cohesive and the rings would close again rapidly. Some results are available from the pure silt but obtaining them proved very difficult.

Finally, with reference to gap control, it became apparent that during some of the longer stages of fast shearing the gap would need adjusting whilst shearing took place to prevent gap friction or excessive soil extrusion. Test 22 provides a perfect example

of the effect on the residual strength of opening and closing the rings. During Stage F of Test 22, see Figure D.68, two small peaks and a small trough occurred. These were a result of gap adjustments. The peaks correspond to the raising of the upper rings and are presumably a result of temporary suction increasing the effective normal stress. It is important to note that the normal stress used to calculate the stress ratio would include the decrease in normal stress as a result of upward side friction. The opposite mechanism operates when the upper rings are lowered causing temporary undrained loading and a decrease in effective stress owing to pore water pressure, this causes a small drop in residual strength such as the one in Stage F of Test 22. It is apparent from Figure D.68 that adjusting the rings has a short term effect on the residual strength associated with positive and negative pore pressures. Furthermore once these excess pressures have dissipated the fast residual strength returns to its stable drained value.

5.2.3 Variation Of Slow Residual Strength

In Chapter 4 the results were analysed by comparing typical fast strengths to the average slow drained residual strength. In some tests the slow residual strength varied throughout the test making comparisons difficult and possible explanations of this behaviour are needed.

The soils in which these variations tended to take place were mixtures of clay and sand or clay and silt, Tests 1 and 22 for example, where slow residual strengths rose by 8.0° and 4.7° respectively. These were some of the biggest increases but other small fluctuations of the order 1° to 3° occurred in some of the other tests. It is proposed that the soil grading may vary in the shear zone throughout the test in comparison with the grading of the original sample. As the strengths always tended to increase it is postulated that the proportion of silt or sand particles in the shear zone might increase as the test progresses. Two potential mechanisms for this are envisaged. One, the clay particles are more likely to be squeezed out of the granular soil matrix between the gap in the confining rings than the actual granular particles, a process which will be enhanced by fast shearing. Two, during fast shearing pore pressure gradients develop between the shear zone and the free water outside the

confining rings which wash the finer particles out of the granular soil matrix. The larger increase in strength in Test 1 than in Test 22 may be related to the differing size of the void spaces with the sand and silt particle matrix. The voids would be larger in the sand thus promoting more clay loss than from the silt and hence a larger increase in strength.

The two ideas put forward in the previous paragraph are really based on circumstantial evidence. Ideally grading analyses should be performed on the extruded soil and the soil in the shear zone after testing was complete. The results could then be compared to the initial grading of the sample. However, to carry out particle size distribution tests, around 20g to 50g of dry sample are required and these quantities were not available from the shear zone of a test using the IC/NGI apparatus. Perhaps the best evidence available for clay particle migration from this research was provided by Test 22. The test was performed against Interface 5 (planar stainless steel), using Soil KBS2, a mixture of the dark grey ball clay and the buff coloured crushed flint. When the shear zone was examined after the test a clearly defined pattern schematically represented in Figure 5.1 was observed. The dark band of colour in the centre of the annulus is almost certainly the ball clay and it appeared to be shiny and slickensided. The outer bands appeared to be Soil KBS2. Previous unpublished work performed by the authors academic supervisor, Dr D.J. Petley, suggested that the polished failure planes in actual landslides may have a slightly higher clay content than the surrounding soil. It is believed that the particles are deposited by the slide during movement. Extrapolating this idea it is possible to envisage the ball clay being squeezed into the shear zone and deposited on the surface. This would imply that the whole shear surface should be coated with ball clay, however, if radial clay particle migration is taking place this coating may be removed from the sample around the edges of the annulus. This would then generate the pattern shown in Figure 5.1. This theory is not conclusive and would require much more evidence to fully support it, but it does offer a potential explanation for the displacement of clay particles and the variations observed in slow drained residual strength.

Test 6 also illustrated an increase in the slow residual angle by 10.8° during the test, yet the test was performed on pure kaolin, not a mixture. The reason for this

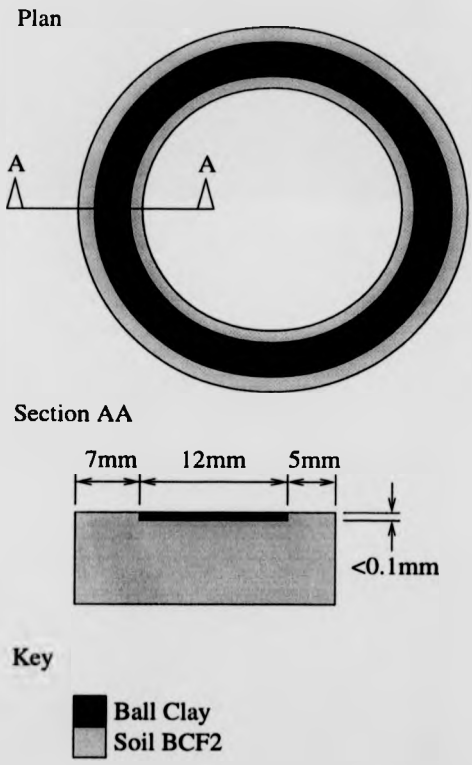

Figure 5.1: Pattern observed in the shear zone after test 22.

was that the soil was mixed to a state just above its plastic limit and placed in the apparatus, but the water bath was not flooded, henceforth the sample gradually dried out. Parathiras [4] conducted some tests on completely dry Brown London Clay and Cowden Till and recorded very high slow residual strengths for both (37.4° for the clay and 42.0° for the till). Therefore as the kaolin dried it is reasonable to assume that its strength would have risen. This conclusion is vindicated in Test 6 because when the water bath was flooded the slow residual strength fell to the level recorded at the start of the test.

5.2.4 Pore Pressure Transducers

The installation of pore pressure transducers into the IC/NGI apparatus is described in Subsection 3.2.4. There were many difficulties associated with this which severely limited the operation of the transducers.

The transducers were fitted into a very tight space in the shearing interface, which then required very sharp angles in the tube containing the cables to get the tube out through the lower confining rings and then over the water bath to the data logger. This appears to have severely limited the reliability of the transducers. As shearing commenced the transducers gradually stopped working generating flat line signals. This is attributed to kinking of the cable tube which contains the atmospheric reference pressure and separation of this tube from the back of the transducer, resulting in no pressure difference across the transducers diaphragm. Unfortunately the timescale of the research prevented the resolution of these problems. Potential solutions could include sealing the tubes to the back of the transducers with epoxy resin and assembling the apparatus without the bottom confining ring, reducing the amount of kinking in the cables.

Assembling the IC/NGI apparatus was also made significantly more complicated when the pore pressure transducers were installed. Once the transducers had been de-aired under water in a vacuum, the whole assembly of the instrumented interface, the sample and the confining rings was performed with the pore pressure transducers under water to prevent air re-entering the porous plates. The process was further complicated by the need to extract the cable tubing through holes in the lower confining

rings, which involved removing and re-soldering electrical connections. However, the assembly was successful with almost immediate responses occurring from the pressure transducers during the consolidation stages of Tests 14 and 15. The laboratory time required to set up these tests was significantly more than the standard tests, involving 6 to 8 hours of intensive work.

Further problems associated with the pore pressure transducers include the limited shear displacement available and the influence of the ceramic porous plates on the shear zone. The transducers are mounted on the rotating table of the IC/NGI apparatus, which means that the cables have to be wrapped around the apparatus during shearing. Whilst theoretically the cables can be made as long as necessary, there is a limit to the amount of cable that can be wrapped around the table without interfering with the operation of the apparatus and its instrumentation and this limits the number of rotations possible and therefore the shear displacement. This limit was not reached during Tests 14 and 15, but it is estimated that the limit would be five to seven rotations or approximately 2000 *mm* to 2800 *mm* of shearing. In between each stage the cables were unplugged and unwound ready for the next stage. Finally there is the problem of assessing the influence of the pore pressure transducers on the shear zone and its rate behaviour. Tests 14 and 15 suggest that in an undulating surface the presence of the transducers may trigger negative rate effects at lower rates than usual.

5.3 Uneven Shear Load And Settlement Across The Annular Sample

Uneven shear loads on the tangential proving rings and differential settlements of the top platen did occur during a number of tests. The implications of these occurrences are reviewed in Subsection 3.2.9. It is possible to reduce uneven settlements by ensuring uniform placement of the sample, however the tilting or *"wobbling"* of the top platen noted during fast shearing in Chapter 4 is difficult to prevent without performing constant volume tests which are not possible in the IC/NGI apparatus.

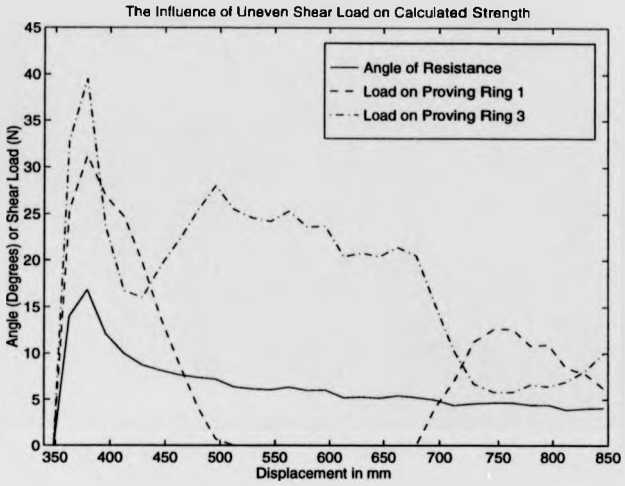

Figure 5.2: Shear loads and strength during stage H, 1000 mm/min, of test 4.

Further evidence beyond that supplied in Subsection 3.2.9 showing uneven shear loads do not effect recorded strengths is provided in Figure 5.2, which illustrates a typical imbalance of shear force without any notable effect on the calculated strength.

5.4 Discussion Of Behaviour

5.4.1 Slow Residual Strength

The study of residual strength escalated rapidly following the Fourth Rankine Lecture by Skempton [1] who was the first person to present correlations between residual strength and soil properties. These early results still provide the benchmark against which later works are compared. Further correlations were proposed by other authors and a comprehensive review of these is provided in Section 2.2. The levels of residual strength observed in this study are reviewed with respect to these earlier works for soil on soil shearing. Furthermore the influence of planar and undulating interfaces are also considered. It is well established that slow drained residual strength is independent of placement conditions and stress history but is a function of normal stress,

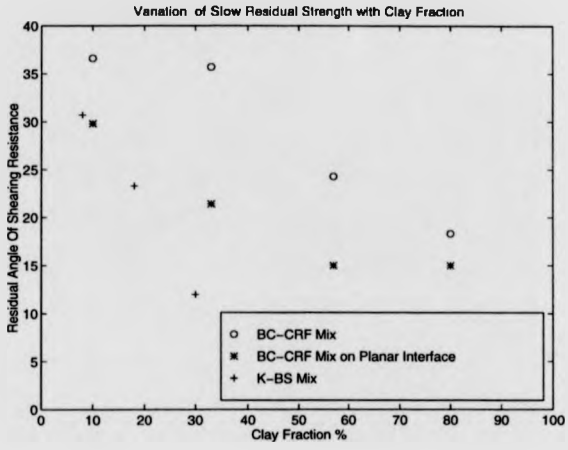

Figure 5.3: Variation of slow residual strength with clay fraction.

particle grading, particle shape, mineralogy and pore water chemistry. This is why these are not considered as part of this research. Moreover an in-depth discussion is not presented as the slow residual strength has usually only been determined at one level of normal stress, thus preventing an analysis of the non-linearity of the failure envelope.

Figure 5.3 illustrates the variation of the slow residual strengths observed during Phases 1, 3 and 4 of testing with clay fraction. The Figure illustrates a general downward trend in strength with increasing clay fraction as would be expected. The shear mode gradually changes from high strength turbulent shearing involving rotund particles displacing and rolling over one another to a sliding low resistance shear involving clay particles orientating themselves parallel to the shear direction and developing slickensides. A more detailed inspection reveals three wide ranging but similar behaviour patterns. The mixtures of ball clay and crushed flint (80% silt) illustrate an upper bound to the observed results. The strength falls steadily from 36.6° when the pure crushed flint was used to 18.3° when the pure ball clay was used. Strengths measured in between these values using mixtures of the clay and the flint followed an S-curve trend. When identical mixtures were tested against a planar

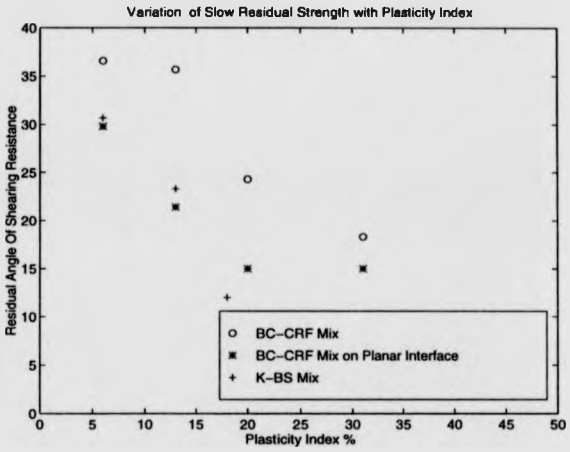

Figure 5.4: variation of slow residual strength with plasticity index.

stainless steel interface the residual strength still fell with increasing clay fraction but the behaviour was slightly different to the soil on soil testing. All of the strengths were lower than during soil on soil shearing and an S-curve was not observed. When the clay fraction reached 57% the residual strength had fallen to 15° a further increase in clay fraction to 80% did not cause further loss of strength. Finally some soil on soil tests were conducted on mixtures of kaolin and fine sand. These illustrated an almost linear decrease in residual strength with increasing clay content. The strength decreased from 30.7°, with an 8% clay fraction, to 12°, with a 30% clay fraction. Figure 5.4 shows the variation of the strengths with plasticity index. This graph illustrates the same trends as seen in Figure 5.3, this is because the activity of each of the individual soils is constant and provides the relationship between clay content and plasticity index. The graph is included here because previous researchers have defined upper and lower bounds for slow residual strength in relation to plasticity index. These will be illustrated presently.

For soil on soil testing, the variation in ϕ'_r with clay fraction observed in this research is compared with the work of Skempton [1] and latterly the summary made by Lupini [44] in Figures 5.5 and 5.6 respectively. On Figure 5.5 the new results

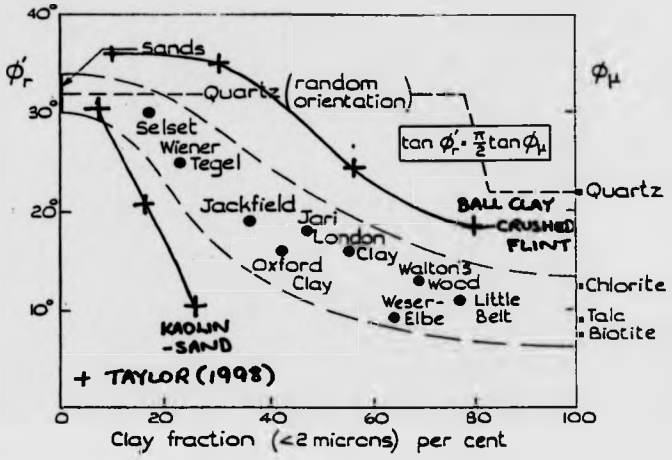

Figure 5.5: Decrease in ϕ'_r with increasing clay fraction, from Skempton 1964 [1].

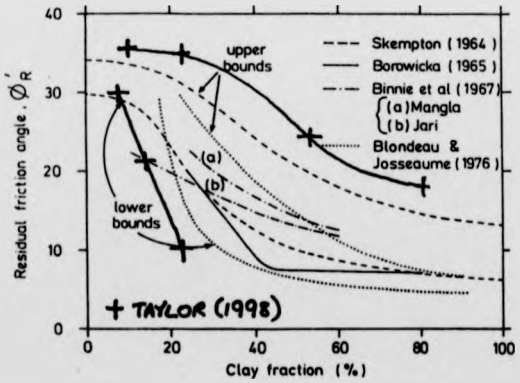

Figure 5.6: Residual strength: correlations with clay fraction, from Lupini et al 1981 [22].

exceed the upper and lower bounds proposed by Skempton in 1964, whilst on Figure 5.6 the upper bound only exceeds previous research. A clue to the position of the lower bound provided by mixtures of kaolin (Soil K) and fine sand (Soil BFS) lies in the grading of the kaolin. Kaolin is a pure clay mineral and would be expected to have clay fractions well above 50%. However, hydrometer tests revealed the actual clay fraction was only 30%. This may be due to incomplete dispersion of the particles during testing. Such an error would lead to an underestimation of clay content and correction of this error would translate the points in Figures 5.5 and 5.6 towards the centre of the bounds postulated in previous research. Alternatively Soil K may have a high proportion of particles which fall on the classification border between clays and fine silts. This could lead to low values of ϕ'_r with low clay contents.

An explanation for the high strengths observed with the mixtures of ball clay (Soil BC) and crushed flint (Soil CF) is more problematic. The initial high value of ϕ'_r for the crushed flint was not surprising, as the particles are likely to be very angular, thus promoting interlocking in the shear zone. It is also possible to argue that this angular phase prevented strength decreasing rapidly with increasing ball clay content so that the behaviour fell within the limits illustrated on Figures 5.5 and 5.6. However even when pure ball clay was used, the strength did not fall between these limits. The high value of residual strength for the ball clay, around $\phi'_r = 18°$, was observed repeatedly in a number of slow stages during different tests and is therefore thought to be correct. Best and Fookes [174] stated that the values they observed in Devon Ball Clays fell in the range 10° to 15°, which suggests that the recorded value of 18° is too high. One reason for this may be in the differences in sample preparation. Best and Fookes [174] performed tests on undisturbed samples, whereas the samples used in this research were mixed from a dry powder which had been mined and presumably pre-treated for the ceramics industry. It is possible that the prepared sample may have contained *"flocs"* of clay particles as a result of the manufacturing process, thus increasing the effective particle size and strength of the sample. Hydrometer grading tests on the powder do not, however, support this idea. Alternatively the manufacturing process may have altered the shape of the clay particles, but this seems unlikely.

A study of Figure 5.7 reveals that the mixtures of kaolin and sand still form a

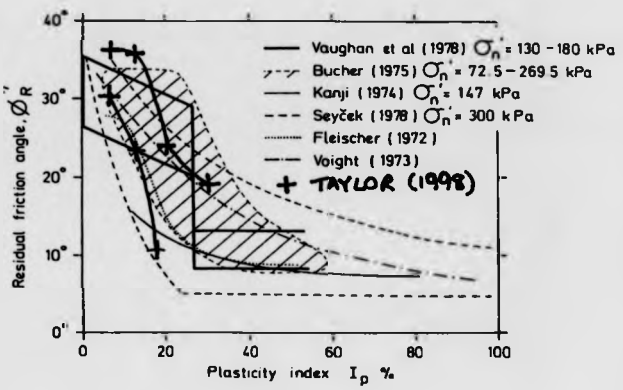

Figure 5.7: Residual strength: correlations with plasticity index, from Lupini et al 1981 [22].

lower bound when ϕ'_r is correlated with plasticity index. The mixtures of ball clay and crushed flint are not problematic in this case and agree very well with previous research. The key to this is the low activity of the ball clay, which means that for the high clay content (80%) the soil has a low plasticity index (31%) resulting in an activity of 0.39, a value in close agreement with Best and Fookes [174] who reported that the Devon ball clays were inactive with activities in the range 0.3 to 0.5. Therefore, explaining the good correlation with previous research in terms of plasticity index, even though the recorded slow residual strengths appear to be high when considered in relation to the clay fraction.

Figures 5.3 and 5.4 illustrate that lower strengths were obtained when the mixtures of ball clay and crushed flint were sheared against a plane stainless steel interface. This is a result of the smooth interface and was intentional, ensuring truly planar shear surfaces developed. The reason for the lower strength was that very few particles became trapped on the smooth surface and hence the recorded friction was a result of the surface roughness and not inter-particle contacts. Interface test results in Appendix D indicate similar behaviour to soil on soil shearing thus implying that the stages of dilation, critical state and particle orientation do still occur against the

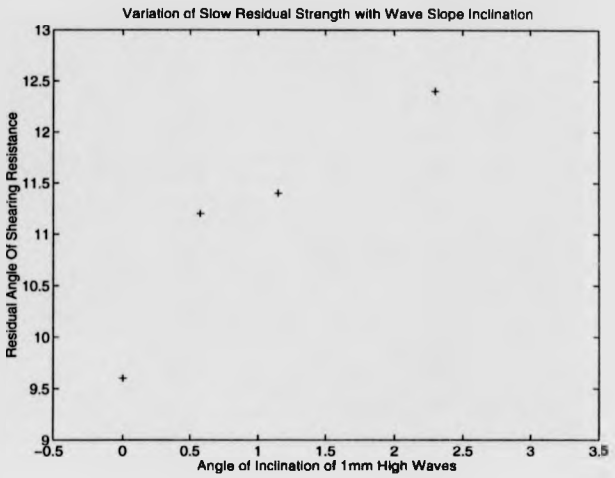

Figure 5.8: Variation of slow residual strength with angle of wave inclination.

interface.

During the series of tests using kaolin against plane and undulating shear surfaces with similar surface roughnesses (Interfaces 1-4), a study of the variation of the slow residual strength with wave inclination was made. The four points plotted on Figure 5.8 correspond to plane, 2, 4 and 8 waves around the annulus all of height 1 mm. These have been approximated to a straight line correlation between angle of slope inclination, i, and slow residual strength, ϕ'_r. The result of this yields the approximate solution,

$$\phi'_r = \phi'_{rplane} + 1.5i \tag{5.1}$$

This result is not in close agreement with Patton [162] [163], whose work in the shear box suggests that the effect of the up slope and down slope should negate one another. In conclusion, whilst the main aim of this research was the investigation of fast residual strengths, valuable information has been obtained with respect to slow residual strengths. Comparisons have been made between the strengths observed in this work with those reported by previous researchers. Furthermore the affects on slow residual strength of smooth planar and non-planar interfaces have been considered.

5.4.2 Fast Peak Strength

There is a limit to the accuracy of the data on fast peak strengths as a result of the limited scan interval outlined in Section 3.2.5, the implications of this are reported in Subsection 4.4. The most recent research by Parathiras [4] did not include a report on fast peak strengths. Previous works, summarised by Tika [2], found the following:

- In soils exhibiting turbulent shear the fast peak strengths correspond to the threshold strengths.
- In soils exhibiting transitional or sliding shear the fast peak strengths rose above the threshold strengths.
- Fast peak strength was attributed to disordering of the shear zone.
- The magnitude of the fast peak strength increased with rate of shearing.
- Finally at a given rate the fast peak strength was higher at lower normal stresses.

The following paragraphs present a study from Phase 2 on the effects of the undulating shear surfaces on the fast peak strength and a study from Phase 3 on the effects of mixtures and interfaces. These results are then compared to the conclusions provided by Tika [2]

Figures 4.8 and 4.11 provide a summary of fast peak behaviour during Phase 2. It can be seen that, generally, the fast peak strengths observed with the kaolin increases with rate of shearing above rates of 10 mm/min. Below this rate fast peaks are not normally recorded. Tests 4,7 and 8 were performed using 4, 2 and 8 $\times$ 1mm wave-form interfaces respectively and Figure 4.8 illustrates that no significant variations in fast peak strength behaviour occurred as a result of varying wave-forms. Generally the fast peak strength rose to around 50% more than the slow residual strength at a rate of 1000 mm/min. The unusual result from Test 8 probably results from poor sampling. Tests 9, 11 and 12 on Figure 4.11 illustrate the quality of the data being obtained by this stage.

Test 6 was performed using Interface 2 4 $\times$ 1mm wave-form), but unlike the other Phase 2 tests the sample was not submerged. Test 6 did not exhibit any fast peak

strengths until the water bath was flooded towards the end of the test, then a significant fast peak occurred at a rate of 1000 mm/min. This implies that fast peak strengths are somehow connected to pore water availability. The results from Tests 14 and 15 are provided in Figure 4.11, and seem unremarkable. The relevance of these tests is more apparent when Stage F of Test 14 and Stages C and E of Test 15 are studied in Figures D.43, D.45 and D.46. Each of the fast peaks observed during these tests is accompanied by negative pore water pressure recordings on the transducers. The average values of these pressures almost exactly mirrors the fast peak on the corresponding strength displacement graph. This provides compelling evidence that shear zone disruption may not be the only mechanism creating fast peaks, but that negative pore water pressures appear also to have a significant role.

The behaviour of fast peak strengths for a variety of mixtures is provided on Figure 4.15 for soil on soil testing and Figure 4.22 for soil against plane interface testing. The first thing to note is that unlike with the slow residual strengths the magnitudes of the fast peaks do not vary between soil on soil and interface testing.

The mixtures were designed so that Tests 16-18 were performed on soils containing 80% clay, this was then reduced through Tests 19-22 by adding silt until finally Tests 23-25 were conducted on a soil containing 80% silt. Figures 4.15 and 4.22 do not illustrate a perfect correlation between the magnitudes of the fast peak and the clay content. However it can be argued that there is a trend for the fast peak strength at a given rate to fall with clay content.

The magnitudes of the fast peak strengths observed with the ball clay tended to be slightly higher than those observed for the kaolin. Furthermore, the onset of fast peak strengths occurred at lower rates during Phase 3, the boundary rate appearing to be of the order of 1 mm/min.

In conclusion on fast peak strengths, many of the ideas proposed by Tika [2] have been corroborated, however her ideas on the reasons for fast peak strengths omit the influence of negative pore water pressures which increase the magnitude of the fast peak. There is also now some evidence to suggest that fast peaks decrease in magnitude with decreasing clay content. Finally the boundary rate at which fast peaks start to occur varies between soils but appears to be around 1 mm/min to

$10mm/min$.

5.4.3 Fast Residual Strength

Prior to this investigation two schools of thought existed on fast residual strength. Tika [2] attributed variations between positive and negative rate behaviour to soil grading and plasticity, whereas Parathiras [4] postulated that rate behaviour depended on shear surface morphology and the availability of water to the shear zone. Further details can be found in Subsection 2.3.2. This section initially considers the rate behaviour observed with undulating shear surfaces to investigate Parathiras' ideas, this is then followed by comparisons between tests on ball clay and crushed flint to investigate Tika's ideas on the influence of grading and plasticity. Finally in this section, a brief summary of the observed behaviour of the fast residual strength is provided.

Tests 3 and 4 were performed using kaolin against Interface 1 (planar) and Interface 2 ($4 \times 1mm$ wave-form) respectively, with both samples submerged. They provided typical curves for the behaviour of fast residual strength with increasing rate of shearing, observed in every test conducted in this research, except Test 2 on the predominantly sandy clay soil KBS2, which illustrated neutral rate behaviour. The curves are illustrated in Figure 4.4 and idealised with additional notation in Figure 5.9. The type of curve resulting from Test 3 will be annotated as a Positive Effect (PE) Curve and the type of curve resulting from Test 4 will now be annotated as a Critical Effect (CE) Curve. Furthermore the critical effect curve can essentially be defined by two points, the Fast Residual Maximum (FRM) point and the Critical Rate (CR) point. The FRM point corresponds to the rate at which the maximum fast residual strength was observed and the CR point corresponds to the rate at which rate behaviour switches from being positive to negative.

The results from Tests 3 and 4 suggested that Parathiras' idea that undulations of the shear zone could induce negative rate behaviour appeared correct. Whereas Test 3 using the planar interface had generated a PE curve, Test 4 using an undulating interface generated a CE curve, with an FRM rate of 40 mm/min and a CR point at 150 mm/min. To corroborate Parathiras' ideas further, Test 6 was performed using

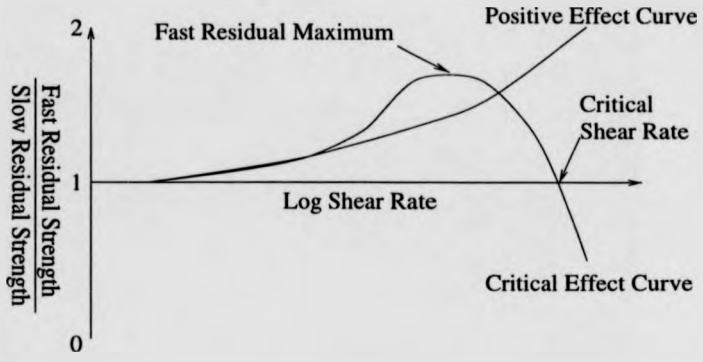

Figure 5.9: Idealised behaviour of fast residual shear strength.

the same soil and interface as Test 4, but without water in the water bath. Figure 4.7 shows that this generated a PE curve, even with an undulating shear surface. Towards the end of Test 6 the sample was submerged and fast shearing then took place. The result of this was negative rate behaviour similar to that observed at higher rates on the CE curve for Test 4. This provides strong evidence that a combination of undulations and available water will induce CE curves. Parathiras attributed this behaviour to pore water pressures, this is investigated in the following chapter.

Parathiras postulated that the magnitude of the negative rate behaviour induced by undulations increased with wave amplitude. Instead of repeating this work a constant amplitude with varying wavelength has been investigated in this study. Tests 4, 7 and 8 were conducted using 4, 2 and 8, 1 mm wave-form interfaces respectively, corresponding to approximate wavelengths of 100 mm, 200 mm and 50 mm at the mid-width of the annulus. Figure 4.7 illustrates that below the CR points in these tests there is a tendency for the FRM points to fall with increasing wavelength a trend similar to that observed for slow residual strengths. It is difficult to exactly define the rates at which the FRM points occur, however with a 50 mm wavelength the rate would appear to be 10 mm/min, for longer wavelengths the rate is around 20-40 mm/min. Above the critical rates, which appear to be of the order 100-200 mm/min, no real trends can be observed. This is probably due to inaccuracies in the levels of the fast residual strength as tests were curtailed because of soil loss.

Below the CR point stable fast residual strengths were attained in short displacements, however, as the CR point is approached and exceeded larger shear displacements are required and soil loss limits multistage testing. Therefore, Tests 9, 11 and 12 were conducted using kaolin (Soil K) and Interface 2 ($4 \times 1mm$ wave-form) over long displacements to establish true fast residual conditions. The results from these tests are presented in Figure 4.10 and illustrate that the CR points may be lower than indicated in Figure 4.7. The results suggest that in the multistage tests true fast residual strengths had not been attained beyond the critical rate point which would now appear to be at a rate of 50 mm/min. The result of this is to steepen the decline of the CE curve beyond the FRM point. Finally Tests 9, 11 and 12 do indicate the continuity available between tests during fast rates of shearing with the modified IC/NGI apparatus, as long as sufficient shear displacements are permitted.

The aim of Phase 3 was to investigate Tika's theories on fast residual strengths and grading. In this phase only CE curves were noted across a variety of soil gradings, this does not agree with Tika's work, which classifies five types of behaviour. This may be because Tika's work involved natural soils and limited shear displacements prevented accurate assessment of fast residual strengths or Tika managed to obtain truly planar shear surfaces with soil on soil tests, because again non-planar shear surfaces appear to have developed during Phase 3 testing. To try to prevent undulations in Phase 3, a planar interface was used as well as soil on soil testing, these tests will be considered presently.

Firstly the soil on soil results, illustrated in Figure 4.13. Tests 16 and 17 were performed on pure ball clay, Soil BC (80% clay), then the clay fraction and plasticity of each sample was reduced through Tests 19 and 21 by adding crushed flint until reaching Tests 13 and 23 which were conducted on pure crushed flint. As a result of Tika's work a PE curve was expected from Test 16, but this did not occur, so the faster rates were repeated with Test 17, which confirmed critical rate (CR) behaviour. Chapter 4 noted that this behaviour was associated with unusual oscillations of the top plate, also when the rings were dismantled some non-linearity was noted around the edges of the shear zone. A study of these *"wobbles"* and pore pressure effects are presented in Chapter 6.

The FRM point for all these tests appears to correspond to a rate of 50 mm/min. However the level of the FRM point varies between soils, see Figure 4.13. With the pure ball clay an FRM point 1.7 times the slow residual strength was attained. When the clay was mixed with the crushed flint the FRM point fell by half, then increasing the silt content further reduces the FRM point again. Eventually when a soil with 80% silt and 10% clay was used the FRM value was barely above the slow residual value. Therefore the magnitude of positive rate effects before the CR point increases with clay content and plasticity.

Because of the large displacements required as the critical rate is approached, as discussed previously, it is difficult to observe any clear trends when rate behaviour becomes negative. For all tests on Figure 4.13 the critical rate appears to be of the order 200-300 mm/min. One point which may merit discussion is the final one of Test 23, the strength of the silt did not fall as dramatically as the strengths of the more cohesive soils.

Secondly the planar interface tests illustrated in Figure 4.20. Test 18 was conducted on pure ball clay and then as testing continued the clay contents were decreased until Tests 24 and 25 where pure crushed flint was used. These tests illustrated very similar results to the soil on soil testing. The levels of the FRM values for Tests 18 and 20 corresponds closely to those observed in Tests 16, 17 and 19, with a tendency for the FRM value to fall with clay content or plasticity index. Tests 21 and 22 differ, despite being performed on the same soil. Test 22 illustrates no FRM value, yielding neutral rate behaviour until the CR point is reached. Any apparent negative rate effects prior to the CR point are a result of averaging fluctuations in the slow residual strength, this also applies to Tests 24 and 25.

The fact that CE curves were observed against a planar interface instantly creates problems for Parathiras' undulations theory, because it would appear unlikely that internal undulating shear surfaces would develop in the soil when the slow residual angle of friction between the soil and the interface is lower than for soil on soil shearing. However Subsection 4.4.3 reveals that *"wobbles"* were noted on the top platen even when the plane interface was used and that these were associated with strength loss beyond the FRM point. This raises the question whether these *"wobbles"* are a result

of undulations or possibly a dilate-contract mechanism, an area explored further in Chapter 6. So instead of preventing these undulations and therefore CE curve behaviour, it appears that the effect of the planar interface in comparison with soil on soil testing is to delay the onset of fast residual strength loss, that is, it increases the rate at which the FRM and CR points occur. For the interface tests the FRM value appears to be attained in Figure 4.20 at a rate around 300 mm/min, compared with 20-50 mm/min for the soil on soil tests. Similarly the CR point for the plane interface test now occurs at around 1000 mm/min (except Test 22, 50 mm/min) compared with 200-300 mm/min for the soil on soil testing.

Finally it should be appreciated that the accuracy of the fast residual strengths is improved with the interface tests, because soil loss was reduced and this allowed longer shear displacements.

To summarise on fast residual strengths, the work has found supporting evidence for the work of Parathiras [4], but has found little evidence in support of Tika [2]. Two types of behaviour have been identified, Positive Effect (PE) Curves which occur in cohesive soils with truly planar shear surfaces and shear surfaces where no free water is available to the shear zone and Critical Effect (CE) Curves which occur whenever oscillations of the top plate or undulations occur in conjunction with free water. Furthermore, the shape and position of the CE curve varies with grading, plasticity and the shape of the shear surface. The mechanisms behind this behaviour will be discussed in Chapter 6.

5.4.4 Strength Recovery After The Resumption Of Slow Shearing

Previous research by Tika [2] noted that the time taken for strength to recover once fast shearing stopped and slow shearing restarted was similar to the time for complete primary consolidation, that is, the time taken for full pore water pressure dissipation. Towards the end of the fast Stages O and J from Tests 6 and 7 respectively, this was investigated using the Variable Fast Speed Method described in Subsection 4.3.2. The shear rate was reduced rapidly from around 1000 mm/min to as slow a rate as

Table 5.1: Calculation of t_{90} from stages O and J of tests 6 and 7 respectively.

Test	Stage	Depth, d mm	σ_n kPa	c_v m^2/yr	t_{90} s
6	O	3.66	74	6.456	55
7	J	2.89	82	6.808	33

possible with the variable speed drive, approximately 8 mm/min. Ideally the change from fast to slow would be instant and the slow rate would be 0.005 mm/min.

Consolidation theory provides the equation required to calculate the degree of pore pressure dissipation after a given time, using,

$$c_v = \frac{T_v d^2}{t} \tag{5.2}$$

where c_v is the coefficient of consolidation, T_v is the time factor, d is the sample depth and t is the actual time. For 90% of the consolidation (pore pressure dissipation) to be complete, the time factor, $T_v = 0.848$ and therefore Equation 5.2 may be expressed as,

$$t_{90} = \frac{0.848 d^2}{c_v}. \tag{5.3}$$

From the data files for Test 6 and Test 7, it was possible to determine both the depth of the sample and the normal stress when the fast shear rate ceased and the slow shear rate commenced. The normal stress is required to obtain a value of c_v. In this case consolidation tests were performed on kaolin as part of this research, see Section 7.2, and the values of c_v used here were obtained from Figure 7.1 in that section. The required data and results from Equation 5.3 are presented in Table 5.1.

The calculated values of t_{90} in Table 5.1, may now be compared to the times illustrated on Figure 5.10. The times given on this figure represent the time taken for 90% of the strength lost below the average slow residual value to be recovered. If the recovery of the strength from the negative rate effect to the slow residual value is associated with pore pressure dissipation, the times on Figure 5.10 should equal those calculated in Table 5.1. The values are not identical for either test, but they are of the same order. For Test 6 the discrepancy between the calculated and observed

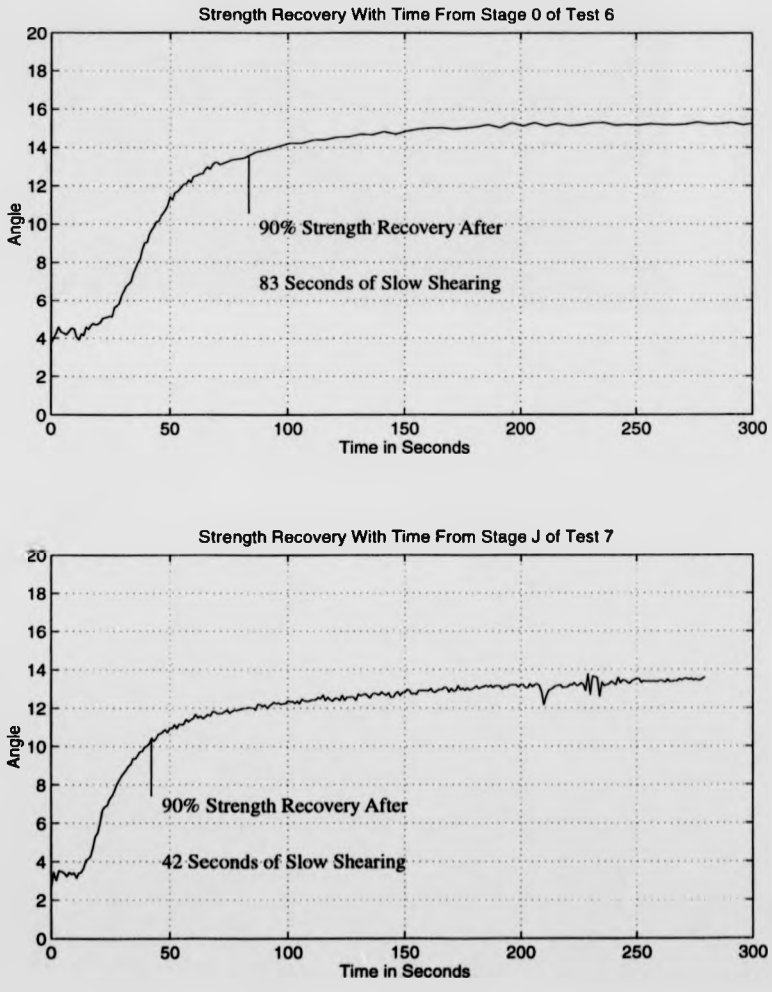

Figure 5.10: Illustration of strength recovery with time from tests 6 and 7.

times is 28 seconds, which is quite substantial. This may be associated with the fact that the sample had previously dried out during an earlier non-submerged phase of testing, this may have altered the consolidation properties of the soil, possibly by not completely saturating when the water bath was flooded. The discrepancy from Test 7 is only 9 seconds and provides a level of agreement that suggests that pore water pressure dissipation is the mechanism behind the strength recovery. Because of the time taken to slow the shear rate from 1000 mm/min to 8 mm/min it is difficult to estimate when pressure dissipation actually started. The zero times on Figure 5.10 were estimated from the shape of the S-shaped curve of the graph, however it may be likely that pressure dissipation started before estimated *"time zero"* and this could explain why both of the recorded values are slightly too small.

5.4.5 The Effect Of Normal Stress Variations On The Shear Strength At Fast Rates Of Shearing

A minor investigation into the influence of increasing or decreasing normal stress was carried out during the final stage of Test 22, see Figures D.69 and D.70, using the Variable Normal Stress Method described in Subsection 4.3.3. The test was not performed using standard multistage testing techniques, but involved adding or removing 10 kg weights to the hanger whilst fast shearing continued.

Figure 5.11 illustrates all the data points recorded during the 1000 mm/min shearing in Test 22, once a fast residual condition had been established. The test was performed against a plane steel interface to minimise soil loss. The main clusters of points represent the true fast residual condition, and during the loading (increasing normal stress) phase of the test these are joined by the dashed line, and during the unloading phase they are joined by the dash dot line. The reason the loading clusters have points tailing off to lower shear stresses is associated with the generation of additional pore water pressures when the next 10 kg is added, thus reducing the effective normal stress. The reverse appears to happen for the unloading points, i.e shear stresses temporarily increase when additional negative pore water pressures are generated when weight is removed from the hanger, thus increasing the effective

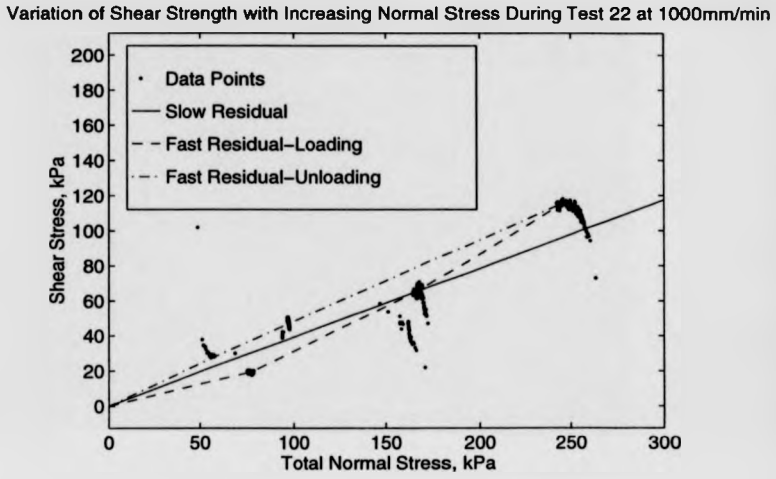

Figure 5.11: The influence of normal stress on negative rate behaviour.

normal stress.

Figure 5.11 illustrates that in this case the type of rate effect at 1000 mm/min changes from being negative at normal stress levels below approximately 170 kPa to positive at normal stress levels above 170 kPa during the increasing normal stress phase of the test. On unloading the rate effect is always positive and illustrates a linear fast residual strength envelope. However, the fast residual strength envelope during loading appears to be concave, thus providing the change from negative to positive behaviour as the fast envelope crosses the slow residual strength envelope. The non-linearity of the envelope during loading suggests that the increases in normal stress, affect the mechanisms behind rate effects; it appears that the negative mechanism may be suppressed by increasing the normal stress, whilst the positive rate effect mechanism is either increased by normal stress increases or at least suppressed less than the negative mechanism. The linearity and increased angle of the unloading curve suggests that positive rate effects may be directly proportional to increases/decreases in normal stress, whereas negative rate behaviour may only occur when the sample is normally consolidated. This questions current knowledge on the independence from stress history of residual strengths.

5.4.6 Slow Peak Strength After Fast Shearing

Slow peaks were observed after many fast shearing stages once a shear stress free pause had occurred to allow consolidation of the sample. The data on slow peaks is largely complete but in some cases soil loss prevented a final stage of slow shearing. Furthermore some of the initial slow remoulded peak strengths were lost because of data logging problems.

Figure 4.3 illustrates slow peaks were observed after fast shearing during the first two tests on mixtures of kaolin and sand. No peaks were noted with normal stress levels of 98 kPa, but under 196 kPa slow peaks were observed after rates of 300 mm/min and higher. Moreover their was a slight tendency for the sandier soils to illustrate higher slow peaks after fast shearing.

The variation of slow peaks after fast shearing with shear zone undulations is illustrated by Tests 4, 6, 7, and 8 on Figure 4.9. It would be reasonable to assume that slow peak strengths should increase with decreasing wavelength in a similar fashion to that illustrated in Figure 5.8 for slow residual strength. There is not enough data to confirm this and Figure 4.9 suggests no link between wavelength and slow peak strength after fast shearing.

Valuable information can be attained from these tests against interfaces. The preceding rate of shearing which first generates slow peaks is 10 mm/min and there is also a tendency for a maximum slow peak value to be attained at rates of around 300 mm/min, above this value the curves flatten or even decrease slightly, further testing would be required to confirm this. Generally the maximum slow peaks after fast shearing average around 50% of the slow remoulded peaks. One exception to this occurred in Test 6 after non-submerged shearing at 1000 mm/min when the slow peak after fast shearing was approximately 1.5 times the slow remoulded peak strength. This suggests that, as with the slow residual strength, slow peak strengths after fast shearing increase as the sample dries.

The variation of slow peaks after fast shearing with soil grading and plasticity with both soil on soil shearing and planar interface shearing was investigated in Tests 16 to 25 illustrated in Figure 4.16 for soil on soil shearing and Figure 4.23 for plane

interface shearing.

The soil on soil testing provides a strong indication that slow peak behaviour is a function of clay fraction and plasticity. The maximum slow peaks were observed with ball clay and the lowest with the silt. The mixtures fell in order between the maximum and minimum values, thus providing evidence that the magnitudes of slow peak strengths decrease with clay fraction and plasticity. There is also evidence to suggest that the preceding fast rate which generates slow peaks increases with falling clay content. The ball clay developed slow peaks after shearing at 1 mm/min compared with the crushed flint were only a slight slow peak was noted after 10 mm/min and a more significant peak after 50 mm/min shearing. Figure 4.16 also illustrates that slow peak strengths do fall slightly at faster preceding rates. During these tests maximum slow peaks were recorded after shearing at speeds around 300 mm/min. Whatsmore there is a constant ratio between the maximum observed slow peak after fast shearing and the slow remoulded peak strength. The slow peak after fast shearing was 25-30% of the slow remoulded peak strength for each soil on soil test.

The planar interface testing provided similar test results for the higher clay content soils, illustrating decreases in slow peak strengths after fast shearing with decreasing clay content and plasticity. The levels of the slow peaks were comparable to the soil on soil tests, but the slow remoulded peaks are different and no corresponding ratio exists between the two peaks. Whilst limited data is available for the lower clay content tests because of soil loss, the minimum preceding rate of fast shearing required to trigger slow peaks appears to increase from 0.5 mm/min for the ball clay (Soil BC) and Soil BCF1 to around 50 mm/min for Soil BCF2, unfortunately no data is available for the crushed flint.

This concludes the section on slow peaks after fast shearing. An analysis of the mechanisms behind these observed behaviours is presented in Chapter 6.

5.4.7 Time Taken For Negative Rate Behaviour To Occur

Any soil exhibiting a critical effect curve as described in Subsection 5.4.3, has the potential to allow a landslide to accelerate to catastrophic failure with long run-out

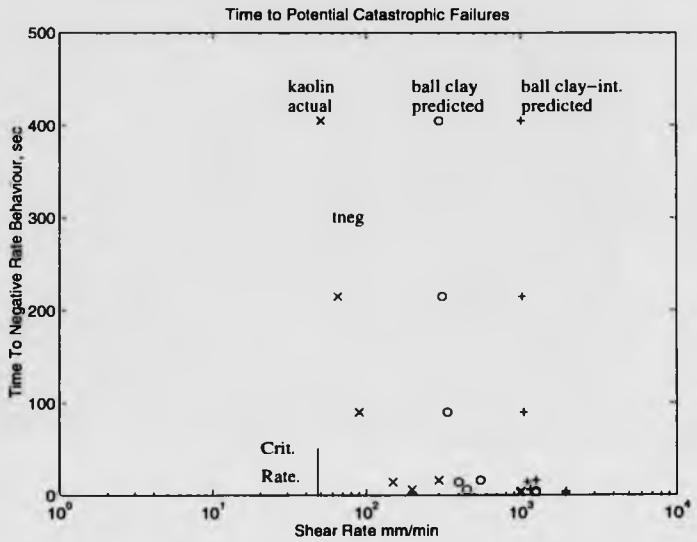

Figure 5.12: Time taken to induce negative rate behaviour.

distance once the rate of shearing exceeds the critical rate. However fast residual strengths above the critical rate do not develop instantly when shearing commences. This section studies the time necessary to generate a negative rate effect across a range of shear speeds and considers the implications of the findings.

Because of the large quantities of testing required to attain accurate data on the subject, this study is confined to a series of tests from Phase 2 performed using kaolin against Interface 2 ($4 \times 1mm$ wave-form). Initially during Test 4 it was noted that at 1000 mm/min negative rate behaviour occurred almost instantly, whereas at 300 mm/min it took around 15 seconds for the strength to fall below the slow residual value. Tests 9, 11 and 12 were performed to investigate further whether or not time to negative rate effect did increase as rate of shearing decreased. Furthermore Test 12 confirmed the critical rate was around 50 mm/min.

The results of these investigations are illustrated in Figure 5.12. This illustrates a smooth curve relating shear rate to the time taken to induce negative rate behaviour. At faster rates above 300-400 mm/min the curve starts to attain values close to

$time = 0$, however as rate decreases the curve climbs until becoming assymptotal to the critical rate. Results of this nature from Phase 3 testing are patchy, but they do suggest similar trends with the times to negative effects much lower at 1000 mm/min than at 300 mm/min. Therefore it is reasonable to speculate that the curve obtained for kaolin against Interface 2 ($4 \times 1mm$ wave-form) can be translated in the x-direction according to the critical rate of any soil illustrating a critical effect curve. An example of this is supplied in Figure 5.12 for the ball clay in both soil on soil and plane interface shearing.

The implications of these curves relates to the triggering of long run-out landslides. Consider as an example a triggering event which reactivates a shear zone identical to the kaolin against Interface 2 ($4 \times 1mm$ wave-form) at a rate of 80 mm/min for a period of 75 seconds. Plotting this point on Figure 5.12 reveals that such an event would not generate negative rate effects and catastrophic failure, even though the shear rate is above the critical value. However, if the duration of the triggering event or the induced rate of displacement was increased so the point fell to the right of the t_{neg} line, negative rate effects would occur causing catastrophic failure. This gives an idealised example of how knowledge of rate effects could be used to identify dangerous combinations of soils and events. To apply this to real events such as earthquakes would require the establishment of a relationship between earthquake type and magnitude to induced shear rates and large quantities of fast rate testing on field samples. Then it may be possible to predict catastrophic slope failures under seismic loading.

5.4.8 Summary Of Idealised Behaviour

To conclude Chapter 5, a series of graphs illustrating the idealised behaviour of the typical strengths associated with fast shearing is presented in Figure 5.13. The plots also include indications the effects variations in grading, plasticity and shear surface morphology are likely to have on these curves. The mechanisms associated with this behaviour are explored and discussed in Chapter 6.

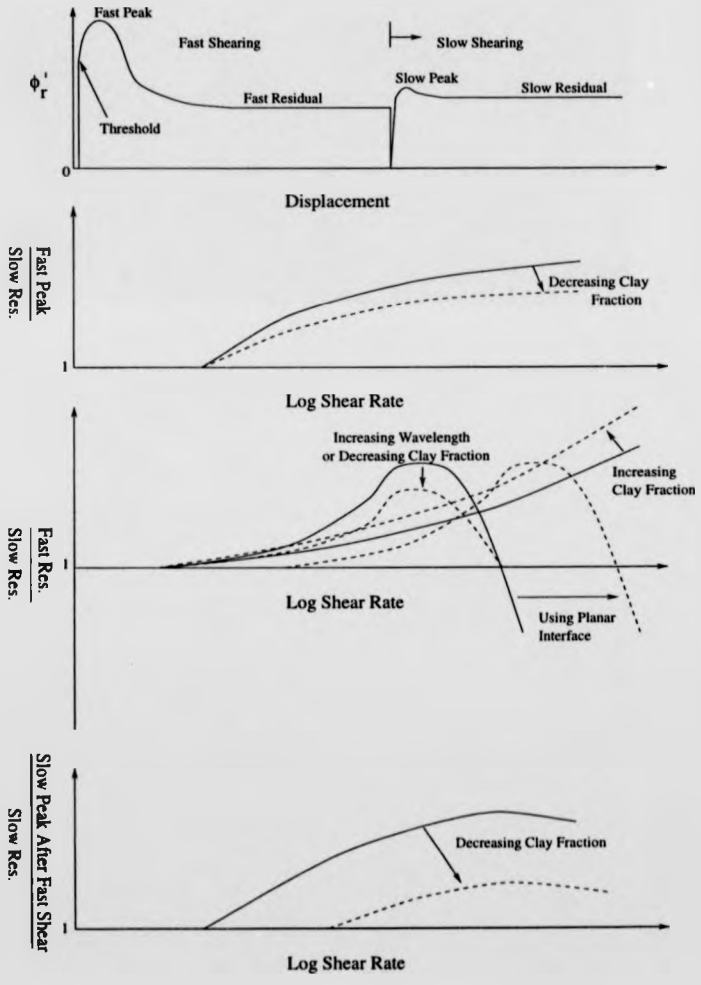

Figure 5.13: Summary of behaviour of typical strength effects.

Chapter 6

Hypotheses And Models For The Observed Variations In Strength

6.1 Introduction

The objective of this chapter is to propose theories and mechanisms which explain the behaviour of the typical strengths discussed in the previous chapter. The main body of this chapter focuses on the loss of residual strength at fast rates of shearing. Fast peak and slow peak after fast shearing strengths are also discussed as well as positive rate behaviour.

6.2 Fast Peak Strength

As a result of the findings in Subsection 5.4.2, which state that water was required to generate fast peak strengths and that negative pore water pressures had been recorded during fast peak strengths, it is postulated that shear zone disruption associated with initial shear zone volume change as proposed by Tika [2] and Tika et al [3] does not fully account for fast peak strengths. The following sequence of events provides a fuller explanation of the observed fast peak behaviour.

- As soon as shear displacement commences the shear zone starts to dilate.

- This dilation continues creating the disorder noted by Tika, but also it rapidly induces negative pore water pressures in the shear zone, generating higher effective normal stresses and resulting in an apparent increase in strength.
- These negative pressures dissipate almost as quickly as they were generated due to the increased porosity of the shear zone.
- This results in a drop in effective normal stress leading to the decline of the fast peak strength towards the fast residual condition.

This overcomes one of the major problems with Tika's work which implies that the magnitude of the fast peak strengths and the slow remoulded peak strengths should be similar, whereas in reality fast peaks nearly always exceed slow remoulded peaks at speeds above 50 mm/min.

The generation of fast peak strength with negative pore pressures only is unlikely owing to the dilation required to generate the pressures. Figure 6.1 Part (i) however, explains the effect of negative pore water pressure. Once residual conditions have been established at Point A, yielding the equation,

$$\tan \phi_r = \frac{\tau_r}{\sigma_n}, \tag{6.1}$$

fast shearing commences generating a negative pore water pressure -u, which increases the effective normal stress to Point B on the failure envelope. Thus generating an apparent shear stress $\tau_{apparent}$, where,

$$\tan \phi_r = \frac{\tau_{apparent}}{\sigma_n - u}. \tag{6.2}$$

Equating Equations 6.1 and 6.2 yields,

$$\tau_{app} = \frac{\tau_r(\sigma_n - u)}{\sigma_n}. \tag{6.3}$$

If the total stress conditions at Point C are now considered it can be seen that,

$$\tau_{app} = \sigma_n \tan \phi_{apparent} \tag{6.4}$$

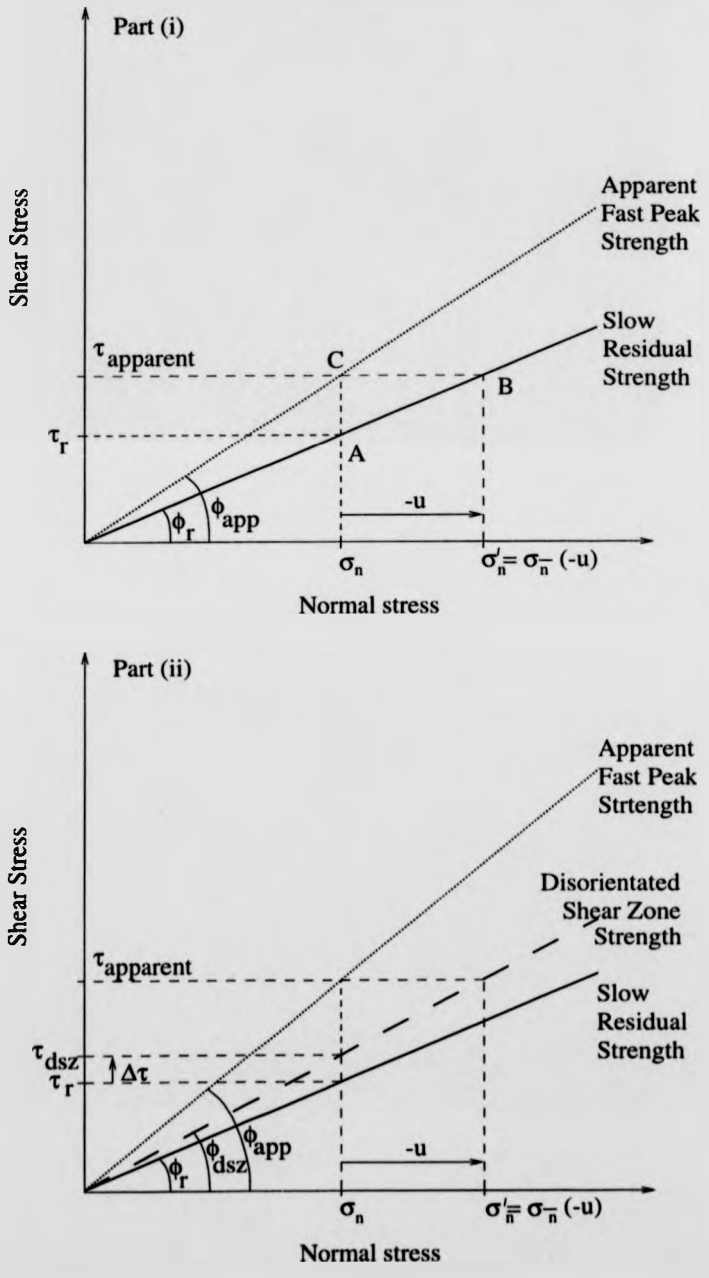

Figure 6.1: Generation of fast peak strength.

and

$$\tau_r = \sigma_n \tan \phi_r. \tag{6.5}$$

Substituting Equations 6.4 and 6.5 into Equation 6.3 yields the solution,

$$\tan \phi_{apparent} = \frac{\tan \phi_r(\sigma_n - u)}{\sigma_n}. \tag{6.6}$$

This solution can then be used to calculate the negative pore water pressures required to generate the observed fast peaks. Where the pore water pressures have been recorded it allows the proportion of the fast peak generated by negative pore water pressures to be found. As an example, consider Test 15 Stage C from which the following data was attained for the fast peak:

Average pore water pressure $u = -11.1kPa$
Slow residual angle $\phi_r = 11.3°$
Total normal stress $\sigma_n = 88.1kPa$
Placing these numbers into Equation 6.6 yields,

$$\tan \phi_{app} = \frac{\tan 11.3°(88.1 + 11.1)}{88.1} = 0.2244996 \tag{6.7}$$

and therefore $\phi_{app} = 12.7°$. In Stage C the recorded fast peak angle was 13.0° suggesting that the main reason for fast peak strengths is negative pore water pressure. Further reliable data from the pore pressure transducer tests is not available, the other data obtained from Tests 14 and 15 on fast peaks does not fit so well, mainly because the fast peaks have not been accurately recorded at a higher rate. The proportion of the fast peak strength which can be attributed to particle disorientation is difficult to measure, but would probably not exceed the ratio of the slow remoulded peak strength to the slow residual strength, the former of which is assumed to correspond to completely random orientation. Slow peak after fast shearing results suggest that disorientation increases with rate and therefore it may become more significant than the previous example. The effect of having a disorientated shear zone strength envelope instead of a residual strength envelope is considered in Figure 6.1 Part (ii),

which illustrates that the effect is an increase in the apparent fast peak envelope. In reality the nature and position of the disorientated shear zone envelope is uncertain and difficult to record.

Finally two further points, the trend observed in Section 5.4.2 and illustrated in Figure 5.13 for fast peaks to decrease with falling clay fraction, adds further evidence to this argument for negative pore water pressures. As the clay content of the soil falls it will become more permeable thus allowing faster rates of pore water flow in the soil. This would reduce the magnitude and duration of any negative pore water pressures as the shear zone dilates, thus reducing the magnitudes of the fast peaks. Secondly, Tika [2] suggested that fast peaks decrease in size with increasing normal stress and, whilst this has not been investigated here, such behaviour would agree with the negative pore water pressure concept. Increased normal stress would reduce sample dilation and therefore decrease generated void space, thus reducing the magnitude of any negative pore pressures.

6.3 Slow Peak Strength After Fast Shearing

Slow peak strengths during the first few millimetres of slow shearing after a fast shearing stage and a pause for consolidation have been noted in most investigations into rate effects. The traditional explanation for this behaviour is that the clay particle orientation parallel to the shear direction associated with slow residual strength, is disturbed by fast shearing. Therefore, when slow shearing recommences a peak above the slow residual strength occurs as a result of the shear zone disruption. This peak falls as the clay particles become realigned by the slow shearing until the slow residual strength is reattained. These ideas were initially presented by Lupini in 1981 [44] and have more recently been reiterated by Tika in 1989 [2] and Tika et al in 1996 [3]. Tika went on to propose that these peaks only occurred in soils with transitional or sliding shear modes and usually within the first 2 mm of shearing. They further proposed that critical fast rates occurred which first caused shear zone disruption and therefore slow peaks. For soils of plasticity index 17-25% they suggested the critical rate was 1 mm/min and for higher plasticity index soils (37-45%) that the critical rate was

10 mm/min to 100 mm/min. They also suggested that rotund particles played a part in the disruption of the shear zone and that to a point increasing rotund particle content increased slow peak strengths.

This research does not conform to the critical rate boundaries proposed by previous researchers, this work has found critical rates increase with falling plasticity. For example, the critical rate for the ball clay (plasticity index 31%) was 1 mm/min compared with the critical rate for the crushed flint (plasticity index 6%) of 10 mm/min to 50 mm/min. The reason for this discrepancy is probably associated with the lack of rotund particles in these tests, few sands were present in any of the tests in Phase 2,3 and 4. The slow peaks observed in these tests were generally smaller than those observed in previous works on rotund plate like particle mixtures, suggesting that Tika et al [3] were correct in their observations. However, disruption to a lesser degree still occurs without the presence of rotund particles. In this case it is logical that higher clay contents and plasticities, and, therefore, proportionally more plate like particles, would lead to higher strengths being developed from particle disruption. This work also noted that slow peaks after fast shearing tended to peak at preceding rates in the region of 300 mm/min, this has not been observed previously and again may be associated with the lack of rotund particles.

Unlike the fast peak strength, the slow peak strength after fast shearing rarely exceeds the slow remoulded peak strength and therefore clay particle disorientation appears to be a valid theory. However by drawing an analogy with other materials this idea seems illogical. In many solid materials the faster you polish them, the shinier the surface becomes and so in the clay soils it would seem reasonable to assume that faster shearing would encourage more particle alignment, thus invalidating many of the ideas surrounding fast rate behaviour. The crucial difference is that the soils are plastic. In solid materials the energy from the polishing (shearing) is dissipated mainly in the form of heat, whereas soils do not tend to heat up as dramatically. It is likely that the energy is dissipated into plastic deformations within the soils and it is these deformations that lead to disruption in the shear zone. As suggested earlier the effect of having a two or three phase soil with rotund particles is also to encourage further deformations. However without rotund particles and over long displacements

at higher rates, it may be theoretically possible for the particles to become partially reorientated. It is reasonable to speculate that this may account for the slight fall in slow peak strength at higher rates observed in this research. Further research would be needed to accurately account for this behaviour.

In conclusion, it has been asserted that the presence of rotund particles play an important role in the behaviour of this slow peak strength. Whilst there is a case for particle alignment to occur at high rates in high clay fraction soils, it has not been substantiated in this research. Therefore, for slow peak strengths after fast shearing the standard ideas relating to the disruption of clay particle orientation by fast shearing would appear to be the mechanism behind the behaviour.

6.4 Positive Rate Effect

Positive rate effects have occurred in virtually every test conducted in this research, whether throughout the tests illustrating positive effect curves or before the critical rate is reached during tests illustrating critical effect curves. Therefore this section contains reports on particle disorientation and viscous effects which are the main mechanisms behind positive rate behaviour. The term *"viscous effects"* which has been used for over a decade without detailed description, is also explored in more detail.

6.4.1 Particle Disorientation

The disruption of particle orientation during fast shearing has previously been discussed in Section 6.3, in which it was found that disruption did occur whether rotund particles were present or not and despite the fact that it could be viewed as illogical. Particle orientation during slow shearing is responsible for the loss of strength from the critical state strength to the residual strength and therefore fast shearing effectively reverses this process causing an increase in strength which is one component of the positive rate effect. The increase in strength is a result of the clay particles no longer sliding over one another on a distinct plane, instead they are partially interlocked generating the increase in strength and a more turbulent form of shearing.

Particle disorientation can not singularly explain positive rate effects because it is likely that the maximum strength available from this mechanism would correspond to the slow peak strengths observed after fast shearing and, in many of the tests, the positive rate effects observed were significantly higher than these slow peaks.

6.4.2 Viscous Effects

The second component of strength increase in the positive rate effect has been termed as a *"viscous effect"* by previous researchers, notably Parathiras [4] and Tika [2]. Tika performed some work using a rotary viscometer to confirm viscous increases in strength, yet little consideration for the theory behind this viscosity has been undertaken. Previous research has attempted to confirm the presence of a viscous component of strength by rapidly reducing fast shearing rates and observing a similar rapid loss of strength. Whilst this investigation has not included such tests, a theoretical proposal relating to viscous effects is now presented.

At this point the disciplines of Geotechnics and Fluid Mechanics meet along a border which appears to be very relevant to rate behaviour. Little research appears to have been conducted in this area which certainly appears to have potential for further work between the two disciplines. The shear zone of a soil would appear to be closely analogous to flow conditions against a boundary in fluid mechanics. The problem is however that most fluid mechanics theories involve Newtonian fluids, which a saturated soil obviously is not. Pursuing this analogy does, however, provide an insight into the viscous effects which occur during fast shearing. Consider Figure 6.2 which illustrates the velocity distribution of a fluid flow against a boundary. The reader should also consider:

- (i) the boundary to represent a soil shear plane,
- (ii) the velocity distribution to represent soil velocities above the plane in what might be termed the shear zone.

Fluid mechanics provides an equation for the shear stress, τ, in the fluid near a wall,

$$\tau = \mu \frac{du}{dy}, \tag{6.8}$$

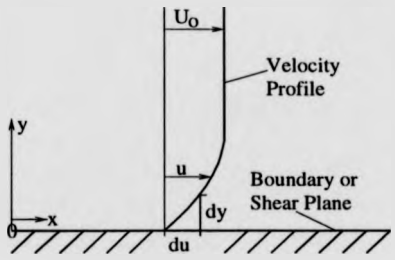

Figure 6.2: Laminar velocity distributions next to a boundary or shear plane

where, μ is the dynamic viscosity, u is the velocity and, y is the distance from the wall. The term du/dy is known as the velocity gradient and has a finite value at the wall. The work of Prandtl [175] in 1905 first established laminar boundary layer theory and then one of his students, Blasius [176], produced a solution for the velocity gradient at the wall, that is when $y = 0$, thus:

$$\left.\frac{du}{dy}\right|_{y=0} = 0.332\frac{U_0^{3/2}}{x^{1/2}\nu^{1/2}} \tag{6.9}$$

where U_0 is the free stream velocity, x is the distance from the start of the boundary and ν is the kinematic viscosity where $\nu = \mu/\rho$ and ρ is the mass density. As x and ν can be considered constant at a given displacement during fast ring shearing, it can be seen from Equation 6.9 that the velocity gradient increases with the free stream velocity (or shear rate). Considering this result in association with Equation 6.8 it is obvious that increasing free stream velocity increases the shear stress at the boundary. Therefore, if the analogy is correct and the flow pattern is laminar this provides the mechanism for a viscous effect generating a positive rate effect.

However another explanation may be possible, consider Figure 6.3 [177] which illustrates the shear stress on a thin plate when a laminar flow breaks down and becomes turbulent. Figure 6.3 illustrates that when the flow becomes turbulent a large increase in shear stress is observed which again could provide the viscous effect. The reason being that if the flow becomes turbulent it is still possible to approximate a velocity gradient close to the wall as shown in Figure 6.4 which has a much higher

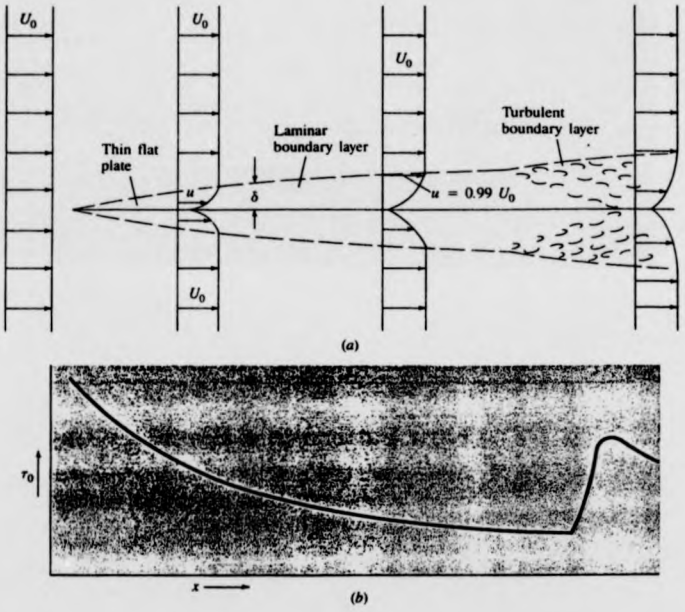

Figure 6.3: Shear stress variation as a function of boundary layer condition, from Roberson and Crowe 1993 [177].

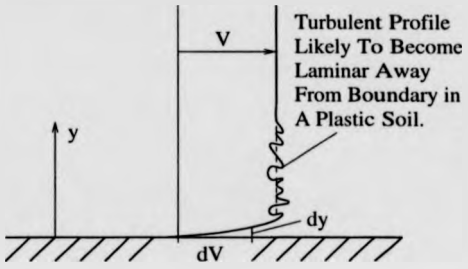

Figure 6.4: Turbulent velocity distribution next to a boundary or shear plane.

magnitude than those illustrated in Figure 6.2.

It appears likely that mechanisms such as these do account for viscous effects, yet it is difficult to assess the comparability of Newtonian fluid flows with what are essentially multi-phase plastic flows. It is possible to speculate that laminar flows occur at slow rates thus encouraging particle orientation and that if the flow degenerates into turbulence at higher rates this disrupts the particle orientation. It is beyond the scope of this research to predict at what speed the laminar-turbulent transition would take place and whether it corresponds to particle disorientation and the onset of slow peaks after fast shearing. The critical velocity would be a function of the geometry of the flow, a rectangular section around an annulus, and the Reynolds number of the flow, which would be difficult to predict for a multi-phase plastic soil.

6.5 Negative Rate Effects

Negative rate effects occurred in all the tests illustrating critical effect curves, but only at shearing speeds above the critical rate. The causes of negative rate behaviour is a contentious issue and is likely to remain so. The reasons for this uncertainty are that a number of different mechanisms may apply in different situations. This section will briefly consider the concept of mechanical fluidization and also the dilation-flow concept proposed by Tika et al [3]. The rest of this section is dedicated to three theories for negative rate effects which this research has found evidence of, these include a pore water pumping effect, shear zone separation and a dilation-contraction

mechanism.

6.5.1 Mechanical Fluidization

The concept of mechanical fluidization results from the early work of Bagnold [115] and further details on this and other previous research is provided in Subsection 2.4.2. The idea of the theory is that as shear rate is increased the nature of shearing changes from continuous particle contacts to a series of brief impacts and when this transition occurs there is a dramatic loss of shear strength. These ideas may account for *"liquefied rock flows"* which are dry and contain particles up to boulder size. However, it is unlikely that this behaviour would occur in this testing on two counts. Firstly the soils used were predominantly cohesive containing mainly clay and silt sized particles, secondly the rates of shearing used would probably not be high enough to achieve the transition from continuous contact to brief impact shearing.

6.5.2 Dilation-Flow Concept

Tika et al in 1996 [3] amassed a quantity of evidence against liquefaction of the shear zone being the cause of negative rate behaviour, see Subsection 2.4.6. Whilst they noted that indirect procedures like dry tests or comparing strength recovery times to consolidation times indicated that positive pore water pressure was the mechanism, facts that have also been observed in this research, attempts to directly measure any large pressures were unsuccessful. They believed, therefore, negative rate effects to be generated by the following procedure:

- (i) dilation of massive particles on fast shearing yielding,
- (ii) an increase in shear zone void ratio and,
- (iii) an increase in shear zone water content,
- (iv) therefore above a critical rate a low strength is attained whilst a steady state of shearing exists,
- (v) this low strength is because of the soils increased ability to flow as a result of points (i) to (iii).

In principal there is no reason why this mechanism should not apply to many shear zones. However, negative rate behaviour has been observed in this testing during Tests 16 and 17 on a pure ball clay containing no massive particles. All negative rate behaviour has been associated with either non-planar shear zones or unusual displacements of the top platen and significant pore water pressures were recorded during Tests 14 and 15 in association with these undulations.

6.5.3 Pore Water Pumping Effect

The ability of undulating shear surfaces to induce negative rate behaviour was first noted by Parathiras [4], who postulated that the undulations had a pumping effect which generated excess pore water pressures reducing effective stress and generating negative behaviour.

Similar behaviour was observed during this testing when undulating shear surfaces were enforced by rigid boundaries. A typical fast stage of shearing using Interface 2 ($4 \times 1mm$ wave-form) is illustrated in Figure 6.5. In this case a dramatic negative rate effect is illustrated and it is accompanied by wavy vertical displacements on the top platen of around 0.1 mm total height and a wavelength identical to that of the waves on the interface (100 mm). The total height of the waves on the interface was 1 mm implying that, as the sample passed over the peaks of the waves it had been compressed or squeezed by 0.9 mm. This is effectively attempting to consolidate the sample and therefore, as the sample is compressed up the slope of the wave-form excess pore water pressures will be generated. This is confirmed during Tests 14 and 15 on the up slope pore pressure transducers during the fast stages illustrated in Figures D.42, D.43, D.45 and D.46. Once the soil has past the wave peak it will commence swelling, allowing the positive pore water pressures to dissipate and possibly inducing negative pore water pressures. However these are unlikely to be as large as the positive pore pressures because the sample cannot be forced to swell unlike when it was compressed. It is likely that the net effect of this around the whole annulus is a positive pore water pressure and, therefore, a fall in effective stress creating a negative rate effect. Unfortunately Tests 14 and 15 were unable to definitely confirm this behaviour conclusively because of the difficulties encountered with the

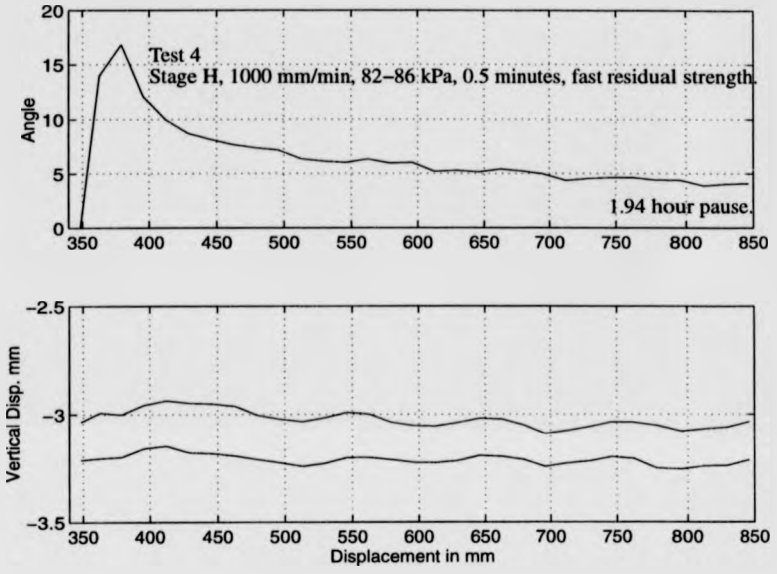

Figure 6.5: Top platen displacements from test 4 (soil on 4x1mm interface).

pore pressure transducers. However, when considering these results and allowing for the offset errors and failed transducers, it is apparent that a net positive pore water pressure is likely. The next question to answer is whether the pore pressures required to account for the losses of strength match those recorded. Again this is open to interpretation due to the incomplete results. Consider Equation 6.10,

$$\tan \phi_{apparent} = \tan \phi_r \frac{\sigma_n - u}{\sigma_n} \tag{6.10}$$

where $\tan \phi_{apparent}$ is the negative rate effect strength in this case and u is the excess pore water pressure. This can then be rearranged in terms of the pore water pressure u, yielding,

$$u = \sigma_n - \sigma_n \frac{\tan \phi_{apparent}}{\tan \phi_r} \tag{6.11}$$

Now studying Stage F (50 mm/min) of Test 14 in Figure D.43, it is difficult to obtain exact values for $\phi_{apparent}$, yet towards the end of the stage it can be assumed to be

of the order of 5°. The average normal stress during Stage F was 79.5 kPa and the preceding slow residual strength in Stage E was 13°. Therefore, substituting these values into Equation 6.11 yields,

$$u = 79.5 - 79.5 \times \frac{\tan 5°}{\tan 13°} = 49kPa. \tag{6.12}$$

Comparing this value, 49 kPa, with the average pore water pressure represented by the circles in Figure D.43, it can be seen that the agreement is poor, with the average pressure being approximately 0 kPa. However, two of the pressure transducers have malfunctioned and only the ones on the up slope (dashed line) and the wave peak (dotted line) are working correctly. Their average value is around 25 kPa, which could account for approximately half of the negative rate effect, however the correct average pressure is uncertain and it may have been lower than 25 kPa if the pressures on the down slope and at the wave trough were known, as these were more likely to be negative. This stage suggests that positive pore water pressures do play a significant role in negative rate behaviour against undulating shear surfaces, but other mechanisms such as the dilation-flow concept may also be in operation.

For a further example consider Stage E ($300mm/min$) of Test 15 in Figure D.46, where the following readings were substituted into Equation 6.11, $\phi_{apparent} = 3°$, $\sigma_n = 84kPa$ and $\phi_r = 9.5°$ yielding an average pore water pressure on the interface of $u = 58kPa$. In Figure D.46 it is apparent that only one pressure transducer was working and therefore the average value means very little. However, the one transducer that was functioning on the wave peak recorded a range of pressures during the fast residual strength from 25 kPa to 100 kPa with an average value which is very close to 58 kPa. This indicates that pore pressures do account for negative rate behaviour.

It is difficult to draw solid conclusions without accurate knowledge of the true average pressure but it is likely that Parathiras' [4] idea on pumping behaviour was correct and that positive pore water pressure reducing the effective stress is a major cause of negative rate behaviour. This is supported further by the indirect evidence provided in Subsections 5.4.4 and 5.4.5. The fact that the time taken for strength to

recover from a negative rate effect is very similar to the time taken for full consolidation indicates that pore pressure dissipation is the mechanism behind the strength recovery. Also, the implication from Figure 5.11 that negative rate behaviour does not occur during decreases in normal stress, may correspond with pore water pressure generation. Any likely compression of the sample thus generating positive pore water pressures will be countered by expansion of the sample under reduced normal stress, the net effect of which may be no pore water pressures and therefore no negative rate effect.

6.5.4 Shear Zone Separation

In the preceding Subsection (6.5.3) it was noted that when a rigid undulating interface was used, a soil could not be forced to swell once it had passed a wave peak. This then indicates that the soil may separate from the interface on the down slope of the undulations. Consider Figure 6.6, which illustrates average data obtained from a series of oedometer tests performed on remoulded kaolin. The graph illustrates the variation of the void ratio, e, with the normal stress (pressure, p) for a loading and unloading sequence where complete primary consolidation or swelling was allowed before changes were made to the normal stress. The hysteresis between the loading and unloading curve represents the soils inability to swell by the same amount that it was previously compressed by. Although during fast shearing complete primary consolidation or swelling is never achieved, this phenomenon explains how and why shear zone separation needs consideration.

As soon as fast rates of shearing are used there is a possibility of developing uneven normal stresses around the annulus and zones of separation on any down slope surfaces. Initially the effect of any separation would appear to be a reduction in the shear force generated by the shear surface and henceforth a negative rate effect. However by considering an extreme example it can be illustrated that this would not necessarily be the case. If this behaviour is considered as the sole mechanism behind negative rate behaviour, pore pressures around the annulus would be zero. Whatsmore if on all the down slopes the soil is separated from the shearing interface, no normal force would be transmitted through these areas. This implies that all the

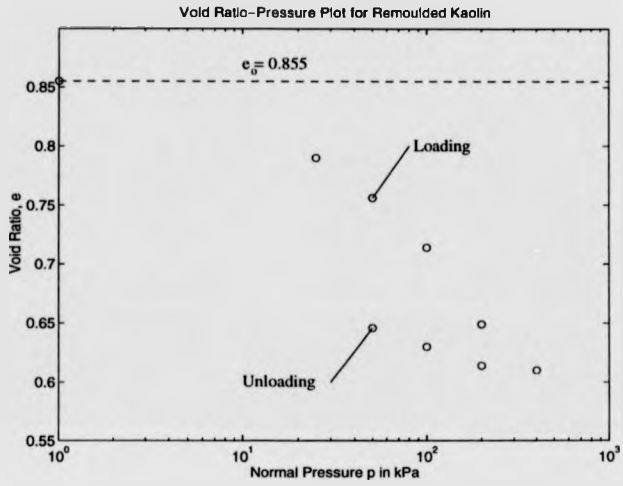

Figure 6.6: An illustration of the differential consolidation/swelling of remoulded kaolin.

normal force would be transmitted through the up slope sections which, as the areas of the up and down slopes are equal, effectively doubles the normal stress on the up slopes. Then assuming a linear failure envelope, this doubles the shear strength on the up slopes generating a shear force identical to that obtained from an even distribution of normal stress on both the up and down slopes. This illustrates that if no pore water pressures exist to transmit a proportion of the normal stress, shear zone separation could not be a mechanism for negative rate behaviour.

Finally the previous discussion makes wide ranging assumptions which imply that the sample is always being compressed in one dimension only. In reality the levels of normal stress and the fast rates of shearing are likely to lead to significant three dimensional deformations in the soil. Therefore it is unlikely that shear zone separation would actually occur, but the deformations are likely to lead to significant variations in normal stress. Finally during testing no direct physical evidence was obtained in support of shear zone separation.

6.5.5 Tilted Shear Zone Concept

During soil on soil testing unusual displacements of the top platen were noted during all shearing stages exhibiting negative rate behaviour. A good example of this is provided in Figure 6.7, representing a fast stage of testing from Test 17 on a pure ball clay. There are many significant differences between this result for a soil on soil test compared with the result shown in Figure 6.5 from a test using Interface 2 ($4 \times 1mm$ wave-from). The observed vertical displacements on Figure 6.5 have a total height of around 0.1 mm and wavelength corresponding to the undulation of the interface. During Test 17 it can be seen from Figure 6.7 that the observed wave-forms had varying total heights, but were generally much larger than in the interface test, at times approaching 0.5 mm. Furthermore, even though there was no interface to control the lengths of the waves, they all have a fixed wavelength of 400 mm which corresponds to the shear displacement at the centre of the soil annulus during one revolution of the IC/NGI apparatus. Such behaviour was always observed to a greater or lesser extent during all stages of soil on soil testing when negative rate behaviour occurred, no such patterns were observed during positive rate behaviour.

One potential mechanism explaining the displacements illustrated in Figure 6.7 is shown in Figure 6.8. The soil annulus contains a plane shear zone which is not horizontal, but is inclined at a significant angle about the axis A-B. The diagrams in Figure 6.8 all assume that no compression or internal deformations occur within the soil, i.e the upper and lower parts of the soil are behaving as separate rigid bodies. However, in reality under a normal stress, the effect of this inclined shear plane is to generate another pumping effect. Consider again Figure 6.8 with vertical movements of the top platen partially restricted by a normal stress, this will have the effect of generating two opposite zones of rapid compression and expansion travelling around the annulus at the rate of shearing. If Figure 6.8 Part(ii) is considered as a snapshot of this behaviour, the zone of compression is on the right hand side and the expansion zone is on the left hand side. As with the undulating interfaces the result of this is the likely generation of positive pore water pressures in the compression zone and negative pore water pressures in the expansion zone. Again the net effect of this

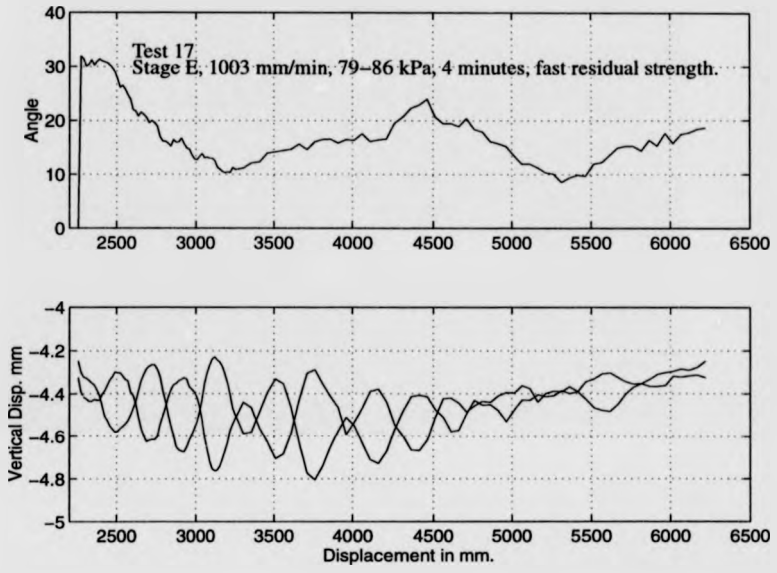

Figure 6.7: Top platen displacements from test 17 (soil on soil).

will be a positive pore water pressure because the negative pressures are likely to be smaller in magnitude because the sample cannot be forced to swell. Therefore, pore water pressure reducing the effective normal stress appears to be the mechanism behind the negative rate effects observed in these soil on soil tests. Furthermore the issue of shear zone separation now reoccurs in the expansion zone, but it is felt that this is unlikely owing to the reasons discussed in Subsection 6.5.4.

In the majority of the tests evidence of the shear plane position, shape and inclination was very difficult to preserve when the apparatus was dismantled. However, an inclined shear surface was noted at the end of Test 21 (soil on soil) with the difference in height across the annulus being of the order of 1 *mm*. Having established how inclined planar surfaces can induce negative rate behaviour, it is now important to study why they develop. It is difficult to imagine what might cause an inclined shear surface in the IC/NGI ring shear apparatus, however, two of the problems discussed in Section 5.2 on testing difficulties , uneven shear load and uneven gap size, may have caused this problem. There is no direct reason why an imbalance in the shear

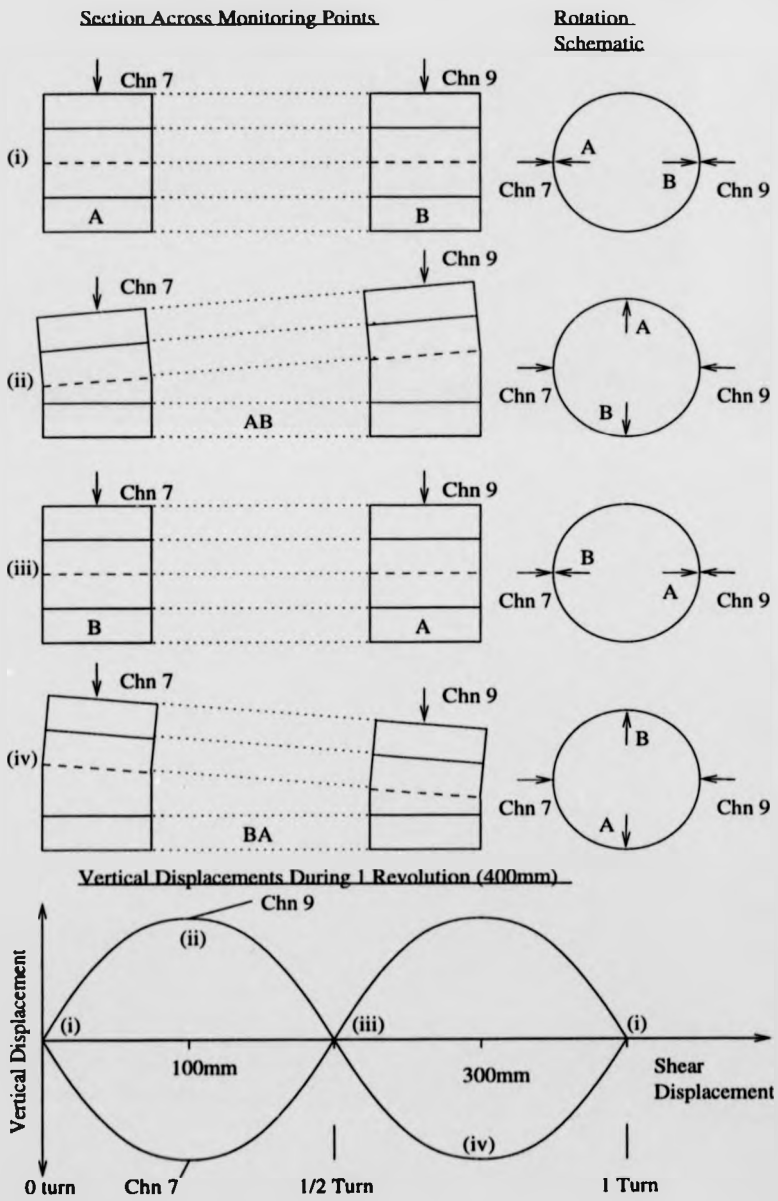

Figure 6.8: The influence of a shear zone inclined about the axis A-B on the displacement of the top platen.

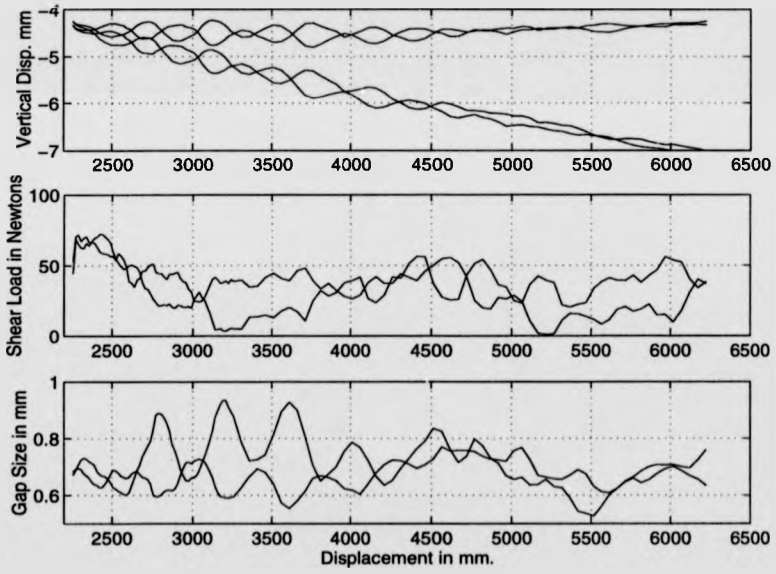

Figure 6.9: Potential causes for the development of an inclined shear surface, an example from Test 17.

load should cause an inclined shear plane but it is intuitive that any imbalance in forces could disrupt the test. A study of the second graph on Figure 6.9 shows that the two recorded shear forces were approximately equal when the wave-forms began, suggesting that uneven shear loads are not responsible for shear plane inclination. It is possible to argue that the biggest difference between the two shear loads occurred when the 'wobbles' were at their largest heights, but it is felt that this is probably a coincidence. Uneven gap size could promote soil loss from one side of a sample thus causing the shear zone to tilt. The third graph on Figure 6.9 illustrates the difference in gap size at two points on opposite sides of the annulus. Again the gap is relatively even when the *"wobbles"* commence, indicating that normal stress distribution and soil loss is likely to be even around the annulus. The fluctuation of the gap size in a similar fashion to the vertical displacements is not surprising as the upper rings are likely to move with the sample because of side friction. Further evidence against uneven gap size leading to uneven soil loss can be found on the first graph of Figure 6.9. This graph illustrates the *"wobbles"* of the top platen before and after soil loss correction. The similar gradients of the two falling levels before soil loss correction illustrates that rates of soil loss were similar on both sides of the sample. Therefore, the reason for the development of an inclined shear surface are unclear, however they are likely to be a function of the IC/NGI apparatus when used at fast rates of shearing. The implications of the inclined surface extend beyond the apparatus, as there is strong evidence that inclined or undulating surfaces will generate net positive pore water pressures, thus inducing negative rate behaviour.

6.5.6 Dilating-Contracting Shear Zone Concept

So far all the potential mechanisms considered for undulation/incline induced negative rate behaviour have assumed that shearing takes place along a very narrow shear plane. In reality it may be more accurate to consider a wider shear zone, especially at faster rates of shearing and this could supply one further mechanism for the generation of the behaviour illustrated in Figure 6.5. In fast testing it has been established that the shear zone dilates and becomes disorientated, however as soon as shearing stops the zone contracts generating positive pore pressures. It might be possible for the

shear zone to attempt to contract during fast shearing as a result of a triggering mechanism which could potentially be variations in the normal or shear stresses. This would then lead to the generation of positive and negative pore water pressures around the annulus and displacements of the top platen similar to those observed in testing. It is unlikely in a virtually pure clay soil such as that used in Test 17 that the degree of dilation and contraction would be large enough to generate wave heights of the order 0.5 *mm*. Whatsmore, it seems unlikely that this mechanism would maintain a constant wavelength of 400 *mm* which was observed during all the tests. Therefore, it is felt that the most likely cause of the negative rate behaviour and oscillation of the top platen observed during soil on soil, testing is the development of net positive pore water pressures developed by the compression of the sample during rotation as a result of the development of a planar but non-horizontal shear surface.

DX
230144
vol.1

DX
230144
vol.2

Fast Shearing Of Cohesive Soils Using Ring Shear Apparatus

Volume Two Of Two

Paul Taylor

Thesis submitted to the University of Warwick
for the degree of Doctor of Philosophy

Department of Engineering
University of Warwick

September 1998

Contents

List of Figures

List of Tables

Chapter 7

Basic Modelling Of The Pumping Effect

7.1 Introduction And Initial Concept

Once the testing using the IC/NGI apparatus began to indicate that undulating shear surfaces and pore water pressures were the likely mechanisms behind the onset of negative rate behaviour, an effort was made to develop a simple model which could predict pore water pressures on an undulating shear surface at different velocities. The main idea behind the model was that if a saturated soil was compressed by a known distance, the change in effective normal stress, $\Delta\sigma'$, could be found from the following relationship:

$$s_c = m_v \Delta\sigma' H, \tag{7.1}$$

where s_c is the compression distance, m_v is the the coefficient of volume compressibility and H is the depth of the sample. By assuming that the change in effective stress is initially accounted for in pore water pressures, it is possible to calculate the pressure generated immediately after the compression. Furthermore using one dimensional consolidation theory, it is possible to find the amount of pressure dissipation after a given time as long as the coefficient of consolidation, c_v, is known. This allowed a technique to be developed where a soil being compressed as it was sheared up a slope could be modelled as a slice of soil moving up a series of short steps. The

slice was assumed to spend a finite amount of time on each step but moved instantaneously from one step to another. Under the instantaneous compression resulting from moving up a step, a pore water pressure, u, was calculated using Equation 7.1 in the form:

$$u = \frac{s_c}{m_v H} \tag{7.2}$$

assuming that initially $u = \Delta\sigma'$. Then during the finite period of time while the soil was assumed to be stationary on the step, this pore water pressure gradually dissipated until the next move up a step occurred. The amount of excess pore water pressure remaining immediately before the next compression was then added to the further excess pore water pressure generated by the compression, giving a new level of pore water pressure which would then start to dissipate. This method was initially tried with hand calculations for an up slope with dimensions identical to those of Interface 2 ($4 \times 1mm$ wave-form), assuming values of m_v and c_v and dividing the slope into 10 steps. This supplied encouraging results and programming commenced to allow the use of many more steps, thus improving the accuracy of the model. The finite period of time spent on each step was calculated according to the slope geometry and the rate of shearing, both of which could be varied in the software. However, before any model results could be compared with IC/NGI tests, values of m_v and c_v were determined for remoulded kaolin and also the problems of down slope sample swelling were addressed.

7.2 Determining m_v And c_v for Remoulded Kaolin

The values of m_v and c_v were determined from standard Oedometer Tests as described in Section 3.4. Three tests were performed on remoulded kaolin and the results of these tests and the calculations of m_v and c_v from these tests are provided in Tables 7.1, 7.2 and 7.3. The test results were compared graphically and showed relatively good agreement and from these plots typical average values of m_v and c_v for remoulded kaolin were obtained, these are provided in Table 7.4 and Figure 7.1.

The swelling values of m_v and c_v are probably open for discussion, they are not standard derivations. The swelling value, $m_{v_{swell}}$ was simply determined by expressing

Table 7.1: Void ratio data for remoulded kaolin.

Oedometer Test Results: Calculation of Voids Ratio, e					
Consolidation Ring Number	Increment Number	Pressure, p in kPa	Settlement ΔH in mm	$\Delta e = \frac{\Delta H}{H_s}$	Void Ratio $e = e_0 - \Delta e$
Ring 3, where:	0	0	0	-	-
$H_s = 10.377$mm	1	25	0.62	0.0597	0.771
$e_0 = 0.831$	2	50	0.96	0.0925	0.738
	3	100	1.36	0.1311	0.700
	4	200	1.84	0.1773	0.654
	5	400	2.41	0.2322	0.599
	6	*200*	*2.38*	*0.2294*	*0.602*
	7	*100*	*2.22*	*0.2139*	*0.617*
	8	*50*	*2.08*	*0.2000*	*0.631*
Ring 6, where:	0	0	0	-	-
$H_s = 10.186$mm	1	25	0.53	0.0520	0.833
$e_0 = 0.885$	2	50	0.86	0.0844	0.801
	3	100	1.30	0.1276	0.757
	4	200	1.75	0.1718	0.713
	5	400	2.33	0.2287	0.656
	6	*200*	*2.27*	*0.2229*	*0.662*
	7	*100*	*2.11*	*0.2071*	*0.678*
	8	*50*	*1.94*	*0.1905*	*0.695*
Ring 8, where:	0	0	0	-	-
$H_s = 9.848$mm	1	25	0.80	0.0812	0.767
$e_0 = 0.848$	2	50	1.16	0.1178	0.730
	3	100	1.60	0.1624	0.686
	4	200	2.13	0.2163	0.632
	5	400	2.70	0.2742	0.574
	6	*200*	*2.66*	*0.2701*	*0.578*
	7	*100*	*2.50*	*0.2539*	*0.594*
	8	*50*	*2.33*	*0.2366*	*0.611*
Italics denote unloading or swelling data					

Table 7.2: Volume compressibility data for remoulded kaolin.

Oedometer Test Results: Calculation of Volume Compressibility, m_v					
Consolidation Ring Number	Increment Number	δe (incremental)	δp in kPa (incremental)	$1 + e_1$	$m_v = \frac{\delta e}{\delta p} \times \frac{1000}{1+e_1}$ in m^2/MN
Ring 3	0	-	-	-	-
	1	0.0597	25	1.831	1.304
	2	0.033	25	1.771	0.745
	3	0.038	50	1.738	0.437
	4	0.046	100	1.700	0.271
	5	0.055	200	1.654	0.166
	6	*-0.003*	*-200*	*1.599*	*0.0094*
	7	*-0.015*	*-100*	*1.602*	*0.0936*
	8	*-0.014*	*-50*	*1.617*	*0.173*
Ring 6	0	-	-	-	-
	1	0.0520	25	1.885	1.103
	2	0.032	25	1.833	0.698
	3	0.044	50	1.801	0.489
	4	0.044	100	1.757	0.250
	5	0.057	200	1.713	0.166
	6	*-0.006*	*-200*	*1.656*	*0.0181*
	7	*-0.016*	*-100*	*1.662*	*0.0963*
	8	*-0.017*	*-50*	*1.678*	*0.2026*
Ring 8	0	-	-	-	-
	1	0.0812	25	1.848	1.758
	2	0.037	25	1.767	0.838
	3	0.044	50	1.730	0.509
	4	0.054	100	1.686	0.320
	5	0.058	200	1.632	0.178
	6	*-0.004*	*-200*	*1.574*	*0.0124*
	7	*-0.016*	*-100*	*1.578*	*0.1020*
	8	*-0.017*	*-50*	*1.594*	*0.2132*
Italics denote unloading or swelling data					

Table 7.3: Coefficient of consolidation data for remoulded kaolin.

Oedometer Test Results: Calculation of the Coefficient of Consolidation, c_v							
Consol. Ring No.	Inc.	$H = H_0 + \Delta H$	$\bar{H} = \frac{H_1+H_2}{2}$ mm	t_{50}* min.	t_{90}* min.	$c_{v50} = \frac{0.026\bar{H}^2}{t_{50}}$ m^2/yr	$c_{v90} = \frac{0.112\bar{H}^2}{t_{90}}$ m^2/yr
Ring 3	0	-	-	-	-	-	-
$H_0 =$	1	18.38	18.69	2.25	6.25	4.037	6.260
19.0mm	2	18.04	18.21	1.50	5.76	5.748	6.461
	3	17.64	17.84	1.00	2.89	8.275	12.334
	4	17.16	17.40	0.74	3.24	10.638	10.466
	5	16.59	16.88	0.40	1.96	18.521	16.282
	6	*16.62*	*16.61*	*0.40*	*1.16*	*17.93*	*26.64*
	7	*16.78*	*16.70*	*0.42*	*1.27*	*17.26*	*24.59*
	8	*16.93*	*16.85*	*1.10*	*3.06*	*6.71*	*10.39*
Ring 6	0	-	-	-	-	-	-
$H_0 =$	1	18.67	18.94	1.60	10.24	5.829	3.924
19.2mm	2	18.34	18.51	1.60	8.41	5.568	4.563
	3	17.90	18.12	1.10	4.00	7.761	9.193
	4	17.25	17.58	0.69	2.56	11.646	13.520
	5	16.87	17.06	0.43	1.69	17.598	19.288
	6	*16.93*	*16.90*	*0.30*	*0.81*	*24.75*	*39.49*
	7	*17.09*	*17.01*	*0.44*	*1.29*	*17.10*	*25.12*
	8	*17.26*	*17.18*	*0.80*	*2.85*	*9.59*	*11.60*
Ring 8	0	-	-	-	-	-	-
$H_0 =$	1	17.40	17.80	2.80	12.96	2.942	2.738
18.2mm	2	17.04	17.22	2.00	6.76	3.855	4.913
	3	16.60	16.82	1.00	4.00	7.356	7.923
	4	16.07	16.34	0.76	2.56	9.134	11.681
	5	15.50	15.79	0.44	1.44	14.723	19.39
	6	*15.54*	*15.52*	*0.34*	*0.90*	*18.41*	*29.97*
	7	*15.70*	*15.62*	*0.65*	*2.33*	*9.76*	*11.73*
	8	*15.87*	*15.79*	*1.20*	*4.10*	*5.40*	*6.81*

Italics denote unloading or swelling data
* Determined using the method outlined in Section 3.4

Table 7.4: Average values of m_v and c_v determined graphically from the oedometer tests.

Effective Normal Stress kPa	m_v m^2/MN	c_v m^2/yr	$m_{v_{swell}}$ m^2/MN	$c_{v_{swell}}$ m^2/yr
0	2.50	3.0	-	-
25	1.38	4.2	-	-
50	0.76	5.4	-	-
100	0.48	7.6	-	-
200	0.28	11.2	-	-
400	0.17	17.8	-	-
200	-	-	0.015	26.20
100	-	-	0.095	17.60
50	-	-	0.200	8.42
0	-	-	1.5	0

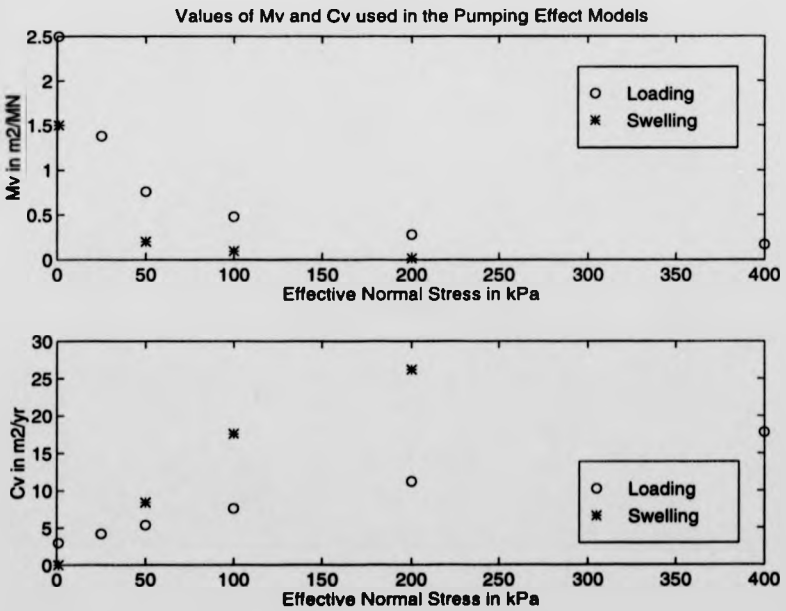

Figure 7.1: Average values of m_v and c_v used in the pumping effect models, determined graphically from the oedometer test results.

the incremental changes in void ratio and pressure as negatives. Values of $c_{v_{swell}}$ were determined by plotting the swelling of the sample against the logarithm and square root of time. This procedure produced two curves which were very similar to the standard consolidation plots used to determine t_{50} and t_{90} and hence $t_{50_{swell}}$ and $t_{90_{swell}}$ were determined in a similar fashion. Two values of c_v were then obtained using the equations shown in Table 7.3 and the average of these values was taken as the value to be used in the models, $c_{v_{swell}}$.

Having now determined the relevant values of volume compressibility and coefficient of consolidation, it is possible to develop a detailed programme. This development is covered in the next section.

7.3 Defining The Slope Geometry

Consider Figures 7.2 and 7.3 which illustrates how a wave-form is defined in all the versions of the program. The model illustrated in Figure 7.3 is very crude and because of the wide step width and large step height would provide inaccurate results. Generally this technique is very basic involving a wide range of assumptions, these will be presented in Subsection 7.4.1. Initially the programs ask for the sample depths, slope length, number of steps, rate of shear and number of wave-forms. They then conduct four preliminary calculations combining the slope geometry and the rate of shearing to determine the height and width of each step, the total time taken to move the soil strip from h_1 to h_2 and the time spent on each step. These are then output to the screen for the users information. Before the main program commences, the user is required to enter the total normal stress on the sample prior to shearing. This provides all the data required to run the model as values of m_v and c_v for remoulded kaolin are stored within the program. The following section, Section 7.4, now discusses the modelling of the up slope shearing involving soil compression and all the assumptions associated with this model.

Figure 7.2: The initial inputs and calculations performed by all of the modelling programs.

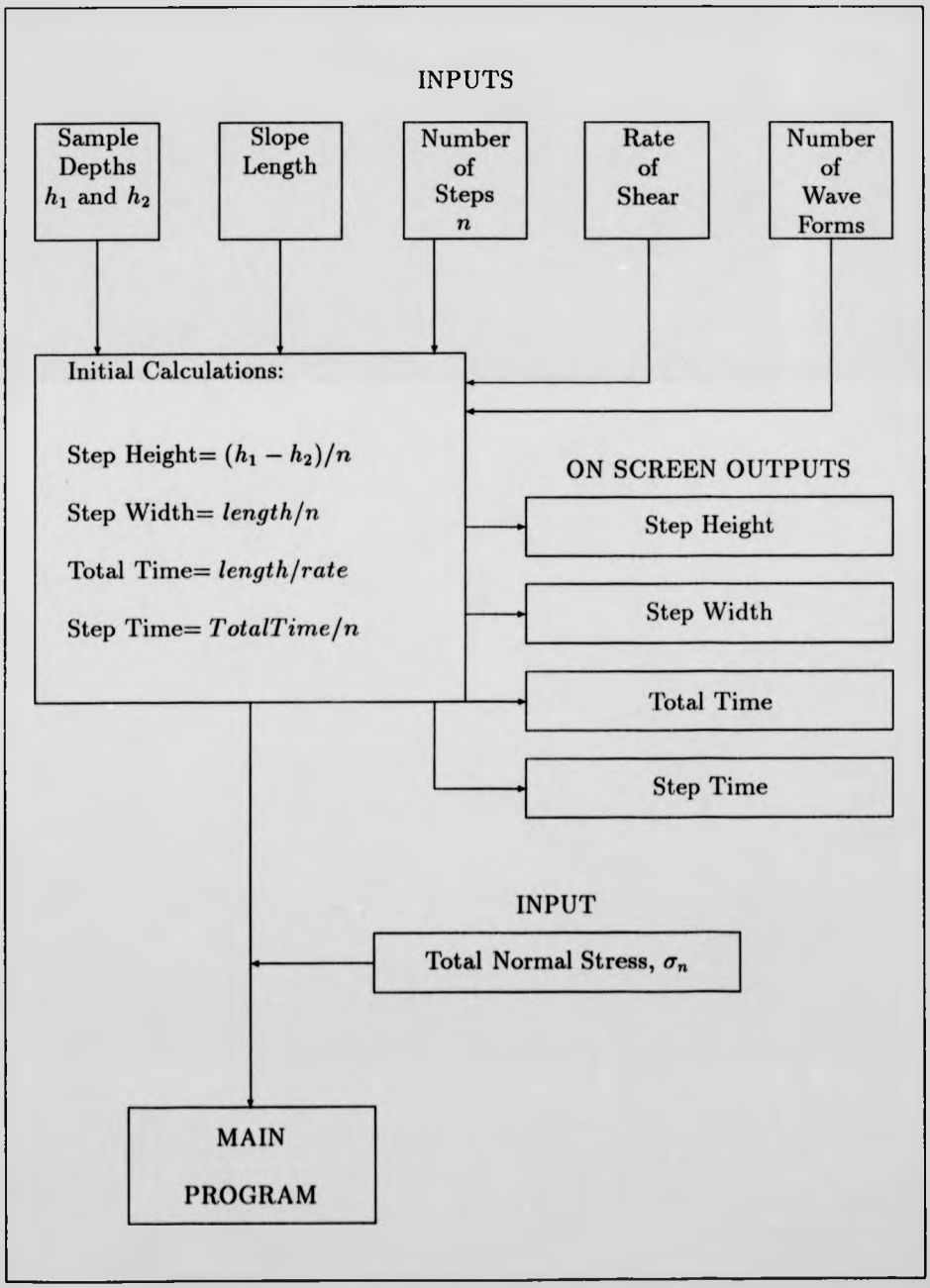

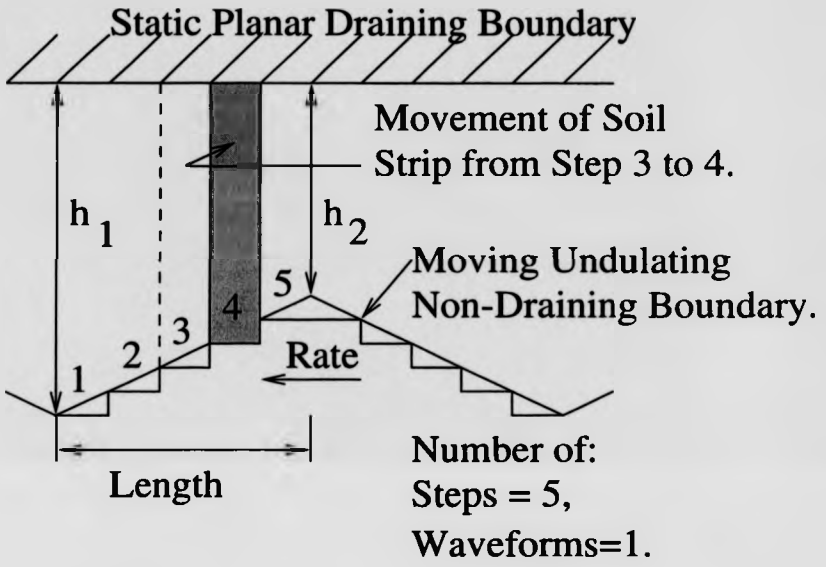

Figure 7.3: Illustrative example of the wave-form model used in the programs.

7.4 Modelling Up Slope Compression

7.4.1 The General Assumptions

As with all models a number of assumptions need to be made. In this case these are wide ranging and obviously make the model somewhat crude. The first major assumption is that the top platen is fixed and therefore the total volume of the sample remains constant. The model is based on Terzaghi's theory of One-Dimensional Consolidation all of the assumptions of his theory apply to this model. These are provided by Craig [178] and are listed here for completeness:

- 1. The soil is homogeneous.
- 2. The soil is fully saturated.
- 3. The solid particles and water are incompressible.
- 4. Compression and flow are one-dimensional (vertical).

- 5. Strains are small
- 6. Darcy's law is valid at all hydraulic gradients.
- 7. The coefficient of permeability and the coefficient of volume compressibility remain constant throughout the process.
- 8. There is a unique relationship, independent of time, between void ratio and effective stress.

Whilst Craig [178] discusses some problems with assumptions 6, 7 and 8, the main problems in relation to this model occur with assumptions 4 and 5. To conform with assumption 4, the model focuses on one strip of soil that is only compressed or swelled vertically. The strip is considered to be a single isolated unit that is unconfined laterally but will not deform in this direction. Furthermore, there are no inter-strip forces between this strip and the surrounding soil and no shear forces or dilation as a result of the instantaneous movements from one step to the next. This is obviously unrealistic as the soil in the ring shear apparatus or indeed in the field is likely to be under going plastic flow with three dimensional effects subjected to significant shear forces. However, as stated previously, the model is crude and is only intended to give an indication of the likely pore pressure distribution on inclined surfaces during fast shearing. Assumption 5, regarding small strains, is open to interpretation. If the user selects a sensible number of steps for the slope geometry the strain resulting from a one step compression will be small, however total strains from h_1 to h_2 are dependent on the slope geometry and the net effect may be that large strains will occur. As long as the results of the models are only used to give a general indication of the likely variation in pore pressure and are not used to determine accurate values, the influence of the assumptions is reasonable.

7.4.2 The Model

The flow chart representing the modelling of the up slope compression of the soil strip is provided in Figure 7.4. The names of the variables used in the flow chart are similar to those in the actual programs provided in Appendix B, however some

Figure 7.4: The modelling of the up slope consolidation performed by all three versions of the software.

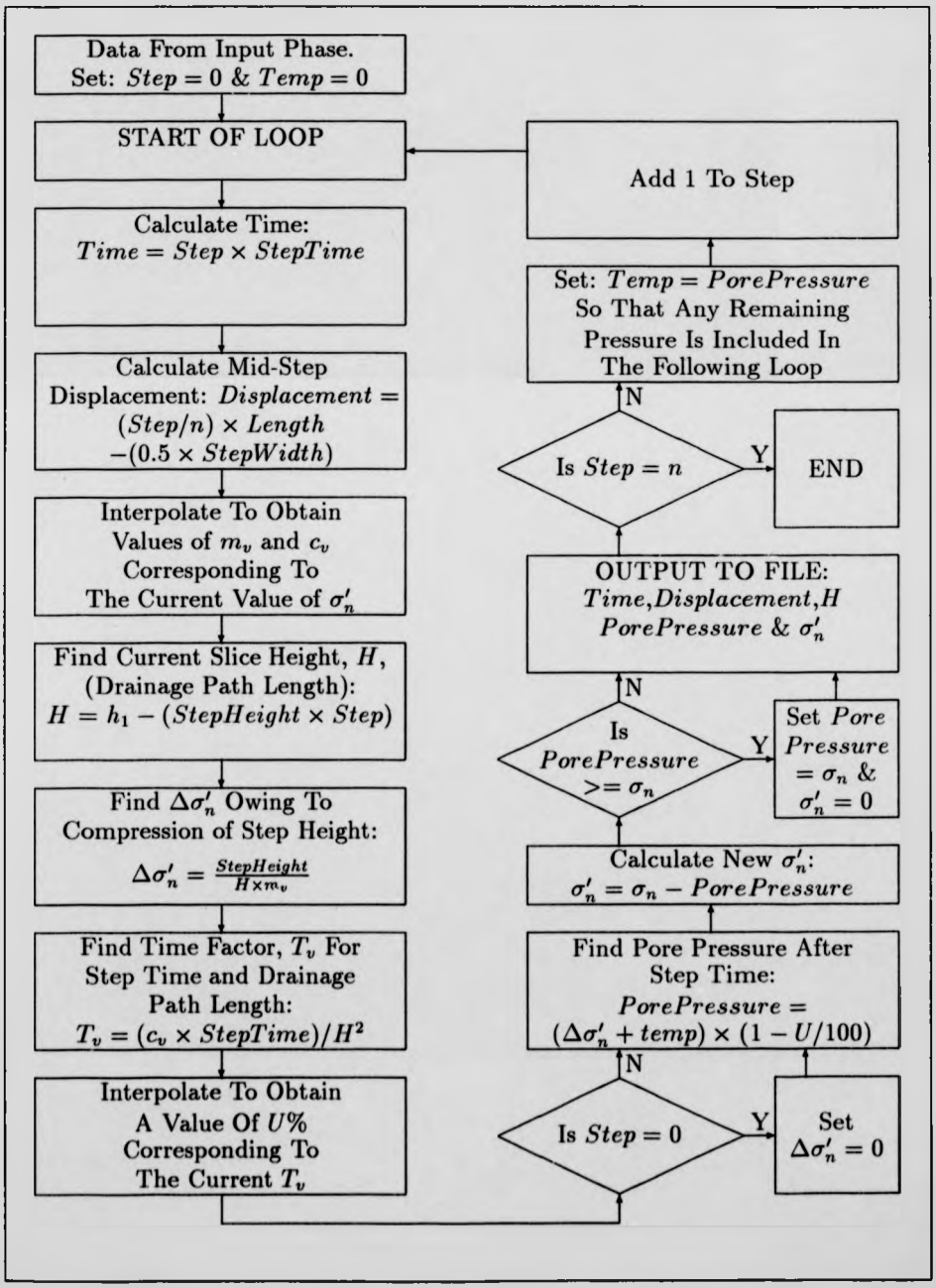

symbols have been used in the flow chart for the sake of brevity. This loop structure is used in all three versions of the software to model the pore pressures generated by the compression of the soil strip up the slope.

Initially the data obtained from the input phase of the programs as illustrated in Figure 7.2 is available at the start of the loop. Before the loop runs the step number and the temporary value for storing remaining pore pressure are also set to zero. The first stages in the loop involve the calculation of the time immediately before the next compression and the horizontal displacement at the middle of the step. This is followed by a subroutine which interpolates values of m_v and c_v corresponding to the current level of the effective normal stress which on the first loop equals the normal stress. The interpolation takes place between the points illustrated by the circles in Figure 7.1. The next stage involves calculating the current height of the strip corresponding to the current step number. Once this is obtained the change in the effective stress due to the compression by the step height for the current strip height and m_v value is calculated from Equation 7.1. This change in effective normal stress is now assumed to be supported totally by pore water pressure, which then equals this increase in stress. Having generated an excess pore water pressure, the amount it dissipates during the time the strip is stationary on one step needs to be calculated. The first stage of this is to calculate the time factor T_v where,

$$T_v = \frac{c_v t}{d^2} \tag{7.3}$$

In this case t is equal to the step time and the length of the drainage path d corresponds to the height of the strip for this single drainage case. Knowing T_v it is then possible to interpolate a value of $U\%$, that is the percentage of pore water pressure that will have dissipated whilst the strip was on one step. The next stage is a decision box which sets the change in effective stress to zero on the first loop when the step number is zero. This prevents pore water generation on the first loop, that is before the soil strip is compressed. The level of the pore water pressure instantly before the next compression is then calculated by adding any remaining pore pressure from the previous step to the change in effective normal stress due to the compression

(further increase in pore pressure) and then reducing this value by $U\%$. This really completes the calculation giving a pore pressure at a given horizontal displacement or time. However before the data can be output a check is required to see if the equations have generated a pore pressure greater than the normal stress, that is, to see if the soil has liquefied. If it has, then the pore pressure is equated to the total normal stress and henceforth the effective normal stress becomes zero. This prevents the generation of negative effective stresses. Now the information is output into five separate columns in a file called "conoutdat" which then contains the current time, the horizontal displacement, the strip height, the current pore pressure and the current effective normal stress. The next stage is to see if the top of the slope has been reached by checking to see if the step number equals the total number of steps. If it does, the loop is interrupted and the up slope consolidation is complete. If the step number is less than total number of steps, the loop continues. At this point the pore pressure is equated to a temporary value so that it can be added to the additional pore pressure which will be generated by the next compression in the following loop. The final stage is to add one to the step number which effectively triggers the next loop and compresses the soil to a new strip height.

7.5 Modelling Down Slope Expansion

Modelling down slope expansion is a more difficult proposition using this technique. Whilst it was possible to force the sample to compress during the up slope phase, the strip cannot be forced to expand on the down slope phase. This has lead to the development of three different programs each using a different technique and involving different assumptions. None of these programs are ideal, their relative merits will be discussed later.

7.5.1 The Free Swell Model

The free swell model assumes that Terzaghi's theory of one dimensional consolidation applies equally to swelling as it does to consolidation and therefore all the assumptions made in Subsection 7.4.1 still apply. The sample is allowed to swell resulting in pore

pressure dissipation but is not forced to stay in contact with the wave-form. This leads to three problems. One is that the sample is still assumed to be under an effective normal stress even though once separation has occurred there is no support to transmit this stress, secondly all pore pressure dissipation is associated with sample expansion not drainage and thirdly the sample does not stay in contact with the wave-form. Therefore, when the up and down slope models are looped together the soil would not start to compress at the bottom of the up slope because of the separation on the previous down slope. To avoid this, at the bottom of every down slope the height of the soil strip is set to equal h_1 without changing the pore pressure regime and therefore the normal effective stress.

The modelling of this swelling process is performed in another loop structure which is illustrated in Figure 7.5. This loop follows the data input phase of the program and the modelling of the up slope consolidation process and all the data from these phases is available at the start of the loop. The important values which are transferred from the up slope loop to the down slope loop are *Temp*, which is the current pore water pressure at the wave peak, H the strip height and σ'_n the current effective stress on the soil strip.

Although the soil strip is no longer forced to contact the wave-form it is still analysed using the strip method. The strip is displaced horizontally by a strip width after each step time period. Therefore the initial calculations for *Time* and *Displacement* are identical to those on the consolidation loop. The next stage is to interpolate values of $m_{v,swell}$ and $c_{v,swell}$ corresponding to the current effective normal stress, this is done using an interpolation subroutine containing the data illustrated by the stars in Figure 7.1. At this point the similarity between the up slope consolidation loop and the down slope swelling loop ends. In the swelling loop the pore pressure dissipation during the step time is now calculated, firstly by determining the value of T_v using Equation 7.3 and then using a subroutine to interpolate a new value for $U\%$. Having found $U\%$ it is then possible to calculate the level of pore pressure after the soil strip has remained static for the *StepTime* period. This pore pressure is found by reducing the temp value from the previous loop by $U\%$. It is now possible to equate the change in the pore water pressure to a change in effective normal stress $\Delta\sigma'_n$ which now has

Figure 7.5: The free swell modelling of the down slope expansion.

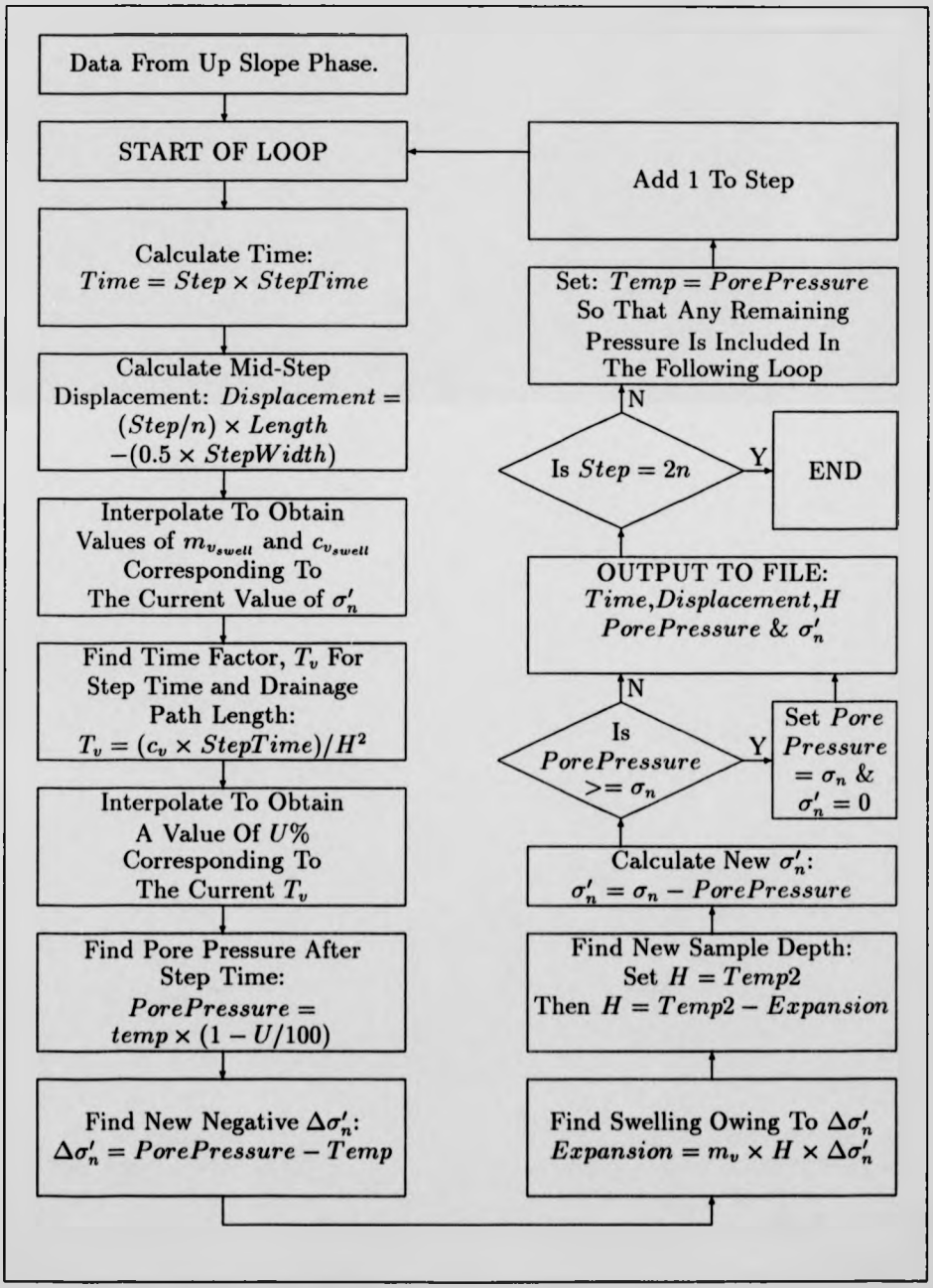

a negative value. The next stage is to calculate the expansion of the sample due to this change in effective stress. Unlike the first loop this involves a major problem, the pore pressure dissipation owing to single drainage has been calculated, but it will now be assumed that the dissipation of the pore pressure is due to sample expansion. This poses major questions for the validity of this model, but appears to be one way round the problem of modelling the swelling. Henceforth the expansion of the sample is calculated from the drop in effective normal stress, the volume compressibility and the strip height using Equation 7.1. Once the expansion is known the new strip height is calculated as is the new effective normal stress as a result of the pore pressure distribution. As with the up slope loop a check is then applied for liquefaction so that the pore pressure is not greater than the total normal stress and henceforth the effective normal stress is always positive. The same results as the up slope loop are then output to file "conoutdat". The next stage is to check whether the bottom of the slope has been reached and this is performed by checking whether or not the step number has reached $2n$ or multiples of $2n$ if multiple wave-forms are being studied. The final stage is to set the pore pressure to the temporary value to be incorporated in to the next loop and to add one to the step number.

These flow charts are designed to be studied for one wave-form, there is some difference in the actual step commands in the programs in Appendix B because the up slope and down slope loops were nested in another loop which controlled the total number of wave-forms to be analysed. Hence, in the actual programs the step number is a function of the total steps on an up slope n and the total number of wave-forms *wave*, this has not been included on these charts for the sake of clarity.

7.5.2 The Forced Swell Model

The forced swell model involves making the soil strip stay in contact with the wave-form. The method used to model this is illustrated in Figure 7.6 and is virtually identical to the up slope consolidation model. The difference being that the change in the effective stress due to the sample expansion is negative and this is equated to a negative pore pressure which gradually dissipates as drainage occurs. Two versions of the software exist using the forced swell model. The difference between the two

Figure 7.6: The modelling of the down slope consolidation by forced swelling.

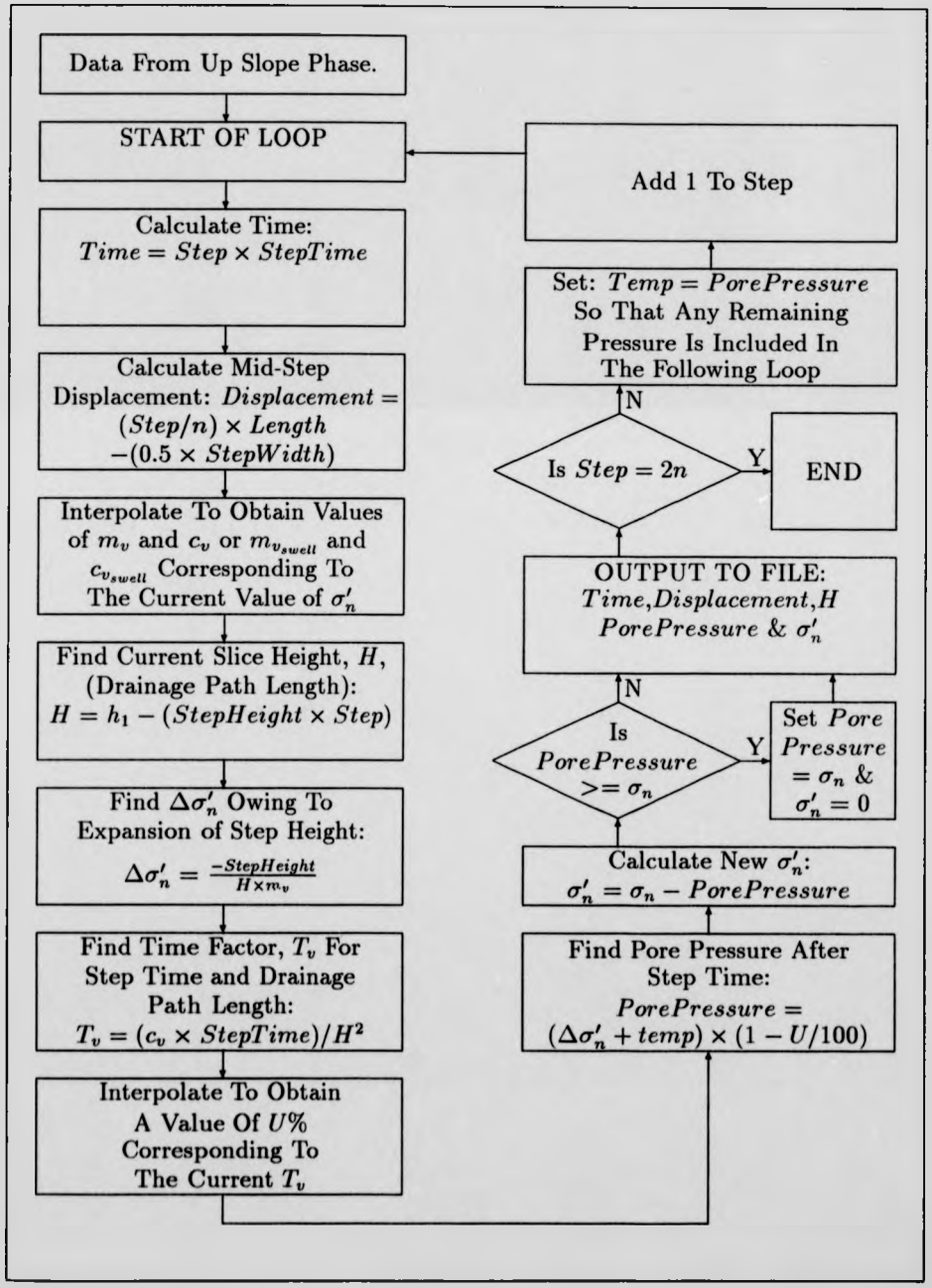

concerns the values of volume compressibility and the coefficients of consolidation. In one version, possibly the theoretically more accurate version, the values $m_{v_{swell}}$ and $c_{v_{swell}}$ are used. This, however, caused the program to generate very large negative pore water pressures which were obviously unrealistic, these will be illustrated presently. A second version was developed which reduced the magnitude of the pore pressures by using the compression values of m_v and c_v, to provide more realistic values. A comparison between all three versions of the software will be made in the next section. The forced swell versions of the model also include the assumption that pore water pressure dissipation owing to single drainage can be equated to swelling, again posing major problems for the validity of the model, but providing one solution to a difficult problem.

7.6 Model Results

The aim of this section is to present results obtained from the three different versions of the program,

- v1.0 The Free Swell Model (using $c_{v_{swell}}$ and $m_{v_{swell}}$)
- v2.0 The Forced Swell Model (using $c_{v_{swell}}$ and $m_{v_{swell}}$)
- v3.0 The Forced Swell Model (using c_v and m_v)

Initially the minimum number of steps required to converge on a steady value is determined. A comparison is made between the three models and their likely agreement with actual behaviour is discussed. Finally in this section an assessment of the influence of shear rate, wave height and sample depth is made using the best model.

7.6.1 Investigating the Number of Steps

Because all three versions of the software operate on identical principles for up slope consolidation and similar principles for down slope swelling, it is reasonable to assume that the influence of the number of steps will be the same in each model therefore for this investigation v1.0 The Free Swell Model will be used. The majority of these

investigations will focus on the wave-form on Interface 2 ($4 \times 1mm$ wave-form) as the widest range of test results are available for this interface. To investigate the number of steps the following wave geometry, shear rate and stress level were defined as constants:

Initial Sample Depth, $h_1 = 9mm$
Final Sample Depth, $h_2 = 8mm$
Horizontal Slope Length, $Length = 50mm$
Number of Wave-Forms, $Wave = 4$
Number of Steps, $n = Variable$
Rate of Shearing, $Rate = 50mm/min$
Total Normal Stress, $\sigma_n = 100l\ Pa$.

These values represent one revolution of shearing with Interface 2 ($4 \times 1mm$) wave-form) in the IC/NGI apparatus before any major soil loss has occurred. It should be noted that all three versions of the model are essentially one-dimensional because of their founding in Terzaghi's theory. Therefore whilst a second dimension is introduced in terms of horizontal displacement the model does not account for the three-dimensional annular shape of the sample in the IC/NGI apparatus.

Running this simulation in v1.0 for a variety of different numbers of steps produces the results illustrated in Figure 7.7. Part 1 of the figure illustrates that the number of steps selected does affect both the shape and positioning of the pore pressure curves. Ideally the analysis would be carried out with an infinite number of steps yet this is obviously not possible, but the results shown in Figure 7.7 suggest that as the number of steps increased the results tend to converge to a fixed level. Whilst this ideal level is not well defined by the use of 10 steps, Part 2 of Figure 7.7 suggests that using 50 or 100 steps provides a good approximation when compared with the levels obtained using 3000 steps. Indeed the range of maximum pressure differences between 50 and 3000 steps is less than $2\ l\ Pa$. Therefore when the crudeness of the model is considered the use of 100 steps appears reasonable, thus providing useful results without excessive quantities of data.

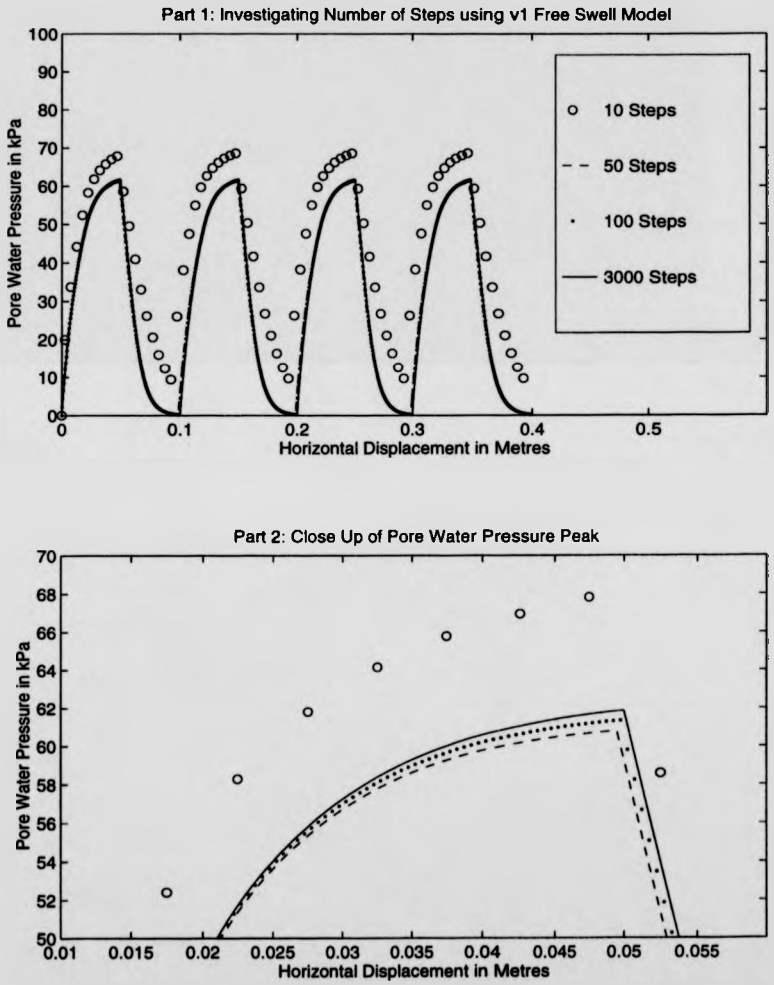

Figure 7.7: The influence of the number of steps on the calculated pore water pressure for a constant set of variables using v1.0 the free swell model.

Always using 100 steps as general value may not be justifiable. It would seem reasonable to create a criterion to ensure relatively accurate results based on either the shear rate or the wavelength. With regard to shear rate; this would involve defining a minimum step time. The problem with this would be that as the rate of shearing was increased the total time for one wavelength would decrease and so would the number of steps required to meet the step time criterion. For example, for 100 steps in the previous example the step time was 0.01 minutes, applying this criterion to the general case yields:

$$n \geq \frac{Length}{0.01 \times Rate} \tag{7.4}$$

where n is the number of steps. Then if the wavelength remained the same (0.05 m) but the rate was increased to 1 m/min this would yield a value of $n = 5$ which is obviously far too low. This criterion may be of use at really slow rates of shear, but as these programs are focused on fast shearing this concept will be rejected. Applying the criterion to the wavelength is a more reasonable option. If the step width is confined to be less than or equal to that in the above case for 100 steps, i.e. $StepWidth = 5 \times 10^{-4}$m the following criterion can then be generated:

$$n \geq \frac{Length}{5 \times 10^{-4}} \tag{7.5}$$

This provides a criterion independent of shear rate and purely dependent on the wavelength, whilst it may be desirable to develop a criterion allowing for the rate of shearing, Criterion 7.5 will be used in the rest of this study as it appears to be appropriate.

7.6.2 Comparing The Three Versions Of The Model

This section provides a brief review of the results available from the three versions of the software and assesses which one is likely to be most realistic.

Figures 7.8 and 7.9 illustrate the variation in pore water pressure and sample height at two different rates given the following data:

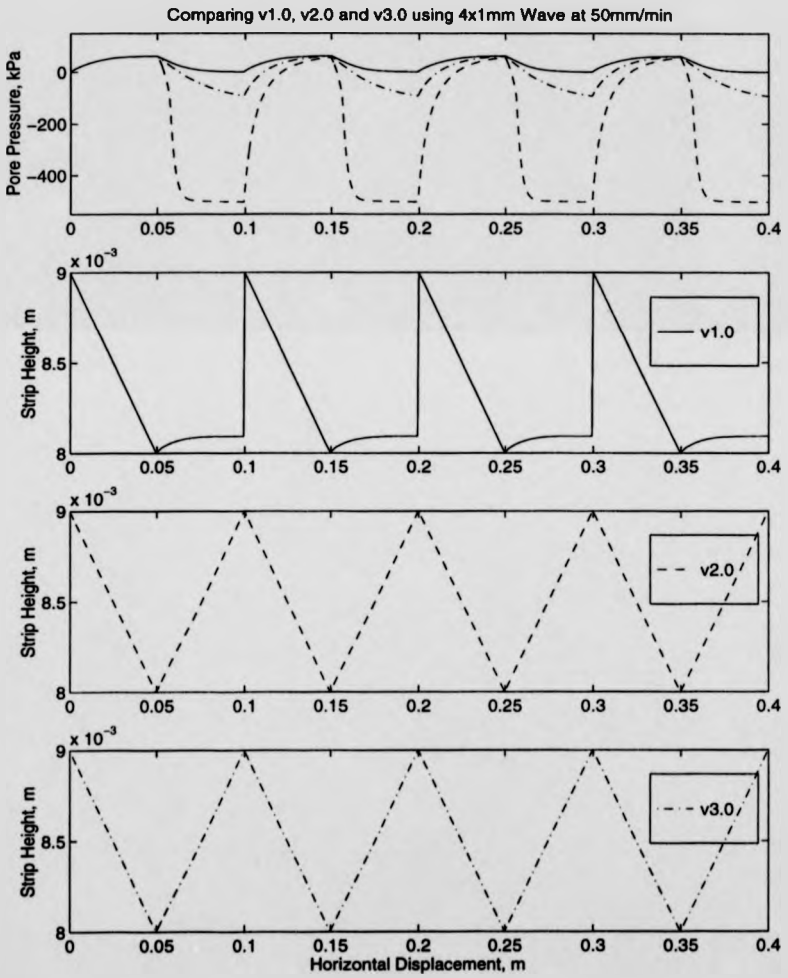

Figure 7.8: Comparison between the three versions of the model using a $4 \times 1mm$ wave-form at $50mm/min$.

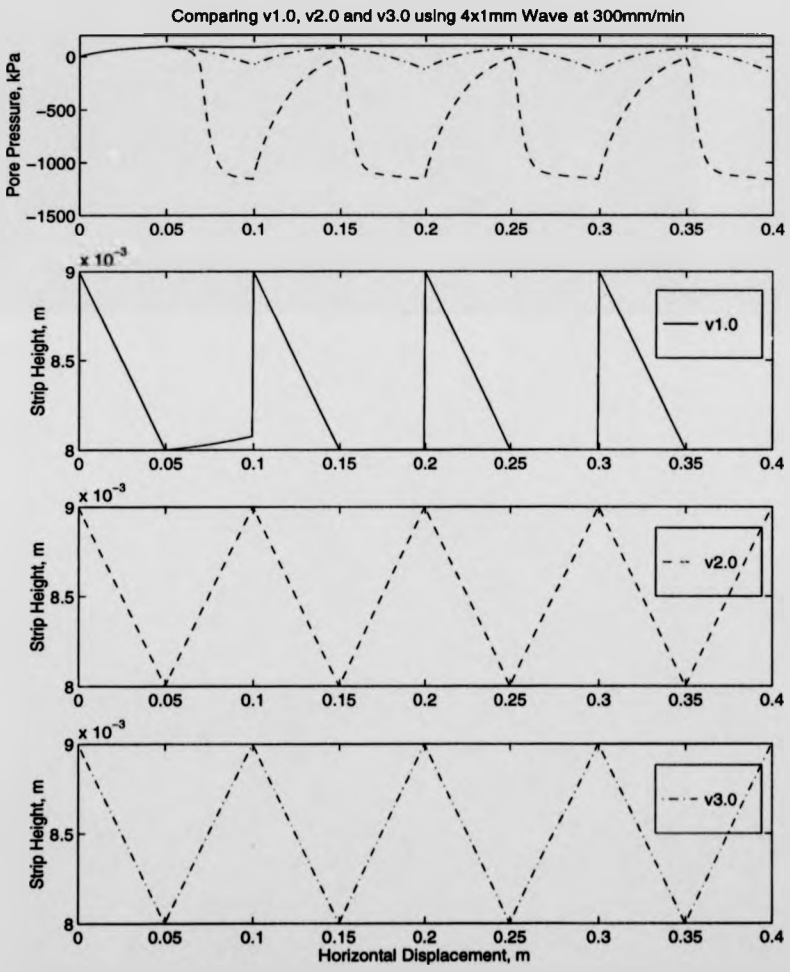

Figure 7.9: Comparison between the three versions of the model using a $4 \times 1mm$ wave-form at $300mm/min$.

Initial Sample Depth, $h_1 = 9mm$

Final Sample Depth, $h_2 = 8mm$

Horizontal Slope Length, $Length = 50mm$

Number of Wave-Forms, $Wave = 4$

Number of Steps, $n = 100$, from Equation 7.5

Rate of Shearing, $Rate = 50mm/min$ and $Rate = 300mm/min$

Total Normal Stress, $\sigma_n = 100l\ Pa$.

The first thing to note from Figures 7.8 and 7.9 is that all the versions of the software produce identical results during the first up slope compression phase, which provides evidence that they are all functioning correctly. The up slope compression phase is probably the most accurate section of the program; the theory and the model results combine well to generate what appears to be reasonable pore pressure distributions on the up slope. Figures 7.8 and 7.9 illustrate that the magnitudes of these pore pressures do increase with rate of shearing and this effect will be discussed in more detail in Subsection 7.6.3.

Secondly, v2.0 of the model generates very large negative pore water pressures on the down slope expansion phases and this is obviously in disagreement with observed test results. The result of these pressures, down to -500 $l\ Pa$ at 50 mm/min and -1200 $l\ Pa$ at 300 mm/min, would be very large increases in effective normal stress and therefore permanent positive rate behaviour at a magnitude significantly higher than that observed. V2.0 is based on the assumption that the sample stays in contact with the interface and uses swelling values $m_{v_{swell}}$ and $c_{v_{swell}}$ to calculate the pore pressures. The use of $m_{v_{swell}}$ and $c_{v_{swell}}$ is theoretically correct and therefore this questions the assumptions made in the model regarding the sample staying in contact with the wave-form and the pressure dissipation by drainage being accounted for by sample expansion. In reality the sample is likely to stay in contact with the wave-form probably because of internal three dimensional plastic deformations, not because of the swelling of the sample. Assuming the sample stays in contact using the one-dimensional model generates results which probably do not accurately represent real tests.

Because of the large negative pressures generated by v2.0, v3.0 was developed which used the standard values of m_v and c_v in the analysis. This version still assumes that the sample stays in contact with the wave-form despite the conclusions drawn in the previous paragraph. This is why this model has little theoretical founding and can only be described as an attempt to generate reasonable behaviour from the model. The results illustrated in Figures 7.8 and 7.9 do appear more reasonable than those obtained from v2.0. However, the net effect of the pressure distribution would be a negative pore water pressure, again resulting in increases in the effective normal stress and therefore positive rate behaviour.

Whilst there are still problems associated with using a one dimensional model on a three dimensional test, the best solution is provided by v1.0 The Free Swell Model. The assumptions and limitations of this model are discussed in Subsection 7.5.1 and whilst some of these have serious implications for the validity of the model, it is felt that when used in conjunction with values of $m_{v_{swell}}$ and $c_{v_{swell}}$ the results obtained are probably the closest to the actual behaviour. The free swell model allows the sample to separate from the wave-form and this is clearly illustrated on the second plot of Figure 7.8 at displacements corresponding to the down slopes. However because this is not likely in reality at the end of the down slope the soil strip is instantly expanded back to its maximum height. This maintains the geometric integrity of the model, whilst changes in stress associated with this instant expansion are neglected. The net pore pressure effects observed with v1.0 are generally positive and therefore, this provides a model which actual test results illustrating negative behaviour can be compared to. Therefore despite of the assumptions, v1.0, The Free Swell Model, will be used in the rest of this chapter, but it is important to remember the crudeness and likely inaccuracies of the model.

7.6.3 Investigating Rate With v1.0 The Free Swell Model

If positive pore water pressures are the mechanism behind the generation of negative rate effects, it would be expected that the magnitude of these pressures would increase with rate of shearing. The following data was used in v1.0 of the software:

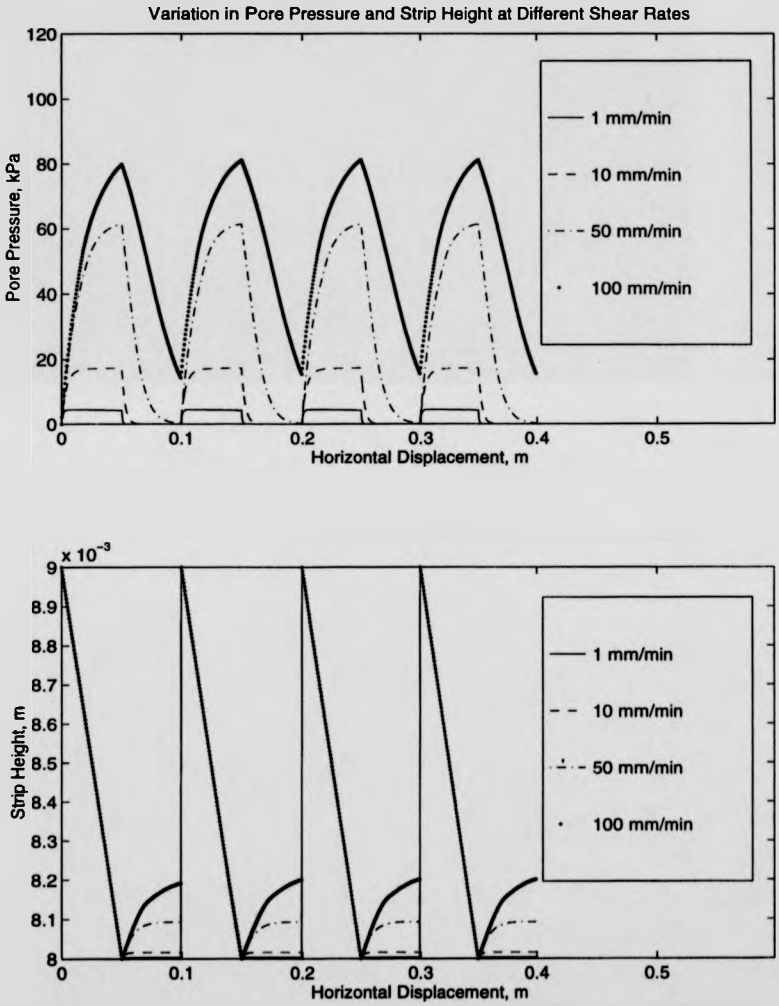

Figure 7.10: The variation in pore pressure and strip height according to v1.0 the free swell model at rates from 1 mm/min to 100 mm/min.

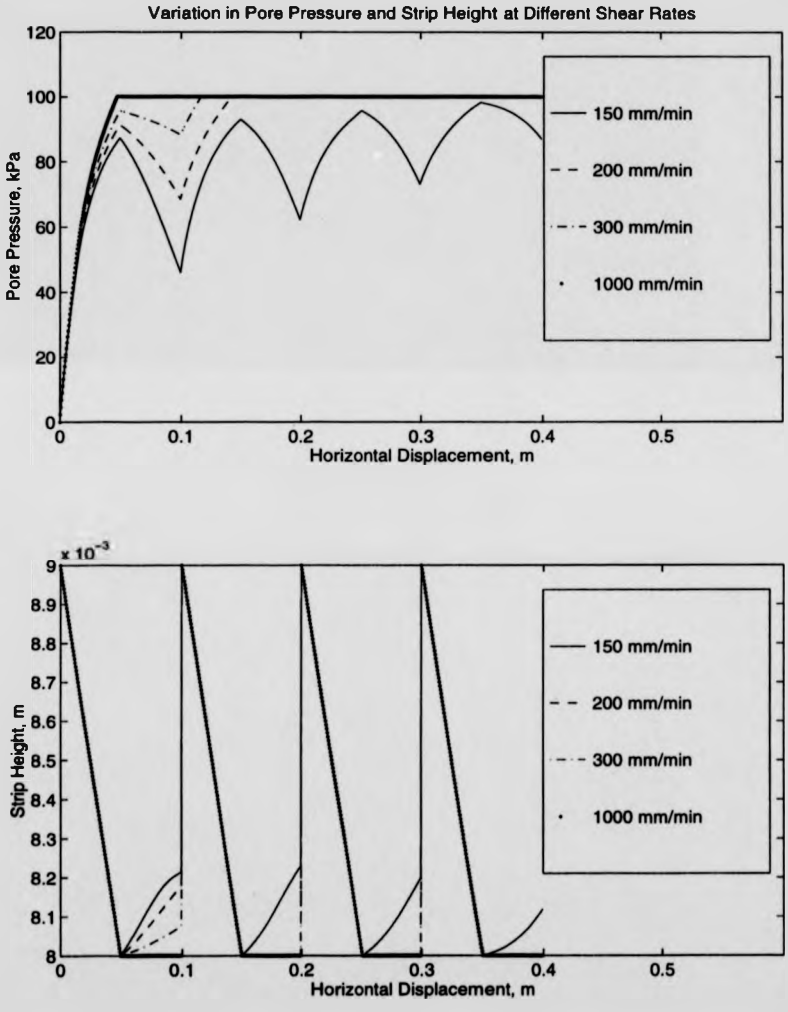

Figure 7.11: The variation in pore pressure and strip height according to v1.0 the free swell model at rates from 150 mm/min to 1000 mm/min.

Initial Sample Depth, $h_1 = 9mm$
Final Sample Depth, $h_2 = 8mm$
Horizontal Slope Length, $Length = 50mm$
Number of Wave-Forms, $Wave = 4$
Number of Steps, $n = 100$, from Equation 7.5
Rate of Shearing, $Rate = Variable$
Total Normal Stress, $\sigma_n = 100l\ Pa$.

A study of Figure 7.10 reveals that the net pore water pressures generated by v1.0 are indeed positive. The pressures vary in a cyclic nature corresponding to the compression and expansion due to the wave-form. The magnitude of the pore pressures increase with rate of shearing, as would be expected. This is not because higher pressures are initially generated from faster compression but because the time factor, T_v, is reduced by the faster shearing. This reduces the amount of pore pressure dissipation and therefore the higher pore pressures accumulate during fast shearing. This could be expressed more simply by stating that at faster rates there is less time for the sample to drain. Figure 7.10 illustrates that at rates up to 50 mm/min the shearing is slow enough to allow full pore pressure dissipation, therefore the wave pattern repeats at a constant level between zero pressure and the peak pressure obtained at a given rate.

The sample swelling actually increases with rate of shearing up to a rate of 100 mm/min; this is perhaps surprising, but these rates are low enough to allow most of the pore water pressure to be dissipated by swelling. This is probably not an accurate representation of swelling, because one might expect the maximum swelling to occur at the slowest rate where there is time for full expansion to occur. However the plots in Figure 7.10 suggest that at rates up to 50 mm/min full swelling does occur. This discrepancy is associated with the assumptions made in Subsection 7.5.1.

At rates above 50 mm/min a slightly different type of behaviour is occurring, there is not enough time to allow full pore water pressure dissipation and therefore once one wave cycle is complete pore pressures start to accumulate from a level above zero pressure. In Figure 7.10, it is illustrated that at 100 mm/min this level is around

18 *l Pa*. It is barely perceptible but the level of the pressure peaks and troughs is creeping up slowly. If the same wave-form is repeated for 20 cycles, the pressure peaks and troughs level to two constant values at approximately 82 *l Pa* and 20 *l Pa* respectively.

The behaviour of the pore pressure at rates above 100 *mm/min* is illustrated in Figure 7.11. It is shown that within four wave cycles, that is one revolution of the IC/NGI apparatus, the sample liquefies at rates of 200 *mm/min* and over. At 150 *mm/min* the tendency for the levels of the pressure peaks and troughs to increase with wave cycle is illustrated more clearly than at 100 *mm/min*. The reason for this increase is that after each wave a higher pore pressure remains as a result of a shortage of drainage time. Therefore, with each wave cycle an accumulative affect is observed until an equilibrium is reached. At 150 *mm/min* the sample does not liquefy within four cycles, but additional testing shows that it does liquefy if the number of wave cycles is increased to five. This implies that there is a specific rate for this total stress level above which the sample will liquefy. The influence of total normal stress will be studied later.

Finally the swelling of the sample at higher rates decreases as rate increases because of the reduced time available for swelling at higher rates, this is shown on the second plot in Figure 7.11. Furthermore, once the sample has liquefied no swelling takes place because there is no longer a change in the effective normal stress from which a change in the pore pressure can be obtained. Therefore with no change in pore water pressure this model cannot predict sample swelling. Once the sample liquefies it remains in that state.

7.6.4 The Influence Of Wave Height, Wavelength And Sample Depth On The Pore Pressure Predictions

The work of Parathiras [4] suggested that the magnitude of the negative rate effects increased with the height of the shear surface undulations, this was investigated given the following data:

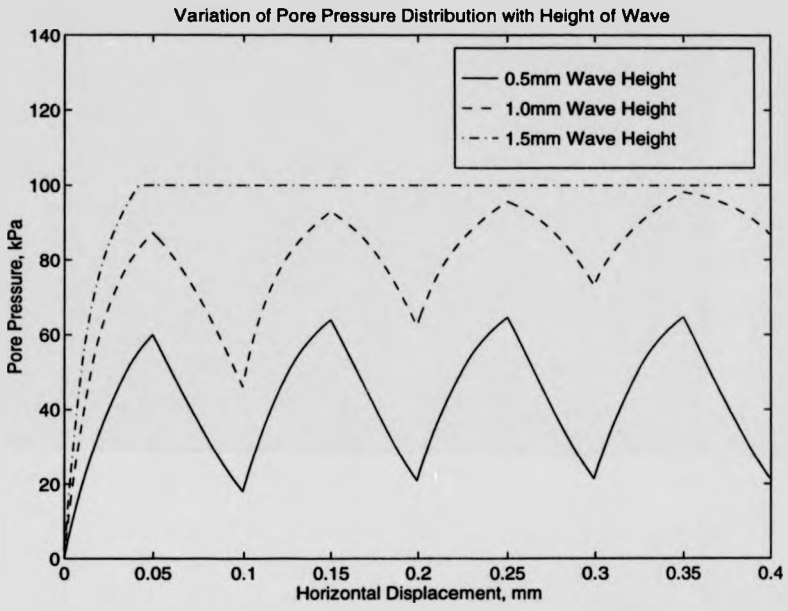

Figure 7.12: The variation in pore pressure distribution as a result of a change in the wave heights.

Initial Sample Depth, $h_1 = 9mm$

Final Sample Depth, $h_2 = Variable$

Horizontal Slope Length, $Length = 50mm$

Number of Wave-Forms, $Wave = 4$

Number of Steps, $n = 100$, from Equation 7.5

Rate of Shearing, $Rate = 150mm/min$

Total Normal Stress, $\sigma_n = 100l\ Pa$.

A rate of 150 mm/min was selected because of the interesting behaviour observed in the previous section. Unsurprisingly Figure 7.12 illustrates that the software generates an increasing pore pressure distribution as wave height increases, this all stems from Equation 7.1. The greater the compression the soil strip is subjected to, the higher the change in effective normal stress and hence pore pressure. It appears there-

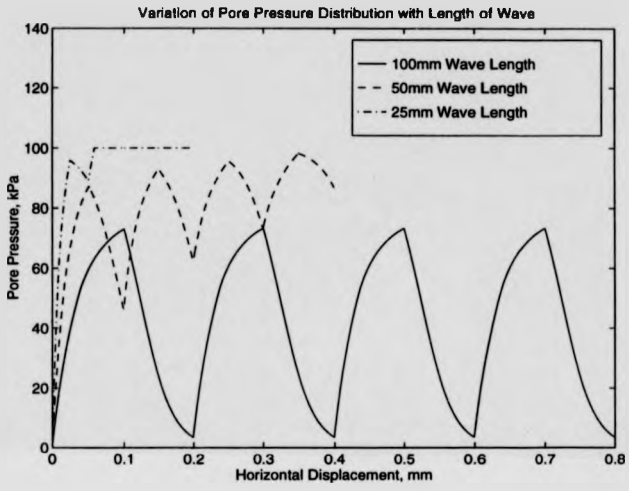

Figure 7.13: The variation in pore pressure distribution as a result of a change in the wavelengths.

fore, Parathiras' [4] theory was correct. The effect of increasing the wave height is very similar to that of increasing the rate of shearing.

This study has suggested that increasing the wavelength of the shear surface has the effect of translating a critical effect curve along the x-axis thus delaying the onset of negative rate behaviour, as illustrated in Figure 5.13. If this is the case as the wavelength is increased the magnitude of the pore pressure distribution should decrease. Now consider Figure 7.13 which has been generated given the following input:

Initial Sample Depth, $h_1 = 9mm$

Final Sample Depth, $h_2 = 8mm$

Horizontal Slope Length, $Length = Variable$

Number of Wave-Forms, $Wave = 4$

Number of Steps, $n = Variable$, from Equation 7.5

Rate of Shearing, $Rate = 150mm/min$

Total Normal Stress, $\sigma_n = 100l\ Pa$.

The wavelengths were selected to correspond to Interfaces 2,3 and 4 the $4 \times 1mm$, $2 \times 1mm$ and $8 \times 1mm$ wave-form interfaces respectively. It should be noted that the wavelengths given on Figure 7.13 are those defined on Figure 7.3 which are really one half of the true wavelength.

The results show that the level of pore pressure generation is indeed lower at higher wavelengths, thus agreeing with the trend illustrated in Figure 5.13. The reason is that whilst the total compression is equal in all three cases, the time taken to travel from trough to peak is longer, given a constant rate, as the wavelength is increased. This allows more time for drainage and thus reduces cumulative levels of pore pressure. Again the effect of increasing the wavelength is similar to that of decreasing rate or decreasing wave height.

The final investigation associated with the geometry of the sample involves a study of the influence of sample depth. Soil loss from the IC/NGI apparatus has been highlighted as a potential problem throughout this study. One of the effects of this will be to shorten the drainage path as the depth of the sample decreases. This should allow more drainage to take place by increasing the time factor T_v, therefore potentially decreasing the cumulative levels of pore water pressure. However, this effect may be offset by the initial higher levels of pore water pressure calculated from Equation 7.2, in which soil loss reduces the value of H and therefore increases pore pressure generation. The effect of soil loss was studied given the following data:

Initial Sample Depth, $h_1 = Variable$
Final Sample Depth, $h_2 = h_1 - 1mm$
Horizontal Slope Length, $Length = 50mm$
Number of Wave-Forms, $Wave = 4$
Number of Steps, $n = 100$, from Equation 7.5
Rate of Shearing, $Rate = 150mm/min$
Total Normal Stress, $\sigma_n = 100 Pa$.

The value of h_1 is initially 9 mm because this is approximately the sample depth at the outset of an IC/NGI apparatus test. Towards the end of testing once excessive

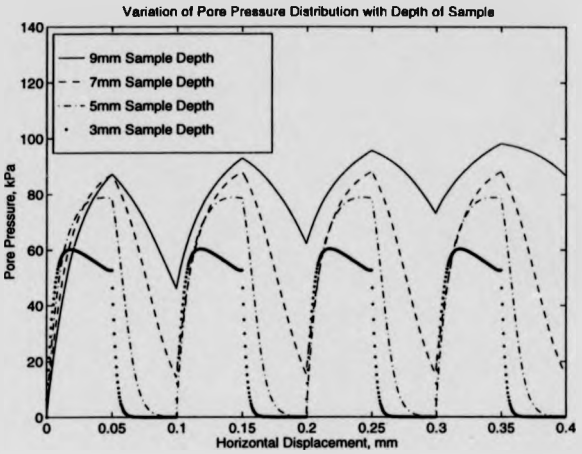

Figure 7.14: The variation in pore pressure distribution as a result of a change in the sample depths.

soil loss has occurred, this value could potentially be as low as 3 *mm*. Figure 7.14 illustrates the results obtained from this investigation. It is apparent that cumulative pore pressure generation is reduced by decreasing the sample depth, indicating that the effect of increased drainage is larger than the effect of increased pressure generation as a result of reducing H in Equation 7.2. The graph clearly illustrates that drainage increases as sample depth is reduced. During the up slope consolidation the curvature of the pore pressure graphs increases significantly as sample depth is reduced from 9 *mm* to 5 *mm*. At 5 *mm* when the wave peak is reached the gradient of the plot is virtually zero. Below this depth the degree of drainage is so high that pore pressures actually start to dissipate on the up slope, this is illustrated on the 3 *mm* initial sample height plot where once the strip height is reduced below around 2.6 *mm* cumulative pore pressures actually start to decrease. This has some important implications to the IC/NGI tests as many of the negative rate effects were observed towards the end of testing, when the sample depth was significantly lower than 9 *mm*.

7.6.5 Investigating The Influence Of Normal Stress On The Pore Water Pressure Distribution And The Effective Normal Stress

Previous research, Tika [2] and Parathiras [4], has suggested that the magnitude of rate effects decreases with increasing normal stress. For this to apply to the pore water pumping mechanism for negative rate behaviour, the pore water pressure cannot be studied directly. The important result is the average effective normal stress, $\bar{\sigma}'_n$, and more specifically its magnitude compared with the total normal stress. If the model is correct and the pumping mechanisms is the cause of negative rate behaviour, the ratio, $\bar{\sigma}'_n/\sigma_n$, should increase with the normal stress. The effect of increasing the normal stress was investigated using the following data:

Initial Sample Depth, $h_1 = 9mm$
Final Sample Depth, $h_2 = 8mm$
Horizontal Slope Length, $Length = 50mm$
Number of Wave-Forms, $Wave = 4$
Number of Steps, $n = 100$, from Equation 7.5
Rate of Shearing, $Rate = 150mm/min$
Total Normal Stress, $\sigma_n = Variable$

The results of the investigation are illustrated in Figure 7.15. The first plot shows the variation in pore pressure distribution with normal stress. A trend of increasing pore water pressures is observed as normal stress is increased. This is a result of the variation of m_v with effective normal stress illustrated in Figure 7.1, m_v falls towards zero with increasing effective stress and this yields higher pore water pressure generation from Equation 7.2. Opposing these increases in pore pressure is improved drainage as a result of c_v increasing with normal effective stress and therefore increasing the time factor T_v. The results in Figure 7.15 suggest this effect is less significant. Further information can be obtained from this plot, under 50 l Pa of total normal stress the sample liquefies during the first compression phase, whereas under 100 l Pa the

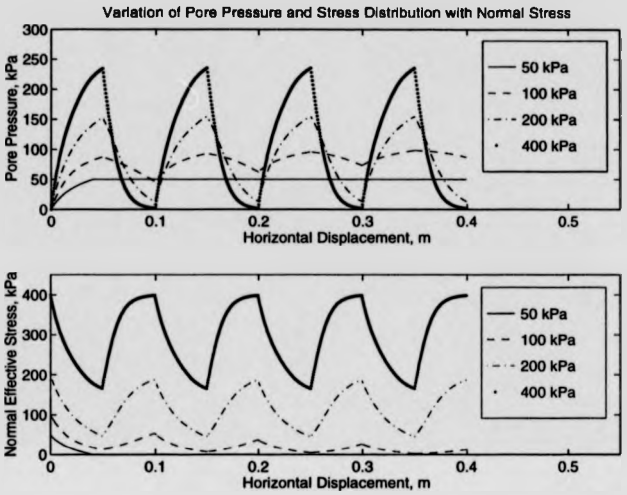

Figure 7.15: The Variation in Pore Pressure Distribution and Effective Normal Stress Distribution as a Result of a Change in the Total Normal Stress

sample does not liquefy within four wave cycles but the results suggest that it would within five or six cycles. When the normal stress is increased to 200 $l\,Pa$ and 400 $l\,Pa$ the samples do not approach a liquefied state. The implications of this are best considered in terms of effective stress.

As stated previously the critical ratio with these results is $\bar{\sigma}'_n/\sigma_n$, which gives an indication of the magnitude of any negative rate behaviour, where $\bar{\sigma}'_n/\sigma_n = 1$ indicates no negative rate effect and $\bar{\sigma}'_n/\sigma_n = 0$ indicates soil liquefaction and hence a dramatic negative rate effect. Unfortunately v1.0 The Free Swell Model does not calculate the mean effective normal stress, $\bar{\sigma}'_n$ and therefore a different measure is used. The value of $\bar{\sigma}'_n$ is replaced with the value $\sigma'_{n_{min}}$ the minimum value of the effective normal stress shown in Figure 7.15, this does not then supply accurate results but does provide an indication of the level of negative rate effects. At 50 $l\,Pa$ and 100 $l\,Pa$ the value of $\sigma'_{n_{min}}$ is zero and therefore the ratio $\sigma'_{n_{min}}/\sigma_n$ is zero indicating dramatic negative rate effects. At total stresses of 200 $l\,Pa$ and 400 $l\,Pa$, $\sigma'_{n_{min}} = 47\ l\,Pa$ and 166 $l\,Pa$ respectively, this leads to values of $\sigma'_{n_{min}}/\sigma_n = 0.235$

at 200 $l\,Pa$ and $\sigma'_{n_{min}}/\sigma_n = 0.415$ at 400 $l\,Pa$. This illustrates that the magnitude of the negative rate effects resulting from effective normal stresses decreases as the total applied stress increases. This observation is in agreement with the previous research performed by Tika [2] and Parathiras [4]. Whilst this investigation has not experimentally investigated the influence of normal stress, the results of the modelling and previous research suggests that increasing normal stress does suppress rate effects.

7.7 Discussion

The aim of this section is to compare the model results to a number of actual tests and to go on and discuss the validity of the model and its implications to the pumping theory.

7.7.1 Comparing Model Results With Monitored Pore Water Pressures Observed During Tests 14 And 15

Making direct comparisons between the model results and the recorded results is very difficult, because the test results take snap shots of the pore pressures at four locations around the annulus and the model provides results from one strip of soil travelling around the annulus. Furthermore, the model always assumes that the soil strip commences from the bottom of a wave-form and is therefore always compressed first. In reality half of the sample starts on a down slope and is subject to expansion first which could potentially generate negative pore pressures. With these difficulties in mind two shearing stages, one from Test 14 and one from Test 15, will be compared with results from the model using the parameters that applied during the tests.

First consider Stage F of Test 14, the results of which are illustrated in Figure D.43, on which only the dashed line (transducer halfway along the up slope) and the dotted line (transducer at the wave peak) will be considered, as the other transducers malfunctioned. To model this stage of fast shearing the following parameters were determined from the results file:

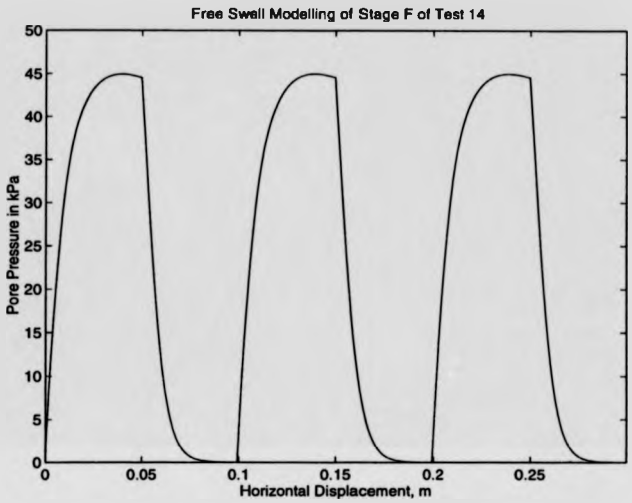

Figure 7.16: The Variation in Pore Pressure Distribution from Modelling the Parameters from Stage F of Test 14

Initial Sample Depth, $h_1 = 6.9mm$

Final Sample Depth, $h_2 = 5.9mm$

Horizontal Slope Length, $Length = 50mm$

Number of Wave-Forms, $Wave = 3$, approximately 300mm of shearing

Number of Steps, $n = 100$, from Equation 7.5

Rate of Shearing, $Rate = 50mm/min$

Total Normal Stress, $\sigma_n = 79.5l\ Pa$

The results of running this through the model are displayed in Figure 7.16. According to these results the transducer on the up slope should be recording a constant pore water pressure equal to that predicted at displacements of 0.025 m, 0.125 m and 0.225 m on Figure 7.16, this pressure is equal to 43 $l\ Pa$. The transducer reading is not constant, however its average value is of the order 30-40 $l\ Pa$ and therefore the agreement with the model is relatively good, when the crudeness of the model is considered along with the difficulties associated with the pore pressure transducers. It should be noted that the negative pore pressures recorded during the early phase

of Stage F are associated with sample dilation, which is not modelled in the software. The agreement between the model and the test results is not so good for the pore pressure transducer on the wave peak. According to the model at displacements of 0.05 m, 0.15 m and 0.25 m the pore pressures were 45 $l\ Pa$, whereas in the measured pressure varied in an approximate range of 20-40 $l\ Pa$.

Secondly consider Stage E of Test 15, the results of which are illustrated in Figure D.46, on which only the dotted line (transducer on the wave peak) will be considered, as the other transducers malfunctioned. To model this stage of fast shearing the following parameters were determined from the results file:

Initial Sample Depth, $h_1 = 6.7mm$
Final Sample Depth, $h_2 = 5.7mm$
Horizontal Slope Length, $Length = 50mm$
Number of Wave-Forms, $Wave = 15$, approximately 1500mm of shearing
Number of Steps, $n = 100$, from Equation 7.5
Rate of Shearing, $Rate = 300mm/min$
Total Normal Stress, $\sigma_n = 84l\ Pa$

The results of running this through the model are displayed in Figure 7.17. At first glance the model appears to provide a poor representation of the actual behaviour and this can be explained by studying the assumptions of the model. Initially in Test 15 Stage E the sample dilates rapidly developing significant suction and these are not allowed for in the model. But then the recorded pore pressure rises to a level higher than the normal stress, implying that in this region the sample has liquefied. A similar result is observed in Figure 7.17, then in reality some of the excess pore pressure drains, but the model does not allow this once liquefaction has occurred and this explains the discrepancy between the two.

In summary, the model appears to be generating pore water pressures which are of similar values to those observed in actual tests. The fact that the results do not correlate more accurately is not surprising, because the model is very simple and dependent on many assumptions outlined in this chapter. Therefore the level of

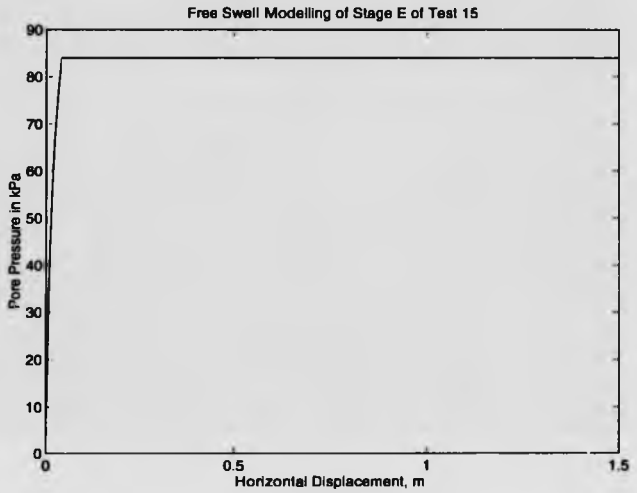

Figure 7.17: The variation in pore pressure distribution by modelling the parameters from stage E of test 15.

agreement attained should be considered as a positive result.

7.7.2 Comparing The Pore Pressure Model Results With The Actual Rate Behaviour Observed In Test 4

The aim of this section is to see if the magnitude of the pore pressures predicted by the model correlate with the observed rate behaviour in Test 4. One difficulty with this task is that the mechanisms behind positive rate effects, viscous effects and particle disorientation, are still likely to be in operation when pore pressures are reducing the effective stress ultimately causing negative rate behaviour. Therefore they will have the effect of reducing the magnitude of the negative rate behaviour. Test 4 (Interface 2, $4 \times 1mm$ wave-form) was selected because this offset could be estimated from Test 3 (Interface 1, planar), during which a positive effect curve was observed.

The variation of fast residual strength with increasing rate is illustrated in Figure 4.4 and these results are summarised in the first three columns of Table 7.6. The next column in Table 7.6 illustrates the percentage of fast residual strength lost as a

Table 7.5: The parameters used to model test 4.

h_1 mm	h_2 mm	Horizontal Slope Length mm	Number of Waves	Steps	Rate of Shearing mm/min	Total Normal Stress kPa
7.45	6.45	50	4	100	10	95.5
7.10	6.10	50	4	100	50	84
6.72	5.72	50	4	100	300	82.5
5.88	4.88	50	4	100	1000	84

result of changing from a planar interface in Test 3 to a $4 \times 1mm$ wave-form interface in Test 4. The fourth column provides the pore pressure increase required to cause this loss of strength, this is calculated using the following equation,

$$u = \sigma_n - \sigma_n(1 - \%loss/100) \tag{7.6}$$

When using Equation 7.6 to calculate the values for u, the total normal stress applied to the sample neglecting side friction which equalled 98 $l\,Pa$ for both Tests 3 and 4 was used. This has induced an error into the calculations, but it does help to keep things simple.

Having calculated the pore pressures required to create the observed loss in strength during Test 4, the next step is to run the model, using the parameters from Test 4 to see if the model can predict the pore pressures derived from the test results. For the four stages of fast shearing, the parameters listed in Table 7.5 were obtained from the results file and then used in the free swell model. The results obtained from the parameters in Table 7.5 are illustrated in Figure 7.18. As one would expect, the pore pressures increased with rate of shearing and at rates of 300 mm/min and 1000 mm/min the pore pressure reached the total normal stress causing the sample to liquefy. When the sample liquefies the average pore pressure is equal to the normal stress and this is shown in the sixth column of Table 7.6. Problems arise however when the sample does not liquefy and the pore pressure distribution is cyclic. In this case an exact average value is not important because of the inaccuracies in the model, therefore an approximate average was attained at rates of 10 mm/min

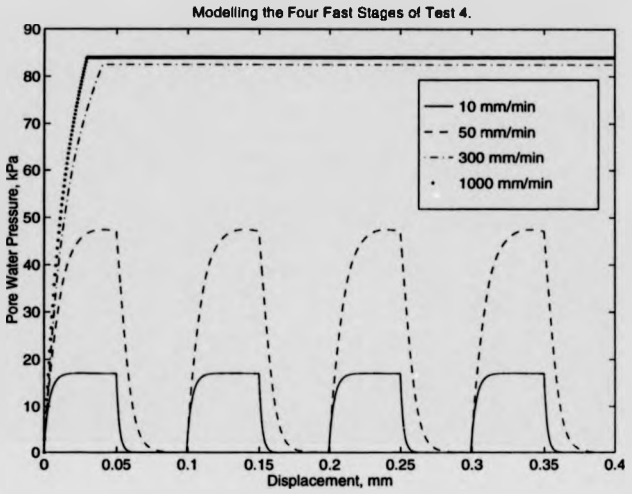

Figure 7.18: Prediction of pore water pressures during test 4 using v1.0 the free swell model.

and 50 mm/min, by assuming the average pore pressure to fall halfway between the maximum and minimum values observed. This enabled Table 7.6 to be completed.

Comparing the required and predicted pore water pressures in Table 7.6 reveals that the values are not in close agreement, which is surprising considering the good match obtained in Section 7.7.1. There are two major reasons for this, one relating to the model and the other to Test 4.

The average predicted pore pressures in Table 7.6 are calculated for one soil strip which always starts off with a full wave height compression, thus generating a maximum pore pressure at the wave peak. In reality many *"strips"* of soil start off from the wave peaks or from the down slopes, these will all initially generate negative pore water pressures, thus reducing the average pore water pressure around the annulus. The model does not account for this and for it to do so would require a different approach and a higher level of programming. If this is conducted in the future, a better approximation of the average pressure would be available and this value would be lower than those provided in Table 7.6, thus providing a closer match to the required pore pressure values.

Table 7.6: Comparing actual results with model results.

Test	Rate of Shearing mm/min	Fast Residual/ Slow Residual	% Decrease in Fast Residual From T3 to T4	Pore Pressure Required For % Decrease	Pore Pressure Predicted By Model
3	10	1.21	-	-	-
	50	1.32	-	-	-
	300	1.40	-	-	-
	1000	1.50	-	-	-
4	10	1.19	2%	2 *l Pa*	8 *l Pa*
	50	1.19	10%	10 *l Pa*	23 *l Pa*
	300	0.80	43%	42 *l Pa*	82 *l Pa*
	1000	0.36	76%	74 *l Pa*	84 *l Pa*

During the early tests including Test 4, shear displacement was limited by soil loss and it is likely that true fast residual conditions were not properly established, especially when negative rate behaviour was occurring. It is likely that the levels of the ratio $FastResidual/SlowResidual$ provided in Table 7.6 are too high. Lowering these values for Test 4 would have the effect of increasing the required pore water pressure and so providing a closer match to the predicted values.

7.7.3 Implications To The Pumping Theory And Conclusions

This chapter has introduced a method for modelling the likely pore pressure build up as a sample is compressed by up slope shearing. It has gone on to develop a method for modelling pore pressure dissipation on down slopes, thus creating a system which can be looped together to model shearing over a symmetrical wave cycle. The methods used in this model are very basic, as is the programming used to operate the model. However, the limitations of the model have been discussed and the assumptions made by the model have been highlighted and are understood, thus making the model meritable.

The investigations undertaken in Section 7.6 using v1.0 The Free Swell Model, studied the influence of rate, wave geometry, sample depth and normal stress. As reported in Section 7.6, the model produced variations in pore water pressure which

would have produced negative rate behaviour by reducing the effective normal stress. The predicted variations in negative rate behaviour appear to be in accordance with the previous research, examples of this include:

- Negative rate effect magnitude increasing with rate
- Negative rate effect magnitude increasing with wave height
- Negative rate effect magnitude decreasing under increased total normal stresses
- The onset of negative rate behaviour being delayed by increasing the wavelength

These supply further evidence that the pumping effect of non-planar shear surfaces does generate positive pore water pressures and therefore negative rate effects. Also as the model results behave in accordance with current understanding of negative rate behaviour, it is a good indication that whilst the model is crude, the underlying principles behind it are functioning correctly.

Finally in this chapter, two comparisons were made; firstly between pore water pressures predicted in the model and those recorded by the pore pressure transducers during Tests 14 and 15, secondly between the magnitude of the rate effects observed in Tests 3 and 4 and the pore water pressures predicted by the model. The level of agreement between the model and the recorded pressures was encouraging, providing more evidence for the merit of the model. However, the correlation between observed negative rate behaviour and predicted pore pressures was not as close. Reasons for this have been explored and possible explanations have been put forward.

In conclusion, v1.0 The Free Swell Model is a crude method for predicting pore pressures on a wavy surface, but it is of some merit and generally produces results in the area of some actual recorded values. It does support the idea that pore pressures are the mechanism behind negative rate effects. The model has several limitations and stretches basic consolidation theory close to the limits of its practical applications. In the authors opinion further development of the model using these techniques would be of limited use as the whole theory is undermined by a large number of assumptions. Further work in this area may be possible using other computational techniques

which could include finite element modelling or even potentially computational fluid dynamics, this however is beyond the scope of this work.

Chapter 8

The Influence Of Undulations Parallel To The Direction Of Shearing

8.1 Introduction

The use of the IC/NGI ring shear apparatus is widely accepted as being an accurate method for finding the residual shear strength of soils. However, it has often been noted that the shear plane that develops in the test samples is not perfectly planar and that curved shear surfaces do develop parallel to the direction of shearing. This may lead to inaccuracies in the calculated angle of shearing resistance, as the standard calculations assume the shear surface to be perfectly planar. This chapter postulates that lateral earth pressure theory may be utilised to derive equations which calculate the true angle of shearing resistance developed across non-planar shear surfaces. This allows a comparison between the true angle of shearing resistance and that calculated by assuming a planar shear surface. It also allows the development of correction curves for a variety of different wave-forms, which will permit the original standard calculations to be adjusted to give the true angle of shearing resistance according to the height of the wave-form and the lateral earth pressure coefficient. The chapter develops to analyse the effect of wave function on the correction curves and concludes

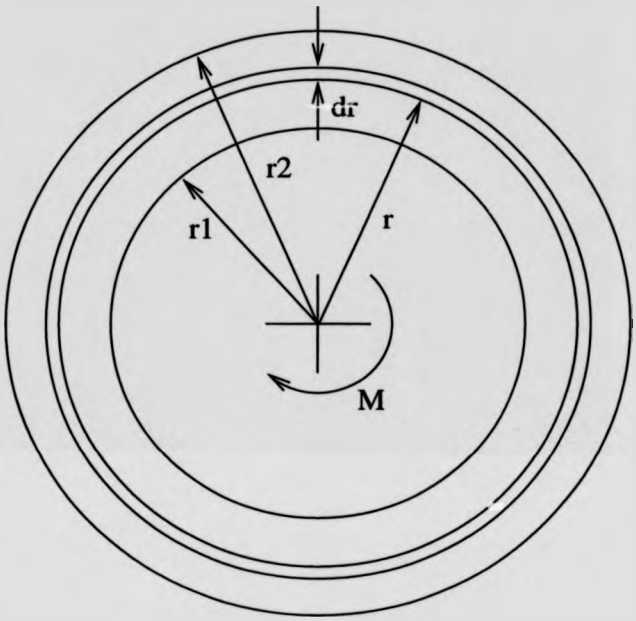

Figure 8.1: A typical annular shear surface.

that one curve applies equally to any wave function.

Before commencing the main analysis performed in this chapter, the origins of Equation 3.2 need to be fully comprehended as the derivation of the equation is fundamental to this chapter. Consider Figure 8.1 which represents a planar annular shear surface with shear strength τ. The moment of resistance generated from the annular element of width dr is supplied by,

$$M_{element} = 2\pi r^2 \tau dr \tag{8.1}$$

therefore integrating radially across the whole annulus gives the total moment,

$$M = \int_{r_1}^{r_2} 2\pi r^2 \tau dr \tag{8.2}$$

and performing the integration yields,

$$M = \frac{2}{3}\pi\tau(r_2^3 - r_1^3). \tag{8.3}$$

Rearranging Equation 8.3 yields Equation 3.2 which forms the basis for the presentation of all ring shear test results.

8.2 Derivation Of The General Solution

Consider an annular sample from a ring shear machine as shown in Figure 8.2 Part (i). If a section is taken through the annulus perpendicular to the direction of shearing, a wavy shear surface such as that shown in Figure 8.2 Part (ii) could be observed. If an infinitely small step on that shear surface is now considered as illustrated in Figure 8.2 Part (iii), it can be seen that the standard normal stress σ_n acts on the horizontal section of the step. However there is also a horizontal stress acting on the vertical face of the step, $k\sigma_n$, it is this stress that is not included in calculations that assume a planar shear surface. If lateral earth pressure theory is utilised the additional shear strength as a result of this horizontal stress will equal $k\sigma_n \tan\phi_r$ assuming that residual strengths are being recorded across a fully developed shear surface. Henceforth, if the shear strength of the horizontal plane is τ, the shear strength of the vertical plane will be $k\tau$, where k is a lateral earth pressure coefficient.

The implications of a non-planar shear surface are that the moment generated will be higher than from a planar one. Therefore Equation 8.2 for the moment from a planar surface can be modified for a non-planar one thus,

$$M_{np} = \int_{r_1}^{r_2} 2\pi r^2 \tau dr + M_v, \tag{8.4}$$

where M_v is the additional moment generated as a result of the shear strength from the vertical planes illustrated in Figure 8.2 Part (iii). The moment generated from the vertical planes M_V can be found from first principles in conjunction with Figure 8.2. Consider an infinitely small vertical element around the annulus of height dh.

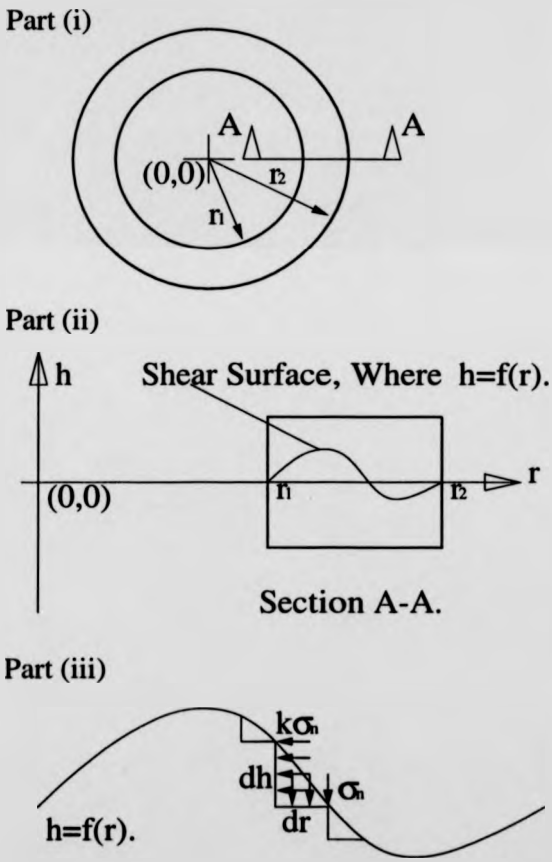

Figure 8.2: The geometry of and the assumed stresses on an undulating shear surface.

The area of the strip A_v is given by,

$$A_v = 2\pi r dh \tag{8.5}$$

therefore the force developed from the element F_v is given by,

$$F_v = 2\pi r k \tau dh. \tag{8.6}$$

Multiplying this force by the radius of the element r and integrating from r_1 to r_2 gives the vertical component of the moment,

$$M_v = \int_{r_1}^{r_2} 2\pi r^2 k \tau dh. \tag{8.7}$$

As $h = f(r)$ the above expression has to be modified so that the integration is performed with respect to r not h. From Figure 8.2 Part(iii) it can be seen that,

$$dh = \frac{dh}{dr} dr. \tag{8.8}$$

The lateral earth pressure $k\sigma_n$ acts in all directions horizontally, therefore if the shear surface has a negative gradient, a negative shear strength will be produced using this substitution. To prevent this from happening the following constraint is applied,

$$dh = \left|\frac{dh}{dr}\right| dr. \tag{8.9}$$

Therefore the vertical component of the moment can be expressed as,

$$M_v = \int_{r_1}^{r_2} 2\pi r^2 k \tau \left|\frac{dh}{dr}\right| dr. \tag{8.10}$$

Furthermore it is now possible to calculate the total moment generated from a non-planar surface by substituting Equation 8.10 into Equation 8.4 yielding,

$$M_{np} = \int_{r_1}^{r_2} 2\pi r^2 \tau dr + \int_{r_1}^{r_2} 2\pi r^2 k \tau \left|\frac{dh}{dr}\right| dr, \tag{8.11}$$

where the the height of the shear surface above or below the true planar level h is a function of the radius r.

8.3 Application Of The General Solution To Specific Wave-Forms

The general solution for the moment developed from a non-planar shear surface derived in Section 8.2, can be applied to a variety of shear surface wave-forms, these include v-shapes, parabolas, sine curves and circular arcs. The aim of this section is to outline the use of the general solution for a variety of different curves.

8.3.1 The V-Shape Wave-Form

Consider the wave-form illustrated in Figure 8.3. The shear surface is formed by the intersection of two straight lines

$$h_1 = a_1 r + b_1 \tag{8.12}$$

and

$$h_2 = a_2 r + b_2. \tag{8.13}$$

As the surface is composed of two different functions h_1 and h_2 the second integral of the general solution can be split into two parts, giving the solution,

$$M_{np_{vshape}} = \int_{r_1}^{r_2} 2\pi\tau r^2 dr + \int_{r_1}^{r_a} 2\pi k\tau r^2 \left|\frac{dh_1}{dr}\right| dr + \int_{r_a}^{r_2} 2\pi k\tau r^2 \left|\frac{dh_2}{dr}\right| dr \tag{8.14}$$

Differentiating the functions given in Equations 8.12 and 8.13 yields,

$$\frac{dh_1}{dr} = a_1 \tag{8.15}$$

and

$$\frac{dh_2}{dr} = a_2. \tag{8.16}$$

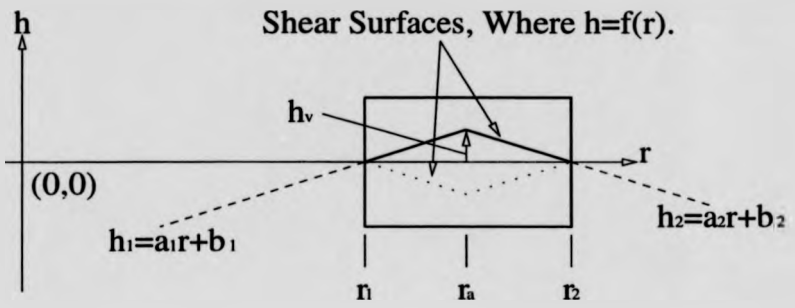

Figure 8.3: The geometry of a v-shape wave-form.

In Figure 8.3, a_1 will have a positive value and a_2 a negative one. Henceforth,

$$\left|\frac{dh_1}{dr}\right| = a_1 \tag{8.17}$$

and

$$\left|\frac{dh_2}{dr}\right| = -a_2, \tag{8.18}$$

also in this case the wave-form is symmetrical so

$$a_1 = -a_2 = \left|\frac{dh_2}{dr}\right| \tag{8.19}$$

therefore substituting Equations 8.17 and 8.19 into Equation 8.14 and rearranging supplies the solution,

$$M_{np_{vshape}} = 2\pi\tau\left\{\int_{r_1}^{r_2} r^2 dr + \int_{r_1}^{r_a} ka_1 r^2 dr + \int_{r_a}^{r_2} ka_1 r^2 dr\right\}. \tag{8.20}$$

Performing the integration with respect to r completes the solution for the v-shape wave-form,

$$M_{np_{vshape}} = \frac{2\pi\tau}{3}\left\{(r_2^3 - r_1^3) + ka_1(r_2^3 - r_1^3)\right\}. \tag{8.21}$$

During ring shear tests Equation 3.2 is always used to calculate the shear strength and if the shear surface is non-planar this produces an apparent shear strength $\tau_{apparent}$

instead of the true shear strength τ. Equation 3.2 should actually be expressed thus,

$$\tau_{apparent} = \frac{3M}{2\pi(r_2^3 - r_1^3)} \tag{8.22}$$

which rearranges to give,

$$M = \frac{2\pi\tau_{apparent}}{3}(r_2^3 - r_1^3). \tag{8.23}$$

Then equating Equations 8.21 and 8.23 provides an expression relating true and apparent shear strengths thus,

$$\tau_{apparent} = \tau(1 + ka_1), \tag{8.24}$$

where

$$a_1 = \frac{2h_v}{r_2 - r_1}. \tag{8.25}$$

Henceforth, if a v-shape wave-form is observed once ring shear testing is complete, the apparent shear strength which will already have been calculated can be converted to the true shear strength by dividing it by $(1 + ka_1)$. Alternatively the correction can be applied to the stress ratio $\tan\phi_r$, yielding,

$$\tan\phi_r = \frac{\tan\phi_{r_{apparent}}}{1 + ka_1}. \tag{8.26}$$

8.3.2 The Parabolic Wave-Form

Consider the wave-form illustrated in Figure 8.4, a parabola, where the height of the wave h is a function of the radius r thus,

$$h = ar^2 + br + c. \tag{8.27}$$

To use this equation in conjunction with the general solution, it is first necessary to define a, b and c. Simultaneously solving three equations defining the position of the

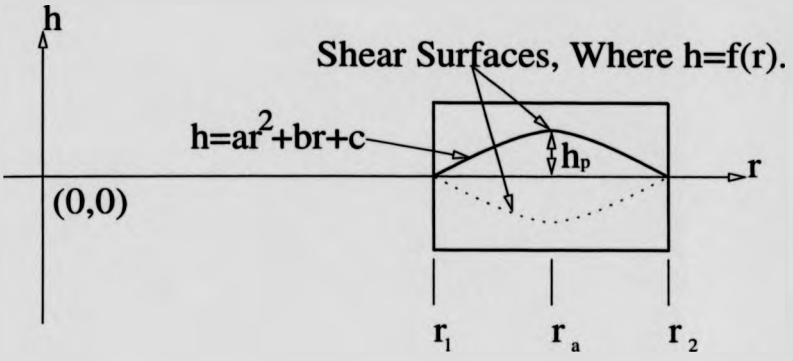

Figure 8.4: The geometry of a parabolic wave-form.

parabola on the axes, provides the coefficients a, b and c thus,

$$a = \frac{-h_p}{r_1^2 - 2r_a r_1 + r_a^2}, \tag{8.28}$$

$$b = \frac{2r_a h_p}{r_1^2 - 2r_a r_1 + r_a^2} \tag{8.29}$$

and

$$c = h_p - \frac{r_a^2 h_p}{r_1^2 - 2r_a r_1 + r_a^2}. \tag{8.30}$$

Differentiating Equation 8.27 gives,

$$\frac{dh}{dr} = 2ar + b. \tag{8.31}$$

Now for the case shown in Figure 8.4 from r_1 to r_a the gradient is positive, therefore

$$\left|\frac{dh}{dr}\right| = 2ar + b \tag{8.32}$$

and from r_a to r_2 the gradient is negative, therefore

$$\left|\frac{dh}{dr}\right| = -(2ar + b). \tag{8.33}$$

Splitting the second integral of the general solution (Equation 8.11) at r_a, then substituting Equations 8.32 and 8.33 and simplifying provides the exact solution for a parabolic wave-form as

$$M_{np_{parabolic}} = 2\pi\tau \left\{ \int_{r_1}^{r_2} r^2 dr + \int_{r_1}^{r_a} k(2ar + b)r^2 dr - \int_{r_a}^{r_2} k(2ar + b)r^2 dr \right\}. \quad (8.34)$$

Completing the integration gives the solution,

$$M_{np_{parabolic}} = \frac{2\pi\tau}{3} \left\{ (r_2^3 - r_1^3) + \frac{3}{2}ka(2r_a^4 - r_1^4 - r_2^4) + kb(2r_a^3 - r_1^3 - r_2^3) \right\}. \quad (8.35)$$

Checking this equation by making $h_p = 0$ yields $a = 0$ and $b = 0$ from Equations 8.28 and 8.29, this then reduces Equation 8.35 to Equation 8.3 the standard one for a plane shear surface as would be expected. A further confirmation can be made by checking the units in Equation 8.35. Coefficients k and b are dimensionless and a has dimensions mm^{-1} this means that all the terms inside the curly brackets have dimensions in mm^3 which, when multiplied by the shear stress, provide the dimensions of moment.

Equating Equations 8.23 and 8.35 yields the solution,

$$\tau = \frac{\tau_{apparent}(r_2^3 - r_1^3)}{(r_2^3 - r_1^3) + \frac{3}{2}ka(2r_a^4 - r_1^4 - r_2^4) + kb(2r_a^3 - r_1^3 - r_2^3)} \quad (8.36)$$

or alternatively,

$$\tan\phi_r = \frac{\tan\phi_{r_{apparent}}(r_2^3 - r_1^3)}{(r_2^3 - r_1^3) + \frac{3}{2}ka(2r_a^4 - r_1^4 - r_2^4) + kb(2r_a^3 - r_1^3 - r_2^3)}. \quad (8.37)$$

8.3.3 The Sine Wave-Form

The derivation of the exact solution for a sine curve of height, h_s, is more complicated than the first two solutions. The method is exactly the same, but defining the parameters in the equation,

$$h = a\sin(br - c), \quad (8.38)$$

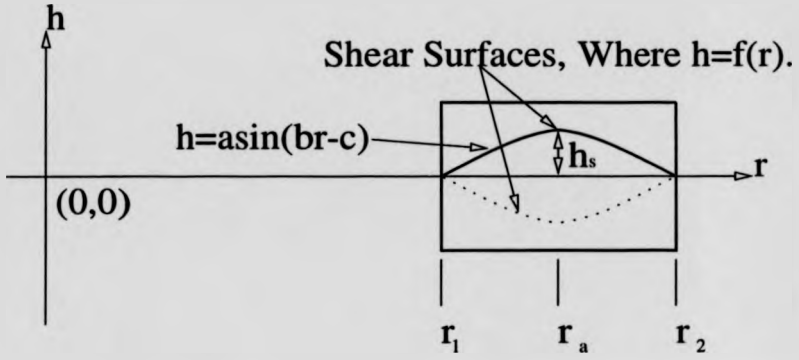

Figure 8.5: The geometry of a sine wave-form.

performing the integration and applying the limits is significantly more complicated. Consider the wave-form illustrated in Figure 8.5. The parameter a is equal to the height of the wave-form h_s and the other parameters are defined as,

$$b = \frac{\pi}{r_2 - r_1} \tag{8.39}$$

and

$$c = \pi \left(\frac{r_2}{r_2 - r_1} - n_{int} \right) \tag{8.40}$$

where n_{int} is the whole part of the value $\frac{r_2}{r_2 - r_1}$. For example if $\frac{r_2}{r_2 - r_1} = 3.782$ then $n_{int} = 3$. Differentiating Equation 8.38 results in,

$$\frac{dh}{dr} = ab\cos(br - c). \tag{8.41}$$

For the case shown in Figure 8.5 from r_1 to r_a the gradient is positive, therefore

$$\left| \frac{dh}{dr} \right| = ab\cos(br - c) \tag{8.42}$$

and from r_a to r_2 the gradient is negative, therefore

$$\left| \frac{dh}{dr} \right| = -ab\cos(br - c). \tag{8.43}$$

Splitting the second integral of the general solution at r_a and substituting for $\left|\frac{dh}{dr}\right|$, gives the exact solution for the sine wave-form as,

$$M_{np_{sine}} = 2\pi\tau\left\{\int_{r_1}^{r_2} r^2 dr + kab\left[\int_{r_1}^{r_a} r^2\cos(br-c)dr - \int_{r_a}^{r_2} r^2\cos(br-c)dr\right]\right\}. \tag{8.44}$$

To solve this equation for the sine wave-form it is necessary to perform the integration, $\int r^2\cos(br-c)dr$. Integrating by parts twice gives the following result,

$$\int r^2\cos(br-c)dr = \frac{r^2}{b}\sin(br-c) + \frac{2r}{b^2}\cos(br-c) - \frac{2}{b^3}\sin(br-c) \tag{8.45}$$

Which simplifies to give,

$$\int r^2\cos(br-c)dr = \frac{2r}{b^2}cos(br-c) + \frac{r^2b^2-2}{b^3}\sin(br-c). \tag{8.46}$$

This allows the completion of all the integration in the above equation for $M_{np_{sine}}$ giving,

$$M = 2\pi\tau\left\{\frac{1}{3}\left[r^3\right]_{r_1}^{r_2} + abk\left[\frac{2r}{b^2}cos(br-c) + \frac{r^2b^2-2}{b^3}\sin(br-c)\right]_{r_1}^{r_a} - \right.$$

$$\left. abk\left[\frac{2r}{b^2}cos(br-c) + \frac{r^2b^2-2}{b^3}\sin(br-c)\right]_{r_a}^{r_2}\right\}. \tag{8.47}$$

Careful application of the limits yields the solution,

$$M_{np_{sine}} = 2\pi\tau\left\{\frac{1}{3}(r_2^3 - r_1^3) + \frac{ka}{b^2}\left[4r_a b\cos(br_a-c) + 2(r_a^2b^2-2)sin(br_a-c) - \right.\right.$$

$$\left.\left. 2r_1 b\cos(br_1-c) - (r_1^2b^2-2)\sin(br_1-c) - 2r_2 b\cos(br_2-c) - (r_2^2b^2-2)\sin(br_2-c)\right]\right\}. \tag{8.48}$$

Checking the units of the equation reveals no errors, the dimensions of a and b are mm and mm^{-1} respectively, c is dimensionless. Therefore the term $\frac{ka}{b^2}$ has dimensions mm^3 and henceforth all terms inside the square brackets should be dimensionless, which they are. Also making $h_s = 0$ makes $a = 0$ and then Equation 8.48 reduces to Equation 8.3 the standard planar one.

Finally equating Equation 8.23 to Equation 8.48 yields the correction equation,

$$\tau = \tau_{apparent}(r_2^3 - r_1^3)/\left\{(r_2^3 - r_1^3) + \frac{3ka}{b^2}\left[4r_a b\cos(br_a - c) + 2(r_a^2b^2 - 2)sin(br_a - c) - \right.\right.$$

$$\left.\left. 2r_1 b\cos(br_1 - c) - (r_1^2b^2 - 2)\sin(br_1 - c) - 2r_2 b\cos(br_2 - c) - (r_2^2b^2 - 2)\sin(br_2 - c)\right]\right\}, \tag{8.49}$$

where τ and $\tau_{apparent}$ can be replaced with $\tan\phi_r$ and $\tan\phi_{r_{apparent}}$ respectively. Finally it should be noted that each of the specific solutions derived in this chapter apply equally to both the solid and dotted wave-forms in Figures 8.3, 8.4 and 8.5 as long as the value of h_v, h_p or h_s is positive.

8.4 Interpretation Of The Specific Solutions

8.4.1 Correction Curves For The IC/NGI Ring Shear Apparatus

In order to compare the solutions for the v-shape, parabolic and sine wave-forms in the IC/NGI ring shear apparatus, it becomes necessary to compute correction curves from the equations derived in Section 8.3. The aim of the curves is that for a given wave-form of height h and a soil with a lateral earth pressure coefficient k, a correction factor C can be obtained where the true shear strength

$$\tau = C\tau_{apparent} \tag{8.50}$$

where, $\tau_{apparent}$ is given by Equation 8.22. The equations were processed in a Turbo Pascal program which computed values of C_v(v-shaped wave-form), C_p(parabolic) and C_s(sine) for a range of values of h and k. The results were then written to a text file which was directly plotted using Matlab. The values of C_v, C_p and C_s were calculated using the following equations derived from Equations 8.24, 8.36 and 8.49.

$$C_v = \frac{1}{1 + ka} \tag{8.51}$$

where $a = \frac{2h_v}{r_2 - r_1}$.

$$C_p = \frac{(r_2^3 - r_1^3)}{(r_2^3 - r_1^3) + \frac{3}{2}ka\,(2r_a^4 - r_1^4 - r_2^4) + kb\,(2r_a^3 - r_1^3 - r_2^3)} \tag{8.52}$$

where $a = \frac{-h_p}{r_1^2 - 2r_a r_1 + r_a^2}$ and $b = \frac{2r_a h_p}{r_1^2 - 2r_a r_1 + r_a^2}$. Finally,

$$C_s = (r_2^3 - r_1^3)/\left\{(r_2^3 - r_1^3) + 3ka/b^2\left[4r_a b\cos(br_a - c) + (2r_a b^2 - 4)\sin(br_a - c) - \right.\right.$$

$$\left.\left. 2r_1 b\cos(br_1 - c) - (r_1^2 b^2 - 2)\sin(br_1 - c) - (r_2^2 b^2 - 2)sin(br_2 - c) - 2r_2 b\cos(br_2 - c)\right]\right\} \tag{8.53}$$

where $a = h_s$, $b = \frac{\pi}{r_2 - r_1}$ and $c = \pi\left(\frac{r_2}{r_2 - r_1} - n_{int}\right)$ where n_{int}, is the whole part of the value $\frac{r_2}{r_2 - r_1}$. In the IC/NGI ring shear apparatus the values for the internal and external radii are 2 and 3 inches respectively. Therefore $r_1 = 50.8mm$, $r_2 = 76.2mm$ and $r_a = (r_1 + r_2)/2 = 63.5mm$. The required data was generated using loop structures in which the values of k were increased by 0.1 in the range 0.1 to 1.0 and values of h were increased at intervals of 0.05 mm to give the curves a smooth appearance through the range 0.0 mm to 8.0 mm. The production of the curves would have been a very long and tedious business without the use of computers. However they were generated in a matter of hours and the results can be seen in Figures 8.6, 8.7 and 8.8.

8.4.2 Implications Of The Correction Curves.

The immediate reaction to the correction curves is that they are all identical. This is true for the accuracy that could be attained by reading values from the curves. In fact a study of the data files reveals that the values of C_v, C_p and C_s are identical to at least two decimal places. A study of the third decimal place (tenths of 1%) shows that in most areas of the curves the values of C_v, C_p and C_s vary by only 0.001 to 0.004, only at the extremities of the curves is this range exceeded. This allows a powerful conclusion to be drawn, the function of the wave-form is not a controlling parameter in the solution of non-planar problems, but the height of the wave-form and the lateral earth pressure coefficient are crucial. It is reasonable to

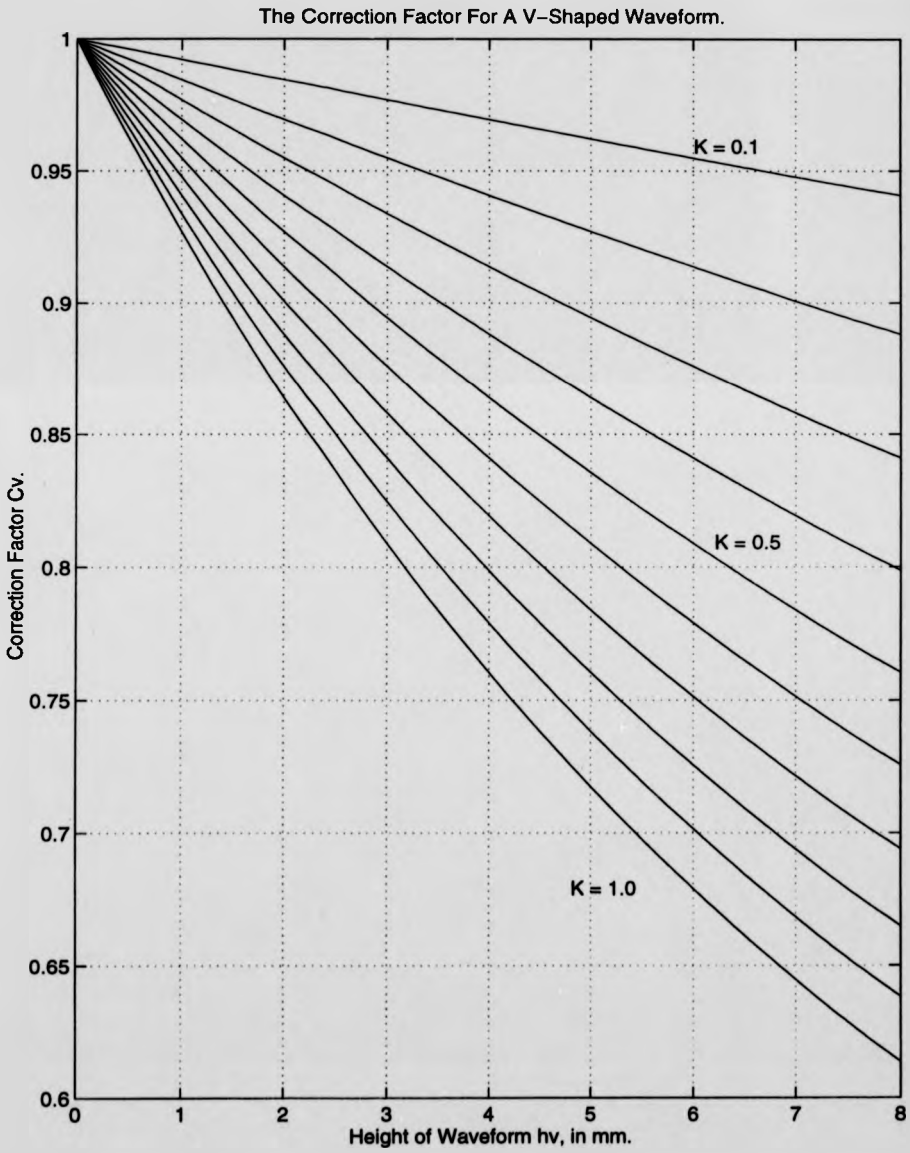

Figure 8.6: The correction factor for a v-shaped wave-form.

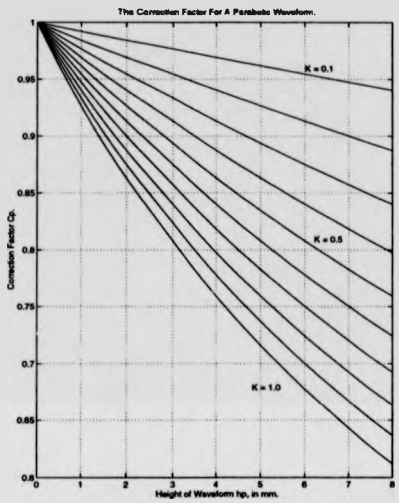

Figure 8.7: The correction factor for a parabolic wave-form.

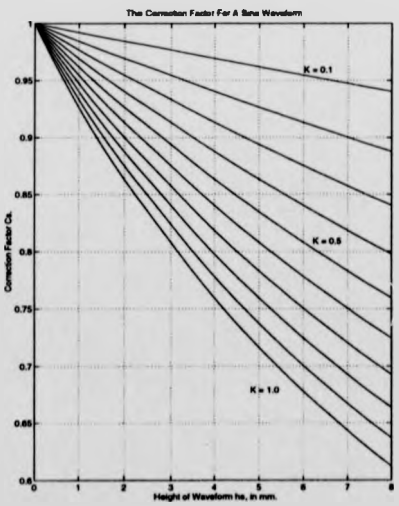

Figure 8.8: The correction factor for a sine wave-form.

assume that any wave-form can be modelled using the simple equation derived for the v-shaped wave-form, Equation 8.24. So the long equations derived for parabolic and sine wave-forms can now be discarded.

Taking Figure 8.6 as the definitive curve for the IC/NGI ring shear apparatus, it can be seen that depending on the value of k used, wave-forms of heights as small as 2 mm can cause 10% errors in the calculated shear strength which is a significant difference. The correction curve suggests that the magnitude of the error is large enough to be recorded in the laboratory and therefore an investigation was conducted by enforcing planar and wavy shear surfaces with artificial shearing interfaces. This investigation is covered in the following chapter.

Chapter 9

Laboratory Validation Of The Mathematical Model And Extension Of The Theory To Field Problems

9.1 Prediction Of Laboratory Strengths

The aim of these tests was to attempt to validate the use of Equation 8.24 for all heights and shapes of wave-form, by obtaining true shear strengths τ from a planar perspex interface and then predicting and observing apparent shear strengths $\tau_{apparent}$ from controlled non-planar surfaces developed against the interfaces illustrated and described in Subsection 3.3.2. Equation 8.24,

$$\tau_{apparent} = \tau(1 + ka_1)$$

can be expressed as

$$\tau = C\tau_{apparent} \tag{9.1}$$

or in terms of the residual stress ratio

$$\tan \phi_r = C \tan \phi_{r_{apparent}} \tag{9.2}$$

where

$$C = \frac{1}{1 + ka} \tag{9.3}$$

This means that prior to testing two parameters need to be defined, the lateral earth pressure coefficient k and the geometric factor a.

Defining the exact value for k was very difficult. At this stage it was decided that k_0, the *"at rest"* parameter should be used. Laboratory measurement of this is difficult because the condition corresponds to zero lateral strain, this makes stress recording almost impossible. Therefore, it was decided to use the following expression proposed by Jaky [179] for normally consolidated soils:

$$k_0 = 1 - \sin \phi'. \tag{9.4}$$

The peak angle of friction, ϕ', for the kaolin used was likely to fall in the range $15 - 20°$, which, using Equation 9.4, yields values of k_0 from 0.66 to 0.74 respectively. Henceforth a value of $k = 0.7$ was adopted in Equation 9.3.

The geometric factor a is defined by the size of the annulus and the height of the wave-form and was stated in Equation 8.25 as

$$a_1 = \frac{2h_v}{r_2 - r_1}.$$

Now that the v-shape correction equation is being used for any wave-form of height h, the equation can now be written thus,

$$a = \frac{2h}{r_2 - r_1}. \tag{9.5}$$

For the interfaces used during the testing h was either 2 mm or 4 mm and therefore, as the inner and outer radii of the Bromhead annulus are 35 mm and 50 mm respectively, $a_{2mm} = 0.266$ and $a_{4mm} = 0.533$. Substituting these values and $k = 0.7$ into Equation

9.3 yields,

$$C_{2mm} = \frac{1}{1 + (0.7 \times 0.266)} = 0.843 \tag{9.6}$$

and

$$C_{4mm} = \frac{1}{1 + (0.7 \times 0.533)} = 0.728. \tag{9.7}$$

Henceforth, when the 2 mm v-shape or circular arc interfaces, see Figure 3.6, are used the apparent average residual angles multiplied by 0.843 should give the true average residual angle recorded from the planar interface. Similarly, when the 4 mm interfaces are used, multiplying the apparent residual angles by 0.728 should reduce them to the true value.

9.2 Laboratory Testing

9.2.1 Procedure

The main testing procedure including descriptions of the apparatus, interfaces, sample preparation, testing techniques, data acquisition, and testing errors is provided in Section 3.3. The investigation consisted of five tests, each one being performed at a rate of 0.0237 mm/min through three increasing levels of normal stress, 50, 100 and 150 kPa, thus ensuring that the sample was always normally consolidated. Test WF1 was performed against a planar interface to obtain the true residual strength. Tests WF2 and WF3 were performed against 2 mm and 4 mm v-shape interfaces respectively and tests WF4 and WF5 were performed against the 2 mm and 4 mm circular arc interfaces. The results from each test were processed to yield slow drained residual angles and by comparing these an assessment was made on the accuracy of the theory.

9.2.2 Test Results

The first test in the series conducted in the Bromhead ring shear apparatus, WF1, used the planar perspex interface. The aim of the test was to develop a truly planar shear surface and hence find the true shear strength of kaolin against a perspex

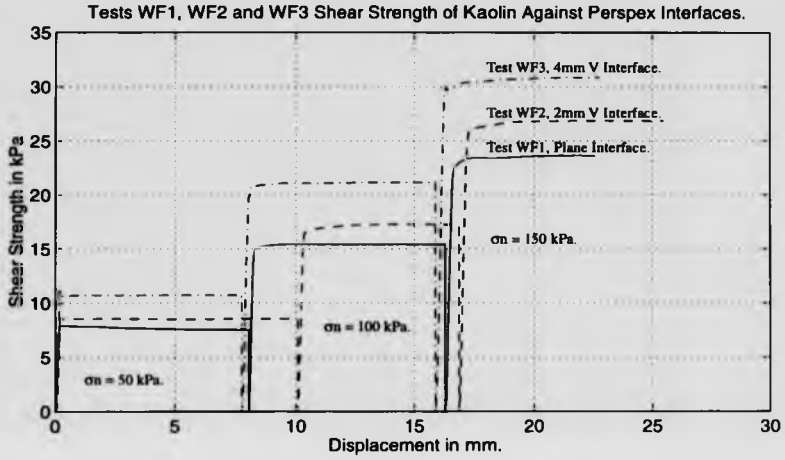

Figure 9.1: Tests WF1, WF2 and WF3, levels of residual strength.

interface.

The results of the first test are represented by the solid lines in Figure 9.1, a plot of shear strength against displacement illustrating the levels of residual strength and in Figure 9.2, illustrating the residual angles of shearing resistance. For Test WF1 the observed residual shear strengths were, 7.50, 15.42 and 23.56 kPa corresponding to normal stress levels of 50, 100 and 150 kPa respectively. This gives a range of residual angles from 8.5° at 50 kPa to 8.9° at 150 kPa, the average value being 8.7°. The results of Test WF2, using a 2 mm v-shaped interface, are illustrated by the

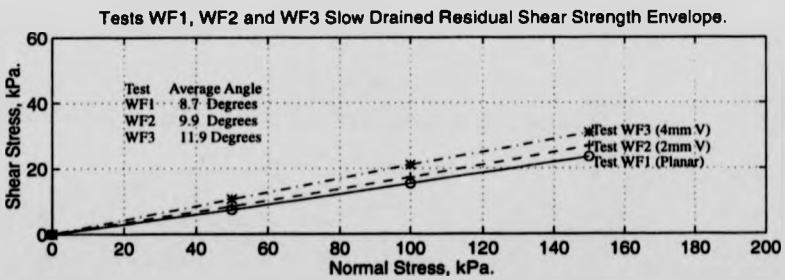

Figure 9.2: Tests WF1, WF2 and WF3, residual angles of shearing resistance.

dashed lines on Figures 9.1 and 9.2. This test proved for the first time that non-planar wave-forms would generate higher shear strengths than planar interfaces. For Test WF2 the observed apparent residual shear strengths were 8.55, 17.27 and 26.83 kPa corresponding to the three standard levels of normal stress (50, 100 and 150 kPa, respectively). This gives a range of apparent residual angles significantly higher than those in Test WF1. The values ranged from 9.7° at 50 kPa to 10.1° at 150 kPa, the average apparent value being 9.9° over 1° higher than the true residual angle of friction.

The results of Test WF3, using a 4 mm v-shaped interface, are illustrated by the dash-dot line on Figures 9.1 and 9.2. According to the new theory, a further increase in shear strength above the levels recorded from the 2 mm v-shaped interface should be observed. This proved to be the case, the observed apparent residual shear strengths were 10.73, 21.13 and 30.85 kPa corresponding to the three standard levels of normal stress. This gives a range of residual angles of friction from 11.6° at 150 kPa to 12.1° at 50 kPa, the average value being 11.9°, again a level significantly higher than both Tests WF1 and WF2.

The first three tests have indicated that the levels of residual shear strength do increase with the height of the wave-form on the interface. This is the first indication that the new theory may be valid, although the magnitudes predicted by the theory and those observed in the tests have, as yet, to be analysed. The next two tests were conducted using circular arc interfaces to see if almost identical behaviour could be observed, as predicted by the new theory. The results of Test WF4, using a 2 mm circular arc interface, are illustrated in Figure 9.3, a plot of shear strength against displacement illustrating levels of residual strength and in Figure 9.4, illustrating the residual angle of shearing resistance. In both Figures 9.3 and 9.4, Test WF4 is represented by the dashed line. Test WF4 produced results encouragingly similar to Test WF2, the apparent residual shear strengths were 9.23, 18.21 and 27.26 kPa at the three standard levels of normal stress. The apparent residual angles ranged from 10.3° at 100 kPa to 10.5° at 50 kPa, the average value being 10.3°. This is significantly higher than the true planar angle (8.8°) and similar to the value recorded for the 2 mm v-shaped interface (9.9°), indicating that wave-form is not a major parameter in

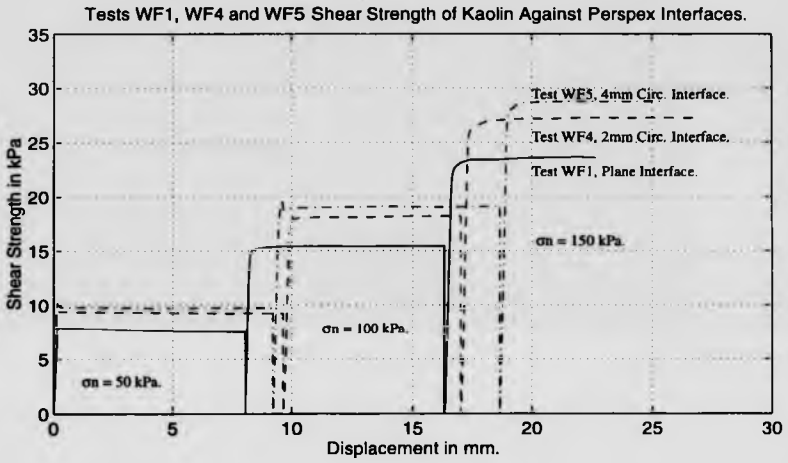

Figure 9.3: Tests WF1, WF4 and WF5, levels of residual strength.

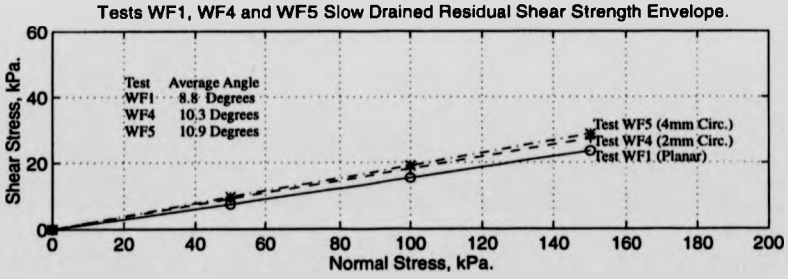

Figure 9.4: Tests WF1, WF4 and WF5, residual angles of shearing resistance.

these tests.

Test WF5 however, was not quite as encouraging. The test was performed using a 4 mm circular arc and therefore similar results to Test WF3 using the 4 mm v-shape wave-form were predicted. However, the apparent residual angle of friction is around 1° lower in Test WF5 than in Test WF3. The results from Test WF5 are illustrated by the dash-dot lines in Figures 9.3 and 9.4. The apparent residual shear strengths in Test WF5 were 9.72, 19.11 and 28.75 kPa at the three standard levels of normal stress. The residual angles of friction ranged from 10.8° at 150 kPa to 11° at 50 kPa, the average value being 10.9°. As stated earlier, not quite the expected value. However these five tests do illustrate the trend of increasing shear strength with waviness predicted by the theory. A closer analysis of the results is performed in the following section.

9.3 Analysis Of Results And Conclusions

To simplify the analysis of the results, the average residual angle of shearing resistance was used in place of the shear strength recorded over a range of normal stresses. The legitimacy of this assumption needs to be examined in relation to the variation of the recorded angles at different normal stress levels. A study of the results illustrated in Figures, 9.1, 9.2, 9.3 and 9.4 reveals that the largest variation in residual angle for any test with normal stresses in the range 50-150 kPa was 0.5° in Test WF3. This small variation could be attributed to many minor effects such as side friction or the problems associated with testing at low levels of normal stress. As the variations are relatively insignificant and certainly smaller than the fluctuations that have been observed in the tests as a result of the non-planar interfaces, it is reasonable to use the average value of the residual angle of friction in the analysis of the test results.

A convenient way to compare the results is presented for Test WF1 in Table 9.1 and Tests WF2 to WF5 in Table 9.2. A study of Table 9.2 reveals that the predicted values did not exactly match the observed values. However this would not be expected and the quality of the correlation will be discussed presently. If the results of Tests WF3 and WF4 were studied alone, it would be possible to conclude that the calculated

Table 9.1: Results from test WF1.

Test No. and Description	σ_n kPa	τ kPa	ϕ_r Degrees	ϕ_{range} Degrees	ϕ_r Average
WF1	50	7.50	8.5		
Plane	100	15.42	8.8		
	150	23.56	8.9	0.4	8.7

Table 9.2: Results from tests WF2 to WF5.

Test No. and Description	σ_n kPa	$\tau_{app.}$ kPa	$\phi_{r_{app.}}$ Deg.	ϕ_{range} Deg.	$\phi_{r_{app.}}$ Ave.	C Obs.	C Pred.	$\phi_{r_{app.}}$ Pred.
WF2	50	8.55	9.7					
2mm V	100	17.27	9.8					
	150	26.83	10.1	0.4	9.9	0.879	0.843	10.4
WF3	50	10.73	12.1					
4mm V	100	21.13	11.9					
	150	30.85	11.6	0.5	11.9	0.739	0.728	12.1
WF4	50	9.23	10.5					
2mm circ.	100	18.21	10.3					
arc	150	27.26	10.3	0.2	10.4	0.846	0.843	10.4
WF5	50	9.72	11.0					
4mm circ.	100	19.11	10.8					
arc	150	28.75	10.9	0.2	10.8	0.815	0.728	12.1

correction factors and henceforth Equations 9.1 to 9.3 were accurate. In Test WF4 the predicted strength was attained during the test to within 0.1°, indicating that if the theory was accurate, the correct value of k_0 had been selected. In Test WF3 the angle attained in the test was only 0.2° lower than the predicted angle, a discrepancy which is relatively small if the accuracy of the testing and the range of recorded residual angles are considered. These two tests illustrate that accurate predictions can be made for both 2 *mm* and 4 *mm* wave-forms and also for v-shape and circular wave-forms. On the basis of these two tests therefore, it is reasonable to assume that the correction factor defined in Equation 9.3 is useful for a wide range of wave heights and, although derived for a v-shape wave-form, is equally applicable to any wave-form when Figures 8.6 to 8.8 are considered in conjunction with these results.

Nevertheless just because the results from Tests WF2 and WF5 do not match the theory quite as well as Tests WF3 and WF4 does not mean that they should be ignored. In Test WF2 the average residual angle recorded was 9.9°, with results ranging from 9.7° to 10.1°, yet the predicted value was 10.4°, thus illustrating a discrepancy of 0.5° from the average value and 0.3° from the closest value recorded during the test. This result with the 2 *mm* v-shape interface is a borderline case, using Equations 9.1 to 9.3 to correct the apparent strength provides a solution closer to the true strength than Equation 3.2 would, the result however is not accurate. Test WF5 also illustrates this trend. In this case the discrepancy from the average angle is greater than 1° and as such is not acceptable.

It is difficult to reach any significant conclusions from these tests, as both 2 *mm* and 4 *mm* wave-forms have provided results which match both well and poorly the predicted values. Similarly, the same can be said for the type of wave-form. Tests WF3 and WF4 do provide encouraging results which have helped to validate Equations 9.1 to 9.3.

There are three main practical considerations which may explain the discrepancies in the results. The first one being that the analysis of Tests WF2 through to WF5 depends on the accuracy of Test WF1, where the true planar strength is obtained. Therefore, any errors made during Test WF1 are likely to be reflected in the predictions for the other four tests.

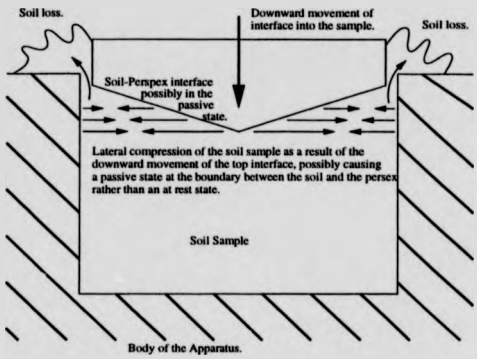

Figure 9.5: A potential mechanism for the development of passive conditions at the soil-perspex interface.

Secondly, and possibly more significantly, is the effects of the scale of the testing apparatus. Lateral earth pressure theory is supposed to relate to problems in earth retaining structures, which are on a vastly different scale to the Bromhead ring shear apparatus and do not involve longitudinal shearing at residual conditions. The effects on the influence of k_0 by the close proximity of four rigid boundaries is uncertain and the direct application of k_0 in this problem is not ideal. However some of these problems will be overcome when the theory is expanded and applied to large scale slope stability problems. Thirdly, and probably most significantly, is the ubiquitous use of k_0, with little consideration of the possibilities of having active (k_a) or passive (k_p) conditions at the soil-perspex interface. In three of the four tests the predicted values fell below the observed values. This suggests that the values of k may have been low. One way of correcting this underestimation would be to consider the possibility of passive conditions at the interface and using a value of k_p in place of k_0. By doing this, one is assuming that the sample is being compressed laterally during shearing. A mechanism for this could be envisaged when the loss of soil from the body of the apparatus is considered. This mechanism is outlined in Figure 9.5. Theoretically the value of k_p in operation would be controlled by the amount of lateral compression and this would ultimately relate to the downward movement of the interface as a result of soil loss, the value of k_p increasing with downward displacement.

Whilst the tests do not completely vindicate the use of the new theory, there are many potential reasons for the discrepancies as outlined above. It is reasonable to assume that the new theory is of some merit, and its potential larger scale applications and increasing power are considered in Sections 9.4 and 9.5.

9.4 Expansion Of The Theory

9.4.1 Simplifying The Derivation

In order to widen the scope and applications of this theory it is first important to see how the application of the general solution to the v-shape wave-form to yield equations 9.1 to 9.3 can be simplified.

The derivation can actually be completed in four lines of working. Consider Figure 9.6, as lateral earth pressure acts equally in all horizontal directions, the v-shape wave-form with gradients plus and minus a in Figure 9.6 Part (i) can be modelled as a single gradient of value a as shown in Figure 9.6 Part (ii). Applying the general solution, Equation 8.11,

$$M_{np} = \int_{r_1}^{r_2} 2\pi r^2 \tau dr + \int_{r_1}^{r_2} 2\pi r^2 k\tau \left|\frac{dh}{dr}\right| dr$$

to the gradient shown in Figure 9.6 Part (ii) yields,

$$M_{np_{vshape}} = 2\pi\tau \left[\int_{r_1}^{r_2} r^2 dr + \int_{r_1}^{r_2} kar^2 dr\right] \tag{9.8}$$

and therefore

$$M_{np_{vshape}} = \frac{2}{3}\pi\tau \left[(r_2^3 - r_1^3) + ka(r_2^3 - r_1^3)\right]. \tag{9.9}$$

Equating this to the standard planar solution, Equation 8.23,

$$M = \frac{2\pi\tau_{apparent}}{3}(r_2^3 - r_1^3)$$

yields the identical solution,

$$\tau = \frac{\tau_{apparent}}{1 + ka}. \tag{9.10}$$

Apart from simplifying the derivation this concept of modelling a wave with an ef-

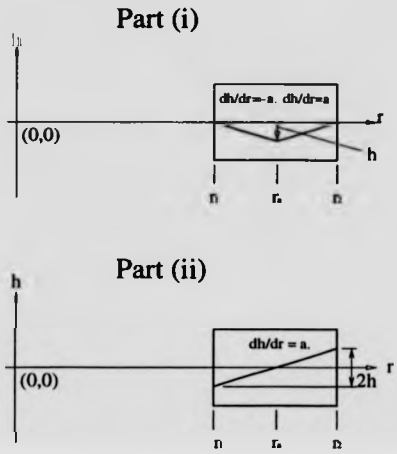

Figure 9.6: The simple modelling of a v-shape wave-form.

fective gradient could make this a powerful tool in the analysis of slope stability, where multiple wave-forms may exist in actual shear zones. Despite the fact that this solution was derived for the ring shear apparatus it is identical to the reduction factor proposed by Skempton [5] which allows for the influence of side shear in actual landslides, thus providing further evidence that this technique could be expanded to apply to real slope stability problems.

9.4.2 Multiple Wave-Forms And The Concept Of Effective Gradient

Whilst it is unlikely that multiple wave-forms will develop during ring shear testing it is quite likely that they might develop along actual shear surfaces. So as a first step to developing a theory which applies to real landslides, problems in the ring shear apparatus are considered. The concept of effective gradient introduced in Subsection 9.4.1 can be used to model any number of wave-forms, as long as the wavelength and amplitude remain constant. Consider the wave-form shown in Figure 9.7 Part (i). Attempting to model this using the technique adopted in Section 8.3 would prove virtually impossible. However, by using the effective gradient, a_e, which is equal to

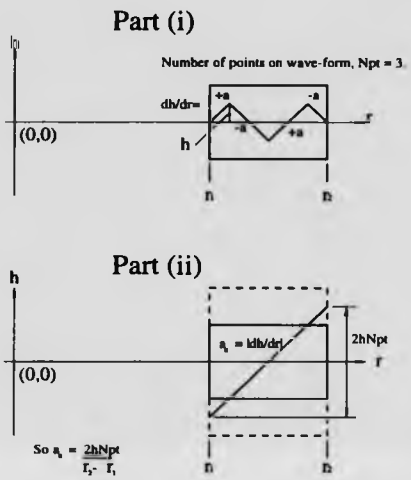

Figure 9.7: The simple modelling of a multiple v-shape wave-form.

the modulus of dh/dr, the problem becomes simple as shown in Figure 9.7 Part (ii) which illustrates the effective gradient a_e of the wave-form shown in Figure 9.7 Part (i). The effective gradient

$$a_e = \left|\frac{dh}{dr}\right| \tag{9.11}$$

is calculated thus,

$$a_e = \frac{2hN_{pt}}{r_2 - r_1}, \tag{9.12}$$

where N_{pt} is the total number of peaks and troughs along the wave-form. Once the effective gradient a_e has been calculated, it can then be used in the correction equation thus,

$$r = \frac{r_{apparent}}{1 + ka_e}. \tag{9.13}$$

Therefore any number of peaks and troughs can be dealt with very easily. As an example of the effect of multiple wave-forms consider Figure 9.8. This illustrates the relationship between the correction factor C and the number of peaks and troughs N_{pt} for a wave of height 1 mm and a k value of 0.5. It can be seen that the value of C falls steadily from being 1.0 when $N_{pt} = 0$ to a level that eventually becomes assymptotal with $C = 0$. This means that as the number of wave-forms increases the accuracy of

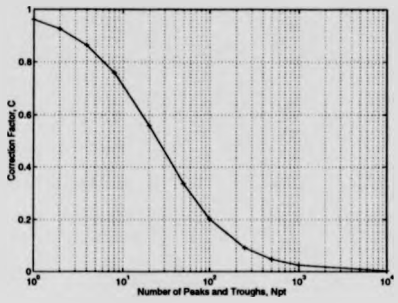

Figure 9.8: The relationship between the number of peaks and troughs of a wave-form and the correction factor for the IC/NGI ring shear apparatus (assuming $k = 0.5$ and $h = 1mm$).

the shear strength calculated using Equation 3.2 falls steadily, rendering the results to be very inaccurate unless they are corrected. If similar results are discovered for translational sliding, the presence of wavy shear surfaces will almost certainly need to be accounted for in some slope stability problems. The potential applications relate to landslides where undulating shear surfaces have been observed parallel to the direction of shearing. Initially it is anticipated that this idea of using lateral earth pressure coefficients and effective gradients could be applied to translational land sliding, if undulating surfaces were observed. Corrected shear strengths allowing for the effects of the undulations could provide an insight into the accuracy of factors of safety where slope failure was predicted but slope stability occurred. The application of this theory to rotational slides or slides with internal shear planes will not be as easy, owing to the more complicated geometries and the variation in the orientation and magnitude of the normal stress over the shear surface. However, if the technique is found to be of use with translational slides, it may be possible to approach these problems in the future using computational techniques.

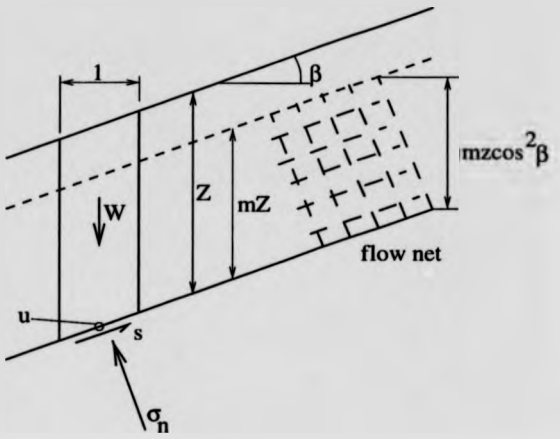

Figure 9.9: Plane translational landslide.

9.5 Field Applications

9.5.1 Undulating Translational Slip Analysis

The analysis of a plane translational landslide using the infinite slope method is well documented, a good example being provided by Craig [178]. Consider the slope illustrated in Figure 9.9, in which the potential failure surface is planar and parallel to the surface as is the phreatic surface. The potential failure surface is at a depth Z, which is small compared to the overall slope dimensions, henceforth the slope can be considered infinite and end and side effects can be ignored.

The shear strength of the soil on the failure plane is,

$$\tau = c' + (\sigma_n - u)\tan\phi' \tag{9.14}$$

and then the factor of safety for the slope is then given by,

$$FOS = \frac{\tau}{s} \tag{9.15}$$

where s is the shear stress on the surface. In association with Figure 9.9, σ_n, s and

u can be derived to give,

$$\sigma_n = [(1-m)\gamma + m\gamma_{sat}]Z\cos^2\beta, \tag{9.16}$$

$$s = [(1-m)\gamma + m\gamma_{sat}]Z\sin\beta\cos\beta \tag{9.17}$$

and

$$u = mZ\gamma_w\cos^2\beta \tag{9.18}$$

where γ, γ_{sat} and γ_w are the unit weights of the unsaturated soil, the saturated soil and water respectively. Substituting Equations 9.16 and 9.18 into Equation 9.14 and then substituting the result of that with Equation 9.17 into Equation 9.15 yields the result,

$$FOS = \frac{c'}{[(1-m)\gamma + m\gamma_{sat}]Z\sin\beta\cos\beta} + \left\{1 - \frac{m\gamma_w}{(1-m)\gamma + m\gamma_{sat}}\right\}\frac{\tan\phi'_p}{\tan\beta}. \tag{9.19}$$

This provides the solution for the full case for an infinite slope. In this research other special cases have been considered. If $m = 0$ there are no significant pore water pressures and Equation 9.19 reduces to,

$$FOS = \frac{c'}{\gamma Z\sin\beta\cos\beta} + \frac{\tan\phi'_p}{\tan\beta}. \tag{9.20}$$

If the shear surface is in a residual strength condition then $c' = 0$ henceforth Equation 9.19 reduces to give,

$$FOS = \left\{1 - \frac{m\gamma_w}{(1-m)\gamma + m\gamma_{sat}}\right\}\frac{\tan\phi'_r}{\tan\beta} \tag{9.21}$$

and finally if there are no pore water pressures $m = 0$ and residual conditions exist $c' = 0$, the result simply becomes,

$$FOS = \frac{\tan\phi'_r}{\tan\beta}. \tag{9.22}$$

Now consider the slope illustrated in Figure 9.10 on which end and side effects are still ignored and l_{max} and w_{max} are much greater than Z but no longer considered

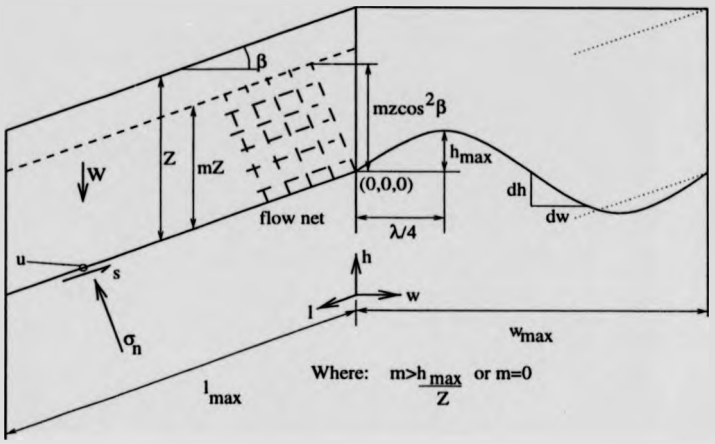

Figure 9.10: Section through an undulating translational landslide.

infinite. The slope contains an undulating shear surface along which $h = f(w)$ and the shear strength of the soil is τ. A similar analysis to that in Section 8.2 can now be performed.

Firstly consider the force, F_h, generated by the summation of all the horizontal elements of width dw,

$$F_h = \int_0^{w_{max}} \tau l_{max} dw. \tag{9.23}$$

Then consider the force, F_v, generated by the summation of all the vertical elements of height dh,

$$F_v = \int_0^{w_{max}} \tau_v l_{max} dh, \tag{9.24}$$

where τ_v is the shear strength on the vertical planes differing from τ because of the difference in the vertical stress, σ_n, and the horizontal stress, $k\sigma_n$. Substituting

$$dh = \frac{dh}{dw} dw \tag{9.25}$$

and applying the constraint

$$dh = \left| \frac{dh}{dw} \right| dw \tag{9.26}$$

to prevent negative gradients yielding negative forces gives,

$$F_v = \int_0^{w_{max}} \tau_v l_{max} \left|\frac{dh}{dw}\right| dw \tag{9.27}$$

Therefore adding Equations 9.23 and 9.27 gives the total down slope force that can be resisted as,

$$F_{total} = \int_0^{w_{max}} \tau l_{max} dw + \int_0^{w_{max}} \tau_v l_{max} \left|\frac{dh}{dw}\right| dw. \tag{9.28}$$

Dividing Equation 9.28 by the total area of the slope $l_{max} w_{max}$ yields the shear strength of the undulating surface, τ_u,

$$\tau_u = \frac{\int_0^{w_{max}} \tau l_{max} dw + \int_0^{w_{max}} \tau_v l_{max} \left|\frac{dh}{dw}\right| dw}{l_{max} w_{max}} \tag{9.29}$$

It was shown previously in Subsections 8.4.2 and 9.4.2 that any wave-form developed in ring shear tests could be modelled by an inclined shear surface with an effective gradient a_e. This assumption is now applied to undulating translational slides with undulations of constant amplitude and wavelength. The effective shear surface is defined in the $h - w$ plane by

$$h = a_e w + b. \tag{9.30}$$

Therefore, if the effective shear surface has a positive gradient in the $h - w$ plane,

$$\left|\frac{dh}{dw}\right| = a_e. \tag{9.31}$$

Substituting Equation 9.31 into Equation 9.29 and completing the integrations yields the solution,

$$\tau_u = \tau + a_e \tau_v \tag{9.32}$$

where in general terms,

$$a_e = \frac{4 h_{max}}{\lambda} \tag{9.33}$$

Then τ_u can be used to determine the factor of safety for the undulating shear surface thus,

$$FOS = \frac{\tau_u}{s}, \tag{9.34}$$

where τ and τ_v are dependent on shear surface conditions.

9.5.2 Peak Strength Conditions

The analysis for peak strength conditions follows, its merits however are debatable because clearly defined shear zones only develop after peak strengths have been obtained and the strength is starting to approach residual levels. Nevertheless the technique may be of use in the back analysis of first time slides.

Two peak strength conditions will be considered, firstly, the no pore water pressure case. If the water table is completely below the shear surface at all points $m = 0$ and therefore,

$$\tau = c' + \sigma_n \tan \phi'_p \tag{9.35}$$

and

$$\tau_v = c' + k\sigma_n \tan \phi'_p \tag{9.36}$$

Equation 9.32 becomes,

$$\tau_u = c' + \sigma_n \tan \phi'_p + a_e(c' + k\sigma_n \tan \phi'_p) \tag{9.37}$$

and the factor of safety is given thus,

$$FOS = \frac{\tau_u}{s} = \frac{c'(1 + a_e) + \gamma Z \cos^2 \beta \tan \phi'_p (1 + ka_e)}{\gamma Z \sin \beta \cos \beta} \tag{9.38}$$

which can be rearranged into a form similar to Equation 9.20 thus completing the solution for peak strength with no pore water pressures,

$$FOS = \frac{c'(1 + a_e)}{\gamma Z \sin \beta \cos \beta} + \frac{\tan \phi'_p}{\tan \beta}(1 + ka_e) \tag{9.39}$$

Secondly in the case where the water table is not below the shear surface but

actually exists in or above the undulations. This analysis currently assumes that the pore water pressure is constant across the undulations, which implies that the phreatic surface undulates parallel to the shear surface. This is obviously not correct, but the assumption will be made to keep the analysis simple. Therefore if the phreatic surface occurs anywhere between the wave peaks and troughs, the value of m should correspond to the wave peaks, that is $m > h_{max}/z$. This is a cautious approach and will lead to an underestimation of the factor of safety. So if $m \neq 0$,

$$\tau = c' + (\sigma_n - u)\tan\phi'_p \tag{9.40}$$

and

$$\tau_v = c' + k(\sigma_n - u)\tan\phi'_p. \tag{9.41}$$

Therefore Equation 9.32 becomes,

$$\tau_u = c' + (\sigma_n - u)\tan\phi'_p + a_e[c' + k(\sigma_n - u)\tan\phi'_p] \tag{9.42}$$

Henceforth for these conditions,

$$FOS = \frac{\tau_u}{s} = \frac{c'(1+a_e) + [(1-m)\gamma + m\gamma_{sat} - m\gamma_w]Z\cos^2\beta\tan\phi'_p(1+ka_e)}{[(1-m)\gamma + m\gamma_{sat}]Z\sin\beta\cos\beta}, \tag{9.43}$$

which can be rearranged into a form similar to Equation 9.19 thus completing the solution for peak strength with pore water pressures,

$$FOS = \frac{c'(1+a_e)}{[(1-m)\gamma + m\gamma_{sat}]z\sin\beta\cos\beta} + \left\{1 - \frac{m\gamma_w}{[(1-m)\gamma + m\gamma_{sat}]}\right\}\frac{\tan\phi'_p}{\tan\beta}(1+ka_e). \tag{9.44}$$

Comparing Equations 9.19 and 9.20 to Equations 9.39 and 9.44, it is apparent that the effect of the undulations is to increase the value of $\tan\phi'_p$ by the factor $1 + ka_e$ and the value of c' by $1 + a_e$.

9.5.3 Residual Strength Conditions

This technique is more applicable to residual strengths and reactivated landslides where shear surfaces are clearly defined.

When the water table is completely below the undulating shear surface the analysis can be performed for the case where $m = 0$ and therefore,

$$\tau = \sigma_n \tan \phi'_r \tag{9.45}$$

and

$$\tau_v = k\sigma_n \tan \phi'_r. \tag{9.46}$$

Substituting into Equation 9.32 yields,

$$\tau_u = \sigma_n \tan \phi'_r + a_c k\sigma_n \tan \phi'_r \tag{9.47}$$

and therefore,

$$FOS = \frac{\tau_u}{s} = \frac{\gamma Z \cos^2 \beta \tan \phi'_r (1 + ka_c)}{\gamma Z \cos \beta \sin \beta} \tag{9.48}$$

which can be rearranged into a form similar to Equation 9.22 thus completing the solution for residual strength with no pore water pressures,

$$FOS = \frac{\tan \phi'_r}{\tan \beta}(1 + ka_c). \tag{9.49}$$

Performing the analysis when the water table is in or above the shear zone requires the same assumptions made in Section 9.5.2, that is $m > h_{max}/Z$. Henceforth for the case when $m \neq 0$,

$$\tau = (\sigma_n - u) \tan \phi'_r \tag{9.50}$$

and

$$\tau_v = k(\sigma_n - u) \tan \phi'_r \tag{9.51}$$

Substituting into Equation 9.32 yields

$$\tau_u = (\sigma_n - u) \tan \phi'_r + a_c k(\sigma_n - u) \tan \phi'_r. \tag{9.52}$$

Therefore

$$FOS = \frac{\tau_u}{s} = \frac{[(1-m)\gamma + m\gamma_{sat} - m\gamma_w]Z\cos^2\beta\tan\phi'_r(1+ka_c)}{[(1-m)\gamma + m\gamma_{sat}]Z\sin\beta\cos\beta} \tag{9.53}$$

which can be rearranged into a form similar to Equation 9.21 thus completing the solution for residual strength with pore water pressures,

$$FOS = \left\{1 - \frac{m\gamma_w}{[(1-m)\gamma + m\gamma_{sat}]}\right\}\frac{\tan\phi'_r}{\tan\beta}(1+ka_c). \tag{9.54}$$

This provides a full set of equations (No. 9.39, 9.44, 9.49 and 9.54) which can be used to establish factors of safety for undulating translational slides, at peak and residual conditions and with or without pore water pressures. For the residual conditions as with the peak conditions, comparing Equations 9.49 and 9.54 to Equations 9.21 and 9.22, reveals that $\tan\phi'_r$ is increased by the factor $1+ka_c$ as a result of the undulating shear surface.

Chapter 10

Conclusions

10.1 Conclusions From The Ring Shear Tests

The main aim of this research has been to investigate the variation of residual strength in cohesive soils at rates of shearing up to 1000 mm/min. Three types of behaviour have been observed, each one having its own implications to slope stability.

- Neutral Effects, where residual strength remains relatively constant with increasing shear rate, as illustrated in Figure 10.1 Part(i). These occur in soils with high sand or silt contents and low clay fraction. These soils are essentially non-plastic in nature. Examples used in this research include Soil KBS2, a sandy clay, and Soil CRF, a pure silt.

- Positive Effect behaviour, as illustrated in Figure 10.1 Part(ii), occurs in cohesive soils when either no free water is available to the sample regardless of shear surface morphology or if water is available and a planar shear surface is maintained using an interface.

- Critical Effect behaviour, as illustrated in Figure 10.1 Part(iii), occurs in cohesive soils when free water is available to the shear zone, when either undulating interfaces are used, or unusual wave type vertical displacements are observed on the top platen during soil on soil or planar interface testing at faster rates of shearing. Critical Effect behaviour occurred in the majority of the tests per-

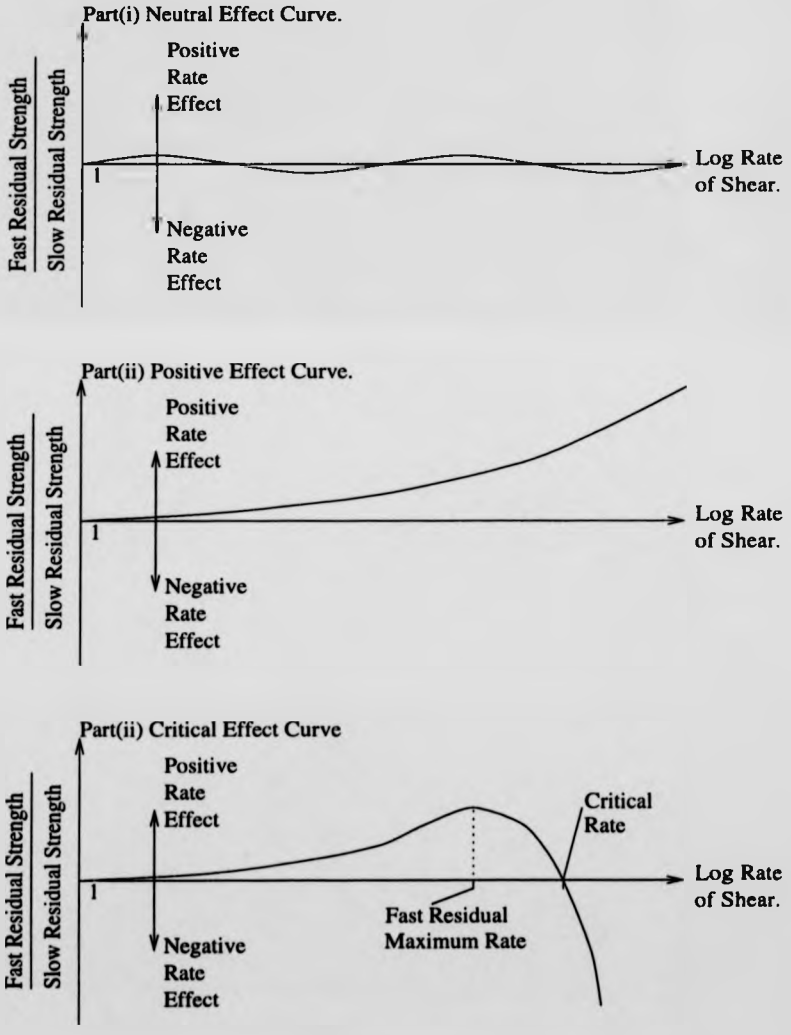

Figure 10.1: The three types of residual strength behaviour observed with increasing rate of shear.

formed in the IC/NGI ring shear apparatus but did not occur in the absence of free water.

The critical effect curve can be essentially defined by two points on the curve. The critical rate and the fast residual maximum rate. The critical rate appears to be independent of soil grading and undulation wavelength, but does vary according to the type of test. Using 1 *mm* wave height undulating interfaces, negative rate effects are induced at shear speeds in the range 50-200 mm/min, compared with 100-400 mm/min for soil on soil testing and approximately 1000 mm/min for plane interface testing. The variation of both the critical and positive effect curves with wave-form and clay fraction is illustrated in Figure 5.13.

The mechanisms behind positive rate behaviour have not been the main focus of this work. The behaviour always occurs at rates up to 1000 mm/min in soils exhibiting a positive effect curve and in soils illustrating a critical effect curve at shear velocities below the critical rate. Previous research has postulated that particle disorientation occurs at faster rates of shearing, thus disrupting the polished fabric of the shear zone. This increases particle contacts and interlocking and therefore leads to a rise in the fast residual strength. This is supported by the observation of slow peaks after fast shearing which occur in short displacements before strength falls to the slow residual value as the particles become realigned. This research has found no evidence in opposition to this idea, but a theoretical discussion suggesting that higher rates could cause increased particle alignment is undertaken in Section 6.2, the conclusion of which is that particle disorientation is more likely at higher rates.

Particle disorientation cannot be the only mechanism involved in positive rate effects for two reasons:

- Increases in fast residual strength exceed the slow peak strength after fast shearing (an indirect measure of the strength available from particle disorientation).
- Increases in fast residual strength exceed the slow remoulded peak strength, which is assumed to correspond to maximum disorientation.

The additional increase in strength at fast rates results from a viscous effect, which has been confirmed by Tika [2], directly using a rotary viscometer and indirectly by

observing virtually instant strength loss when shear rate was reduced during ring shear testing. Again this research has no evidence in opposition to a viscous component of strength and has undertaken a theoretical explanation of the behaviour. An analogy between a soil shear zone and a Newtonian fluid flow along a rigid boundary is described in Subsection 6.4.2, in which the shear stress at the boundary (shear zone) increases with flow velocity in laminar flows. The analogy is then extended to postulate that the breakdown from laminar to turbulent flow may correspond to the onset of particle disorientation.

Negative rate behaviour occurs in soils displaying a critical effect curve at shear velocities higher than the critical rate. Indirect testing methods, testing without water and testing with water to compare t_{90} consolidation times to strength recovery times, indicate that pore water pressure generation, reducing the effective normal stress and hence the shear strength is the likely mechanism behind negative rate behaviour. Tika et al [3] also observed these facts but could not measure any significant pore water pressures, possibly because they installed their pore pressure instrumentation into planar interfaces. This lead them to propose the dilation-flow concept described in Subsection 6.5.2, which relies on massive particle dilation, causing increased shear zone moisture content and therefore an increased ability for the soil to flow. Whilst this mechanism may occur in some soils, this research contains soil on soil tests on pure clays, Tests 16 and 17 for example, which contain no massive particles but still illustrate negative rate behaviour. Therefore a different mechanism is required.

The results of this research all indicate that the most likely cause of negative rate behaviour is positive pore water pressure generation as a result of rapid compression of the sample during fast shearing. The mechanism of the compression varies according to the type of test, whether soil on soil, planar interface or undulating interface. This pumping effect was initially observed during testing against undulating rigid interfaces, the compression being caused by shear displacements along the up slope, as discussed in more detail in Subsection 6.5.3. The pumping effect was partially confirmed by the measurement of significant pore pressures using transducers installed in an undulating interface.

Negative rate behaviour was also observed during soil on soil testing in which a planar surface should have developed. Unusual vertical displacements of the top platen occurred in these tests and usually corresponded to significant strength loss. These vertical displacements could represent the development of an undulating shear surface similar to those obtained with wavy rigid interfaces, but the geometry of the wave-forms observed on the top platen suggest that the shear zone had tilted but remained relatively planar, possibly as a result of uneven soil loss. This again would cause compression and expansion in the shear zone, the net effect of which was likely to be positive pore pressures. This concept is discussed in more detail in Subsection 6.5.5. Similar behaviour was observed during testing against a planar interface, this raises questions with regard to the tilted shear zone concept. The critical rate during these planar tests was much higher, 1000 mm/min, this could have triggered a different type of behaviour. The high viscous forces at the interface may have encouraged the development of secondary inclined shear planes, or possibly a wider shear zone undergoing an opposing dilation-contraction effect. This is thought to be unlikely but is discussed in more detail in Subsection 6.5.6.

Further evidence for pore water pressure generation was sought by developing a computational model, which, although quite crude, did predict levels of pore pressure generation. Using the model the effects of wave dimension, shear rate, normal stress level and sample depth on pore water pressure generation were investigated. These results correlated well with known facts about negative rate behaviour, that is, the relative magnitude of the effect increases with wave height and shear rate and decreases as normal stress is increased.

The author is confident that pore pressure generation by a pumping effect is a major cause of negative rate behaviour in cohesive soils. A strong body of both direct and indirect test evidence has been obtained in support of this theory but further direct measurements of pore water pressure are required to provide totally conclusive evidence. Where massive particles are present, the dilation-flow concept proposed by Tika et al [3] should not be discarded. This may act in conjunction with a pore pressure effect on undulating surfaces or singularly on a truly plane surface. Combinations of different mechanisms should never be discounted.

Two other typical strengths have been studied as part of this research.

- Fast Peak Strengths occur very rapidly during the first few millimetres of fast shearing and may be significantly higher than the slow remoulded peak strength. They tend to start to occur at rates in the range 1-10 mm/min and then increase in magnitude with increasing rate of shearing. The strengths attained at a given shear rate fall as clay content is decreased, but are independent of shear surface wave-form. Fast peak strengths were not observed in Test 6 when no water was available to the shear zone. Negative pore water pressures were observed during Tests 14 and 15 in association with fast peak strengths.

- Slow Peak Strengths After Fast Shearing occur in the first few millimetres of slow shearing once a fast shearing stage is complete. The preceding rate which triggers the onset of slow peaks increases as clay fraction falls from around 1 mm/min in pure clays up to 50 mm/min in silts. Slow peaks increase in magnitude up to a preceding rate of 300 mm/min and then tend to stay at this level or even decrease slightly as the preceding rate is increased to 1000 mm/min. During the kaolin on interface tests, maximum slow peak after fast shearing strength was around 50% of the slow remoulded peak strength. This value fell to around 25-30% with the mixtures of ball clay and crushed flint. In Test 6 (no water available), slow peaks after fast shearing 50% higher than the slow remoulded peaks were observed, this may be associated with the sample drying out.

The variation of both Fast Peak and Slow Peak After Fast Shearing Strengths with increasing rate and clay fraction is illustrated on Figure 5.13.

The mechanism generating fast peak strength is outlined in detail in Section 5.4.2. The results of this research indicate that the sample dilates rapidly as soon as it is subjected to fast shearing. This causes a small increase in strength as the particle alignment is disrupted, but a much larger increase in strength occurs as a result of negative pore pressures generated by the rapid dilation. This increases the effective normal stress and therefore the shear strength. The peak strength diminishes quickly as the shear zone reaches constant volume shearing and the negative pressures

dissipate. The mechanism for the slow peak strength after fast shearing is particle disorientation during the preceding fast shearing. This is discussed previously in this section and at length in Subsection 6.4.1.

10.2 Implications For Long Run-Out Landslides

This research has revealed that cohesive soils generally exhibit some form of rate effect. A Positive Effect Curve will be exhibited if a shear surface is absolutely planar, which is unlikely in the field, or if there is no free water available to the shear zone. A Critical Effect Curve will be exhibited in any undulating shear surface where free water is available to the shear zone. Furthermore, there are two peak strengths which occur in association with fast shearing. The fast peak strength occurs as soon as rapid shearing commences and the slow peak strength after fast shearing occurs once the shear zone is fully consolidated and slow shearing has resumed. The implications of all these effects to the triggering of long run-out landslides in cohesive soils now follows.

Fast peak strengths can be significantly higher than the slow drained residual strength and usually occur within the first few millimetres of shearing. Fast peaks are higher when free water is available to the shear zone, but may also occur to a lesser extent when no water is available. Therefore if a stable shear surface is subjected to a short rapid disturbing action, a single shock wave for example, the fast peak strength may prevent significant mobilisation of the landslide and therefore prevent the possibility of a negative rate effect fast residual strength occurring. However, if a more prolonged disturbing action occurs the fast peak strength will then decrease to the fast residual strength and this could encourage landslide acceleration.

Slow Peak strengths after fast shearing are associated with the disruption of the shear zone caused by fast shearing. When free water is available testing shows that slow peaks may be 15% to 20% higher than the slow residual strength and potentially 2 or 3 times more than this when free water is not available. The implications of this relate to reactivation of existing landslide masses which have previously experienced rates of movement above a value of approximately 50 mm/min. The slow peak

strength means that an extra disturbing force would be needed to overcome this peak, before prolonged slow shearing at slow residual conditions could recommence. Therefore, in the analysis of a well established shear zone which has experienced fast shearing in the past, the effect of the slow peak strength is to increase the factor of safety. However, because of the margins and uncertainties involved, the slow peak strength should not be included in slope stability calculations for design purposes.

A Positive Effect Curve basically implies that shear strength will continuously increase with the rate of shearing, in the field this is only likely where water is not freely available to induce negative rate effects. Whilst a positive rate effect is always desirable because it will tend to decelerate a mass movement, it may only occur in non-fissured intact clays which prevent water reaching the shear zone. There are other potential sources of water which should be considered and these include ground water and the possibility of the mass moving onto saturated material such as alluvium. This implies that, as with all other landslides, the risk of catastrophic slides can be reduced by draining the slope, but because of the scale of most large slope failures which degenerate into rapid flows this may be uneconomic even if potentially dangerous slopes could be identified. An interesting corollary of the positive effect curve is that, whilst it discourages catastrophic landslide mass acceleration, as soon as a slide starts to decelerate the available shear strength will fall, thus encouraging renewed acceleration. Therefore the effect of the positive effect curve may not be to stop rapid mass movements, but rather to limit their velocities.

The results of this research have shown that undulations on the shear surface of height 1 *mm* are large enough in the IC/NGI apparatus to generate pore water pressures which cause negative rate behaviour when water is available to the shear zone. Whilst there may be some scaling effect, it is reasonable to assume that most field shear zones are uneven enough to generate this pore water pressure effect, as long as free water is available. The most important factor then becomes the Critical Effect Curve and more particularly the critical rate of the shear zone. If a triggering action such as an earthquake causes rates of displacement above the critical rate, the slide will accelerate to potentially catastrophic failure even if the earthquake ceases. Shear rates below the critical rate will cause positive rate effects and will

encourage stability assuming that prior to the triggering action the slope was stable under slow drained residual conditions. A further extension of these ideas relates to the time taken to generate the negative rate behaviour and this is discussed in more detail in Subsection 5.4.7. Summarising these ideas, negative rate behaviour does not happen instantaneously but requires a finite period of time to develop. Therefore, if a triggering action causes rates of displacement above the critical rate, this will not accelerate the slide mass until this finite period of time passes. Thus, short term triggers such as shock waves or short earth tremors may not causes slide mass acceleration where as an earthquake similar in magnitude but of longer duration might.

Finally, whilst this work has focused on the initiation of rapid flows, the study may help to explain the phenomena of slide debris flowing up hill. Whilst it is the belief of the author that once a slide is initiated at fast rates of displacement it accelerates and eventually breaks down and flows under a different mechanism at much higher velocities, probably either mechanical fluidization or liquefaction flow on a saturated soil. It is possible that up hill flow may be aided by a pore water pumping effect, similar to that postulated on the up slope sections of the undulating shear surfaces used in this research.

10.3 Further Work

The immediate priority as a result of this work would be the final confirmation that undulating surfaces do indeed generate net positive pore water pressures and therefore negative rate behaviour. It is felt that this fact could be established using Interface 2 ($4 \times 1mm$ wave-form) instrumented with pore water pressure transducers as used in Tests 14 and 15. The reliability of the transducers has been a problem but the following techniques in conjunction with correct de-airing and underwater assembly could help to improve the quality and continuity of the data obtained:

- Omitting the bottom outer confining ring, thus reducing the kinking of the transducer cables between the interface and the data logger.

- Using epoxy resin to seal the cable housing which supplies the atmospheric reference pressure to the back of the transducer body. This will prevent the development of excess pore pressures behind the silicon diaphragm of the transducer.

- Making a small hole in the cable housing just outside the ring shear apparatus water bath, thus ensuring an atmospheric reference pressure behind the transducer diaphragm.

If successful these techniques would supply continuous pore pressure readings from four points around the annulus during fast shearing, thus allowing a more accurate assessment of the average pore water pressure and more definite conclusions. Furthermore, accurate comparisons could then be made between the magnitudes of negative rate effects and the observed pore water pressures.

The IC/NGI ring shear apparatus is undoubtedly complicated and during testing a number of problems may occur which incorporate uncertainties into the test results. *Soil loss, gap control, uneven shear loads* and *uneven settlement* have all been noted during this research and they all add an element of uncertainty to the test results. These topics are discussed in more detail in Section 5.2. With care and attention, however, it is possible to obtain repeatable results. Soil loss is the biggest limitation to ring shear testing at high velocities. Recently attempts have been made to prevent soil loss from the IC/NGI apparatus by Parathiras [4]. These were largely successful but involved closing the gap completely and losing the direct method of recording side friction. A mechanism is required which overcomes the problem of soil loss without giving rise to further uncertainties. It may be that the IC/NGI apparatus has been used at or close to its limits in the investigation of rate effects and that to gain further knowledge a totally new method is required. The continuous development of ring shear apparatus by Sassa and his team at Kyoto University, see Subsection 2.2.9, has lead to several impressive pieces of apparatus which are mostly fully automated devices with feedback systems, these prevent soil loss by maintaining a constant gap which is sealed by a rubber flange subject to a known compression and the friction force from the flange is known and remains constant. These apparatus are a new level

of technology beyond the IC/NGI ring shear apparatus and would be prohibitively expensive to develop in Europe, but because slope instability in association with earthquake loading is such a problem in Japan, substantial government funding is available at Kyoto. It is possible that even a relatively early version of Sassa's ring shear apparatus could help the progress of research into rate effects in the UK and Europe. The author feels that greater international cooperation would help to expand the understanding of catastrophic slope failures and that obtaining a version of Sassa's apparatus in the UK or Europe is the next logical and financially viable step.

A wide base of knowledge is now available on rate effects observed in the laboratory using the IC/NGI apparatus. As yet no significant work has been conducted on comparing this knowledge to real case studies. The problem with this is finding a suitable failure to investigate, then obtaining adequate field data and samples from the major shear zone, not just from the debris at the bottom of the slope. Further problems would also be encountered when trying to establish ground water levels in the slope prior to the failure; estimation may be possible by extrapolating from surrounding areas. Once a sample has been obtained, IC/NGI ring shear tests could be performed to determine the slow residual strength and also the strength behaviour with increased shear rate, which this research suggests would follow the Critical Effect Curve illustrated in Figure 10.1 Part(iii). Back analysis of the failure could then commence, but traditional quasi-static slope stability analysis would not be suitable. A dynamic analysis would be required probably involving continuous feedback from the fast test results and calculating the energy dissipation from the moving debris. This is undoubtedly a difficult task and probably involves many more years of research.

Finally, on further work the author believes there may be some merit in exploring the possibility of overlapping the fields of Geotechnics and Fluid Mechanics, by comparing fluid flows along a boundary to shear zones in soils. Most Fluid Mechanics focuses on Newtonian fluids in which shear stress is directly proportional to the rate of shear strain, which is obviously not the case in Soil Mechanics. A field of study exists on Bingham plastic fluids, which according to Roberson and Crowe [177], *"act like a solid for small values of shear stress and then behave as a fluid at higher shear stress"*, a situation which may be analogous with Soil Mechanics. A starting point

for this analogy may be the references suggested by Roberson and Crowe [177], these being Harris from 1977 [180] and Schowalter from 1978 [181].

10.4 Other Applications

The study of rate effects has applications beyond slope stability and long run-out landslides. Anything that involves either soil on soil shearing or soil shearing against a solid material could benefit from the knowledge presented in this thesis. Tika [98] acknowledged this and applied the results of her fast ring shear testing using steel interfaces to displacement piles. Pipe Jacking is another area that could benefit from this study. Pipe Jacking ranges in scale from the installation of small underground service pipes with diameters of a few centimetres up to the installation of short tunnels through pre-existing embankments. Whilst the scales differ vastly rate effects could significantly affect the jacking forces required, and this is one example where a negative rate effect may be advantageous. Finally a research program is in progress at Warwick University into the continuous extrusion of soil bricks from tapered concrete dies. The aim of this being to provide a sustainable alternative technology for developing countries. The aim is to extrude bricks at a rate of around 1 m/min and therefore an understanding of rate behaviour and pore pressure development along the taper may help with the attainment of smooth extrusion thus preventing transverse cracking in the bricks. Currently problems exist with stick slip behaviour which may be associated with rate effects.

10.5 The Influence Of Undulations Perpendicular To The Shear Direction

The stress distributions in a soil annulus subjected to rotational shearing are very complex, even when the shear surface is planar. There is a tendency for concave shear surfaces to develop during soil on soil tests in the IC/NGI apparatus and these complicate the stress distributions further. In an attempt to assess the influence of concave shear zones, lateral earth pressure theory was used to estimate horizontal

stresses in the annulus and this allowed additional shear strength as a result of the horizontal stresses acting on the concave surfaces to be calculated.

The general solution derived in this work allowed the analysis of any wave-form where the wave height was a function of the annular radius, and an investigation of the sensitivity of the solution to the type of wave-form revealed that wave-form was not a major controlling parameter. As a result of this work, the correction curve illustrated in Figure 8.6 was obtained for the IC/NGI apparatus. The solutions of the analysis were then compared to actual testing using non-planar interfaces in the Bromhead ring shear apparatus. Whilst the correlation between observed and predicted results was not perfect, using the correction factor would have provided a better estimation of the true shear strength than just taking the shear strength developed from the non-planar surface.

Finally a technique was developed to allow the influence of multiple wave-forms to be assessed in ring shear apparatus. This concept was then developed to derive factor of safety equations for translational landslides with undulations perpendicular to the direction. These have not yet been used and further work could involve assessing the influence of different wave dimensions and values of lateral earth pressure on the factor of safety. Furthermore comparisons with actual cases studies exhibiting such undulations could help to validate this concept.

References

[1] Skempton A.W. Fourth Rankine Lecture. Long-term stability of clay slopes. *Géotechnique*, 14(2):77–102, 1964.

[2] Tika T.M. *The effect of fast shearing on the residual strength of Soils.* PhD thesis, University of London, 1989.

[3] Tika T.M, Vaughan P.R, and Lemos L.J. Fast shearing of pre-existing shear zones in soil. *Géotechnique*, 46(2):197–233, 1996.

[4] Parathiras A.N. *Displacement rate effects on the residual strength of soils.* PhD thesis, University of London, 1994.

[5] Skempton A.W. Residual strength of clays in landslides, folded strata and the laboratory. *Géotechnique*, 35(1):3–18, 1985.

[6] Hvorslev M.J. Torsion shear tests and their place in the determination of the shearing resistance of soils. *Proceedings of the American Society for Materials and Testing*, 39:999–1022, 1939.

[7] Bishop A.W, Green G.E, Garga V.K, Andresen A, and Brown J.D. A new ring shear apparatus and its application to the measurement of residual strength. *Géotechnique*, 21(4):273–328, 1971.

[8] American Society of Civil Engineers. Progress report on the special committee to codify present practice on the bearing value of soils for foundations, Appendix A. In *Proceedings of the American Society of Civil Engineers, Papers and Discussions*, pages 1174–1191. 1917.

[9] Streck O. Fortschritte auf dem Gebeit des Baugrundforschung [Progress made in the field of foundation soil research]. *Zentralbl Bauverwaltung*, 9, 1928.

[10] Franzius O, Streck A, and Hinderks A. The Experiment Institute for Hydraulics and Foundations at the Technical University atHanover. Hydraulic laboratory practise, pages 599-601, 1929. American Society of Mechanical Engineers.

[11] Tiedmann B. Uber die Schubfestigkeit bindiger Böden. *Bautechnik*, 15(30,33):400–403,433–435, 1937.

[12] Ghani M.A. Determination of shear strcss of a fine cloddy soil with a "guarded" shear head. In *Proceedings of the 2nd International Conference of the International Society for Terrain-Vehicle Systems*, pages 279–310, Toronto, 1966. University of Toronto Press.

[13] Langer C. Propriétés mécaniques et physiques des terrains cohèrents. In *Compte rendu des recherches effectuées durant l'Année 1938*, pages 19–27, Paris, 1938. Laboratories du Bâtiment et des Travaux Publics.

[14] Cooling L.F and Smith D.B. The shearing resistance of soils. *The Journal of the Institution of Civil Engineers*, 3:333–343, 1935.

[15] Cooling L.F and Smith D.B. The shearing resistance of soils. In *Proceedings of the 1st International Conference on Soil Mechanics*, volume 1, pages 37–41, Harvard, 1936.

[16] Gruner H.E and Haefeli R. Beitrag zur Untersuchung des physikalischen und statischen Verhaltens Roharenter Böden [Contribution to the investigation of the physical and static behaviour of cohesive soils]. *Schweizerisch Bauzeitung*, 103:171–174,185–188, 1934.

[17] Hvorslev M.J. Uber die festigkeitseigenschaften gestörter Bindiger Böden [On the strength properties of remoulded cohesive soils]. *Danmarks Naturvidenskabelige Samfund, Ingeniorvidenskabelige Skrifter*, A(45), 1937. Published thesis.

Translated June 1969 by USAE Waterways Experiment Station, Vicksburg, Mississippi.

[18] Hvorslev M.J. Physical components of shear strength of saturated clays. In *Proceedings of the Research Conference on the Shear Strength of Cohesive Soils*, pages 169–273, Boulder, 1960. American Society of Civil Engineers.

[19] Hvorslev M.J and Kaufman R.I. Torsion shear apparatus and testing proceedures. *Bulletin No. 38, USAE Waterways Experiment Station, Vicksburg, Mississippi*, 1952.

[20] Haefeli R. Investigation and measurements of the shear strengths of saturated cohesive soils. *Géotechnique*, 20(3):186–208, 1950.

[21] Haefeli R. Mechanische Eigenschaften von Lockergesteinen. *Schweizerisch Bauzeitung*, 111:299–303,321–325, 1938.

[22] Lupini J.F, Skinner A.E, and Vaughan P.R. The drained residual strength of cohesive soils. *Géotechnique*, 31(2):181–213, 1981.

[23] Horn H.M and Deere D.U. Frictional characteristics of minerals. *Géotechnique*, 12(4):319–335, 1962.

[24] Goldstein M.N, Misumsky V.A, and Lapidus L.S. The theory of probability and statistics in relation to the rheology of soils. In *Proceedings of the 5th International Conference on Soil Mechanics*, volume 1, pages 123–126, Paris, 1961.

[25] Astbury N.F. Science in the ceramic industry. *Proceedings of the Royal Society*, A258:27–46, 1960.

[26] Mitchell J.K. The fabric of natural clays and its relation to engineering properties. *Proceedings of the Highway Research Board*, 35:693–713, 1956.

[27] Morgernstern N.R and Tchalenko J.S. The optical determination of preferred orientation in clays and its application to the study of microstructure in consolidated kaolin. *Proceedings of the Royal Society*, A300:218–250, 1967.

[28] Yong R.N.A and McKyes E. Failure and yield of a clay under triaxial stresses. *Journal of the Soil Mechanics and Foundations Division, American Society of Civil Engineers*, 97(SM1):159–176, 1971.

[29] Caquot A. *Equilibre des massifs à frottement interne.* Gauthier-Villars, Paris, 1934.

[30] Borowicka H. The influence of the colloidal content on the shear strength of clay. In *Proceedings of the 6th International Conference on Soil Mechanics*, volume 1, pages 175–178, Montreal, 1965.

[31] Chandler R.J. The measurement of residual strength in triaxial compression. *Géotechnique*, 16(3):181–186, 1966.

[32] Chandler R.J. The effects of weathering on the shear strength properties of Keuper Marl. *Géotechnique*, 19(3):321–334, 1969.

[33] Herrmann H.G and Wolfskill L.A. Residual shear strength of weak clay shales. Technical Report 3-699, Engineering properties of nuclear craters, Report 5, Massachusetts Institute of Technology, Cambridge, Massachusetts, 1966.

[34] Skempton A.W and Petley D.J. The strength along structural discontinuities in stiff clays. In *Proceedings of Geotechnical Conference, Oslo*, volume 2, pages 29–46, Oslo, 1967. Norwegian Geotechnical Institute.

[35] Binnie M.A, Clarke J.F.F, and Skempton A.W. The effect of discontinuities in clay bedrock on the design of dams in the mangla project. In *Transactions of the 9th International Conference on Large Dams*, volume 1, pages 165–183, Istanbul, 1967.

[36] Early K.B and Skempton A.W. Investigations of the landslide at Walton's Wood, Staffordshire. *Quarterly Journal of Engineering Geology*, 5:19–41, 1972.

[37] Sinclair S.R and Brooker E.W. The shear strength of Edmonton Shale. In *Proceedings of Geotechnical Conference, Oslo*, volume 1, pages 295–299, Oslo, 1967. Norwegian Geotechnical Institute.

[38] Kenney T.C. The influence of mineral composition on the residual strength of natural soils. In *Proceedings of the Geotechnical Conference, Oslo*, volume 1, pages 123–129, Oslo, 1967. Norwegian Geotechnical Institute.

[39] Cullen R.M and Donald I.B. Residual strength determination in direct shear. In *Proceedings of the 1st Australia-New Zealand Conference on Geomechanics*, volume 1, pages 1–10, 1971.

[40] Sembenelli P and Ramirez A.L. Measurement of residual strength of clay with a rotating shear machine. In *Proceedings of the 7th International Conference on Soil Mechanics*, volume 3, pages 528–529, Mexico, 1969.

[41] La Gatta D.P. Residual strength of clay and clay shales by rotation shear tests. *Havard Soil Mechanics Series*, No. 86, 1970. Cambridge, Massachussets.

[42] Garga V.K. *Residual shear strength under large strains and the effect of sample size on the consolidation of fissured clay.* PhD thesis, University of London, 1970.

[43] Lemos L.J. *The effect of rate on residual strength of soil.* PhD thesis, University of London, 1986.

[44] Lupini J.F. *The residual strength of soils.* PhD thesis, University of London, 1981.

[45] La Gatta D.P. The effect of rate of displacement on measuring the residual strength of clay. Contract Report 5-71-5, USAE Waterways Experiment Station, August 1971.

[46] Spears D.A and Taylor R.K. The influence of weathering on the composition and engineering porperties of in-situ Coal Measures rocks. *International Journal of Rock Mechanics and Mineral Science*, 9:729–756, 1972.

[47] Fleischer S. Scherbruch- und Schergleitfestigkeit von Bindigen Erdstoffen. *Neue Bergbautechnik*, 2(2):98–99, 1972. Frieburg: Mining Academy.

[48] Voight B. Correlation between Atterberg plasticity limits and residual shear strength of natural soils. *Géotechnique*, 23(2):265–267, 1973.

[49] Fleischer S and Scheffler H. Problem-oriented shearing technologies for the determination of the drained shear strength of cohesive soils. In *Proceedings of the 7th European Conference on Soil Mechanics*, volume 2, pages 41–48, Brighton, 1979.

[50] Townsend F.C and Gilbert P.A. Tests to measure residual strengths of some clay shales. *Géotechnique*, 23(2):267–271, 1973.

[51] Townsend F.C and Gilbert P.A. Engineering properties of clay shales, Report 2: Residual shear strength and classification indexes of clay shales. Technical Report S-71-6, Soils and Pavement Laboratory, USAE Waterways Experiment Station, Vicksburg, 1974.

[52] Townsend F.C and Gilbert P.A. Effects of specimen type on the residual strength of clays and clay shales. *American Society for Testing and Materials*, STP599:43–65, 1976.

[53] Vaughan P.R and Walbancke H.J. The stability of cut and fill slopes in boulder clay. In *Proceedings of Symposium on Engineering Beahviour of Glacial Materials*, pages 209–219, Birmingham, 1975. Midland Society Soil Mechanics.

[54] Vaughan P.R, Hight D.W., Sodha V.G., and Walbancke H.J. Factors controlling the stability of clay fills in Britain. In *Clay Fills*, pages 203–217. Institution of Civil Engineers, London, 1978.

[55] Kanji M.A. The relationship between drained friction angles and Atterberg limits of natural soils. *Géotechnique*, 24(4):671–674, 1974.

[56] Kanji M.A and Wolle C.M. Residual strength- new testing and microstructure. In *Proceedings of the 9th International Conference on Soil Mechanics*, volume 1, pages 153–154, Tokyo, 1977.

[57] Littleton I. An experimental study of the adhesion between clay and steel. *Journal of Terramechanics*, 13(3):141–152, 1976.

[58] Bucher F. Die Restscherfestigkeit natürlicher Böden, ihre Einflussgrössen und Beziehungen als Ergebnis experimenteller Untersuchungen. Technical Report 103, 99 Pages, Zürich: Institutes für Grundbau und Bodenmechanik Eidgenössische Technische Hochschule, 1975.

[59] Blondeau F and Josseaume H. Mesure de la résistance au cisaillement résiduelle en laboratoire. Technical report, Bulletin de Liason des Laboratoires des Ponts et Chaussées, 1976. Stabilité de talus 1, versants naturels numéro spécial II, 90-106.

[60] Kenney T.C. Residual strengths of mineral mixtures. In *Proceedings of the 9th Inernational Conference on Soil Mechanics*, volume 1, pages 155–160, Tokyo, 1977.

[61] Seyček J. Residual shear strength of soils. *Bulletin of the International Association of Engineering Geology*, 17:17–35, 1978.

[62] Mandl G, De Jone L.N.J, and Maltha A. Shear zones in granular material. *Rock Mechanics*, 9:95–144, 1977.

[63] Bromhead E.N. A simple ring shear apparatus. *Ground Engineering*, 12(5):40–44, 1979.

[64] Bromhead E.N and Dixon N. The field residual strength of london clay and its correlation with laboratory measurements, especially ring shear tests. *Géotechnique*, 36(3):449–452, 1986.

[65] Moore R. The chemical and mineralogical controls upon the residual strength of pure and natural clays. *Géotechnique*, 41(1):35–47, 1991.

[66] Yagi N, Yatabe R, and Enoki M. *Landslides*, chapter Stability analyses for landslides using ring shear results. Balkema, Rotterdam, 1991. Edited by Bell.

[67] Anayi J.F, Boyce J.R, and Rogers C.D.F. Modified Bromhead ring shear apparatus. *Geotechnical Testing Journal, GTJODJ*, 12(2):171–173, 1989.

[68] Taylor P and Petley D.J. A review of the first phase of testing using the modified ring shear apparatus. Technical Report CE 54, University of Warwick, Department of Engineering, October 1996.

[69] Stark T.D and Vettel J.J. Bromhead ring shear test proceedure. *Geotechnical Testing Journal, GTJODJ*, 15(1):24–32, 1992.

[70] Stark T.D and Eid H.T. Modified Bromhead ring shear apparatus. *Geotechnical Testing Journal, GTJODJ*, 16(1):100–107, 1993.

[71] Hungr O and Morgernstern N.R. High velocity ring shear tests on sand. *Géotechnique*, 34(3):415–421, 1984.

[72] Sassa K. The mechanism starting liquefied landslides and debris flows. In *Proceedings of the 4th International Symposium on Landslides*, volume 2, pages 349–354, Toronto, 1984.

[73] Sassa K, Shima M, Hiura M, Nakagawa A, and Suemine A. Development of ring shear type debris flow apparatus. Technical Report 57860028, Japanese Ministry of Education, Science and Culture, 1984. Report of grant-in-aid for scientific research.

[74] Sassa K. The mechanism of debris flow. In *Proceedings of the 11th International Conference on Soil Mechanics and Foundation Engineering*, volume 3, pages 1173–1176, San Francisco, 1985.

[75] Sassa K, Fukuoka H, and Vibert C. A new high-speed high-stress ring shear apparatus and the undrained shear strength during motion. In *Proceedings of the Japan-China Symposium on Landslides and Debris Flows*, pages 93–97, 1989.

[76] Sassa K, Fukuoka H, Vibert C, and Shima M. Development of a high-speed high-stress ring shear apparatus and shear strength reduction at rapid loading in landslides. *Annuals, Disaster Prevention Research Institute, Kyoto University*, 32(B-1):165–182, 1989. (In Japanese).

[77] Sassa K, Fukuoka H, and Zhang D.X. *Landslides*, chapter Measurement of the apparent friction angle during rapid loading by the high-speed high-stress ring shear apparatus–Interpretation of the relationship between landslide volume and the apparent friction during motion. Balkema, Rotterdam, 1991. Edited by Bell.

[78] Sassa K. Access to the dynamics of landslides during earthquakes by a new cyclic loading high-speed ring shear apparatus. In *6th International Symposium on Landslides, Special Session No.1, "Seismicity and Landslides", Draft for theme address*, pages 1–35, Christchurch, 1992.

[79] Shoaei Z and Sassa K. Basic study on the shear behaviour of landslides during earthquakes. –Excess pore pressure generation in the undrained cyclic loading ring shear tests–. *Bulletin of the Disaster Prevention Research institute, Kyoto University*, 44:27–70, 1994.

[80] Nieuwenhuis J.D. *The lifetime of a landslide investigation in the French Alps.* A.A. Balkema, Rotterdam, 1991.

[81] Sassa K. A new intelligent-type dynamic loading ring shear apparatus. *Landslide News*, 10:33, 1997.

[82] Novosad J. Studies on granular materials II. Apparatus for measuring dynamic angle of internal and external friction of granular materials. In *Col-*

lection of Czechoslovakian Chemistry Communications, English Edition, pages 2697–2701. 29th edition, 1964.

[83] Scarlett B and Todd A.C. A split ring annular shear cell for the determination of the shear strength of a powder. *Journal of Scientific Instruments. Series 2*, 1:655–656, 1968.

[84] Ramiah B.K, Davalu N.K, and Purushothamaraj P. Influence of chemicals on residual strength of silty clay. *Soils and Foundations*, 10(1):25–36, 1970.

[85] Petley D.J. *The shear strength of soils at large strains.* PhD thesis, University of London, 1966.

[86] De Beer E. Shear strength characteristics of the 'boom clay'. In *Proceedings of the Geotechnical Conference, Oslo*, volume 1, pages 83–88, Oslo, 1967. Norwegian Geotechnical Institute.

[87] Martins J.P. *Shaft resistance of axially loaded piles in clay.* PhD thesis, University of London, 1983.

[88] Gostelow T.P. *Slope development in stiff overconsolidated clays.* PhD thesis, University of London, 1974.

[89] Savage S.B. Granular flows at high shear rates. In *Theory of dispersed multiphase flow*, pages 339–358. Academic Press, Publication No. 49, Mathematics Research Centre, University of Wisconsin, Madison, 1982. Edited by R.E. Meyer.

[90] Hungr O and Morgernstern N.R. Experiments on the flow behaviour of granular materials at high velocity in an open channel. *Géotechnique*, 34(3):415–421, 1984.

[91] Osipov V.I, Nikolaeva S.K, and Sokolov V.N. Microstructural changes associated with thixotropic phenomona in clay soils. *Géotechnique*, 34(2):293–303, 1984.

[92] Bernander S. Shear strength and deformation properties of clays in direct shear tests at high strain rates. In *Proceedings of the 11th International Conference on Soil Mechanics and Foundation Engineering*, volume 2, pages 987–990, San Francisco, 1985.

[93] Idriss I.M. Evaluating seismic risk in engineering practice. In *Proceedings of the 11th International Conference on Soil Mechanics and Foundation Engineering*, volume 1, pages 255–320, San Francisco, 1985.

[94] Lemos L.J, Skempton A.W, and Vaughan P.R. Earthquake loading of shear surfaces in slopes. In *Proceedings of the 11th International Conference on Soil Mechanics and Foundation Engineering*, volume 4, pages 1955–1958, San Francisco, 1985.

[95] Lemos L.J. Shear strength of shear surfaces under rapid loading. In *Proceedings of the 10th European Conference on Soil Mechanics and Foundation Engineering*, pages 137–141, Firenze, Italy, 1991.

[96] Bracegirdle A, Vaughan P.R, and Hight D.W. *Landslides*, chapter Displacement prediction using rate effects on residual strength. Balkema, Rotterdam, 1991. Edited by Bell.

[97] Skempton A.W, Leadbeater A.D, and Chandler R.J. The Mam Tor Landslide, North Derbyshire. *Philosophical Transactions of the Royal Society of London*, A329:503–547, 1989.

[98] Tika-Vassilikos T.M. Clay-on-steel ring shear tests and their implications for displacement piles. *Geotechnical Testing Journal, GTJODJ*, 14(4):457–463, 1991.

[99] Fukuoka H. Variation of the friction angle of granular materials in the high-speed high-stress ring shear apparatus,–Influence of re-orientation, alignment and crushing of grains during shear–. *Bulletin from the Disaster Prevention Research Institute, Kyoto University*, 41, Part 4(362), 1991.

[100] Steenfelt J.S. Sliding resistance for foundations on clay till. In *Proceedings of the Wroth Memorial Symposium*, St Catherines College, Oxford, 1992. Edited by G.T. Houlsby and A.N. Schofield.

[101] Sassa K and Fukuoka H. Measurement of the internal friction angle of soils during motion by the high-speed ring shear apparatus. *Journal of Japan Landslide Society*, 29(4), 1993. In Japanese.

[102] Howard K. Avalanche mode of motion: implication from lunar examples. *Science*, 180:1052–1055, 1973.

[103] The British Broadcasting Corporation. The runaway mountain, December 1995. Television Programme from the Horizon series.

[104] Heim A. *Bergsturz und Menschenleben.* Fretz und Wasmuth, Zürich, 1932. 218 pages.

[105] Kent P.E. The transport mechanism in catastrophic rock falls. *Journal of Geology*, 74:79–83, 1966.

[106] Habib P. Sur un mode de glissment des massiffs rocheux. *Comptes Rendus Hebdomadaires des Seances. Academie des Science. Serie 2. Mecanique-Physicique, Chimie, Sciences de l'Univers et Sciences de la Terre*, 264:151–153, 1967.

[107] Habib P. Production of gaseous pore pressure during rock slides. *Rock Mechanics*, 7:193–197, 1976.

[108] Goguel J. Scale dependent rockslide mechanisms, with emphasis on the rate of pore-fluid vapourization. In *Rockslides and Avalanches, 1, Natural Phenomena*, pages 693–705. Elsevier, Amsterdam, 1978. Edited by B. Voight.

[109] Shreve R.L. Sherman Landslide, Alaska. *Science*, 154:1639–1643, 1966.

[110] Shreve R.L. The Blackhawk Landslide. *Geological Society of America*, pages 1–47, 1968. Special Paper 108.

[111] Shreve R.L. Leakage and fluidization in air-layer lubricated avalanches. *Geological Society of America Bulletin*, 86:653–678, 1968.

[112] Sharp R.P and Nobles L.H. Mudflow of 1941 at Wrightwood, Southern California. *Geological Society of America Bulletin*, 64:547–560, 1953.

[113] Kojan E. and Hutchinson J.N. Mayunmarca rockslide and debris flow, Peru. In *Rockslides and Avalanches, 1, Natural Phenomena*, pages 315–361. Elsevier, Amsterdam, 1978. Edited by B. Voight.

[114] McSaveney M.J. Sherman Glacier rock avalanche, Alaska. In B. Voight, editor, *Rockslides and Avalanches, 1, Natural Phenomena*. Elsevier, Amsterdam, 1978.

[115] Bagnold R.A. Experiments on a gravity-free dispersion of large solid spheres in a Newtonian fluid under shear. *Proceedings of the Royal Society of London*, A225:49–63, 1954.

[116] Bagnold R.A. The flow of cohesionless grains in fluids. *Proceedings of the Royal Society of London*, A249:235–297, 1956.

[117] Hsü K.J. Catastrophic debris streams (Sturzstroms) generated by rock falls. *Geological Society of America Bulletin*, 86:123–140, 1975.

[118] Körner H.J. Flow mechanisms and resistances in the debris streams of rock slides. *Bulletin of the International Association of Engineering Geology*, 16:101–104, 1977.

[119] Lee J.H and Sassa K. A study on the apparent friction angle mobilized during the undrained loading in long run-out landslides. *Bulletin of the Disaster Prevention Research Institute*, 45(393):99–124, March 1996. Part 4.

[120] Körner H.J. Model conceptions for the rock slide and avalanche movement. In *Proceedings of the International Symposium "INTERPRAEVENT 1980"*, volume 2, pages 15–55, 1980. In German.

[121] Körner H.J. Japanese translation of selected papers. In *Proceedings of the International Symposium "INTERPRAEVENT 1980"*, Japan, 1982. The Erosion Control Engineering (Sabo) Society.

[122] Davies T.R.H. Spreading of rock avalanche debris by mechanical fluidization. *Rock Mechanics*, 15:9–24, 1982.

[123] Melosh H.J. Accoustic fluidization: A new geologic process? *Journal of Geophysical Research*, 84(B13):7513–7520, 1979.

[124] Kobayashi Y. Effect of basal guided waves on landslides. *Pure and Applied Geophysics*, 142(2):329–346, 1994.

[125] Romero S.U and Molina R. Kinematic aspects of the Vaiont slide. In *Proceedings of the 3rd Congress of the International Society of Rock Mechanics*, volume II Part B, pages 865–870, Denver, Colorado, 1974.

[126] Anderson D.L. The Vaiont slide, a geotechnical analysis based on new geologic observations of the failure surface. Technical Report GL-85-5, Geotechnical Laboratory US Army Engineers Waterways Experiment Station, Vicksburg, Mississippi, 1985. Prepared by A.J. Hendron and F.D. Patton, Vol. 2.

[127] Anderson D.L. An earthquake induced heat mechanism to explain the loss of strength of large rock or earth slides. In *International Conference on Engineering or Protection from Natural Disasters*, pages 569–580, Bangkok, 1980.

[128] Voight B and Faust C. Frictional heat and strength loss in some rapid landslides. *Géotechnique*, 32(1):43–54, 1982.

[129] Voight B and Faust C. Frictional heat and strength loss in some rapid landslides: error correction and affirmation of mechanism for the Vaiont landslide. *Géotechnique*, 42(4):641–643, 1992.

[130] Nonveiller E. Private communication, 1982. Transaction between B. Voight and C. Faust reported in their Géotechnique paper, 42(4):641-643, 1992.

[131] Davis R, Smith N.R, and Salt G. Pore fluid frictional heating and stability of creeping landslides. *International Journal of Numerical and Analytical Methods in Geomechanics*, 14:427–443, 1990.

[132] Salt G, Hancox G.T, and Northey R.D. Limit equilibrium analysis of the East Abbotsford landslide and assessment of possible causes of the slide. Technical Report EG 341, N.Z. Geological Survey, 1980.

[133] Salt G. Aspects of landslide mobility. In *Proceedings of the 11th International Conference on Soil Mechanics and Foundation Engineering*, volume 3, pages 1167–1172, San Francisco, 1985.

[134] Smith N and Salt G. Predicting landslide mobility. An application to the East Abbotsford slide, New Zealand. In *Proceedings of the 5th Australia–New Zealand Conference on Geomechanics*, pages 567–573, Sydney, 1988.

[135] Erismann T.H. Mechanisms of large landslides. *Rock Mechanics*, 12:15–46, 1979.

[136] Atakol K and Larew H.G. Dynamic shearing resistance of dry Ottawa sand. *Journal of the American Society of Civil Engineers*, 96(SM2):705–720, 1970.

[137] Terzaghi K. Varieties of submarine slope failures. In *Proceedings of the 8th Texas Conference on Soil Mechanics and Foundation Engineering*, pages 1–15, 1956.

[138] Hutchinson J.N. A sliding-consolidation model for flow slides. *Canadian Geotechnical Journal*, 23(2):115–126, 1986.

[139] Seed H.B. Landslide during earthquakes due to soil liquefaction. *Journal of the American Society of Civil Engineers*, 94(SM5):1053–1122, 1968.

[140] Hutchinson J.N and Bhandari R.I. Undrained loading: a fundamental mechanism of mudflows and other mass movements. *Géotechnique*, 21(4):353–358, 1971.

[141] Casagrande A. Liquefaction and cyclic deformation of sands, a critical review. In *Proceedings of the 5th Pan-American Conference on Soil Mechanics and Foundation Engineering*, volume 5, pages 75–133, Buenos Aires, Argentina, 1975.

[142] Cruden D.M and Hungr O. The debris of the Frank slide and theories of rockslide-avalanche mobility. *Canadian Journal of Earth Science*, 23:425–432, 1986.

[143] Sassa K. The mechanism of high mobility in the Ontake debris avalanche. In *Proceedings of the 8th African Regional Conference of the International Society for Soil Mechanics and Foundation Engineering*, volume 3, pages 1173–1176, Kyoto, Japan, 1987.

[144] Sassa K. The Ontake debris avalanche and its interpretation. *Lanslide News*, 1:5–8, June 1987.

[145] Sassa K, Fukuoka H, Lee J.H, Shoaei Z, Zhang D, Zhengzhang X, Zeng S, and Cao B. Prediction of landslide motion based on the measurement of geotechnical parameters. In *International Workshop on Prediction of Rapid Landslide Motion*, pages 72–106, Kyoto, Japan, 26 July - 5 August 1994. UNESCO Working Party on World Landslide Inventory.

[146] Freudlich H. *Thixotropy.* Hermann and Cie, Paris, 1935.

[147] Freudlich H. Quicksand as a thixotropic system. *Transactions of the Faraday Society*, 31:769–774, 1935.

[148] Freudlich H and Jones A.D. Sedimentation volume, dilatancy, thixotropic and plastic properties of concentrated suspensions. *Journal of Physical Chemistry*, 40(9):1217–1236, 1936.

[149] Seed H.B and Chan C.K. Thixotropic characteristics of compacted clays. *Journal of the American Society of Civil Engineers*, 83(SM4):1–35, 1957.

[150] Mitchell J.K. Fundamental aspects of thixotropy in soils. *Journal of the American Society of Civil Engineers*, 86(SM3):19–52, 1960.

[151] Day P.R. Effect of shear on water tension in saturated clay. Technical Report N-30, Western Regional Research Projects, 1954 and 1955. Annual Reports I and II.

[152] Bishop A.W, Blight G.E, and Donald I.B. Discussion and closure to Section 2. In *Proceedings of the Research Conference on shear strength of cohesive soils*, pages 1027–1042, Boulder, Colorado, 1960.

[153] Kerr P.F and Drew I.M. Quick-clay slides in the U.S.A. *Engineering Geology*, 2(4):215–238, 1968.

[154] Ward S.G and Whitmore R.L. Studies of the viscosity and sedimentation of suspensions. Part 1, the viscosity of suspension of spherical particles. *British Journal of Applied Physics*, 1:286–290, 1950.

[155] Chong J.S, Christiansen E.B, and Baer A.D. Rheology of concentrated suspensions. *Journal of Applied Polymer Science*, 15:2007–2021, 1971.

[156] Casagrande A and Wilson S.D. Effect of rate of loading on the strength of clays and shales at constant water content. *Géotechnique*, 2(3):251–263, 1951.

[157] Richardson A.M. Effects of rate of strain on stress-strain behaviour of saturated soils. The response of soils to dynamic loads. Technical Report 6, Waterways Experiment Station, Vicksburg, Mississippi, 1961.

[158] Blight G.E. Shear stress and pore pressure in triaxial testing. *Journal of the American Society of Civil Engineers*, 91(SM6):25–39, 1965.

[159] Dounias G.T, Potts D.M, and Vaughan P.R. The shear strength of soils containing undulating shear zones - a numerical study. *Canadian Geotechnical Journal*, 25:550–558, 1988.

[160] Bromhead E.N. *The stability of slopes.* Blackie Academic and Professional, 2nd edition, 1992.

[161] Hutchinson J.N. A reconsideration of the coastal landslides at Folkestone Warren, Kent. *Géotechnique*, 19:6–38, 1969.

[162] Patten F.D. *Multiple modes of shear failure in rock related materials.* PhD thesis, University of Illinois, 1966. 282 Pages.

[163] Patten F.D. Multiple modes of shear failure in rock. In *Proceedings of the 1st International Congress on Rock Mechanics*, volume 1, pages 509–513, Lisbon, 1966.

[164] Goodman R.E. The deformability of joints. Technical Report 447, The American Society for Testing and Materials, 1970. Pages 174-196.

[165] Barton N.R. A relationship between joint roughness and joint shear strength. In *Proceedings, International Symposium on Rock Fracture*, pages 1–8, Nancy, France, 1971.

[166] Barton N.R. A review of the shear strength of filled discontinuities in rock. Technical report, Norwegian Geotechnical Institute, 1974. Publication 105.

[167] Davis R.O and Salt G.A. Strength of undulating shearsurfaces in rock. *Géotechnique*, 36:503–509, 1986.

[168] Morgernstern N.R and Tchalenko J.S. Microscopic structures in kaolin subjected to direct shear. *Géotechnique*, 17:309–328, 1967.

[169] Bridle R.C, Vaughan P.R, and Jones H.N. Emphingham dam-Design, construction and performance. *Proceedings of the Institution of Civil Engineers*, Part 1, 78:247–289, 1985. Part 1.

[170] Skempton A.W and Coats D.J. Carsington dam failure. In *Proceedings, Symposium on Failures in Earthworks*, pages 203–220, London, 1985. Institution of Civil Engineers.

[171] Gibson R.E and Henkel D.J. Influence of duration of tests at constant rates of strain on measured 'drained' strength. *Géotechnique*, 4(1):6–15, 1954.

[172] British Standards Institute. BS1377 Soils for civil engineering purposes. Part 5. Compressibility, permeability and durability tests, 1990.

[173] British Standards Institute. BS1377 Soils for civil engineering purposes. Part 2. Classification tests, 1990.

[174] Best R and Fookes P.G. Some geotechnical and sedimentary aspects of ballclays from Devon. *Quarterly Journal of Engineering Geology*, 3:207–238, 1971.

[175] Prandtl L. Über Flussigkeitsbewegung bei sehr kleiner Reibung. In *Verhandlungen des III. Internationalen Mathematiker–Kongresses*, Leipzig, 1905.

[176] Blasius H. Grenzschichten in Flüssigkeiten mit kleiner Reibung. *Zeitschrift fuer Mathematik und Physik*, 1908.

[177] Roberson J.A and Crowe C.T. *Engineering fluid mechanics.* Houghton Mifflin Company, Washington State University, Pullman, 5th edition, 1993.

[178] Craig R.F. *Soil Mechanics.* Chapman and Hall, 5th edition, 1992.

[179] Jaky J. Pressure in soils. In *Proceedings of the 2nd International Conference on Soil Mechanics*, volume 1, pages 103–107, 1948.

[180] Harris J. *Rheology and non-Newtonian flow.* Longman, New York, 1977.

[181] Schowalter W.R. *Mechanics of non-Newtonian fluids.* Pergamon Press, New York, 1978.

Appendix A

Calibrations And Error Assessment

A.1 Force Measurements On The IC/NGI Apparatus

Measurements of force were taken at three locations on the IC/NGI ring shear apparatus. Two transducer-proving ring combinations recorded the shear forces transmitted by the sample, a third combination recorded the side friction on the upper half of the sample. The SGDTs were mounted inside the proving rings to record the deflection of the rings.

Stage 1 of these calibrations involved recording the data logger readings associated with linear displacements of the SGDT spindle across a range of displacements from 0 *mm* (spindle fully out) to 25 *mm* (spindle fully in). This was performed by clamping each transducer in the test rig illustrated on Figure A.1 and then inserting slip gauges to attain a range of displacements. Three separate sets of readings were taken. In between each set of readings the transducer was removed and repositioned in the rig. The average value of these readings was then obtained and is plotted on the first graphs of Figures A.3, A.5 and A.7. The gradient corresponding to each data point was then calculated and the average of these values was found to give a linear approximation of the relationship between data logger reading and SGDT spindle

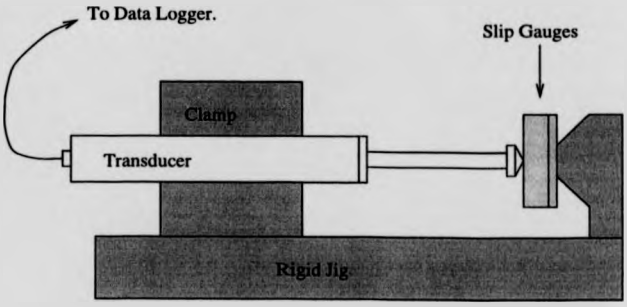

Figure A.1: Test rig used for calibrating strain gauge displacement transducers.

displacement. This completed the first stage of the calibrations.

Stage 2 involves interpreting the proving rings calibration certificates provided in Figures A.2, A.4 and A.6. The apparatus was brand new at the start of this work and therefore there was no need to recalibrate the rings at Warwick. The first step was to convert the number of divisions into actual displacements and then plot these against the corresponding force in newtons. This provides the average data points on the second graph of Figures A.3, A.5 and A.7. Then the gradient corresponding to each data point was calculated and the average of these values was found to give a linear approximation of the relationship between the force on the proving ring and the compression or expansion of the proving ring. This completed the second stage of the calibration.

The final stage of the calibration, Stage 3, combines the two average gradients obtained in Stages 1 and 2 to give the required gradient to convert the data logger reading into a force in newtons. For example consider the calibration of Channel 1, see Figure A.3, where:

Stage 1 gradient $= 0.00191524mm/DIV$
Stage 2 gradient $= 0.002955mm/N.$

Therefore to calculate the required gradient the following equation is used,

$$\frac{0.00191524mm/DIV}{0.002955mm/N} = 0.648135N/DIV. \quad \text{(A.1)}$$

Hence the value of m in the equation $y = mx + c$ in Table 3.2 for Channel 1 is $m = 0.648135N/DIV$, $c = 0$ as there is no intercept on the y-axis. Finally this conversion factor was programmed into the data logger and then the calibration was checked. The forces corresponding to a number of spindle displacements in the range 0 mm to 2 mm were recorded at both limits and the mid-range of the available 25 mm spindle displacement. These values were then compared to forces obtained by interpolating for the spindle displacements from the proving ring calibration certificates. The percentage difference between the data logged value and the value from the calibration certificates was then calculated. The maximum percentage difference is shown on the third plot as the maximum observed error and the average percentage difference is shown as the average observed error. The average values were always below 0.6% and as the shear forces rarely exceed 80 Newtons this corresponds to an error of approximately 0.5 Newtons. The maximum side friction force recorded was of the order of 700 Newtons and again using the 0.6% value this corresponds to an error of around 4 Newtons. These values are acceptable for use in conjunction with the IC/NGI apparatus. The maximum values tended to occur at the limits of the transducer spindle displacements, that is fully in or out, and therefore such positioning was avoided where possible during the testing.

Calibration Certificate

WF No. 25800 Ring No. 100458/3

Capacity. 700 NEWTONS 1 Division = .002 mm

LOAD	COMP.	TENSION
NEWTONS	Division	Division
0	0	
50	73	
100	148	
150	222	
200	298	
250	371	
300	445	
350	517	
400	590	
450	663	
500	737	
550	811	
600	883	
650	956	
700	1029	

A copy of this certificate is retained at our Works for reference and replacement purposes.

For and on behalf of
WYKEHAM FARRANCE ENG. LTD.
Weston Road,
SLOUGH. ENGLAND
Tel - 0753 - 571241
Fax - 0753 - 811313

Date - 27-4-94

41

Figure A.2: Calibration certificate for proving ring 100458/3.

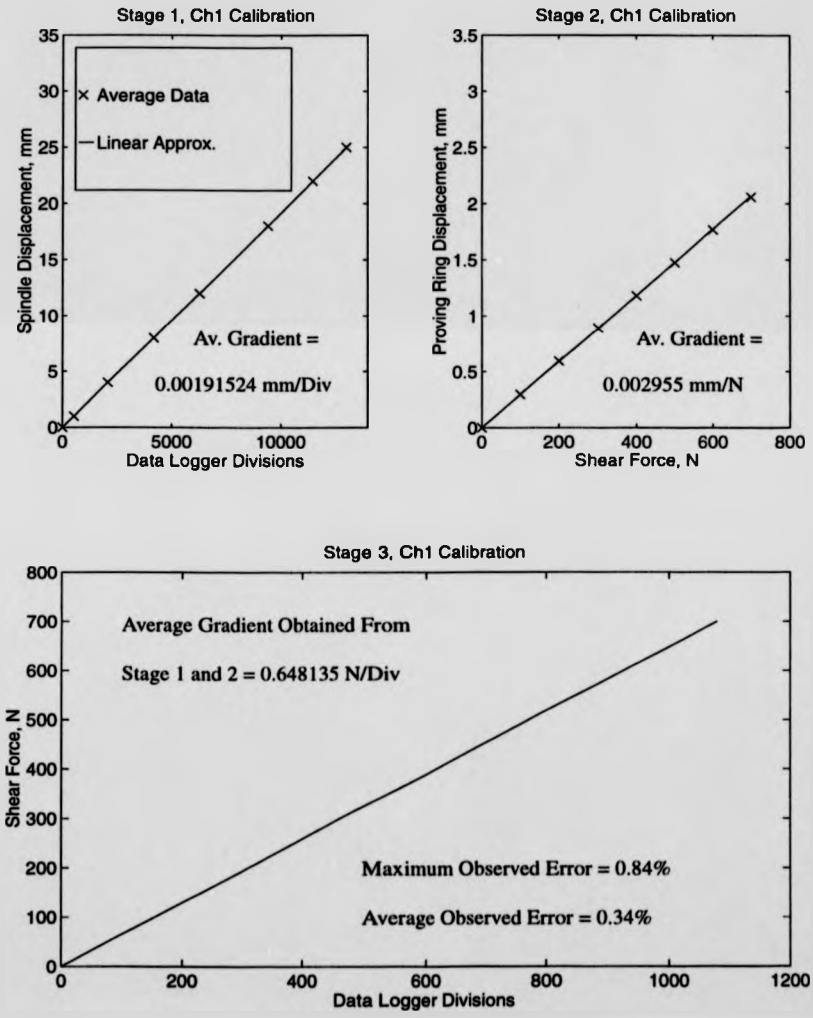

Figure A.3: Calibration combination of SGDT HS25/7721 and proving ring 100458/3 on channel 1.

Calibration Certificate

WF No. 25800 Ring No. 100458/1

Capacity. 700 NEWTONS 1 Division = .002 mm

LOAD	COMP.	TENSION
NEWTONS	Division	Division
0	0	
50	72	
100	143	
150	215	
200	289	
250	360	
300	431	
350	504	
400	576	
450	648	
500	718	
550	791	
600	863	
650	935	
700	1008	

A copy of this certificate is retained at our Works for reference and replacement purposes.

For and on behalf of
WYKEHAM FARRANCE ENG. LTD.
Weston Road,
SLOUGH. ENGLAND
Tel - 0753 - 571241
Fax - 0753 - 811313

Date - 27-4-94

41

Figure A.4: Calibration certificate for proving ring 100458/1.

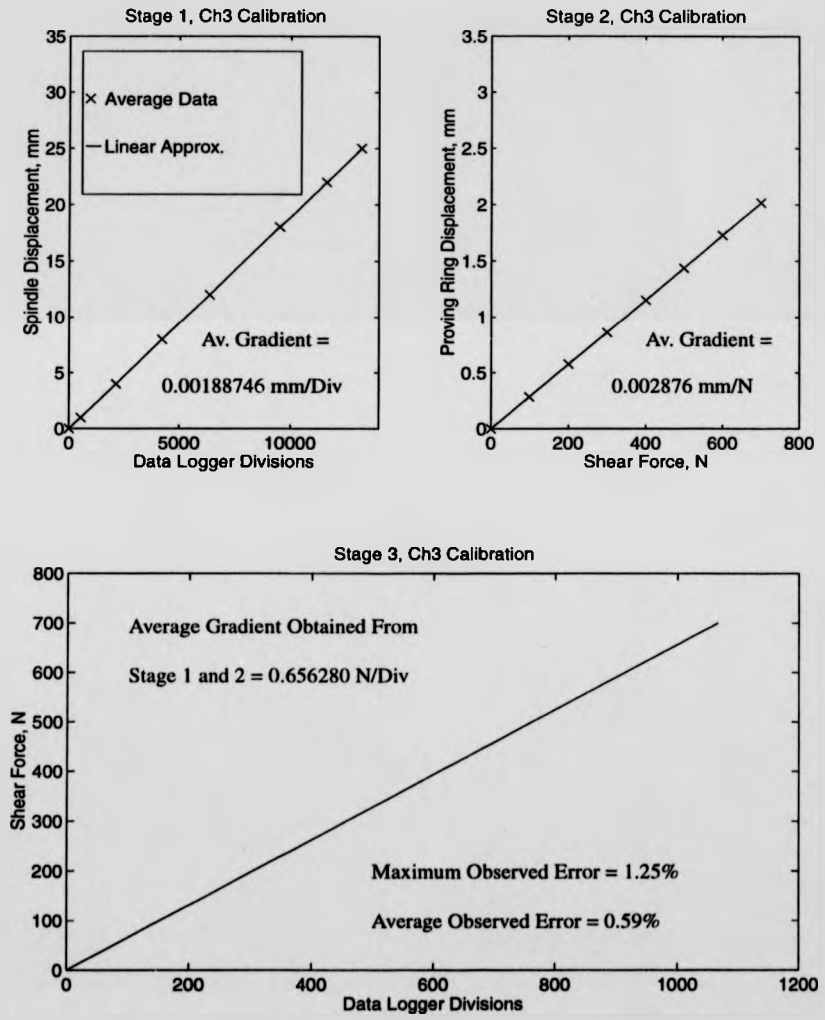

Figure A.5: Calibration combination of SGDT HS25/7716 and proving ring 100458/1 on channel 3.

Calibration Certificate

WF No. 25800 Ring No. 100458/2

Capacity. 700 NEWTONS 1 Division = .002 mm

LOAD	COMP.	TENSION
NEWTONS	Division	Division
0	0	2500
50	77	2422
100	155	2344
150	234	2267
200	310	2191
250	387	2112
300	463	2034
350	541	1957
400	617	1881
450	692	1803
500	768	1727
550	847	1650
600	923	1575
650	999	1498
700	1075	1421

A copy of this certificate is retained at our Works for reference and replacement purposes.

For and on behalf of
WYKEHAM FARRANCE ENG. LTD.
Weston Road,
SLOUGH. ENGLAND
Tel - 0753 - 571241
Fax - 0753 - 811313

Date - 27-4-94

41

Figure A.6: Calibration certificate for proving ring 100458/2.

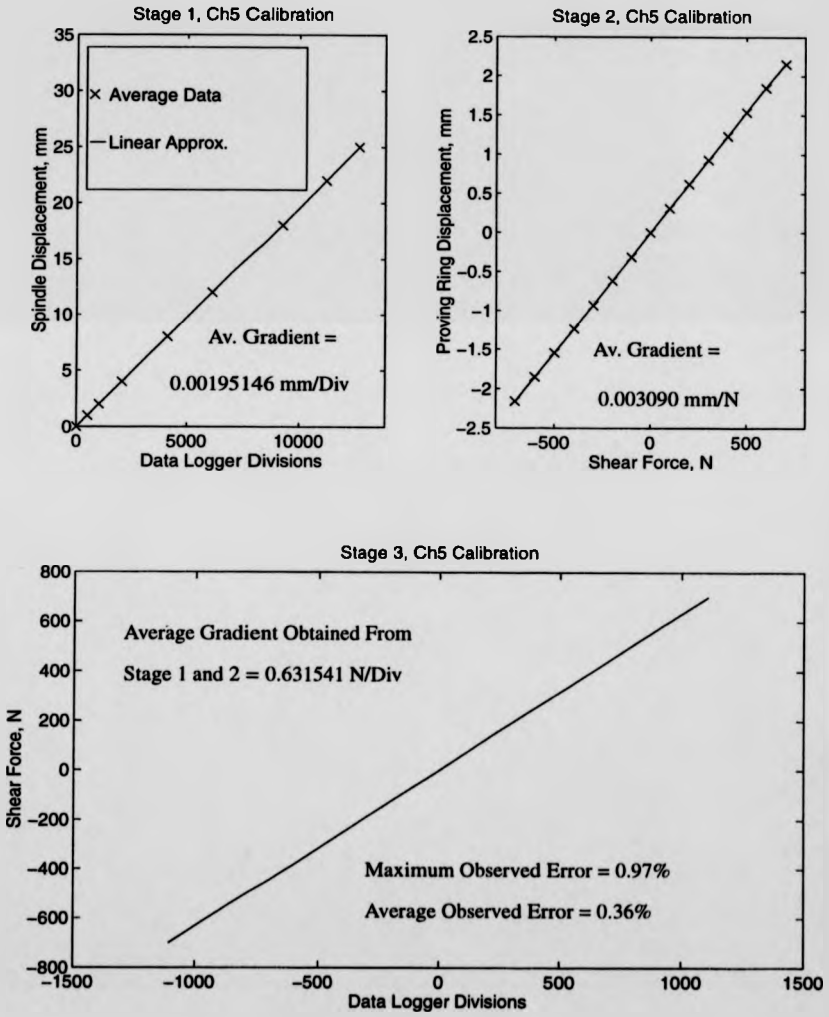

Figure A.7: Calibration combination of SGDT HS25/7715 and proving ring 100458/2 on channel 5.

A.2 Displacement Measurements On The IC/NGI Apparatus

Displacement measurements were taken using SGDTs at four locations on the IC/NGI apparatus. Two measurements of the sample settlement were recorded by SGDTs mounted on each side of the torque arm and two measurements of the gap size were taken by SGDTs mounted on top of the upper confining rings.

The calibration method used was identical to that described in Stage 1 of Section A.1. Once the average gradient had been obtained from three independent sets of recordings using slip gauges, the gradient was programmed into the data logger and checks were carried out by comparing the displacements recorded by the data logger to the widths of the slip gauges used. The percentage differences between the recorded and the actual displacements were calculated and the average and maximum of these percentages across the 25 mm range of the transducers are reported on Figure A.8 along with the average gradients and actual data points. The accuracy attained was always better than $\pm 0.06mm$ and was usually better than $\pm 0.03mm$.

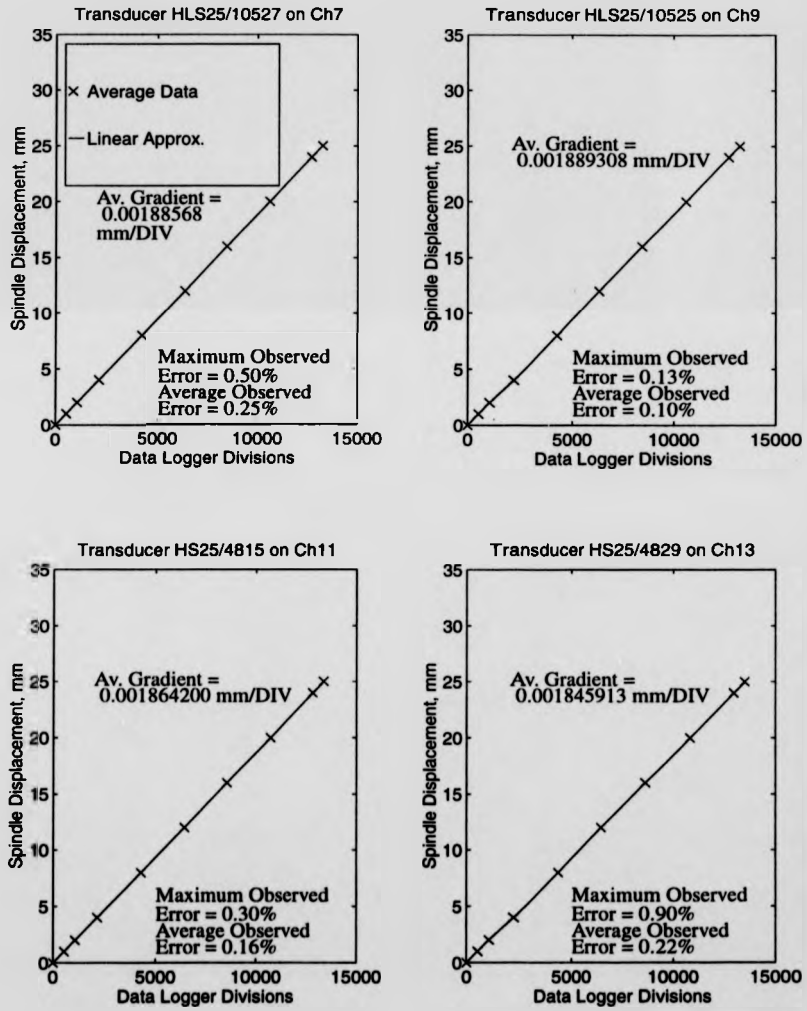

Figure A.8: Calibration of the SGDTs on channels 7, 9, 11 and 13.

A.3 New Drive System Speed Calibration

The calibration of the speed output signal from the new drive system allowed the fast rate of shearing at the mid radius of the annulus to be logged automatically. The calibration was performed by setting the speed of the drive shaft at a range of rates from 0 to 429 rpm, monitoring the output voltage on Channel 15 and recording the time taken for the rotating table of the IC/NGI apparatus to travel through one revolution. From the time taken for one revolution the rate of shear at the mid radius of the annulus was calculated using the geometry of the annulus. The results of this are illustrated by the crosses on Figure A.9. For each point the speed gradient was calculated and the average of all these value was obtained, this is illustrated by the solid line on Figure A.9. The value 99.29638 $(mm/min)/V$ was then programmed into the data logger and checks were then made across the full speed range these revealed that the logged speeds were accurate to within $\pm 4mm/min$ at rates between 120 mm/min and 940 mm/min and to within $\pm 8mm/min$ at 1000 mm/min.

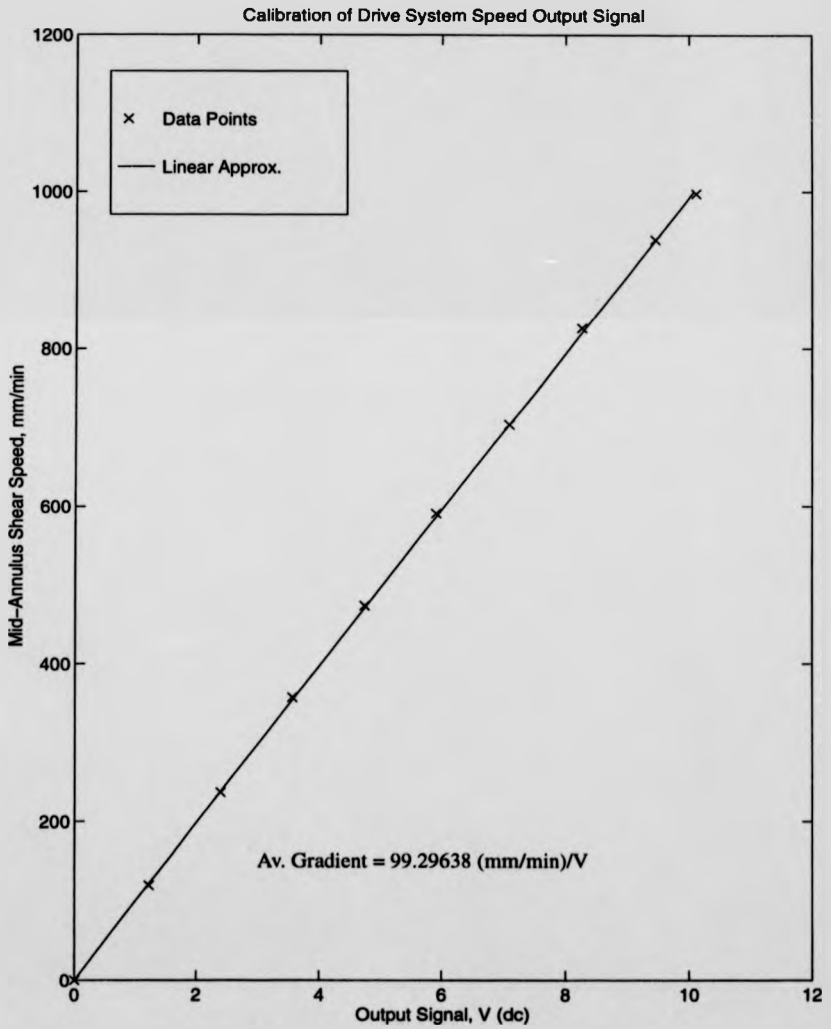

Figure A.9: Calibration Of The New Drive System Speed Output On Channel 15

A.4 Calibration Of The Pore Pressure Transducers

The pore pressure transducers were specially ordered for this investigation and arrived pre-calibrated with a certificate. Each of these certificates is provided in Figures A.10 to A.13. The key value on these certificates, required to convert the transducer signal (in mV) to pore pressures (in kPa) is the sensitivity. To obtain the required gradient (m in kPa/V) for the data logger linear conversion equation, $y = mx + c$ required some simple rearrangement and adjustment to different units. An example is provided here for pore pressure transducer 7762. From Figure A.10 it can be seen that the sensitivity of the transducer is 5.923 $mV/V/Bar$. The supply voltage to the transducer was always maintained at 5 V, this was achieved by constantly monitoring the supply voltage on Channel 16 of the data logger. Therefore the transducer sensitivity becomes $5.923mV/V/Bar \times 5V = 29.615mV/Bar$. Inversing this value and substituting volts for millivolts and $1Bar = 101.325kPa$ yields the value for m thus, $m = 3421.41kPa/V$. Conducting the same conversion for the other transducers yield the results given in Table A.1.

With these transducers zero volts output did not correspond to atmospheric pressure. This meant that values of c were needed in the calibration equation $y = mx + c$. Finding the correct value of c proved to be difficult, and the method used was not ideal, but did provide a solution. When the transducers had been mounted in the undulating interface and this interface had been attached under water to the base plate, the assembly took place in a sink which was filled to the brim, providing a head of water equal to 150 mm above the tops of the transducers. This head should have lead to the transducers recording 1.5 kPa. The actual transducer recordings using the conversion $y = mx$ were taken and values of c were calculated so that each transducer gave a reading of 1.5 kPa under 150 mm of water. This value was then programmed into the data logger, thus giving the full conversion equation $y = mx + c$. This concludes the Appendix on calibration and error assessment.

Table A.1: Pore pressure transducer calibration.

Transducer Number	Range	Sensitivity $mV/V/Bar$	m Value for $y = mx + c$
7762	3 Bar g	5.923	$3421.41kPa/V$
7838	3 Bar g	5.703	$3553.39kPa/V$
9019	7 Bar g	2.547	$7956.42kPa/V$
9020	7 Bar g	2.468	$8211.10kPa/V$

Druck

CALIBRATION CERTIFICATE

Calibration date:	29.1.97 SO: P00534
Transducer type:	PDCR 81
Serial Number:	7762
Range:	3 bar g
Supply:	5 Volts
Sensitivity:	5.923mV/V/bar
Non-linearity & hysteresis:	+/-0.2% BSL
Temperature operating range:	
Temperature compensated range:	-20 to +120°C
Temperature error band:	
Thermal zero shift:	0.05%/FSO/°C
Thermal sensitivity shift:	0.2%/°C
Electrical connection	
Supply positive:	RED
Supply negative:	BLUE
Output positive:	YELLOW
Output negative:	GREEN
Screen:	
Notes:	5 mtrs cable refer to note 6 overleaf

QA11

Druck Limited Fir Tree Lane, Groby, Leicester LE6 0FH, England.
Telephone: (0116) 231 4314. Facsimile: (0116) 287 5022

Figure A.10: Calibration certificate for pore pressure transducer 7762.

Druck

CALIBRATION CERTIFICATE

Calibration date:	29.1.97 SO: P00534
Transducer type:	PDCR 81
Serial Number:	7838
Range:	3 bar g
Supply:	5 Volts
Sensitivity:	5.703mV/V/bar
Non-linearity & hysteresis:	+/-0.2% BSL
Temperature operating range:	
Temperature compensated range:	-20 to +120°C
Temperature error band:	
Thermal zero shift:	0.05%/FSO/°C
Thermal sensitivity shift:	0.2%/°C
Electrical connection	
Supply positive:	RED
Supply negative:	BLUE
Output positive:	YELLOW
Output negative:	GREEN
Screen:	
Notes:	5 mtrs cable refer to note 6 overleaf

321

QA 11

Druck Limited Fir Tree Lane, Groby, Leicester LE6 0FH, England.
Telephone: (0116) 231 4314. Facsimile: (0116) 287 6022

Figure A.11: Calibration certificate for pore pressure transducer 7838.

Druck

CALIBRATION CERTIFICATE

Calibration date:	13.3.1997 SO: P00534
Transducer type:	PDCR 81
Serial Number:	9019
Range:	7 bar g
Supply:	5 volts
Sensitivity:	2.547mV/V/bar
Non-linearity & hysteresis:	+/- 0.2% BSL
Temperature operating range:	
Temperature compensated range:	-20 to 120°C
Temperature error band:	
Thermal zero shift:	0.05%/FS/°C
Thermal sensitivity shift:	0.2%/°C
Electrical connection	
Supply positive:	RED
Supply negative:	BLUE
Output positive:	YELLOW
Output negative:	GREEN
Screen:	

Notes:

5 mtrs cable

REFER TO NOTE 6 OVERLEAF

Druck Limited Fir Tree Lane, Groby, Leicester LE6 0FH, England.
Telephone: (0116) 231 4314. Facsimile: (0116) 287 5022

Figure A.12: Calibration certificate for pore pressure transducer 9019.

CALIBRATION CERTIFICATE

Calibration date:	13.3.1997 SO. P00534
Transducer type:	PDCR 81
Serial Number:	9020
Range:	7 bar g
Supply:	5 volts
Sensitivity:	2.468mV/V/bar
Non-linearity & hysteresis:	+/- 0.2% BSL
Temperature operating range:	
Temperature compensated range:	-20 to 120°C
Temperature error band:	
Thermal zero shift:	0.05%/FS/°C
Thermal sensitivity shift:	0.2%/°C
Electrical connection	
Supply positive:	RED
Supply negative:	BLUE
Output positive:	YELLOW
Output negative:	GREEN
Screen:	

Notes:

5 mtrs cable

REFER TO NOTE 6 OVERLEAF

Druck Limited Fir Tree Lane, Groby, Leicester LE6 0FH, England.
Telephone: (0116) 231 4314. Facsimile: (0116) 287 5022

Figure A.13: Calibration certificate for pore pressure transducer 9020.

Appendix B

Software Programs

Small print

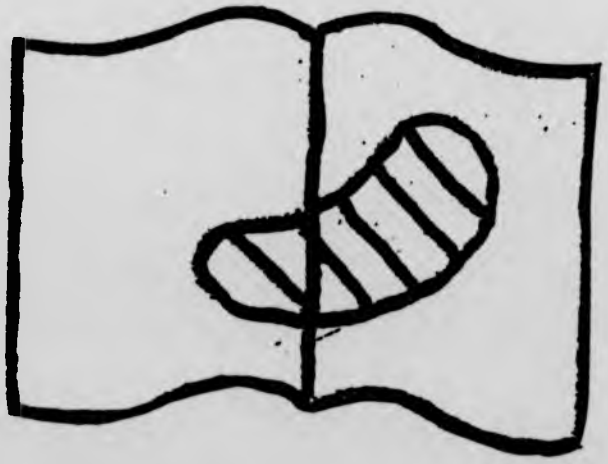

Jul 10 1998 14:09:21 **convert.pas** Page 1

```
program convert(input,output);
var
   line  : string[80];
   temp2 : string[2];
   temp4 : string[4];
   temp8 : string[8];
   filename1,filename2,clock : string[12];
   hour,hour2,min,code,count,count2,count3,check : integer;
   sec,c1,c2,c3,c5,c7,c9,c11,c13,c16,time,time2,disp,disptot,first,1
   ,disptotal,initdisp,maths,angle,natress
   ,natress,gap,settle,timeset,rate : real;
   infile,outfile : text;
begin
   writeln('*************************************');
   writeln('Ring Shear Test.. Data File Handler');
   writeln('*************************************');
   writeln;
   write('Please enter name of input file:');
   readln(filename1);
   assign(infile,filename1);
   reset(infile);
   write('Please enter name for output file:');
   readln(filename2);
   assign(outfile,filename2);
   rewrite(outfile);
   write('Please enter load on hanger arm in newtons:');
   readln(c1);
   writeln('Please enter time in minutes from start of test');
   write('at which this phase of testing began:');
   readln(timeset);
   writeln('Please enter rate of displacement in mm/minute (0 if logged):');
   readln(rate);
   writeln('Please enter total displacement in mm from start of test');
   write('at which this phase began:');
   readln(initdisp);
   disp:=0;
   dispot:=0;
   time2:=timeset;
   count:=0;
   count2:=0;
   count3:=0;
   Writeln(outfile,'Time  ':12,'Time in':12,'Displacement':12,'Channel 1 ':12,'Channe
l 3 ':12,
                   'Channel 5 ':12,'Channel 7 ':12,'Channel 9 ':12,
                   'Channel 11 ':12,'Channel 13 ':12,'Channel 16 ':12
                   'Load ':12,'Shear ':12,
                   'Tan Theta':12,'Theta ':12,
                   'Gap Size ':12,'Settlement':12);
   writeln(outfile,'hh:mm:ss.t':12,'Minutes':12,'mm   ':12,'F1, Newtons':12,'F2, Newto
ns':12,
                   'N, Newtons':12,'mm ':12,'mm ':12,'mm ':12,'mm ':12
                   : 'mm/minute ':12,'Stress kN/m2':12,'Stress,Kn/m2':12,
                   ':12,'Degree''s':12,'mm  ':12,'mm  ':12);
   writeln(outfile);
      while not eof(infile) do begin
         count:=count+1;
         readln(infile,line);
            clock:=copy(line,27,10);
            temp2:=copy(line,27,2);
            val(temp2,hour,code);
            temp2:=copy(line,30,2);
            val(temp2,min,code);
            temp4:=copy(line,33,4);
```

Jul 10 1998 14:09:21 **convert.pas** Page 2

```
            val(temp4,sec,code);
            if (count>1) then count2:=count2+1;
               time:=60*hour+min+sec/60;
               if count=1 then first:=time;
               time:=24*60*count2+time-first+timeset;
                  hour2:=hour;
            readln(infile,line);
            temp8:=copy(line,26,8);
            val(temp8,c1,code);
            if c1<0 then c1:=0;
            temp8:=copy(line,66,8);
            val(temp8,c3,code);
            if c3<0 then c3:=0;
               readln(infile,line);
                  temp8:=copy(line,26,8);
                  val(temp8,c5,code);
                  temp8:=copy(line,66,8);
                  val(temp8,c7,code);
               readln(infile,line);
               temp8:=copy(line,26,8);
               val(temp8,c9,code);
               temp8:=copy(line,66,8);
               val(temp8,c11,code);
               readln(infile,line);
                  temp8:=copy(line,26,8);
                  val(temp8,c13,code);
                  temp8:=copy(line,66,8);
                  val(temp8,c16,code);
                  if rate>0 then c16:=rate;
                     disp:=c16*(time-time2);
                     time2:=time;
                     dispot:=dispot+disp;
                     dispotal:=dispot+initdisp;
               readln(infile,line);
      maths:=(c1+c3)*3.7298/(10*11.6+c5);
      angle:=(180/pi)*arctan(maths);
      natress:=(10*11.6+c5)/10.13414958;
      gap:=(c11-c13)/2;
      settle:=(c7+c9)/2;
         writeln(outfile,clock:12,time:12:3,dispotal:12:2,c1:12:2,c3:12:2,c5:12:2,c7
:12:4,c9:12:4,
            c11:12:4,c13:12:4,c16:12:4,natress:12:2,
            natress:12:2,maths:12:4,angle:12:2,gap:12:4,settle:12:4);
   end;
   close(infile);
   close(outfile);
end
```

Turbo Pascal program: convert.pas.

Jul 10 1998 14:20:27 **convertp.pas** Page 1

```
program convert2(input,output);
var
   line  : string[80];
   temp2 : string[2];
   temp4 : string[4];
   temp8 : string[8];
   filename1,filename2,clock : string[12];
   hour,hour2,min,code,count,count2,count3,check : integer;
       sec,c1,c2,c3,c5,c7,c9,c11,c13,c15,c16,c17,c18,c19,c20,time,time2,disp
       ,disptot,first,initdisp,maths,angle,nstress
       ,stress,gap,settle,rate,apress : real;
       infile,outfile : text;
begin
  writeln('*****************************************');
  writeln('Ring Shear Test. Data File Handler.');
  writeln('*****************************************');
  writeln;
  writeln;
  write('Please enter name of input file:');
      readln(filename1);
  assign(infile,filename1);
  reset(infile);
  write('Please enter name for output file:');
      readln(filename2);
  assign(outfile,filename2);
  rewrite(outfile);
  write('Please enter load on hanger arm in newtons:');
      readln(l);
  writeln('Please enter time in minutes from start of test');
  write('at which this phase of testing began:');
  readln(first);
  write('Please enter rate of displacement in mm/minute (0 if logged):');
      readln(rate);
  writeln('Please enter total displacement in mm from start of test');
  write('at which this phase began:');
      readln(initdisp);
      disptot:=0;
      apress:=0;
  time2:=timeset;
  count:=0;
  count2:=0;
  writeln;
  writeln(outfile,'Time  :12,'Time in':12,'Displacement':12,'Channel 1 ':12,'Channe
1 3 ':12,
                  'Channel 5 ':12,'Channel 7 ':12,'Channel 9 ':12,
                  'Channel 11 ':12,'Channel 13 ':12,'Channel 15 ':12
                  'Normal ':12,'Shear ':12,
                  'Pan Tilt ':12,'Rate ':12,
                  'Gap Size ':12,'Settlement':12,
                  'Supply ':12,'Channel 17 ':12,
                  'Channel 19 ':12,'Channel 20 ':12);
  writeln(outfile,'hh:mm:ss':12,'Minutes':12,'mm ':12,'F1, Newtons':12,'F2, Newto
ns':12,
                  'N, Newtons':12,'mm ':12,'mm ':12,'mm ':12
                  ':mm/minute ':12,'Stress,kN/m2':12,'Stress,Kn/m2':12,
                  'Degrees':12,'mm ':12,'mm ':12,
                  'Volts':12,'KPa ':12,'KPa ':12,
                  'KPa ':12,'KPa':12);
  writeln(outfile);
      while not eof(infile) do begin
          count:=count+1;
              readln(infile,line);
          if count>=first then begin
              temp2:=copy(line,27,2);
                  val(temp2,hour,code);
```

Jul 10 1998 14:20:27 **convertp.pas** Page 2

```
                  temp2:=copy(line,30,2);
                  val(temp2,min,code);
                  temp4:=copy(line,33,4);
                  val(temp4,sec,code);
                      if(hour<hour2) then count2:=count2+1;
                      time:=(hour*60+min+sec/60);
                          if count=1 then first:=time;
                          time:=24*60*count2+time-first+timeset;
                              hour2:=hour;
              readln(infile,line);
              temp8:=copy(line,2,8);
              val(temp8,c1,code);
              if c1<0 then c1:=0;
              temp8:=copy(line,66,8);
              val(temp8,c3,code);
              if c3<0 then c3:=0;
                  readln(infile,line);
                  temp8:=copy(line,26,8);
                      val(temp8,c5,code);
                      temp8:=copy(line,66,8);
                          val(temp8,c7,code);
                  readln(infile,line);
                  temp8:=copy(line,26,8);
                  val(temp8,c9,code);
                  temp8:=copy(line,66,8);
                  val(temp8,c11,code);
                  readln(infile,line);
                  temp8:=copy(line,26,8);
                      val(temp8,c13,code);
                      temp8:=copy(line,66,8);
                          val(temp8,c15,code);
                              disp:=c15*(time-time2);
                                  time2:=time;
                                  disptot:=disptot+disp;
                                      disptotal:=disptot+initdisp;
                  readln(infile,line);
                  temp8:=copy(line,2,8);
                  val(temp8,c16,code);
                  temp8:=copy(line,66,8);
                      val(temp8,c17,code);
                  readln(infile,line);
                  temp8:=copy(line,2,8);
                  val(temp8,c18,code);
                  temp8:=copy(line,66,8);
                  val(temp8,c19,code);
                      readln(infile,line);
                      temp8:=copy(line,2,8);
                          val(temp8,c20,code);
                      readln(infile,line);
              maths:=(c1+c3)*3.7298/(10*1-11.6+c5);
              angle:=(180/pi)*arctan(maths);
              nstress:=(c1+c3)*0.3680424419;
              stress:=(c1+c3)*0.3680424419;
              gap:=(c11+c13)/2;
              settle:=(c7+c9)/2;
              apress:=(c7+c18+c19+c20)/4;
          writeln(outfile,clock:12,time:12:3,disptotal:12:2,c1:12:2,c3:12:2,c5:12:2,c7
:12:4,c9:12:4,
              c11:12:4,c13:12:4,c15:12:4,nstress:12:2,
                  stress:12:2,maths:12:4,angle:12:2,gap:12:4,settle:12:4,
              c16:12:4,c17:12:2,c18:12:2,c19:12:2,c20:12:2,apress:12:2);
      end;
      close(infile);
      close(outfile);
end.
```

Turbo Pascal program: convertp.pas.

Jul 10 1998 14:32:17 **wavehunt.pas-SectionA** Page 1

```
program convert2(input,output);

var
   line  : string[80];
   temp2 : string[2];
   temp4 : string[4];
   temp8 : string[8];
   filename1,filename2,filename3,clock : string[12];
       hour,hour2,min,code,count,count2,count3,check : integer;
           sec,c1,c3,c5,c7,c7first,c7last,c7nosoilloss
          ,c9,c9first,c9last,c9nosoilloss
          ,c11,c13,c16,time,time2,disp,disptot,first,1
          ,disptotal,disptotalfirst,disptotallast,initdisp,maths,angle,nstress
          ,sstress,gap,settle,timeset,rate : real;
   infile,outfile : text;
begin
   writeln('**********************************');
   writeln('Ring Shear Test, Data File Handler');
   writeln('**********************************');
   writeln;
   writeln;
   write('Please enter name of input file:');
       readln(filename1);
   assign(infile,filename1);
   reset(infile);
   write('Please enter name for output file 1:');
       readln(filename2);
   assign(outfile,filename2);
   rewrite(outfile);
   write('Please enter load on hanger arm in newtons:');
       readln(l);
   writeln('Please enter time in minutes from start of test');
   write('at which this phase of testing began:');
       readln(timeset);
   write('Please enter rate of displacement in mm/minute (0 if logged):');
       readln(rate);
   writeln('Please enter total displacement in mm from start of test');
   write('at which this phase began:');
       readln(initdisp);
       disptotal:=0;
       disptot:=0;
   time2:=timeset;
   count:=0;
   count2:=0;
   hour2:=0;
   writeln(outfile,'Time  ':12,'Time in':12,'Displacement':12,'Channel 1 ':12,'Channe
l 3 ':12,
                   'Channel 5 ':12,'Channel 7 ':12,'Channel 9 ':12,
                  ,'Channel 11 ':12,'Channel 13 ':12,'Channel 16 ':12
                   ,'Normal   ':12,'Shear    ':12,
                   'Tan Theta':12,'Theta  ':12
                   ,'Gap Size ':12,'Settlement':12);
  writeln(outfile,'hh:mm:ss.t':12,'Minutes':12,'mm   ':12,'F1, Newtons':12,'F2, Newto
ns':12,
                   'W, Newtons':12,'mm  ':12,'mm  ':12,'mm  ':12,'mm  ':12
                  ,'mm/minute ':12,'Stress,kN/m2':12,'Stress,Kn/m2':12,
                  ' ':12,'Degree''s':12,'mm  ':12,'mm  ':12);
  writeln(outfile);

      while not eof(infile) do begin
          count:=count+1;
              readln(infile,line);
              clock:=copy(line,27,10);
              temp2:=copy(line,27,2);
              val(temp2,hour,code);
              temp2:=copy(line,30,2);
```

Jul 10 1998 14:32:17 **wavehunt.pas-SectionA** Page 2

```
              val(temp2,min,code);
              temp4:=copy(line,33,4);
              val(temp4,sec,code);
                    if(hour<hour2) then count2:=count2+1;
                    time:=60*hour+min+sec/60;
                    if count=1 then first:=time;
                    time:=24*60*count2+time-first+timeset;
                    hour2:=hour;
              readln(infile,line);
              temp8:=copy(line,26,8);
              val(temp8,c1,code);
              if c1<0 then c1:=0;
              temp8:=copy(line,66,8);
              val(temp8,c3,code);
              if c3<0 then c3:=0;
                  readln(infile,line);
                  temp8:=copy(line,26,8);
                  val(temp8,c5,code);
                  temp8:=copy(line,66,8);
                  val(temp8,c7,code);
              readln(infile,line);
              temp8:=copy(line,26,8);
              val(temp8,c9,code);
              temp8:=copy(line,66,8);
              val(temp8,c11,code);
                  readln(infile,line);
                  temp8:=copy(line,26,8);
                  val(temp8,c13,code);
                  temp8:=copy(line,66,8);
                  val(temp8,c16,code);
                   if rate>0 then c16:=rate;
                   disp:=c16*(time-time2);
                    time2:=time;
                   disptot:=disptot+disp;
                   disptotal:=disptot+initdisp;
              readln(infile,line);
     maths:=(c1+c3)*3.7298/(10*l+11.6+c5);
     angle:=(180/pi)*arctan(maths);
     nstress:=(10*l+11.6+c5)/10.13414958;
     sstress:=(c1+c3)*0.368042419;
     gap:=(c11+c13)/2;
     settle:=(c7+c9)/2;
        writeln(outfile,clock:12,time:12:3,disptotal:12:2,c1:12:2
       ,c3:12:2,c5:12:2,c7:12:4,c9:12:4,
       c11:12:4,c13:12:4,c16:12:4,nstress
       :12:2,sstress:12:2,maths:12:4,angle:12:2,gap:12:4,settle:12:4);
end;
reset(infile);
 write('Please enter name for output file 2:');
     readln(filename3);
assign(outfile,filename3);
rewrite(outfile);
c7last:=c7;
c9last:=c9;
disptotallast:=disptotal;
count:=0;
disptotal:=0;
disptot:=0;
time2:=timeset;
count2:=0;
hour2:=0;
  writeln(outfile,'Time':12,'Time, mins':12,'Displacement':12,
  'Channel 7':12,'Ch 7, cortd':12,'Channel 9':12,'Ch 9, cortd':12);
  writeln(outfile);
while not eof(infile) do begin
```


Turbo Pascal program: wavehunt.pas.

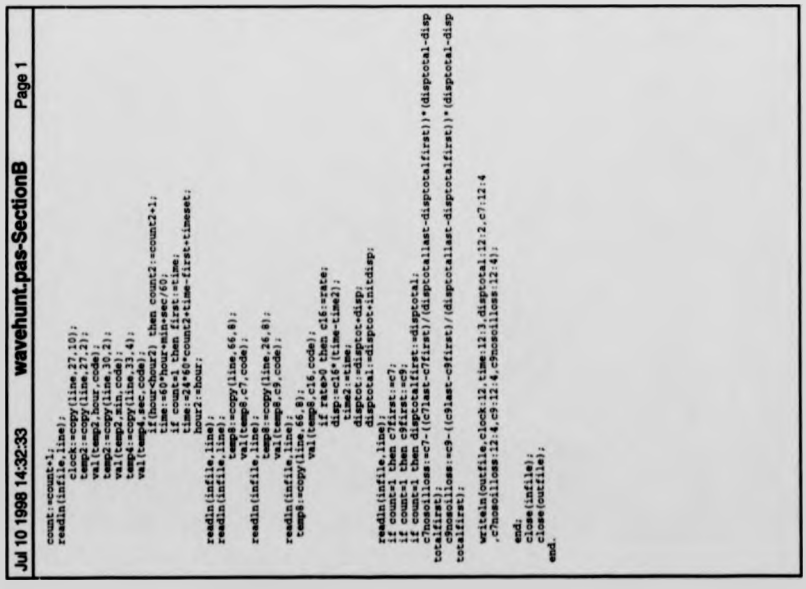

Jul 10 1998 14:32:33 wavehunt.pas-SectionB Page 1

```
  count:=count-1;
  readln(infile,line);
        clock:=copy(line,27,10);
        temp2:=copy(line,27,2);
          val(temp2,hour,code);
        temp2:=copy(line,30,2);
          val(temp2,min,code);
        temp4:=copy(line,33,4);
        val(temp4,sec,code);
              if(hour<hour2) then count2:=count2+1;
        time:=60*hour+min+sec/60;
              if count=1 then first:=time;
              time:=24*60*count2+time-first-timeset;
                    hour2:=hour;
  readln(infile,line);
  readln(infile,line);
        temp8:=copy(line,66,8);
          val(temp8,c7,code);
  readln(infile,line);
          temp8:=copy(line,26,8);
            val(temp8,c9,code);
  readln(infile,line);
  temp8:=copy(line,6,8);
          val(temp8,c16,code);
                if rate>0 then c16:=rate;
                    disp:=c16*(time-time2);
                          time2:=time;
                    disptot:=disptot+disp;
                    disptotal:=disptot+initdisp;
  readln(infile,line);
  if count=1 then c7first:=c7;
  if count=1 then c9first:=c9;
  if count=1 then disptotalfirst:=disptotal;
  chosenillions:=c7-((c7last-c7first)/(disptotallast-disptotalfirst))*(disptotal-disp
totalfirst);
    chosenillions:=c9-((c9last-c9first)/(disptotallast-disptotalfirst))*(disptotal-disp
totalfirst);

  writeln(outfile,clock:12,time:12:3,disptotal:12:2,c7:12:4
  ,c7chosenillions:12:4,c9:12:4,c9chosenillions:12:4);

  end;
  close(infile);
  close(outfile);
end.
```

Turbo Pascal program: wavehunt.pas.

```
Jul 10 1998 13:45:23          v1.c-SectionA          Page 1

/* Consolidation v12, Multiple Upslope Downslope Consolidation Programme*/
/* Version 12 - Linear interpolation of mv and cv values */
/* analysis by linearly interpolating values of U from Tv */
/* interpolating values of mv and cv from oedometer tests on remoulded */
/* and outputs the results to file 'conoutdat'.  Therefore any slope */
/* dimensions, shear rates, and normal stresses may be used but the */
/* results will always be for remoulded kaolin.  The sample is not forced */
/* to fail (failure will not be allowed) under the applied normal */
/* normal effective stress, resulting in shear zone separation */
/* swelling values of mv and cv are used in this stage */
#include <stdio.h>
#include <math.h>
#define FILENAME "conoutdat"

main()
{

/* Define Variables */

    float h_1, h_2, length, rate, delta_h, step_width,
          total_time, step_time, normal_stress, mv, cv,
          pore_pressure, Tv, temp, temp2, expansion, U, step, H;
    int n, flag, flag0, flag1, wave, wavenu;
    FILE *conoutdat;

    /* Open output file */
    conoutdat = fopen(FILENAME,"w");

    /* Slope Data Input Phase */

    printf("\n\n##########################################\n");
    printf("\n Slope Data Input Phase #1a\n");
    printf("##########################################\n\n");
    printf("When entering data please use units in KPA, METRES and MINUTES.\n\n");

    printf("%s", "Input initial sample depth:");
    scanf("%f", &h_1);
    printf("%s", "Input final sample depth:");
    scanf("%f", &h_2);
    printf("%s", "Input horizontal slope length:");
    scanf("%f", &length);
    printf("%s", "Input number of wave forms to be analysed:");
    scanf("%d", &wavenu);
    printf("%s", "Input number of calculation steps:");
    scanf("%d", &n);
    printf("%s", "Input rate of sample displacement:");
    scanf("%f", &rate);

    /* Initial Calculations:  Step Height, Step Width, */
    /*                        Total Time, Step Time */

    printf("\nData calculated from slope geometry, dynamics and number of steps.\n");
    delta_h = (h_1-h_2)/n;
    step_width = length/n;
    total_time = length/rate;
    step_time = total_time/n;
    printf("\nStep Height = %g\n", delta_h);
    printf("Step Width  = %g\n", step_width);
    printf("Total Time  = %g\n", total_time);
    printf("Step Time   = %g\n", step_time);

    /* Sample Data Input Phase */

    printf("\n\n##########################################\n");
```

```
Jul 10 1998 13:45:23          v1.c-SectionA          Page 2

    printf("# Sample Data Input Phase #1a\n");
    printf("# Tv, U, mv, cv\n");
    printf("##########################################\n");
    printf("\nEnter initial normal effective stress in kPa, wherein the pore water pr
essure is equal to zero:");
    scanf("%f", &normal_stress);
    printf("\n\nCOMMENCING ANALYSIS\n");
    eff_normal_stress = normal_stress;

    /* Wave Loop */

for (wave=0; wave<wavenu-1; wave+=1)
    {

    /* Loop Structure 1 Forced Consolidation */

for (step=(2*n*wave); step<((2*n*wave)+n); step+=1)
    {

    /*Calculate Time*/
        time = step * step_time;

    /*Calculate Displacement*/
        displacement=((step/n)*length)-(step_width/2);

    /*Find mv And cv Consolidation Values Corresponding */
        /*To Effective Normal Stress*/
            if (eff_normal_stress>=0 && eff_normal_stress<25)
                {mv=0.0025-(((eff_normal_stress-0)/25)*0.00112);
                 cv=3;
                 flag=1;}
            if (eff_normal_stress>=25 && eff_normal_stress<50)
                {mv=0.00138-(((eff_normal_stress-25)/25)*0.00062);
                 cv=4.2;
                 flag=2;}
            if (eff_normal_stress>=50 && eff_normal_stress<100)
                {mv=0.00076-(((eff_normal_stress-50)/50)*0.00028);
                 cv=2.2;
                 flag=3;}
            if (eff_normal_stress>=100 && eff_normal_stress<200)
                {mv=0.00048-(((eff_normal_stress-100)/100)*0.0002);
                 flag=4;
                 cv=1.6;}
            if (eff_normal_stress>=200 && eff_normal_stress<400)
                {mv=0.00028-(((eff_normal_stress-200)/200)*0.00011);
                 flag=5;
                 cv=1.6;}
            if (eff_normal_stress>400)
                {mv=0.00017;
                 flag=6;
                 cv=1.6;}

    /*Find Increase In Effective Stress Owing To Compression Equal To Step Height*/
            H = h_1-(delta_h*(step-(2*n*wave)));
            delta_eff_normal_stress = delta_h/(H*mv);

    /*Find Time Factor For Current Drainage Path Length*/
            Tv = ((cv/525600)*step_time)/(H*H);
```

C program: v1.c.

C program: v1.c.

Jul 10 1998 13:48:46 **v1.c-SectionB** Page 1

```
  /*Find U% Value Corresponding To Tv*/
                if ( Tv>=0 && Tv<0.0077 )
                   {U=(10*Tv)/0.0077;
                   flag=1;}
                if ( Tv>=0.0077 && Tv<0.031 )
                   {U=10 +((10*(Tv-0.0077))/(0.031-0.0077));
                   flag=2;}
                if ( Tv>=0.031 && Tv<0.071 )
                   {U=20 +((10*(Tv-0.031))/(0.071-0.031));
                   flag=3;}
                if ( Tv>=0.071 && Tv<0.126 )
                   {U=30 +((10*(Tv-0.071))/(0.126-0.071));
                   flag=4;}
                if ( Tv>=0.126 && Tv<0.196 )
                   {U=40 +((10*(Tv-0.126))/(0.196-0.126));
                   flag=5;}
                if ( Tv>=0.196 && Tv<0.286 )
                   {U=50 +((10*(Tv-0.196))/(0.286-0.196));
                   flag=6;}
                if ( Tv>=0.286 && Tv<0.403 )
                   {U=60 +((10*(Tv-0.286))/(0.403-0.286));
                   flag=7;}
                if ( Tv>=0.403 && Tv<0.567 )
                   {U=70 +((10*(Tv-0.403))/(0.567-0.403));
                   flag=8;}
                if ( Tv>=0.567 && Tv<0.848 )
                   {U=80 +((10*(Tv-0.567))/(0.848-0.567));
                   flag=9;}
                if ( Tv>=0.848 && Tv<1.129 )
                   {U=90 +((10*(Tv-0.848))/(1.129-0.848));
                   flag=10;}
                if ( Tv>=1.129 )
                   {U=100;
                   flag=11;}

/*Sets Displacement And Change In Effect Normal Stress To Zero For First Loop*/
      if (step == 0)
                  {
                   delta_eff_normal_stress = 0;
                  displacement = 0;
                  }

/*Calculate Pore Pressure At Step*/
     pore_pressure = (delta_eff_normal_stress + temp)*(1-(U/100));

/*Calculate Effective Normal Stress*/
    eff_normal_stress=normal_stress-pore_pressure;

/*Check For Liquefaction*/
       if (pore_pressure>=normal_stress)
         {
          eff_normal_stress = 0;
          pore_pressure = normal_stress;
         }
/*Output*/
      printf("  %f   %f   %f   %f   %f   %f\n", time, displacement, H, pore_pressure, eff
_normal_stress);
      fprintf(conoutdat,"  %f   %f   %f   %f   %f\n", time, displacement, H, pore_pr
essure, eff_normal_stress);

/*Set temp = pore pressure so that it can be added to next increase in stress*/
      temp = pore_pressure;
 }
 /* Loop Structure 2 Down Slope Expansion */

for (step=((2*n*wave)+(n+1)); step<=((2*n*wave)+(2*n)-1); step+=1)
```

Jul 10 1998 13:48:46 **v1.c-SectionB** Page 2

```
  {
/*Calculate Time*/
     time = step * step_time;

/*Calculate Displacement*/
     displacement=((step/n)*length)-(step_width/2);


 /*Find mv And cv Swelling Values Corresponding To Effective Normal Stress*/
               if (eff_normal_stress>=0 && eff_normal_stress<50)
                  {mv=0.0015-(((eff_normal_stress-0)/50)*0.0013);
                  flagb=1;
                  cv=0.0+(((eff_normal_stress-0;/50)*8.42);
                  flagc=1;}
               if (eff_normal_stress>=50 && eff_normal_stress<100)
                  {mv=0.0002-(((eff_normal_stress-50)/50)*0.00015);
                  flagb=2;
                  cv=8.42+(((eff_normal_stress-50)/50)*9.18);
                  flagc=2;}
               if (eff_normal_stress>=100 && eff_normal_stress<200)
                  {mv=0.000095-(((eff_normal_stress-100)/100)*0.00008);
                  flagb=3;
                  cv=17.6+(((eff_normal_stress-100)/100)*8.60);
                  flagc=3;}
               if (eff_normal_stress>=200)
                  {mv=0.000015;
                  flagb=4;
                  cv=17.6+(((eff_normal_stress-100)/100)*8.60);
                  flagc=4;}

/*Find Time Factor For Current Drainage Path Length*/
     Tv = ((cv/525600)*step_time)/(H*H);

  /*Find U% Value Corresponding To Tv*/
               if ( Tv>=0 && Tv<0.0077 )
                  {U=(10*Tv)/0.0077;
                  flag=1;}
               if ( Tv>=0.0077 && Tv<0.031 )
                  {U=10 +((10*(Tv-0.0077))/(0.031-0.0077));
                  flag=2;}
               if ( Tv>=0.031 && Tv<0.071 )
                  {U=20 +((10*(Tv-0.031))/(0.071-0.031));
                  flag=3;}
               if ( Tv>=0.071 && Tv<0.126 )
                  {U=30 +((10*(Tv-0.071))/(0.126-0.071));
                  flag=4;}
               if ( Tv>=0.126 && Tv<0.196 )
                  {U=40 +((10*(Tv-0.126))/(0.196-0.126));
                  flag=5;}
               if ( Tv>=0.196 && Tv<0.286 )
                  {U=50 +((10*(Tv-0.196))/(0.286-0.196));
                  flag=6;}
               if ( Tv>=0.286 && Tv<0.403 )
                  {U=60 +((10*(Tv-0.286))/(0.403-0.286));
                  flag=7;}
               if ( Tv>=0.403 && Tv<0.567 )
                  {U=70 +((10*(Tv-0.403))/(0.567-0.403));
                  flag=8;}
               if ( Tv>=0.567 && Tv<0.848 )
                  {U=80 +((10*(Tv-0.567))/(0.848-0.567));
                  flag=9;}
               if ( Tv>=0.848 && Tv<1.129 )
                  {U=90 +((10*(Tv-0.848))/(1.129-0.848));
                  flag=10;}
```

Jul 10 1998 13:48:53 **v1.c-SectionC** Page 1

```
if ( Tv>=1.129 )
                {U=100;
                 flag=11;}

/*Calculate Pore Pressure At Step*/
    pore_pressure = (temp)*(1-(U/100));

/*Calculate Delta Effective Normal Stress*/
    delta_eff_normal_stress=pore_pressure-temp;

/*Find Swelling Owing to Drop Delta Normal Effective Stress*/
    expansion = mv*H*delta_eff_normal_stress;

/*Find New Sample Depth*/
    temp2 = H;
    H = temp2 - expansion;

/*Find New Effective Normal Stress*/
eff_normal_stress = normal_stress - pore_pressure;

/*Check For Liquefaction*/
    if (pore_pressure>=normal_stress)
        {
         eff_normal_stress = 0;
         pore_pressure = normal_stress;
        }
/*Output*/
    printf("  %f   %f   %f   %f\n", time, displacement, H, pore_pressure, eff
_normal_stress);
    fprintf(conoutdat,"  %f   %f   %f   %f\n", time, displacement, H, pore_pr
essure, eff_normal_stress);

/*Set temp = pore pressure so that it can be added to next increase in stress*/
    temp = pore_pressure;

    }
fclose(conoutdat);
}
```

C program: v1.c

```
Jul 10 1998 13:20:48          v2.c-SectionA          Page 1

/* Consolidation v13 Multiple Upslope Downslope Consolidation Programme*/
/* Note this version does not use Tv */
/* analysis by linearly interpolating values of U from Tv */
/* interpolating values of mv and cv from oedometer tests on remoulded Kaolin*/
/* and outputs the results to file "consoutdat".  Therefore any slope */
/* dimensions, shear rates, and normal stresses may be used but the */
/* results will have to be manually plotted. The soil is fixed */
/* to swell down the slope resulting in very high negative pore pressures */
/* swelling values of mv and cv are used in this stage */
#include <stdio.h>
#include <math.h>
#include <conio.h>
#define FILENAME "consoutdat"

main()
{

/* Define Variables */

  float h_1, h_2, length, rate, delta_h, step_width,
        total_time, step_time, normal_stress, mv, cv,
        time_factor, Tv, temp2, expansion, U, step, Hi;
  int n, flag, flag2, flag3, wave, wavenc;
  FILE *consoutdat;

/* Open output file */
consoutdat = fopen(FILENAME,"w");

/* Slope Data Input Phase */

  printf("\n\n*************************\n");
  printf("* Slope Data Input Phase *\n");
  printf("*************************\n\n");
  printf("*When entering data please use units in KILONEWTONS, METRES and MINUTES.\n\n
");

  printf("%s","Input initial sample depth:");
  scanf("%f", &h_1);
  printf("%s", "Input final sample depth:");
  scanf("%f", &h_2);
  printf("%s", "Input horizontal slope length:");
  scanf("%f", &length);
  printf("%s", "Input number of wave forms to be analysed:");
  scanf("%d", &wavenc);
  printf("%s", "Input number of calculation steps:");
  scanf("%d", &n);
  printf("%s", "Input rate of sample displacement:");
  scanf("%f", &rate);

/* Initial Calculations: Step Height, Step Width, */
/*                       Total Time, Step Time */

  printf("\nData calculated from slope geometry, dynamics and number of steps.\n");
  delta_h = (h_1-h_2)/n;
  step_width = length/n;
  rate = rate/1440;
  step_time = total_time/n;
  printf("\nStep Height = %g\n", delta_h);
  printf("Step Width = %g\n", step_width);
  printf("Total Time  = %g\n", total_time);
  printf("Step Time   = %g\n", step_time);

/* Sample Data Input Phase */
```



```
Jul 10 1998 13:20:48          v2.c-SectionA          Page 2

  printf("\n\n*************************\n");
  printf("* Soil Input Phase *\n");
  printf("*************************\n\n");
  printf("%s","Input initial normal effective stress in kPa, when\n the pore water pr
essure is equal to zero:");
    scanf("%f", &normal_stress);
  printf("\n\nINCREMENTAL ANALYSIS\n");
  eff_normal_stress = normal_stress;

    /* Wave Loop */

for (wave=0; wave<wavenc-1; wave++)
    {

  /* Loop Structure 1 Forced Consolidation */

for (step=(2*n*wave)+1; step<=(2*n*wave)+n; step+=2)
    {

/*Calculate Time*/
    time = step * step_time;

/*Calculate Displacement*/
    displacement=((step/n)*length)-(step_width/2);

/*Find mv And cv Values Corresponding To Effective Normal Stress*/
        if (eff_normal_stress>=0 && eff_normal_stress<25)
            {mv=0.0025-(((eff_normal_stress-0)/25)*0.00218);
             flag=1;
             cv=3+(((eff_normal_stress-0)/25)*1.2);
             flag=1;}
        if (eff_normal_stress>=25 && eff_normal_stress<50)
            {mv=0.00218-(((eff_normal_stress-25)/25)*0.00062);
             flag=2;
             cv=4.2+(((eff_normal_stress-25)/25)*1.2);
             flag=2;}
        if (eff_normal_stress>=50 && eff_normal_stress<100)
            {mv=0.00076-(((eff_normal_stress-50)/50)*0.00026);
             flag=3;
             cv=5.4+(((eff_normal_stress-50)/50)*2.2);
             flag=3;}
        if (eff_normal_stress>=100 && eff_normal_stress<200)
            {mv=0.00048-(((eff_normal_stress-100)/100)*0.0002);
             flag=4;
             cv=7.6+(((eff_normal_stress-100)/100)*3.6);
             flag=4;}
        if (eff_normal_stress>=200 && eff_normal_stress<400)
            {mv=0.00028-(((eff_normal_stress-200)/200)*0.00011);
             flag=5;
             cv=11.2+(((eff_normal_stress-200)/200)*6.6);
             flag=5;}
        if (eff_normal_stress>=400)
            {mv=0.00017;
             flag=6;
             cv=11.2+(((eff_normal_stress-200)/200)*6.6);
             flag=6;}

/*Find Increase In Effective Stress Owing To Compression Equal To Step Height*/
            Hi = h_1-(delta_h*(step-(2*n*wave)));
        delta_eff_normal_stress = delta_h/(Hi*mv);

/*Find Time Factor For Current Drainage Path Length*/
        Tv = ((cv/525600)*step_time)/(Hi*Hi);
```

C program: v2.c

```
Jul 10 1998 13:25:01        v2.c-SectionB        Page 1

/*Find Uh Value Corresponding To Tv*/
        if ( Tv>=0 && Tv<0.0077 )
                {u=sqrt(Tv)/0.0077;
                flag=1;}
        if ( Tv>=0.0077 && Tv<0.031 )
                {u=10 *((10*(Tv-0.0077))/(0.031-0.0077));
                flag=2;}
        if ( Tv>=0.031 && Tv<0.071 )
                {u=20 *((10*(Tv-0.031))/(0.071-0.031));
                flag=3;}
        if ( Tv>=0.071 && Tv<0.126 )
                {u=30 *((10*(Tv-0.071))/(0.126-0.071));
                flag=4;}
        if ( Tv>=0.126 && Tv<0.196 )
                {u=40 *((10*(Tv-0.126))/(0.196-0.126));
                flag=5;}
        if ( Tv>=0.196 && Tv<0.286 )
                {u=50 *((10*(Tv-0.196))/(0.286-0.196));
                flag=6;}
        if ( Tv>=0.286 && Tv<0.403 )
                {u=60 *((10*(Tv-0.286))/(0.403-0.286));
                flag=7;}
        if ( Tv>=0.403 && Tv<0.567 )
                {u=70 *((10*(Tv-0.403))/(0.567-0.403));
                flag=8;}
        if ( Tv>=0.567 && Tv<0.848 )
                {u=80 *((10*(Tv-0.567))/(0.848-0.567));
                flag=9;}
        if ( Tv>=0.848 && Tv<1.129 )
                {u=90 *((10*(Tv-0.848))/(1.129-0.848));
                flag=10;}
        if ( Tv>=1.129 )
                {u=100;
                flag=11;}

/*Sets Displacement And Change In Effect Normal Stress To Zero For First Loop*/
    if (step == 0)
            {
                delta_eff_normal_stress = 0;
                displacement = 0;
            }

/*Calculate Pore Pressure At Step*/
    pore_pressure = (delta_eff_normal_stress * temp)*(1-(U/100));

/*Calculate Effective Normal Stress*/
    eff_normal_stress=normal_stress-pore_pressure;

/*Check For Liquefaction*/
    if (pore_pressure>=normal_stress)
        {
            eff_normal_stress = 0;
            pore_pressure = normal_stress;
        }
/*Output*/
    printf("%f  %f  %f  %f  %f\n", time, displacement, H, pore_pressure, eff_no
rmal_stress);
    fprintf(consoledat,"%f  %f  %f  %f  %f\n", time, displacement, H, pore_press
ure, eff_normal_stress);

/*Set temp = pore pressure so that it can be added to next increase in stress*/
    temp = pore_pressure;
    }
/* Loop Structure 2  Forced Down Slope Swelling */
```

```
Jul 10 1998 13:25:01        v2.c-SectionB        Page 2

for (steps=((2*n*wave)+(n+1)); steps<=((2*n*wave)+(2*n)-1); step++1)
    {
/*Calculate Time*/
        time = step * step_time;

/*Calculate Displacement*/
        displacement=((step/n)*length)-(step_width/2);

/*Find mv And cv Swelling Values Corresponding To Effective Normal Stress*/
        if (eff_normal_stress>0 && eff_normal_stress<50)
                {mv=0.0015-(((eff_normal_stress-0)/50)*0.0013);
                flag=1;
                cv=(eff_normal_stress-0)/50)*8.42);
                flag=1;}
        if (eff_normal_stress>=50 && eff_normal_stress<100)
                {mv=0.0002-(((eff_normal_stress-50)/50)*0.000105);
                flag=2;
                cv=(((eff_normal_stress-50)/50)*9.18);
                flag=2;}
        if (eff_normal_stress>=100 && eff_normal_stress<200)
                {mv=0.000095-(((eff_normal_stress-100)/100)*0.00008);
                flag=3;
                cv=(((eff_normal_stress-100)/100)*8.60);
                flag=3;}
        if (eff_normal_stress>=200)
                {mv=0.000015;
                flag=4;
                cv=(((eff_normal_stress-100)/100)*8.60);
                flag=4;}

/*Find Decrease In Effective Stress Owing To Swelling Equal To Step Height*/
    H = h_1-(delta_H*(step-(2*n*wave)-n));
    delta_eff_normal_stress = -delta_H/(H*mv);

/*Find Time Factor For Current Drainage Path Length*/
    Tv = ((cv/525600)*step_time)/(H*H);

/*Find Uh Value Corresponding To Tv*/
        if ( Tv>=0 && Tv<0.0077 )
                {u=(10*Tv)/0.0077;
                flag=1;}
        if ( Tv>=0.0077 && Tv<0.031 )
                {u=10 *((10*(Tv-0.0077))/(0.031-0.0077));
                flag=2;}
        if ( Tv>=0.031 && Tv<0.071 )
                {u=20 *((10*(Tv-0.031))/(0.071-0.031));
                flag=3;}
        if ( Tv>=0.071 && Tv<0.126 )
                {u=30 *((10*(Tv-0.071))/(0.126-0.071));
                flag=4;}
        if ( Tv>=0.126 && Tv<0.196 )
                {u=40 *((10*(Tv-0.126))/(0.196-0.126));
                flag=5;}
        if ( Tv>=0.196 && Tv<0.286 )
                {u=50 *((10*(Tv-0.196))/(0.286-0.196));
                flag=6;}
        if ( Tv>=0.286 && Tv<0.403 )
                {u=60 *((10*(Tv-0.286))/(0.403-0.286));
                flag=7;}
```

C program: v2.c.

Jul 10 1998 13:25:07 v2.c-SectionC Page 1

```
    if ( Tv>=0.403 && Tv<0.567 )
            {U=0.4 +((10*(Tv-0.403))/(0.567-0.403));
             flag=8;}
            if ( Tv>=0.567 && Tv<0.848 )
              {U=40 +((10*(Tv-0.567))/(0.848-0.567));
              flag=9;}
            if ( Tv>=0.848 && Tv<1.129 )
              {U=50 +((10*(Tv-0.848))/(1.129-0.848));
              flag=10;}
              if ( Tv>=1.129 )
                {U=100;
                flag=11;}


/*Calculate Pore Pressure At Step*/
    pore_pressure = (delta_eff_normal_stress + temp)*(1-(U/100));
/*Calculate Effective Normal Stress*/
    eff_normal_stress=normal_stress-pore_pressure;

/*Check For Liquefaction*/
    if (pore_pressure>=normal_stress)
      {
       eff_normal_stress = 0;
       pore_pressure = normal_stress;
      }
/*Output*/ printf("%f  %f  %f  %f\n", time, displacement, H, pore_pressure, eff_no
rmal_stress);
         fprintf(conoutdat,"%f  %f  %f  %f\n", time, displacement, H, pore_press
ure, eff_normal_stress);
/*Set temp = pore pressure so that it can be added to next increase in stress*/
    temp = pore_pressure;

  }
fclose(conoutdat);
}
```

C program: v2.c.

Jul 10 1998 13:01:36 v3.c-SectionA Page 1

```
/* Consolidation v3. Multiple Upslope Downslope Consolidation Programme*/
/* Now with provision for interpolating values of U from Tv */
/* analysis by linear interpolation. Also provision for interpolating values of mv and cv from oedometer tests on remoulded kaolin*/
/* and outputs the results to file 'conoutdat'.  Therefore any slope */
/* dimensions, shear rates, and normal stresses may be used but the */
/* results will always be for remoulded kaolin.  The sample is forced */
/* to swell when the stress is reduced below the preconsolidation stress */
/* consolidation values of mv and cv are used in this stage to reduce the*/
/* pressures */
#include <stdio.h>
#include <stdlib.h>
#define FILENAME "conoutdat"

main()
{

/* Define Variables */

   float h_i, h_j, length, rate, delta_h, step_width,
         total_time, step_time, normal_stress, mv, cv,
         time_displacement, eff_normal_stress, delta_eff_normal_stress,
         time_factor, displacement, sum, expression, U, step, H;
   int n, flag, flag2, flag3, wave, wavenu;
   FILE *conoutdat;

/* Open output file */
conoutdat = fopen(FILENAME,"w");

/* Slope Data Input Phase */

   printf("\n\n*********************************\n");
   printf("* Slope Data Input Phase #1a! *\n");
   printf("*********************************\n\n");
   printf("When entering data please use units in KILONEWTONS, METRES and MINUTES.\n\n
");

   printf("%s", "Input initial sample depth:");
   scanf("%f", &h_i);
   printf("%s", "Input final sample depth:");
   scanf("%f", &h_j);
   printf("%s", "Input horizontal slope length:");
   scanf("%f", &length);
   printf("%s", "Input number of wave forms to be analysed:");
   scanf("%d", &wavenu);
   printf("%s", "Input number of calculation steps:");
   scanf("%d", &n);
   printf("%s", "Input rate of sample displacement:");
   scanf("%f", &rate);

/* Initial Calculations: Step Height, Step Width, */
/*                       Total Time, Step Time */

   printf("\nData calculated from slope geometry, dynamics and number of steps.\n");
   delta_h = (h_i-h_j)/n;
   step_width = length/n;
   total_time = length/rate;
   step_time = total_time/n;
   printf("\nStep Height = %g\n", delta_h);
   printf("Step Width = %g\n", step_width);
   printf("Total Time  = %g\n", total_time);
   printf("Step Time   = %g\n", step_time);

/* Sample Data Input Phase */
```

Jul 10 1998 13:01:36 v3.c-SectionA Page 2

```
   printf("\n\n*********************************\n");
   printf("* Sample Data Input Phase #1b! *\n");
   printf("*********************************\n\n");
   printf("%s","Input initial normal effective stress in kPa. When\n the pore water pr
essure is equal to zero:");
   scanf("%f", &normal_stress);
   printf("\nINCOHERENCING ANALYSIS\n");
   eff_normal_stress = normal_stress;

   /* Wave Loop */

for (wave=0; wave<=wavenu-1; wave++)
   {

   /* Loop Structure 1 Forced Consolidation */

for (step=(2*n*wave); step<=((2*n*wave)+n); step++)
   {

   /*Calculate Time*/
      time = step * step_time;

   /*Calculate Displacement*/
      displacement=((step/n)*length)-(step_width/2);

   /*Find mv And cv Values Corresponding To Effective Normal Stress*/
            if (eff_normal_stress>=0 && eff_normal_stress<25)
               {mv=0.0025-(((eff_normal_stress-0)/25)*0.00112);
               flag=1;
               cv=3+(((eff_normal_stress-0)/25)*1.2);
               flag=1;}
            if (eff_normal_stress>=25 && eff_normal_stress<50)
               {mv=0.00138-(((eff_normal_stress-25)/25)*0.00062);
               flag=2;
               cv=4.2+(((eff_normal_stress-25)/25)*1.2);
               flag=2;}
            if (eff_normal_stress>=50 && eff_normal_stress<100)
               {mv=0.00076-(((eff_normal_stress-50)/50)*0.00028);
               flag=3;
               cv=5.4+(((eff_normal_stress-50)/50)*2.2);
               flag=3;}
         if (eff_normal_stress>=100 && eff_normal_stress<200)
            {mv=0.00048-(((eff_normal_stress-100)/100)*0.0002);
            flag=4;
            cv=7.6+(((eff_normal_stress-100)/.00)*3.6);
            flag=4;}
         if (eff_normal_stress>=200 && eff_normal_stress<400)
            {mv=0.00028-(((eff_normal_stress-200)/200)*0.00011);
            flag=5;
            cv=11.2+(((eff_normal_stress-200)/200)*6.6);
            flag=5;}
         if (eff_normal_stress>=400)
            {mv=0.00017;
            flag=6;
            cv=11.2+(((eff_normal_stress-200)/200)*6.6);
            flag=6;}

   /*Find Increase In Effective Stress Owing To Compression Equal To Step Height*/
            delta_eff_normal_stress = (mv*delta_h)/((mv*mv)+(mv*mv));

   /*Find Time Factor For Current Drainage Path Length*/
            Tv = ((cv/525600)*step_time)/(H*H);
```

C program: v3.c

Jul 10 1998 13:05:03 v3.c-SectionB Page 1

```
/*Find Uh Value Corresponding To Tv*/
if ( Tv>=0 && Tv<0.0077 )
    {U=(10*Tv)/0.0077;
     flag=1;}
     if ( Tv>=0.0077 && Tv<0.031 )
        {U=10 +((10*(Tv-0.0077))/(0.031-0.0077));
        flag=2;}
if ( Tv>=0.031 && Tv<0.071 )
    {U=20 +((10*(Tv-0.031))/(0.071-0.031));
     flag=3;}
     if ( Tv>=0.071 && Tv<0.126 )
        {U=30 +((10*(Tv-0.071))/(0.126-0.071));
        flag=4;}
     if ( Tv>=0.126 && Tv<0.196 )
        {U=40 +((10*(Tv-0.126))/(0.196-0.126));
        flag=5;}
     if ( Tv>=0.196 && Tv<0.286 )
        {U=50 +((10*(Tv-0.196))/(0.286-0.196));
        flag=6;}
     if ( Tv>=0.286 && Tv<0.403 )
        {U=60 +((10*(Tv-0.286))/(0.403-0.286));
        flag=7;}
     if ( Tv>=0.403 && Tv<0.567 )
        {U=70 +((10*(Tv-0.403))/(0.567-0.403));
        flag=8;}
     if ( Tv>=0.567 && Tv<0.848 )
        {U=80 +((10*(Tv-0.567))/(0.848-0.567));
        flag=9;}
     if ( Tv>=0.848 && Tv<1.129 )
        {U=90 +((10*(Tv-0.848))/(1.129-0.848));
        flag=10;}
     if ( Tv>=1.129 )
        {U=100;
        flag=11;}

/*Sets Displacement And Change In Effect Normal Stress To Zero For First Loop*/
    if (step == 0)
            {
            delta_eff_normal_stress = 0;
            displacement = 0;
            }

/*Calculate Pore Pressure At Step*/
    pore_pressure = (delta_eff_normal_stress * temp)*(1-(U/100));

/*Calculate Effective Normal Stress*/
    eff_normal_stress=normal_stress-pore_pressure;

/*Check For Liquefaction*/
    if (pore_pressure>=normal_stress)
        {
        eff_normal_stress = 0;
        pore_pressure = normal_stress;
        }
/*Output*/
    printf("%f  %f  %f  %f\n", time, displacement, H, pore_pressure, eff_no
rmal_stress);
    fprintf(conoutdat,"%f  %f  %f  %f  %f\n", time, displacement, H, pore_press
ure, eff_normal_stress);

/*Set temp = pore pressure so that it can be added to next increase in stress*/
    temp = pore_pressure;
    }
    /* Loop Structure 2  Forced Down Slope Swelling */
```


Jul 10 1998 13:05:03 v3.c-SectionB Page 2

```
for (step=((2*n*wave)+(n+1)); step>=((2*n)*wave)+(2*n)-1); step-=1)
    {
/*Calculate Time*/
    time = step * step_time;

/*Calculate Displacement*/
    displacement-=((step/n)*length)-(step_width/2);

/*Find mv And cv Values Corresponding To Effective Normal Stress*/
        if (eff_normal_stress>=0 && eff_normal_stress<25)
                {mv=0.00125-(((eff_normal_stress-0)/25)*0.00112);
                flag=1;
                cv=3-(((eff_normal_stress-0)/25)*1.2);
                flag=1;}
        if (eff_normal_stress>=25 && eff_normal_stress<50)
                {mv=0.00138-(((eff_normal_stress-25)/25)*0.00062);
                flag=2;
                cv=4.2-(((eff_normal_stress-25)/25)*1.2);
                flag=2;}
        if (eff_normal_stress>=50 && eff_normal_stress<100)
                {mv=0.0076-(((eff_normal_stress-50)/50)*0.00228);
                flag=3;
                cv=5.4-(((eff_normal_stress-50)/50)*2.2);
                flag=3;}
        if (eff_normal_stress>=100 && eff_normal_stress<200)
                {mv=0.00648-(((eff_normal_stress-100)/100)*0.0002);
                flag=4;
                cv=7.6-(((eff_normal_stress-100)/100)*3.6);
                flag=4;}
        if (eff_normal_stress>=200 && eff_normal_stress<400)
                {mv=0.00028-(((eff_normal_stress-200)/200)*0.000111);
                flag=5;
                cv=11.2-(((eff_normal_stress-200)/200)*6.6);
                flag=5;}
        if (eff_normal_stress>=400)
                {mv=0.0001;
                flag=6;
                cv=11.2+(((eff_normal_stress-200)/200)*6.6);
                flag=6;}

/*Find Decrease In Effective Stress Owing To Swelling Equal To Step Height*/
    H = H - delta_H*((Tv*cv)/mv);
        delta_eff_normal_stress = -delta_h/(H*mv);

/*Find Time Factor For Current Drainage Path Length*/
    Tv = ((cv/525600)*step_time)/(H*H);

    /*Find Uh Value Corresponding To Tv*/
        if ( Tv>=0 && Tv<0.0077 )
                {U=(10*Tv)/0.0077;
                flag=1;}
                if ( Tv>=0.0077 && Tv<0.031 )
                {U=10 +((10*(Tv-0.0077))/(0.031-0.0077));
                flag=2;}
        if ( Tv>=0.031 && Tv<0.071 )
                {U=20 +((10*(Tv-0.031))/(0.071-0.031));
                flag=3;}
        if ( Tv>=0.071 && Tv<0.126 )
                {U=30 +((10*(Tv-0.071))/(0.126-0.071));
                flag=4;}
        if ( Tv>=0.126 && Tv<0.196 )
                {U=40 +((10*(Tv-0.126))/(0.196-0.126));
                flag=5;}
```

C program: v3.c.

Jul 10 1998 13:06:16 v3.c-SectionC Page 1

```
        if ( Ty>=0.196 && Ty<0.286 )
           {U=50.+((10.*(Ty-0.196))/(0.286-0.196));
           flag=6;}
        if ( Ty>=0.286 && Ty<0.403 )
           {U=60.+((10.*(Ty-0.286))/(0.403-0.286));
           flag=7;}
        if ( Ty>=0.403 && Ty<0.567 )
           {U=70.+((10.*(Ty-0.403))/(0.567-0.403));
           flag=8;}
        if ( Ty>=0.567 && Ty<0.848 )
           {U=80.+((10.*(Ty-0.567))/(0.848-0.567));
           flag=9;}
        if ( Ty>=0.848 && Ty<1.129 )
           {U=90.+((10.*(Ty-0.848))/(1.129-0.848));
           flag=10;}
        if ( Ty>=1.129 )
           {U=100.;
           flag=11;}

     /*Calculate Pore Pressure At Step*/
        pore_pressure = (delta_eff_normal_stress + temp)*(1-(U/100));

     /*Calculate Effective Normal Stress*/
       eff_normal_stress=normal_stress-pore_pressure;

     /*Check For Liquefaction*/
        if (pore_pressure>=normal_stress)
           {
             eff_normal_stress = 0;
             pore_pressure = normal_stress;
           }
     /*Output*/
        printf("%f  %f  %f  %f  %f\n", time, displacement, H, pore_pressure, eff_no
rmal_stress);
        fprintf(conoutdat,"%f  %f  %f  %f  %f\n", time, displacement, H, pore_press
ure, eff_normal_stress);
     /*Set temp = pore pressure so that it can be added to next increase in stress*/
        temp = pore_pressure;
     }
  fclose(conoutdat);
  }
```

C program: v3.c.

Appendix C

Examples Of Complete Test Results

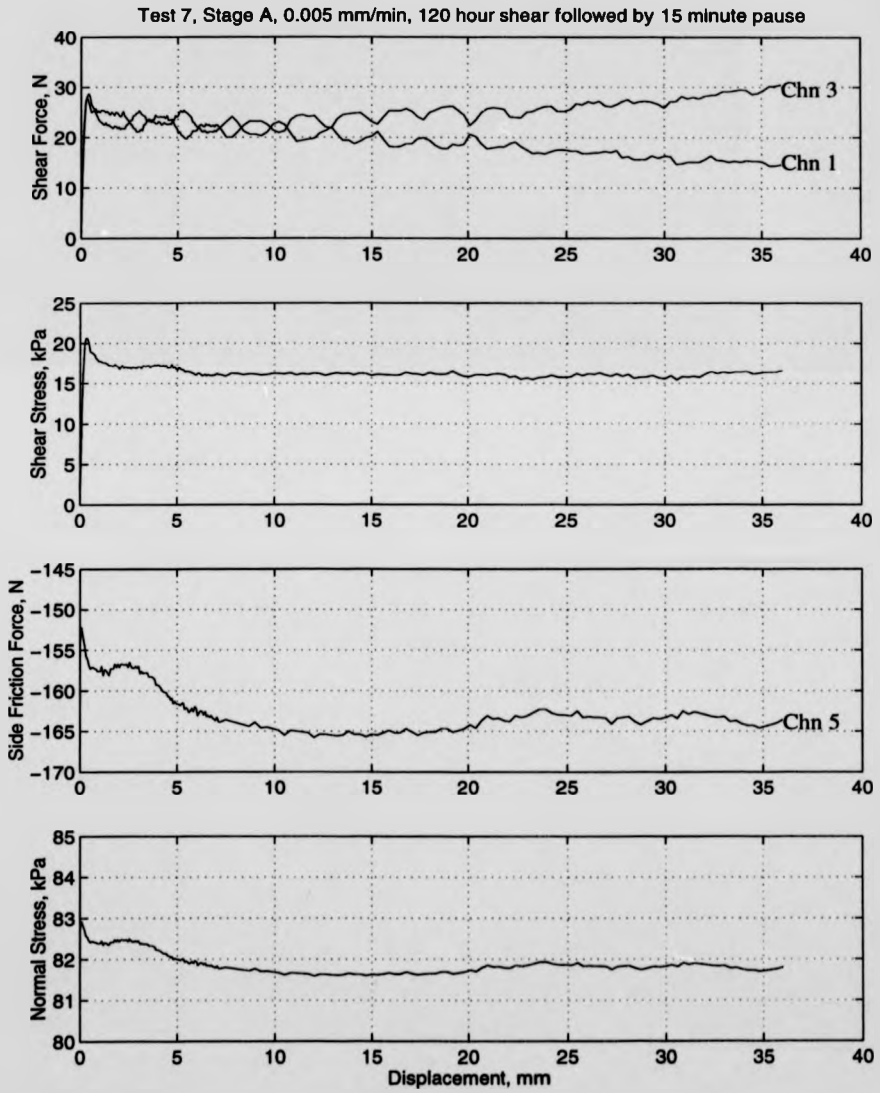

Figure C.1: Test 7, complete test results, stage A.

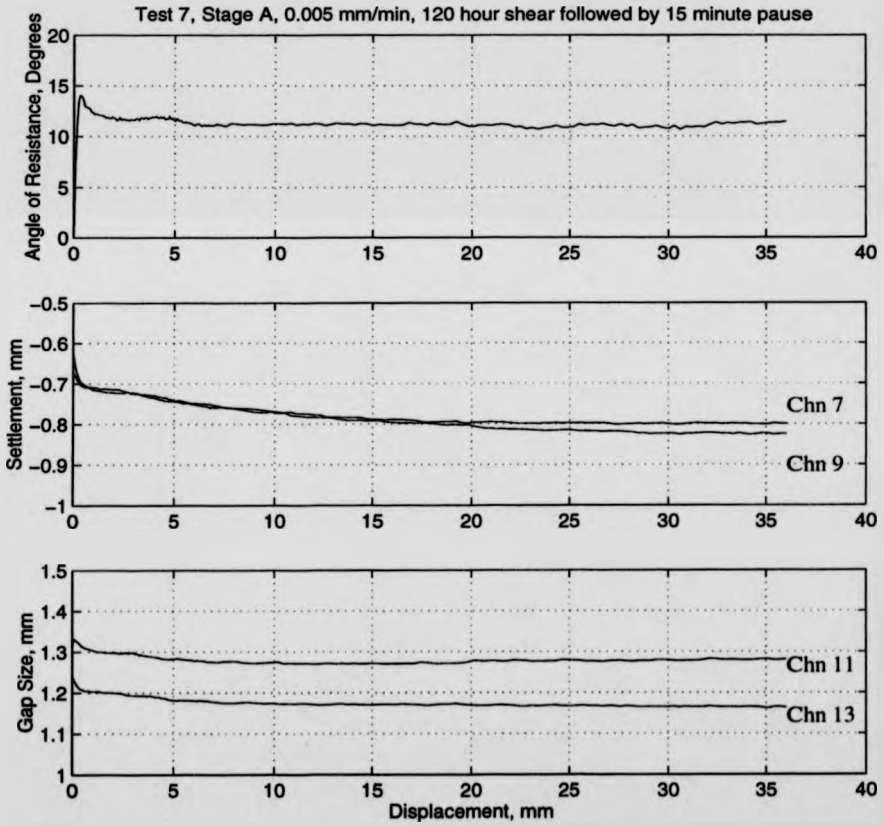

Figure C.2: Test 7, complete test results, stage A.

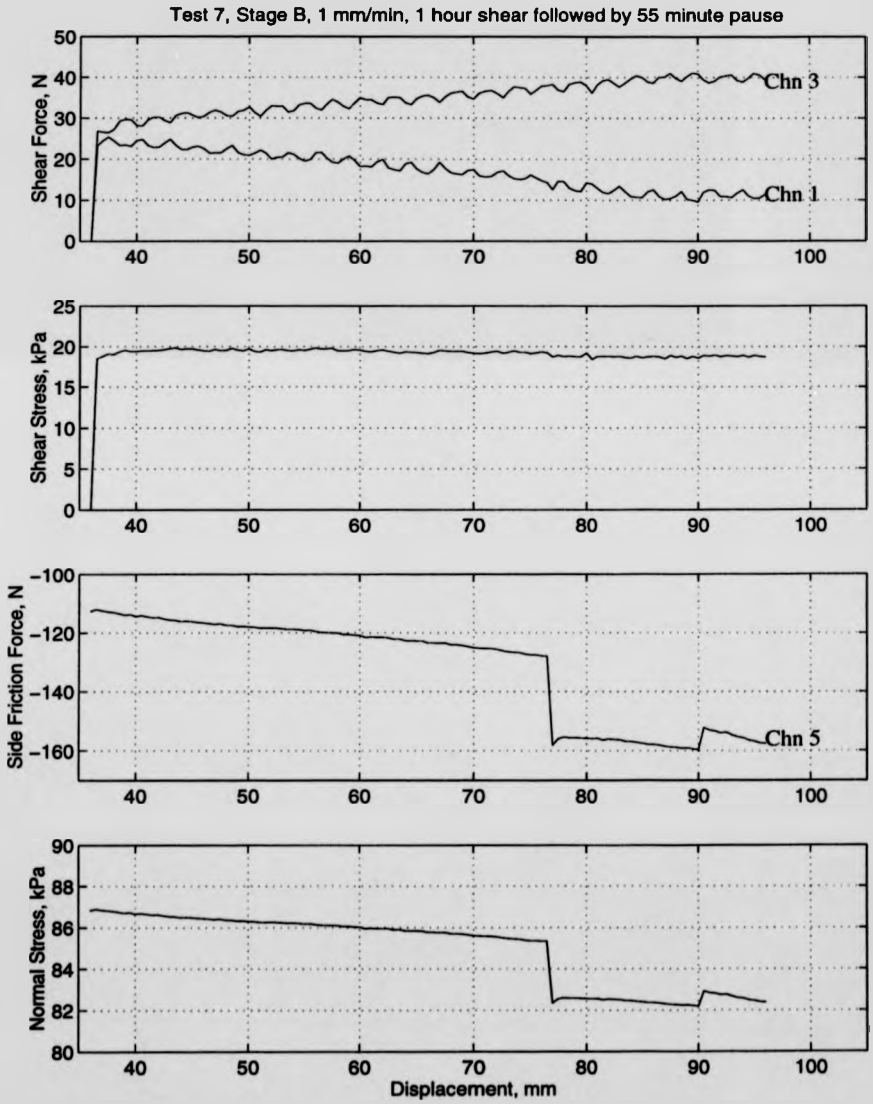

Figure C.3: Test 7, complete test results, stage B.

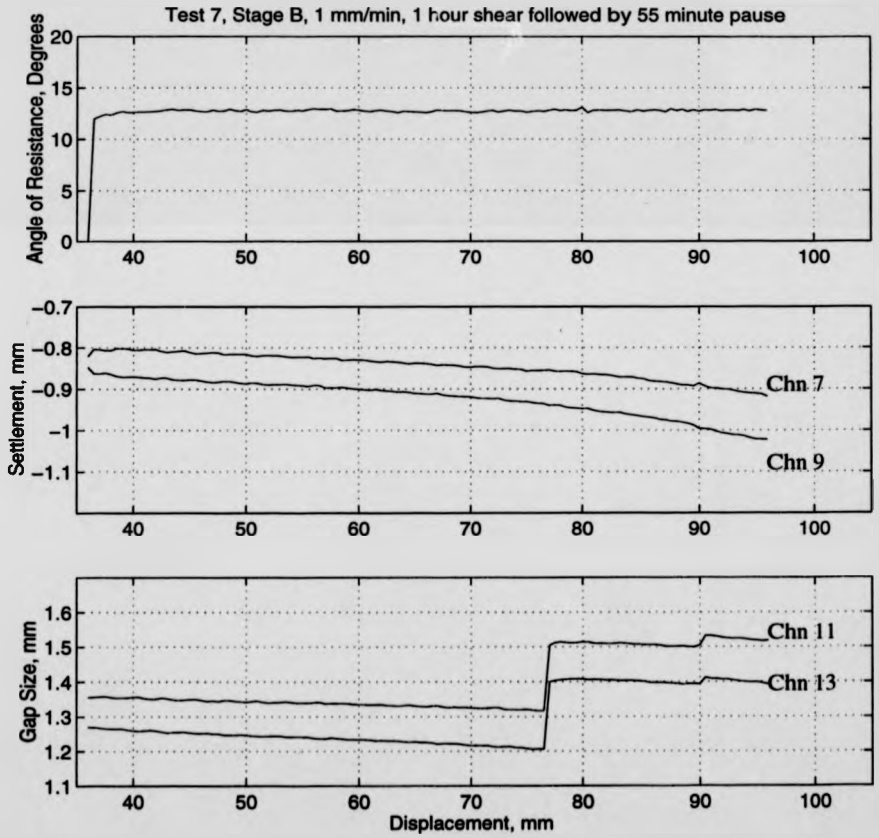

Figure C.4: Test 7, complete test results, stage B.

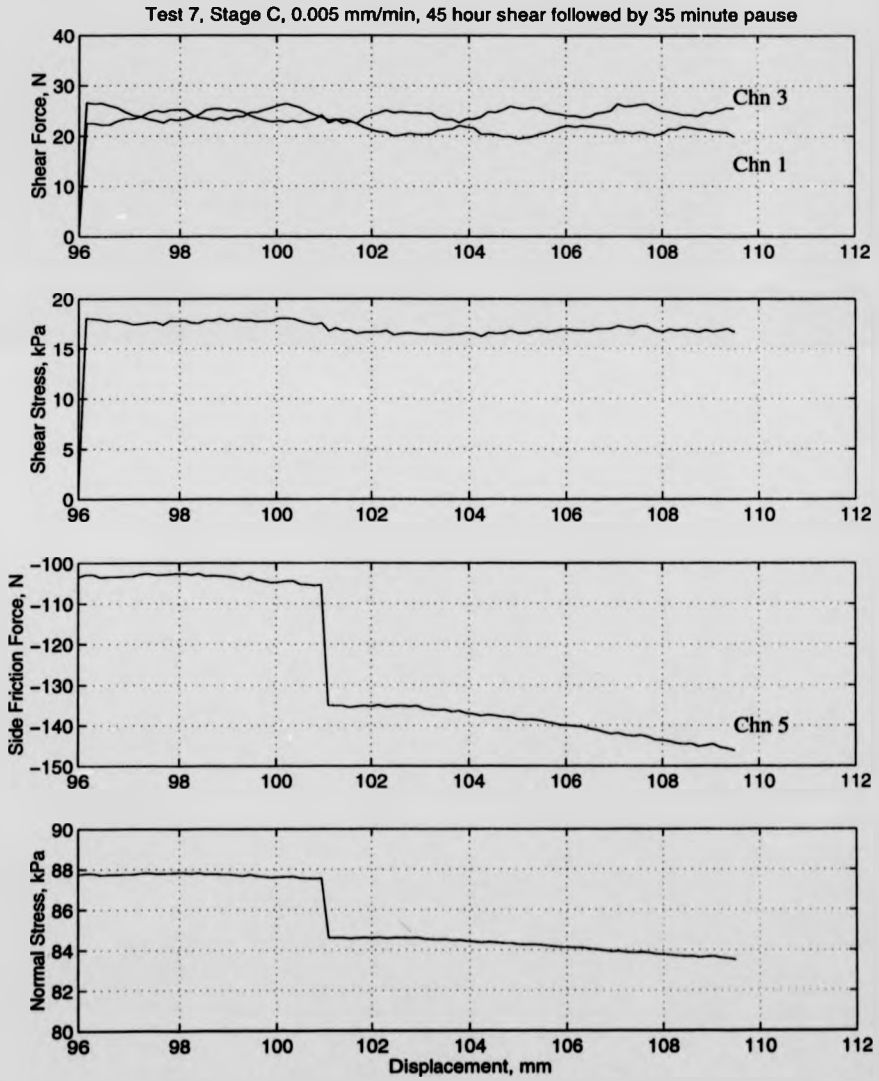

Figure C.5: Test 7, complete test results, stage C.

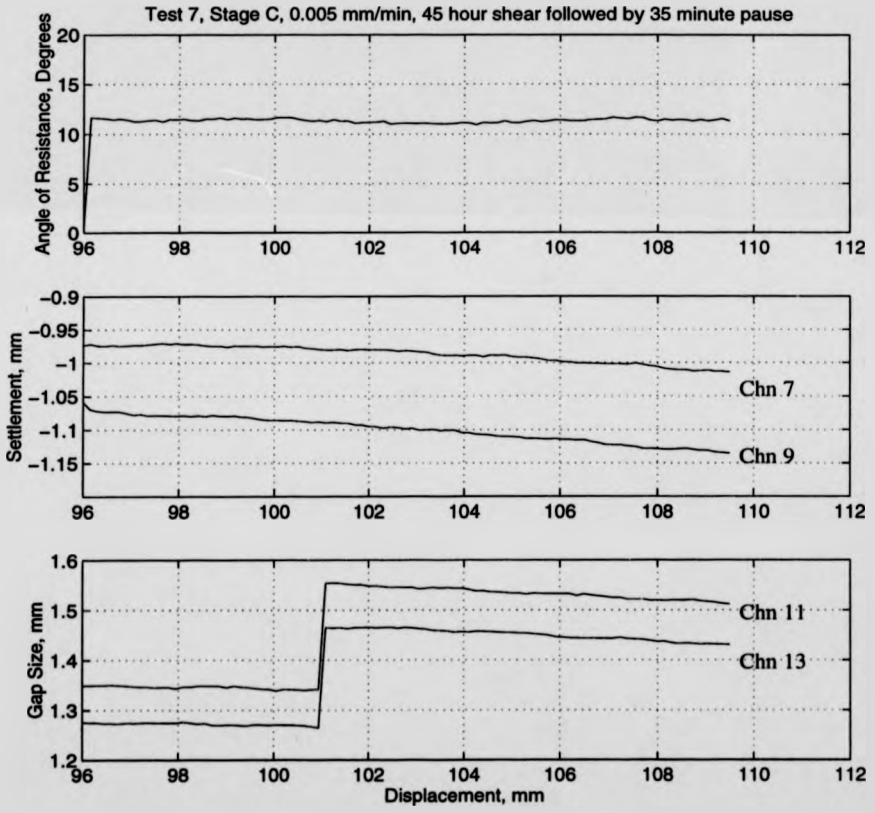

Figure C.6: Test 7, complete test results, stage C.

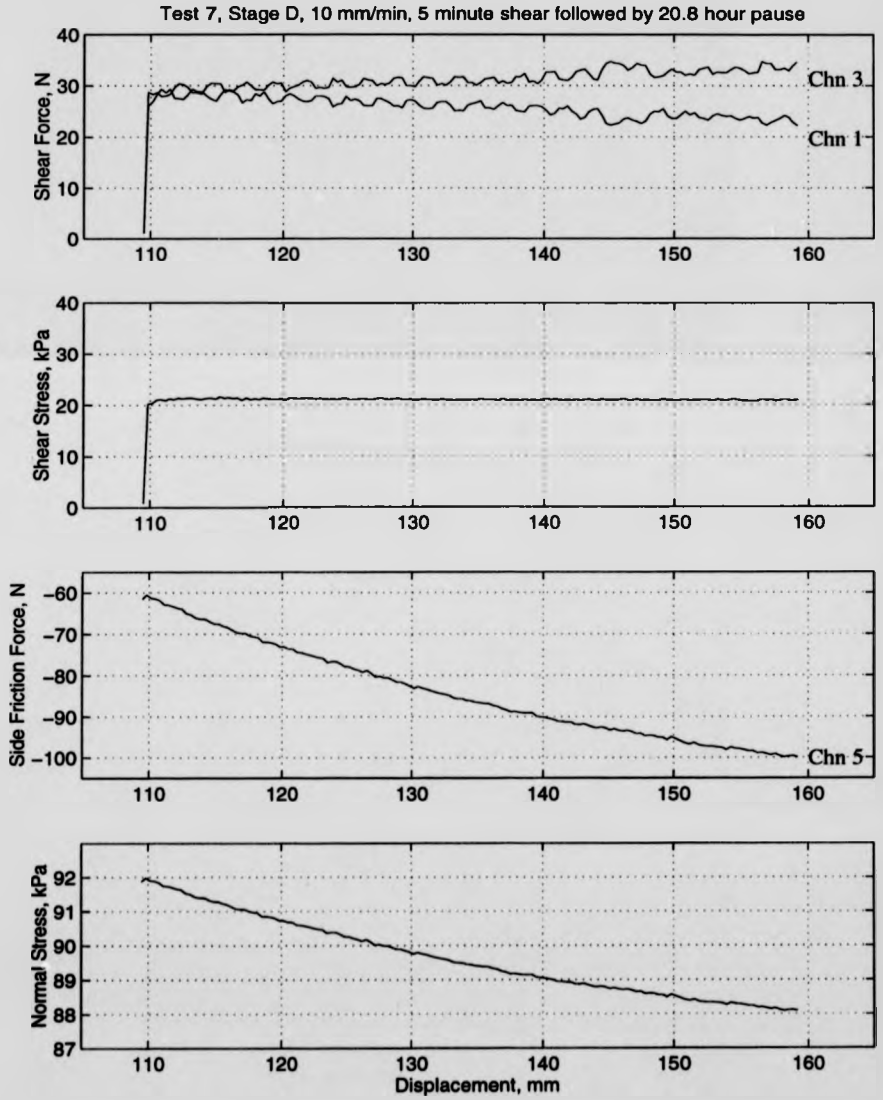

Figure C.7: Test 7, complete test results, stage D.

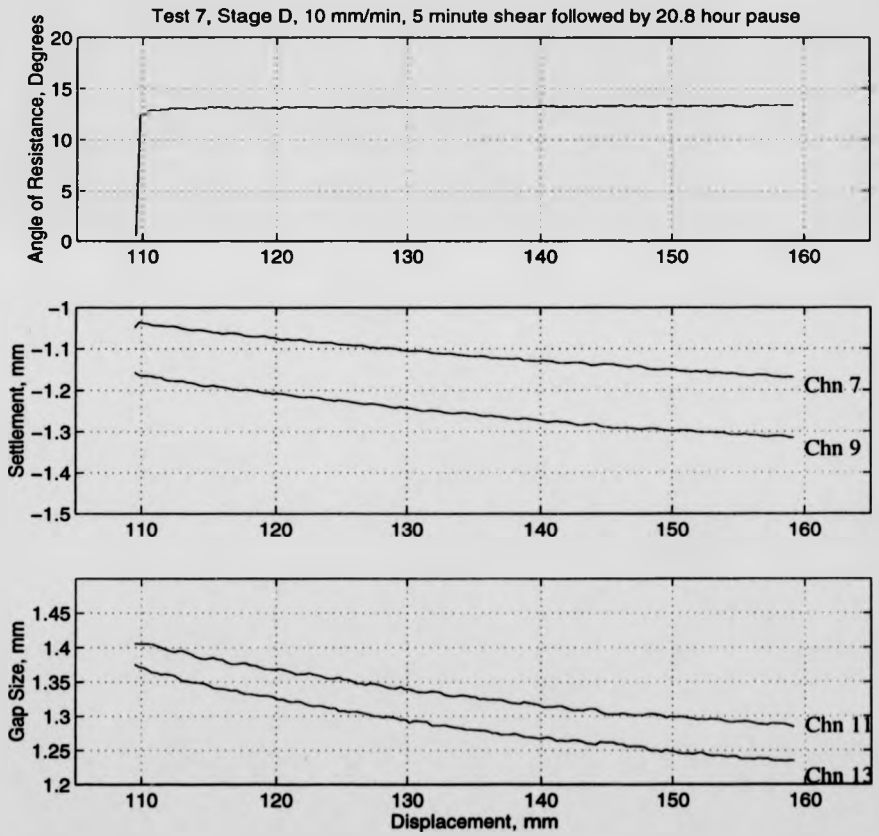

Figure C.8: Test 7, complete test results, stage D.

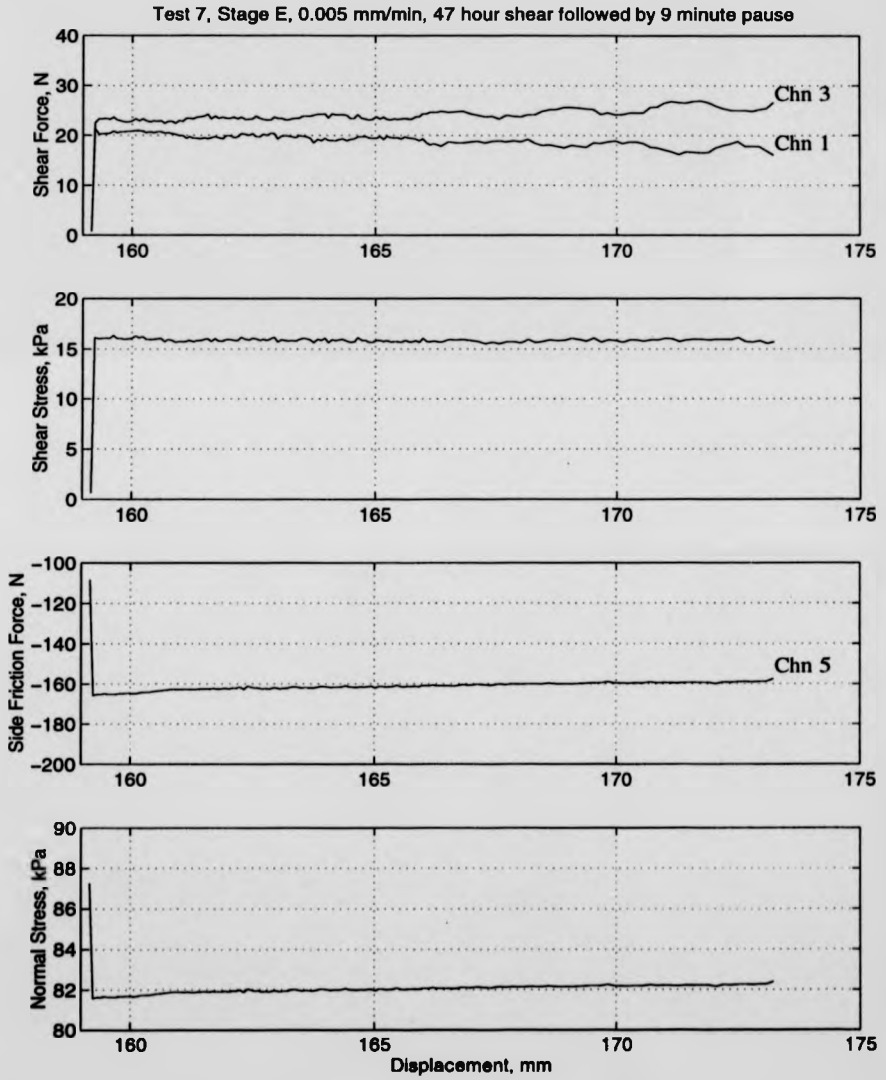

Figure C.9: Test 7, complete test results, stage E.

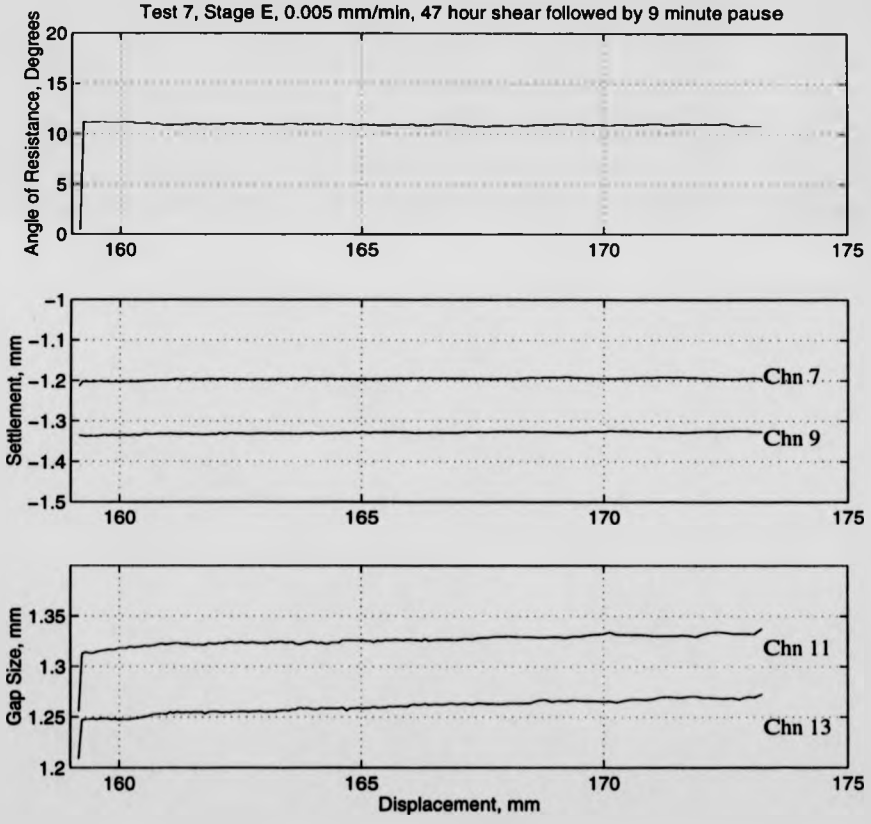

Figure C.10: Test 7, complete test results, stage E.

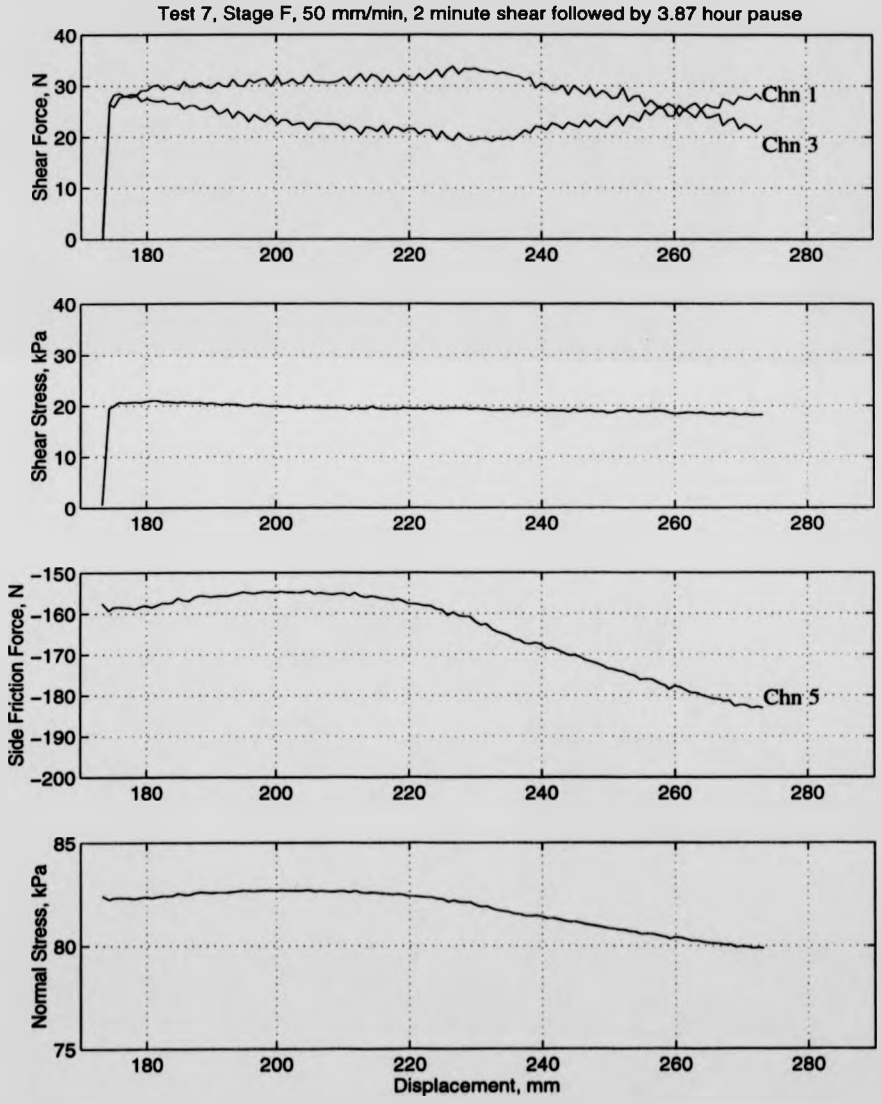

Figure C.11: Test 7, complete test results, stage F.

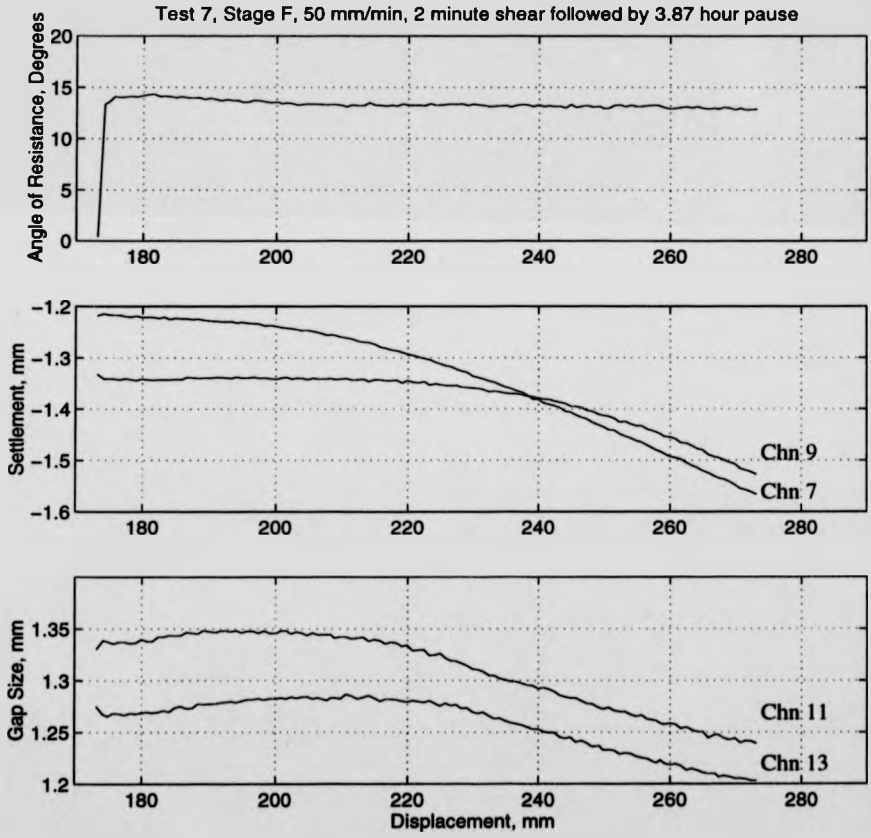

Figure C.12: Test 7, complete test results, stage F.

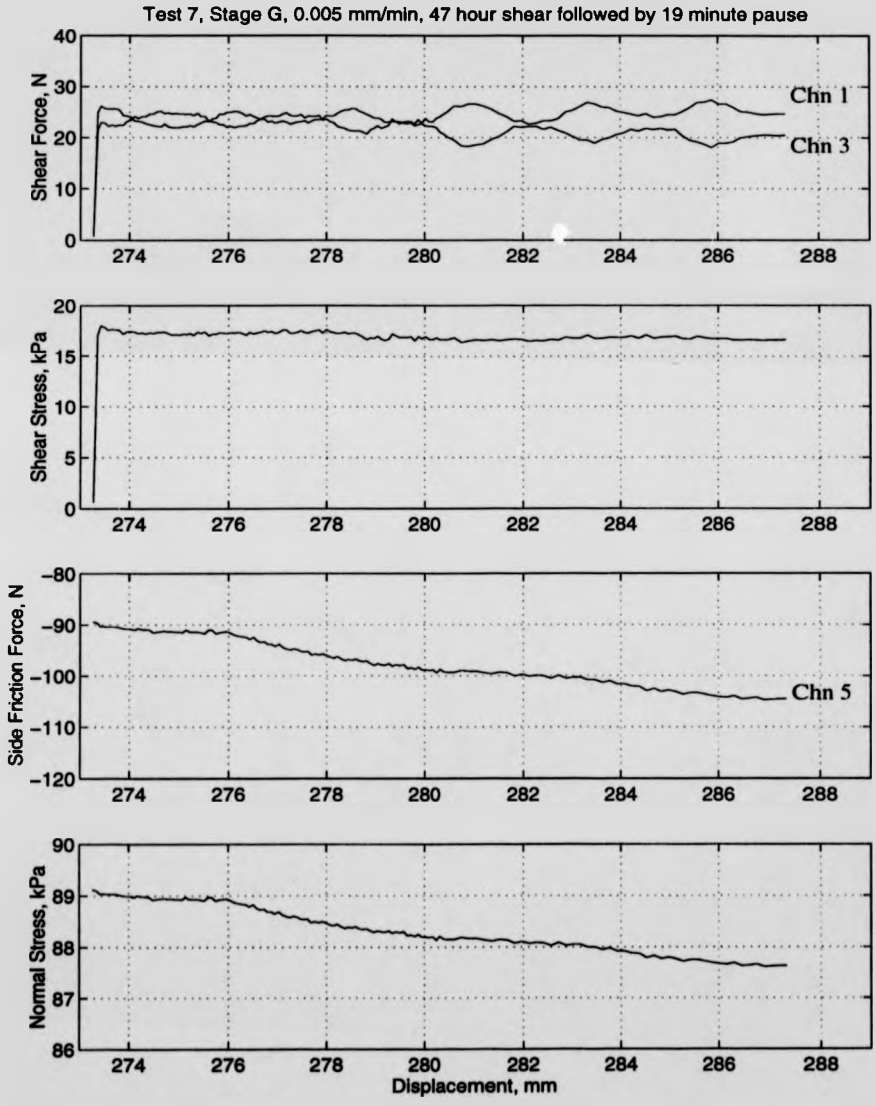

Figure C.13: Test 7, complete test results, stage G.

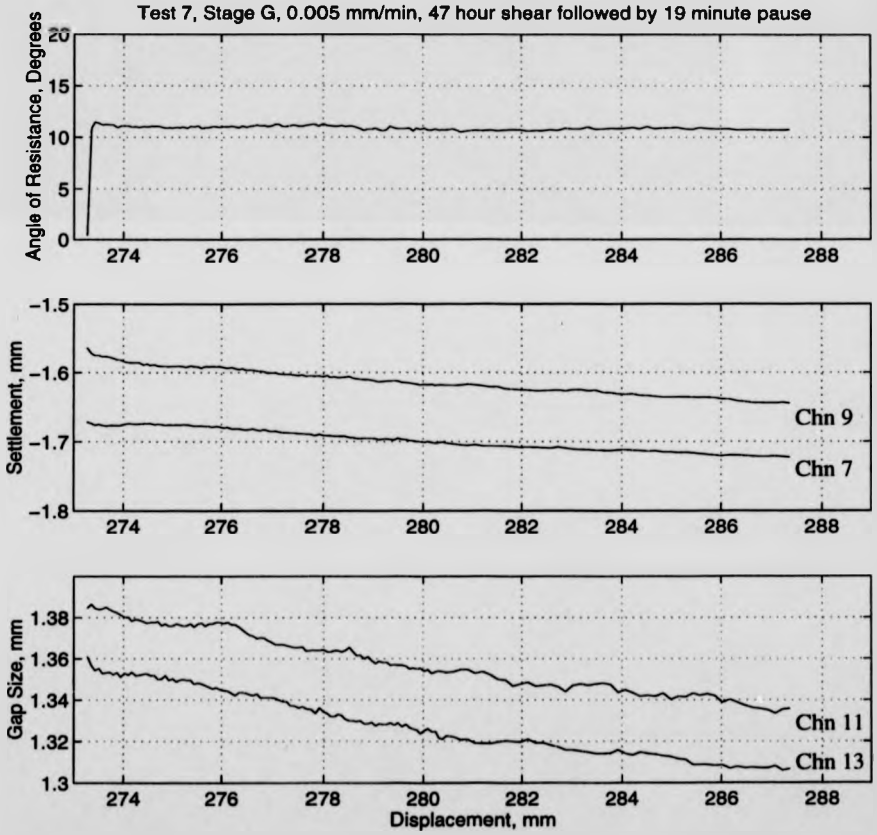

Figure C.14: Test 7, complete test results, stage G.

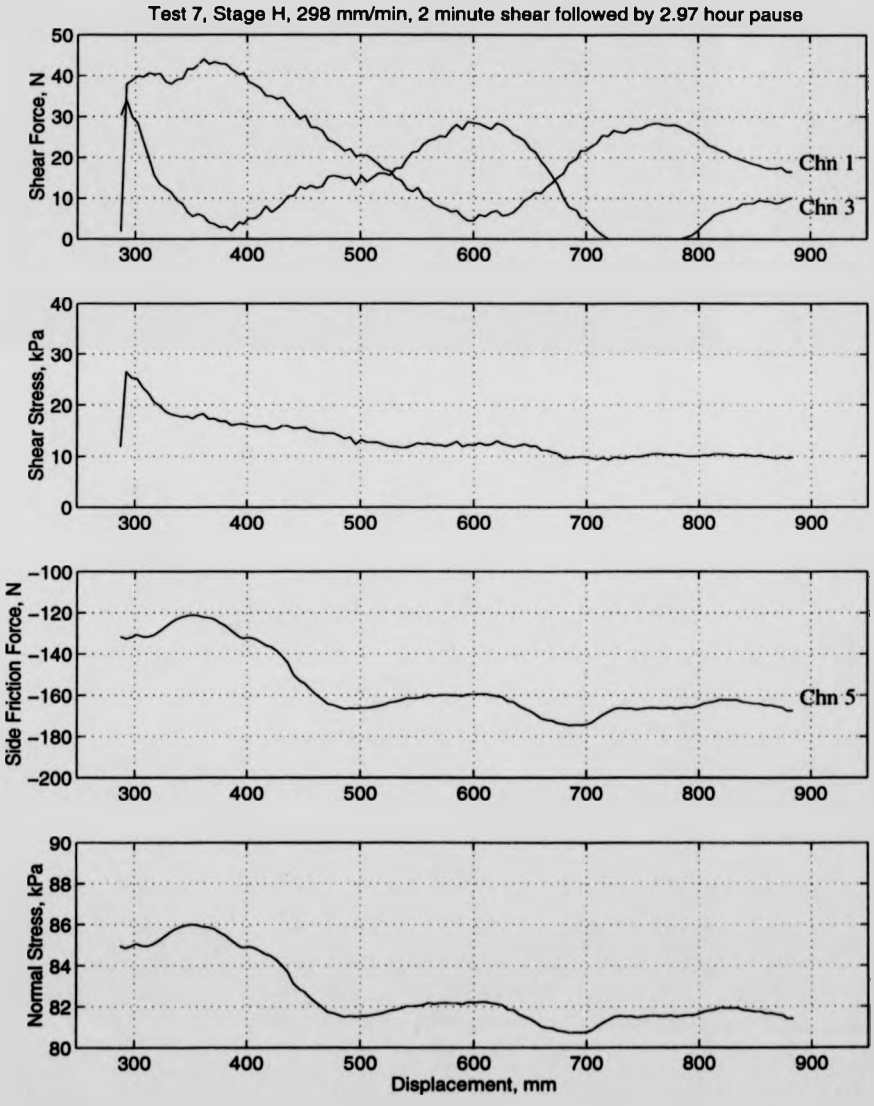

Figure C.15: Test 7, complete test results, stage H.

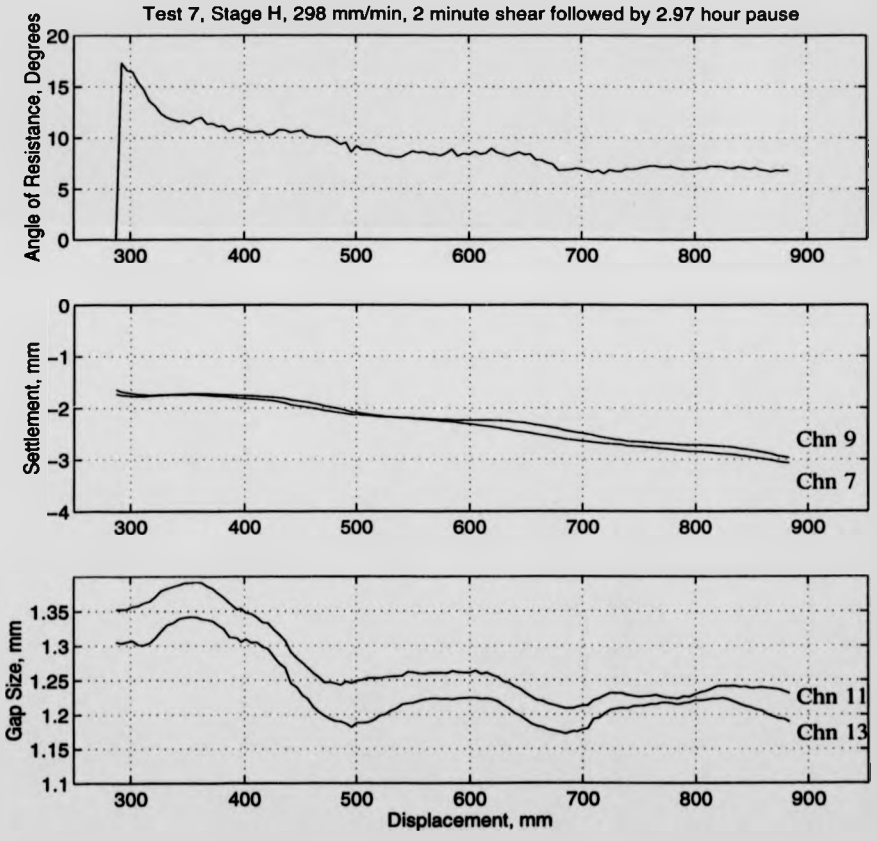

Figure C.16: Test 7, complete test results, stage H.

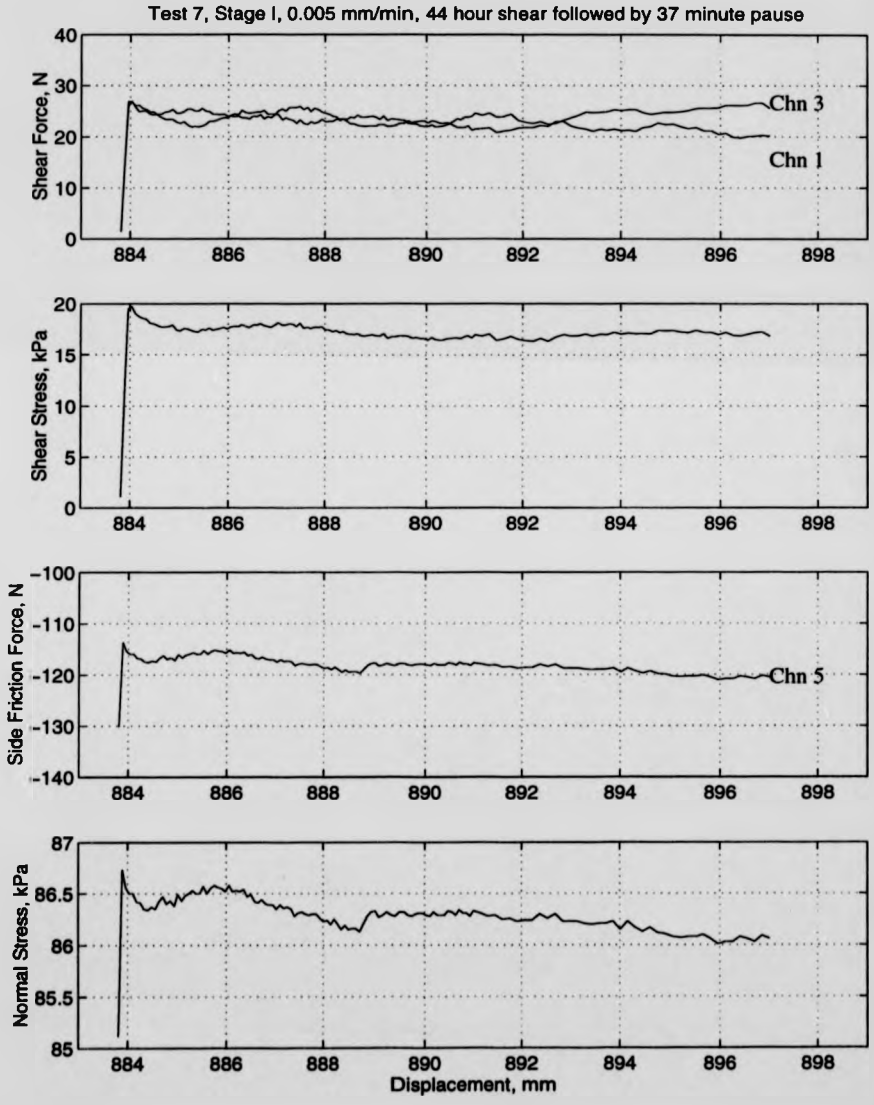

Figure C.17: Test 7, complete test results, stage I.

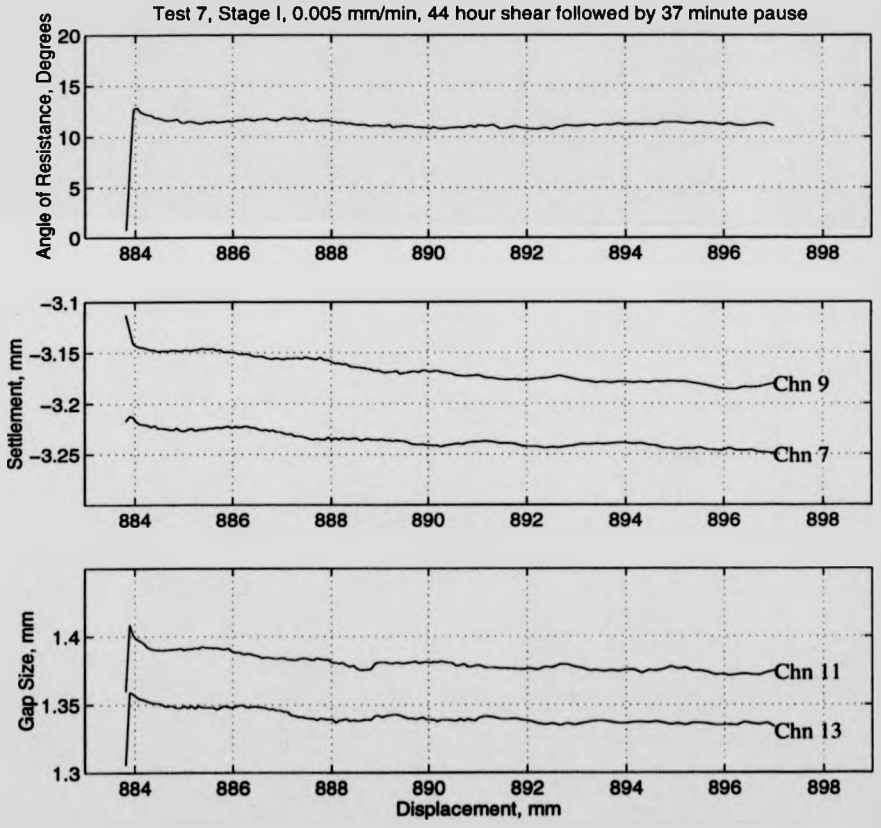

Figure C.18: Test 7, complete test results, stage I.

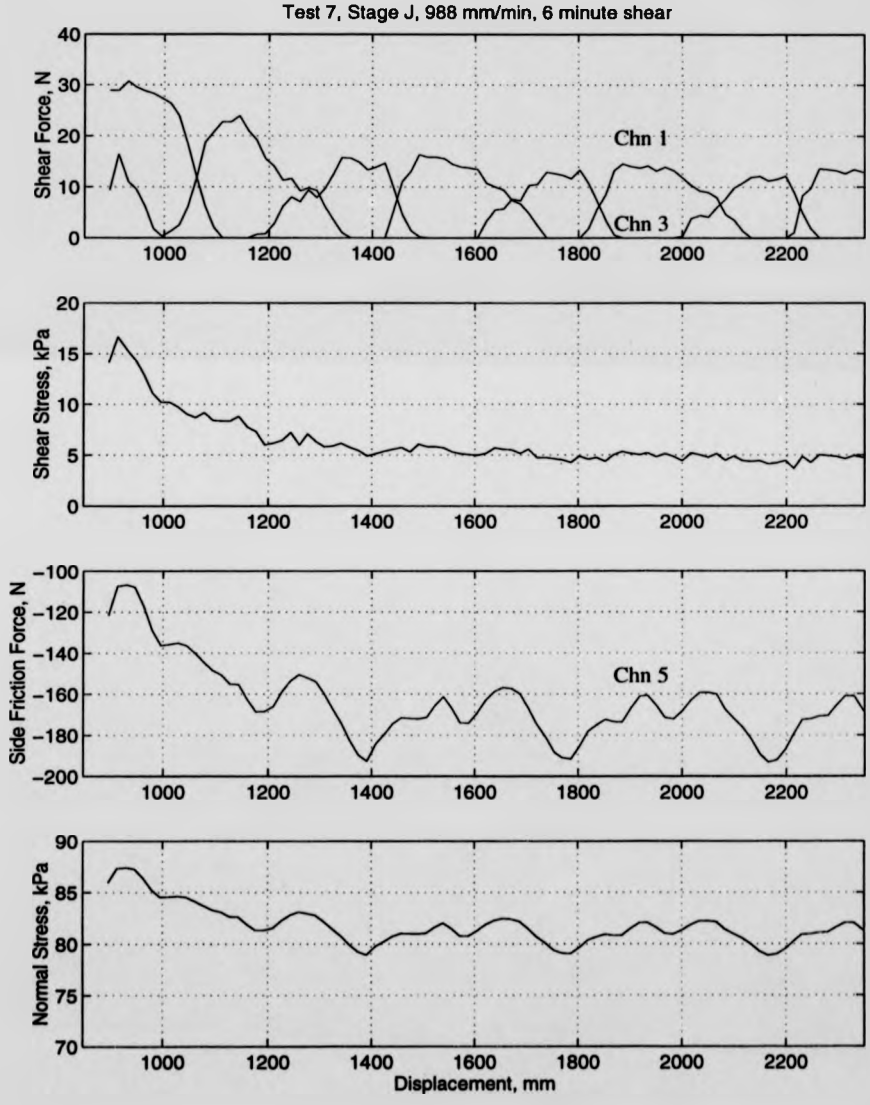

Figure C.19: Test 7, complete test results, stage J.

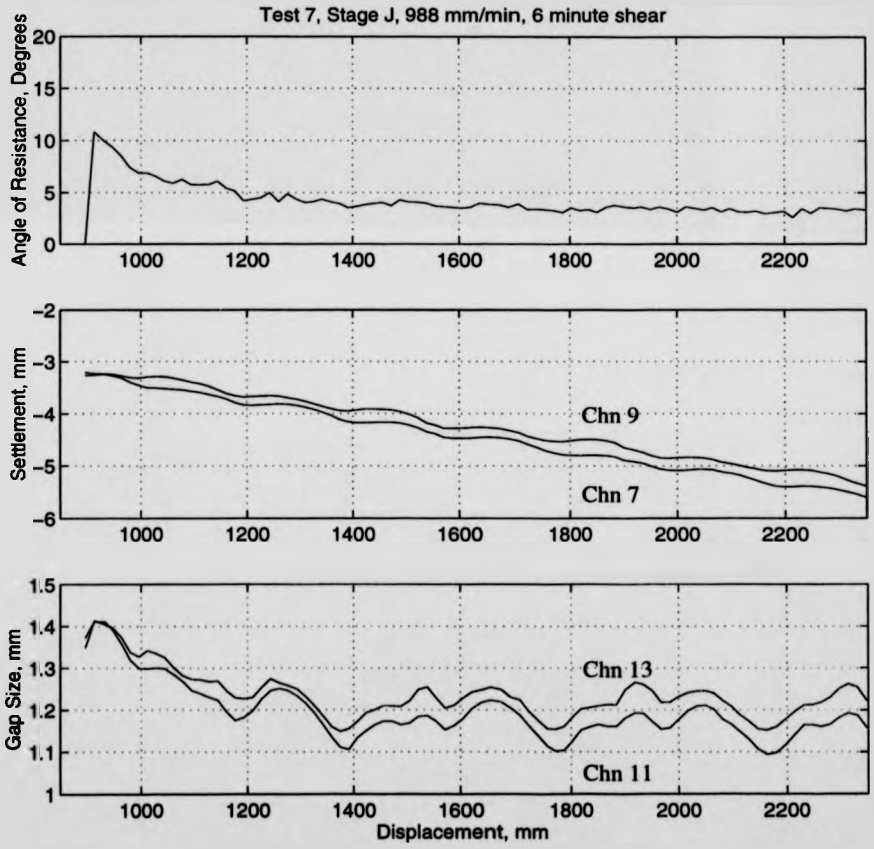

Figure C.20: Test 7, complete test results, stage J.

Test No: WF1			Rate o/min: – (Ro)			Bromhead Ring Shear Test Description: KAOLIN ON PLANE PERSPEX INTERFACE, TO ESTABLISH DRAINED RESIDUAL ANGLE. CONSOLIDATION PHASE				
Date: 25/2/97			Rate mm/min (0.742Ro): –							
Normal Stress kPa: 50(σ)			Platen Weight kg: 0·989 (W)			Mass On Hanger=(0.40831σ -W)/10=19kg				Sht 1 of 6
Time hh:mm;ss	Min.	Settl-ement gauge	Settlement in mm (0.002/div)	Reading on 9717A	Reading on 9717B	F1(N)= 9717Adiv *0.18818	F2(N)= 9717Bdiv *0.19120	Shear Stress τ(kPa)= 0.44186(F1+F2)	Tan ϕ= τ/σ	ϕ Deg.
11:30:00	0	4·00	0							
11:30:10	0·17	4·64	0·128							
11:30:15	0·25	4·71	0·142							
11:30:30	0·50	4·89	0·178							
11:30:45	0·75	5·04	0·208							
11:31:00	1	5·16	0·232							
11:32:00	2	5·46	0·292							
11:34:00	4	5·63	0·326							
11:38:00	8	5·695	0·339							
11:45:00	15	5·72	0·344							
12:00:00	30	5·75	0·350							
12:30:00	60	5·755	0·351							
13:05:00	95	5·76	0·352							
14:30:00	180	5·765	0·353							
14:35:00	START	SHEARING THE								
	SAMPLE OVER 4									
	REVOLUTIONS AT 90°/min									
	TO ESTABLISH A GOOD									
	SHEAR SURFACE									

Test No: WF1			Rate o/min: 0·0320 (Ro)			Bromhead Ring Shear Test Description: KAOLIN ON PLANE PERSPEX INTERFACE, TO ESTABLISH DRAINED RESIDUAL ANGLE.				
Date: 26/2/97			Rate mm/min (0.742Ro): 0·0237							
Normal Stress kPa: 50 (σ)			Platen Weight kg: 0·989 (W)			Mass On Hanger = (0.40831σ - W)/10 = 19 kg				Sht 2 of 6
Time hh:mm;ss	Min. (DISPLACEMENT IN MM)	Settlement gauge	Settlement in mm (0.002/div)	Reading on 9717A	Reading on 9717B	F1(N)= 9717Adiv *0.18818	F2(N)= 9717Bdiv *0.19120	Shear Stress τ(kPa)= 0.44186(F1+F2)	Tan ϕ= τ/σ	ϕ Deg.
09:40:00	0 (0)	7·60	0·720	2·00	2·00	0	0	0	0	0
09:50:00	0 (0)	7·60	0·720	2·00	2·00	0	0	0	0	0
09:55:00	5 (0·12)	7·605	0·721	2·30	2·35	5·64	6·69	5·45	0·10898	6·22
09:57:00	7 (0·18)	7·605	0·721	2·45	2·49	8·47	9·37	7·88	0·15766	8·96
10:00:00	10 (0·24)	7·605	0·721	2·45	2·495	8·47	9·46	7·92	0·15840	9·00
10:10:00	20 (0·47)	7·605	0·721	2·45	2·49	8·47	9·37	7·88	0·15766	8·96
11:00:00	70 (1·66)	7·61	0·722	2·45	2·48	8·47	9·18	7·80	0·15596	8·86
11:40:00	110 (2·61)	7·61	0·722	2·445	2·475	8·37	9·08	7·71	0·15421	8·77
13:50:00	240 (5·70)	7·61	0·722	2·44	2·46	8·28	8·80	7·55	0·15094	8·58
14:20:00	270 (6·41)	7·61	0·722	2·44	2·46	8·28	8·80	7·55	0·15094	8·58
15:30:00	340 (8·07)	7·61	0·722	2·44	2·455	8·28	8·70	7·50	0·15006	8·53

Test No: WF1	Rate o/min: — (Ro)	Bromhead Ring Shear Test Description: KAOLIN ON PLANE PERSPEX INTERFACE, TO ESTABLISH DRAINED RESIDUAL ANGLE, SECOND CONSOLIDATION PHASE	
Date: 26/2/97	Rate mm/min (0.742Ro): —		
Normal Stress kPa: 100(σ)	Platen Weight kg: 0·989 (W)	Mass On Hanger=(0.40831σ -W)/10=3·98kg	Sht 3 of 6

Time hh:mm;ss	Min.	Settl-ement gauge	Settlement in mm (0.002/div)	Reading on 9717A	Reading on 9717B	F1(N)= 9717Adiv *0.18818	F2(N)= 9717Bdiv *0.19120	Shear Stress τ(kPa)= 0.44186(F1+F2)	Tan ϕ= τ/σ	ϕ Deg.
15:50:00	0	7·61	0·722							
15:50:10	0·17	7·89	0·778							
15:50:15	0·25	7·93	0·786							
15:50:30	0·50	8·01	0·802							
15:50:45	0·75	8·05	0·810							
15:51:00	1·00	8·08	0·816							
15:52:00	2	8·12	0·824							
15:54:00	4	8·15	0·830							
15:58:00	8	8·17	0·832							
16:05:00	15	8·185	0·837							
16:20:00	30	8·195	0·839							
16:56:00	66	8·20	0·840							
27/2/97										
09:15:00	1045	8·24	0·848							

Results from Test WF1

Test No: WF1	Rate o/min: 0·0320 (Ro)	Bromhead Ring Shear Test Description: KAOLIN ON PLANE PERSPEX INTERFACE, TO ESTABLISH DRAINED RESIDUAL ANGLE.
Date: 27/2/97	Rate mm/min (0.742Ro): 0·0237	
Normal Stress kPa: 100 (σ)	Platen Weight kg: 0·989 (W)	Mass On Hanger=(0.40831σ -W)/10= 3·08 kg — Sht 4 of 6

Time hh:mm;ss	Min. displacement (mm)	Settl-ement gauge	Settlement in mm (0.002/div)	Reading on 9717A	Reading on 9717B	F1(N)= 9717Adiv *0.18818	F2(N)= 9717Bdiv *0.19120	Shear Stress τ(kPa)= 0.44186(F1+F2)	Tan ϕ= τ/σ	ϕ Deg.
09:20:00	0 (0)	8·25	0·850	2·00	2·00	0	0	0	0	0
09:22:00	0 (0)	8·25	0·850	2·00	2·00	0	0	0	0	0
09:23:00	1 (0·01)	8·25	0·850	2·09	2·10	1·32	1·91	1·43	0·0143	0·82
09:24:00	2 (0·03)	8·25	0·850	2·18	2·24	3·39	4·59	3·53	0·0353	2·02
09:25:00	3 (0·07)	8·25	0·850	2·30	2·37	5·65	7·07	5·62	0·0562	3·22
09:26:00	4 (0·09)	8·25	0·850	2·43	2·50	8·09	9·56	7·80	0·0780	4·46
09:27:00	5 (0·12)	8·255	0·851	2·55	2·62	10·35	11·85	9·81	0·0981	5·60
09:29:00	6 (0·14)	8·255	0·851	2·66	2·73	12·42	13·96	11·66	0·1166	6·65
09:29:00	7 (0·17)	8·26	0·852	2·76	2·84	14·30	16·05	13·41	0·1341	7·64
09:30:00	8 (0·19)	8·26	0·852	2·81	2·89	15·24	17·02	14·25	0·1425	8·11
09:31:00	9 (0·21)	8·265	0·853	2·825	2·905	15·52	17·30	14·50	0·1450	8·25
09:32:00	10 (0·24)	8·265	0·853	2·85	2·92	16·00	17·59	14·84	0·1484	8·44
09:33:00	11 (0·26)	8·265	0·853	2·86	2·92	16·18	17·59	14·92	0·1492	8·49
09:34:00	12 (0·28)	8·27	0·854	2·87	2·92	16·37	17·59	15·01	0·1501	8·53
09:35:00	13 (0·30)	8·27	0·854	2·87	2·93	16·37	17·78	15·09	0·1509	8·58
09:36:00	14 (0·33)	8·27	0·854	2·88	2·92	16·56	17·59	15·09	0·1509	8·58
09:37:00	15 (0·36)	8·27	0·854	2·88	2·92	16·56	17·59	15·09	0·1509	8·58
09:42:00	20 (0·49)	8·27	0·854	2·89	2·92	16·75	17·59	15·17	0·1517	8·63
09:47:00	25 (0·59)	8·27	0·854	2·89	2·925	16·75	17·69	15·22	0·1522	8·65
10:02:00	40 (0·95)	8·28	0·854	2·91	2·92	17·12	17·59	15·34	0·1534	8·72
10:32:00	70 (1·66)	8·285	0·857	2·92	2·92	17·31	17·59	15·42	0·1542	8·77
11:40:00	138 (3·27)	8·295	0·859	2·93	2·91	17·50	17·40	15·42	0·1542	8·77
13:00:00	218 (5·16)	8·30	0·860	2·94	2·90	17·69	17·21	15·42	0·1542	8·77
14:05:00	283 (6·71)	8·305	0·861	2·94	2·90	17·69	17·21	15·42	0·1542	8·77
15:10:00	348 (8·25)	8·315	0·863	2·95	2·89	17·88	17·02	15·42	0·1542	8·77

Results from Test WF1

Results from Test WF1

Test No: WF1	Rate o/min: — (Ro)	Bromhead Ring Shear Test Description: KAOLIN ON PLANE PERSPEX INTERFACE, TO ESTABLISH DRAINED RESIDUAL ANGLE. THIRD CONSOLIDATION STAGE.	
Date: 27/2/97	Rate mm/min (0.742Ro): -		
Normal Stress kPa: 150(σ)	Platen Weight kg: 0·989 (W)	Mass On Hanger=(0.40831σ -W)/10=6.0kg	Sht 5 of 6

Time hh:mm;ss	Min.	Settl-ement gauge	Settlement in mm (0.002/div)	Reading on 9717A	Reading on 9717B	F1(N)= 9717Adiv *0.18818	F2(N)= 9717Bdiv *0.19120	Shear Stress τ(kPa)= 0.44186(F1+F2)	Tan ϕ= τ/σ	ϕ Deg.
15:20:00	0	8.320	864							
15:20:10	0·17	8.54	0·908							
15:20:15	0·25	8.58	0·916							
15:20:30	0·50	8.63	0·926							
15:20:45	0·75	8.67	0·934							
15:21:00	1	8.69	0·938							
15:22:00	2	8.72	0·944							
15:24:00	4	8.74	0·948							
15:28:00	8	8.76	0·952							
15:35:00	15	8.765	0·953							
15:50:00	30	8.77	0·954							
16:05:00	45	8.78	0·956							
16:50:00	90	8.79	0·958							
28/2/97										
10:20:00	1140	8.82	0·964							

Test No: WF1	Rate o/min:0·0320 (Ro)	Bromhead Ring Shear Test Description: KAOLIN ON PLANE PERSPEX INTERFACE, TO ESTABLISH DRAINED RESIDUAL ANGLE.
Date: 28/2/97	Rate mm/min (0.742Ro):0·0237	
Normal Stress kPa:150(σ)	Platen Weight kg:0·989 (W)	Mass On Hanger=(0.40831 σW)/10=6·0kg Sht 6 of 6

Time hh:mm;ss	Min. (DISPLACEMENT IN mm)	Settl-ement gauge	Settlement in mm (0.002/div)	Reading on 9717A	Reading on 9717B	F1(N)= 9717Adiv *0.18818	F2(N)= 9717Bdiv *0.19120	Shear Stress τ(kPa)= 0.44186(F1+F2)	Tan ϕ= τ/σ	ϕ Deg.
10:32:00	0 (0)	8·87	0·974	2·00	2·00	0	0	0	0	0
10:35:00	0 (0)	8·87	0·974	2·00	2·00	0	0	0	0	0
10:37:00	2 (0·05)	8·87	0·974	2·02	2·10	0·38	1·91	1·01	0·0067	0·39
10:39:00	4 (0·09)	8·87	0·974	2·19	2·31	3·58	5·93	4·20	0·0280	1·60
10:41:00	6 (0·14)	8·87	0·974	2·44	2·58	8·28	11·09	8·56	0·0571	3·27
10:43:00	8 (0·19)	8·875	0·975	2·71	2·85	13·36	16·25	13·08	0·0872	4·98
10:45:00	10(0·24)	8·88	0·976	2·90	3·07	16·94	20·46	16·53	0·1102	6·29
10:47:00	12(0·28)	8·89	0·978	3·10	3·29	20·70	24·66	20·04	0·1336	7·61
10:49:00	14(0·33)	8·90	0·980	3·22	3·38	22·96	26·39	21·81	0·1454	8·27
10:51:00	16 (0·38)	8·905	0·981	3·26	3·41	23·71	26·06	22·39	0·1493	8·49
10:53:00	18 (0·43)	8·905	0·981	3·28	3·42	24·09	27·15	22·64	0·1509	8·58
10:55:00	20(0·47)	8·91	0·982	3·29	3·42	24·28	27·15	22·72	0·1515	8·61
11:00:00	25(0·59)	8·915	0·983	3·31	3·43	24·65	27·34	22·97	0·1531	8·71
11:05:00	30(0·71)	8·92	0·984	3·32	3·44	24·84	27·53	23·14	0·1543	8·77
11:20:00	45(1·07)	8·925	0·985	3·34	3·45	25·22	27·72	23·39	0·1559	8·86
12:00:00	85(2·01)	8·94	0·988	3·34	3·45	25·22	27·72	23·39	0·1559	8·86
13:00:00	145(3·44)	8·95	0·990	3·33	3·48	25·03	28·30	23·56	0·1571	8·93
14:35:00	240(5·69)	8·965	0·993	3·34	3·48	25·22	28·30	23·65	0·1577	8·96
15:00:00	265(6·28)	8·970	0·994	3·33	3·48	25·03	28·30	23·56	0·1571	8·93

Results from Test WF1

Appendix D

Full Test Results

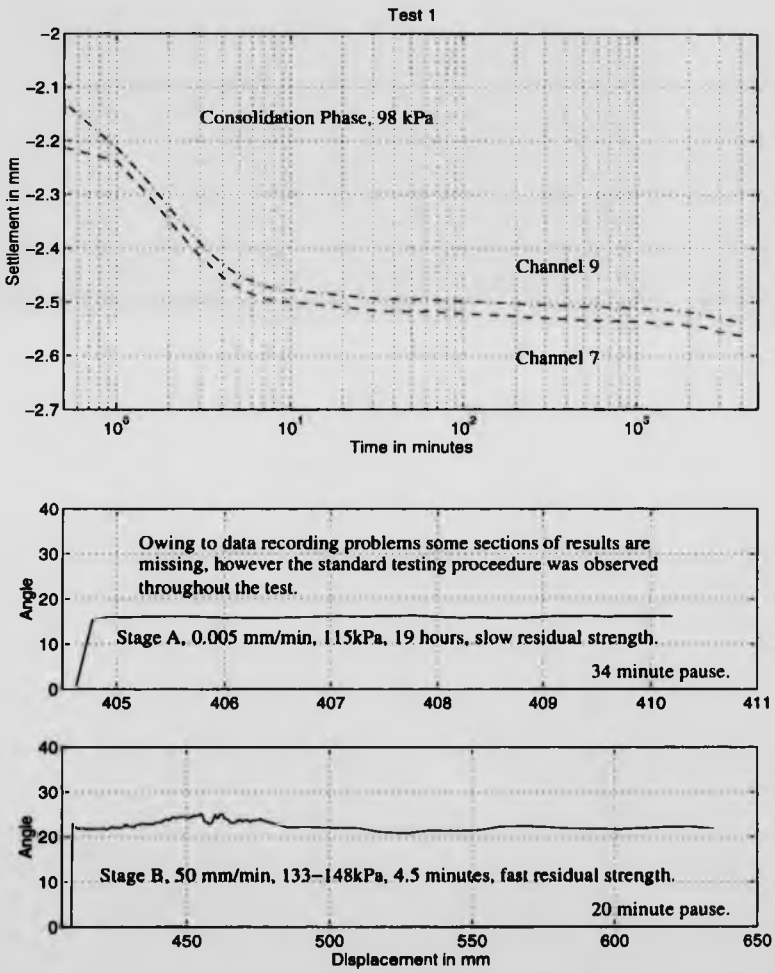

Figure D.1: Test 1, submerged, soil on soil test, 60% kaolin, 40% 30 FG Buckland fine sand.

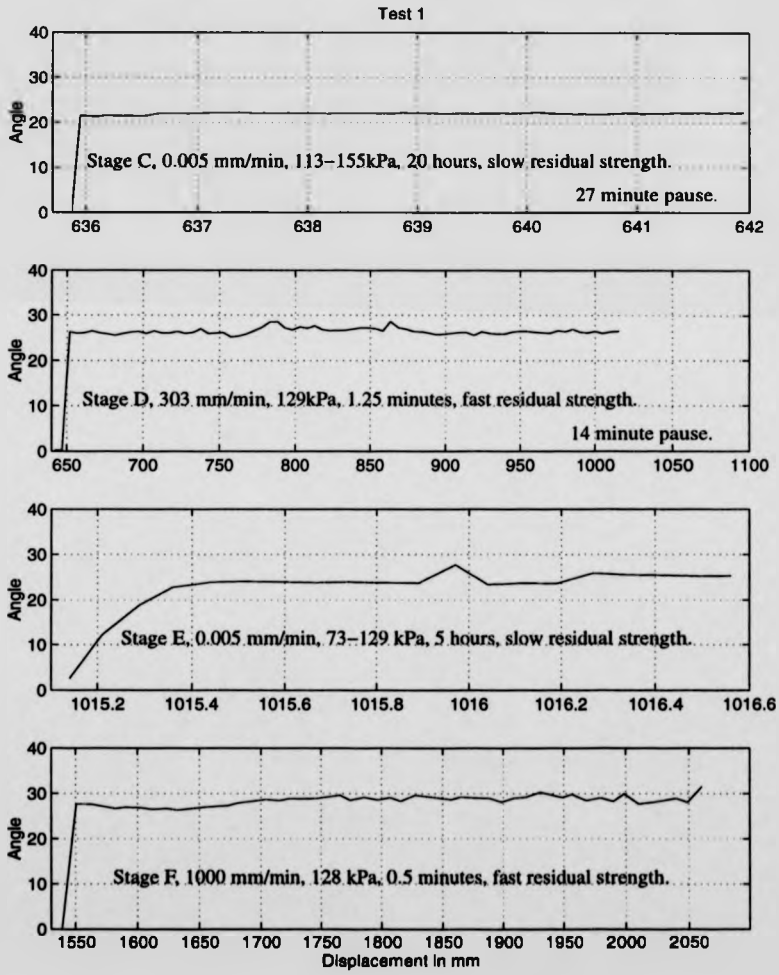

Figure D.2: Test 1, submerged, soil on soil test, 60% kaolin, 40% 30 FG Buckland fine sand.

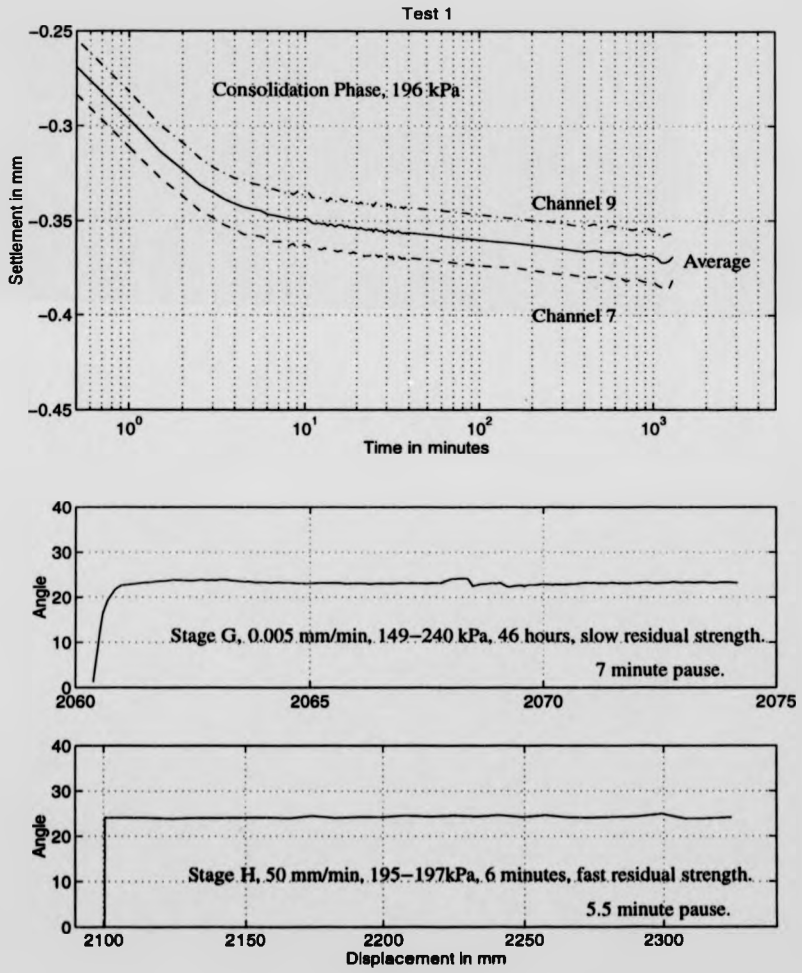

Figure D.3: Test 1, submerged, soil on soil test, 60% kaolin, 40% 30 FG Buckland fine sand.

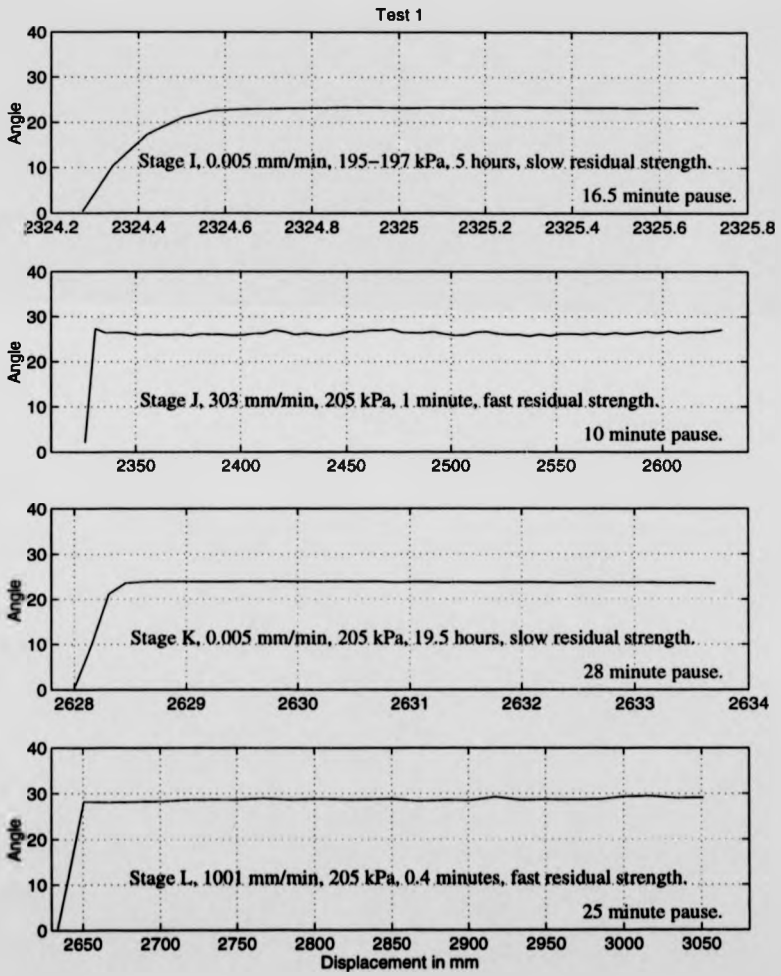

Figure D.4: Test 1, submerged, soil on soil test, 60% kaolin, 40% 30 FG Buckland fine sand.

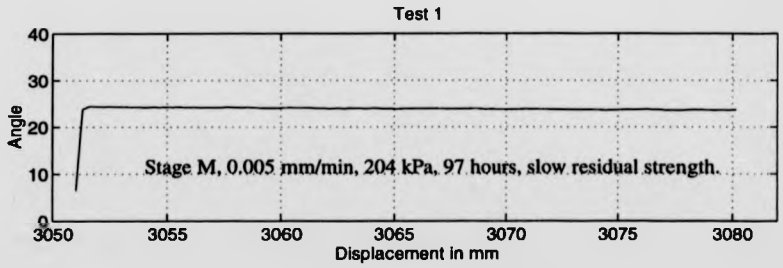

Figure D.5: Test 1, submerged, soil on soil test, 60% kaolin, 40% 30 FG Buckland fine sand.

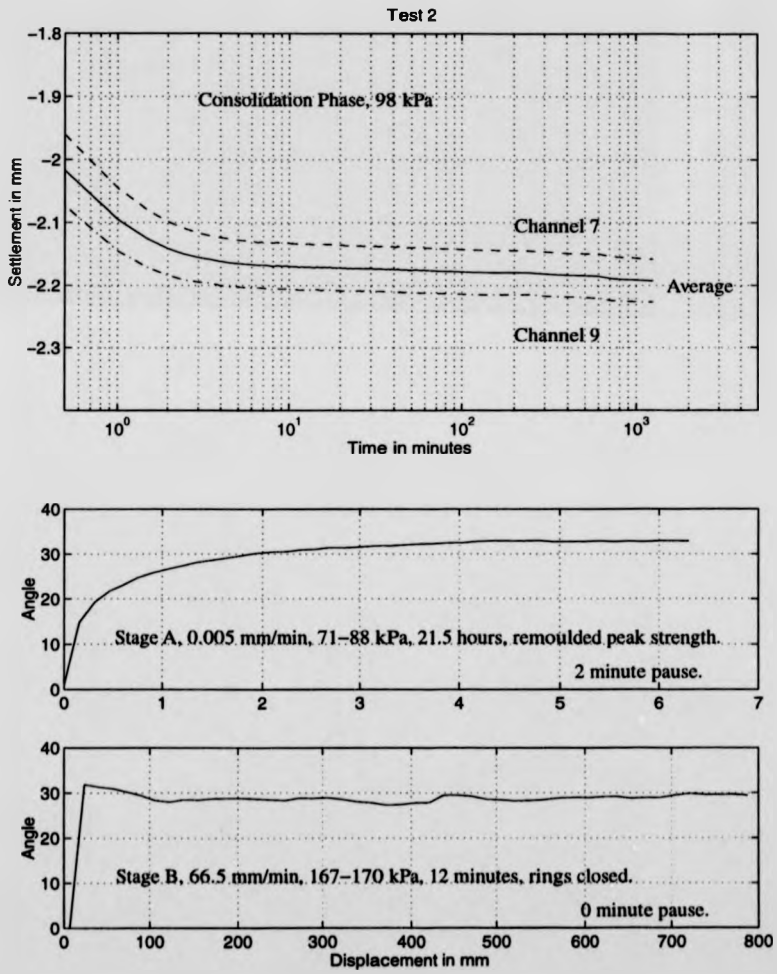

Figure D.6: Test 2, submerged, soil on soil test, 27% kaolin, 73% 30 FG Buckland fine sand.

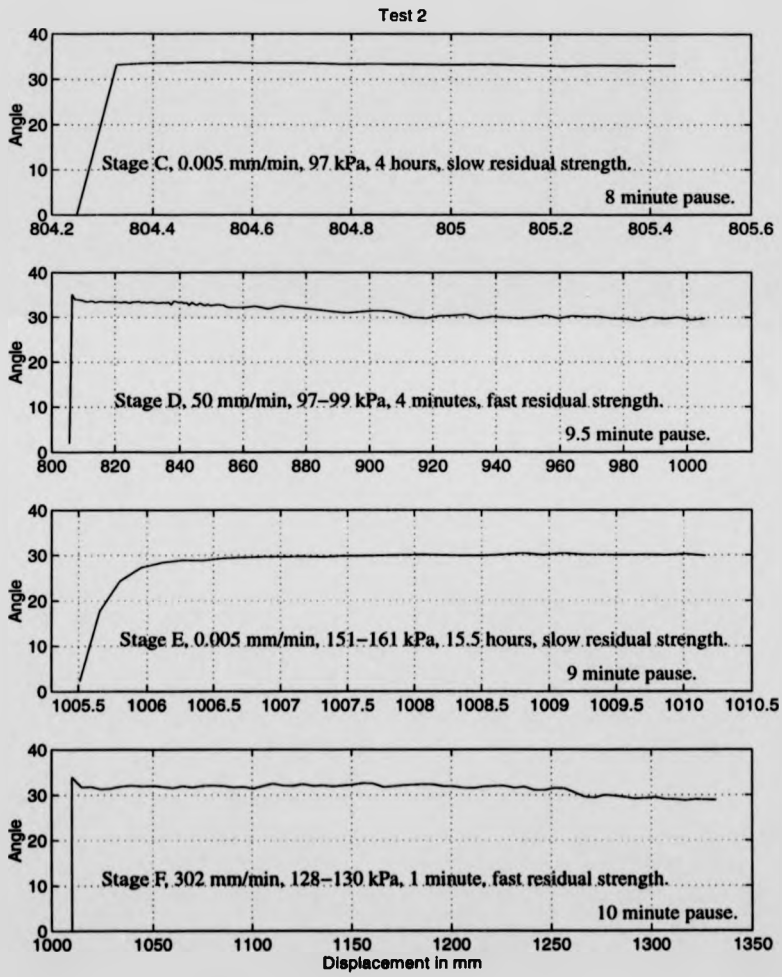

Figure D.7: Test 2, submerged, soil on soil test, 27% kaolin, 73% 30 FG Buckland fine sand.

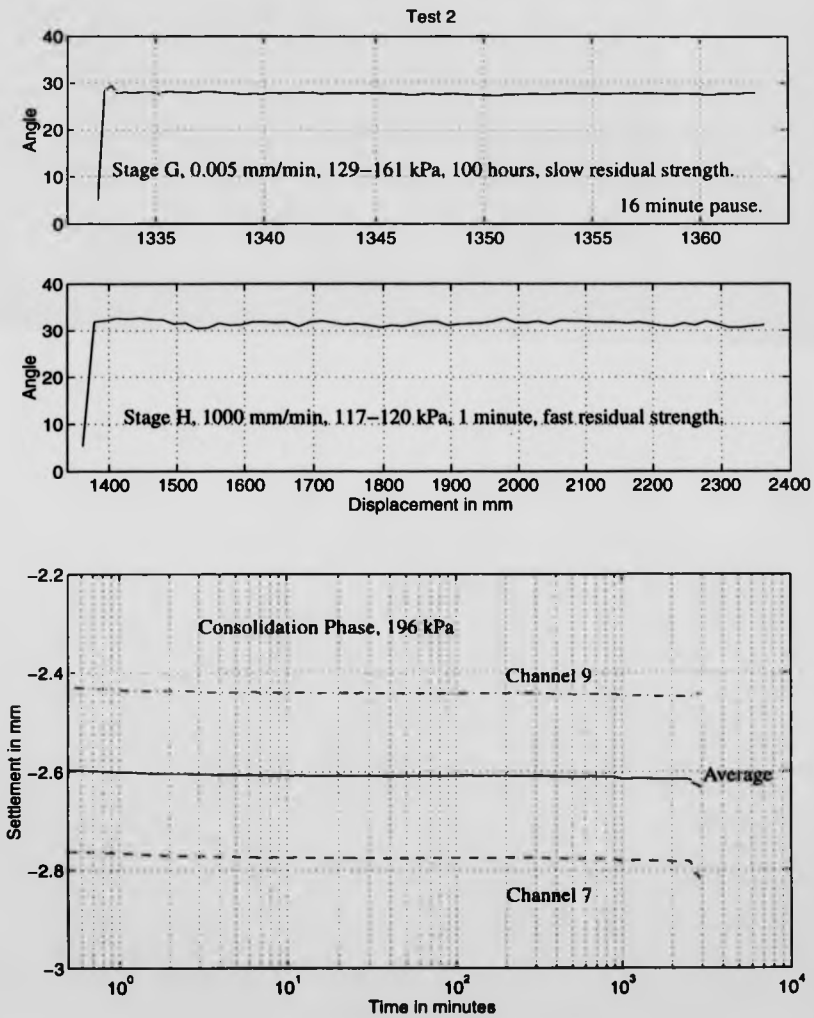

Figure D.8: Test 2, submerged, soil on soil test, 27% kaolin, 73% 30 FG Buckland fine sand.

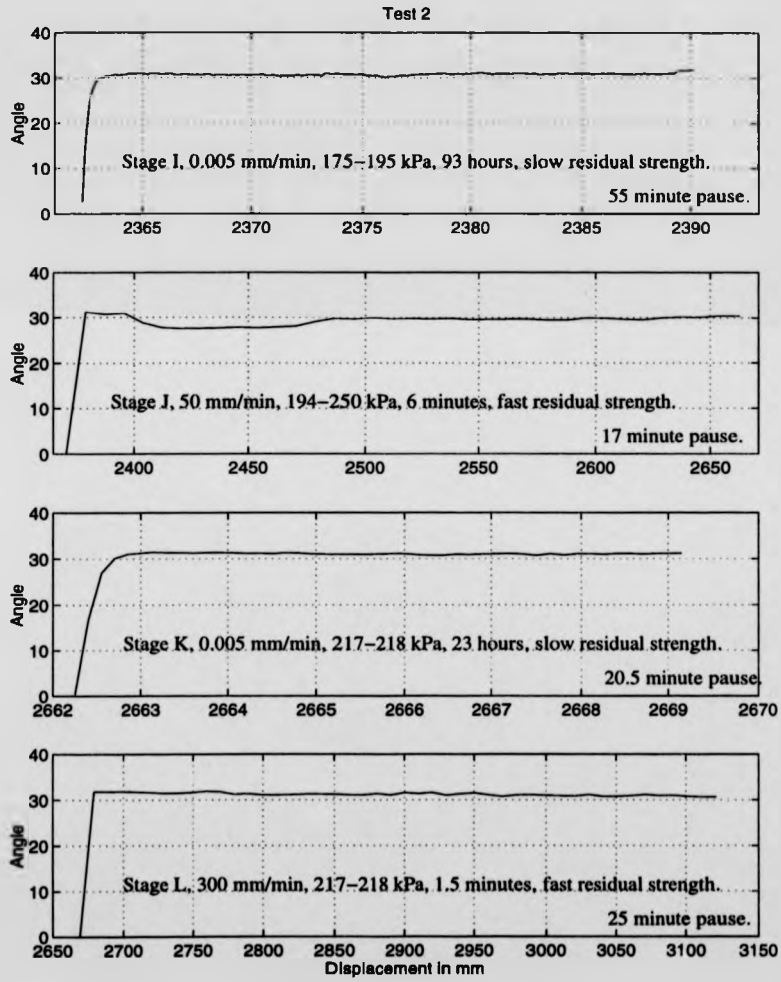

Figure D.9: Test 2, submerged, soil on soil test, 27% kaolin, 73% 30 FG Buckland fine sand.

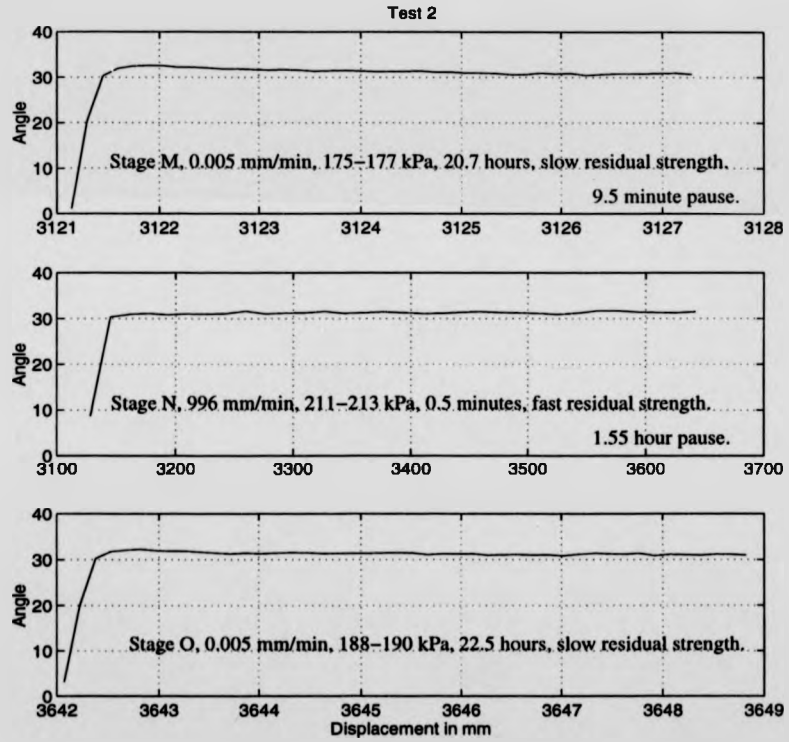

Figure D.10: Test 2, submerged, soil on soil test, 27% kaolin, 73% 30 FG Buckland fine sand.

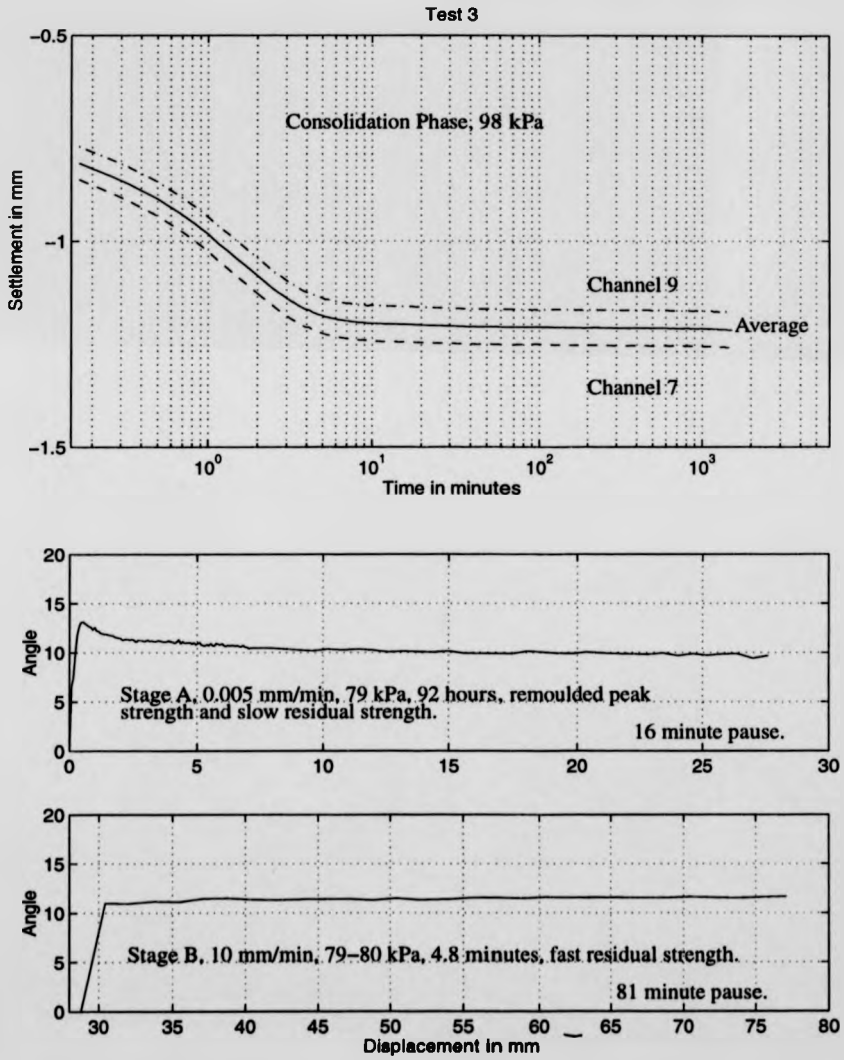

Figure D.11: Test 3, submerged, plane perspex interface test, 100% kaolin.

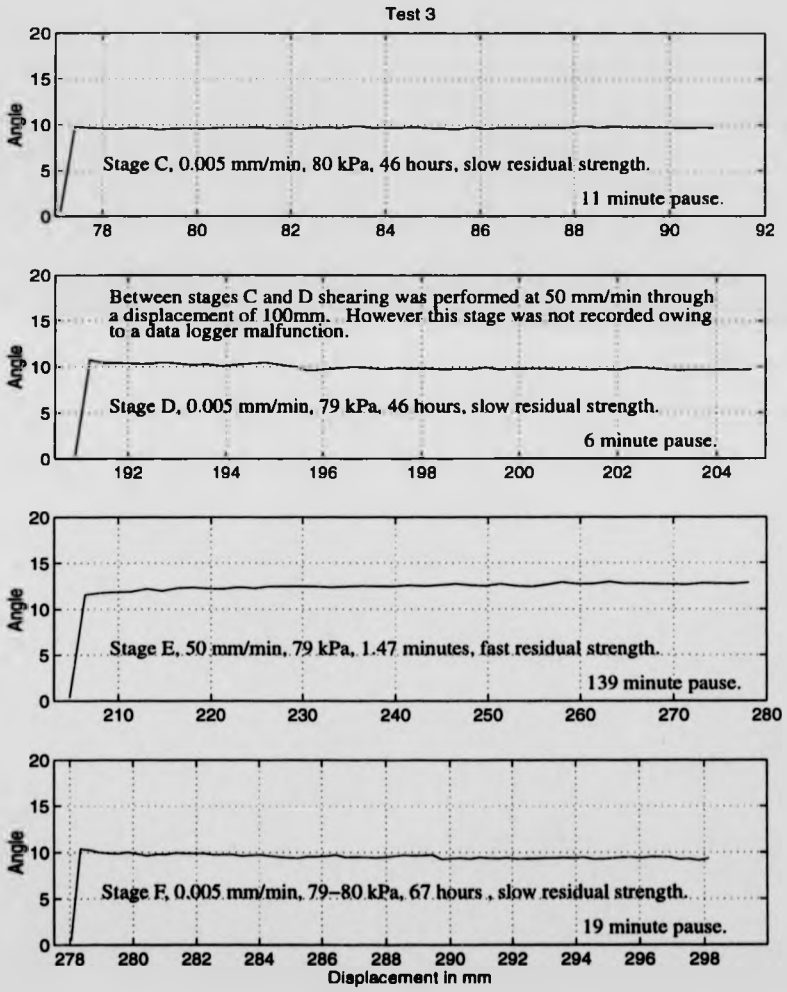

Figure D.12: Test 3, submerged, plane perspex interface test, 100% kaolin.

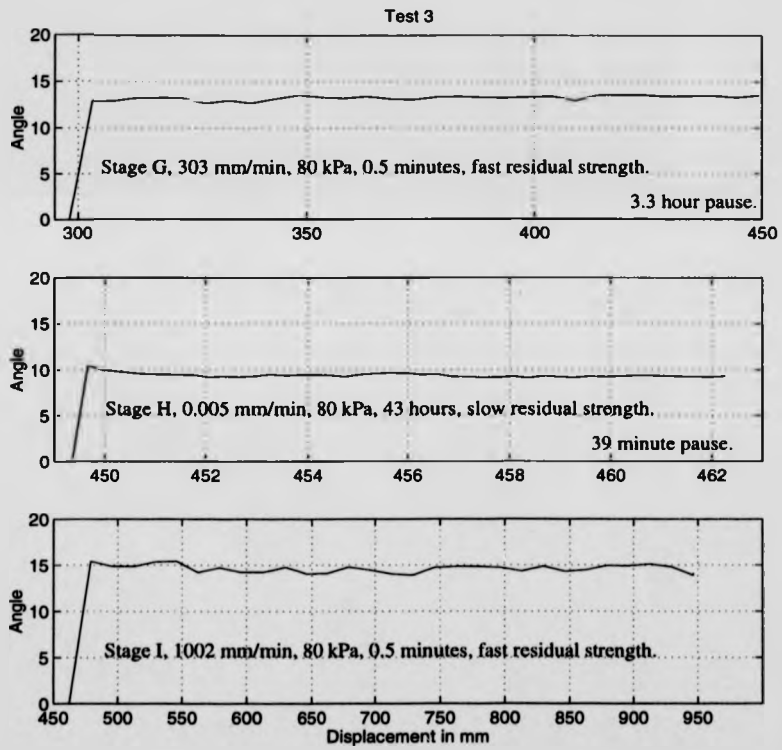

Figure D.13: Test 3, submerged, plane perspex interface test, 100% kaolin.

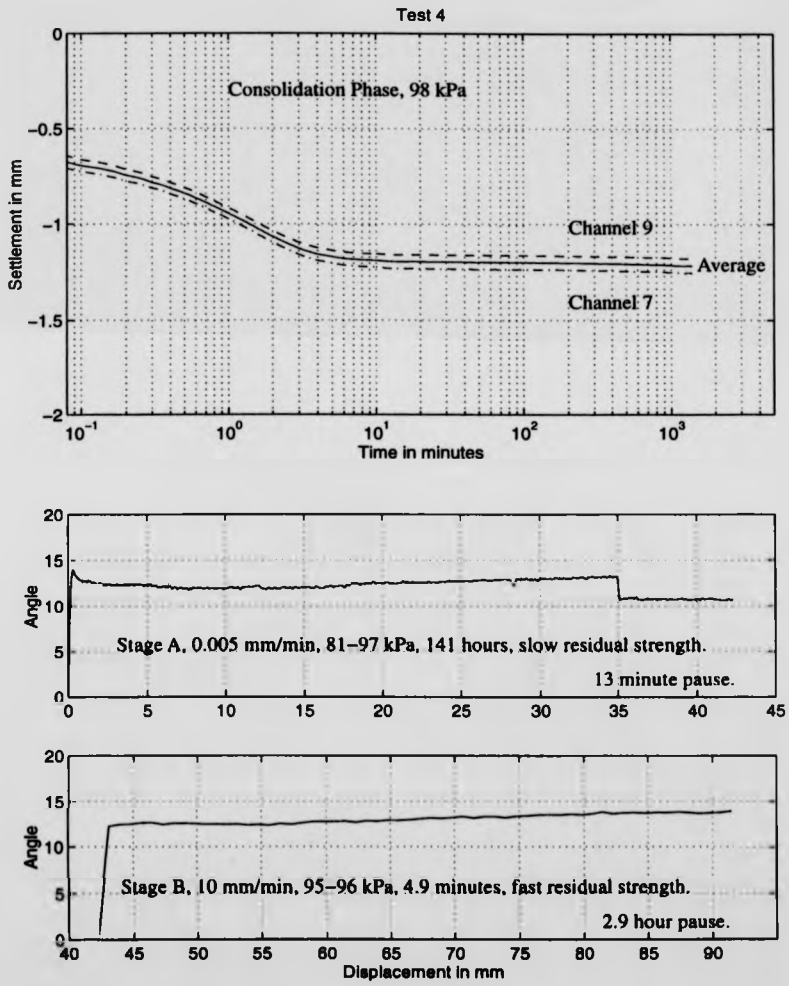

Figure D.14: Test 4, submerged, 4x1mm wave-form perspex interface test, 100% kaolin.

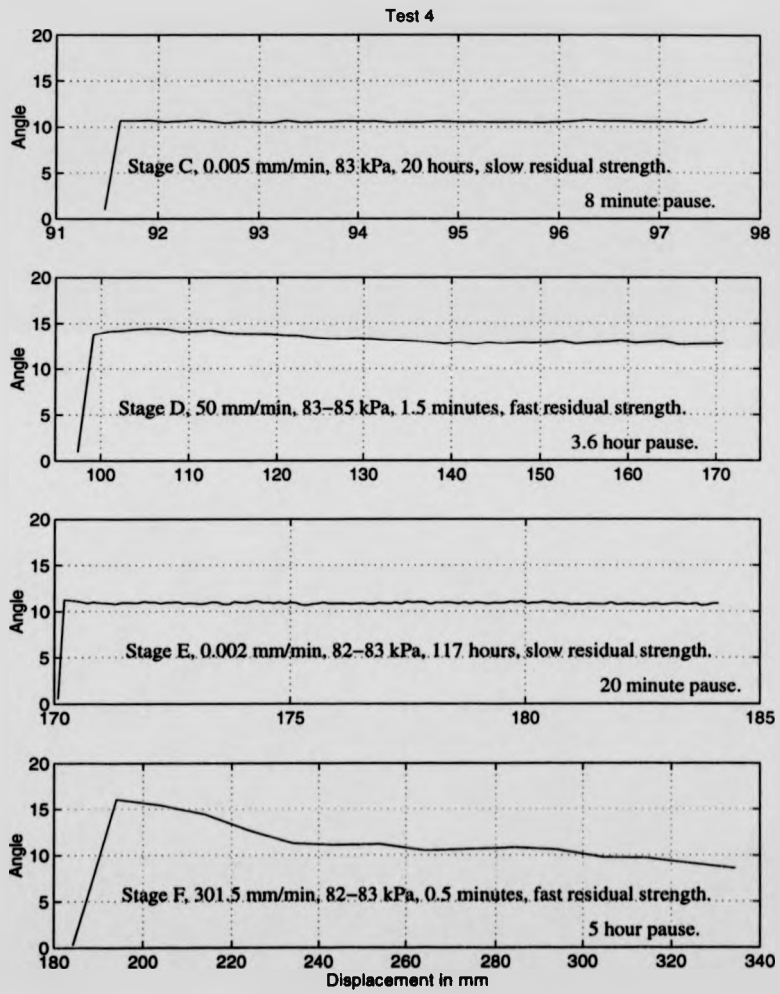

Figure D.15: Test 4, submerged, 4x1mm wave–form perspex interface test, 100% kaolin.

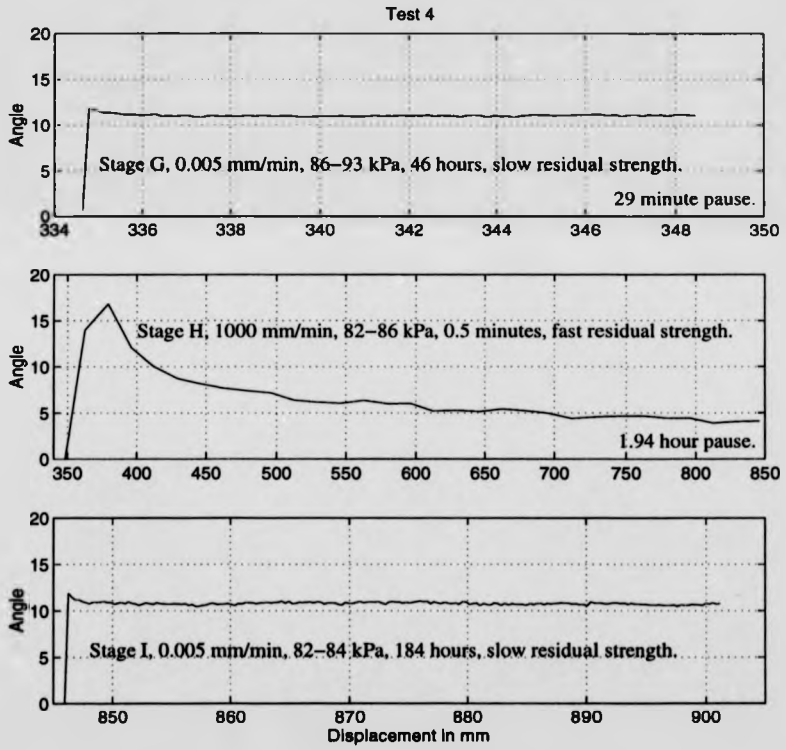

Figure D.16: Test 4, submerged, 4x1mm wave–form perspex interface test, 100% kaolin.

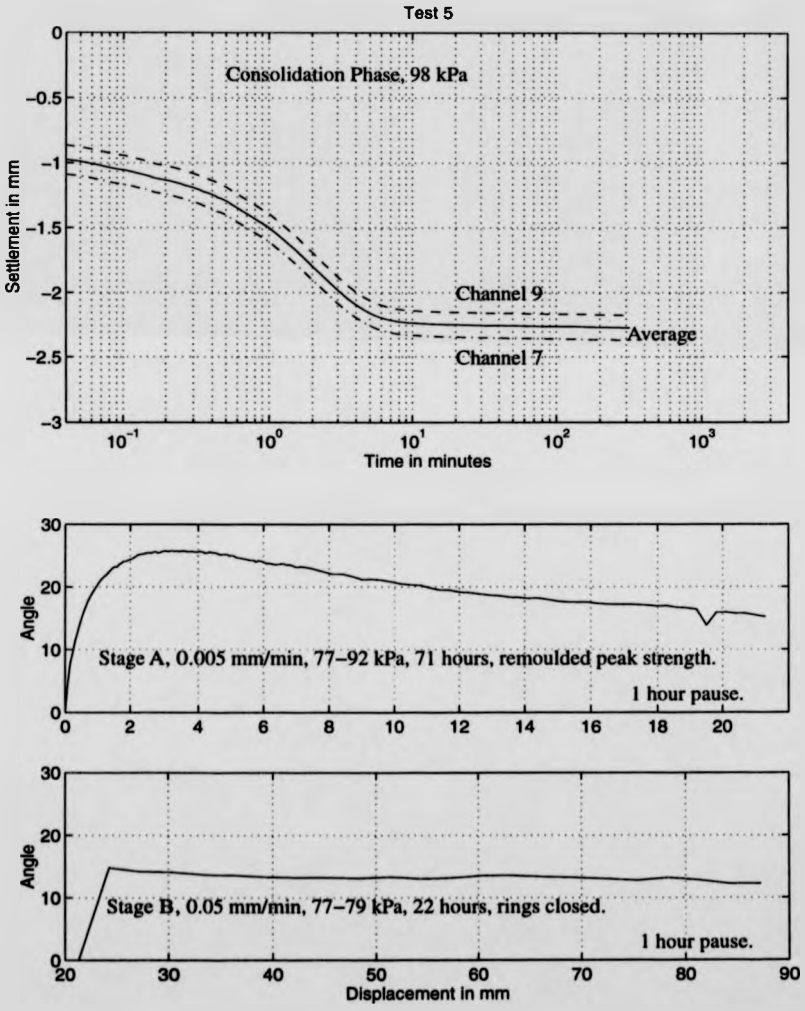

Figure D.17: Test 5, submerged, soil on soil test, 100% kaolin.

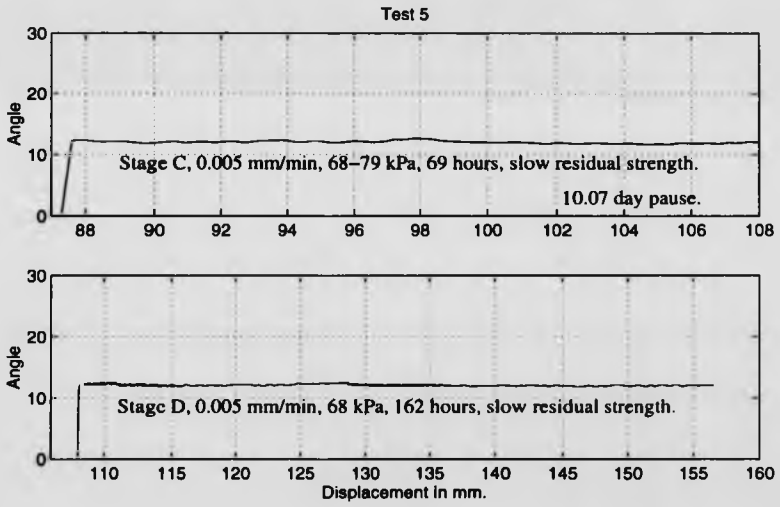

Figure D.18: Test 5, submerged, soil on soil test, 100% kaolin.

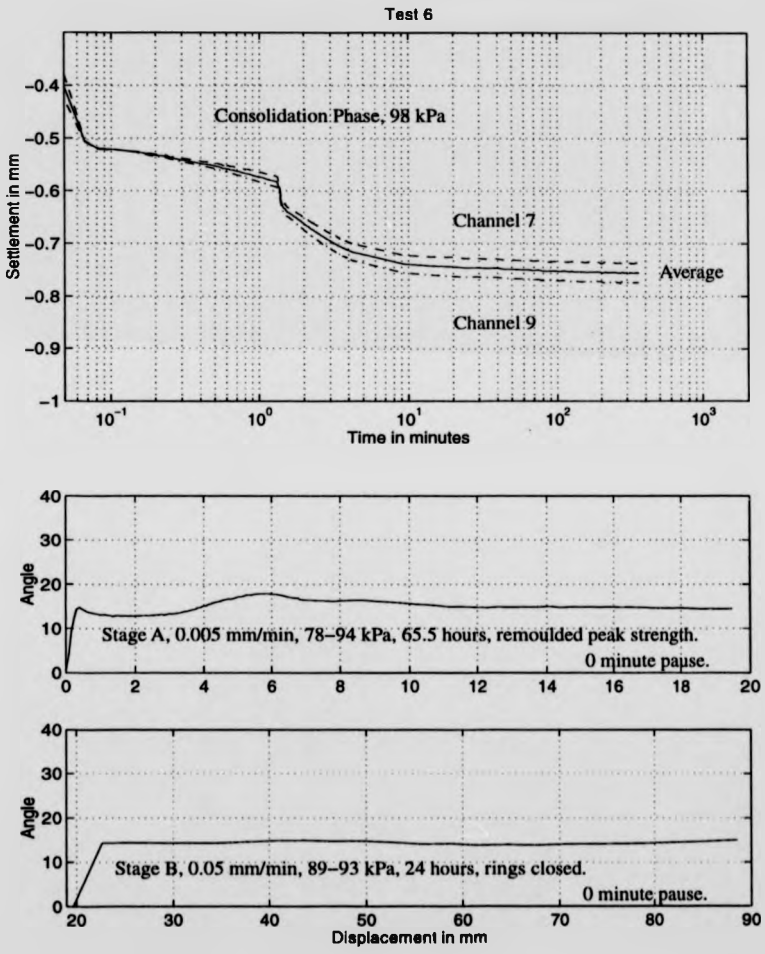

Figure D.19: Test 6, non-submerged, 4x1mm wave-form perspex interface test, 100% kaolin.

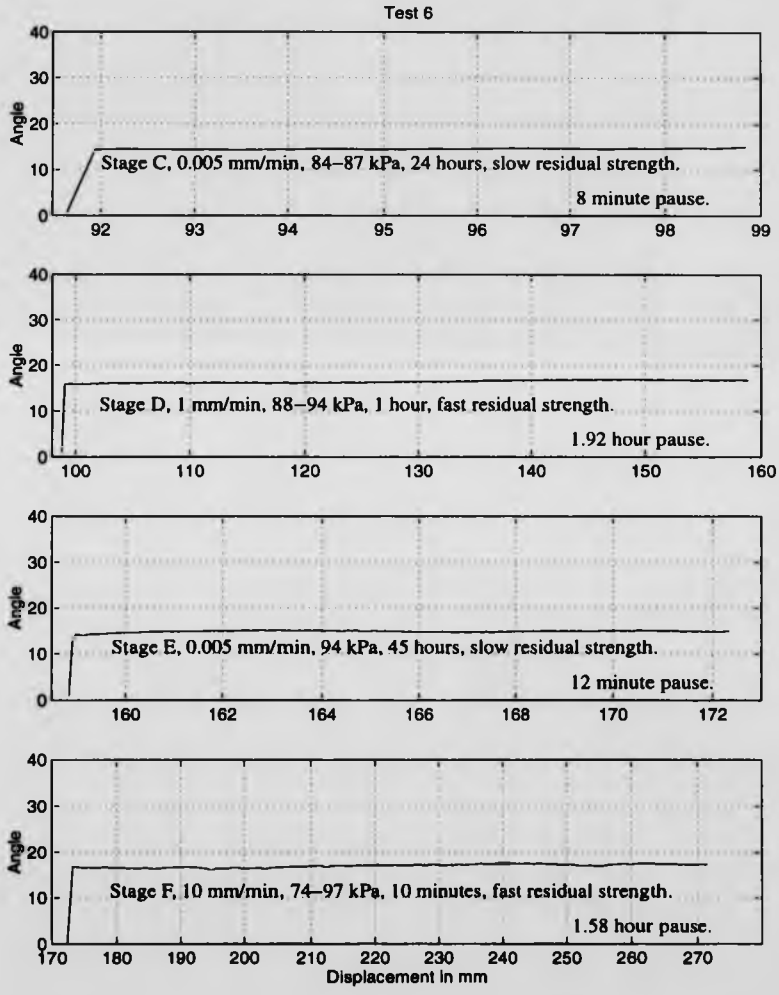

Figure D.20: Test 6, non-submerged, 4x1mm wave-form perspex interface test, 100% kaolin.

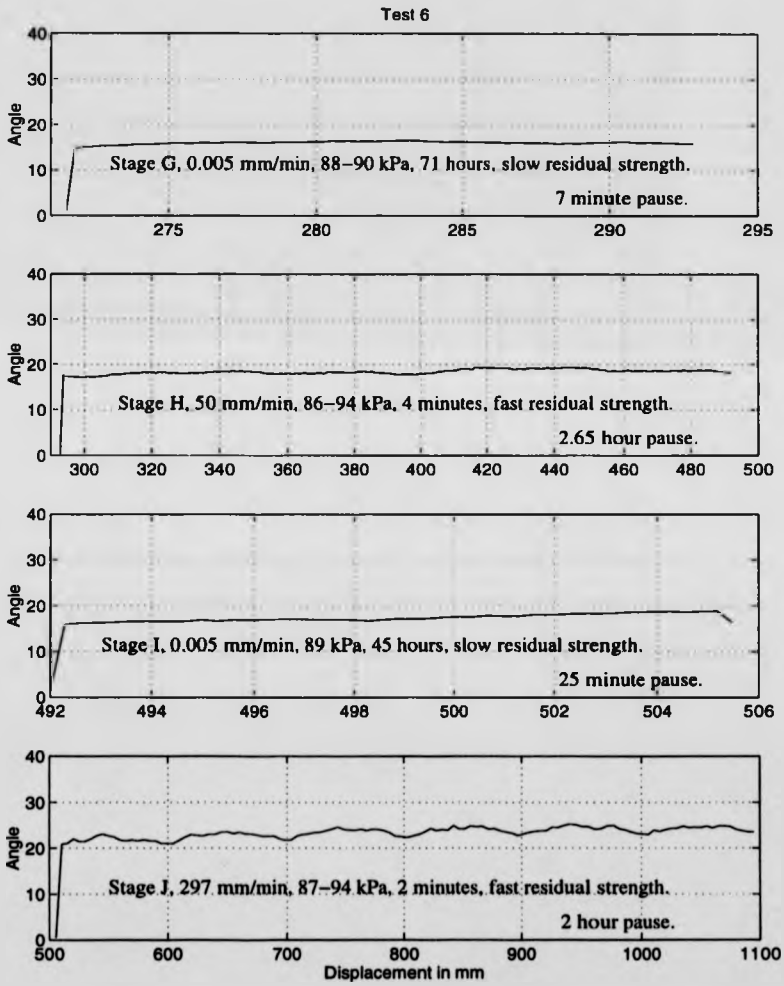

Figure D.21: Test 6, non-submerged, 4x1mm wave-form perspex interface test, 100% kaolin.

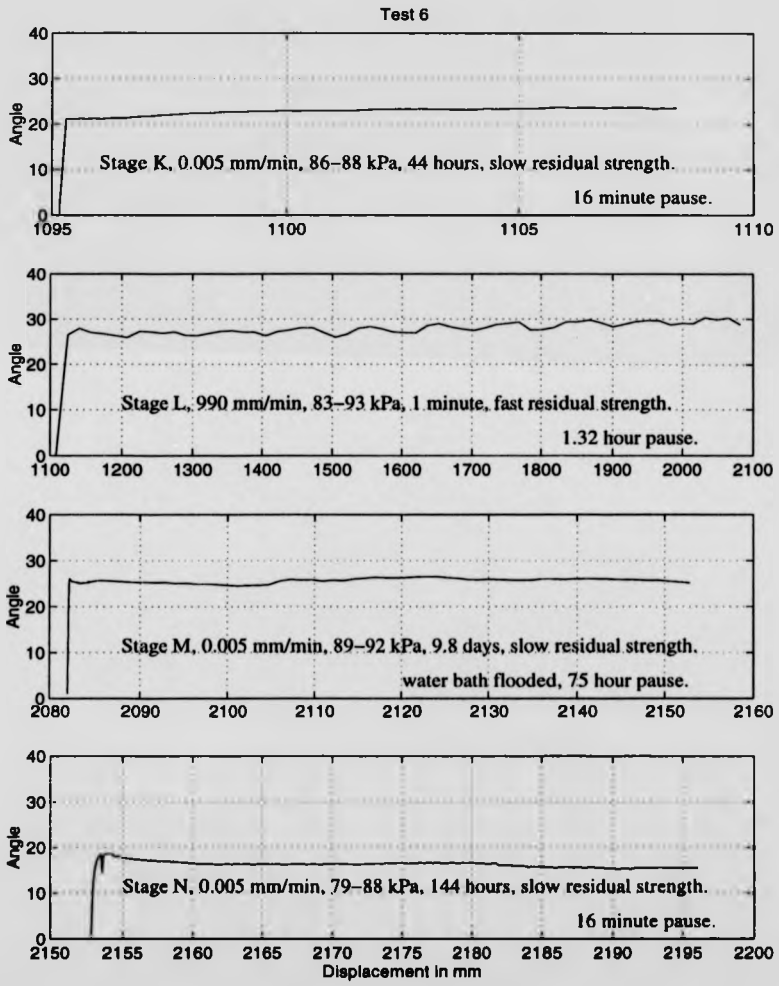

Figure D.22: Test 6, non-submerged becoming submerged, 4x1mm wave-form perspex interface test, 100% kaolin.

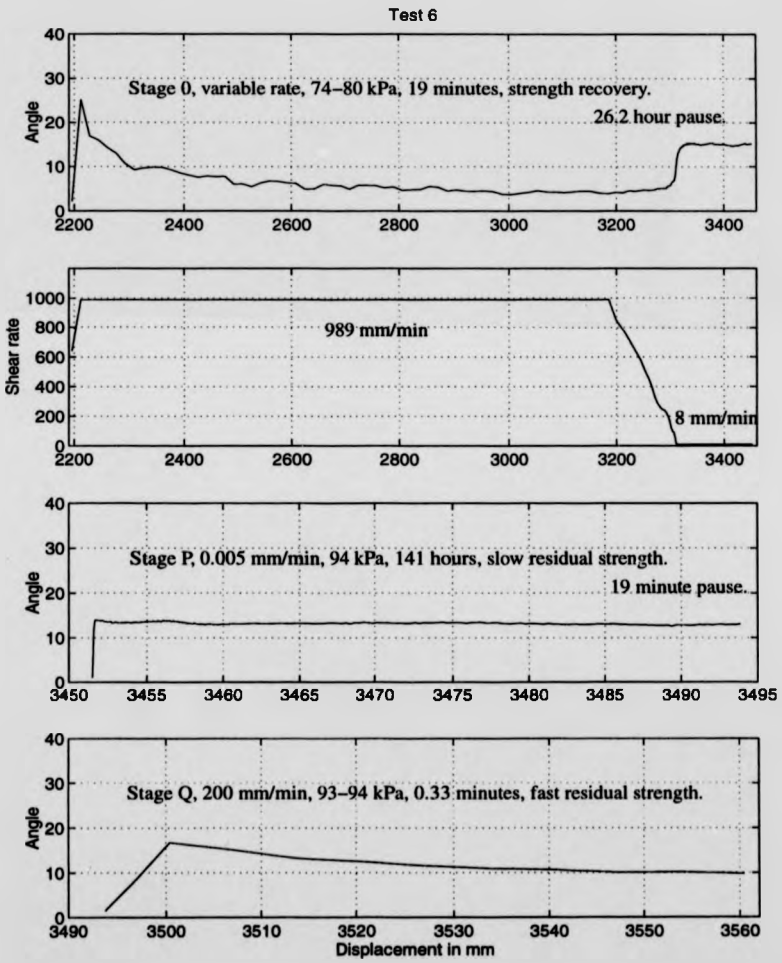

Figure D.23: Test 6, now submerged, 4x1mm wave-form perspex interface test, 100% kaolin.

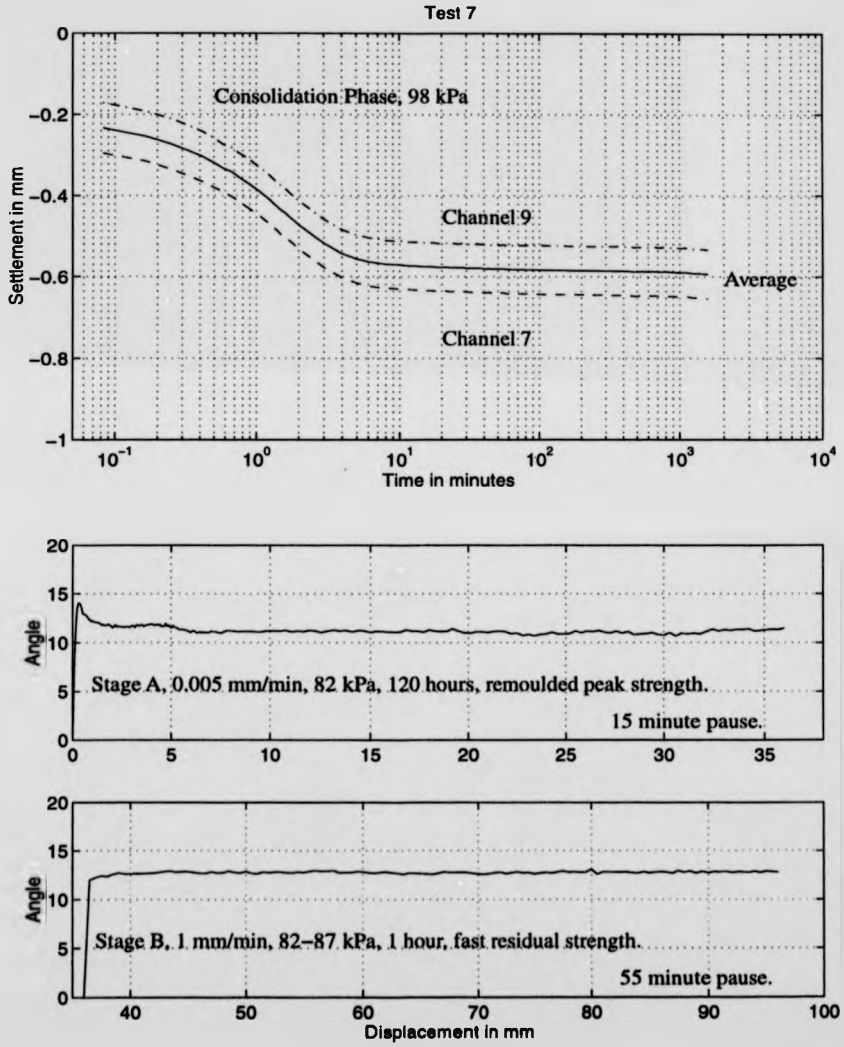

Figure D.24: Test 7, submerged, 2x1mm wave-form perspex interface test, 100% kaolin.

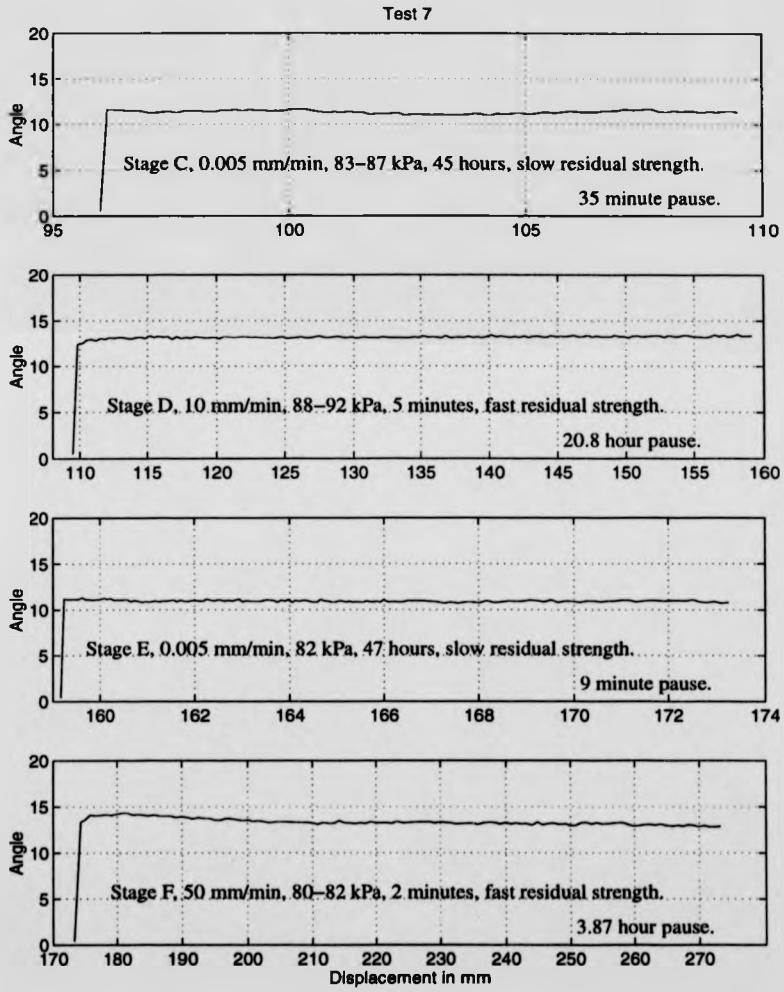

Figure D.25: Test 7, submerged, 2x1mm wave–form perspex interface test, 100% kaolin.

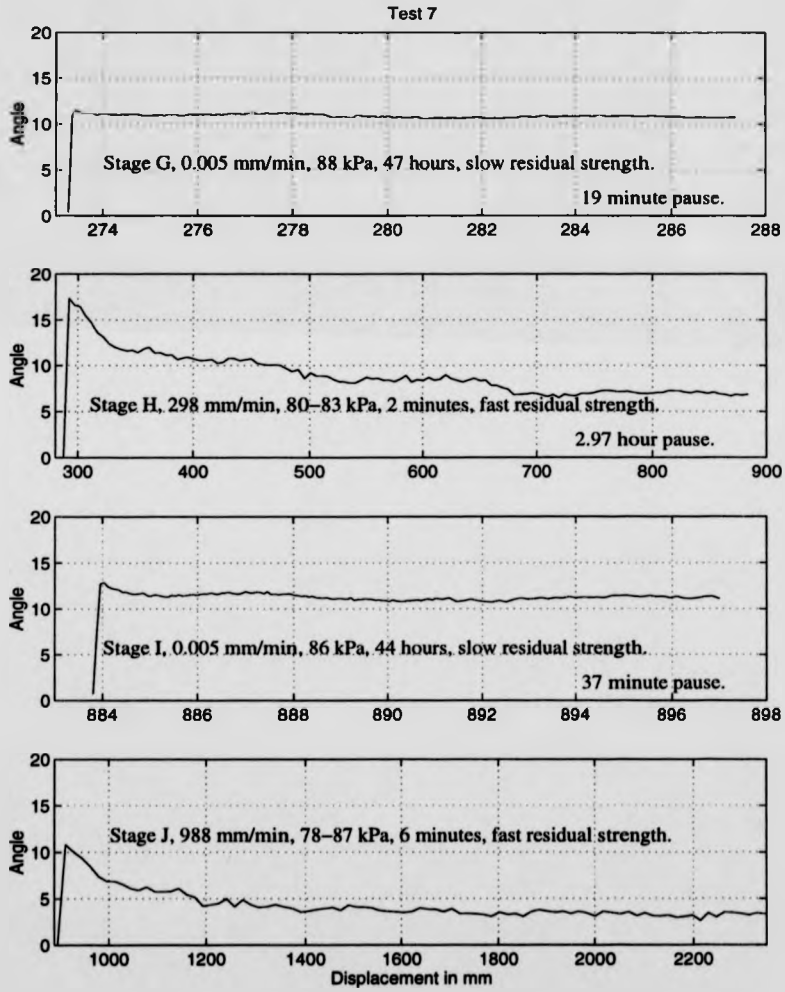

Figure D.26: Test 7, submerged, 2x1mm wave-form perspex interface test, 100% kaolin.

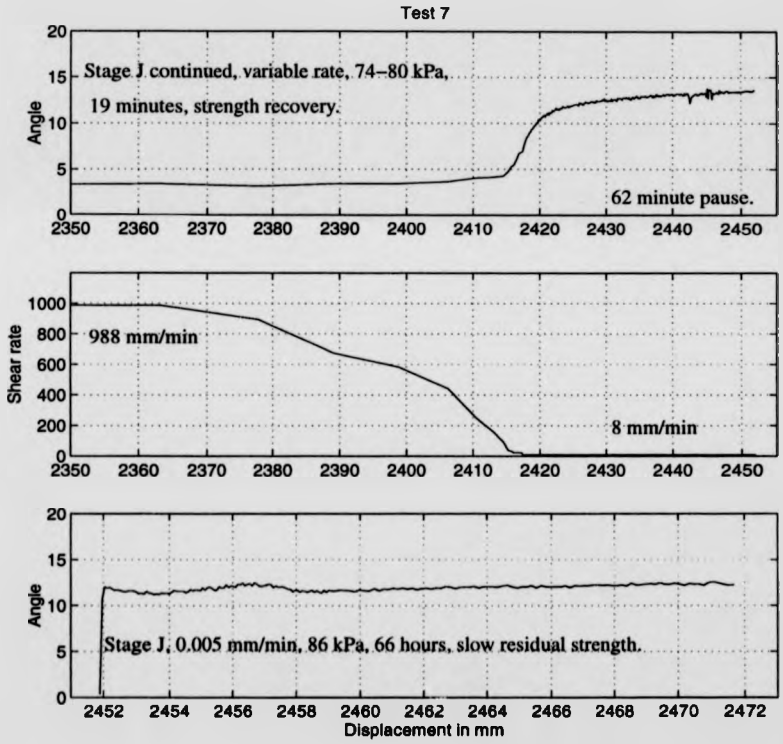

Figure D.27: Test 7, submerged, 2x1mm wave–form perspex interface test, 100% kaolin.

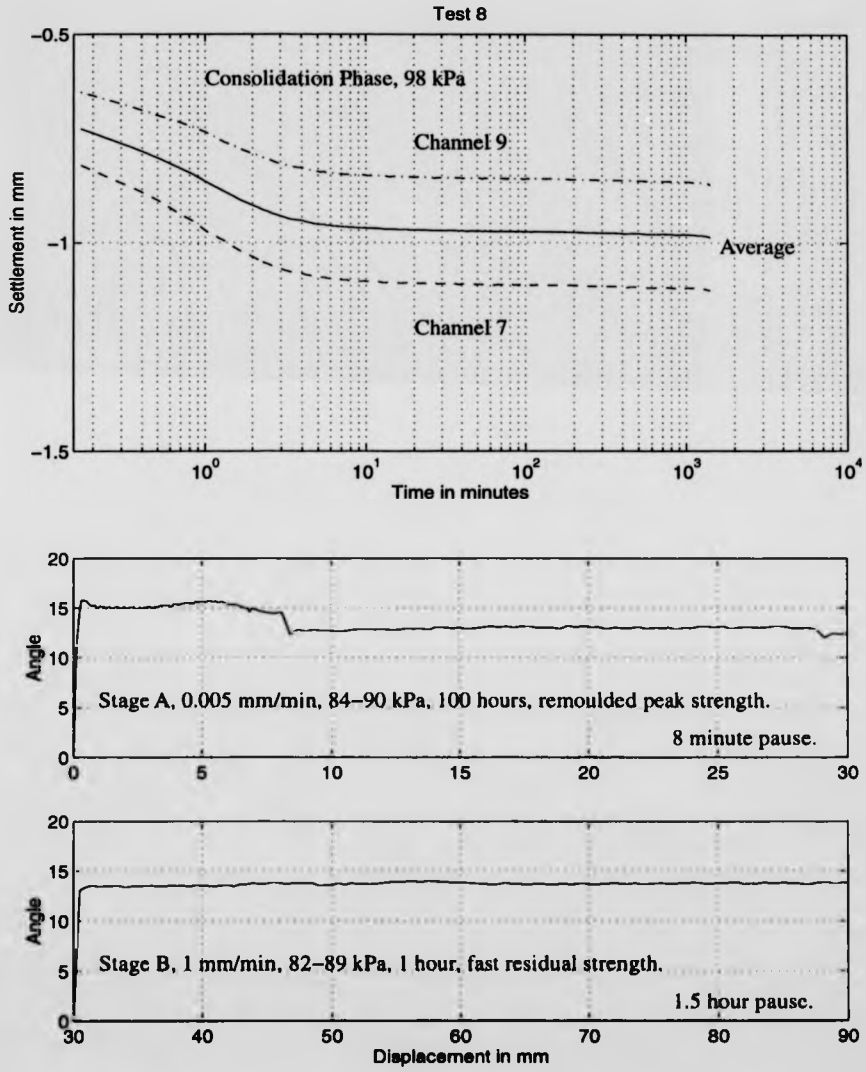

Figure D.28: Test 8, submerged, 8x1mm wave-form perspex interface test, 100% kaolin.

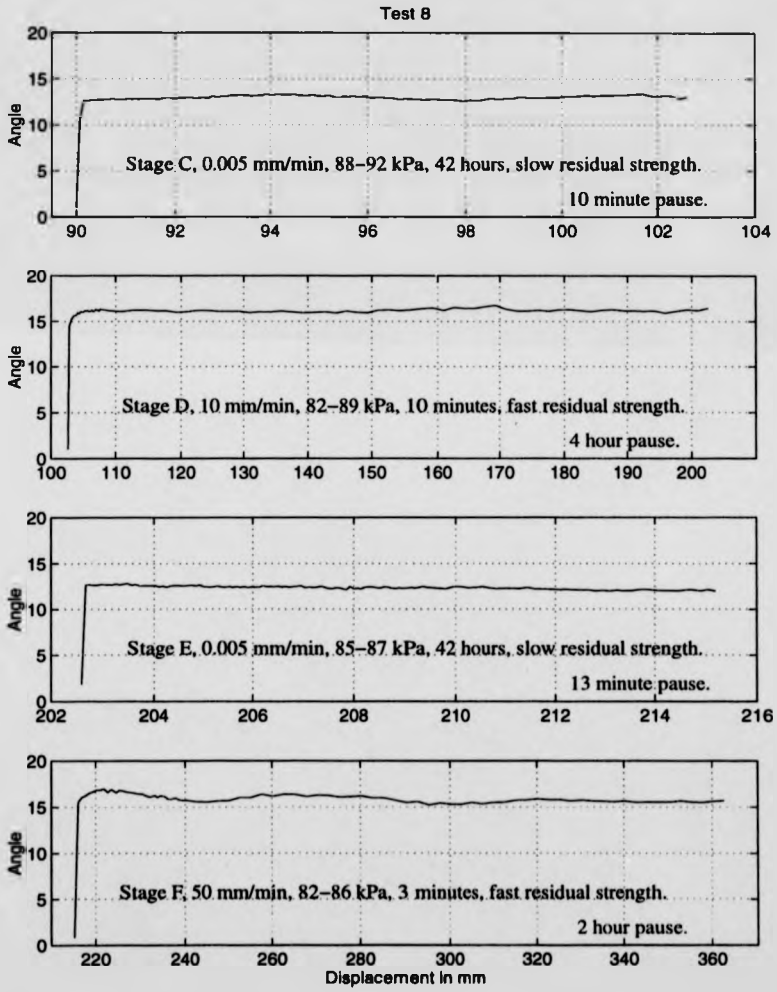

Figure D.29: Test 8, submerged, 8x1mm wave-form perspex interface test, 100% kaolin.

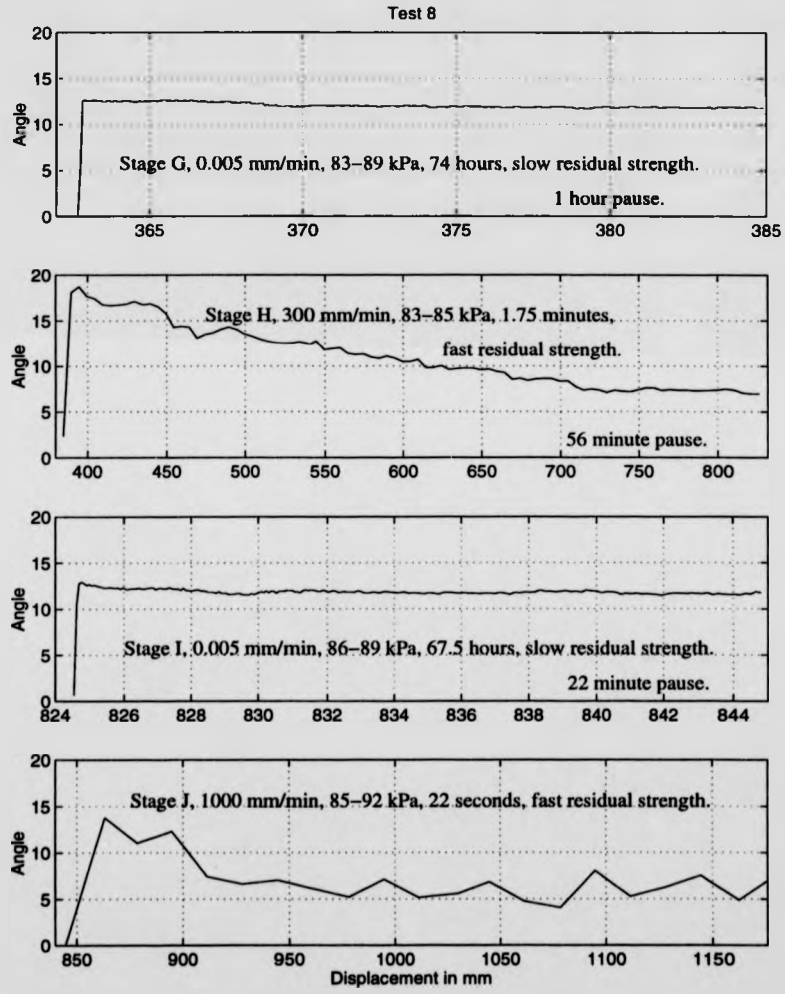

Figure D.30: Test 8, submerged, 8x1mm wave-form perspex interface test, 100% kaolin.

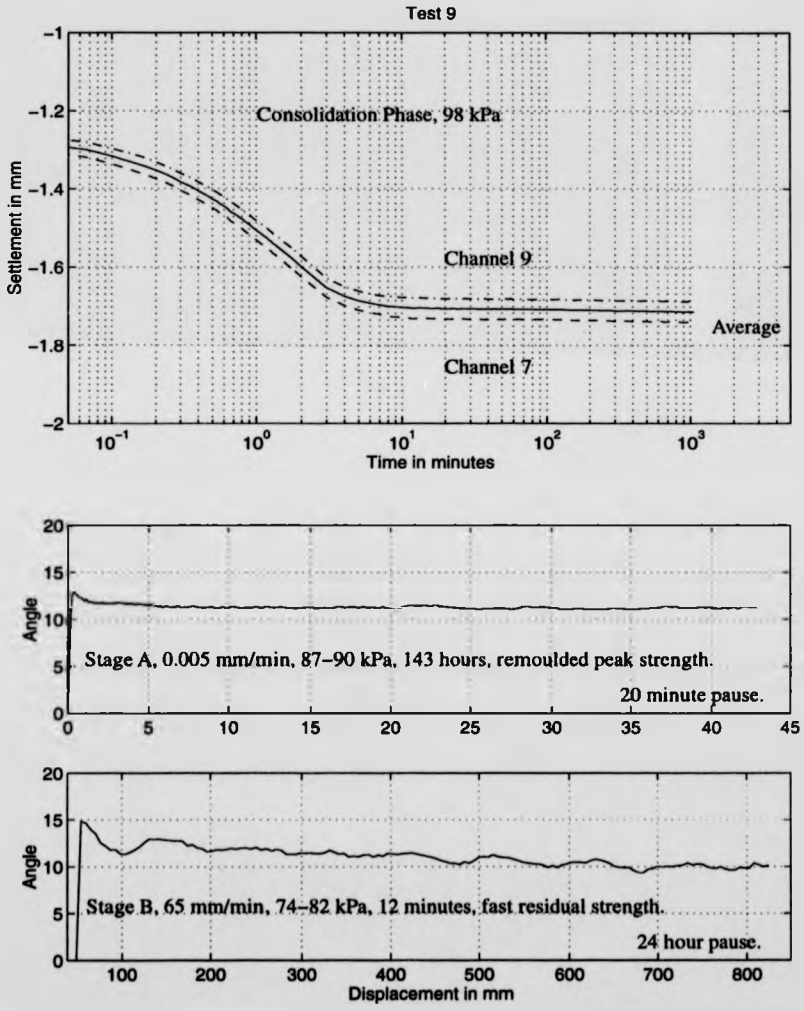

Figure D.31: Test 9, submerged, 4x1mm wave–form perspex interface test, 100% kaolin.

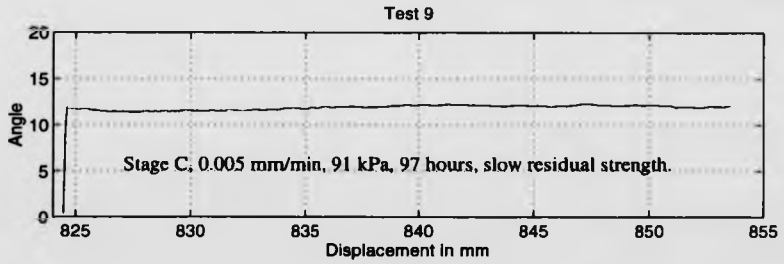

Figure D.32: Test 9, submerged, 4x1mm wave–form perspex interface test, 100% kaolin.

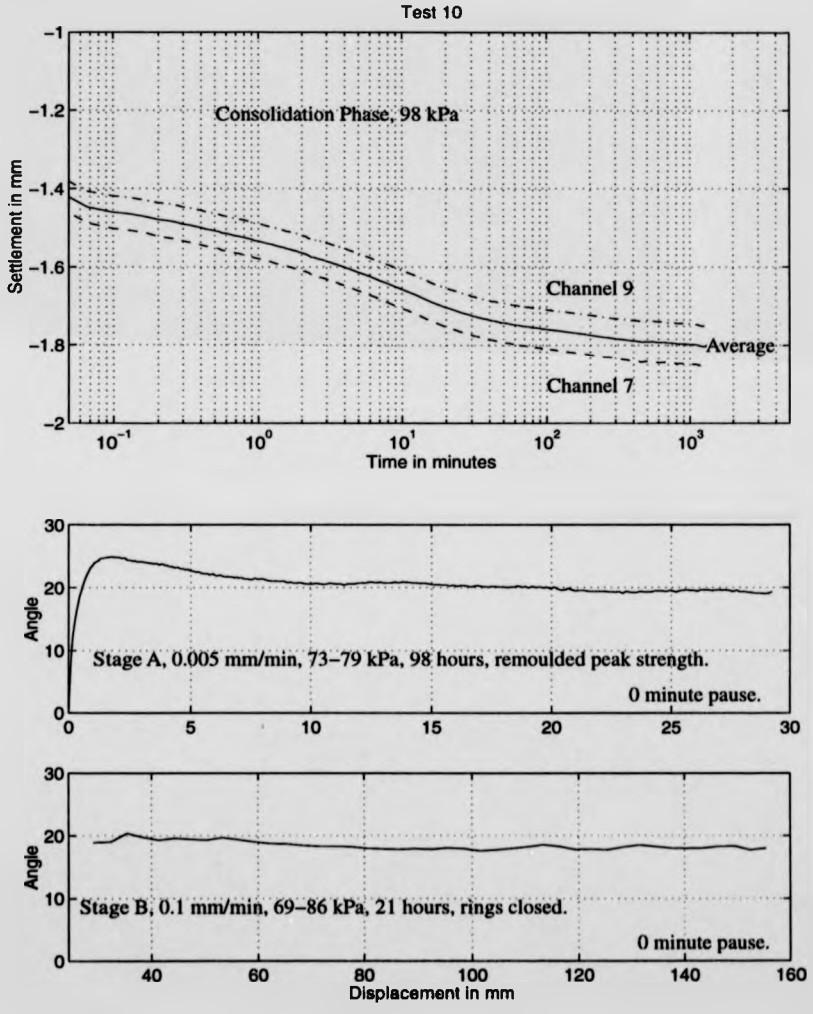

Figure D.33: Test 10, submerged, soil on soil test, 100% ball clay.

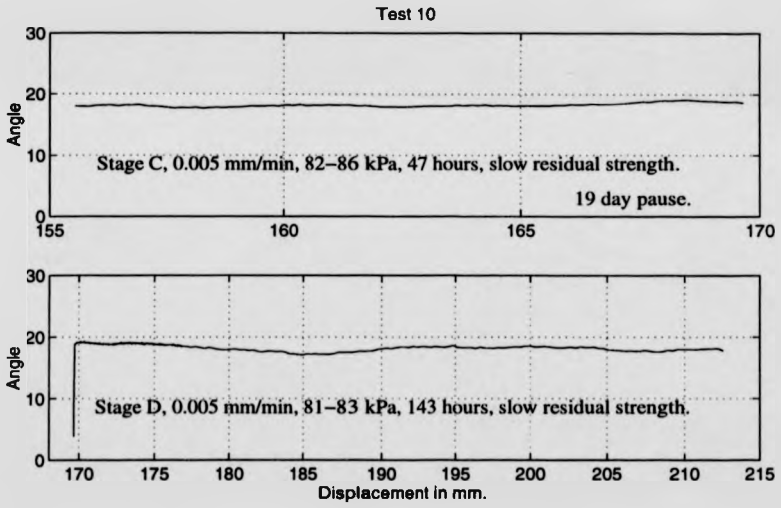

Figure D.34: Test 10, submerged, soil on soil test, 100% ball clay.

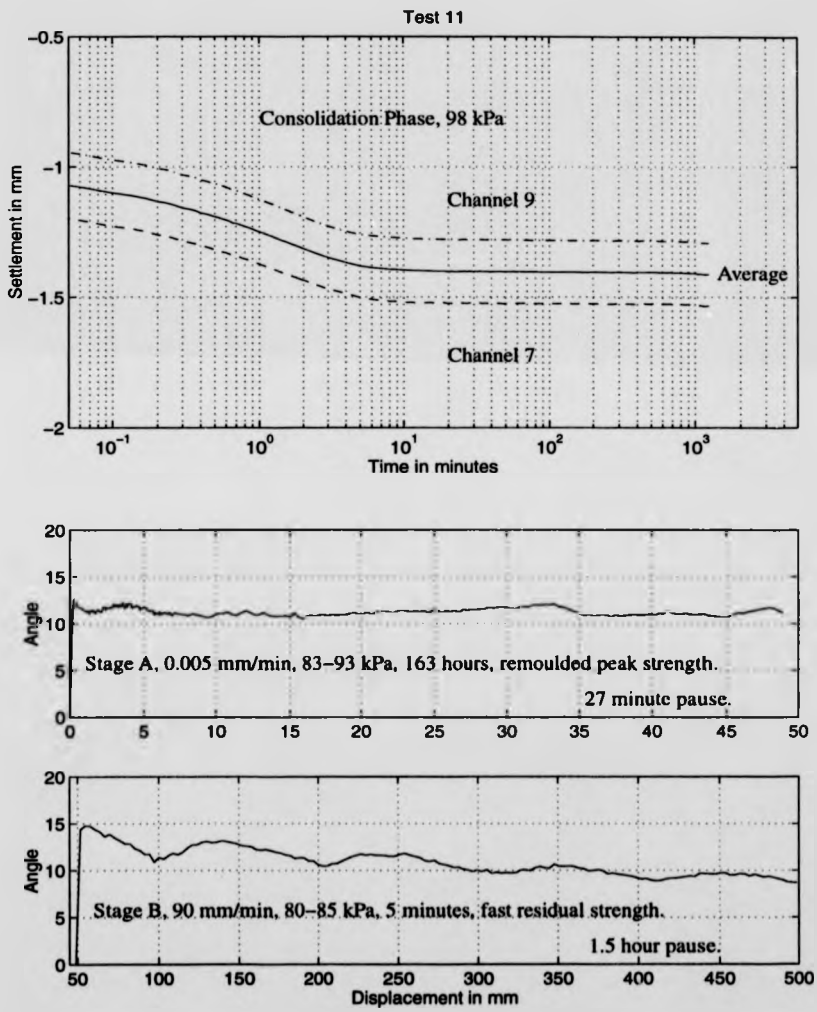

Figure D.35: Test 11, submerged, 4x1mm wave-form perspex interface test, 100% kaolin.

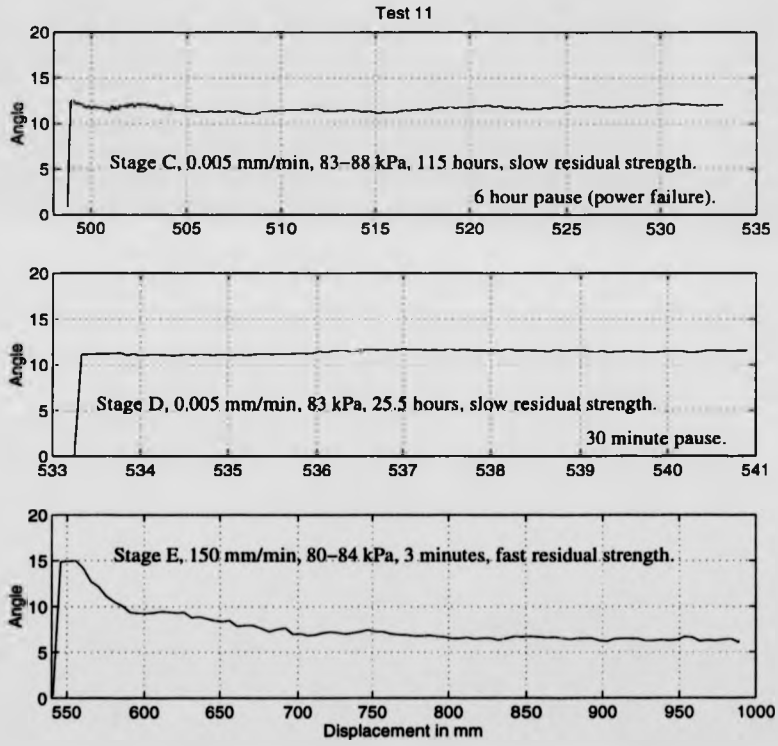

Figure D.36: Test 11, submerged, 4x1mm wave-form perspex interface test, 100% kaolin.

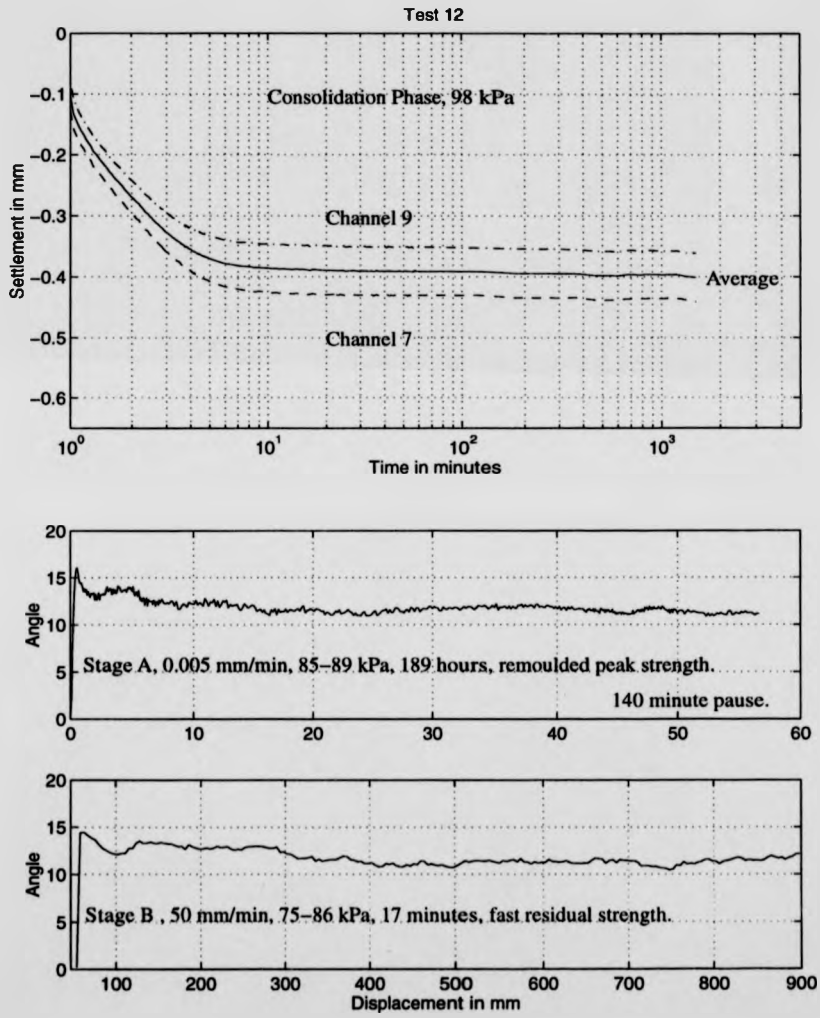

Figure D.37: Test 12, submerged, 4x1mm wave-form perspex interface test, 100% kaolin.

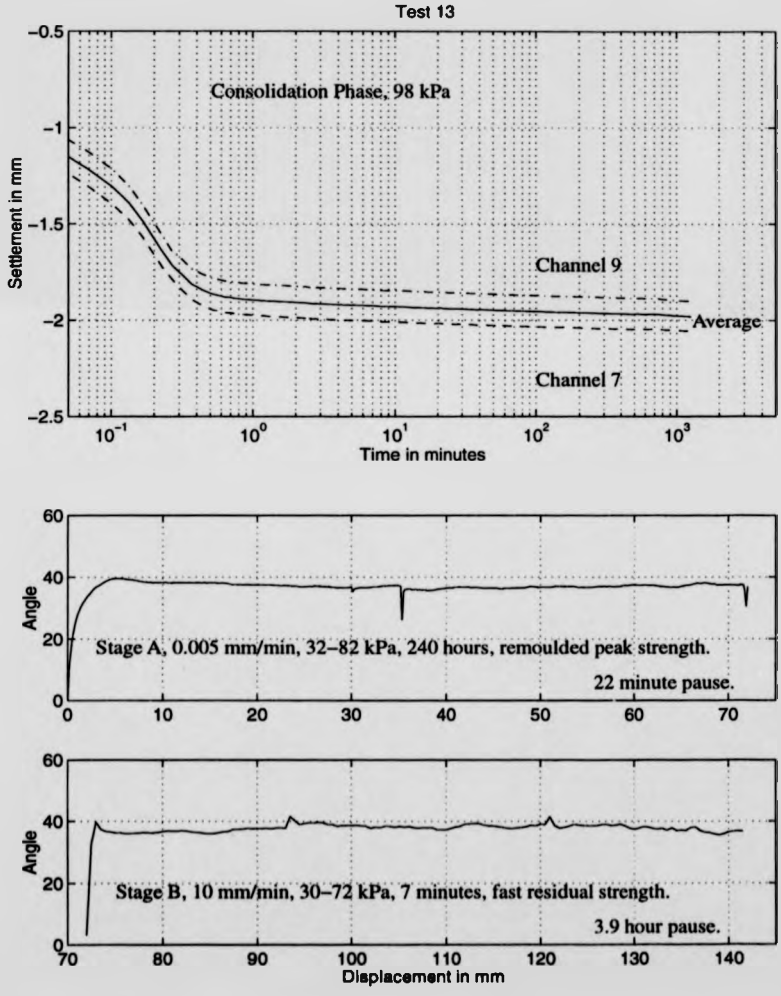

Figure D.38: Test 13, submerged, soil on soil test, 100% crushed flint.

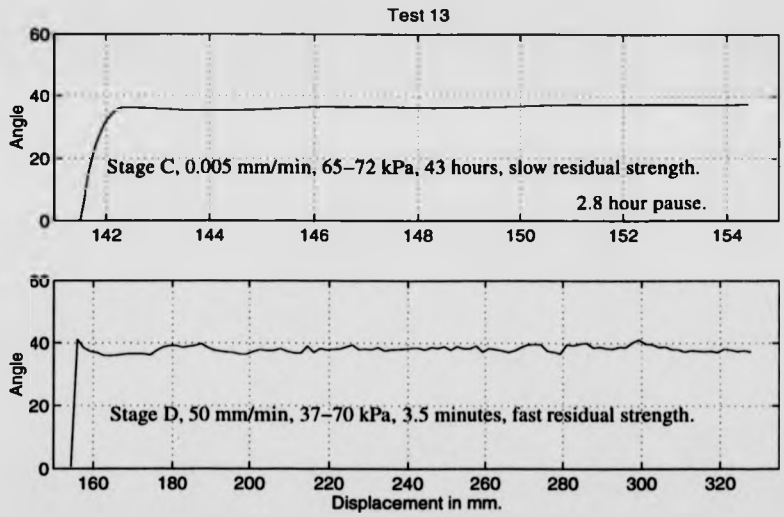

Figure D.39: Test 13, submerged, soil on soil test, 100% crushed flint.

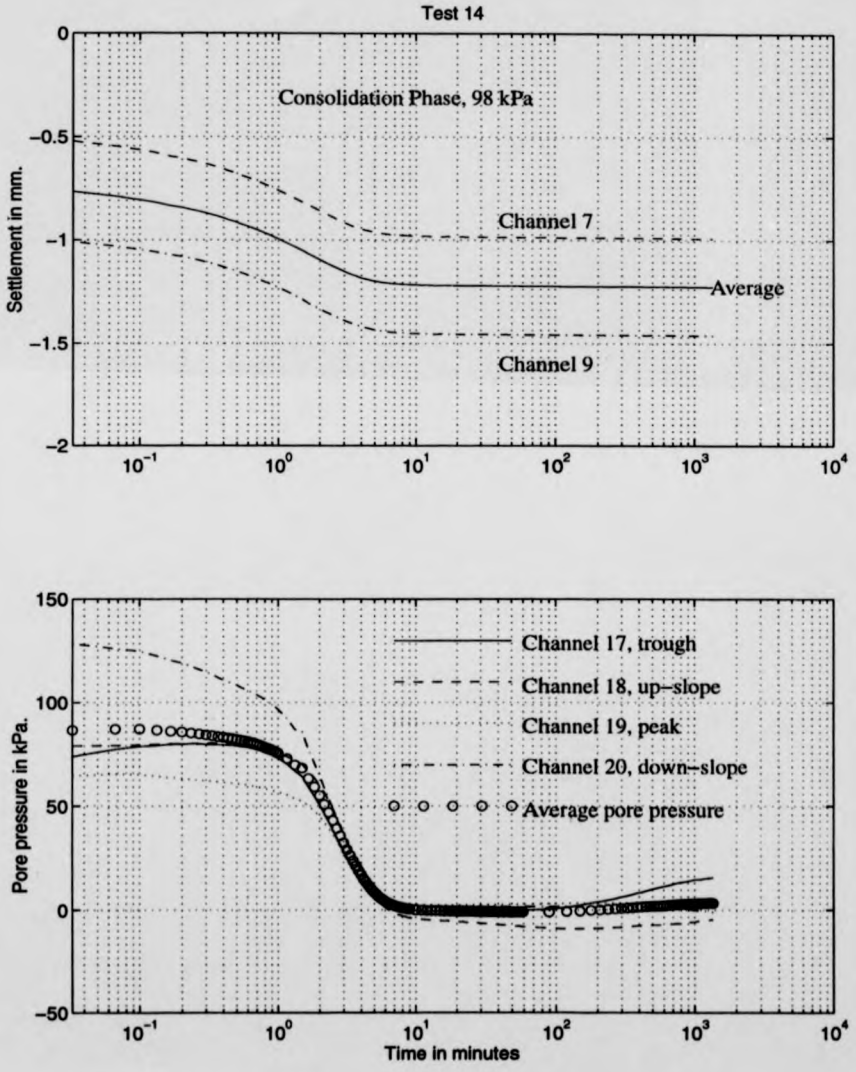

Figure D.40: Test 14, submerged, 4x1mm wave-form perspex interface test, 100% kaolin.

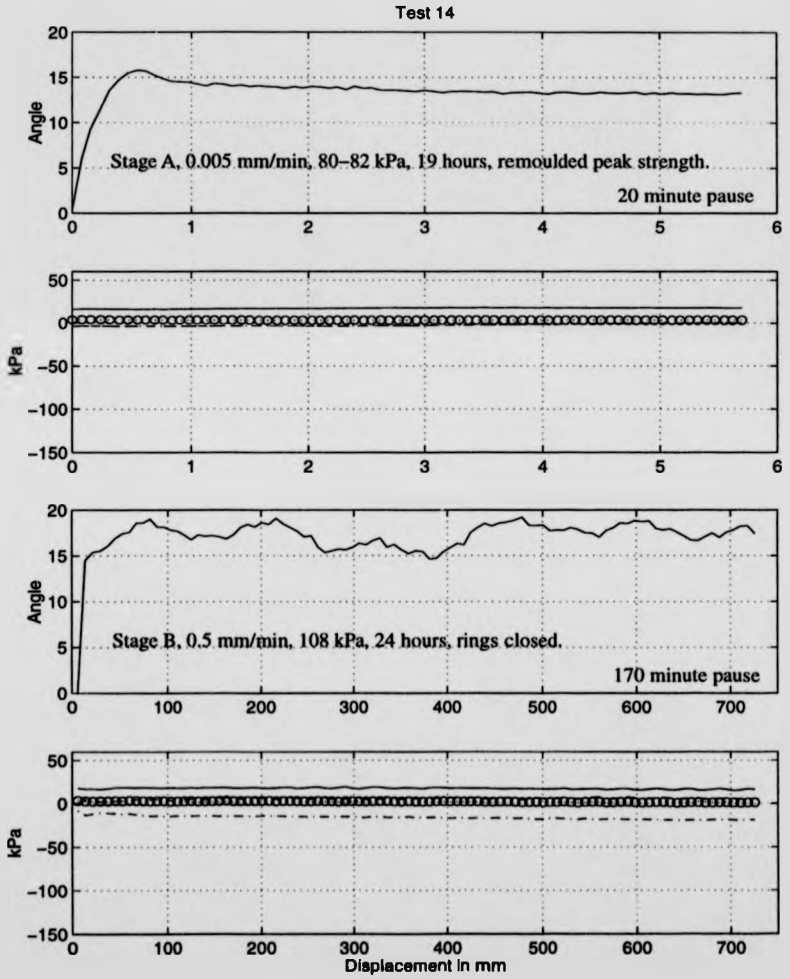

Figure D.41: Test 14, submerged, 4x1mm wave-form perspex interface test, 100% kaolin.

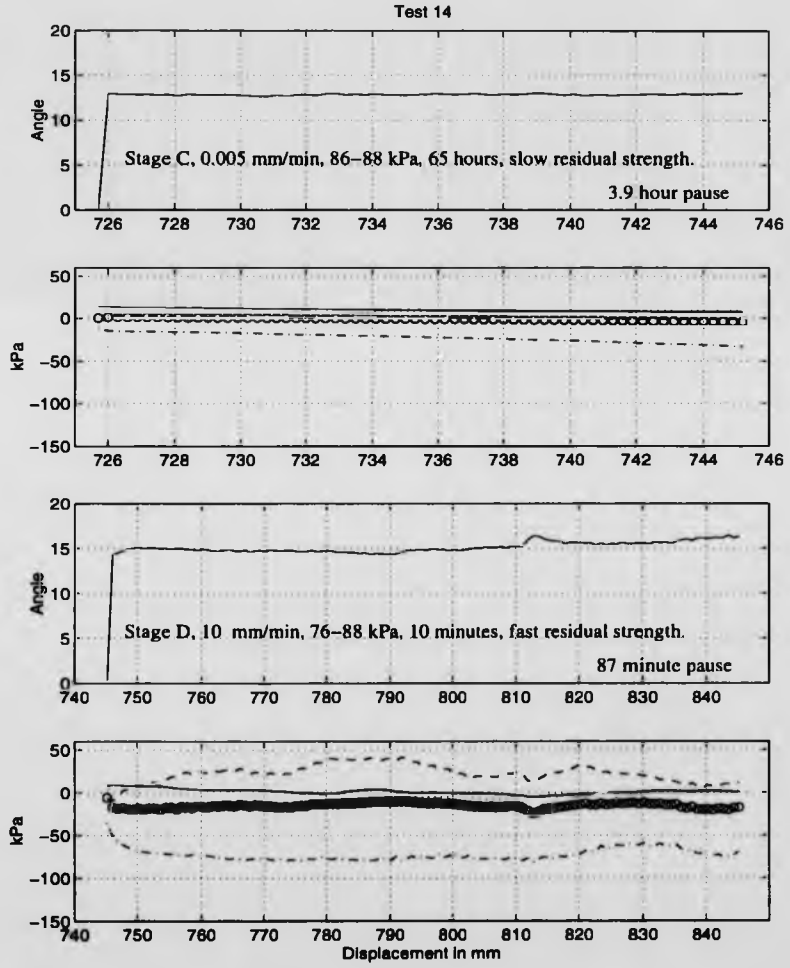

Figure D.42: Test 14, submerged, 4x1mm wave-form perspex interface test, 100% kaolin.

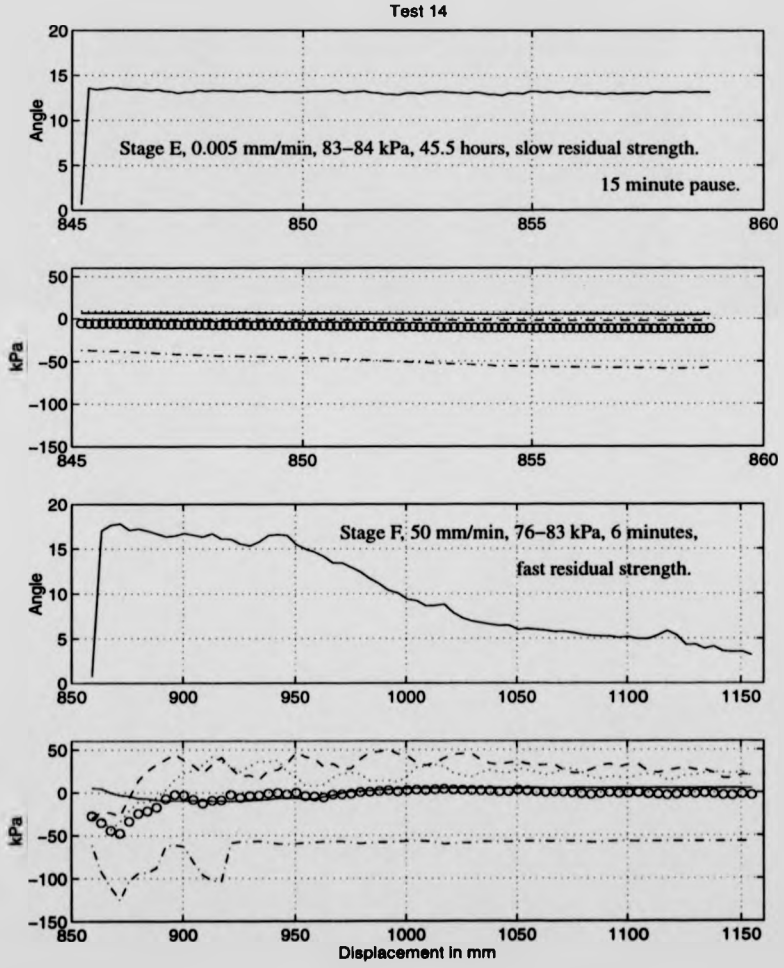

Figure D.43: Test 14, submerged, 4x1mm wave-form perspex interface test, 100% kaolin.

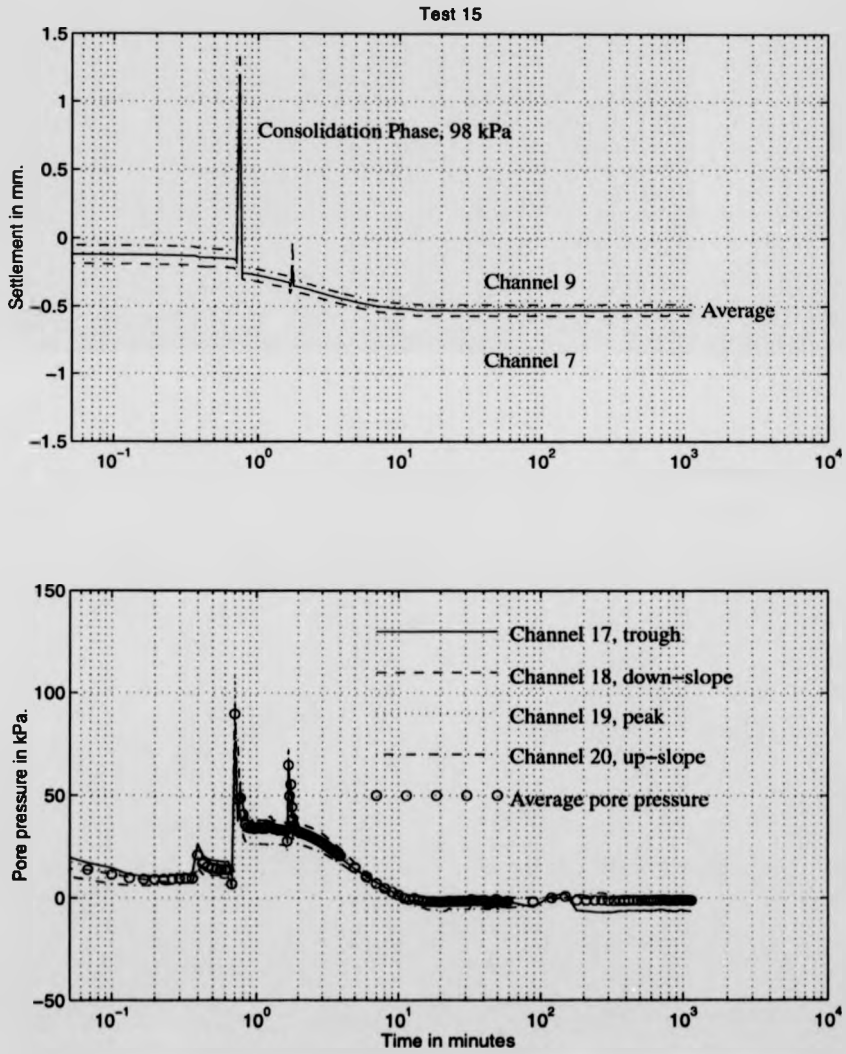

Figure D.44: Test 15, submerged, 4x1mm wave-form perspex interface test, 100% kaolin.

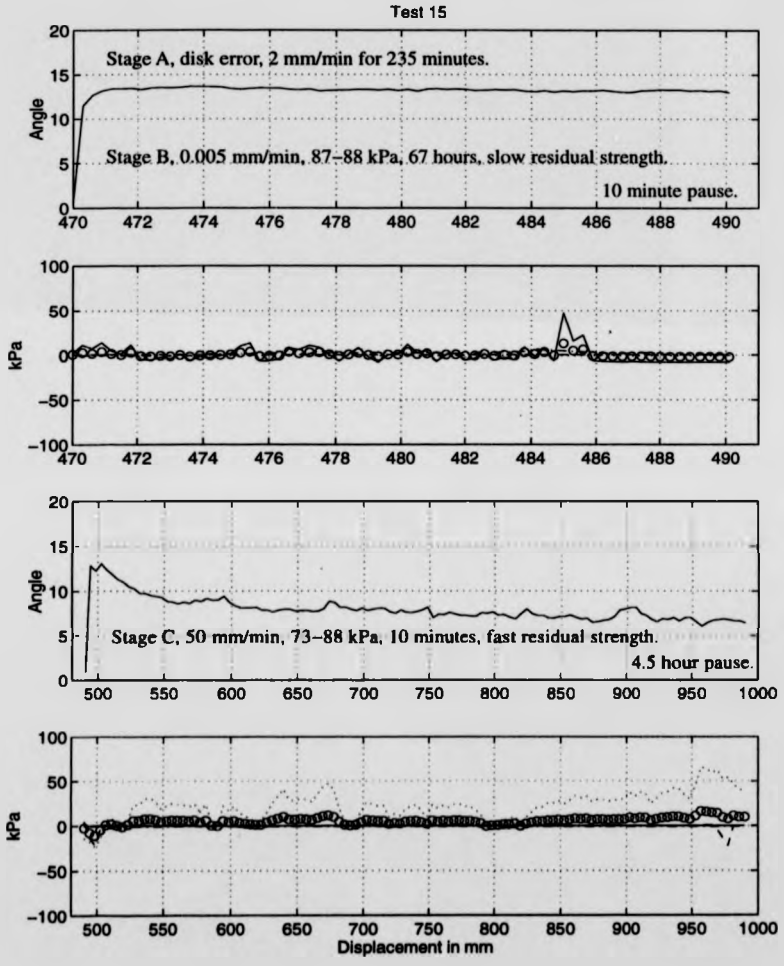

Figure D.45: Test 15, submerged, 4x1mm wave-form perspex interface test, 100% kaolin.

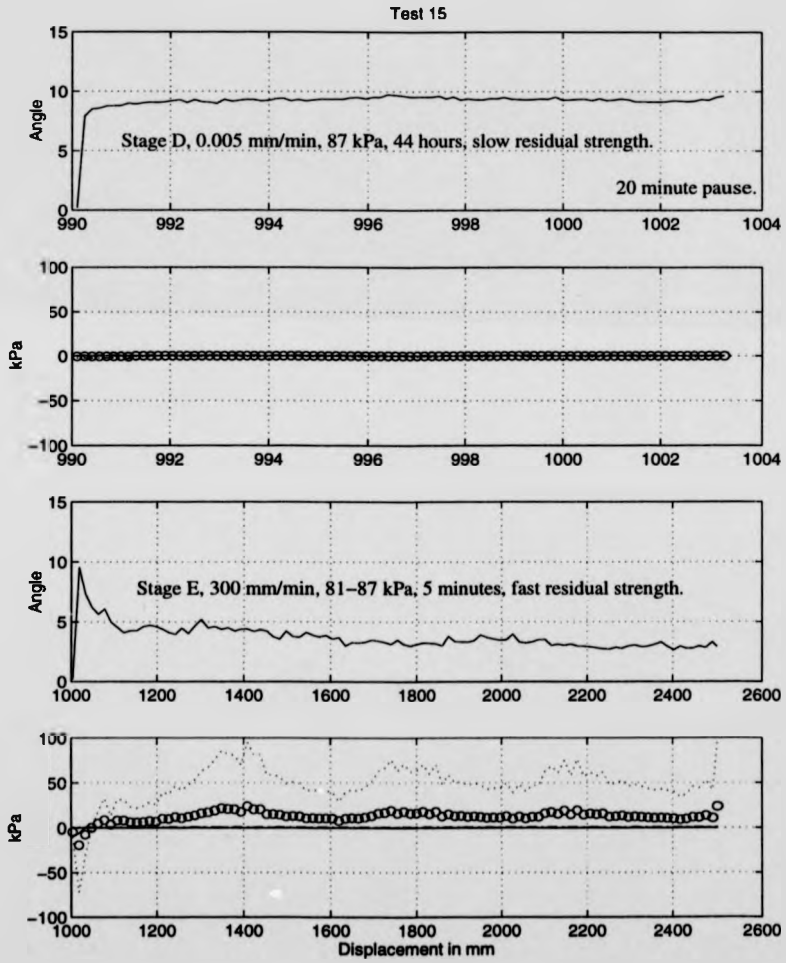

Figure D.46: Test 15, submerged, 4x1mm wave-form perspex interface test, 100% kaolin.

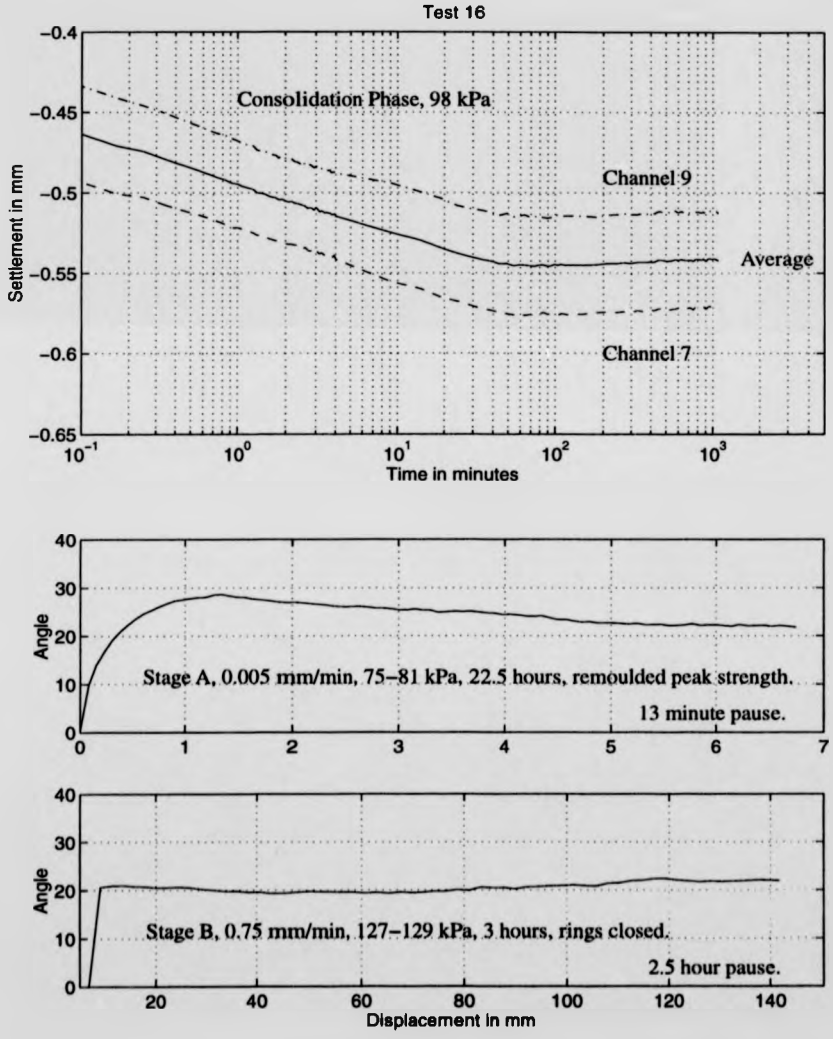

Figure D.47: Test 16, submerged, soil on soil test, 100% ball clay.

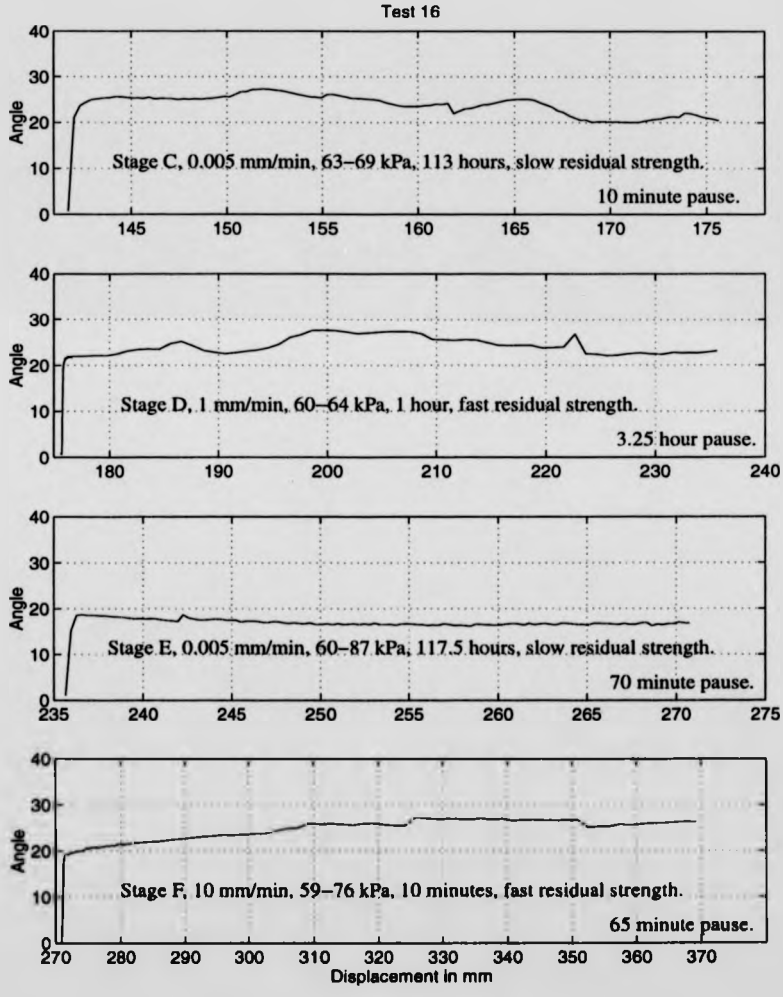

Figure D.48: Test 16, submerged, soil on soil test, 100% ball clay.

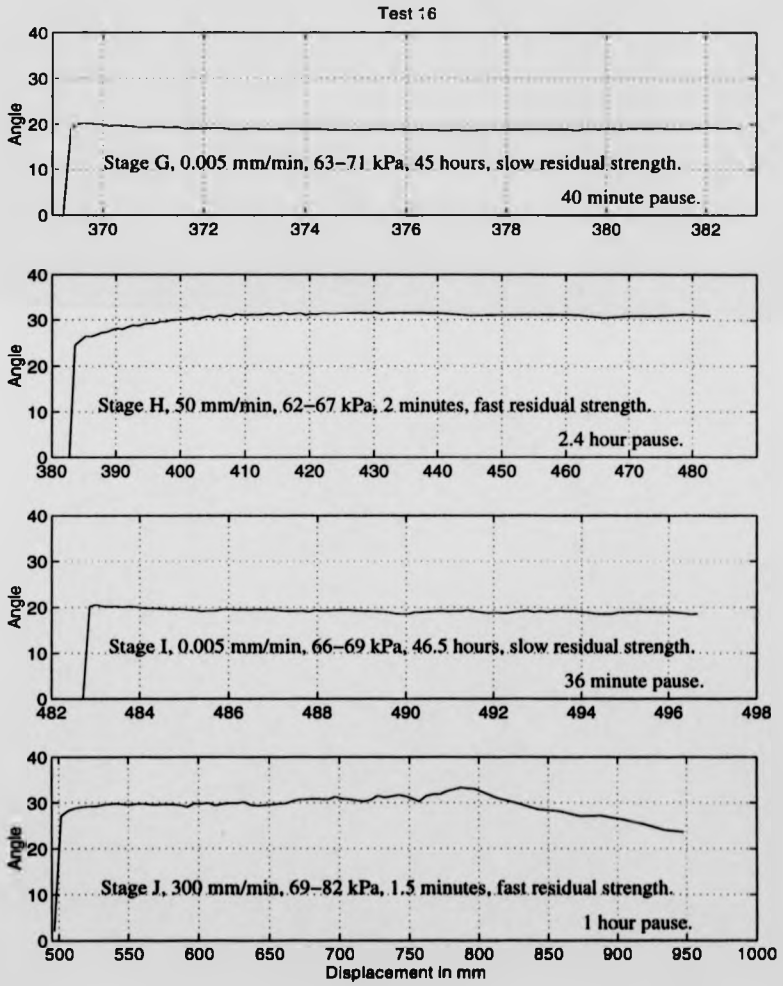

Figure D.49: Test 16, submerged, soil on soil test, 100% ball clay.

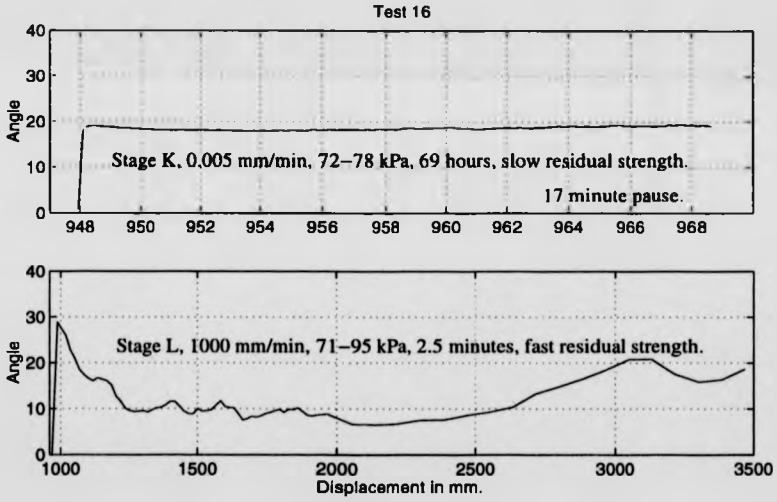

Figure D.50: Test 16, submerged, soil on soil test, 100% ball clay.

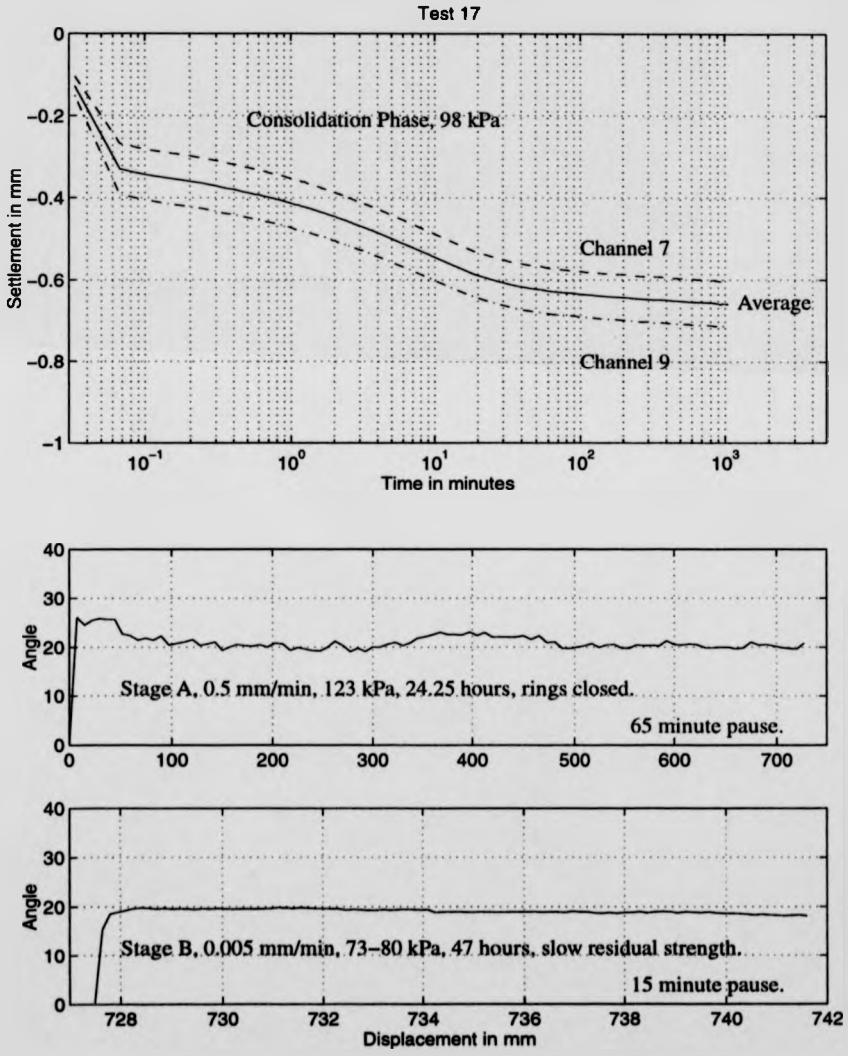

Figure D.51: Test 17, submerged, soil on soil test, 100% ball clay.

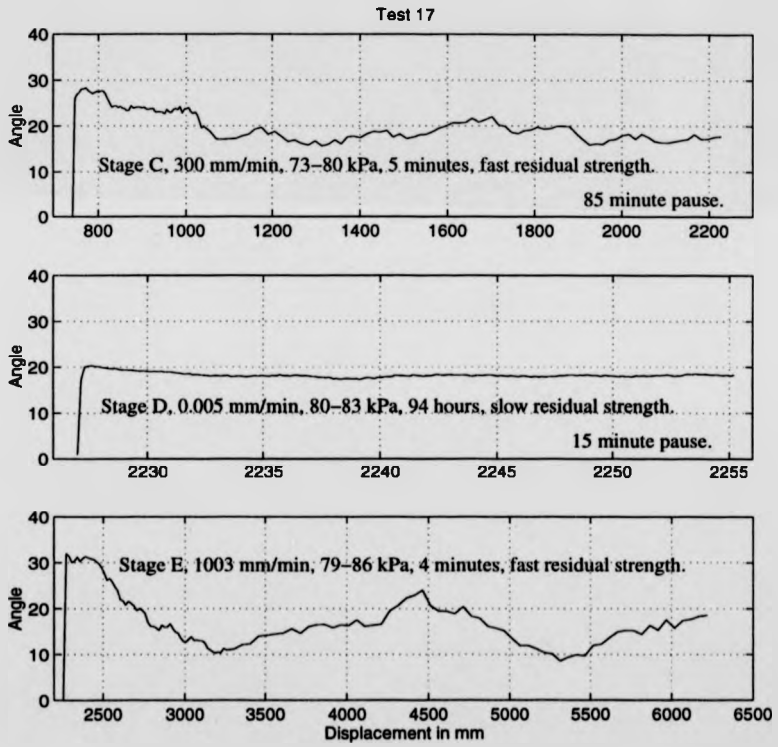

Figure D.52: Test 17, submerged, soil on soil test, 100% ball clay.

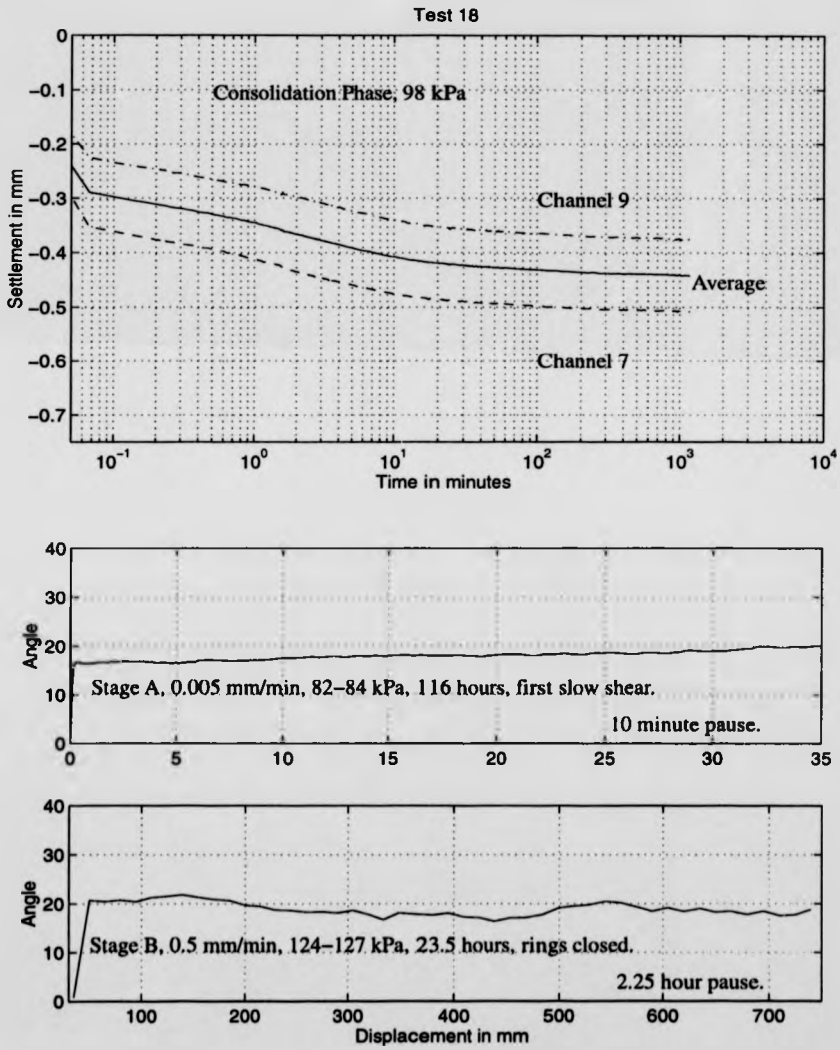

Figure D.53: Test 18, submerged, planar stainless steel interface test, 100% ball clay.

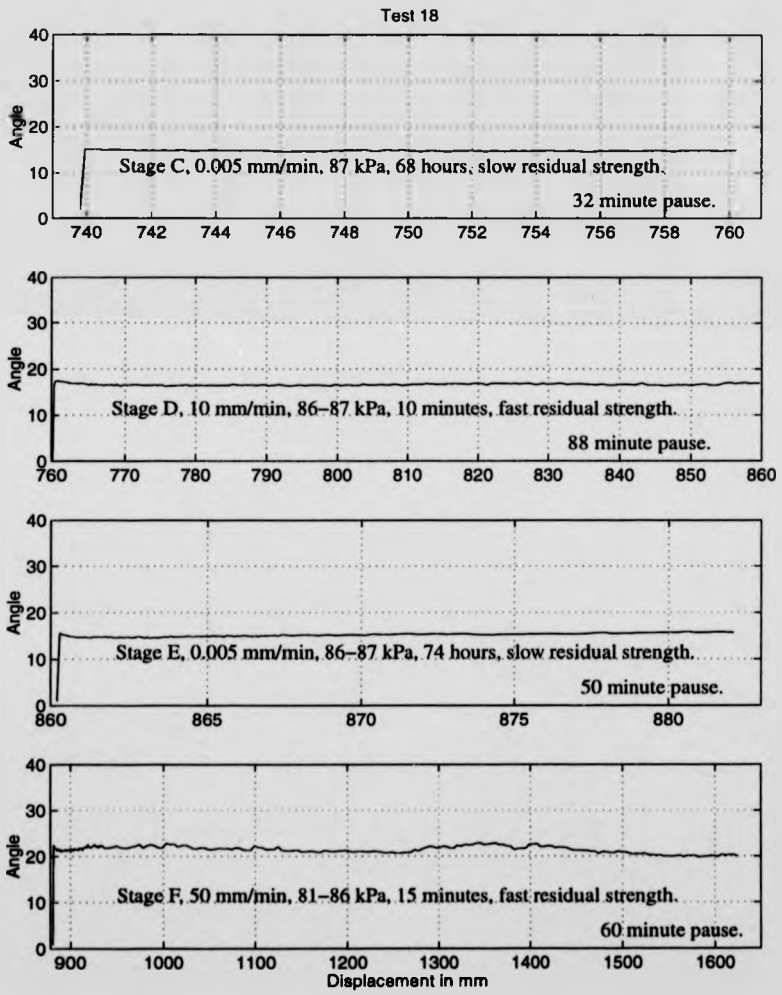

Figure D.54: Test 18, submerged, planar stainless steel interface test, 100% ball clay.

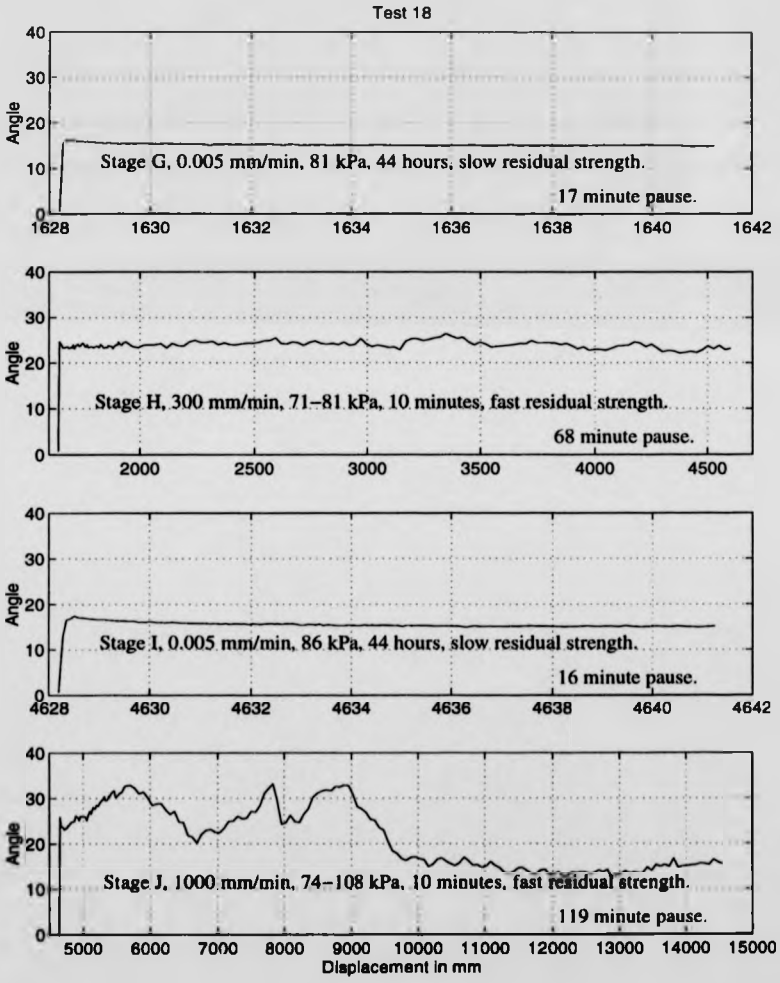

Figure D.55: Test 18, submerged, planar stainless steel interface test, 100% ball clay.

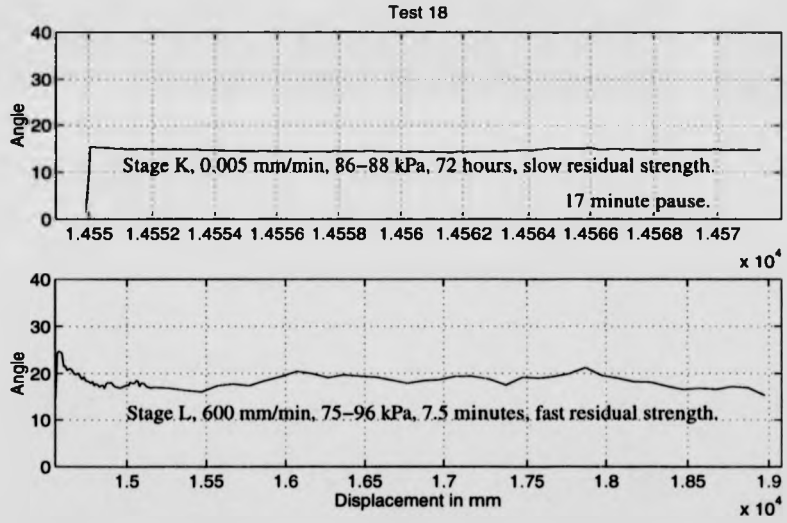

Figure D.56: Test 18, submerged, planar stainless steel interface test, 100% ball clay.

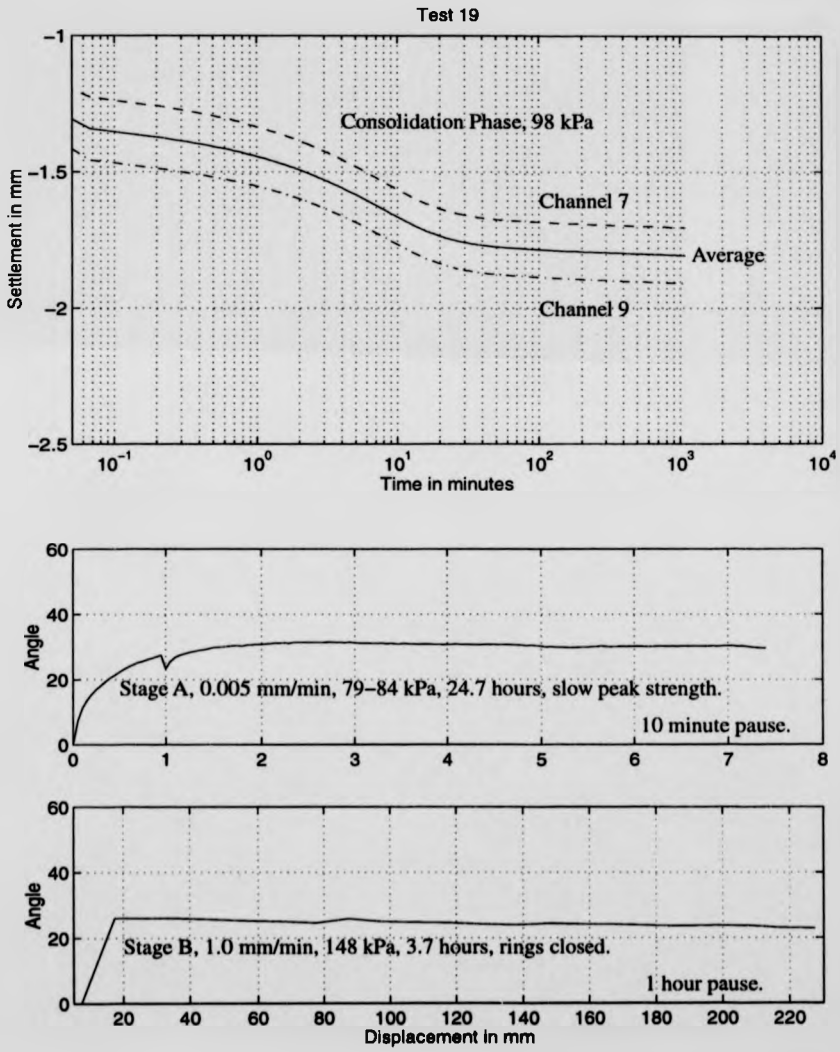

Figure D.57: Test 19, submerged, soil on soil test, 67% ball clay, 33% crushed flint.

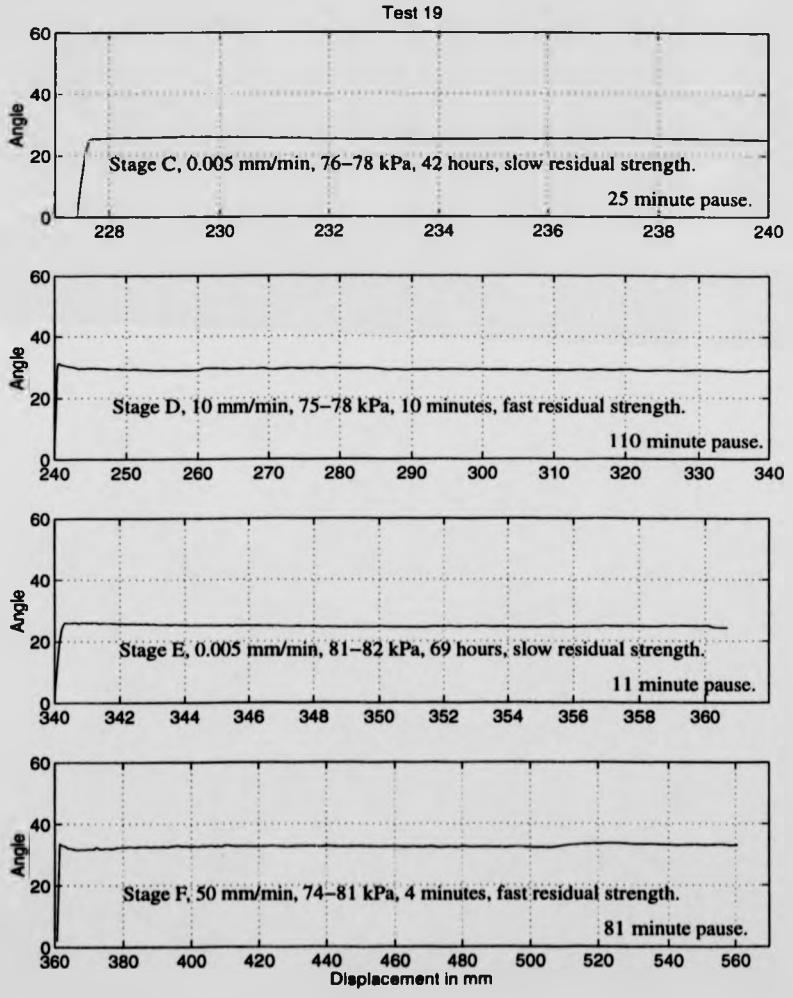

Figure D.58: Test 19, submerged, soil on soil test, 67% ball clay, 33% crushed flint.

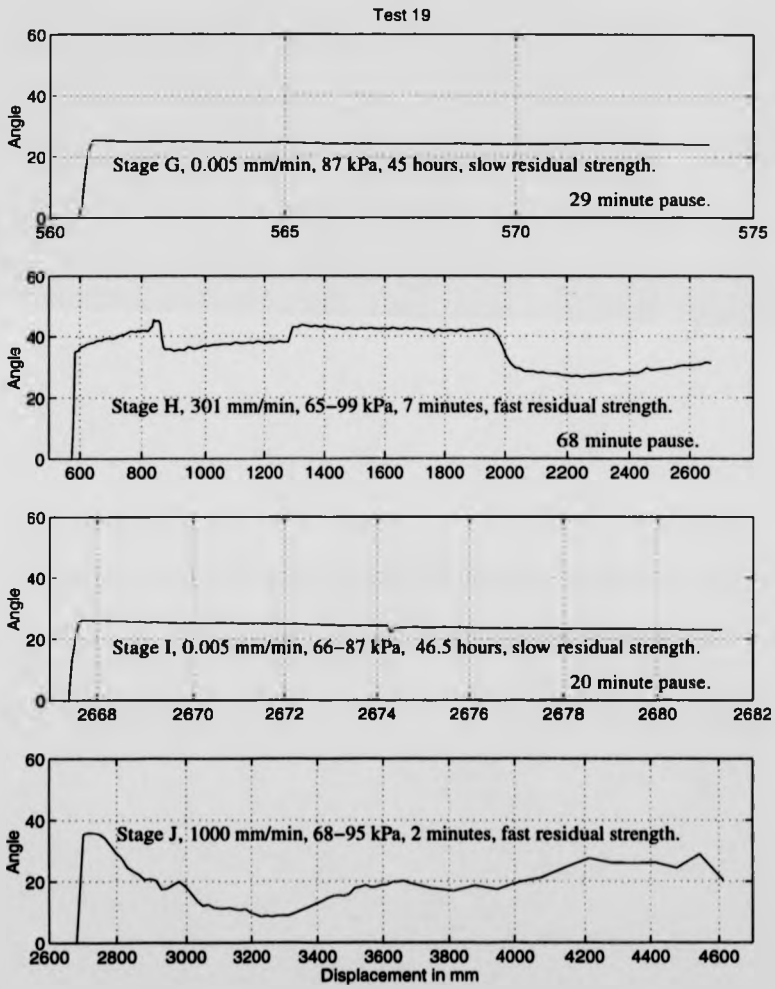

Figure D.59: Test 19, submerged, soil on soil test, 67% ball clay, 33% crushed flint.

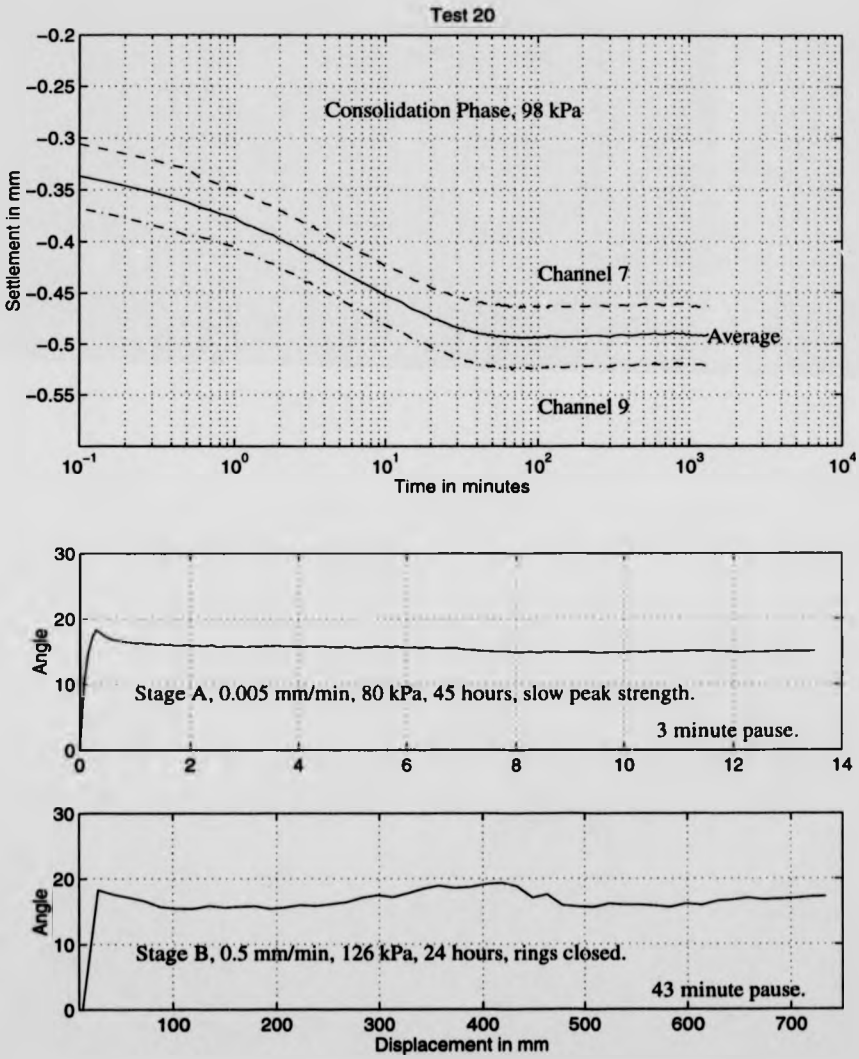

Figure D.60: Test 20, submerged, planar stainless steel interface test, 67% ball clay, 33% crushed flint.

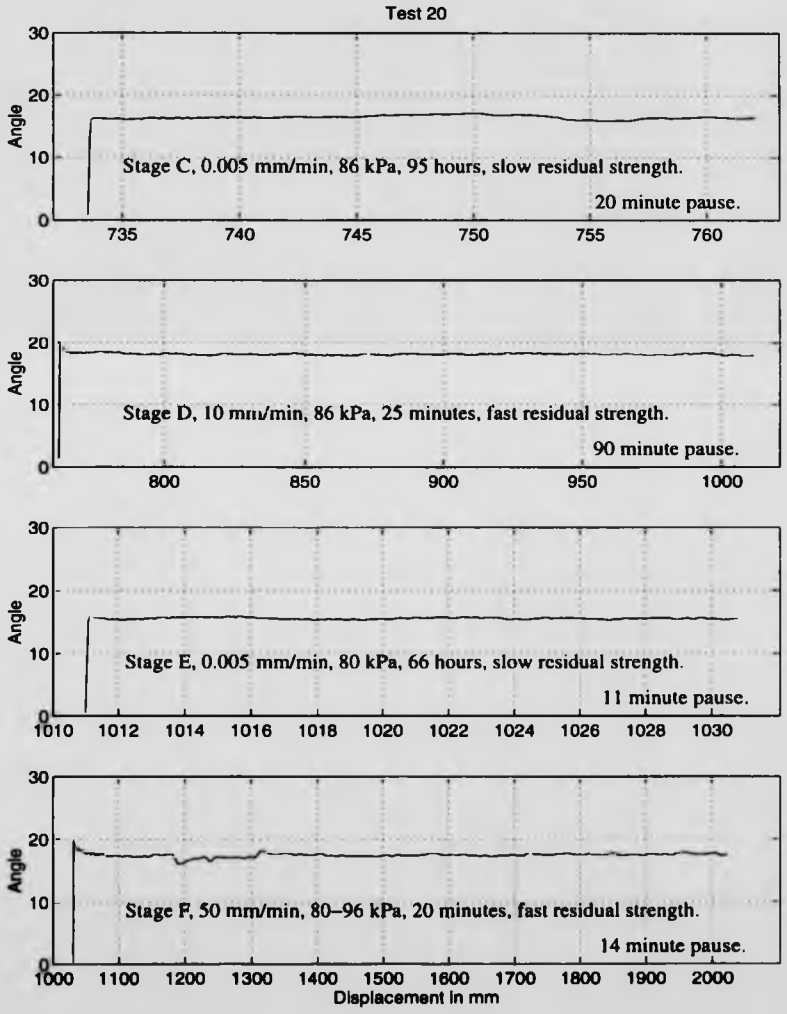

Figure D.61: Test 20, submerged, planar stainless steel interface test, 67% ball clay, 33% crushed flint.

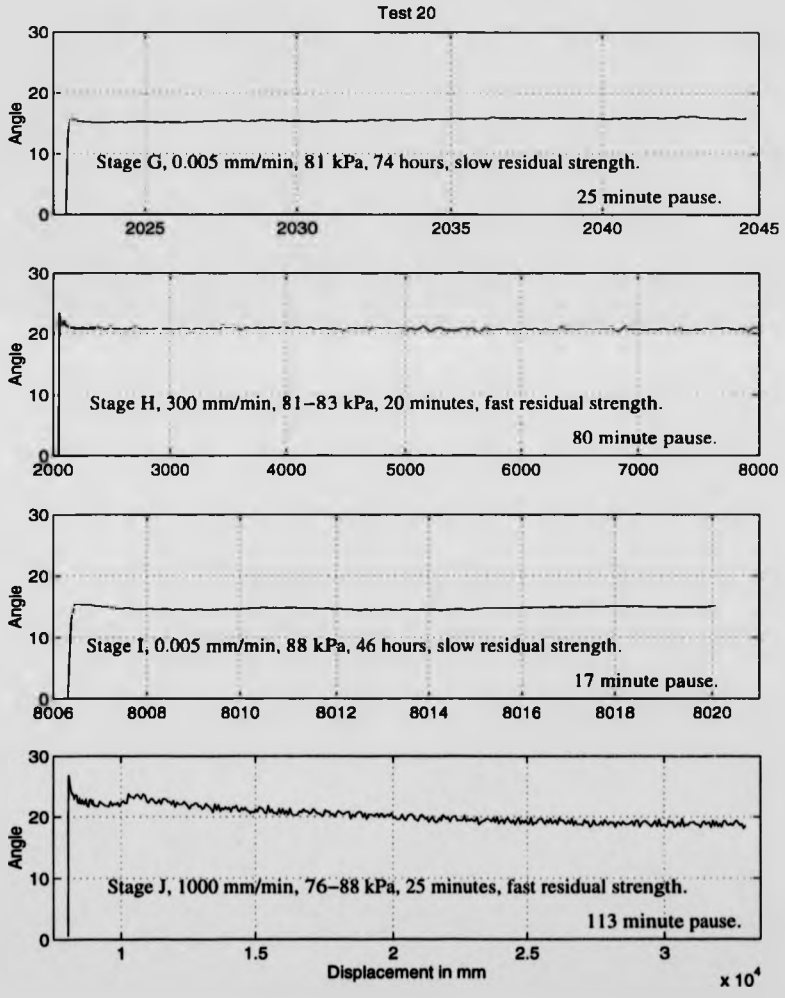

Figure D.62: Test 20, submerged, planar stainless steel interface test, 67% ball clay, 33% crushed flint.

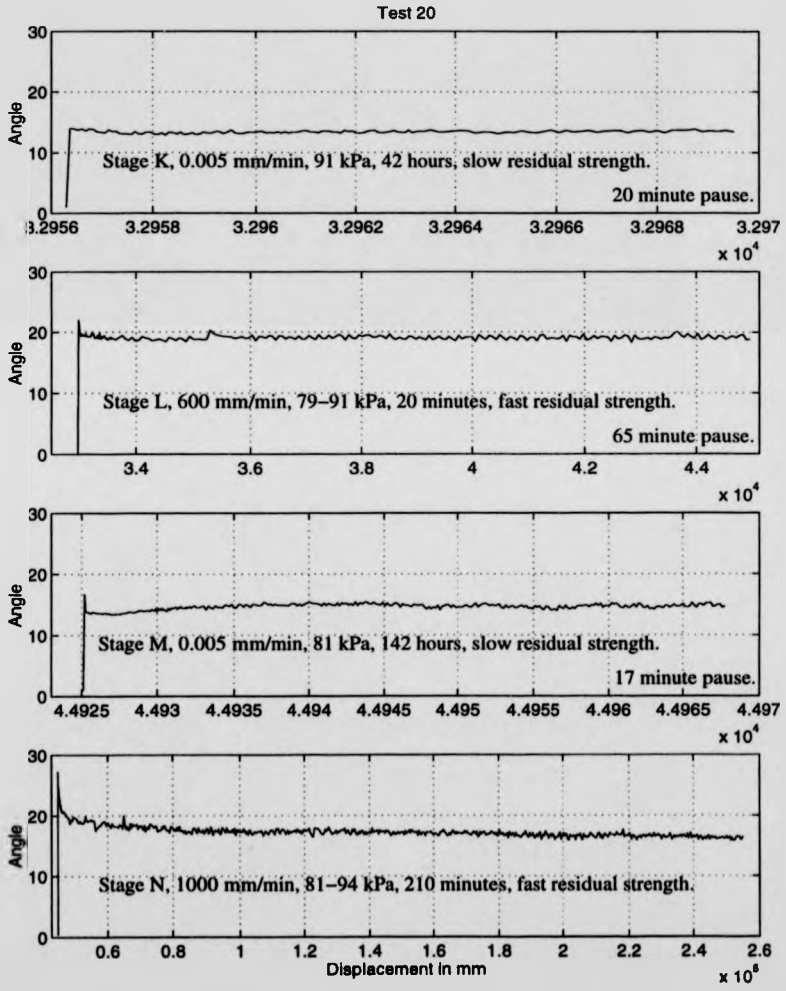

Figure D.63: Test 20, submerged, planar stainless steel interface test, 67% ball clay, 33% crushed flint.

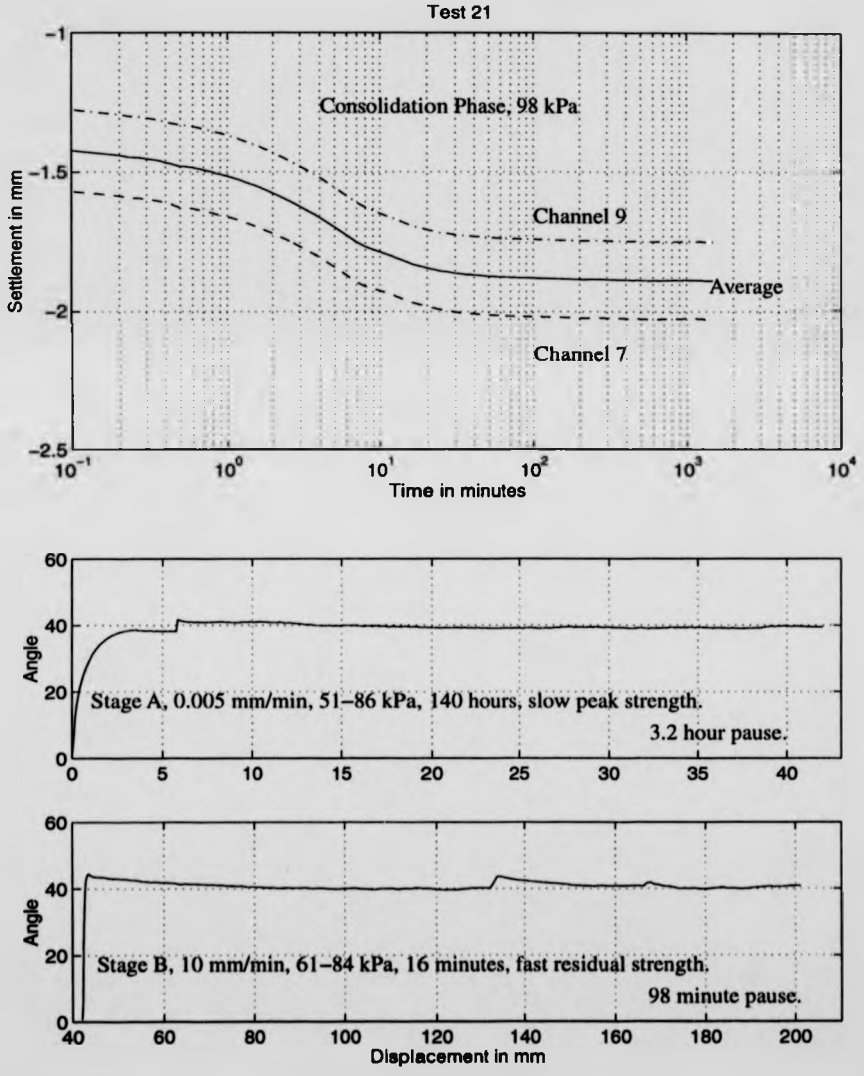

Figure D.64: Test 21, submerged, soil on soil test, 33% ball clay, 67% crushed flint.

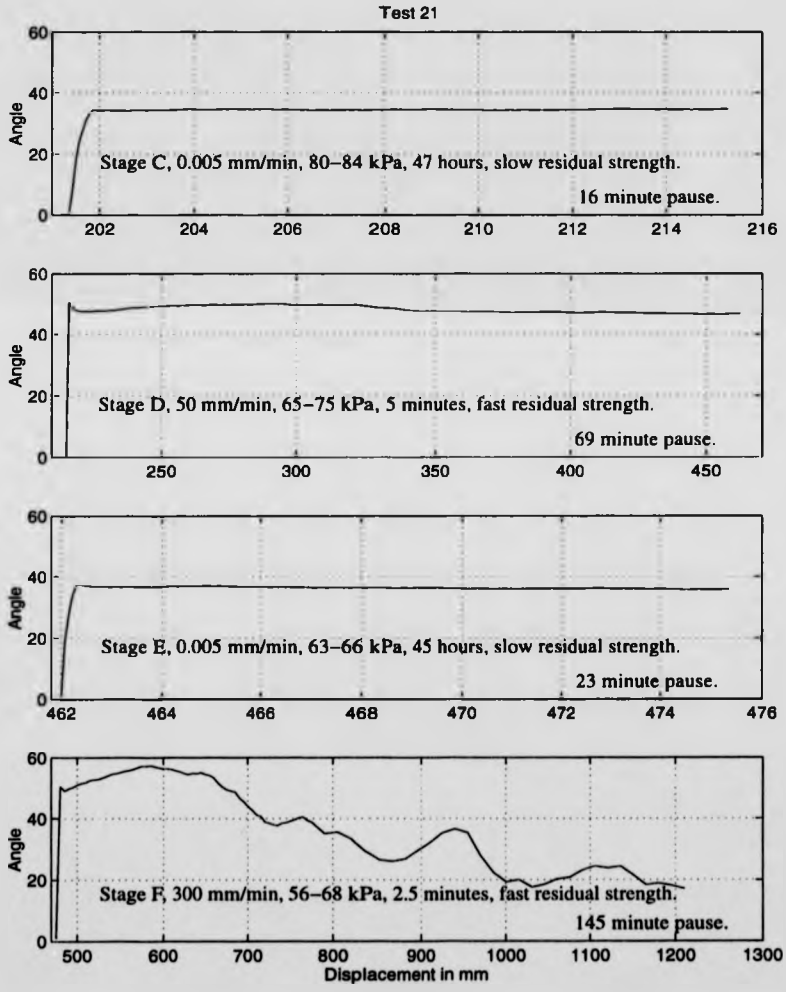

Figure D.65: Test 21, submerged, soil on soil test, 33% ball clay, 67% crushed flint.

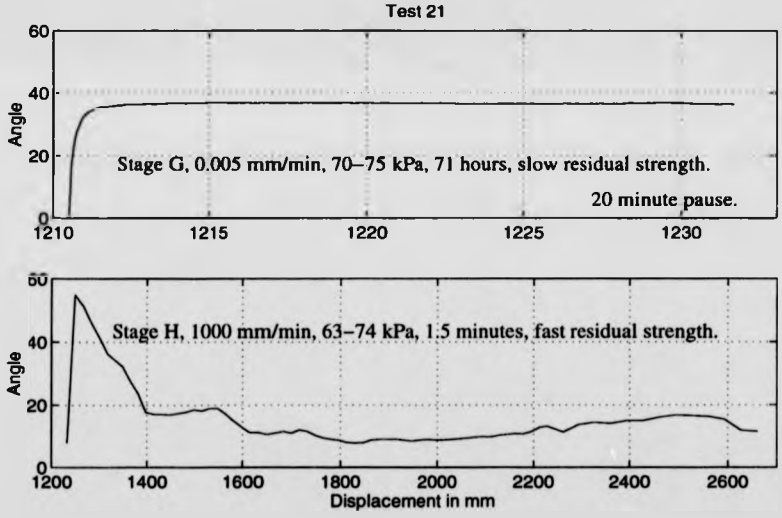

Figure D.66: Test 21, submerged, soil on soil test, 33% ball clay, 67% crushed flint.

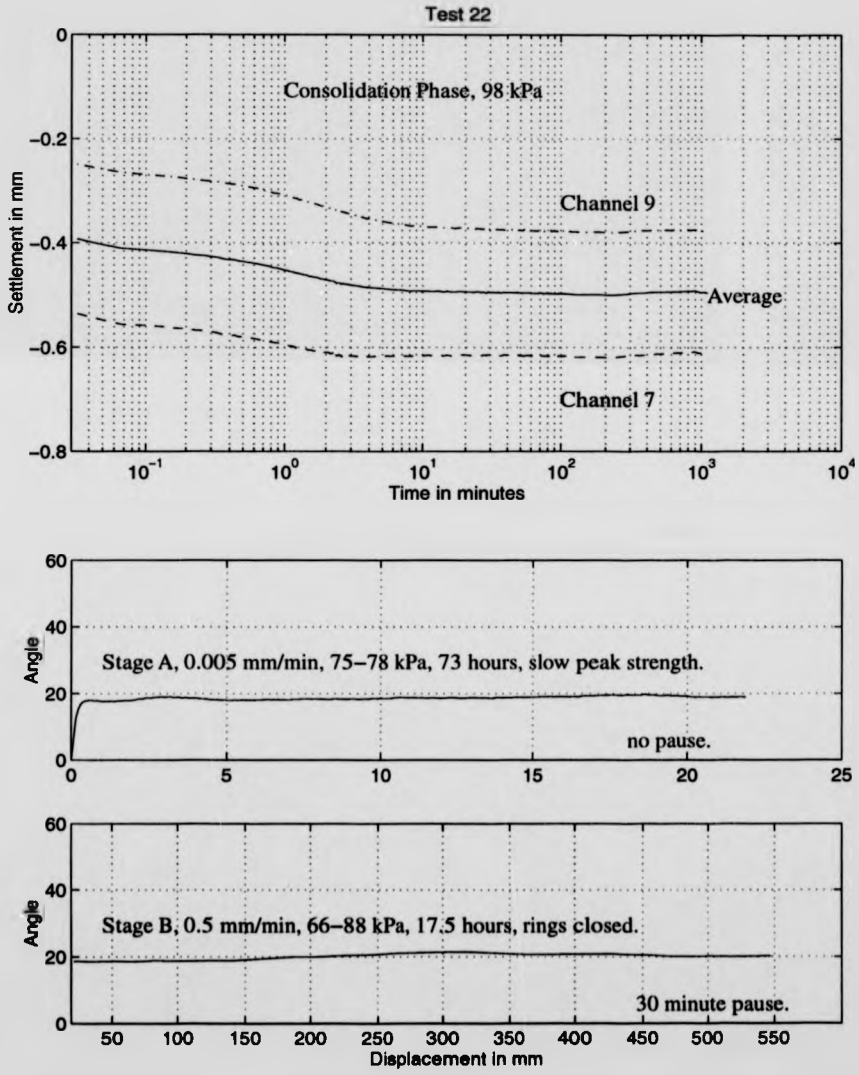

Figure D.67: Test 22, submerged, planar stainless steel interface test, 33% ball clay, 67% crushed flint.

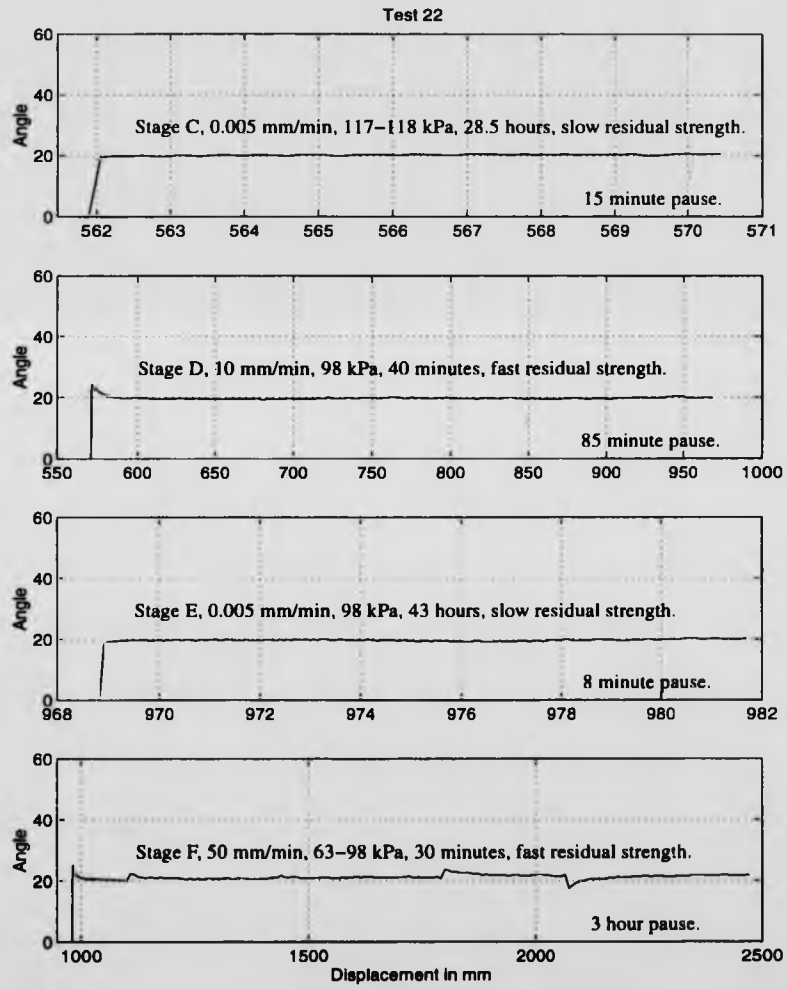

Figure D.68: Test 22, submerged, planar stainless steel interface test, 33% ball clay, 67% crushed flint.

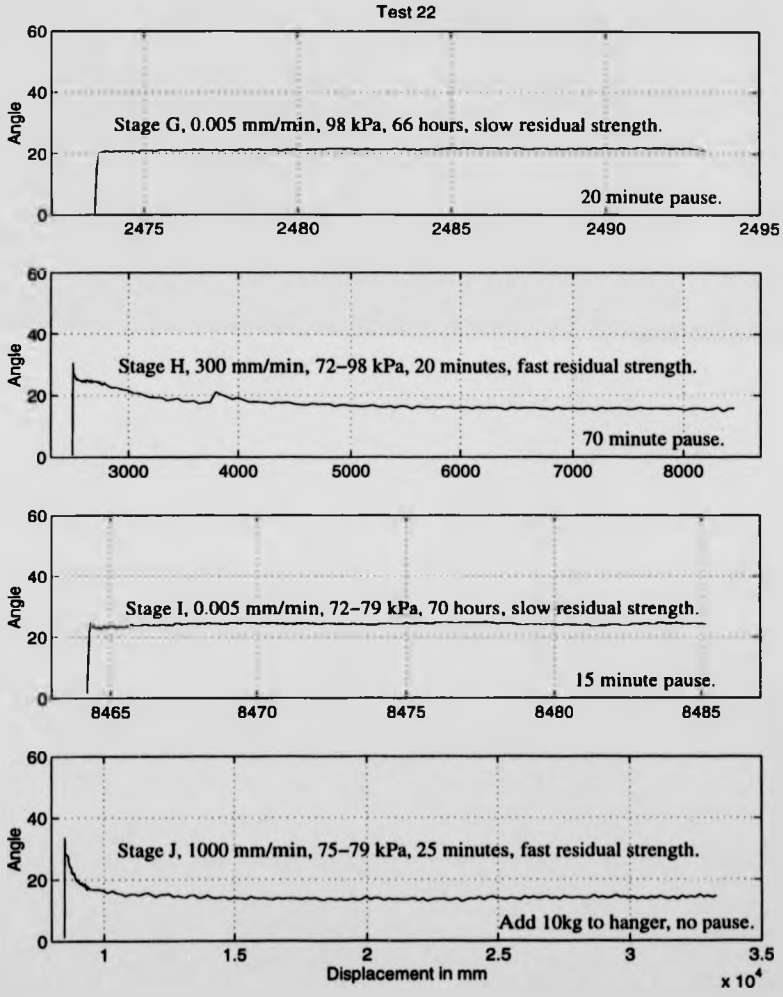

Figure D.69: Test 22, submerged, planar stainless steel interface test, 33% ball clay, 67% crushed flint.

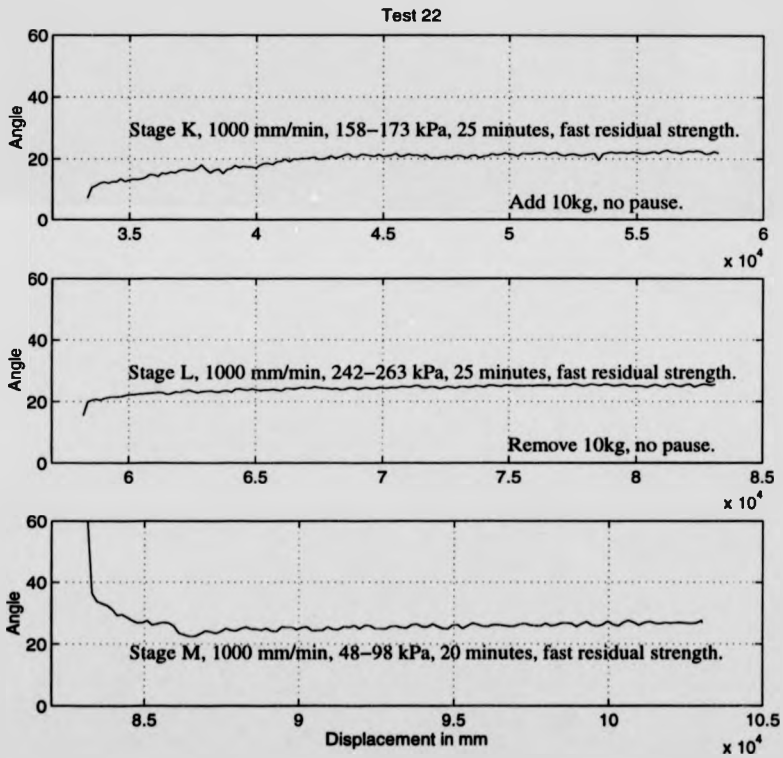

Figure D.70: Test 22, submerged, planar stainless steel interface test, 33% ball clay, 67% crushed flint.

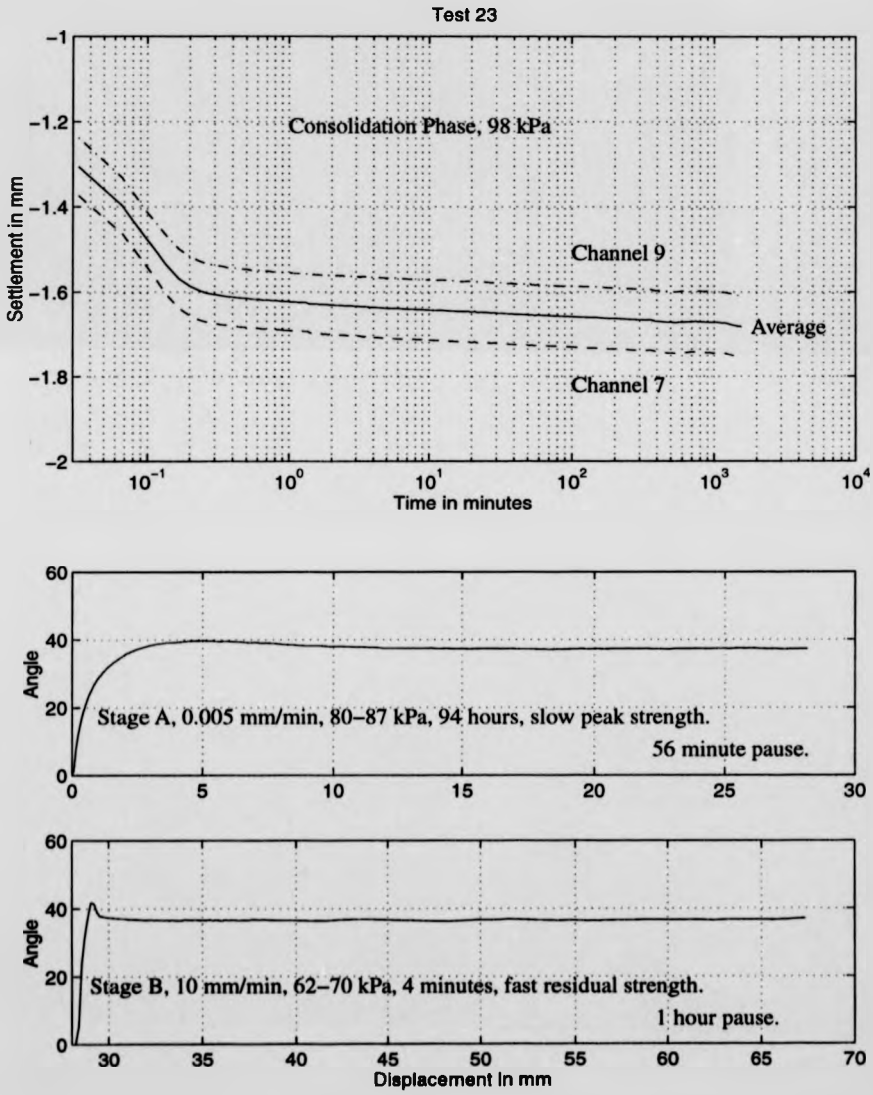

Figure D.71: Test 23, submerged, soil on soil test, 100% crushed flint.

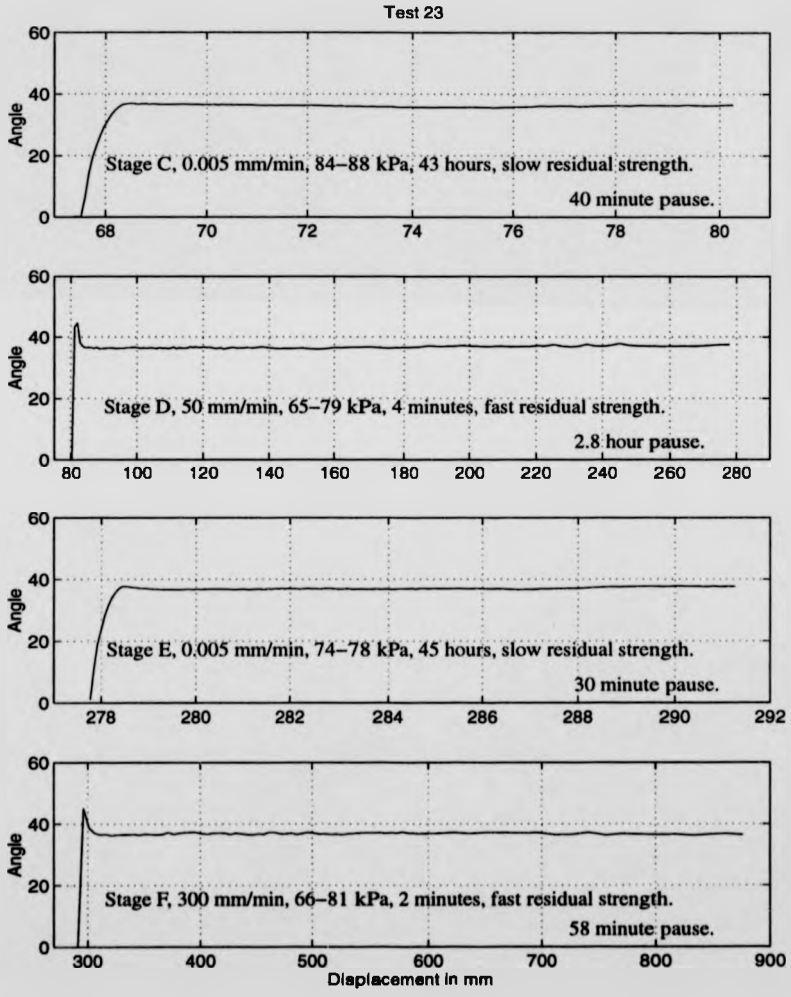

Figure D.72: Test 23, submerged, soil on soil test, 100% crushed flint.

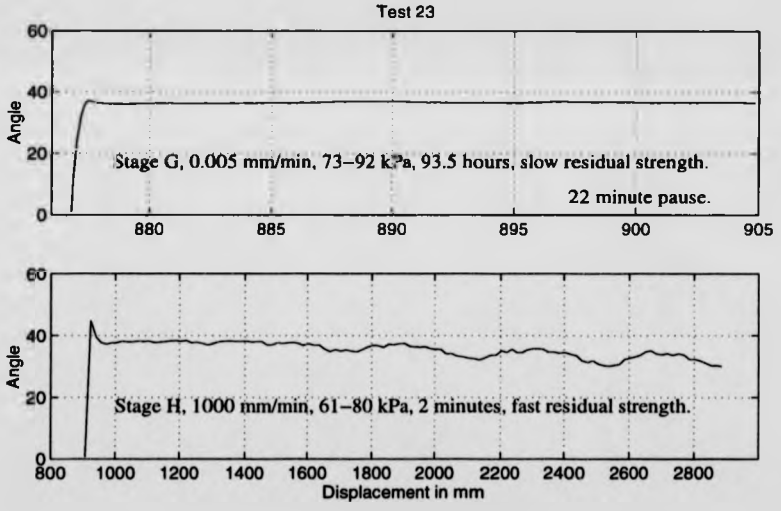

Figure D.73: Test 23, submerged, soil on soil test, 100% crushed flint.

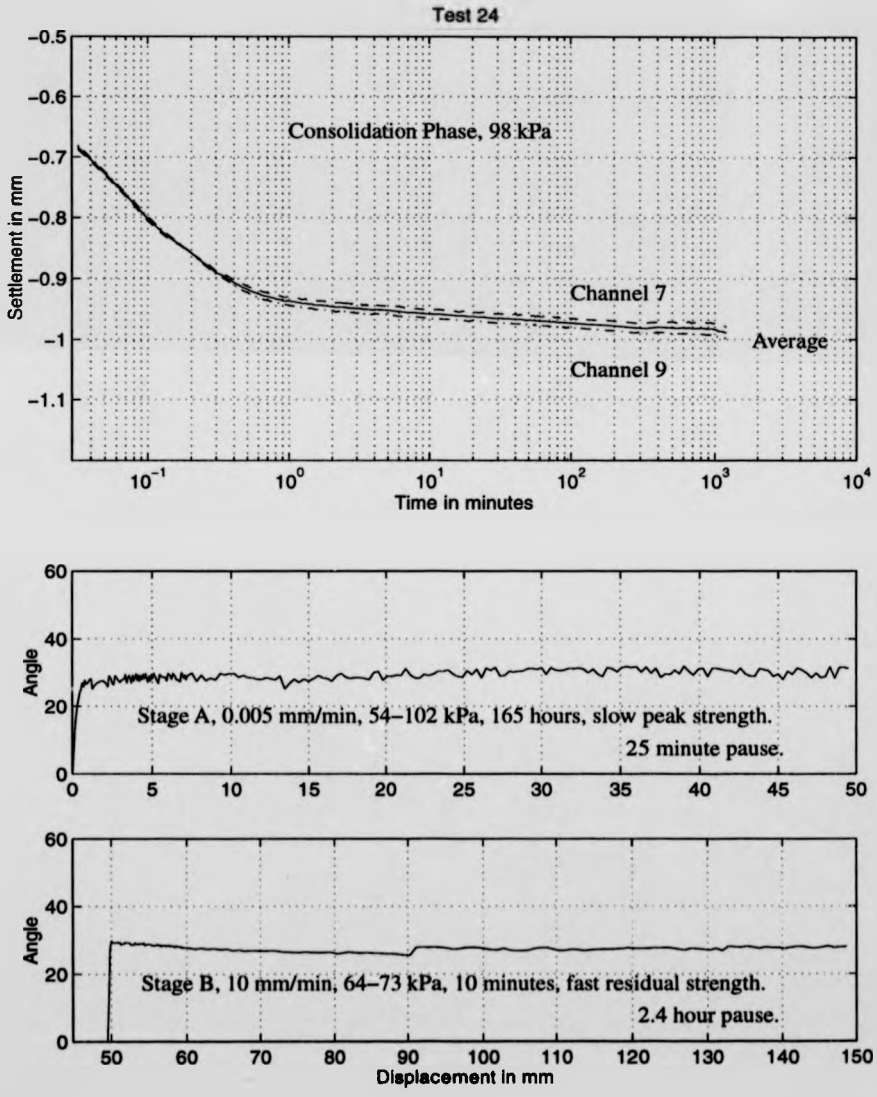

Figure D.74: Test 24, submerged, planar stainless steel test, 100% crushed flint.

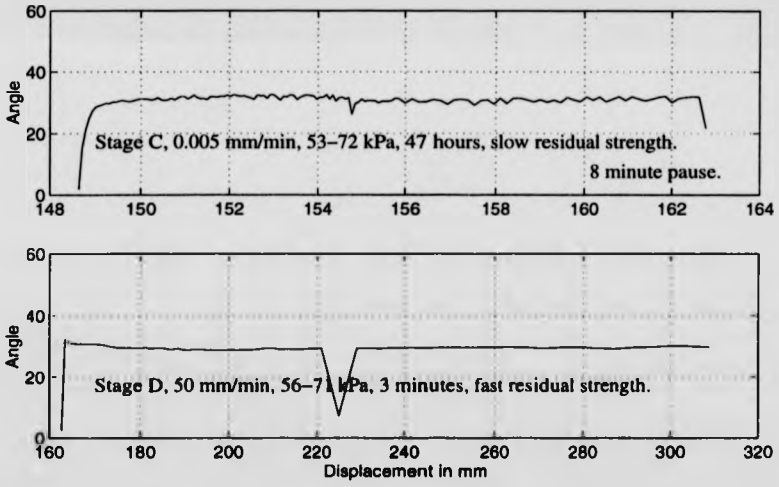

Figure D.75: Test 24, submerged, planar stainless steel test, 100% crushed flint.

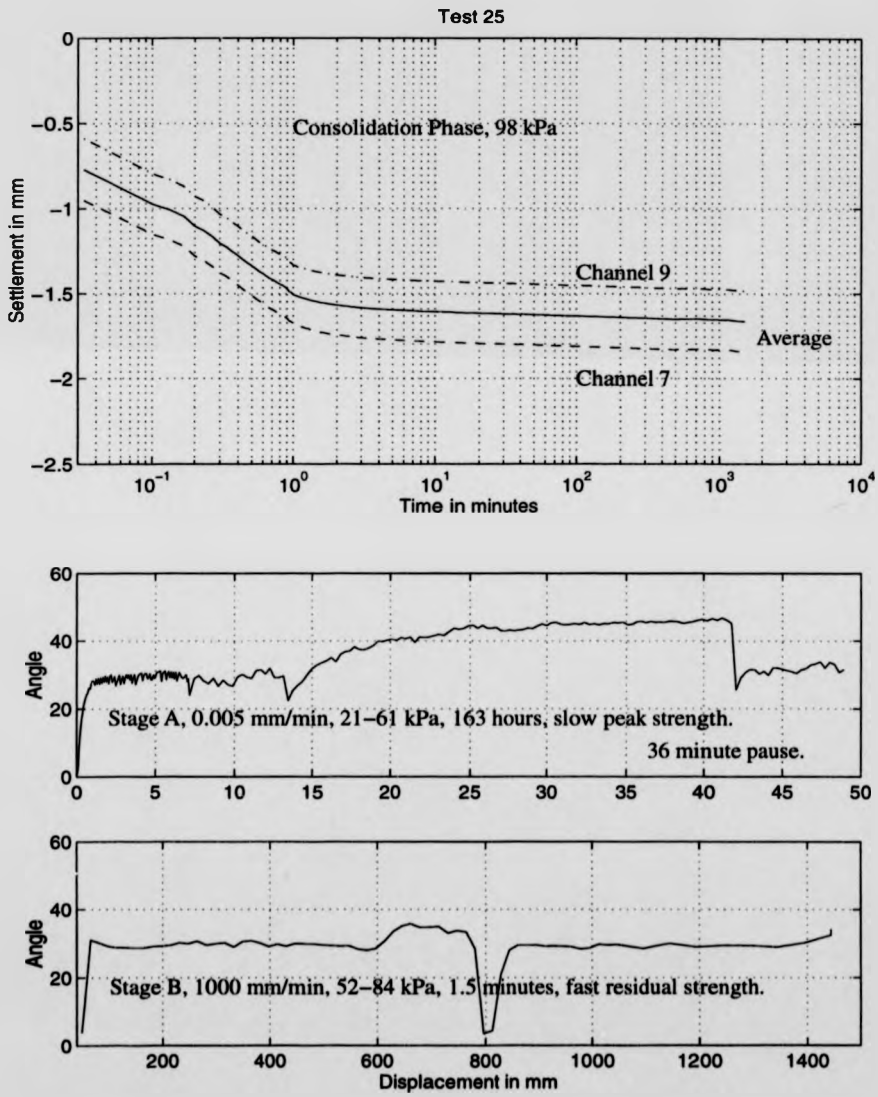

Figure D.76: Test 25, submerged, planar stainless steel test, 100% crushed flint.

DX
230144
vol.2